

Unclassified

SECURITY CLASSIFICATION OF THIS PAGE

2

REPORT

AD-A205 012

IC FILE COPY

1. REPORT SECURITY CLASSIFICATION Unclassified		DTIC	
2. SECURITY CLASSIFICATION AND SECURITY INTERESTS SELECTED		3. DISTRIBUTION/AVAILABILITY OF REPORT Approved for public release: Distribution unlimited	
7. DECLASSIFICATION/DOWNGRADING SCHEDULE 1989		4. MONITORING ORGANIZATION REPORT NUMBER(S) AFOSR-TR- 89-0034	
5. PERFORMING ORGANIZATION REPORT NUMBER(S) D		6. NAME OF PERFORMING ORGANIZATION Airborne Research Associates	
7. OFFICE SYMBOL (If applicable) NC		8. NAME OF MONITORING ORGANIZATION AFOSR/NC	
9. ADDRESS (City, State and ZIP Code) 46 Kendal Common Road Weston, Massachusetts 02193		10. ADDRESS (City, State and ZIP Code) Building 410 Bolling AFB, D.C. 20332-6448	
11. NAME OF FUNDING/SPONSORING ORGANIZATION AFOSR		12. OFFICE SYMBOL (If applicable) NC	
13. ADDRESS (City, State and ZIP Code) Building 410 Bolling AFB, D.C. 20332-6448		14. PROCUREMENT INSTRUMENT IDENTIFICATION NUMBER F49620-86-C-0013	
15. SOURCE OF FUNDING NOS.		16. SOURCE OF FUNDING NOS.	
PROGRAM ELEMENT NO. 61102F		PROJECT NO. 2310	
TASK NO. A1		WORK UNIT NO.	
17. TITLE (Include Security Classification) AIRCRAFT INVESTIGATION OF THE TURBULENT TRANSPORT OF ELECTRIC CHARGE THROUGH THE UNSTABLE PLANETARY BOUNDARY LAYER			
18. PERSONAL AUTHOR(S) Anderson, Bruce, Ralph Markson, Christopher W. Fairall, and John C. Willett			
19. TYPE OF REPORT Final		20. TIME COVERED FROM 15 NOV 85 to 14 NOV 87	
21. DATE OF REPORT (Yr. Mo. Day) 1989 January 5		22. PAGE COUNT 321	
23. SUPPLEMENTARY NOTATION			
24. COSATI CODES		25. SUBJECT TERMS (Continue on reverse if necessary and identify by block number)	
FIELD	GROUP	SUB. GR.	
		Atmospheric electricity; electrode layer; convection current; turbulent charge transport. (JLB) E	
26. ABSTRACT (Continue on reverse if necessary and identify by block number) Experimental results from a two year aircraft investigation of the atmospheric electrical and meteorological properties of the unstable planetary boundary layer (PBL) are reported. The primary objectives of the research were to 1) examine the strength of the electrode effect charge source over land and sea, and 2) obtain simultaneous measurements of meteorological and charge fluxes under varying conditions of atmospheric stability to test predictions of a second order closure model of charge transport (J. Willett, J. Geophys. Res., 84, 703, 1979). Soundings of electric field, conductivity, temperature, condensation nuclei, dew point, and turbulence structure functions for velocity, temperature and humidity along with surface temperatures and wind speeds were obtained over the desert in southeastern New Mexico in May 1986, and over water in the Bahamas in March 1987. Our results indicate 1) strong electrode layers form over the ocean but are often inhibited over land by surface radioactivity and 2) the shape and intensity of convection current profiles are dependent on electrical relaxation and turbulence intensity as predicted by the charge transport model. (Keywords)			
27. DISTRIBUTION/AVAILABILITY OF ABSTRACT UNCLASSIFIED/UNLIMITED <input checked="" type="checkbox"/> SAME AS RPT. <input checked="" type="checkbox"/> DTIC USE <input type="checkbox"/>		28. ABSTRACT SECURITY CLASSIFICATION Unclassified	
29. NAME OF RESPONSIBLE INDIVIDUAL James G. Stobie, Lt Col, USAF		30. TELEPHONE NUMBER (Include Area Code) (202) 767-4960	
31. OFFICE SYMBOL NC			

COMPLETED PROJECT SUMMARY

**TITLE:** Aircraft Investigation of the Turbulent Transport of  
Electric Charge through the Unstable Planetary  
Boundary Layer

**PRINCIPLE INVESTIGATOR:** Dr. Ralph Markson  
Airborne Research Associates  
46 Kendal Common Road  
Weston, Massachusetts 02193

**CO-INVESTIGATORS:** Professor Christopher W. Fairall  
Department of Meteorology  
Pennsylvania State University  
University Park, Pennsylvania 16802

Dr. John C. Willett  
Code 4325  
Naval Research Laboratory  
Washington, DC 20375

**INCLUSIVE DATES:** 15 November 1985 to 14 November 1987

**CONTRACT NUMBER:** F49620-86-C-0013

**TOTAL COST:** \$233,120

**SENIOR RESEARCH PERSONNEL:** Dr. Bruce Anderson  
Airborne Research Associates

**JUNIOR RESEARCH PERSONNEL:** None

**PUBLICATIONS AND PRESENTATIONS:**

"A field Study of the Electrode Effect and Convection Current  
over Land", C.W. Fairall, J.C. Willett, R. Markson and B.  
Anderson, EOS, Trans. Amer. Geophys. Union, 67(44), 891, 1986.

"Electrical Structure in the Marine Boundary Layer", B. Anderson,  
R. Markson, C.W. Fairall, and J.C. Willett, EOS, Trans. Amer.  
Geophys. Union, 68(44), 1218, 1987.

"Aircraft Investigation of Electric Charge Flux over Land and  
Sea", B.E. Anderson, R. Markson, C.W. Fairall, and J.C. Willett,  
Proc. VIII Int. Conf. Atmos. Electricity, 782, Uppsala Sweden,  
(June, 1988), Institute for High Voltage Research at Uppsala  
University, Sweden, (Accepted for publication by the Journal of  
Geophysical Research, December, 1988).

"Comparisons of Ionospheric Potential and Air-Earth Current as  
Indicators of the Global Circuit Current", R. Markson, Proc. VIII  
Int. Conf. Atmos. Electricity, 814, Uppsala, Sweden, (June 1988),  
Institute of High Voltage Research at Uppsala University, Sweden,  
(Accepted for publication by the Journal of Geophysical Research,  
December, 1988).

## ABSTRACT OF OBJECTIVES AND ACCOMPLISHMENTS:

There were two main objectives to the research:

- (1) To examine the strength of the electrode effect charge source over land and sea.
- (2) To obtain simultaneous measurements of meteorological and charge fluxes under varying conditions of convection to test predictions of a second order closure model (Willett, 1979) of the turbulent transport of electrode effect space charge through the planetary boundary layer.

Aircraft soundings of electric field, conductivity, temperature, condensation nuclei, dew point, and turbulence structure functions for velocity, temperature and humidity along with surface temperatures and wind speeds were obtained over the desert in southeastern New Mexico and over water in the Bahamas. Sixteen flights were performed in the desert deployment where, in addition, a ground station was operated to obtain simultaneous measurements of wind speed at two heights, Air-Earth current density, electric field, and turbulence structure functions for temperature and velocity. Eleven flights were carried out over the ocean near Eleuthera, Bahamas.

Our results indicate:

- (1) Strong electrode layers form over the ocean but are often inhibited over land. We attribute this to radioactive emanations from the ground which cause ionization close to surface preventing an accumulation of monopolar ions.
- (2) The shape and intensity of convection current profiles are dependent on the electrical relaxation time and turbulence intensity as predicted by the charge transport model.
- (3) Vertical electric field measurements, because of their sensitivity to volumes of space charge, are a better indicator of organized oceanic convective structure than humidity or other in situ measurements.
- (4) Ionospheric potential is a much better parameter for observing temporal variations in the global electric circuit supply current than Air-Earth current density because of the latter's sensitivity to changes in columnar resistance and convection current.

---

## Reference:

Willett, J.C., 1979: Fair weather electric charge transfer by convection in an unstable planetary boundary layer, J. Geophys. Res., 84, 703.

---

**Final Technical Report  
(Unclassified)**

**"AIRCRAFT INVESTIGATION OF THE TURBULENT TRANSPORT  
OF ELECTRIC CHARGE THROUGH THE UNSTABLE  
PLANETARY BOUNDARY LAYER"**

**Submitted to the**

**AIR FORCE OFFICE OF SCIENTIFIC RESEARCH**

**Contract F49620-86-C-0013**

**by**

**AIRBORNE RESEARCH ASSOCIATES  
46 Kendal Common Road  
Weston, MA 02193**

**5 January 1989**

**Prepared by**

**Bruce Anderson, Senior Scientist**

**Ralph J. Markson, Principle Investigator**

**Christopher W. Fairall, Co-Investigator**

**John C. Willett, Co-Investigator**

**89 2 10 133**

**Approved for public release;  
distribution unlimited.**



# FOREWORD

The work presented in this document was the cooperative effort of Airborne Research Associates, Inc., the Pennsylvania State University and the Naval Research Laboratory and was performed under contract number F49620-86-C-0013 from the Air Force Office of Scientific Research.

Accession For	
NTIS	CRAD <input checked="" type="checkbox"/>
DTIC	US <input type="checkbox"/>
Unann	<input type="checkbox"/>
Dist	<input type="checkbox"/>
By	
Date	
Author	
Dist	Author
A-1	

## TABLE OF CONTENTS

TITLE PAGE.....	i
FORWORD.....	ii
ACKNOWLEDGEMENTS.....	iv
LIST OF PARTICIPANTS.....	v
SUMMARY .....	vi
I. INTRODUCTION .....	1
II. EXPERIMENTAL APPROACH .....	5
A. Flight Procedures .....	5
B. Data Acquisition .....	8
III. MEASUREMENTS.....	9
A. Instrumentation, Calibrations and Conversion Factors .....	9
B. Derived Variables and Parameters .....	17
IV. SURFACE SCALING, FLUXES, AND MODEL PARAMETERS .....	18
A. Electrical Parameters.....	18
B. Turbulence and Meteorological Parameters .....	20
REFERENCES .....	23
V. ELECTRICAL AND METEOROLOGICAL SOUNDINGS .....	24
A. New Mexico Data.....	30
B. Bahamas Data.....	169
VI. DATA SUMMARIES AND CONVECTION CURRENT PROFILES.....	284
VII. APPENDICES.....	309
Appendix A. "Aircraft Investigation of Electric Charge Flux over Land and Sea", Anderson, B., R. Markson, C.W. Fairall and J.C. Willett, <u>Proc. VIII Int. Conf. Atmos. Electricity</u> , 782, Uppsala, Sweden, (June, 1988), Institute of High Voltage Research at Uppsala University, Sweden (accepted for publication J. Geophys. Res.).	
Appendix B. "Comparison of Ionospheric Potential and Air-Earth Current as Indicators of the Global Circuit Current", R. Markson, <u>Proc. VIII Int. Conf. Atmos. Electricity</u> , 814, Uppsala, Sweden,	

#### ACKNOWLEDGEMENTS

We are grateful to the Bahamian government, Mr. Breon Leary and other personnel at the Rock Sound International Airport, members of the National Soaring Society, and, in particular, the late Mr. Jack Gomez, for their logistical support and assistance during the field deployments.

# LIST OF PARTICIPANTS

Principle Investigator: Dr. Ralph Markson  
Airborne Research Associates  
46 Kendal Common Rd.  
Weston, Massachusetts 02193  
ph. (617)-899-1834

Co-investigators: Dr. Christopher W. Fairall  
Dept. of Meteorology  
Pennsylvania State University  
University Park, Pennsylvania 16802  
ph. (814)-863-3934

Dr. John C. Willett  
Code 4325  
Naval Research Laboratory  
Washington, DC 20375  
ph. (202)-767-3350

Senior Personnel: Dr. Bruce E. Anderson  
Airborne Research Associates  
181 West Street  
Waltham, Massachusetts 02154  
ph. (617)-890-2066

## SUMMARY

This document presents experimental results of a two year aircraft investigation of the relationships between the electrical and micrometeorological structure of the unstable planetary boundary layer (PBL). The specific objectives of the research were to 1) quantify the strength of the electrode effect charge source over land and water and 2) obtain simultaneous measurements of the surface fluxes of heat and momentum and profiles of electrical parameters in order to test predictions of a second order closure model of the turbulent transport of electrode effect space charge (Willett; 1979, 1981). In pursuit of these goals, soundings of electric field, polar conductivities, temperature, condensation nuclei, dew point, and turbulence structure function parameters for velocity, temperature and humidity, along with surface temperatures and wind speeds were obtained on flights over the desert in southeastern New Mexico in May 1986, and over water in the Bahamas in March 1987. This report presents these unique data along with a discussion of the experimental techniques, instrumentation, calibrations, and methods used to calculate derived variables, surface fluxes and model parameters.

Analyzed results are discussed in Appendices A and B, two papers given at the Eight International Conference on Atmospheric Electricity in Uppsala Sweden in June of 1988, and are not emphasized in the main body of the report. (Both papers have been accepted for publication in the Journal of Geophysical Research.) Summarizing the findings presented in these papers:

- (1) Strong electrode layers form over the ocean but are often weak or inhibited over land. We attribute this to radioactive emanations from the soil which cause ionization close the surface preventing an accumulation of positive space charge (Appendix A).
- (2) The shape and intensity of convection current profiles are dependent on electrical relaxation and turbulence intensity as predicted by the charge transport model (Appendix A).

(3) Vertical electric field measurements, because of their sensitivity to volumes of space charge, are a better indicator of the structure of organized convection over the ocean than humidity or other in situ measurements (Appendix A).

(4) Ionospheric potential is a much better parameter for observing variations in the global electric circuit than Air-Earth conduction current density because of the latter's sensitivity to changes in columnar resistance and convection current (Appendix B).

We expect to provide more indepth discussions of results and final conclusions in future publications when a more thorough comparison of experimental results with model predictions has been completed.

## I. INTRODUCTION

Briefly, this report is organized into a detailed account of how measurements and variables were obtained or calculated (Sections I, II, III and IV); flight descriptions and tables and graphs of meteorological and electrical soundings (Section V); tables of surface flux, model and electrical parameters and convection current profiles (Section VI); and discussions of results (Appendices A and B).

As indicated in the above summary, the primary motivations for this work were to measure the strength of the electrode layer over land and sea and to test the predictions of a second order closure model of the turbulent transport of space charge in the PBL (Willett, 1979, 1981). The strength of the electrode layer can be assessed from profiles of electric field and conductivity while the model requires as additional inputs the surface fluxes of momentum, heat, and moisture, surface roughness and measurements of conduction current density well above the exchange layer. The simultaneous determinations of all these parameters was made possible by use of ARA's dedicated twin-engine Beechcraft Baron atmospheric research aircraft. This aircraft, shown in Figure 1, has been outfitted with atmospheric electrical, meteorological and turbulence instrumentation and used with success in numerous past field experiments (e.g., Markson, et al., 1981). One additional device, a condensation nucleus counter, was purchased and installed for use in this project so that small ion lifetimes could be estimated.

Measurements were made at two diverse locations, Hobbs, New Mexico, and Rock Sound (RSD), Bahamas (see Figures 2a and 2b for maps of the two areas) in order to access the strength of the electrode effect charge source over land and ocean. The former region is characterized by thick, strongly unstable, cloud-free mixed layers and the latter by intense convection driven by warm ocean currents. In total, 27 data flights of about 2.5 hours average duration were performed; 16 during a 3 week stay at Hobbs in May, 1986, and 11 in just over 2 weeks in the Bahamas in March, 1987. All flights, except ocean Flight 6 and land Flight 16, were made in fine weather. Land Flight 16, conducted in the early morning, was the only one made in a neutral to stable PBL. On several missions, specifically



Figure 1. Turbocharged Beechcraft Baron atmospheric research aircraft. Radioactive probe antennas are located near the left wingtip and the Gardien conductivity tubes are under the right wingtip. A vertical mast holding 5 microthermal sensors was mounted on the right wingtip and the Lyman-Alpha hygrometer was positioned under the left wing. Both digital and analog data acquisition systems are operated by an observer.



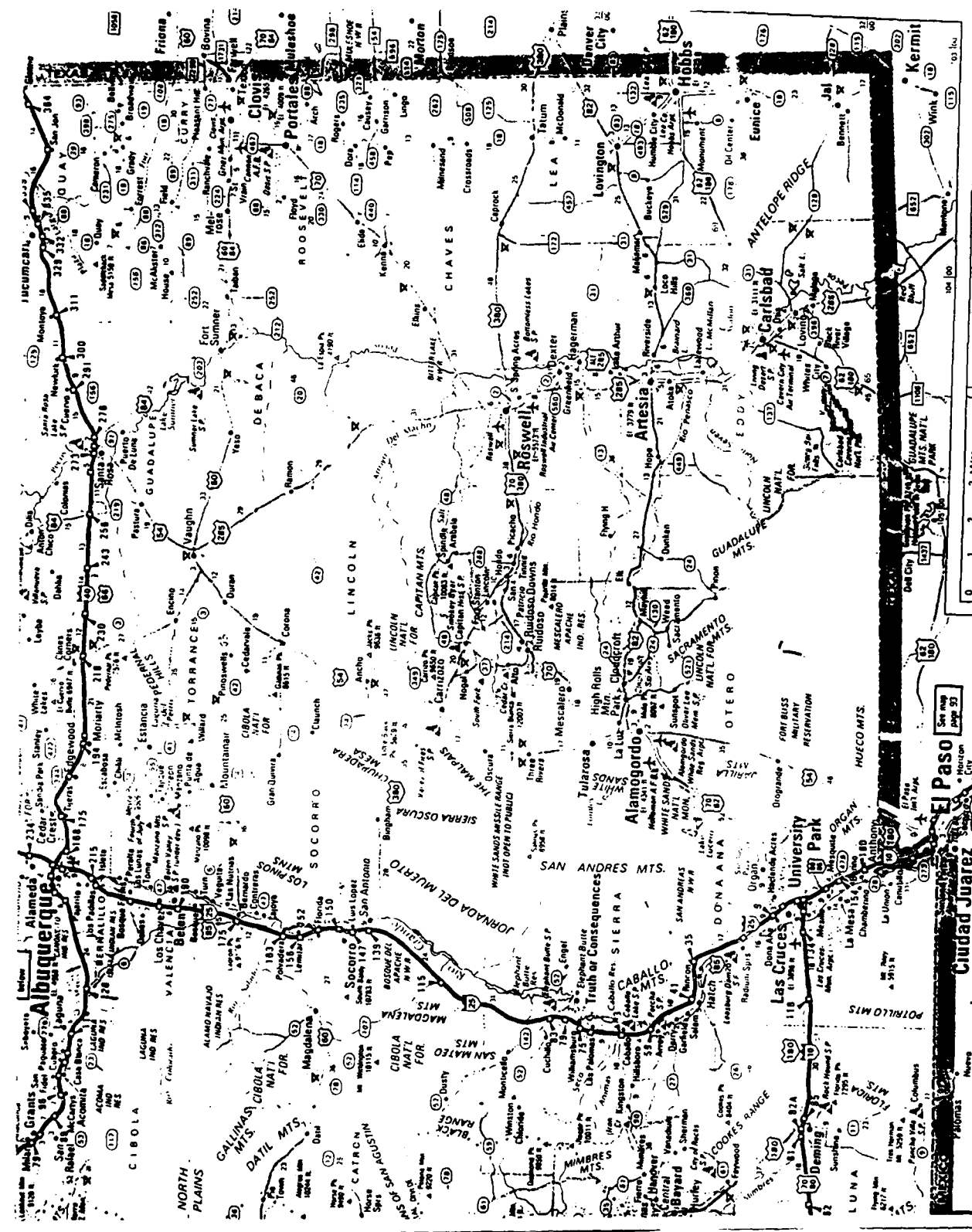


Figure 2a. A map of southern New Mexico showing areas where data were collected during the desert deployment. Missions were flown from the Hobbs Sail Plane Port located 7 miles from the Texas border and 70 miles ENE of Carlsbad.

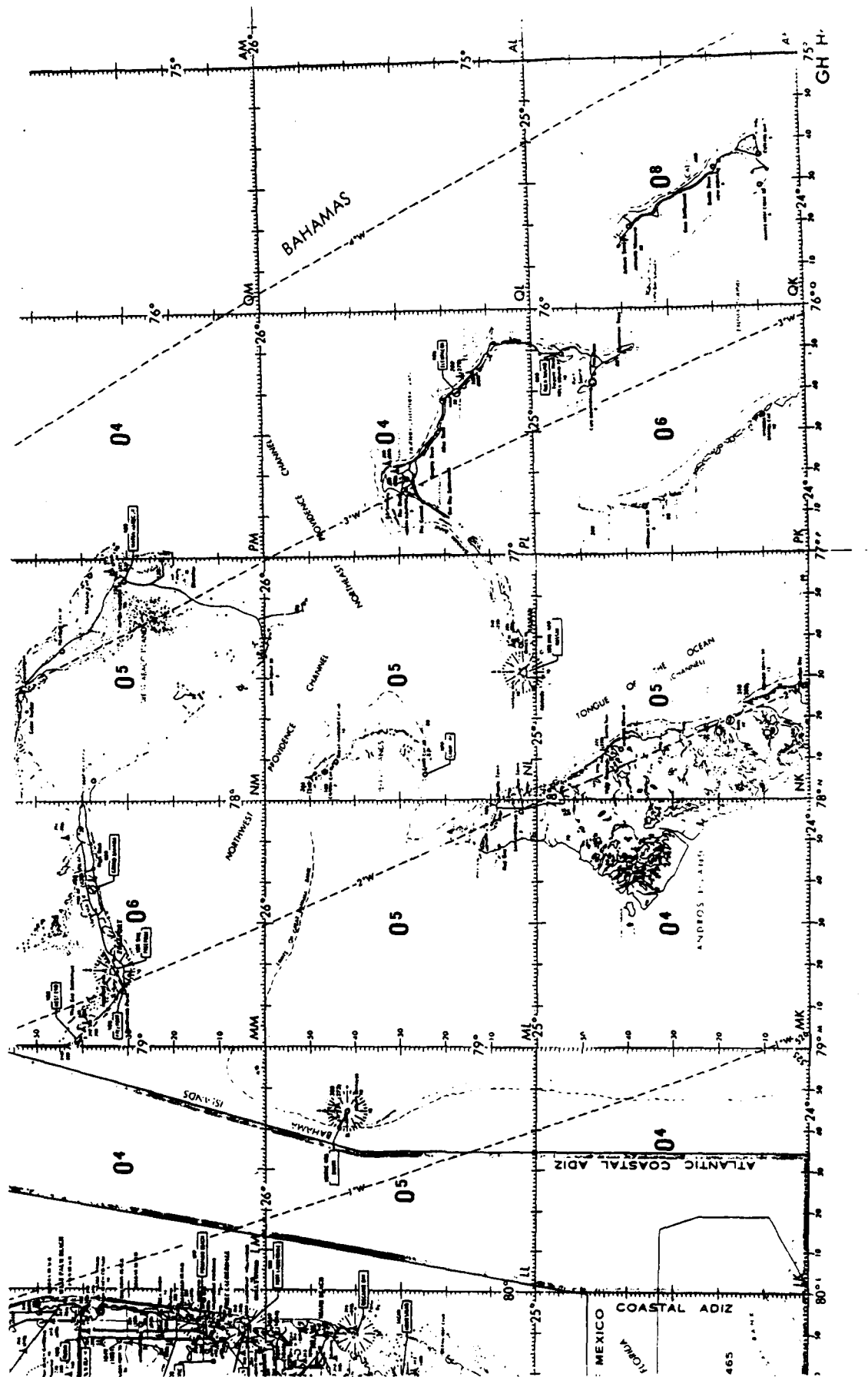


Figure 2b. A map of the Bahama Islands and the southeast coast of Florida showing the areas where oceanic measurements were obtained. The aircraft and crew were based in Rock Sound, Eleuthera (24°53' N, 76°11' W) and most data flights were made within a 60 Nm radius N and E of this point. Flight 9 soundings were performed over the Gulf Stream between Bimini and Miami.

land Flights 1, 2, 10, and 11 and ocean Flights 1 and 4, we failed to acquire complete micrometeorological data sets. This was because of either equipment failure or broken wires on the turbulence instrumentation. At Hobbs, because of the extreme heat and turbulence, the aircraft computer experienced frequent crashes resulting in some data loss.

Early in the land deployment it became evident that surface radioactivity was causing high conductivity near the ground. This ionization retards formation of electrode layers, hence limiting the convective current. Electric field and conductivity soundings were made near Portales, Carlsbad and Roswell, New Mexico, none of which showed significantly less radioactivity than near Hobbs. Tabulated results show the average electrical relaxation time over Hobbs was about one half that found in the marine PBL.

## II. EXPERIMENTAL APPROACH

### A. Flight Procedures

At Hobbs, where a ground station had been set up to measure conduction current and micrometeorological parameters, the usual flight plan was to make a ladder profile (a series of level passes at increasing altitudes) over the ground equipment, then make a slow continuous spiral descent ending with low passes over the same area. This was to allow comparison between the aircraft and the ground station data. Constant altitude passes at reduced power were performed during the ascent since ascending profiles of the turbulence parameters can not be used for analysis because of increased aircraft engine and propeller noise during a climb. Ladder profile rungs were usually at 20, 50, 100, 200, 500, 1000 and 2000 ft heights, then at 2000 to 3000 ft intervals up to the flight apex, and were about 2 min in duration. Descent rates were about 500 ft/min above the inversion, slowing to around 200 ft/min near the ground. Since convection is generated by solar heating of the surface in the desert environment, PBL conditions changed quite rapidly in time. This allowed us to make up to 3 flights a day and to obtain distinctly different profiles on each.

Similar flight plans were followed over the ocean in the Bahamas. Since no ground equipment was involved, the aircraft was simply flown upwind from land to open ocean water and data collection was initiated. Ladder profiles and spiral descent soundings were obtained on all flights with the exception of Flight 1 which was mainly a test flight. Additional low altitude passes were made to examine the convective structure over the ocean and to provide data from which to calculate the 15 m wind velocities. Convection in the marine environment is driven by air-water temperature differences and since ocean water temperatures show only slight diurnal variations, we conducted only 1 mission per day, with Flights 9 and 10 being the exception. The former yielded soundings over shallow water near Bimini, over the Gulf stream between Bimini and Florida, and another between Bimini and Nassau. Flight 10, the return trip from Nassau to Rock Sound, produced entirely different profiles over the shallow water west of Eleuthera.

Near the ocean surface, owing to the plume structure of organized convection in the marine PBL (references), the electrical and meteorological parameters were quite variable. This is illustrated in Fig. 3, a time series of electric field and humidity variations at 6 m height. In order to obtain realistic averages of these quantities, level passes were at least 2 min and typically 3 min in duration. Some error could arise from frequency aliasing, since data were recorded at 3 s intervals, but this would only apply to the electric field instrument which has a temporal response of around 1 s (the humidity, temperature and velocity variations are all fed to RMS units with ca. 10 s time constants). This error, which is anticipated to be small, has not been assessed. The rapid fluctuations in electric field become damped with height and, like convection current density, depend on the stability of the PBL.

The experiment required determinations of conduction current density well above the convective boundary layer. At Hobbs, where the mixed layer depth ranged to over 4 km and averaged 1.8 km, soundings were made to about 7 km altitude, requiring pilot and crew to utilize breathing oxygen. Over the ocean, the inversion height was always below 2 km (averaging 1.1 km) with a weak subsidence inversion between 2 and 3 km. Soundings there were

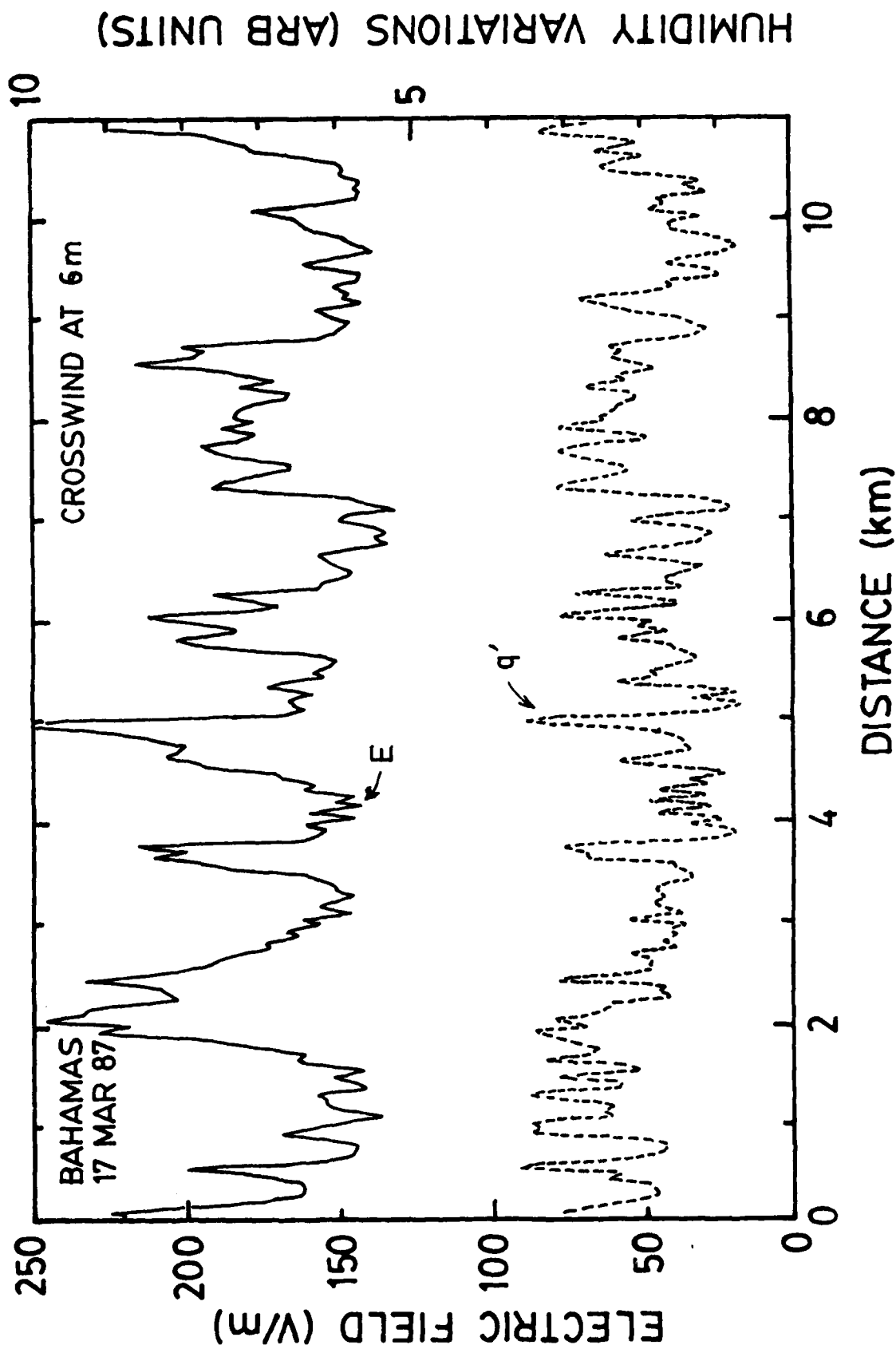


Figure 3. Time series of electric field (solid line) and humidity fluctuations (dashed line) over the ocean at 6m height showing the variability of these parameters caused by organized convection.

obtained to 4.1 km altitude. A general criteria for terminating ascent was the magnitude of the vertical electric field ( $<10$  V/m) and whether conductivity was increasing at an exponential rate with altitude. After initial soundings, apex altitudes were chosen and flown to on subsequent missions.

## B. Data Acquisition

A Hewlett Packard (HP) basic programable 9835B desktop computer coupled through an IEEE488 interface to a HP 3497 20 channel scanner/voltmeter was used to acquire and record data. The scanner sampled all 20 analog channels in about 3.2 seconds. The channel gains were checked with a voltage reference prior to the experiment and found to be accurate to within 0.1% in the worst case; zero offsets were all less than  $\pm 1$  LSB. Loran position and ground speed data entered the computer via a custom BCD interface which was read after every 5 analog data scans (around 16 second intervals). Data was stored on magnetic tape cartridges of about 200 KByte capacity which provided approximately 1.5 hours of data-taking capability. All signals were recorded as raw voltages with corrections and calibrations applied postflight. The system activated a high voltage relay which controlled the voltage on the Gerdien conductivity tubes's capacitor plates.

An 8 channel strip chart recorder was flown in both deployments to monitor instruments and provide realtime display. Flight notes were recorded directly on the chart and transcribed postflight. A second HP9835A computer was provided by NRL to allow ground personnel to perform data reduction and analysis while data was being collected. Plots were produced on a HP 7245 thermal plotter.

### III. MEASUREMENTS

#### A. Instrumentation, Calibrations and Conversion Factors

The following paragraphs provide a detailed description of the aircraft instruments, how calibrations were performed and factors used in converting analog signal outputs to engineering units:

(1) **Air pressure.** The aircraft has 2 pressure transducers onboard, both are solid state, one manufactured by National Semiconductor and the other by Rosemount Engineering. Calibrations were determined from extrapolated sea level pressures given as flight information and by comparison with the aircraft pressure altimeter.

$$P \text{ (mB)} = 100 * V \quad \text{(National Semiconductor)}$$

$$P \text{ (mB)} = 742.8 - 285.8 * V \quad \text{(Rosemount)}$$

The Rosemount sensor data were used to calculate altitude in all the final data analyses.

(2) **Altitude** was calculated from air pressure using the expression:

$$A \text{ (km)} = (1 - (P/P_0)^{-5.256}) T_0 / 6.5$$

where  $P_0$  and  $T_0$  are the pressure and Kelvin temperature at ground level. Altitudes calculated in this manner were in good agreement with those indicated by the aircraft cockpit altimeter.

(3) **Air temperature** was determined from a Rosemount Engineering Platinum resistive sensor designed specifically for aircraft. This device was calibrated versus mercury thermometers and checked periodically by comparison with the aircraft cockpit thermometer.

$$T \text{ (°C)} = (V - .02) * 100$$

The temperature was corrected for dynamic heating of the sensor using the following expression:

$$T_c (K) = T [ (C_p/C_v - 1) M^2 / 2 ]$$

where  $C_p$  and  $C_v$  are the heat capacity of air at constant pressure and volume, respectively, and  $M$  is the Mach number. For our average velocity (60 m/s), this expression reduced to:

$$T_c = T / [1 + 1.8 / T] \quad \text{where all temperatures are Kelvin.}$$

(4) Dew point was measured with an EG&G model 137-C3 aircraft hygrometer system of the chilled mirror type. The mirror was cleaned periodically and the calibration was checked and set by replacing the hygrometer sensor with factory supplied resistors, then adjusting the scale and zero potentiometers to obtain the recommended output voltages.

$$T_{dew} (^{\circ}C) = 23 * V - 65$$

(5) Vertical electric field. Two redundant custom-built radioactive probe systems were used in the desert deployment; only one was used in the Bahamas. Field values are determined as the difference in potential between radioactive probes mounted an equal distance above and below a wingtip in a vertical array. These sensors can be seen on the left wingtip in Fig. 1. Custom electronics using high voltage feedback and driven guard rings provide the system with rapid response. The electric field created by charge on the airframe is rejected as common mode signal by adjusting the gain of one of the input amplifiers until the system is immune to changes in aircraft charge. Empirical calibrations were determined by making low level passes by a ground station, ignoring the effects of image charge.

$$E1 (V/m) = 104 * V \quad (\text{outboard})$$

$$E2 (V/m) = 102 * V \quad (\text{inboard})$$



According to the convention of ordinary physics, the electric field is directed downward in fair weather and should be negative. This document, unfortunately, has mixed conventions; the graphs and tables in Section V. report positive fields in fair weather while the tables in Section VI. present negative values for the same data. The latter section switches convention in order to present convection currents as positive; the 200 to 300 graphs of the former section were completed before this necessity was realized. One should bear in mind that all the data presented herein are from fair weather measurements.

(6) **Positive and negative conductivity.** Two identical custom-built Gerdien tube capacitors mounted under the right wingtip were used for these determinations. Capacitance of the tubes were measured at NRL. The current amplifier gain,  $R_{eff}$ , (the effective feedback resistor value in the op amp circuit) was established for each tube by introducing a known current onto the center plate (anode or cathode) and measuring output voltages. Acceleration voltages ( $V_{acc}$ ) of about  $\pm 90$  V were used throughout. Amplifier offsets ( $V_o$ ) were measured at regular intervals during the flight by grounding the acceleration plates of the tubes and recording the output signals.

$$\lambda_{\pm}(\text{ohm}^{-1}\text{m}^{-1}) = \epsilon_o V / R_{eff} V_{acc} C$$

for most of this work

$$\lambda_{+}(\text{ohm}^{-1}\text{m}^{-1}) = 7.38\text{E-}12 (V - V_o) / V_{acc}$$

$$\lambda_{-}(\text{ohm}^{-1}\text{m}^{-1}) = 7.16\text{E-}12 (V - V_o) / V_{acc}$$

(7) **Conduction current density,  $J$ .**  $J$  is defined as being the product of electric field and total conductivity. Note that in the boundary layer  $J$  will be a superposition of conduction and convection current.

$$J (\text{pA/m}^2) = E ( \lambda_{+} + \lambda_{-} )$$

(8) Cloud condensation nuclei (CCN) were measured with an Environment-One model Rich 200 CCN counter obtained for the project. The calibration curve determined for the instrument from tests at NRL is shown in Figure 4. Corrections were only applied to values used to calculate ion lifetimes and ion production rates. This instrument detects nuclei of 0.0016  $\mu\text{m}$  diameter and larger.

$$\text{CCN (Kcounts/cm}^3\text{)} = \text{Gain } V / 5$$

(9) Surface temperature (TIR) was measured with a Barnes PRT-5 infrared radiation thermometer. Calibrations were found by positioning a pan of water underneath the sensor and making simultaneous measurement of its temperature with a high quality mercury thermometer and the IR thermometer. Curves were produced by adding ice or hot water to the bath while stirring. This sort of calibration suffers from reflections of the aircraft in the pan, but no other suitable approach has been found.

$$\text{TIR (}^{\circ}\text{C)} = 10 (V - 1.43) \quad (\text{medium range})$$

$$\text{TIR (}^{\circ}\text{C)} = 12.6 (V + 1.36) \quad (\text{high range})$$

(10) Indicated airspeed was gauged with a Rosemount Engineering pressure transducer. The unit is calibrated by comparison with the aircraft airspeed indicator while varying the engine power settings in level flight.

$$\text{IAS (kts)} = 96.3 (V - 1.65) / 1.09$$

(11) Ground speed and position were recorded from a Teledyne 711 Loran-C navigation unit. The displayed ground speeds have been verified by timing passes between known landmarks. Hobbs is not covered by the Loran Network; these data were only obtained on the ocean flights. Wind speeds were determined as the difference between the aircraft airspeed and groundspeed, or as one half the difference in ground speed between upwind and downwind runs.

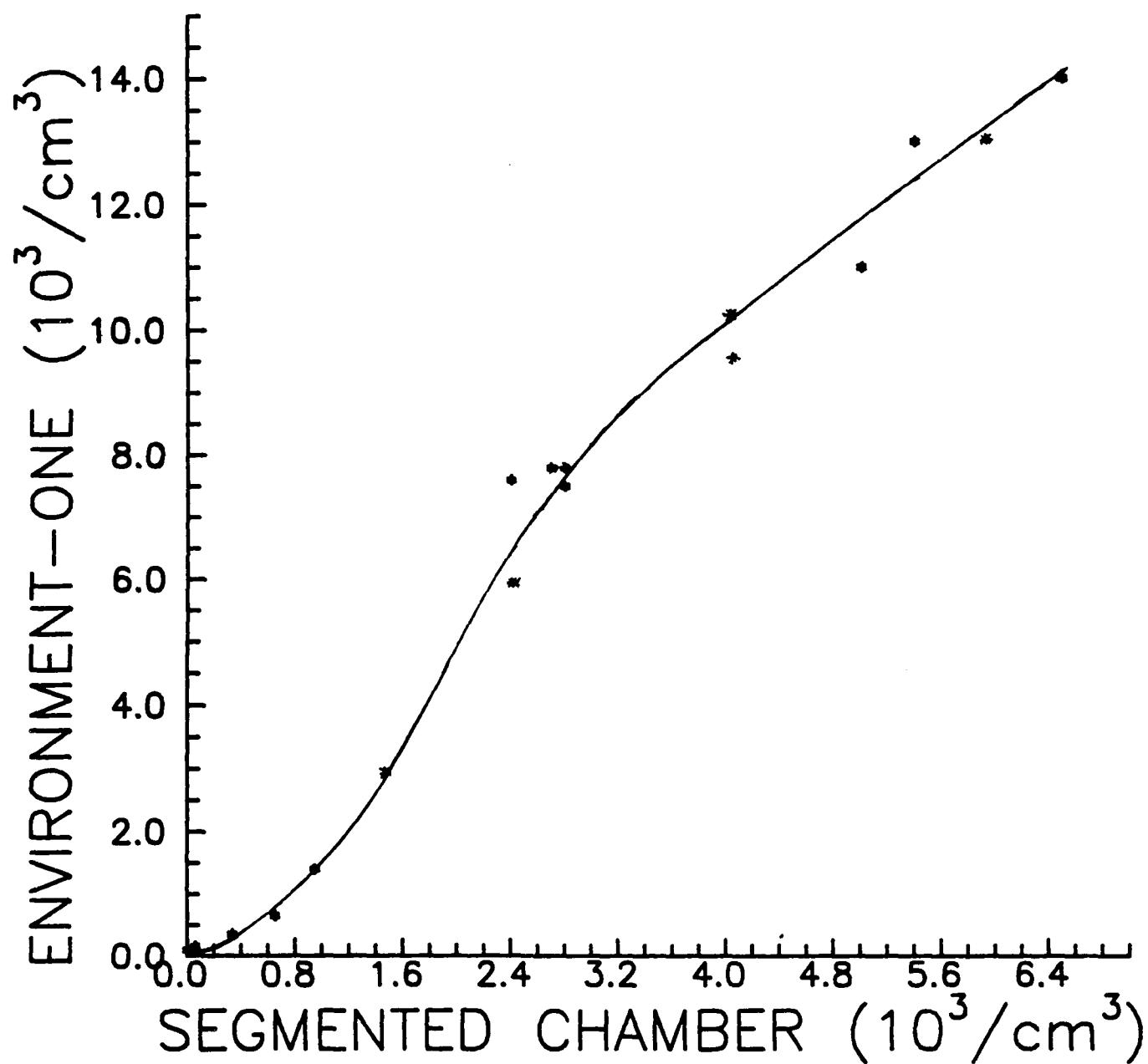


Figure 4. Calibration curve for the Environment One, Rich 200 condensation nuclei detector. Data were obtained at NRL using a well calibrated segmented chamber instrument.

(12) Temperature structure function parameter,  $C_T^2$ . Temperature fluctuations,  $\langle V_T \rangle$ , were measured with a 4.5  $\mu\text{m}$  diameter Tungsten resistive wire sensor (Thermo Systems Inc. (TSI) model T1.5-1210) and a fast response TSI dc Wheatstone bridge. A second resistive probe, left covered during flight, was used to balance the bridge. The probes were arranged on a vertical mast on the aircraft right wingtip. Typical probe resistances were 6 ohms at 0°C, the bridge gain was set at 20 V/ohm using a variable decade resistor, and sensor current was 5 ma. The bridge output was fed to a signal conditioner with band pass filtering and variable gain, then to an RMS unit with gain, before being recorded on the computer system. High and low pass filter settings were 10 and 200 Hz for both deployments and a total gain of 30 was employed. The system's electrical noise was determined by measuring the output with the probes covered. The microthermal sensors are known to change resistance when they become encrusted with sea salt, so each probe was washed in an alcohol/water solution as part of preflight for the ocean flights.

$C_T^2$  was calculated using the single probe, RMS method (Fairall and Marks, 1984) from the bridge measurements of temperature fluctuations described above.

Let

$$X_1 = .11 (f_1^{-2/3} - f_u^{-2/3}) U^{2/3}$$

$$X_2 = [S G R_1 \alpha (1 + \alpha T)]^2$$

$$X_3 = 2 \cdot [.000015 G I^3]^2 (P/1013) (288/(T + 273))^{3/2} \epsilon^{2/3}$$

Then

$$C_T^2 (\text{°C}^2/\text{m}^{2/3}) = [(\langle V_T \rangle^2 - (G V_N)^2)/X_2] - X_3 / .42 X_2$$

Where

$f_1$  = lower frequency limit, 10 Hz in both locations

$f_u$  = upper frequency limit, 200 Hz

U = Aircraft airspeed, usually 60 m/s

$S$  = bridge sensitivity, 20 V/ohm  
 $G$  = total amplifier gain, 30  
 $R_i$  = ice point resistance of the probe, 6 ohms  
 $\alpha$  = probe temperature coefficient,  $.004\text{ }^{\circ}\text{C}^{-1}$   
 $T$  = ambient temperature,  $^{\circ}\text{C}$   
 $I$  = probe current, 5 mA  
 $P$  = pressure at given altitude, mB  
 $V_N$  = system noise, .002 V  
 $\epsilon$  = velocity structure function parameter (see below).

Note that term  $X_3$  is a correction for the microthermal probe velocity sensitivity at the current employed. At higher currents the velocity contribution can become significant.

(13) Velocity structure function parameter or the rate of dissipation of turbulent kinetic energy,  $\epsilon$ . Velocity fluctuations,  $\langle V_v \rangle$ , were measured with a fast response TSI hot-wire anemometer in a constant temperature circuit using the same type of resistive sensor described above. A decade resistor was used to balance the bridge and apply a 50% overheat to the probe. Signals were bandpass filtered, amplified and RMS values recorded. Filter settings of 50 and 200 Hz were used at Hobbs and 20 and 200 Hz over the ocean with the total gain being 300 in both locations. Noise values were determined with the hot wire covered. The bridge DC output was also recorded.

was calculated from the RMS and DC outputs of the Hot-wire anemometer described above using the following equations:

If

$$Y_1 = (f_1^{-2/3} - f_u^{-2/3})^{-3/2}$$

$$Y_2 = B (P/1013)^{1/2} (288/(T + 273))^{1/4} (165 - T)/150$$

then,

$$\epsilon \text{ (m}^2\text{s}^{-3}\text{)} = 619 U^{1/2} \langle V_v \rangle^3 (V/Y_2 G)^3 Y_1$$

where U, T, and P retain the definitions and values given above and

$f_l = 50$  Hz at Hobbs, 20 Hz over the ocean

$f_u = 200$  Hz

B = hot wire sensitivity,  $1.0 \text{ V}^2/(\text{m/s})^{1/2}$

V = hot wire DC output voltage

G = total gain, 300 for both deployments

(14) Humidity structure function parameter,  $C_q^2$ . Humidity variations,  $\langle V_q \rangle$ , were determined with a custom-made Lyman-Alpha hygrometer. The source and detector were mounted under the left wingtip and a path length of 1 cm was employed. The detector output was split, the DC signal being recorded directly and fluctuation between 10 and 200 Hz amplified with a total gain of 30 and RMS values were recorded. The Lyman-Alpha was not used in the desert deployment.

$C_q^2$  was calculated from the Lyman-Alpha DC and RMS outputs using the following expressions.

$$F = .11 (f_l^{-2/3} - f_u^{-2/3}) U^{2/3}$$

$$C_q^2 (g^2/kg^2 \text{ m}^2/3) = ((\langle V_q \rangle^2 - (V \cdot V_N)^2)/G)/(F (V/S)^2)$$

where

$f_l = 10$  Hz

$f_u = 200$  Hz

V = the Lyman-Alpha DC signal, V

$V_N$  = the normalized RMS noise level, 0.0016

G = system gain, 30

S = sensitivity, 6

The Lyman-Alpha source lamp output varies with lens cleanliness, source voltage, etc. By normalizing the above equation by source strength, these variations are effectively removed.

## B. Derived Variables and Parameters

Experimentally determined variables were combined to yield meteorological and electrical parameters useful in elucidating the structure of the troposphere. The paragraphs below describe each and detail their calculation.

(1) Virtual potential temperature,  $\theta_v$  (K), e.g., temperature extrapolated to the surface and corrected for water vapor content, was calculated from:

$$\theta_v = T [1 + .61 Q] (P_o/P)^{0.287}$$

where  $Q$  is the specific humidity.

(2) Specific humidity,  $Q$ , is derived from the air pressure,  $P$ , and dew point temperature saturation water vapor pressure,  $e$ , using the following expression:

$$Q \text{ (g/Kg)} = 622 e / (P - 0.38 e)$$

where  $e \text{ (mB)} = 6.108 (T_d / 273.16)^{-5.14} e^{-(6827 (1/T_d - 1/273.16))}$   
and  $T_d$  is the dew point temperature in degrees Kelvin.

(3) Relative humidity,  $RH$ , is given by:

$$RH = e / e_s \quad (6)$$

where  $e$  and  $e_s$  are the saturation water vapor pressures at the measured dew point and at the ambient air temperature, respectively.

#### IV. SURFACE SCALING, FLUXES AND MODEL PARAMETERS

This section will define the parameters presented in the tables and graphs of Section VI.; most were used in evaluating Willett's model of turbulent electric charge transport in the PBL and are further defined in Willett (1979, 1981). A thorough discussion of surface layer scaling and Monin-Obukhov Similarity Theory can be found in Panofsky and Dutton (1984).

##### A. Electrical Parameters

(1) Convection current,  $J_c$ . In the boundary layer,  $J$  is the sum of the Air-earth conduction current density and convection current. The two were separated using:

$$J_c = J_o - E (\lambda_+ + \lambda_-)$$

where  $J_c$  is the convection or eddy current and  $J_o$  is the average conduction current density above the inversion, where convection current is assumed to be zero. Note that  $E$  and  $J_o$ , following the "Physics" convention, are negative in fair weather while  $J_c$ , the upward flux of positive space charge, is positive.

(2) The electrode effect source efficiency factor,  $\hat{J}_{mx}$ , (a dimensionless parameter) is simply the ratio of the maximum convection current to the conduction current and is given by:

$$\hat{J}_{mx} = -J_c / J_o$$

where  $J_c$  is measured near the surface (6 or 15 m altitude).



(3) The boundary layer electrical relaxation time,  $\tau_\lambda$ , is calculated from the average total conductivity in the surface layer using the expression:

$$\tau_\lambda (\text{seconds}) = \epsilon_0 / (\lambda_+ + \lambda_-)$$

where  $\epsilon_0$  is the dielectric constant of free space.

(4) The small ion lifetime,  $\tau_n$ , can be found from:

$$\tau_n (\text{seconds}) = [\alpha (\lambda_+ + \lambda_-) / 2 e k + \beta (Z)]^{-1}$$

where  $\alpha$  is the small ion recombination coefficient,  $e$  is the charge of a proton or electron ( $1.602 \times 10^{-19}$  C),  $k$  is the mobility of small singly charged ions at constant temperature and pressure,  $\beta$  is the recombination coefficient between small ions and large particles and  $Z$  is the large particle (aerosol) concentration as measured by the OCN counter. Polar conductivities and aerosol concentrations were an average from the lowest 100 m of the PBL. The following numerical values were used for the constants in the above expression (Hoppel, 1985).

$$\alpha = 1.6 \times 10^{-12} \text{ m}^3 \text{ s}^{-1} \text{ for both deployments}$$

$$k = 0.00012 \text{ m}^2 \text{ V}^{-1} \text{ s}^{-1} \text{ at sea level (Bahamas)}$$

$$k = 0.000137 \text{ m}^2 \text{ V}^{-1} \text{ s}^{-1} \text{ at 1.1 km altitude (Hobbs)}$$

$$\beta = 3.18 \times 10^{-12} \text{ m}^3 \text{ s}^{-1} \text{ (Bahamas)}$$

$$\beta = 1.15 \times 10^{-12} \text{ m}^3 \text{ s}^{-1} \text{ (Hobbs)}$$

(5) The volume ionization rate,  $q$ , was calculated using the equation

$$q (\text{m}^{-3} \text{ s}^{-1}) = (\lambda_+ + \lambda_-) / 2 e k \tau_n$$

where  $e$ ,  $k$ , and  $\tau_n$  retain the definitions and values given above. Again, the conductivity values used were from the lower 100 m of the PBL.

(6) The dimensionless potential drop across the boundary layer,  $V$ , is the ratio of the electrical potential at the inversion height ( $Z_i$ ) in the presence of convection current to an estimate of the potential due solely

to conduction current. The following equation was used for its calculation,

$$\hat{V} = [(\lambda_+ + \lambda_-)/(-J_0 Z_1)] [-\int_0^{Z_1} E_z dz]$$

where the polar conductivity values represent measurements in the surface layer. The lower limit of  $\hat{V}$  obtained in the absence of convection is 1.0.

## B. Turbulence and Meteorological Parameters

(1) The inversion height,  $Z_1$ , or thickness of the boundary layer was determined for each sounding from plots of  $C_T^2$  and  $\Theta_v$  supplemented by observations of cloud base altitudes. There generally was an uncertainty of 50 to 100 m in the selection of  $Z_1$  caused by limited sampling.

The surface fluxes were evaluated from ground (at Hobbs) and aircraft measurements using the bulk aerodynamic (Davidson et al., 1981) and dissipation (Fairall et al., 1980) techniques. Both methods rely on Monin-Obukhov Similarity theory (Panofsky and Dutton, 1984) to relate the mean fluctuations of temperature (T), velocity (u) and moisture (q) to scalar surface fluxes. The following equations define the Monin-Obukhov surface scaling parameters (starred quantities) in terms of eddy covariance fluxes:

momentum:  $\rho \overline{(u'w')} = -\rho u_*^2$

sensible heat:  $\rho C_p \overline{(\theta'w')} = -\rho C_p u_* T_*$

latent heat:  $\rho L_e \overline{(q'w')} = -\rho L_e u_* q_*$

Where w is the vertical velocity component,  $L_e$  the latent heat of vaporization of water,  $\rho$  the density of air,  $C_p$  the specific heat of air, and the primed quantities denote fluctuations about the mean.

Using the bulk technique, the surface scaling parameters for velocity, temperature and humidity can be represented by:

$$(2a) \quad u_* = u_z k [\ln(z/Z_0) - \psi_u(z/L)]^{-1}$$

$$(3a) \quad T_* = (T_z - T_s) \alpha k [\ln(z/Z_{0t}) - \psi_T(z/L)]^{-1}$$

$$(4a) \quad q_* = (q_z - q_s) \alpha k [\ln(z/Z_{0T}) - \psi_T(z/L)]^{-1}$$

where  $z$  is the height of the measurement and the subscripts  $s$  and  $z$  denote quantities (wind speed, temperature and moisture) at the surface and at height  $z$ .  $Z_0$  and  $Z_{0t}$  are roughness lengths,  $L$  is the Monin-Obukhov length,  $\alpha$  and  $k$  are constants, and  $\psi_u$  and  $\psi_T$  are empirical functions. The ratio  $z/L$  defines the stability of the layer and is calculated from the surface drag coefficients and roughness lengths in a manner detailed by Davidson, et al., (1981). Another approach to calculating this quantity, using the dissipation technique, is given below.

Fluxes were not calculated by the bulk technique at Hobbs because a) the wind speed gradient measurements yielded unreasonably long roughness lengths and b) surface temperatures were recorded only on the last 6 flights. For the oceanic data, literature values of roughness lengths and drag coefficients were used in all cases.

Using the dissipation method, the scaling parameters were calculated as follows:

$$(2b) \quad u_* = (0.4 z \epsilon)^{1/3} / (1 + 0.5 |S|^{2/3})^{1/2}$$

$$(3b) \quad T_* = -0.45 (C_T^2)^{1/2} [z (1 + 7 |S|)]^{1/3}$$

$$(4b) \quad q_* = -0.45 (C_q^2)^{1/2} [z (1 + 7 |S|)]^{1/3}$$

Where  $z$  is the height of the measurement and  $S$  is the atmospheric stability,  $z/L$ , discussed above.

S was calculated for an unstable surface layer from the following expression using an iterative process:

$$S = S_0 (1 + 0.5|S|^{2/3}) (1 + 7|S|)^{1/3}$$

where  $S_0$  is given by

$$S_0 = 3.26 (z^{2/3}/T) [(C_T^2)^{1/2} + 0.61 T (C_q^2)^{1/2}] / z^{2/3}$$

S is defined to be negative for unstable conditions.

The Monin-Obukhov length, L, is represented by:

$$(5) \quad L = z/S$$

$$\text{or} \quad L = T u_*^2 / k g \theta_{v*}$$

where k is Von Karman's constant (0.4), g is the force of gravity, and  $\theta_{v*}$  is given by  $T_* + 0.61 q_* T$ . The humidity scaling parameter,  $q_*$ , was not included in the Hobbs calculations because it was assumed to be negligible.

The ratio  $-Z_1/L$  is an indicator of convection strength. L denotes the approximate height where mechanical and buoyant generation of turbulence is equal; the larger the buoyant production of turbulence, the smaller L becomes. Therefore,  $-Z_1/L$  is directly proportional to convective strength.

(6) Model parameter, R, the ratio of electric to turbulent time scales, is calculated from:

$$R = u_* \tau_\lambda / Z_1$$

with large values of R favoring large convection currents.

## REFERENCES

- Davidson, K.L., G.E. Schacher, C.W. Fairall and A.K. Goroch,  
1981: Verification of the bulk method for calculating overwater optical  
turbulence, Appl. Optics, 20, 2919.
- Fairall, C.W., R. Markson, G.E. Schacher and K.L. Davidson, 1980: An  
aircraft study of turbulence dissipation rate and temperature structure  
function in the unstable marine atmospheric boundary layer,  
Boundary-Layer Meteor., 19, 453.
- Fairall, C.W., and R. Markson, 1984: Aircraft measurements of atmospheric  
velocity and temperature microturbulence spectra, Dept. of Meteor. Tech.  
Report, Pennsylvania State University, University Park, Pennsylvania.
- Gish, O.H., Evaluation and interpretation of the columnar resistance of the  
atmosphere, Terr. Mag. and Atmos. Electr. 49, 159.
- Hoppel, W.A., 1985: Ion-aerosol attachment coefficients, ion depletion and  
the charge distribution on aerosols, J. Geophys. Res. 90, 5917.
- Markson, R., J. Sedlacek, and C.W. Fairall, 1981: Turbulent transport of  
electric charge in the marine atmospheric boundary layer,  
J. Geophys. Res., 86, 12115.
- Panofsky, H.A. and J.A. Dutton, 1984: Atmospheric Turbulence, John Wiley  
and Sons, New York.
- Willett, J.C., 1979: Fair weather electric charge transfer by convection in  
an unstable planetary boundary layer, J. Geophys. Res., 84, 703.
- Willett, J.C., 1981: Toward an understanding of the turbulent electrode  
effect over land, Naval Res. Lab. Rept. 8519, Sept. 1981, Naval Research  
Laboratory, Washington, DC, 20375, copies can be obtained from the  
author.

## V. ELECTRICAL AND METEOROLOGICAL SOUNDINGS

Tables and plots of meteorological and electrical soundings are presented on the following pages. Data are grouped according to location and flight and include:

- 1) A brief flight description.
- 2) Tables of averages and standard deviations from level runs.
- 3) Plots of ladder profile data and convection current.
- 4) Graphs of continuous ascending or descending soundings.
- 5) Time series of electrical parameters (for selected flights over the desert only).
- 6) Radiosonde soundings of meteorological parameters and wind profiles (for ocean flights only).

The flight descriptions are not exhaustive; they are intended to give a summary of the weather conditions, flight locations and any non-routine observations. More extensive flight logs and data keys are available upon request.

Items 5) and 6) in the above list are only included for selected flights. Time series of aircraft atmospheric electrical parameters are provided on Desert Flights 8 through 16 so that comparisons can be made with groundstation data. MET soundings made at Nassau for several of the ocean flights were obtained from the Bahamian Flight service and are included as an aid to data interpretation; a complete set of soundings for the oceanic flights were not readily available at the time this document was prepared.

A summary of the symbols used in the tables and figures of this section is provided in Table 1. Definitions and references to the pages where each have been discussed are included and differences between the Hobbs and Rock Sound data sets are indicated.

Figures 5a through 5i are examples of the graphs and plots presented in this section. For the sake of brevity, subsequent figures will refer to one these plots for complete explanations of the symbols and formats used.

Ladder profiles and convection current plots are illustrated by Figures 5a through 5d. Data used in these plots are from the tables of level run averages. Ladder profiles were not obtained on Hobbs Flights 1, 2 and 3 and convection current profiles are only included on flights where they could be determined with confidence and when companion flux values were available.

Spiral and continuous soundings are exemplified by Figs. 5e through 5h with each plotted point representing a 5 sample average over about a 16 second time interval. The ascent or descent rates from such soundings were about 3 m/s, yielding a vertical resolution of approximately 50 m.

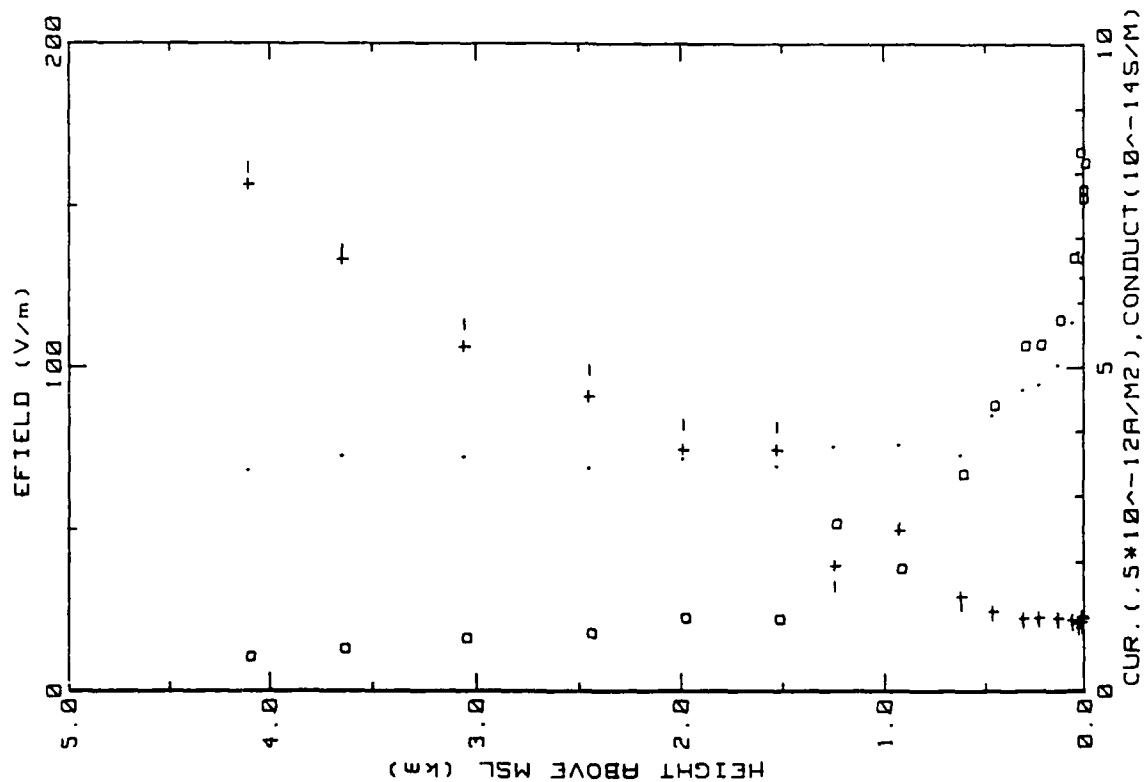
Figure 5i is an example of a time series plot of electrical parameters. Again, each point represents a 5 sample average over about 16 seconds. The aircraft airspeed was usually 60 m/s which yields a horizontal resolution per plotted point of approximately 1 km. Aircraft altitudes have not been included on the graph but can be deduced from the tables and times of the continuous soundings. Again, additional information is available upon request.

Finally, a cautionary note is in order for the turbulence data.  $C_T^2$  values from the ocean deployment are a factor of 3 larger than those expected from air-sea temperature differences. Also, at Hobbs, the aircraft  $\epsilon$  values were 3 times those measured by the ground station. In both cases, a faulty RMS unit is suspected to be the cause. The reader would be advised to divide both parameters by 3 before attempting to use them in further calculations. Oceanic  $\epsilon$  data and desert  $C_T^2$  values are reliable unless otherwise indicated.

Table 1. Summary of Symbols used in graphs and tables.

<u>Variable</u>	<u>Definition</u>	<u>Units</u>	<u>ref. page</u>
Time	Local Time	HHMM	-
N	Number of Samples in average		-
Altitude	Pressure altitude	km	9
Efield	Outboard electric field (RSD)	V/m	10
Efield1	Outboard electric field (Hobbs)	V/m	10
Efield2	Inboard electric field (Hobbs)	V/m	10
+Lam	Positive conductivity	$\text{ohm}^{-1}\text{m}^{-1}$	11
-Lam	Negative conductivity	$\text{ohm}^{-1}\text{m}^{-1}$	11
Con Curr	Conduction current	$\text{pA m}^{-2}$	11
Con Curr1	Calculated from E_field1	"	11
Con Curr2	Calculated from E_field2	"	11
Theta_v	Virtual Potential Temperature	$^{\circ}\text{C}$	17
Rel Hum	Relative humidity in %	-	17
CCN	Cloud Condensation Nuclei	$1000 \text{ cm}^{-3}$	12
Press	Atmospheric pressure	mB	9
EPS	Velocity structure function	$\text{m}^2\text{s}^{-3}$	15
CT	$C_T^2$ , Temperature structure function	$^{\circ}\text{C}^2\text{m}^{-2/3}$	14
Cq2	Humidity structure function	$(\text{g/kg})^2\text{m}^{-2/3}$	16
Q	Specific Humidity	g/Kg	17
Trose	Air temperature	$^{\circ}\text{C}$	9
T_IR	Infrared surface temperature	$^{\circ}\text{C}$	12
T_dew	Dew point temperature	$^{\circ}\text{C}$	10
Z <sub>1</sub>	Boundary layer thickness	km	20
Z/Z <sub>1</sub>	Normalized height	-	20





17MAR87 FLIGHT#11 1116 TO 1234 LST

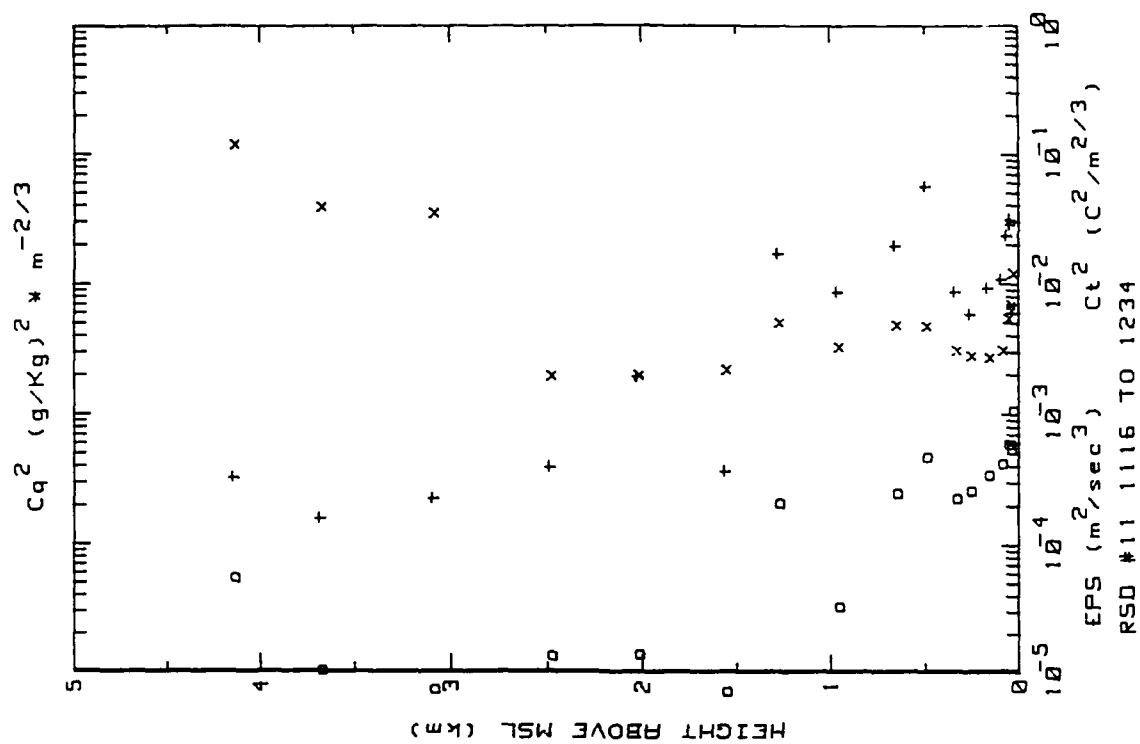


Figure 5b. The data points plotted are the eddy dissipation rate of turbulent kinetic energy,  $\epsilon$  (o), the temperature structure function parameter,  $C_T^2$  (x), and the humidity structure function parameter,  $C_q^2$  (+). The flight number and start and end times of the sounding are given below the graph.

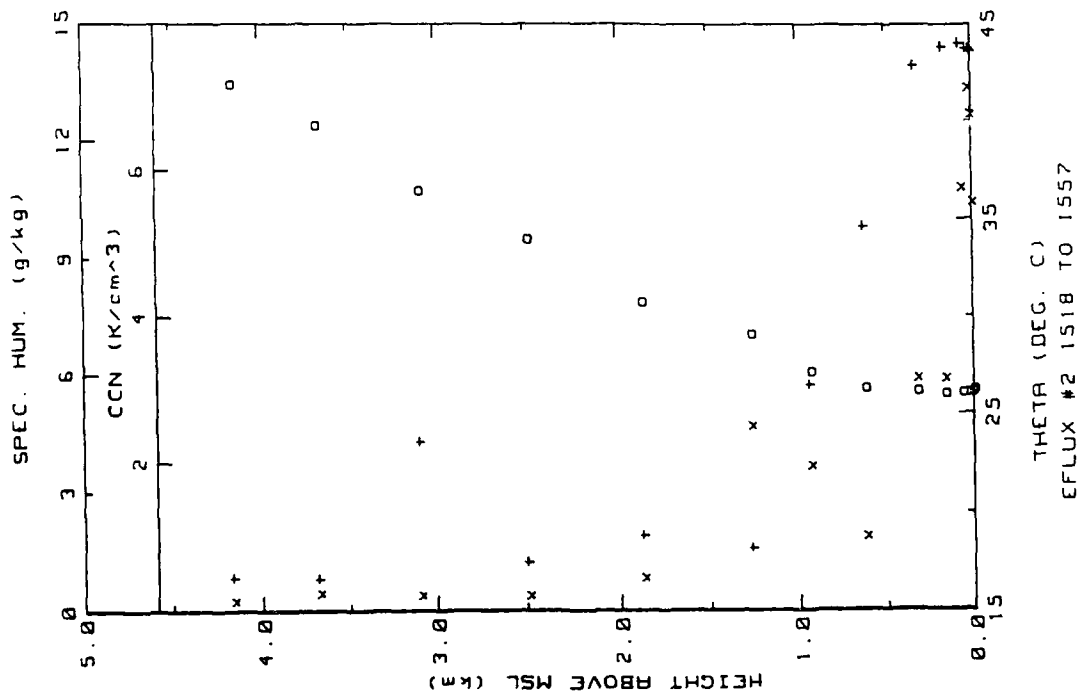


Figure 5c. The data points plotted are virtual potential temperature (O), specific humidity (+) and cloud condensation nuclei (x). The start and end times of the sounding are given below the plot.

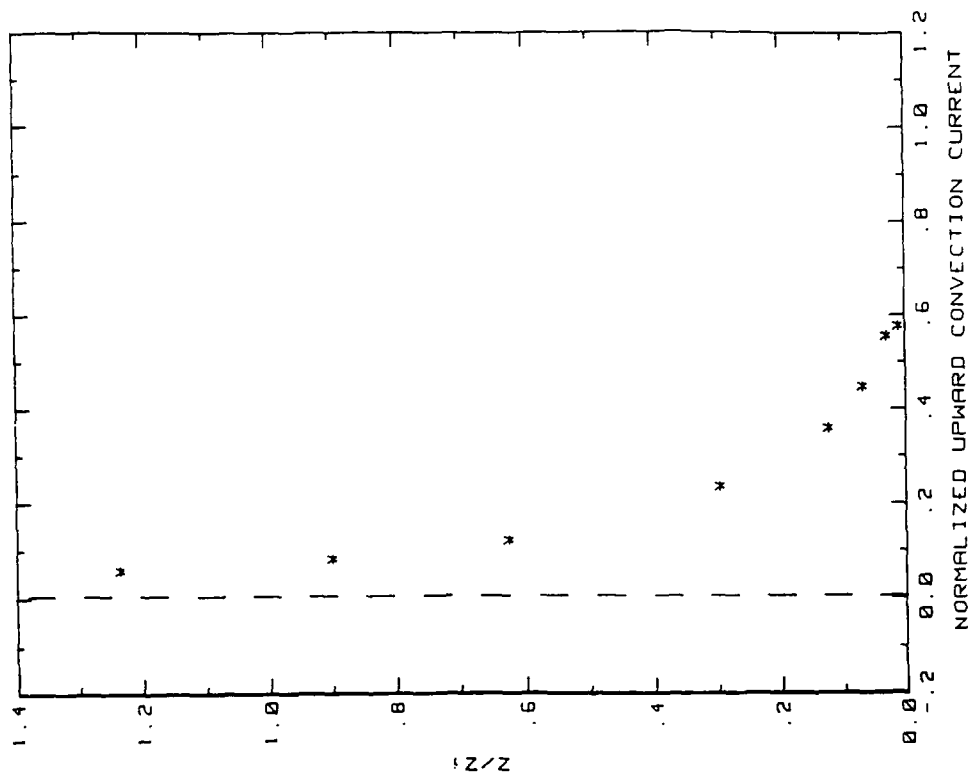


Figure 5d. Plot of normalized convection current ( $-J_c/J_0$ ) versus normalized height obtained by dividing the altitude of the level run ( $Z$ ) by the boundary layer thickness ( $Z_i$ ). The start and end times of the ladder profile along with the boundary layer thickness and Air-Earth conduction current density are given below the plot.

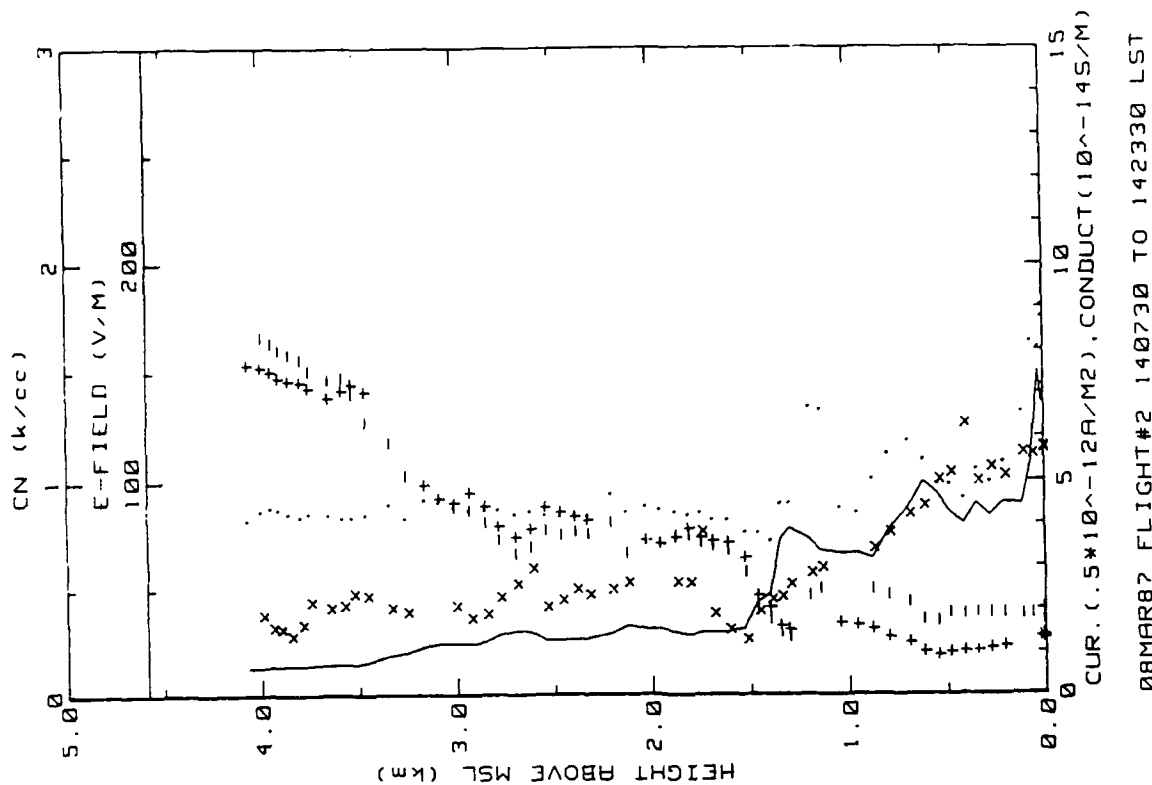


Figure 5f. The data points plotted are electric field (solid line), conduction current (.), positive conductivity (+), negative conductivity (-), and cloud condensation nuclei (x). The start and end times of the sounding are given below the graph. Each point represents a 5 sample average.

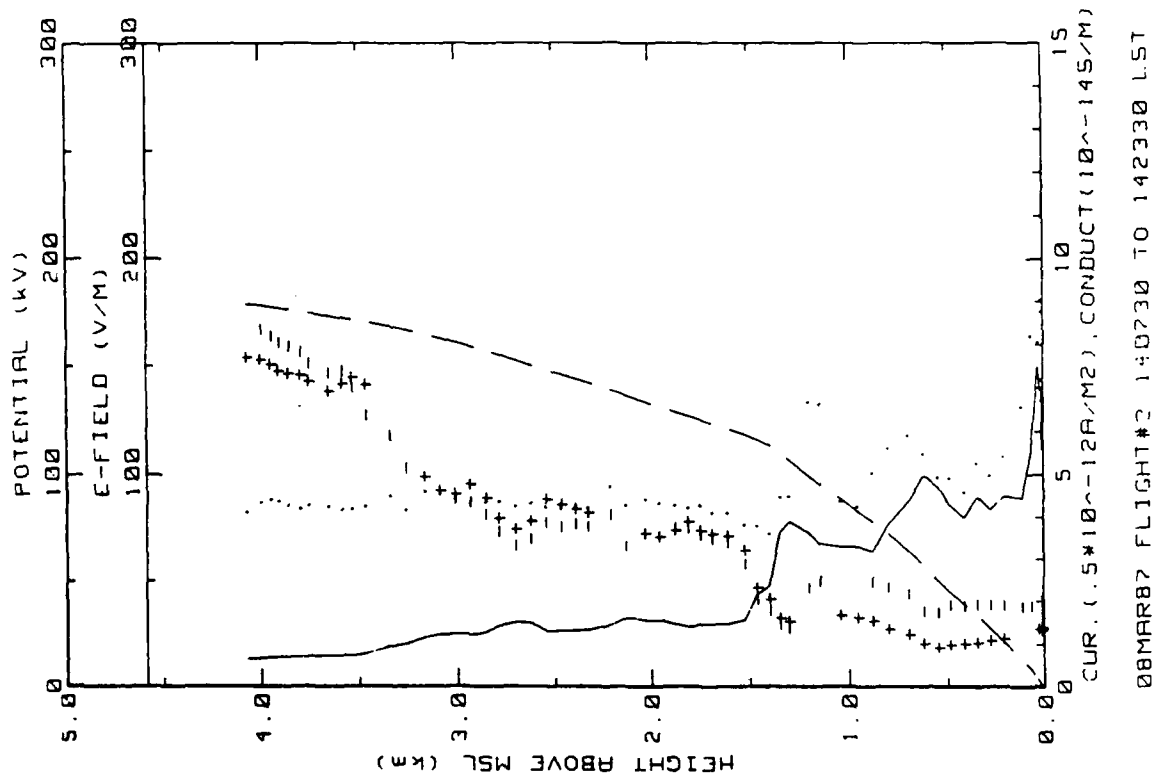


Figure 5e. The data points plotted are electric field (solid line), conduction current (.), positive conductivity (+), negative conductivity (-) and integrated potential (dashed line) using the convention of positive field in fair weather. The start and end times of the sounding are given below the graph. Each point represents a 5 sample average.

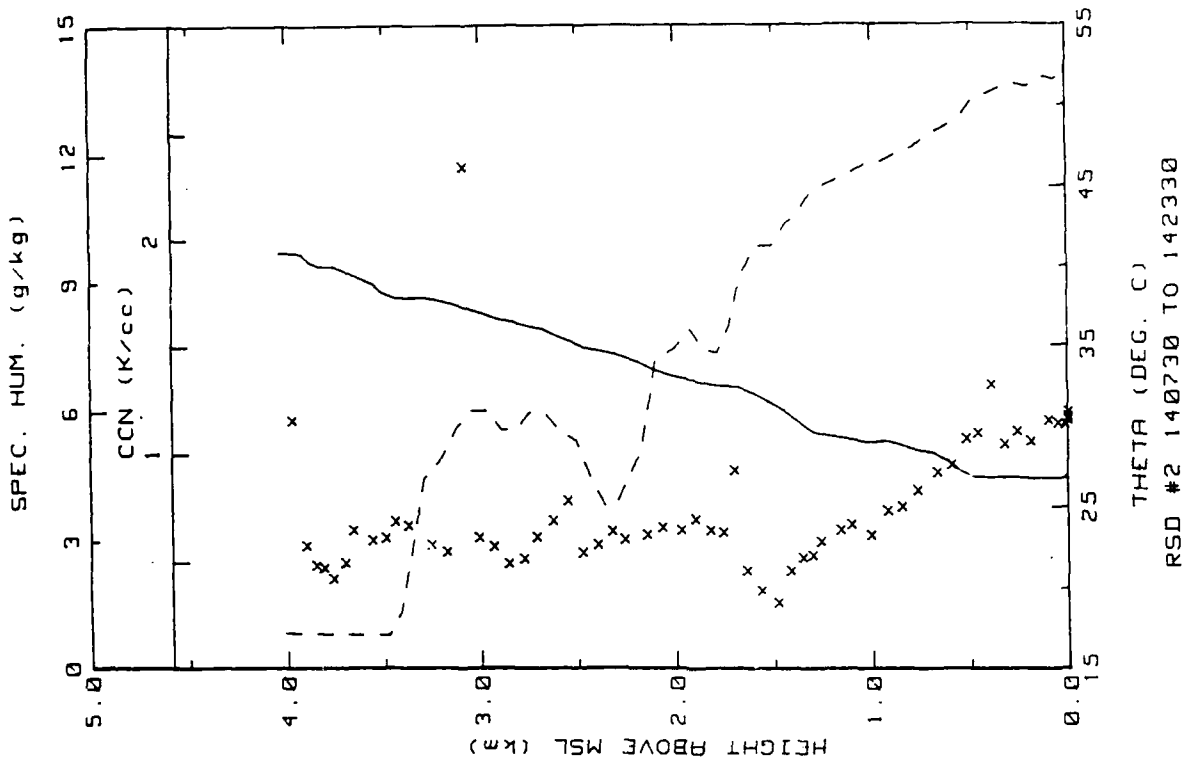


Figure 5h. The data points plotted are virtual potential temperature (solid line), specific humidity (dashed line) and cloud condensation nuclei (x). The start and end times of the sounding are given below the graph. Each point represents a 5 sample average.

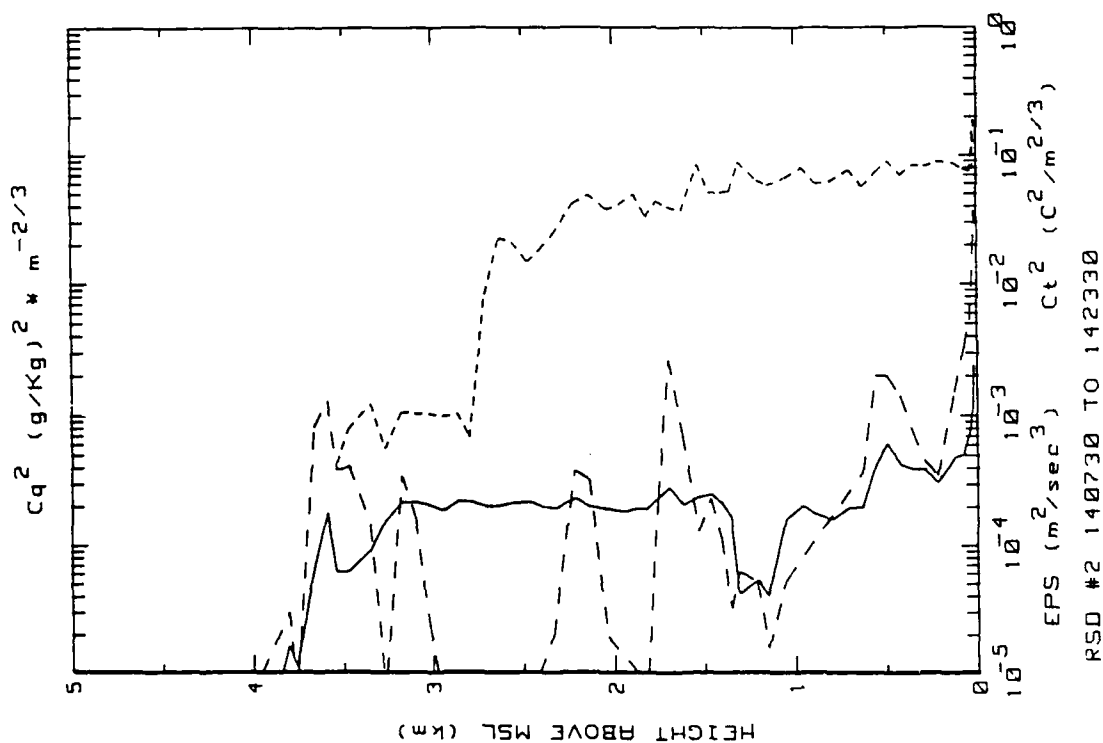
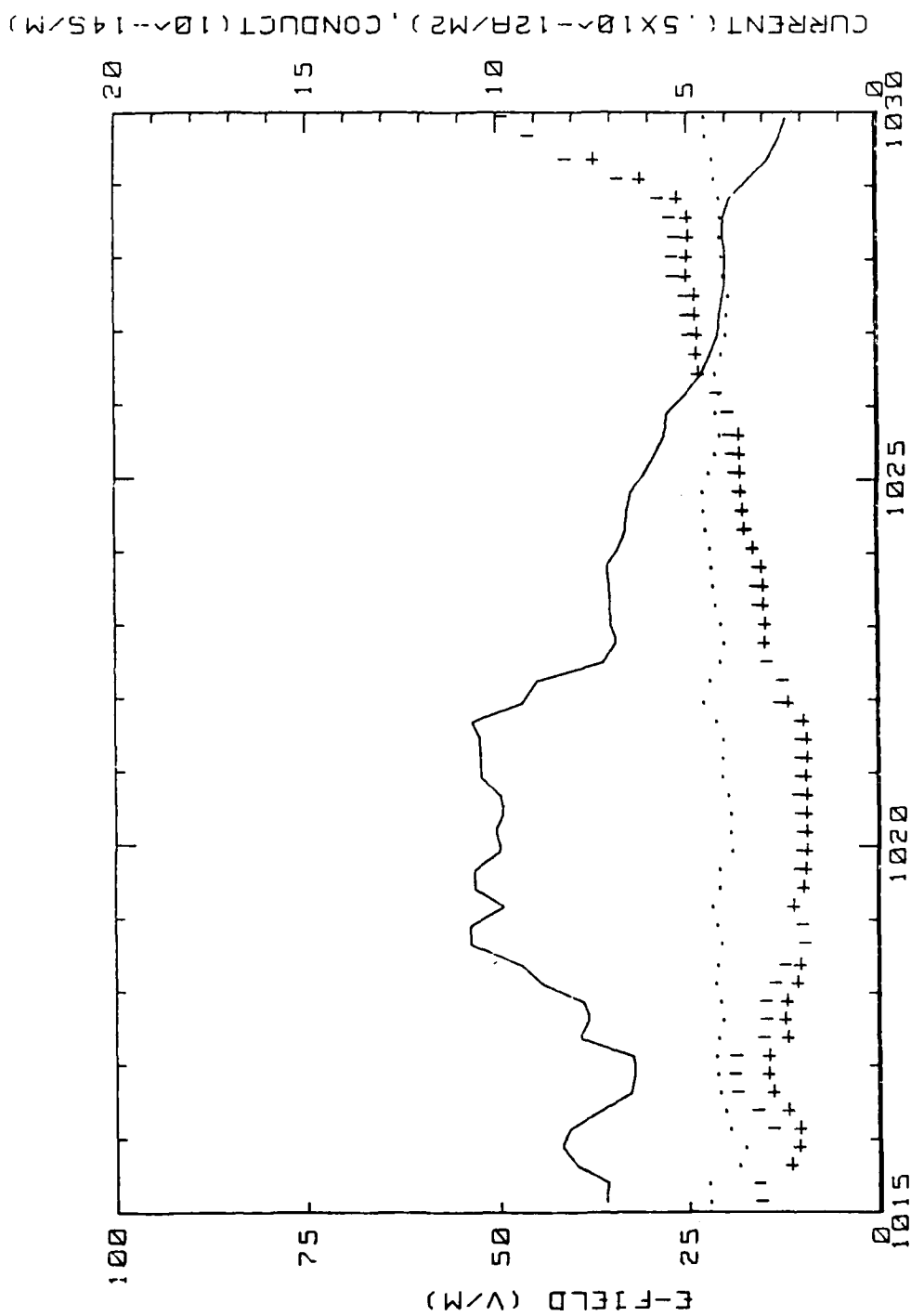


Figure 5g. The data points plotted are the eddy dissipation rate of turbulent kinetic energy,  $\epsilon$ , (solid line) the temperature structure function parameter,  $C_t^2$ , (long dashes) and the humidity structure function parameter,  $C_q^2$  (short dashes). The start and end times of the sounding are given below the plot. Plotted points represent 5 sample averages.



22 MAY 86 FLIGHT#9 101500 TO 103000 LST

Figure 5i. The data points plotted are electric field (solid line), positive conductivity (+), negative conductivity (-), and conduction current (.). Each point represents a 5 point average.

NEW MEXICO DATA

Period: 13 May 1986 to 29 May 1986

Flight: 1

Date: 13 May 1986

Takeoff: 1549 MDST from Hobbs

Landed: 1743 at Hobbs

Conditions: Mostly clear with scattered cumulus at 4.8 km. Light surface winds.

Instruments: Aerosol and turbulence instrumentation were not recorded.

Summary: Primarily a survey flight to determine the best site for the ground station. Low passes were made to measure conductivity, an indicator of surface radioactivity, near Hobbs and Pecos. Soundings of electrical parameters were made from Pecos enroute to Hobbs.

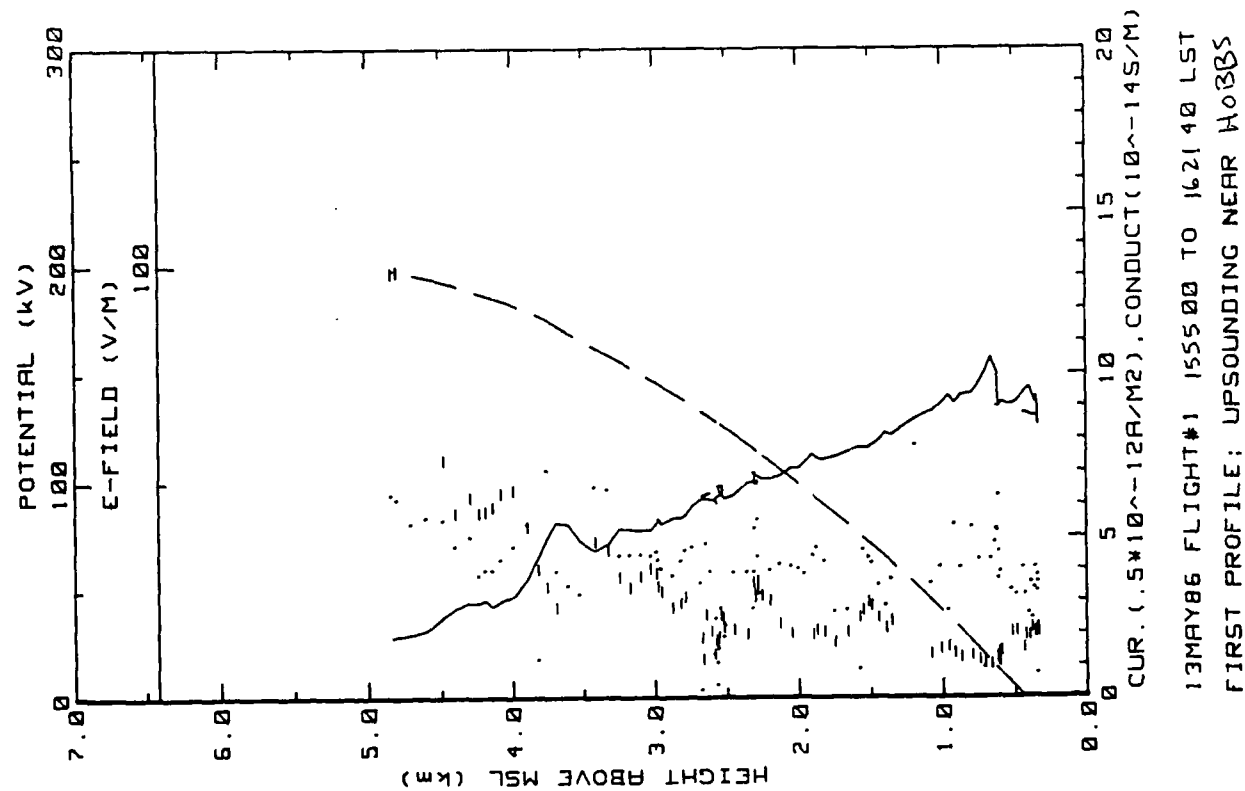


Figure 6a. Hobbs flight 1 continuous upsounding (ref. Fig. 5e).

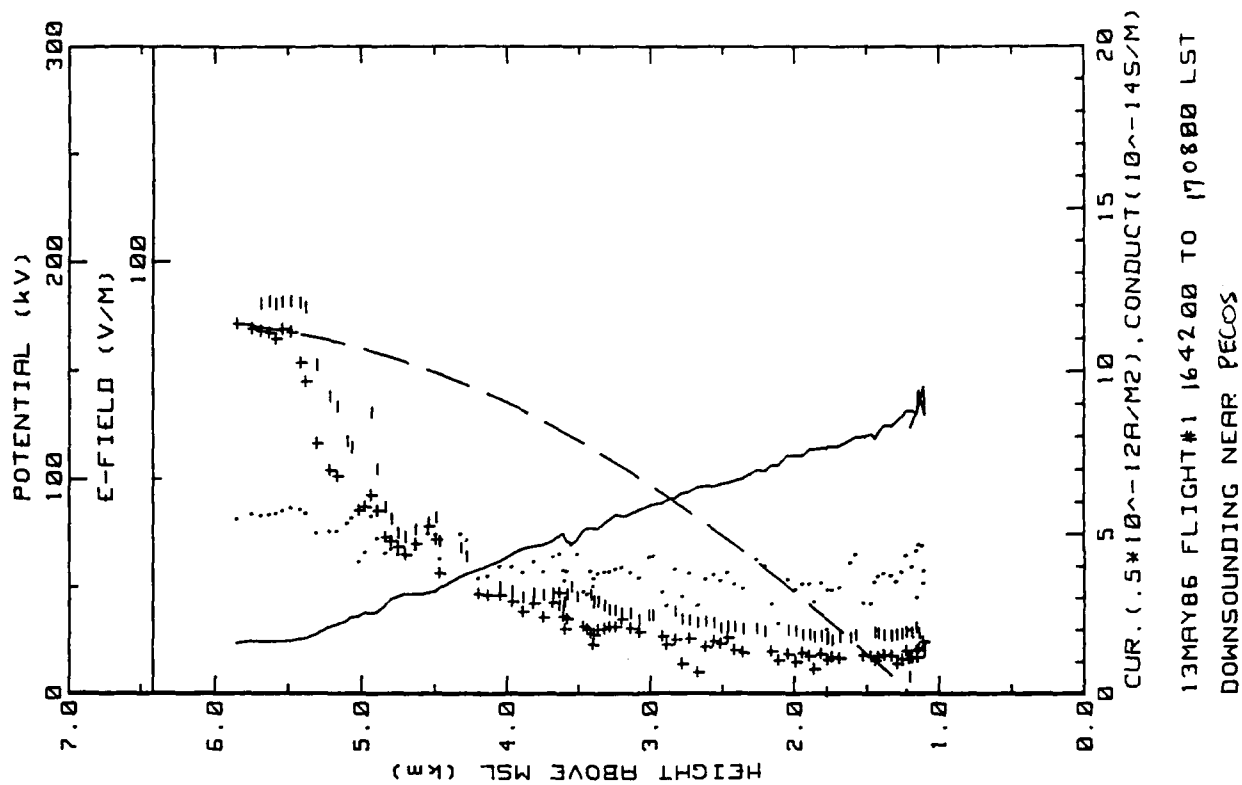


Figure 6b. Hobbs Flight 1 spiral downsounding (ref. Fig. 5e).



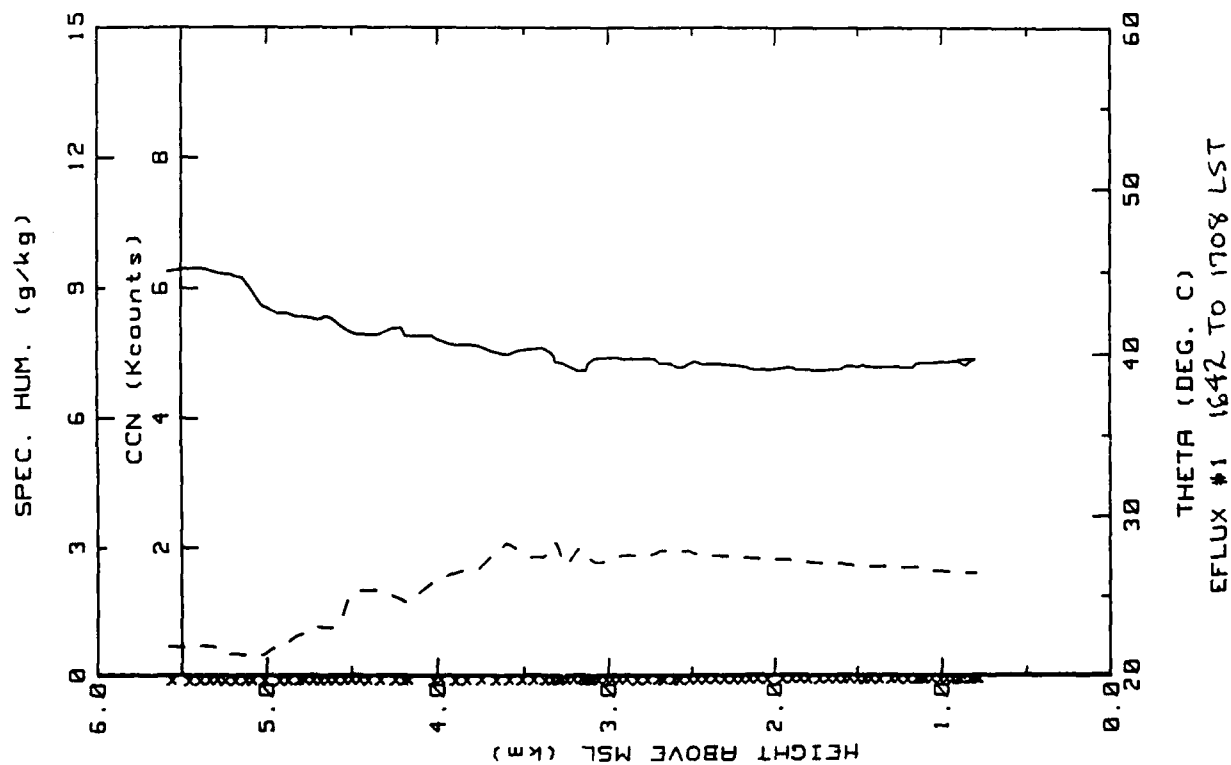


Figure 6c. Hobbs Flight 1 spiral downounding (ref. Fig. 5h).

Flight: 2

Date: 14 May 1986

Takeoff: 1438 LT from Hobbs

Landed: 1753 at Portales, NM

Takeoff: 1843 from Portales

Landed: ca. 1930 at Hobbs

Conditions: Scattered Cumulus with bases at 5.9 km and tops at 6.5 km. Hot and dry with intense convection; light winds.

Instruments: Turbulence instruments not turned on.

Summary: Second scouting trip for possible ground station site. Made spiral descent and constant altitude passes over irrigated farmland about 15 km SW of Portales, NM. On the return flight, an upsounding to 3.2 km was made beginning over plowed land just S of Portales.

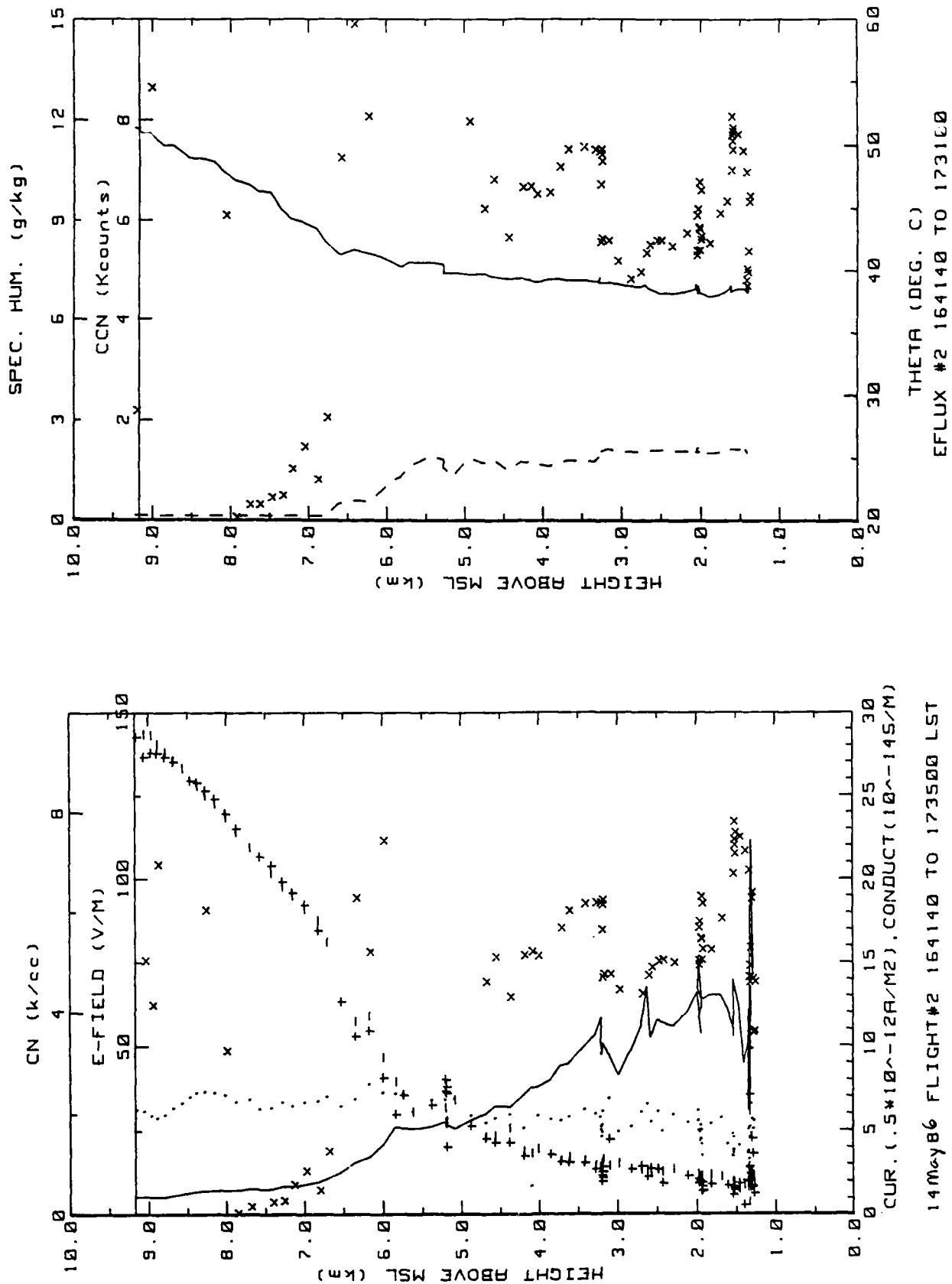


Figure 7a. Hobbs Flight 2 spiral descending (ref. Fig. 5f).

Figure 7b. Hobbs Flight 2 spiral descending (ref. Fig. 5h).

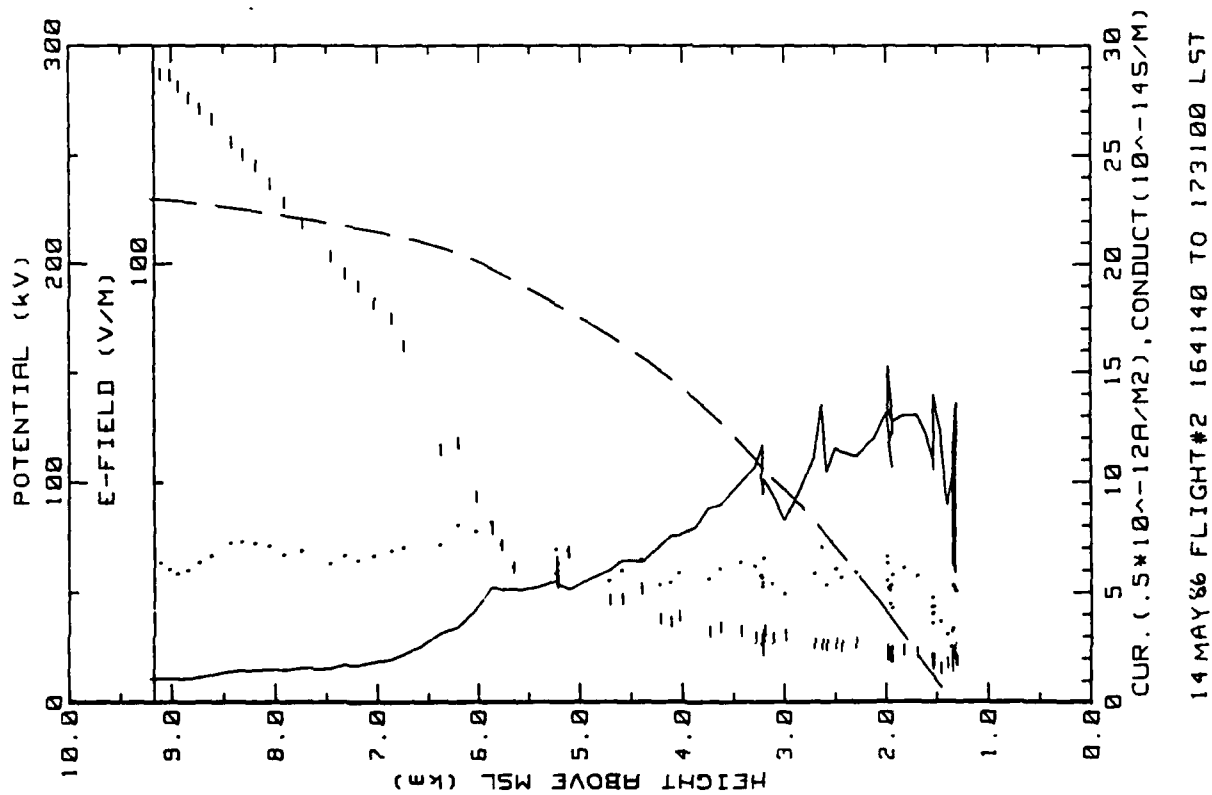


Figure 7c. Hobbs Flight 2 spiral downsonding (ref. Fig. 5e).

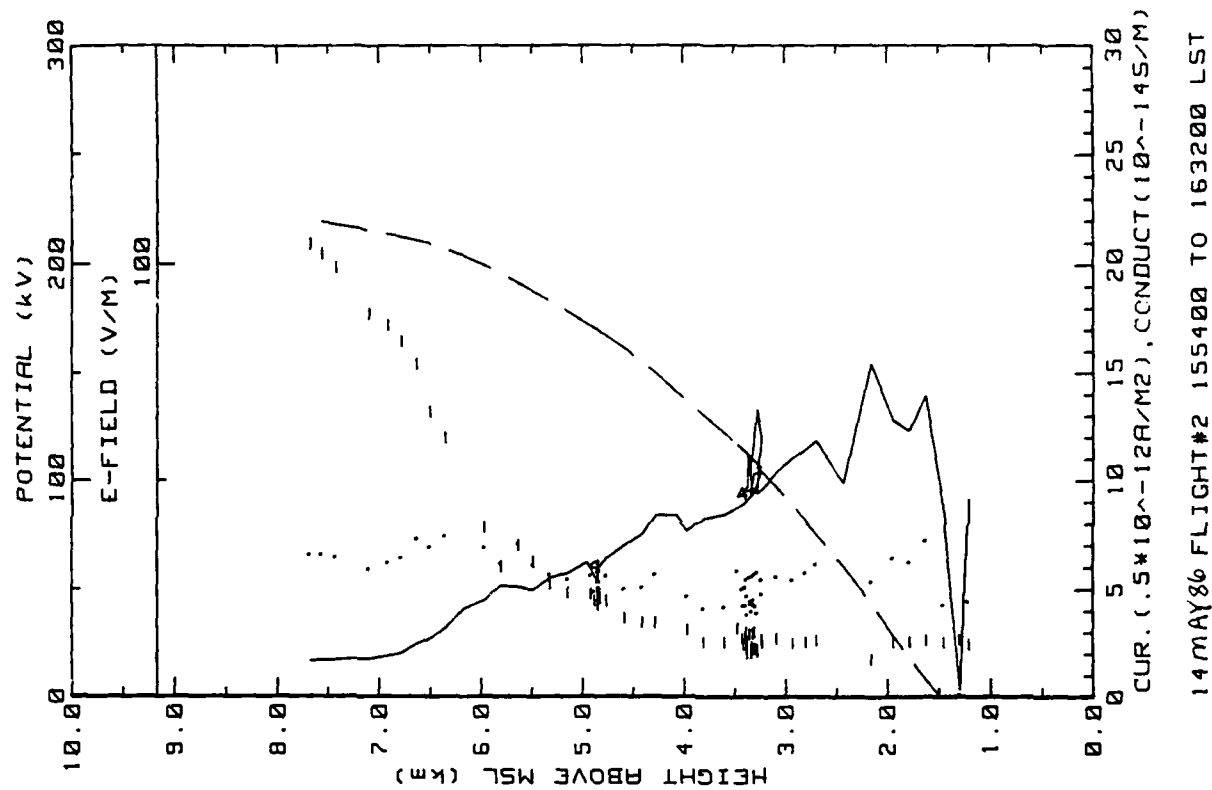


Figure 7d. Hobbs Flight 2 continuous upsonding (ref. Fig. 5e).

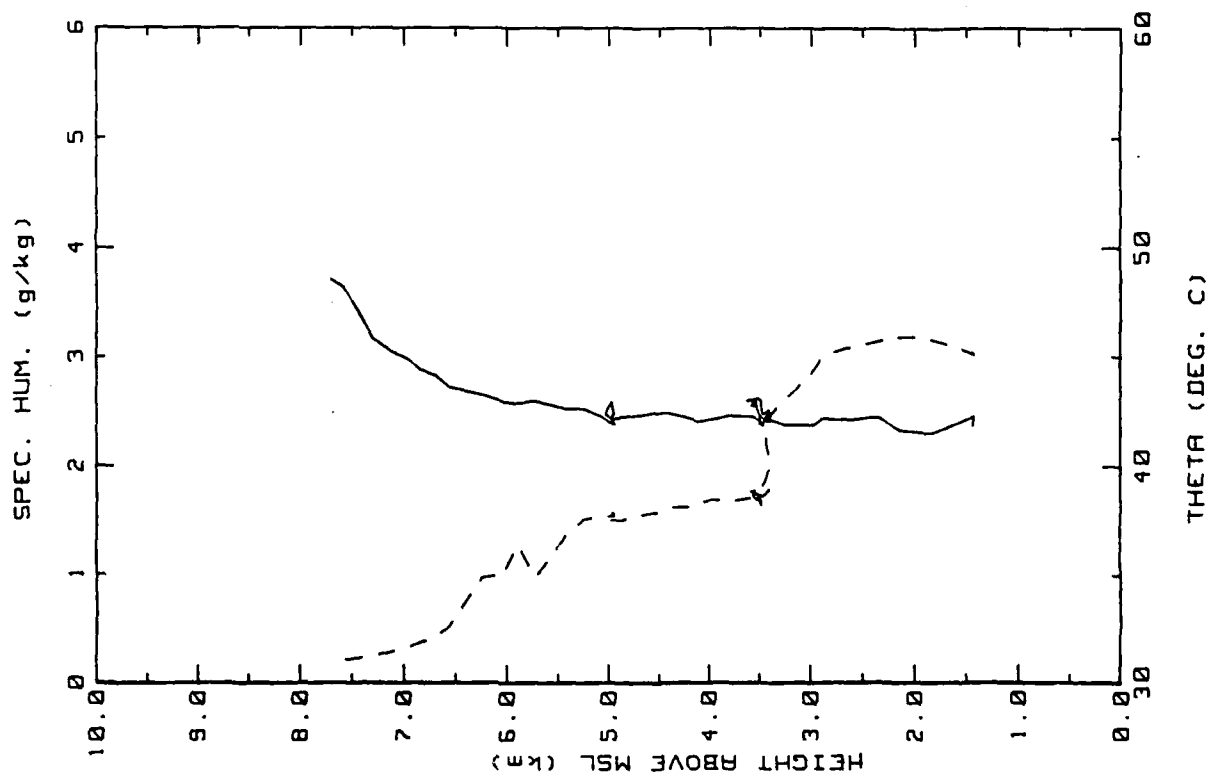


Figure 7e. Hobbs Flight 2 continuous upsounding (ref. Fig. 5h).

Flight: 3

Date: 16 May 1986

Takeoff: 1740 LT from Hobbs

Landed: 1926 at Hobbs

Conditions: Scattered cumulus clouds (<1/10 cover) with bases at 5.5 km. Hot and dry with lots of convection initially, but decreasing toward the end of the flight. Light winds.

Instruments: All worked properly; Barnes Infrared thermometer not turned on.

Summary: Last test flight. Several passes were made by a ground station to calibrate the electric field instruments and a spiral down sounding from 5.5 km was executed over the Hobbs airport.

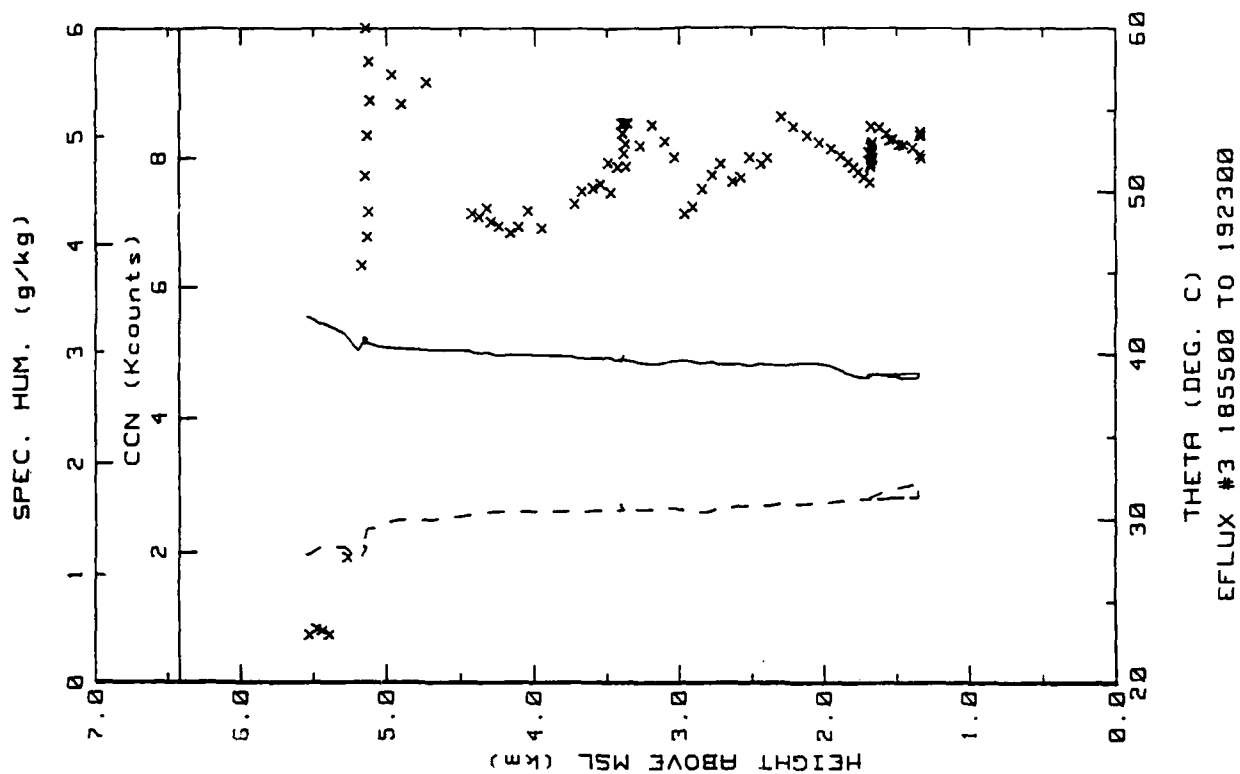


Figure 8a. Hobbs Flight 3 spiral down sounding (ref. Fig. 5e).

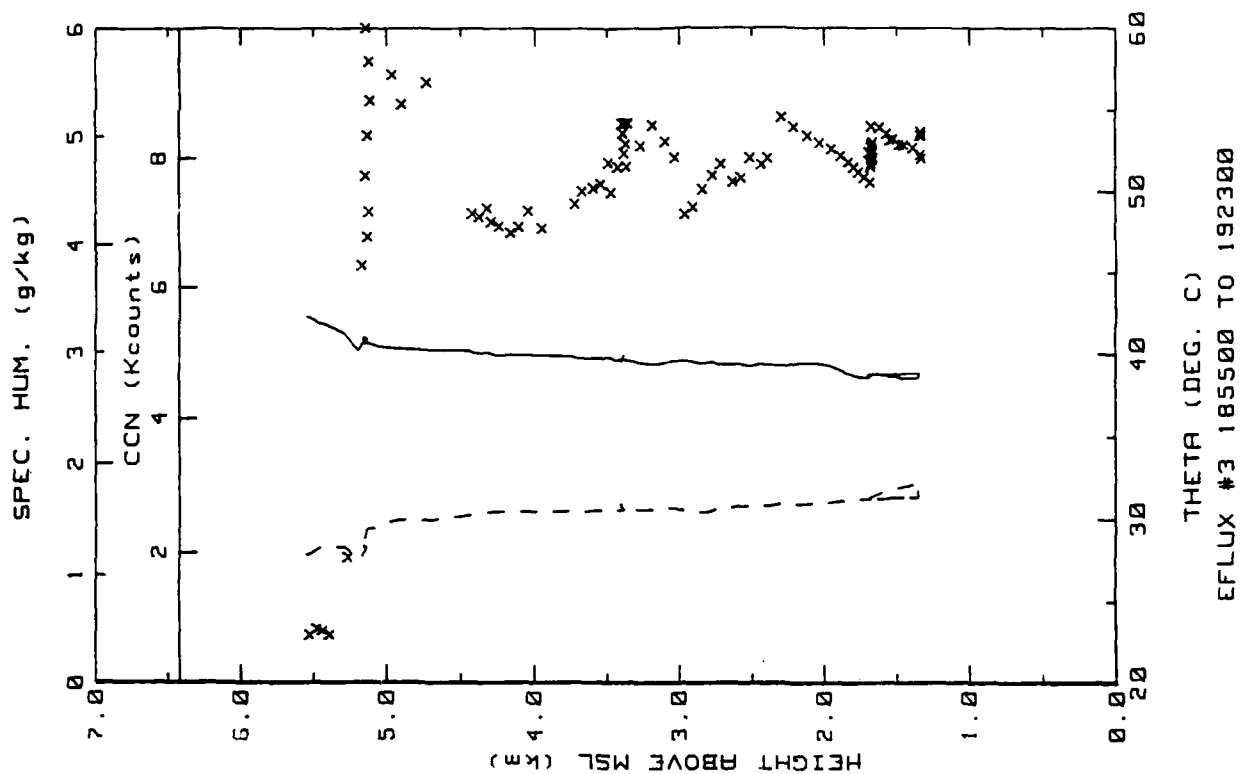


Figure 8b. Hobbs Flight 3 spiral down sounding (ref. Fig. 5h).

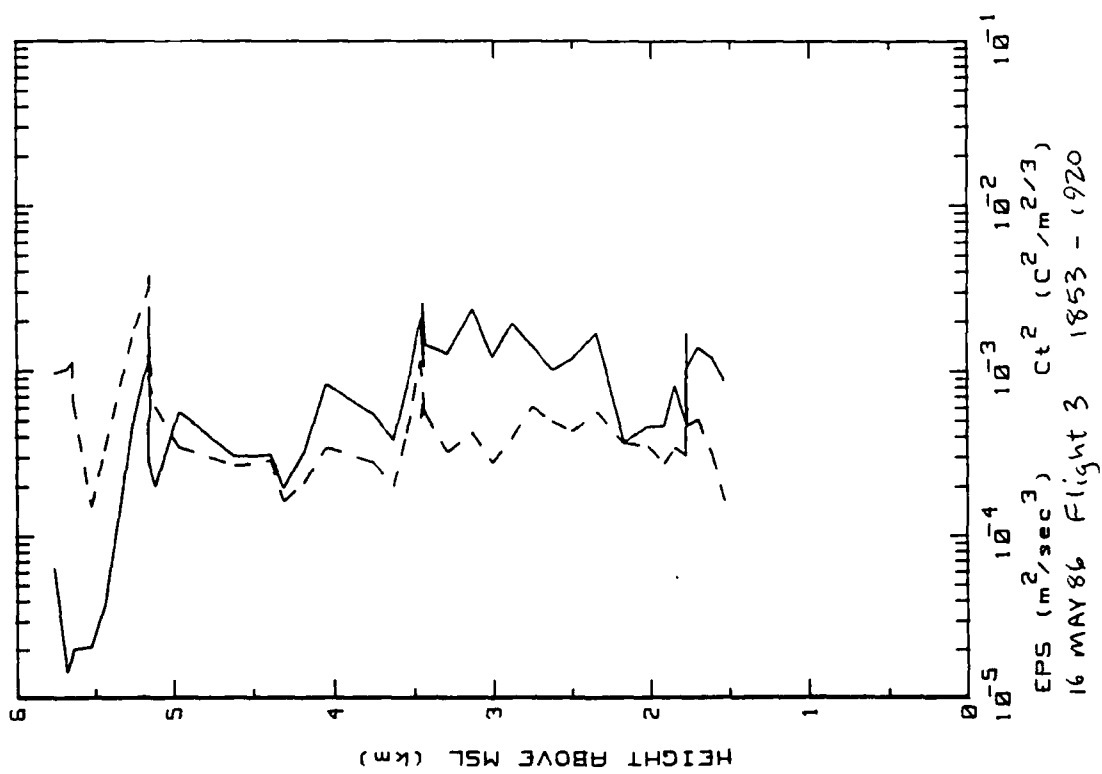


Figure 8c. Hobus Flight 3 spiral downounding (ref. Fig. 5g)



Flight: 4

Date: 18 May 1986

Takeoff: 1035 LT from Lea County Airport.

Landed: 1329 at Hobbs

Conditions: Clear and dry with vigorous convection toward the end of the flight. Winds at Hobbs were from the N at about 5 m/s and visibility was good.

Instruments: All instruments worked properly.

Summary: Several constant altitude passes were made by the ground station at Hobbs then an upsounding was performed enroute to Carlsbad. A ladder profile was obtained on descending from 4.6 km over Carlsbad beginning at 1119 LT and ending at 1200. A spiral profile interspersed with constant altitude runs was performed near Hobbs between 1251 and 1324 ending with low passes over the ground station.



Table 2b. Hobbs Flight 4 averages and (standard deviations)/averages for constant altitude runs over the ground station.

OBIS FLIGHT # 4  
16 MAY 1966

STANDARD DEVIATIONS/MEAN VALUES

MARGINS FROM LEVEL RUNS

Line	N	Altitude ft	Efield1 V/m	Efield2 V/m	t <sub>lam</sub> 10 <sup>-14</sup>	-t <sub>lam</sub> 10 <sup>-14</sup>	Con Cur1 10 <sup>-12</sup>	Con Cur2 10 <sup>-12</sup>	-t <sub>lam</sub> 10 <sup>-14</sup>	Con Cur1 10 <sup>-12</sup>	Con Cur2 10 <sup>-12</sup>	EPS	C12	0
------	---	----------------	----------------	----------------	---------------------------------------	--	-------------------------------	-------------------------------	--	-------------------------------	-------------------------------	-----	-----	---

Line	N	Altitude ft	Efield1 V/m	Efield2 V/m	t <sub>lam</sub> 10 <sup>-14</sup>	-t <sub>lam</sub> 10 <sup>-14</sup>	Con Cur1 10 <sup>-12</sup>	Con Cur2 10 <sup>-12</sup>	t <sub>relat</sub> C
------	---	----------------	----------------	----------------	---------------------------------------	--	-------------------------------	-------------------------------	-------------------------

Line	N	Press mb	Rel Hum %	CON k/cc	EPS m/s	C1 C2/C3	g/kg	t <sub>rose</sub> C	LJR C	t <sub>des</sub> C
------	---	-------------	--------------	-------------	------------	-------------	------	------------------------	----------	-----------------------

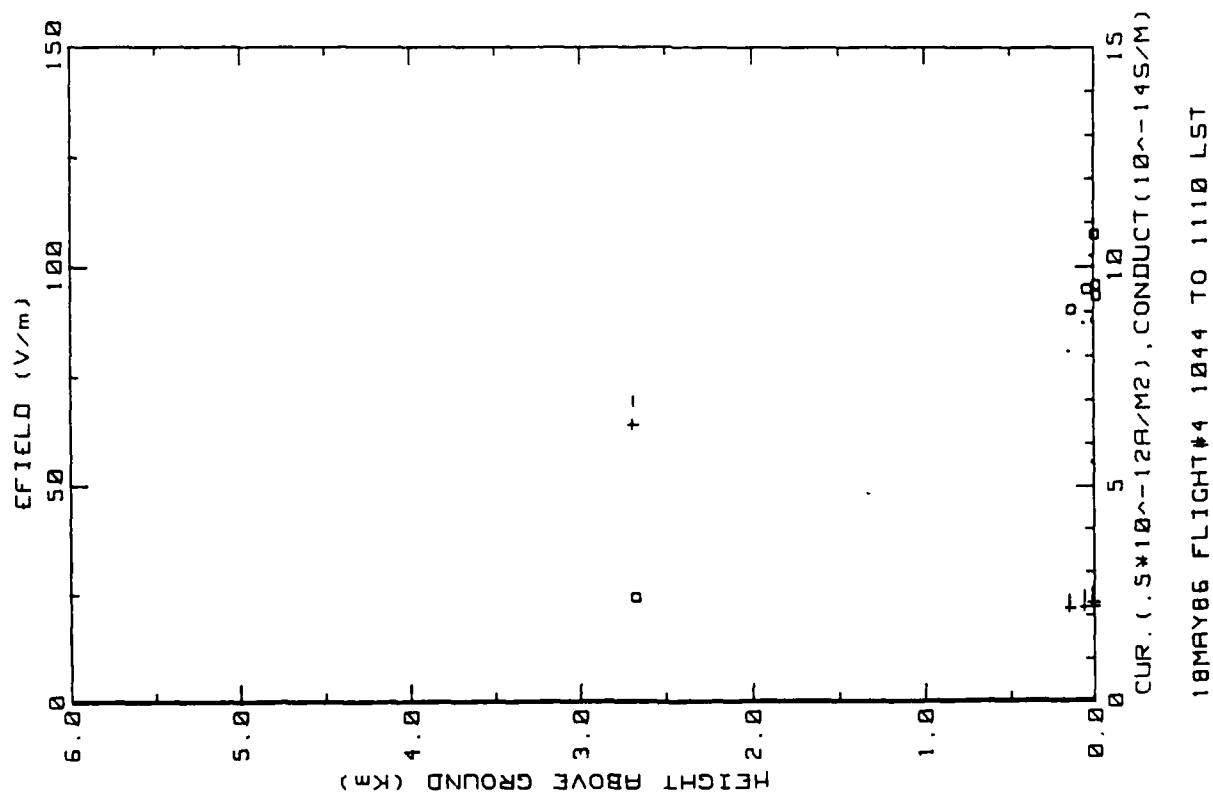


Figure 9a. Hobbs Flight 4 ladder profile (ref. Fig. 5a)

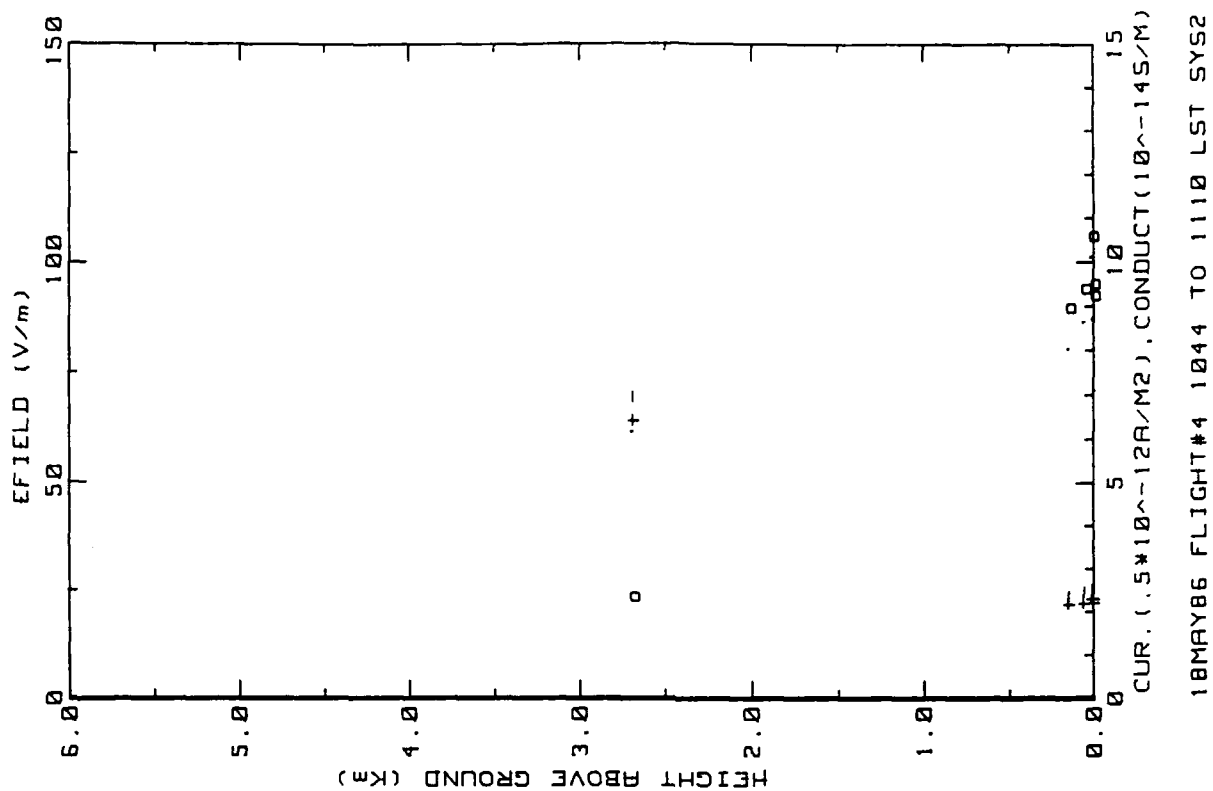


Figure 9b. Similar to 9a. but for inboard E-field system.

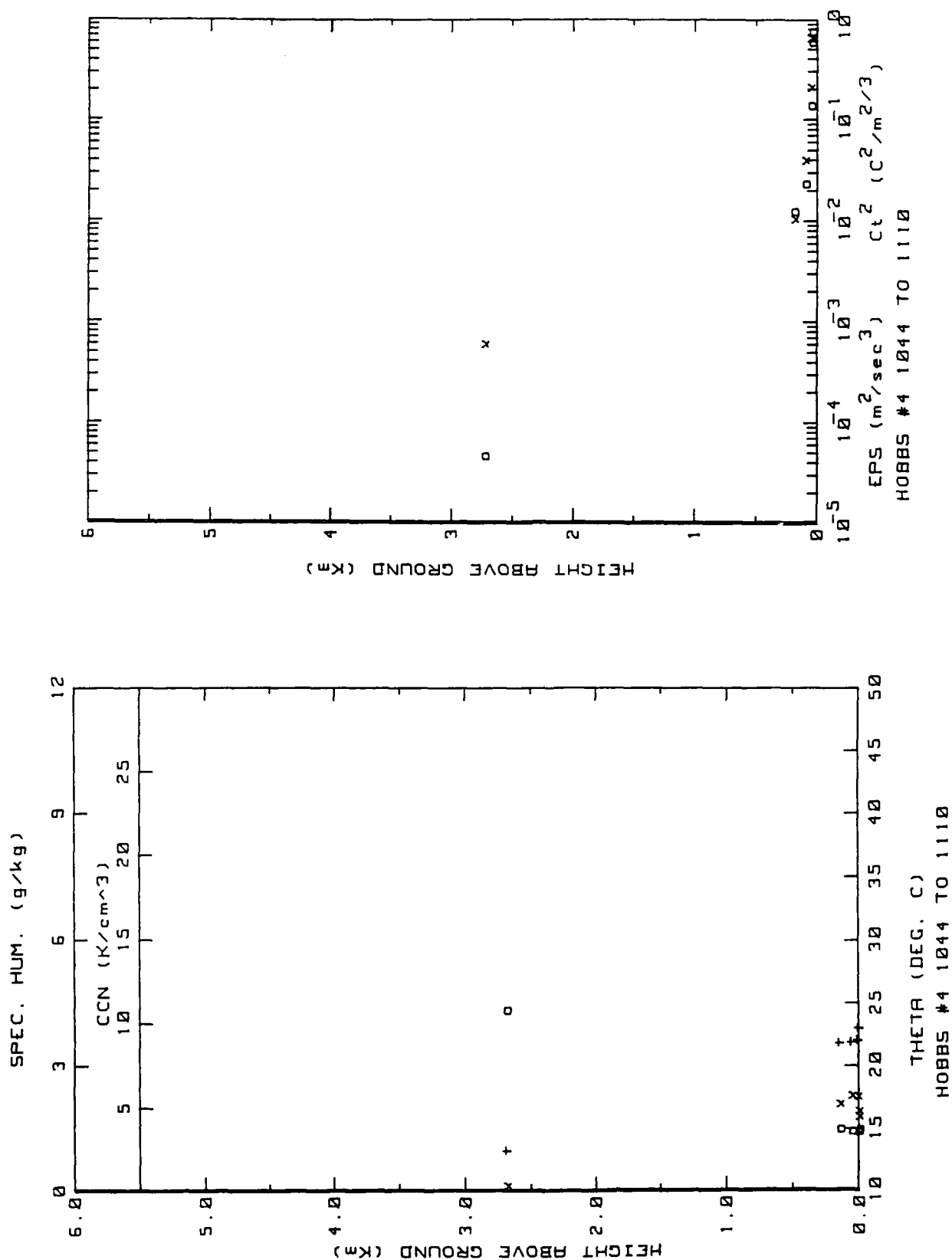


Figure 9c. Hobbs Flight 4 ladder profile (ref. Fig 5c).

Figure 9d. Hobbs Flight 4 ladder profile (ref. Fig 5b).

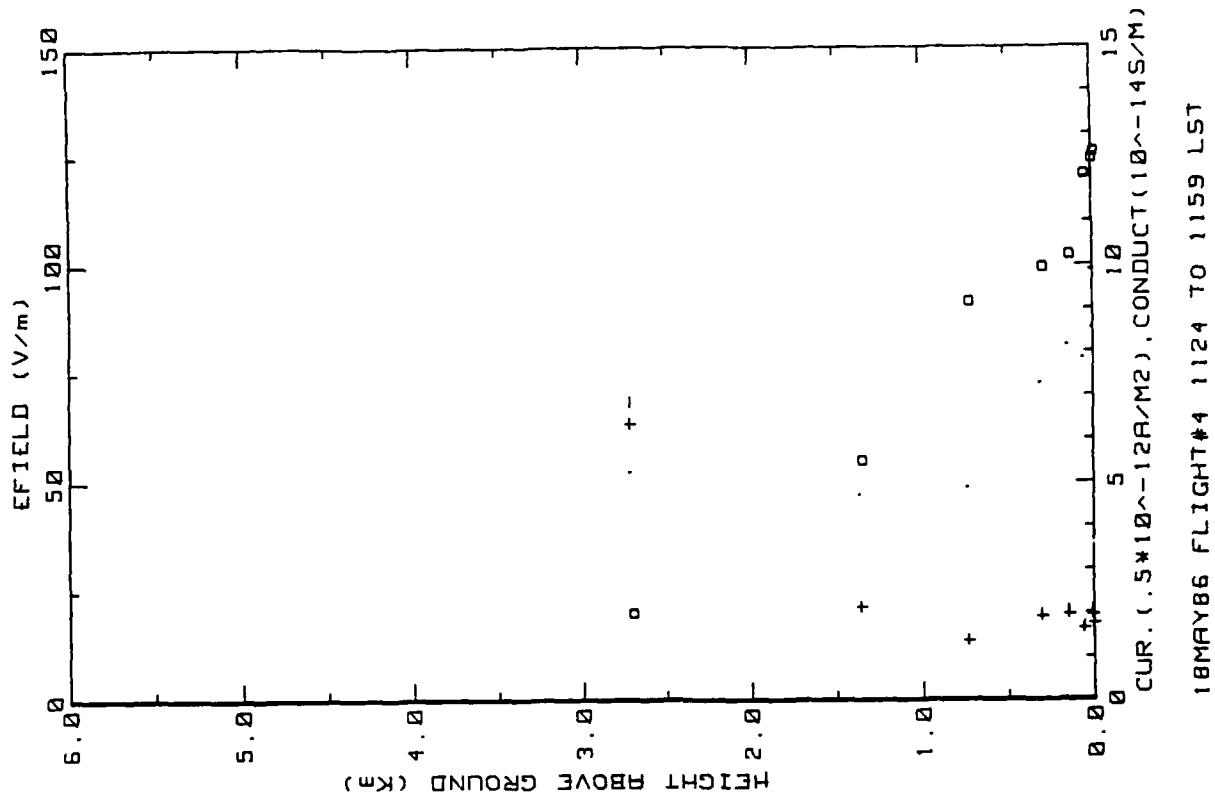


Figure 9f. Hobbs Flight 4 ladder profile near Carlsbad, NM  
(ref. Fig. 5a).

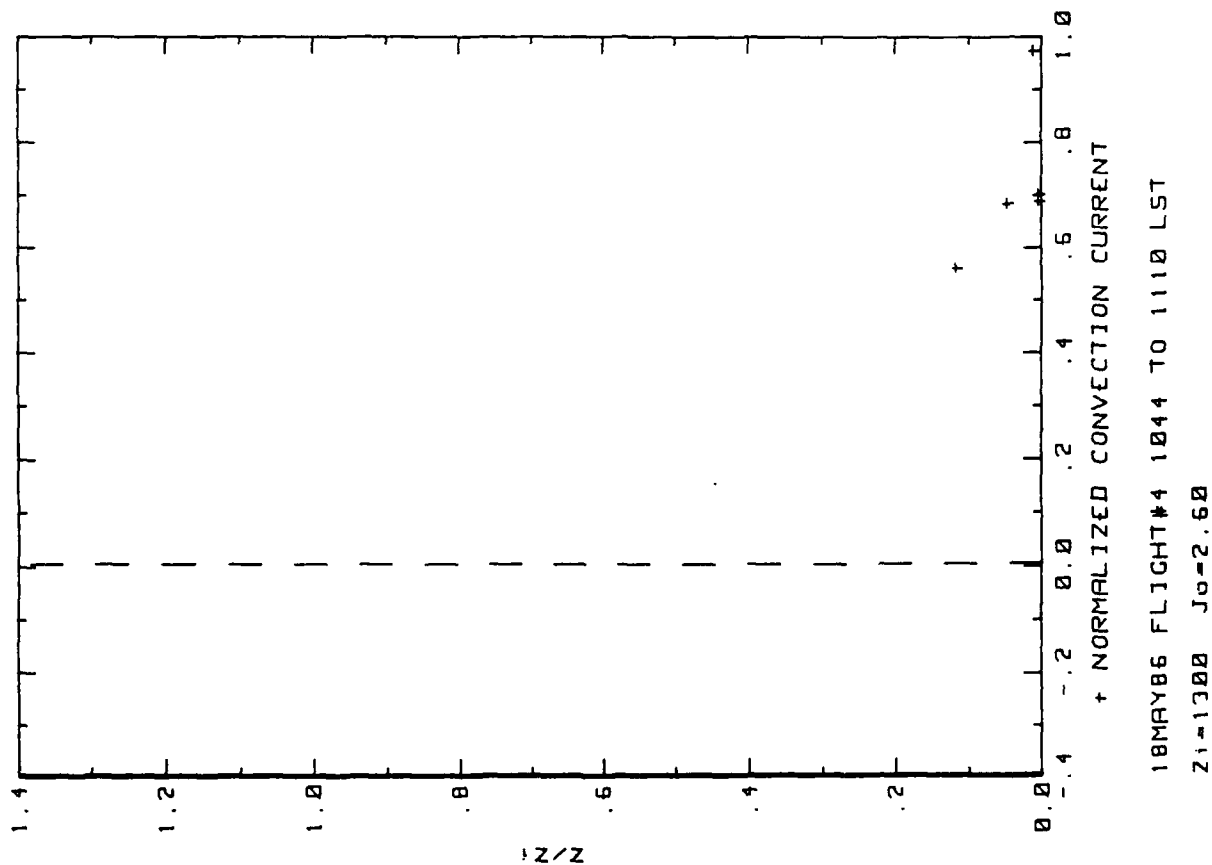


Figure 9e. Hobbs Flight 4 convection current profile  
(ref. Fig. 5d).

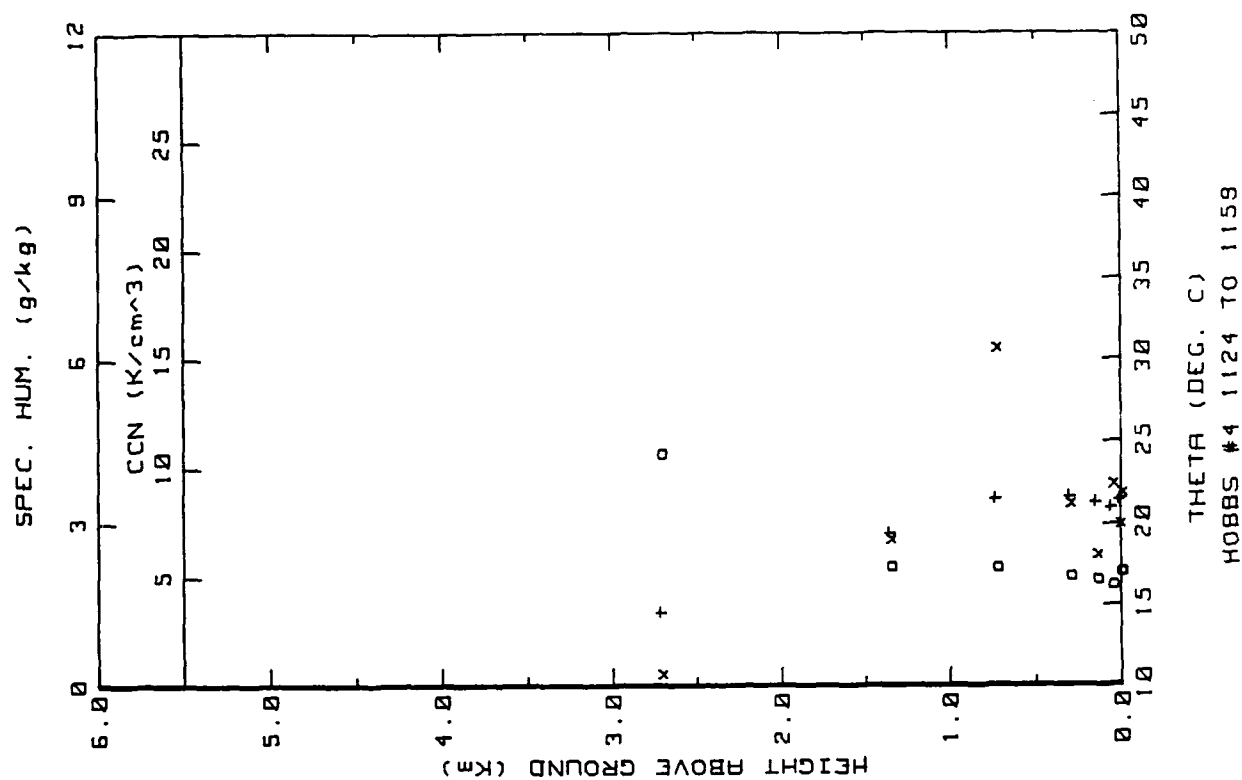
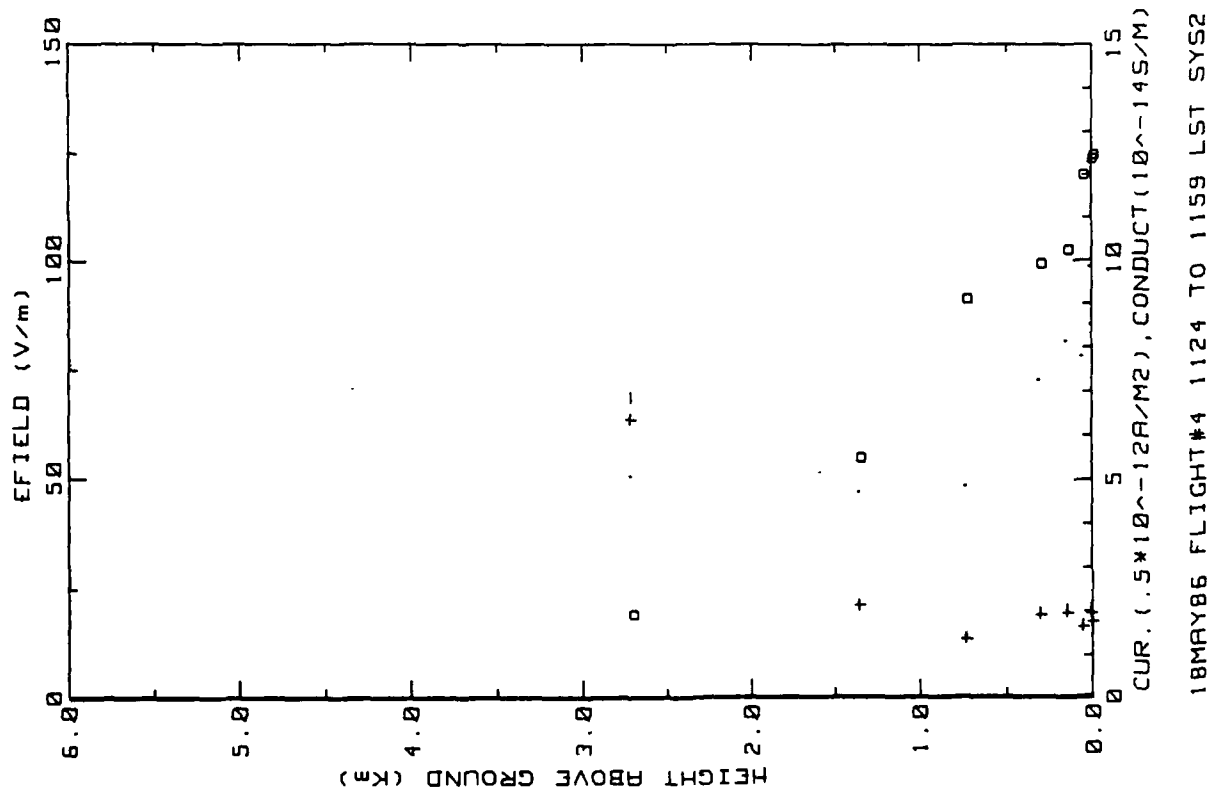


Figure 9g. Similar to Fig. 9f but for inboard E-field system.

Figure 9h. Hobbs Flight 4 ladder profile near Carlsbad, NM (ref. Fig. 5c)

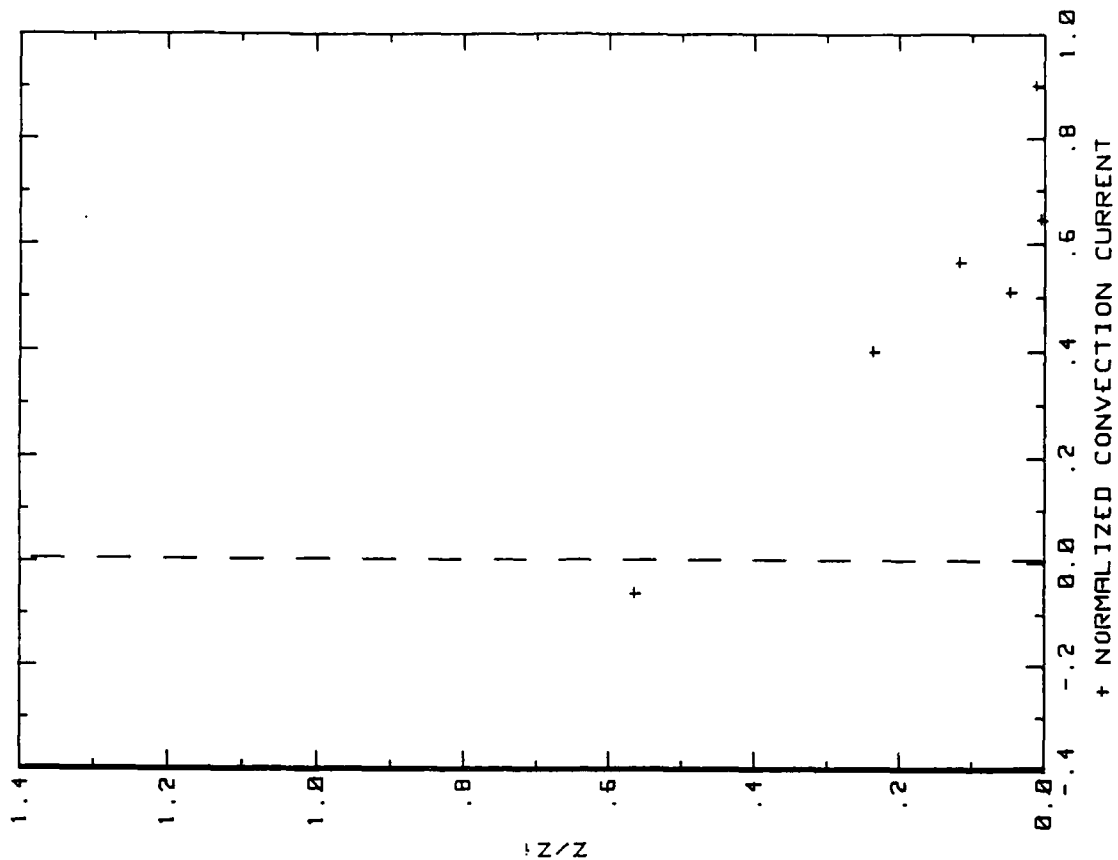


Figure 9j. Hobbs Flight 4 convection current profile near Carlsbad, NM. (ref. Fig. 5d)

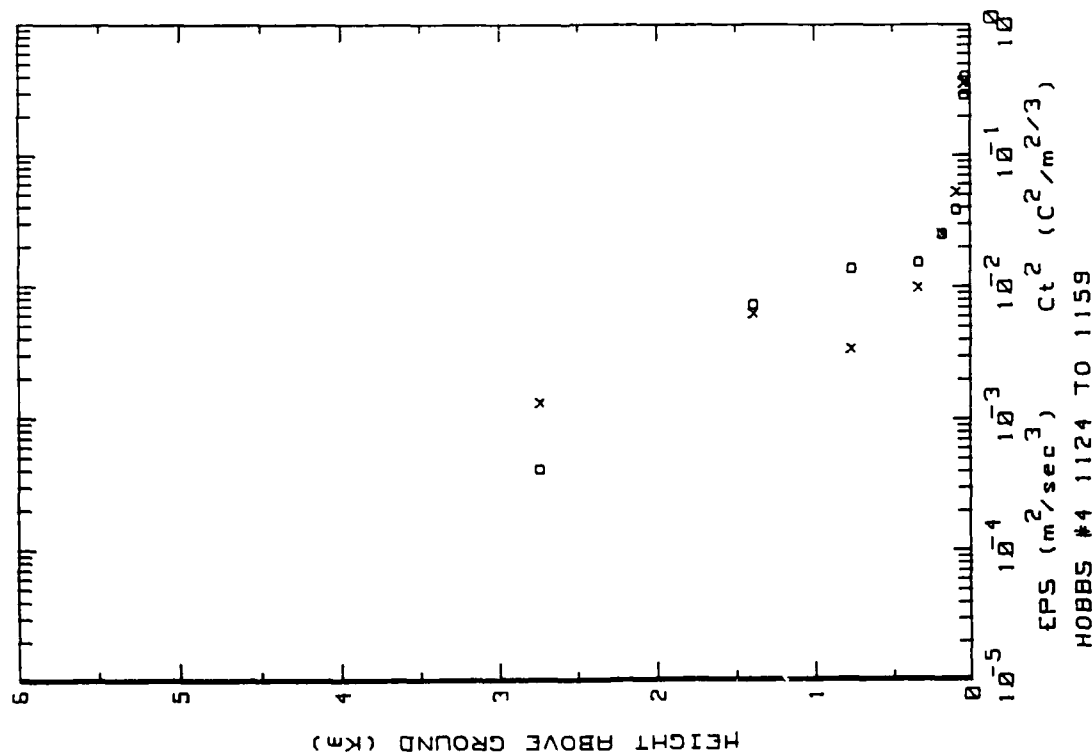


Figure 9i. Hobbs Flight 4 ladder profile near Carlsbad, NM (ref. Fig. 5b)



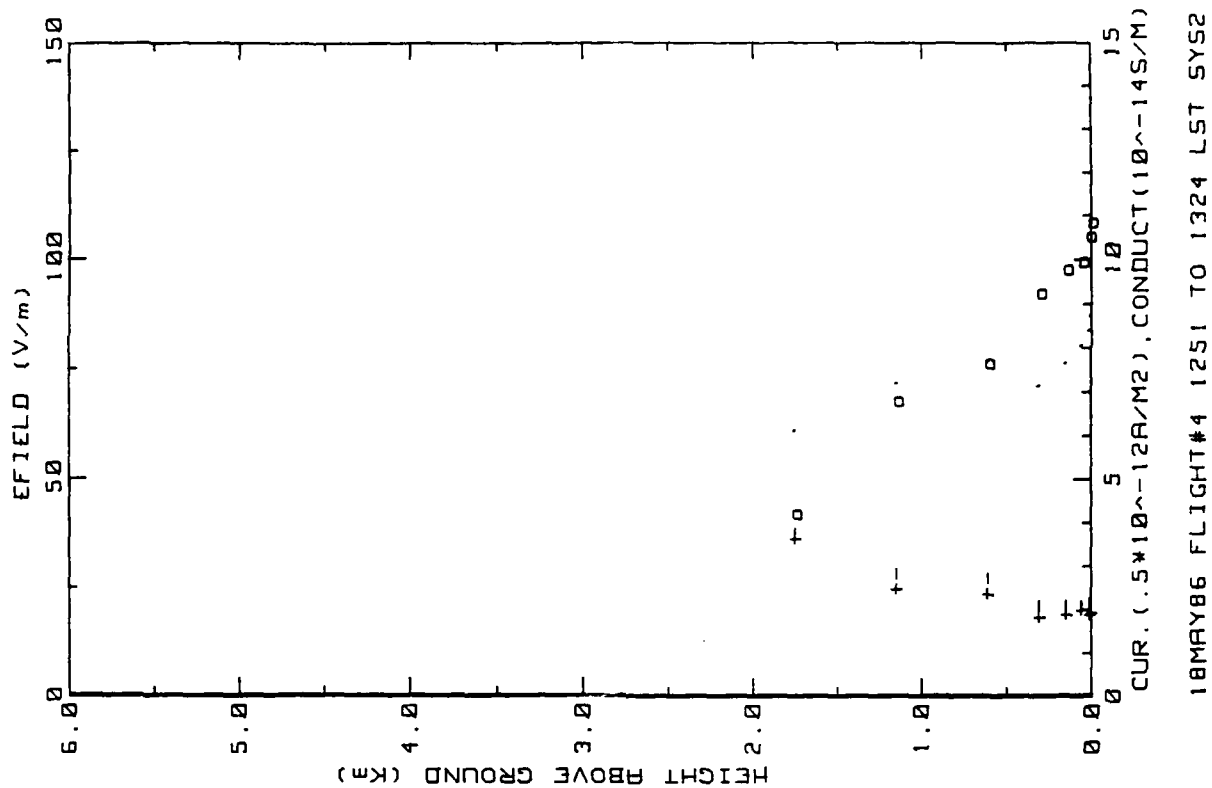


Figure 9k. Same as Fig. 9k but for inboard E<sub>field</sub> system.

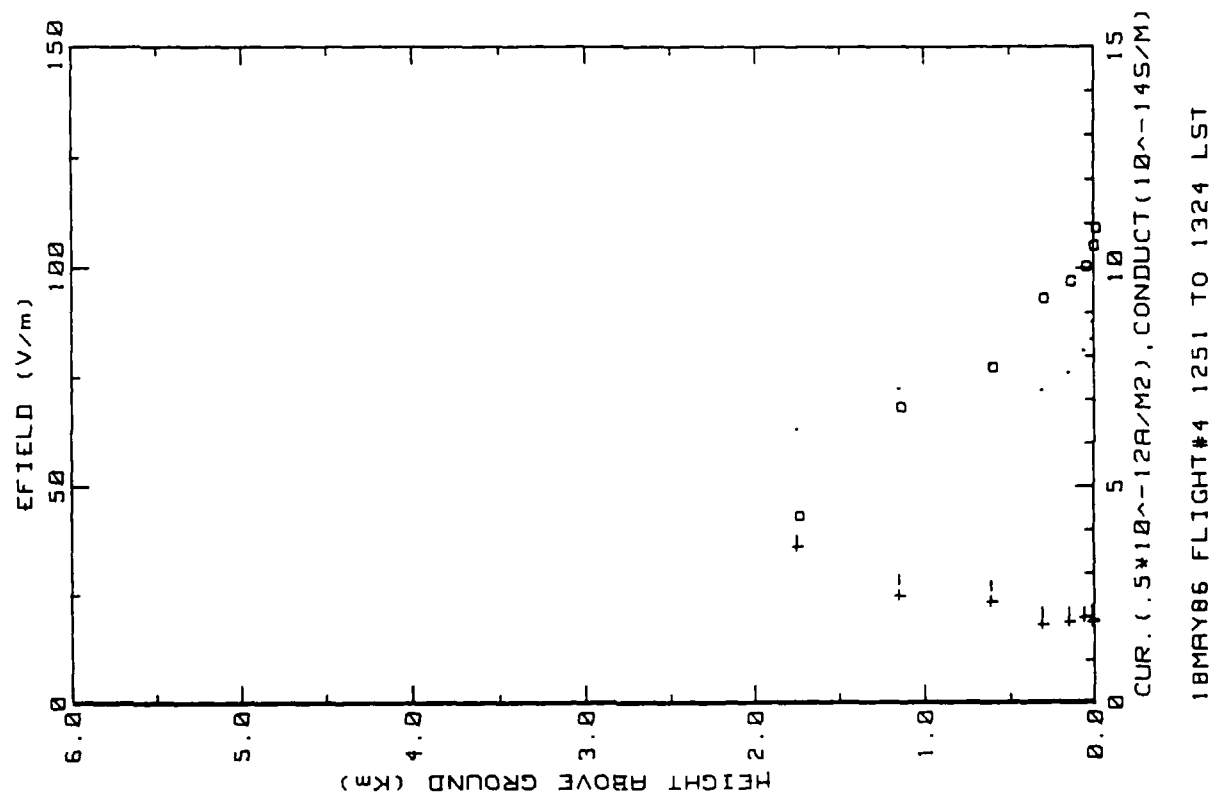
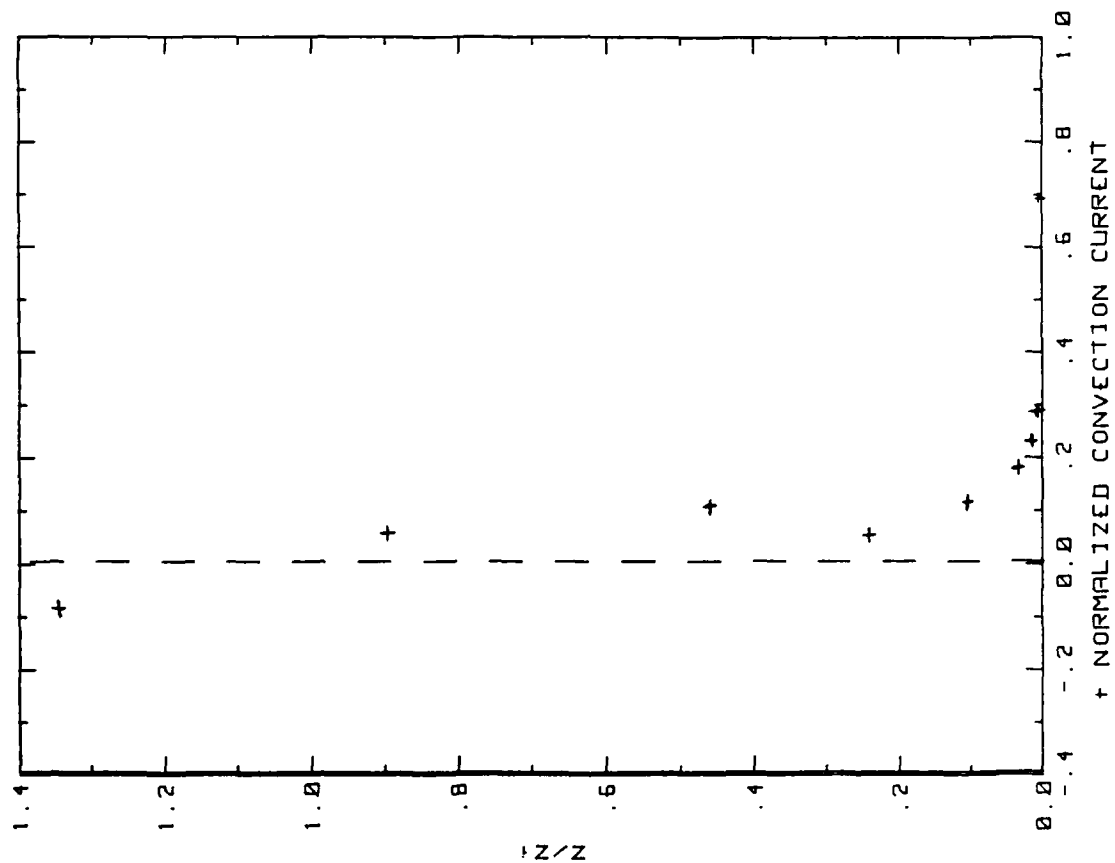


Figure 9k. Hobbs Flight 4 ladder profile (ref. Fig. 5a)



18MAY86 FLIGHT#4 1251 TO 1324 LST

Z<sub>1</sub>=1300 J<sub>0</sub>=3.4

Figure 9m. Hobbs Flight 4 convection current profile  
(ref. Fig. 5d)

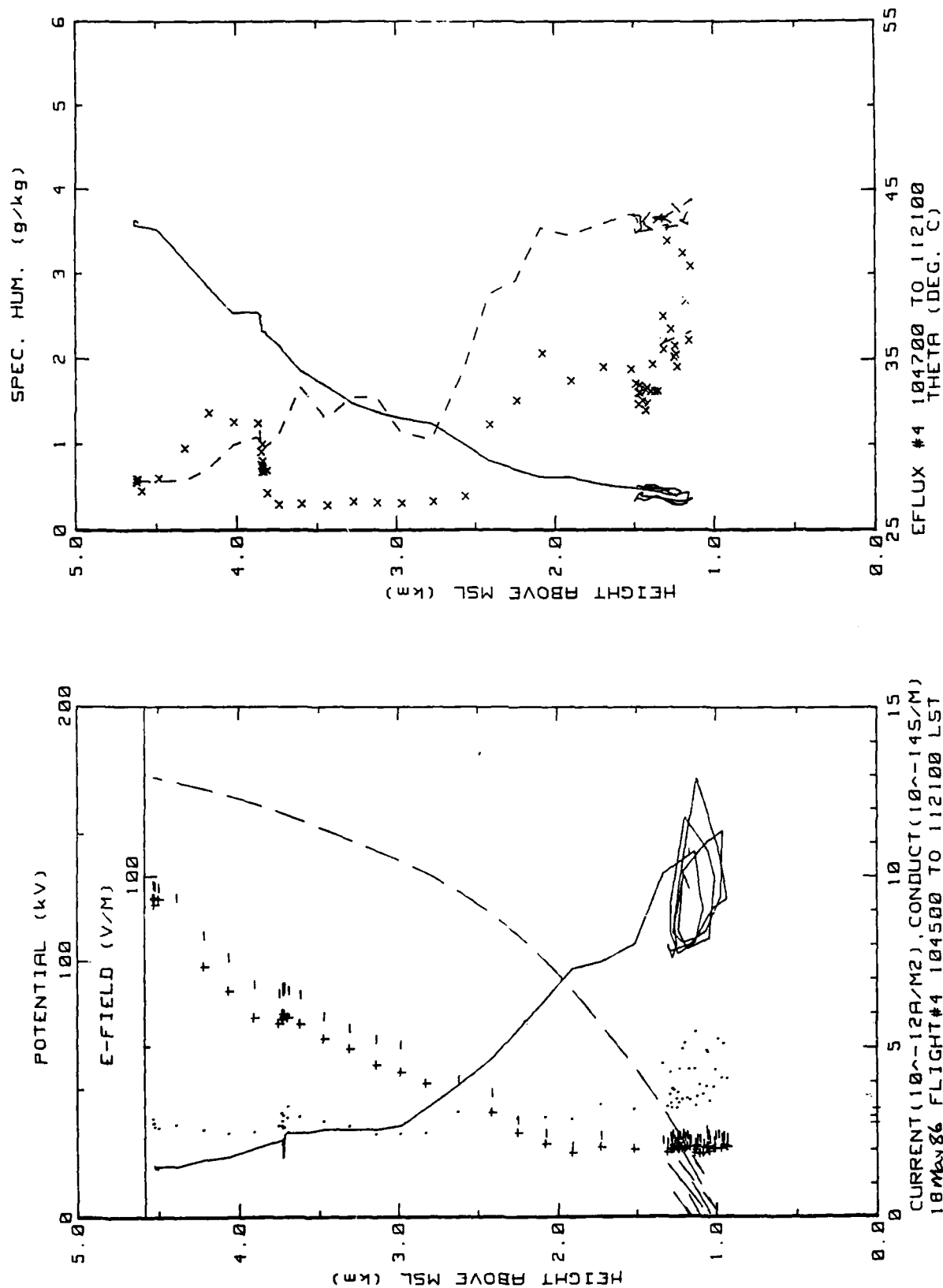


Figure 9n. Hobbs Flight 4 continuous upsonding (ref. Fig. 5a).

Figure 9o. Hobbs Flight 4 continuous upsonding (ref. Fig. 5h).

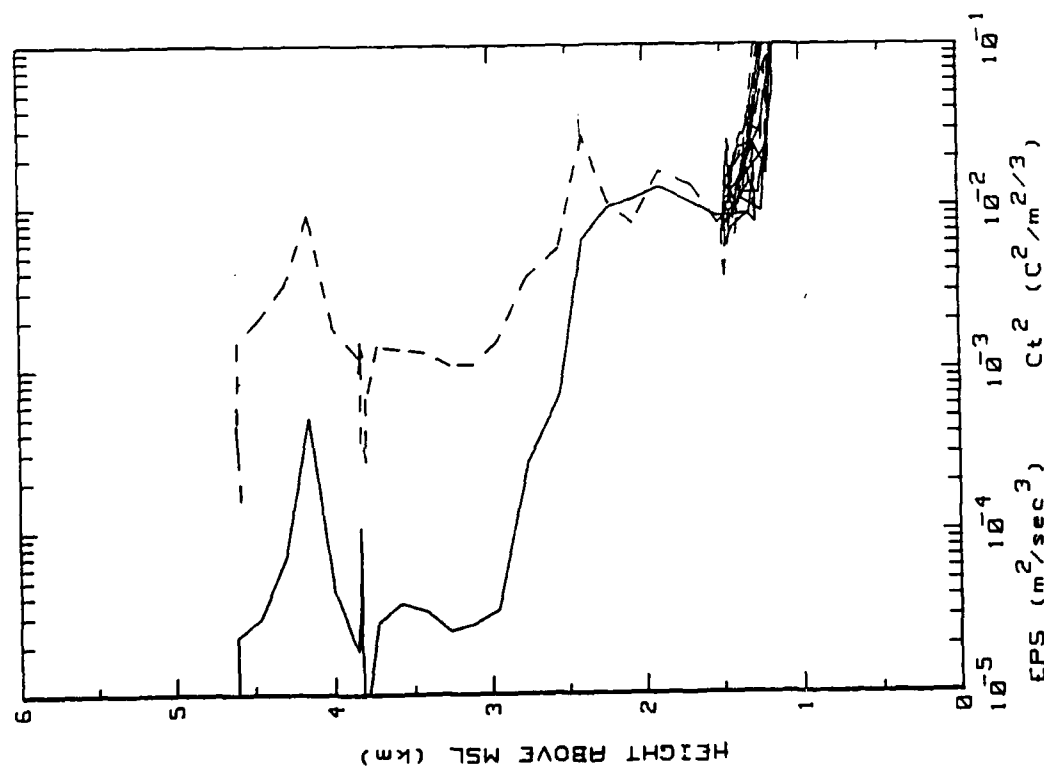


Figure 9p. Hobbs Flight 4 continuous upsounding (ref. Fig. 5g; see Fig. 9a for times).

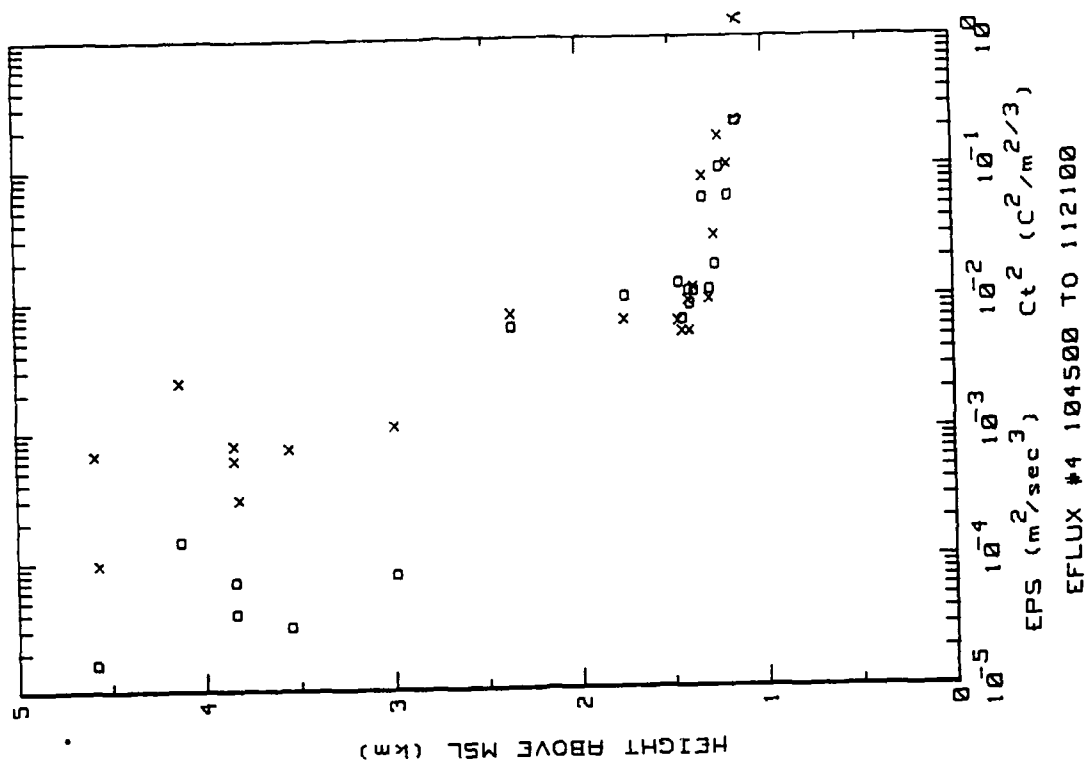


Figure 9q. Hobbs Flight 4 continuous upsounding (ref. Fig. 5b).

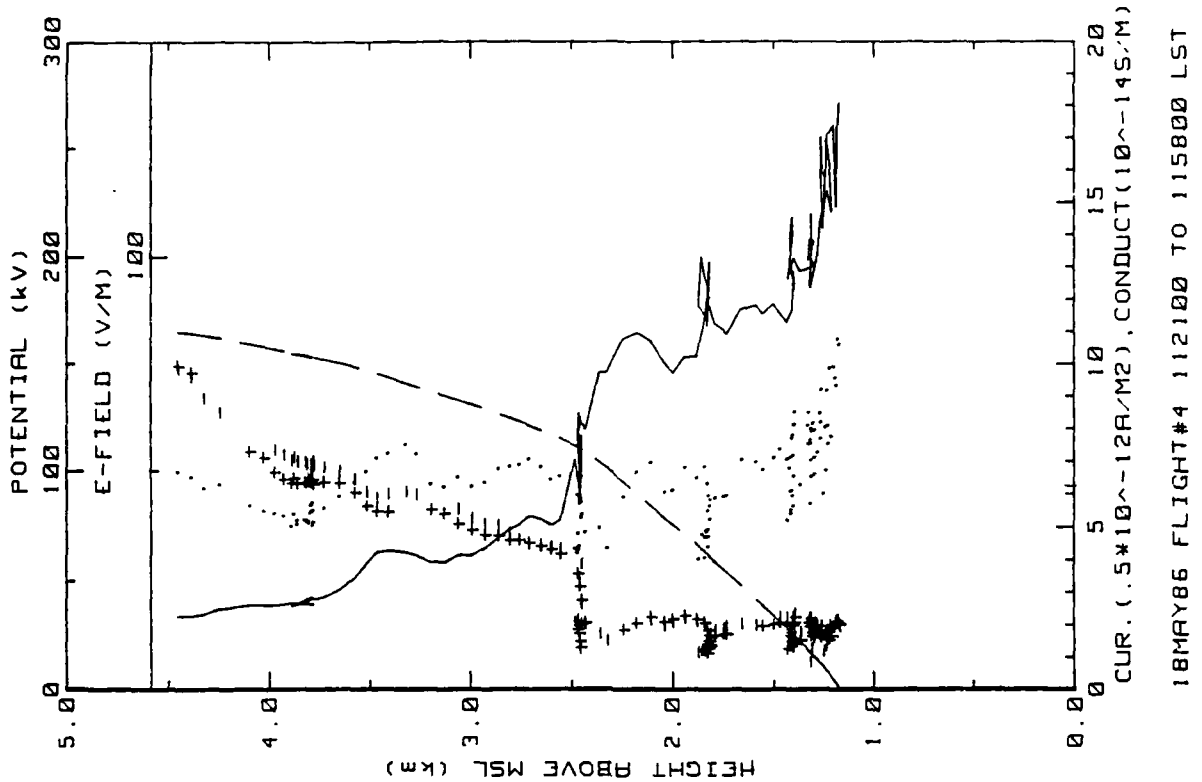


Figure 9r. Hobbs Flight 4 spiral descending into Carlsbad, NM (ref. Fig. 5e).

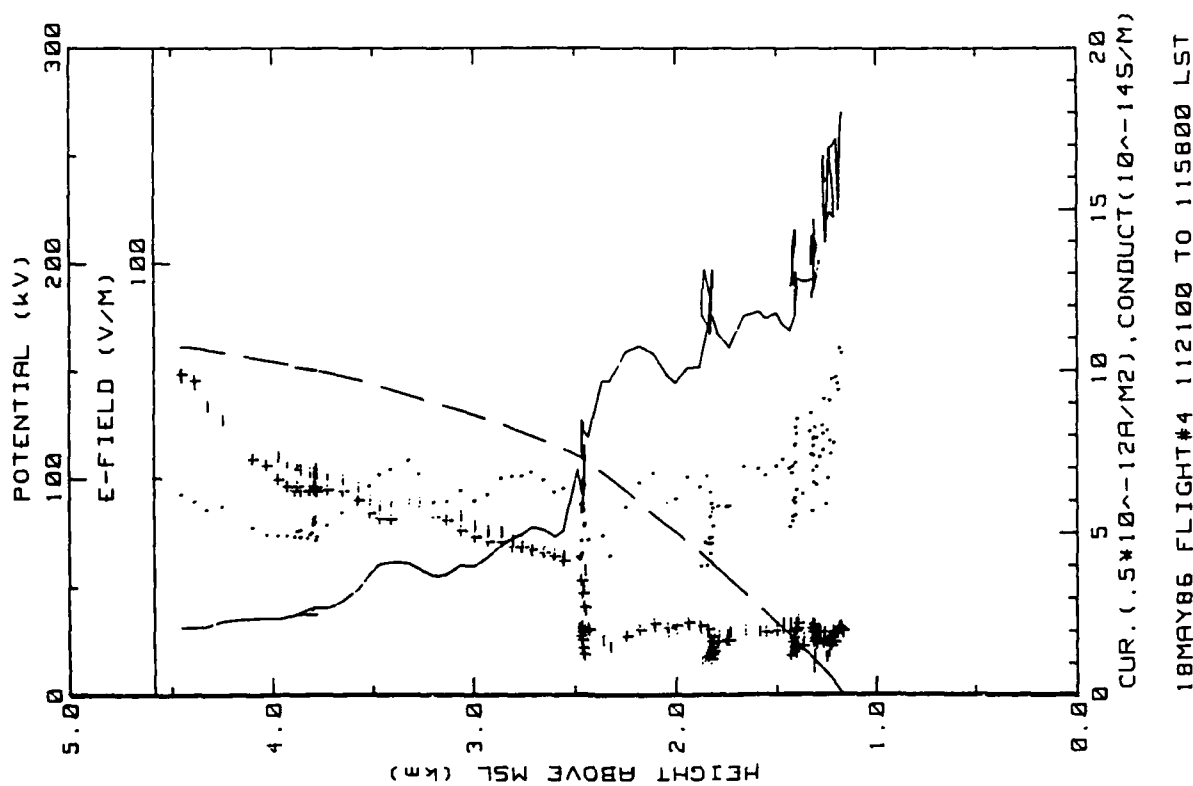


Figure 9s. Same as Fig 9r. but for outboard E-field system.

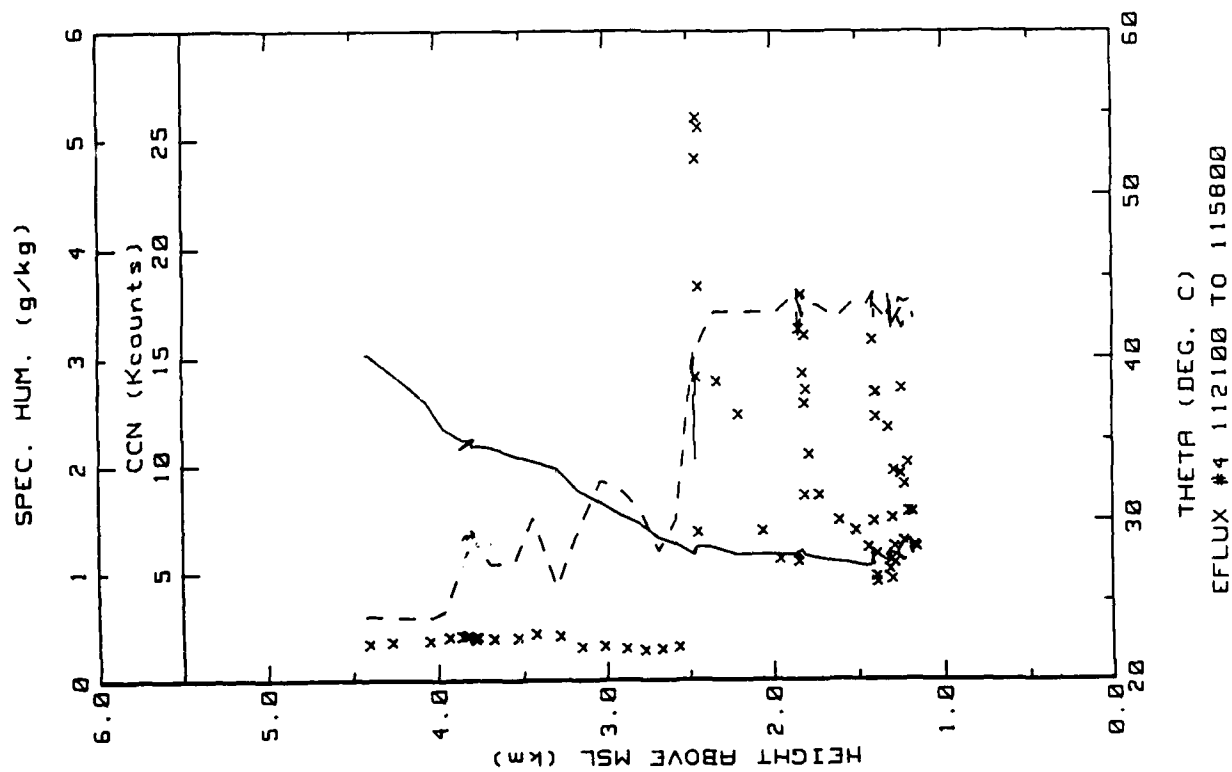


Figure 9t. Hobbs Flight 4 spiral down sounding into Carlsbad, NM (ref. Fig. 5h).

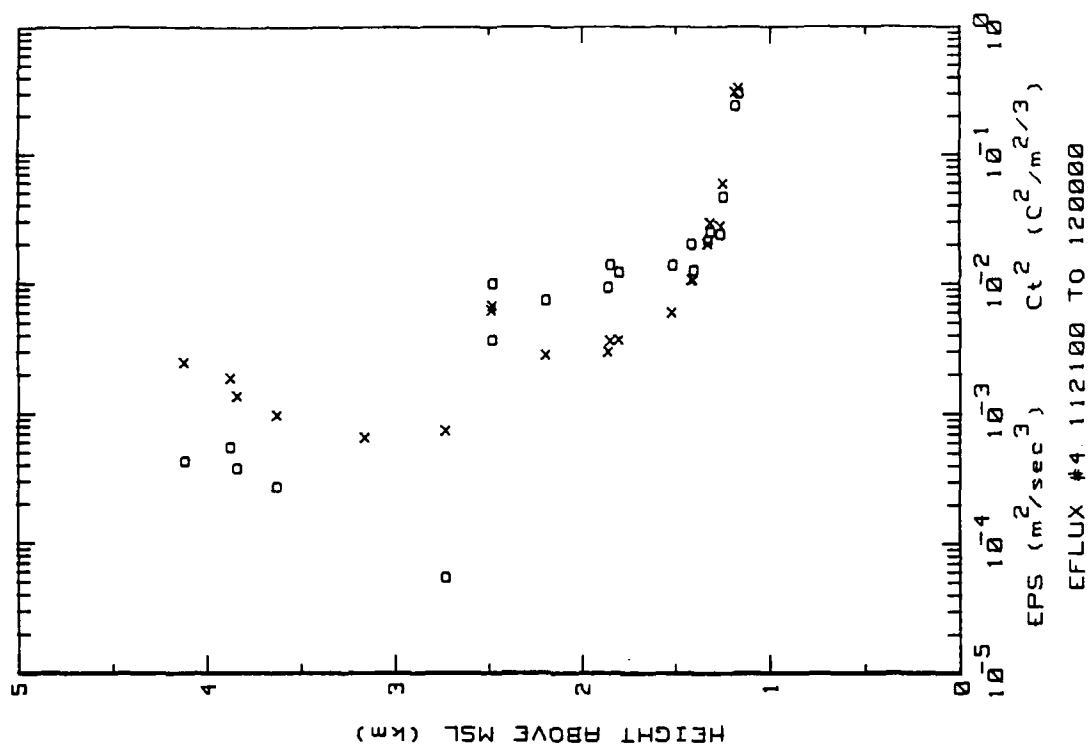
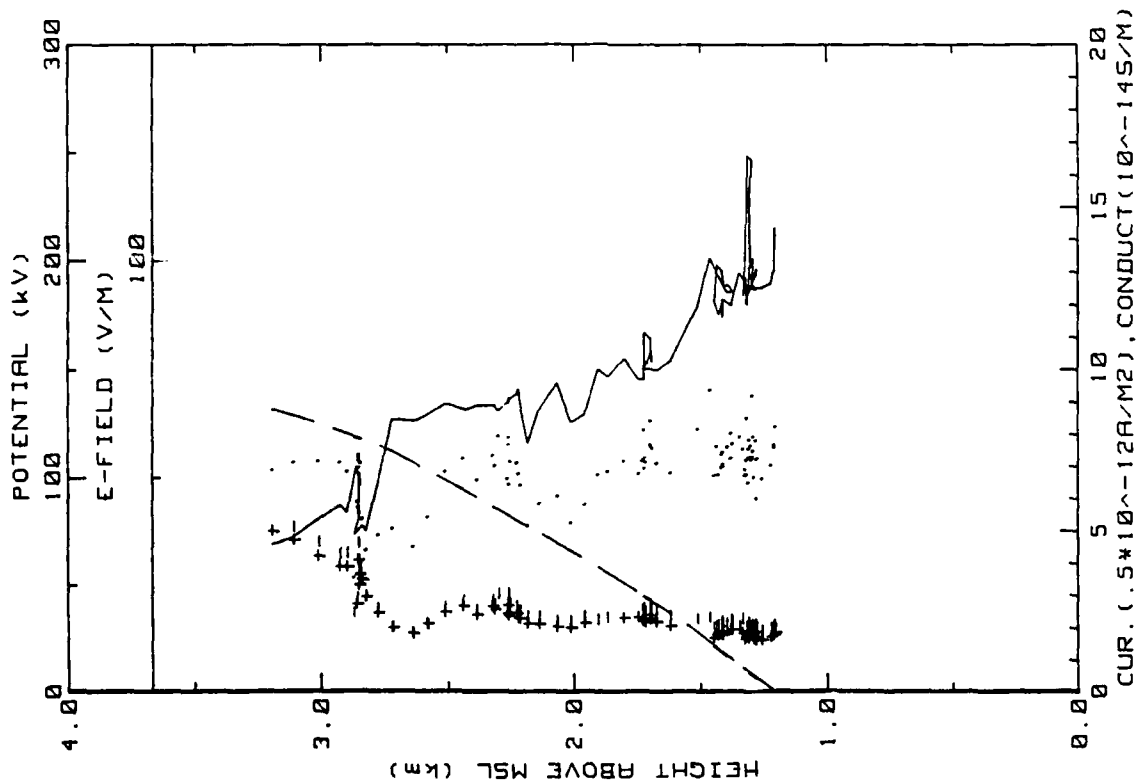
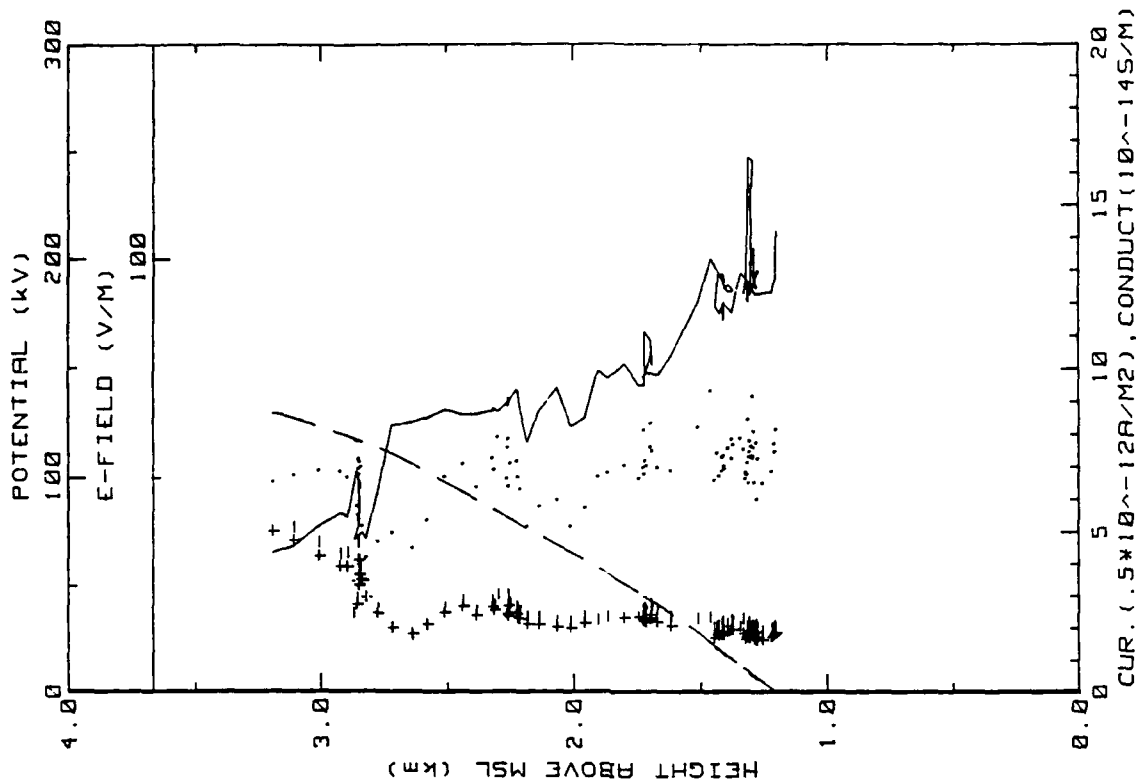


Figure 9u. Hobbs Flight 4 spiral down sounding into Carlsbad, NM (ref. Fig. 5b).



18MAY86 FLIGHT#4 124900 TO 131400 LST

Figure 9v. Hobbs Flight 4 spiral down sounding (ref. Fig. 5e).



18MAY86 FLIGHT#4 124900 TO 131400 LST

Figure 9w. Same as Fig. 9u. but for inbound E-field system.

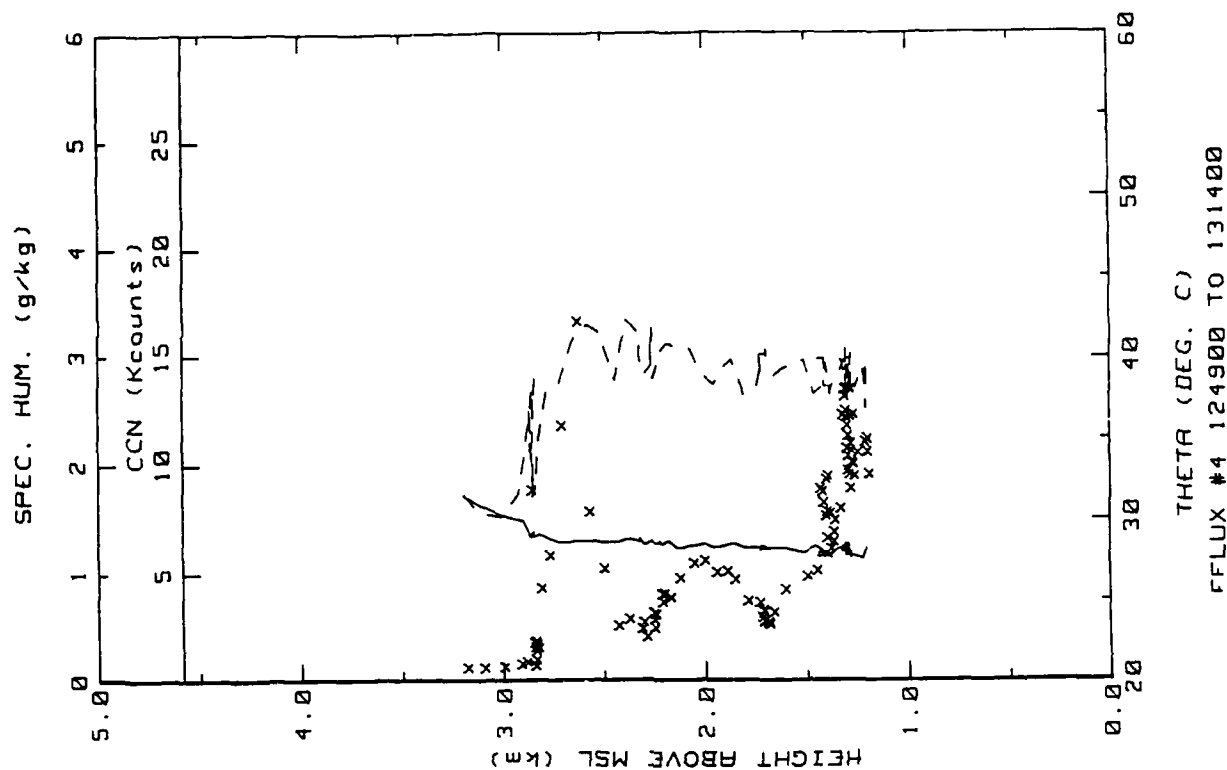


Figure 9x. Hobbs Flight 4 spiral downwinding (ref. Fig. 5b).

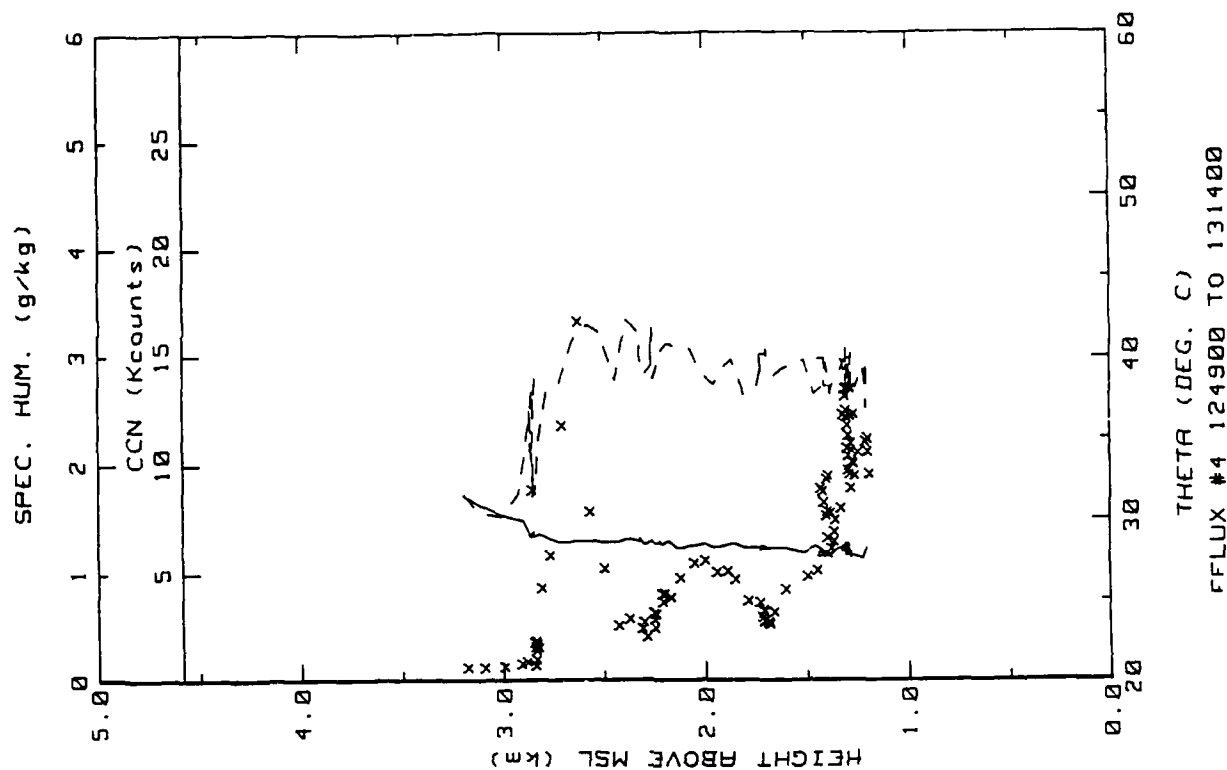


Figure 9y. Hobbs Flight 4 spiral downwinding (ref. Fig. 5h).



Flight: 5

Date: 18 May 1986

Takeoff: 1522 LT from Hobbs

Landed: 1620 at Hobbs

Conditions: No clouds; variable winds mostly from the NE at 5 m/s. Dry with good convection as evidenced by bumpy aircraft ride. Good visibility.

Instruments: All worked properly.

Summary: Executed slow spiral ascent to 4 km followed by a spiral descent and constant altitude runs over the ground station.

Table 3. Hobbs Flight 5 averages and (standard deviations)/averages for constant altitude runs over the ground station.

AVERAGES FROM LEVEL RUNS

Time HHH	N	Altitude km	Efield1 V/m	Efield2 V/m	+Lam 10 <sup>-14</sup>	-Lam 10 <sup>-14</sup>	Con Cur1 10 <sup>-12</sup>	Con Cur2 10 <sup>-12</sup>	Theta_v C
1531	35	2.780	24.24	20.01	5.10	7.01	3.28	2.71	26.8
1540	55	2.093	39.35	37.76	5.21	3.72	2.56	2.45	22.0
1546	48	1.525	58.98	58.00	2.32	2.40	2.74	2.75	20.6
1551	41	.890	68.16	69.09	1.94	2.00	2.74	2.70	19.7
1558	47	.285	77.74	78.58	1.75	2.21	3.11	3.15	19.6
1602	46	.151	80.20	80.16	1.74	2.04	3.02	3.02	18.9
1606	24	.061	84.62	84.55	1.82	1.94	3.18	3.18	19.1
1610	11	.015	87.56	87.53	1.94	2.21	3.64	3.64	19.4
1614	15	.006	86.67	86.80	1.85	2.20	3.52	3.53	19.4

Time HHH	N	Press mb	Rel Hum %	CON c/cc	EPS m2/s3	CI C2/m2/s	G g/kg	frose C	T_DR C	T_dew C
1531	35	617	20.3	.6	4.83E-05	1.17E-03	1.00	-3.0	0.0	-22.7
1540	55	678	43.8	5.4	5.20E-03	9.42E-03	2.40	-3	0.0	-11.1
1546	48	733	41.9	7.6	5.95E-03	1.52E-03	2.97	4.4	0.0	-7.4
1551	41	796	31.0	8.4	7.57E-03	1.21E-03	3.02	10.3	0.0	-6.1
1558	47	858	21.8	9.2	1.62E-02	6.69E-03	2.91	16.2	0.0	-5.6
1602	46	871	21.1	9.9	1.17E-02	9.47E-03	2.90	16.9	0.0	-5.5
1606	24	881	19.8	9.8	5.79E-02	5.77E-02	2.87	18.0	0.0	-5.4
1610	11	886	18.4	9.3	1.23E-01	1.99E-01	2.80	18.8	0.0	-5.7
1614	15	885	18.8	9.0	2.58E-01	3.48E-01	2.85	18.8	0.0	-5.4

STANDARD DEVIATIONS/MEAN VALUES

Time	Efield1	Efield2	+Lam	-Lam	Concur1	Concur2	CON	EPS	CI2	G
1531	.040	.053	.014	.027	.042	.050	.604	.309	.254	.068
1540	.212	.222	.300	.355	.177	.182	.615	.023	.838	.253
1546	.034	.034	.101	.124	.113	.112	.187	1.010	.543	.077
1551	.027	.025	.055	.062	.025	.024	.102	.535	.421	.028
1558	.043	.035	.084	.025	.022	.037	.089	.545	.623	.047
1602	.040	.037	.056	.046	.025	.020	.080	.534	.607	.033
1606	.037	.031	.070	.050	.021	.030	.101	.793	.757	.017
1610	.079	.063	.050	.031	.104	.094	.067	.542	.448	.008
1614	.035	.029	.041	.033	.106	.114	.026	.524	.418	.030

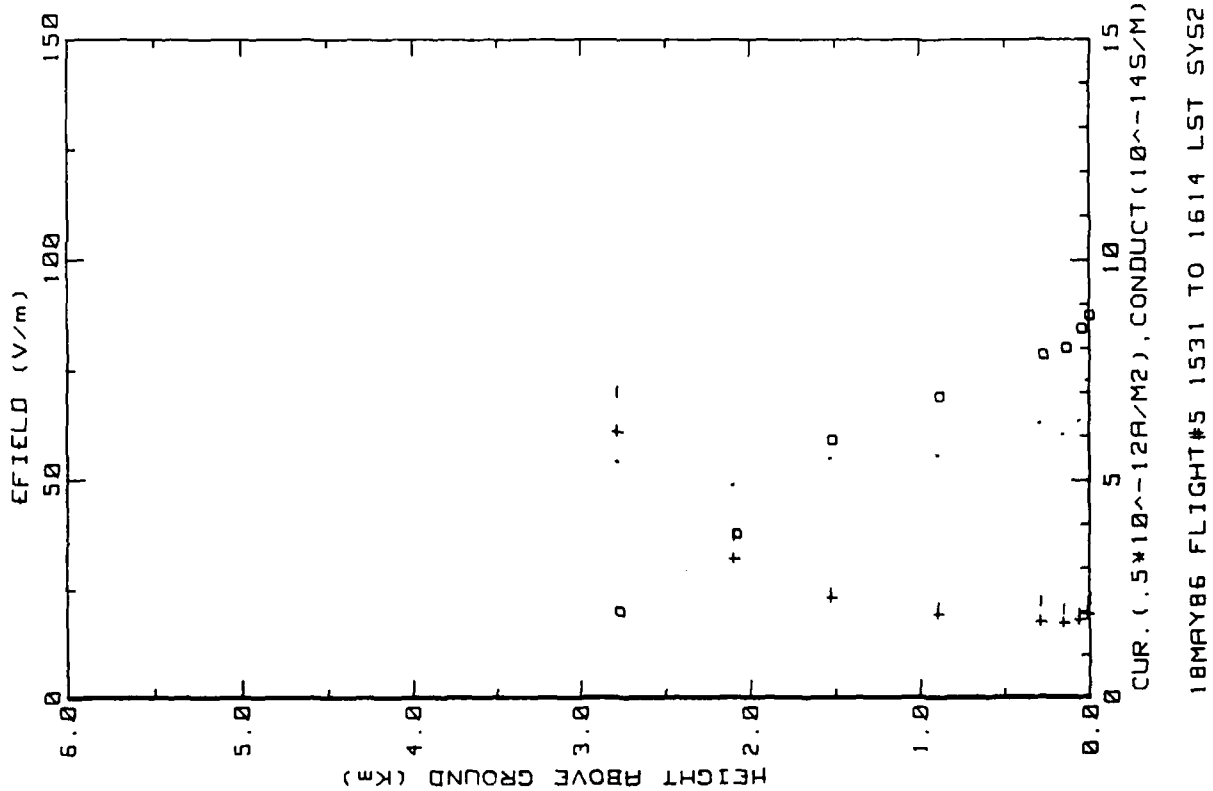


Figure 10a. Hobbs Flight 5 ladder profile (ref. Fig. 5a)

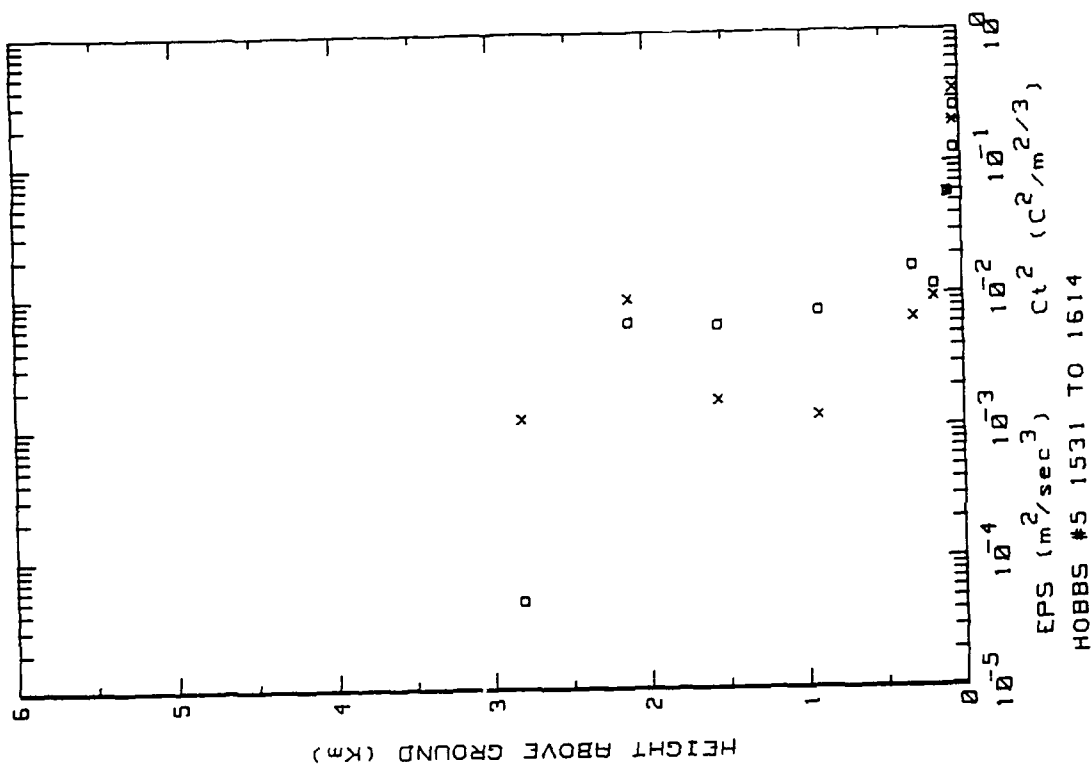


Figure 10b. Hobbs Flight 5 ladder profile (ref. Fig. 5b).

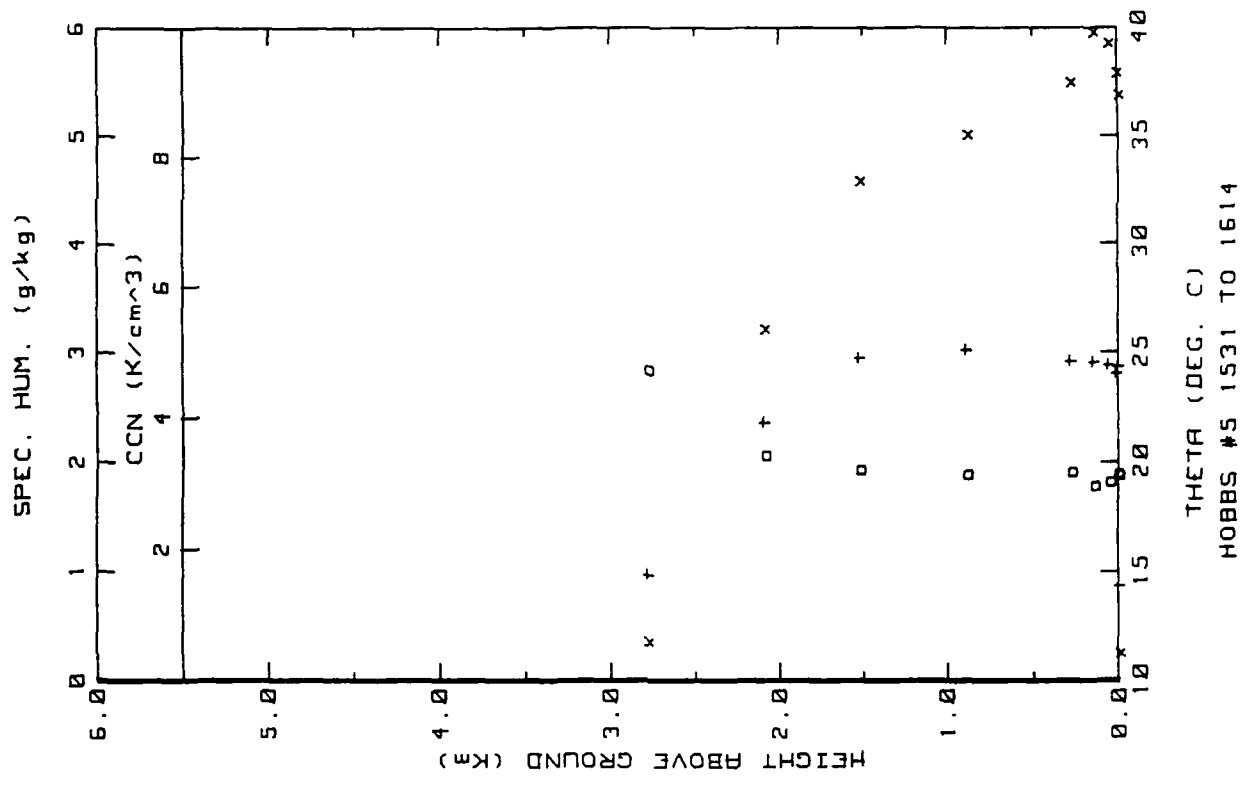


Figure 10c. Similar to 10a. but for outboard E<sub>field</sub> system.

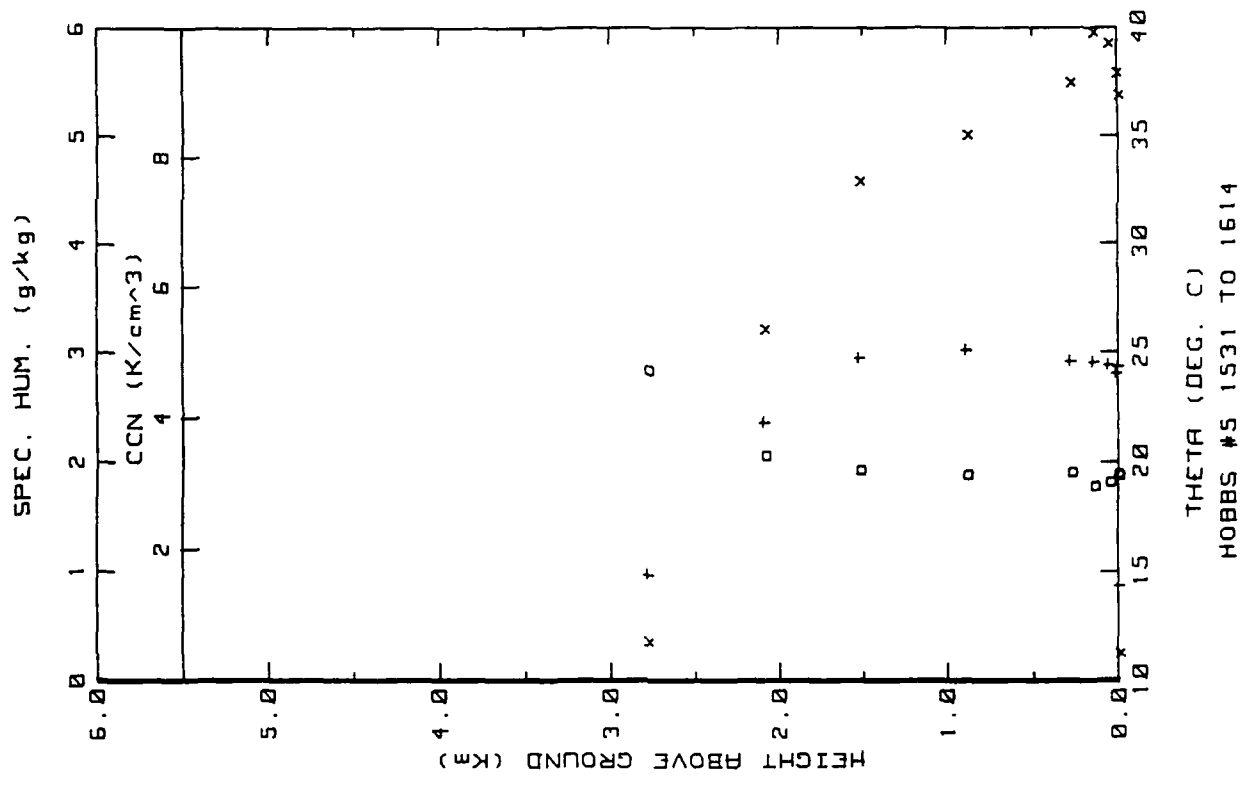
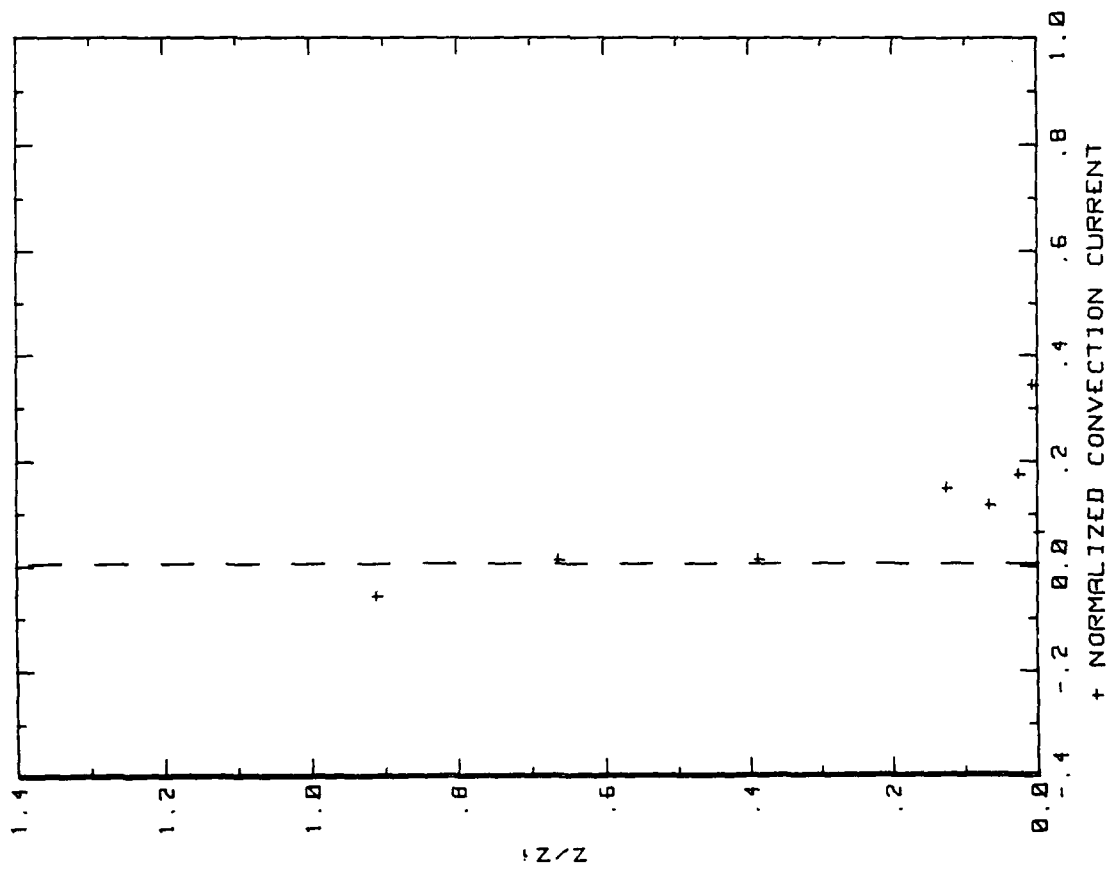


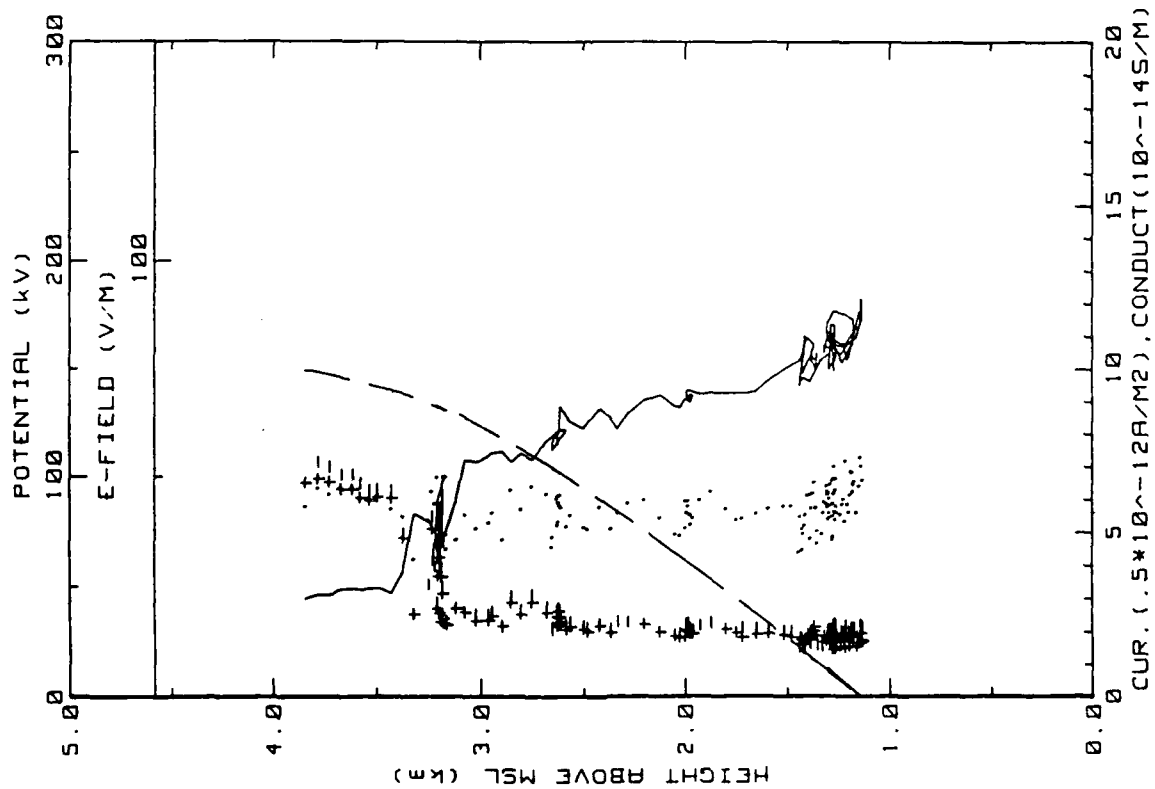
Figure 10d. Hobbs Flight 5 ladder profile (ref. Fig. 5c).



18MAY86 FLIGHT#5 1531 TO 1614 LST

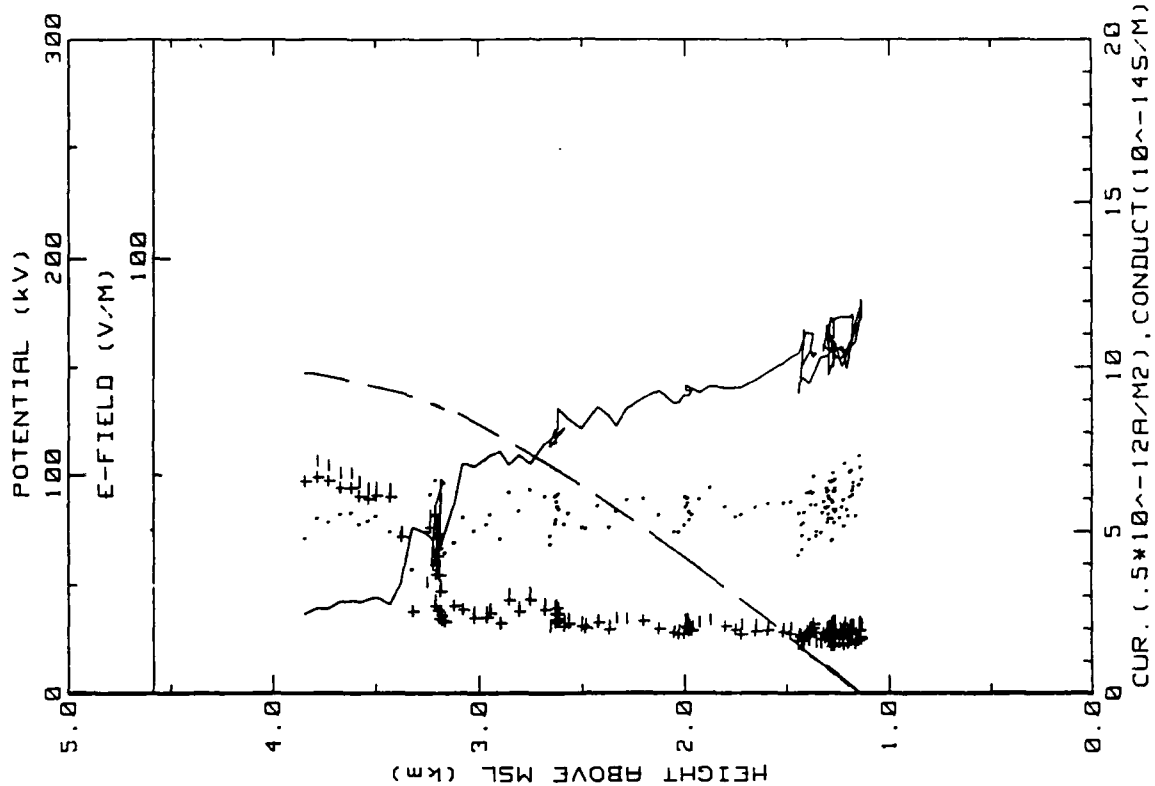
Z1=2300 J0=2.71

Figure 10e. Hobbs Flight 5 convection current profile  
(ref Fig. 5d)



18MAY86 FLIGHT#5 153530 TO 161400 LST

Figure 10f. Hobbs Flight 5 spiral downsonding (ref. Fig. 5e).



18MAY86 FLIGHT#5 153530 TO 161400 LST

Figure 10g. Same as Fig. 10f. but for inboard E<sub>field</sub> system.

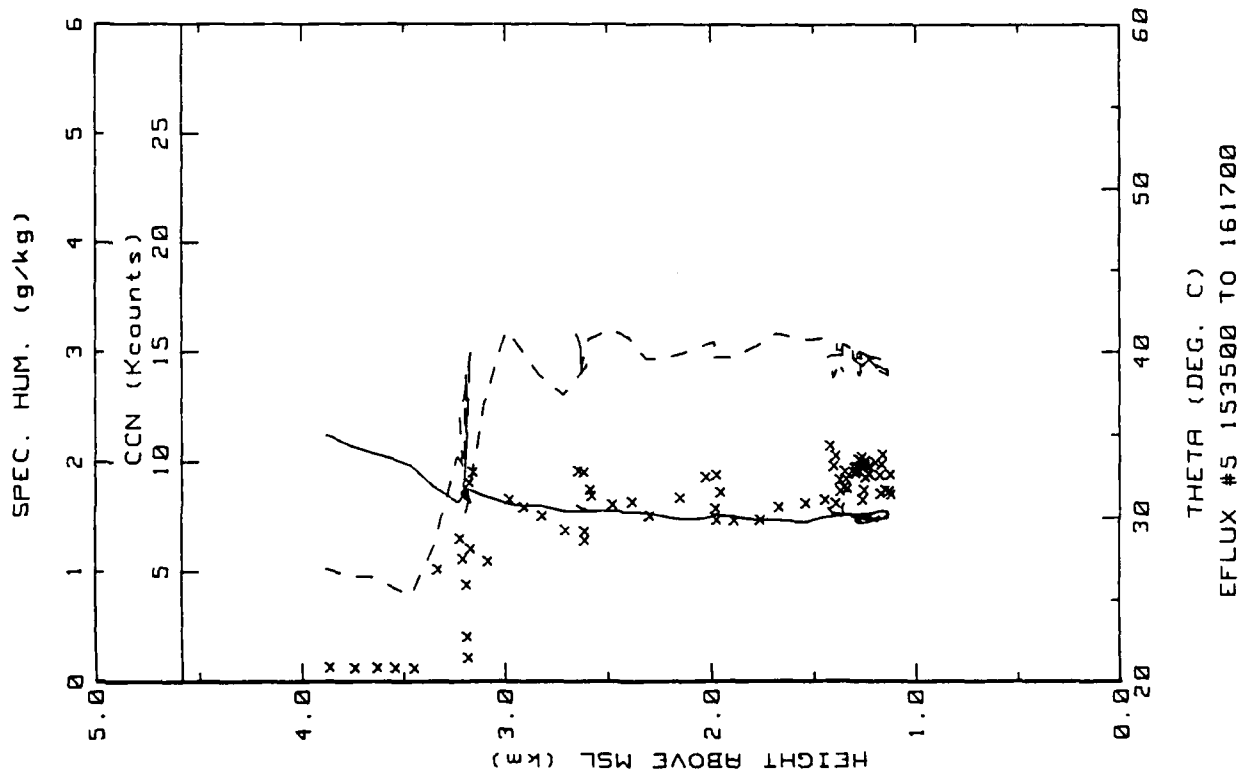


Figure 10h. Hobbs Flight 5 spiral down sounding (ref. Fig. 5h).

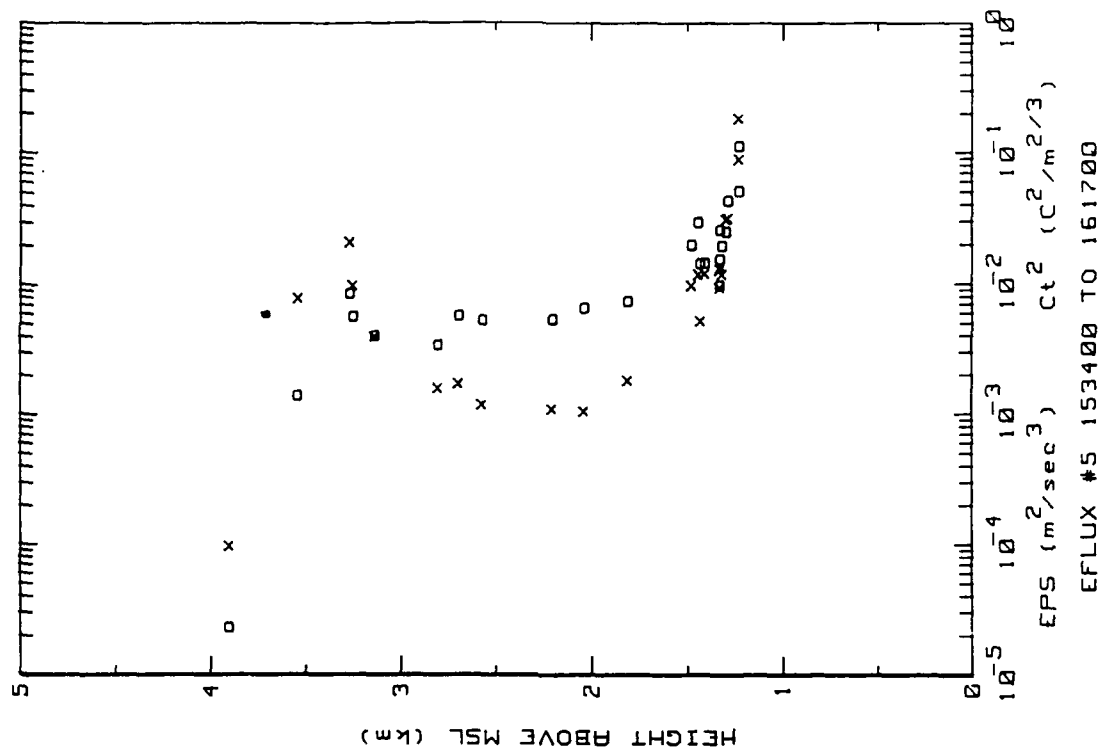


Figure 10i. Hobbs Flight 5 spiral down sounding (ref. Fig. 5b).

Flight: 6

Date: 19 May 1986

Takeoff: 1021 LT from Hobbs

Landed: 1120 at Hobbs

Conditions: Clear skies, cooler than normal. Visibility was reduced because of high aerosol density. Winds were from the SSE at 5 m/s.

Instruments: Both conductivity tubes were slightly noisy.

Summary: Low altitude passes were made over the ground station at the beginning of the flight followed by a slow spiral descent from 4.6 km over the Hobbs airport.



Table 4. Hobbs Flight 6 averages and (standard deviations)/averages for constant altitude runs over the ground station. Data from 1107 LT are not reliable.

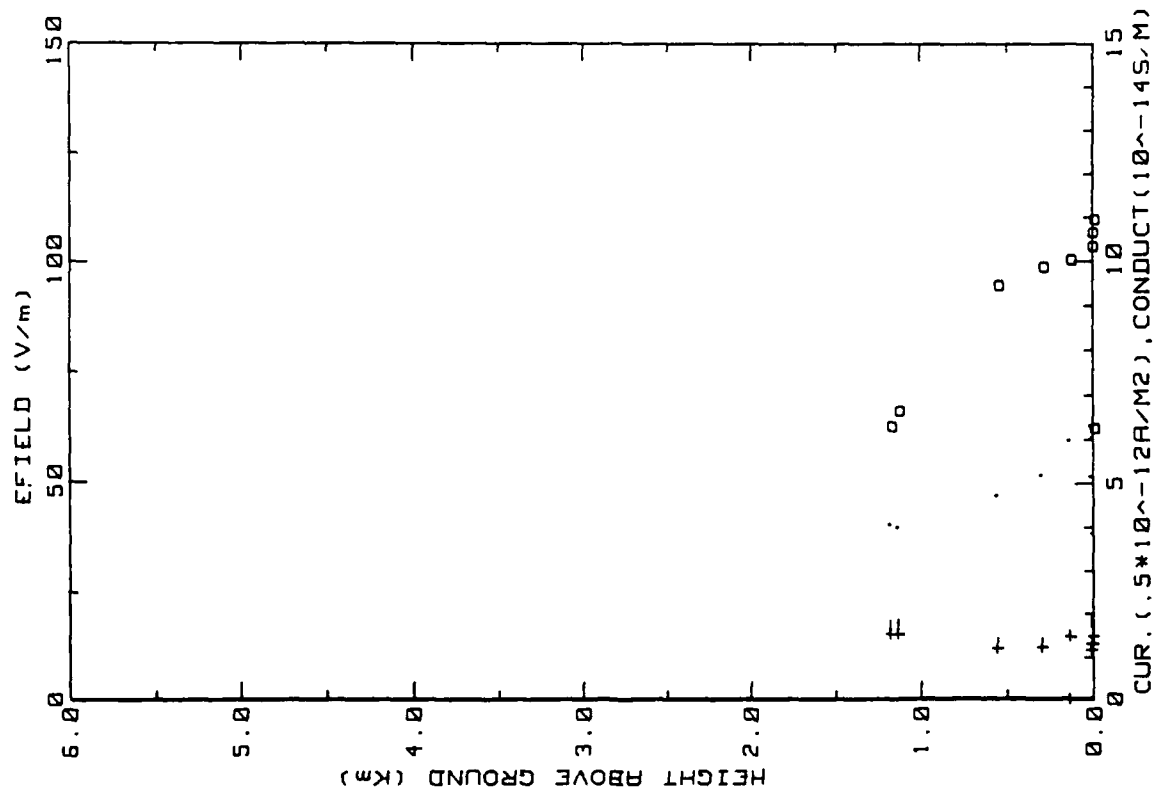
AVERAGES FROM LEVEL RUNS

Time HHH	N	Altitude km	Efield1 V/m	Efield2 V/m	+Lam 10 <sup>-14</sup>	-Lam 10 <sup>-14</sup>	Con Cur1 10 <sup>-12</sup>	Con Cur2 10 <sup>-12</sup>	11eta_v C
1031	35	.558	94.66	92.85	1.20	1.31	2.56	2.34	19.4
1036	44	1.180	62.90	61.32	1.53	1.71	2.02	1.97	20.3
1046	31	1.135	66.42	65.02	1.53	1.74	2.00	1.95	20.2
<del>1107</del>	<del>13</del>	<del>.896</del>	<del>62.57</del>	<del>60.81</del>	<del>1.48</del>	<del>1.62</del>	<del>1.94</del>	<del>1.88</del>	<del>20.3</del>
1110	11	.015	106.54	106.37	1.17	1.80	3.16	3.15	20.1
1113	13	.005	109.50	109.98	1.30	1.46	3.03	3.04	20.2
1116	10	.140	100.38	99.72	1.47	0.00	2.99	2.96	20.6
1118	25	.300	98.75	99.32	1.23	1.31	2.60	2.61	21.2
1120	39	.015	103.42	102.87	1.31	1.20	2.58	2.57	17.1

Time HHH	N	Press mb	Rel Hum %	CON k/cc	EPS m2/s3	CT C2/m2/s3	Q g/kg	Trose C	T <sub>DR</sub> C	T <sub>dev</sub> C
1031	35	830	28.6	19.0	8.69E-03	2.39E-03	3.26	13.3	0.0	-4.6
1036	44	767	34.1	14.2	2.84E-03	8.12E-03	2.93	7.9	0.0	-7.0
1046	31	771	34.2	.5	2.86E-03	6.77E-03	2.99	8.2	0.0	-6.7
<del>1107</del>	<del>13</del>	<del>985</del>	<del>34.4</del>	<del>14.0</del>	<del>3.06E-03</del>	<del>1.15E-02</del>	<del>2.55</del>	<del>7.0</del>	<del>0.0</del>	<del>6.9</del>
1110	11	886	22.3	26.7	1.36E-01	1.68E-01	3.50	19.3	0.0	-2.8
1113	13	867	22.2	26.0	4.51E-01	4.68E-01	3.52	19.5	0.0	-2.7
1116	10	873	23.7	27.9	4.31E-02	5.73E-02	3.60	18.5	0.0	-2.6
1118	25	856	24.4	29.4	2.39E-02	2.02E-02	3.57	17.6	0.0	-2.9
1120	39	886	26.1	28.5	1.26E-02	5.78E-03	3.33	16.3	0.0	-3.2

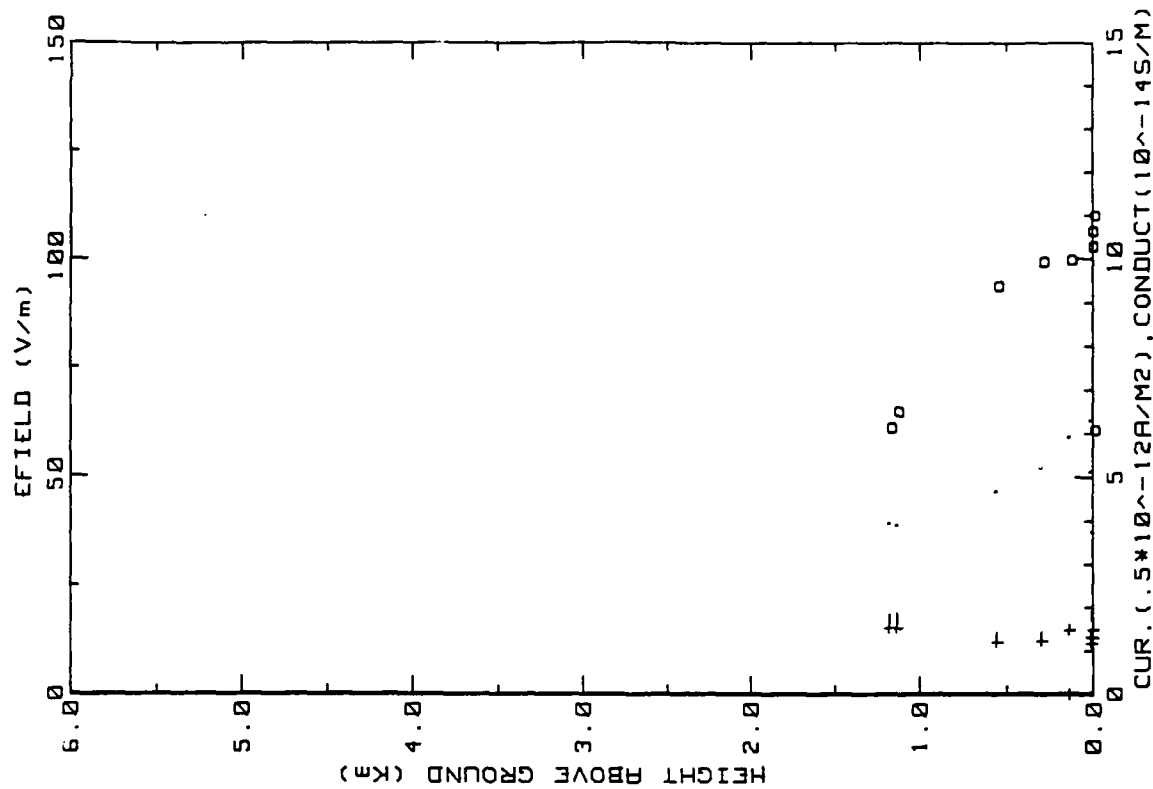
STANDARD DEVIATIONS/MEAN VALUES

Time	Efield1	Efield2	+Lam	-Lam	Concur1	Concur2	CON	EPS	CT2	Q
1031	.037	.041	.057	.059	.042	.045	.091	.430	.423	.019
1036	.091	.088	.138	.153	.142	.134	.250	.395	.791	.075
1046	.132	.138	.128	.229	.129	.126	.305	.755	.587	.077
1107	.077	.074	.062	.155	.099	.099	.296	.056	.727	.070
1110	.058	.050	.063	.097	.097	.093	.003	.307	.387	.006
1113	.042	.035	.050	.107	.105	.109	.025	.464	.332	.010
1116	.055	.039	.282	0.000	.346	.323	.113	.308	.317	.010
1118	.084	.079	.239	.056	.113	.104	.154	.554	.869	.014
1120	.040	.037	.217	.141	.104	.108	.171	.441	.547	.020



19MAY86 FLIGHT#6 1031 TO 1120 LST

Figure 11a. Hobbs Flight 6 ladder profile (ref. Fig. 5a)



19MAY86 FLIGHT#6 1031 TO 1120 LST SYS2

Figure 11b. Similar to 11a. but for inboard E-field system.

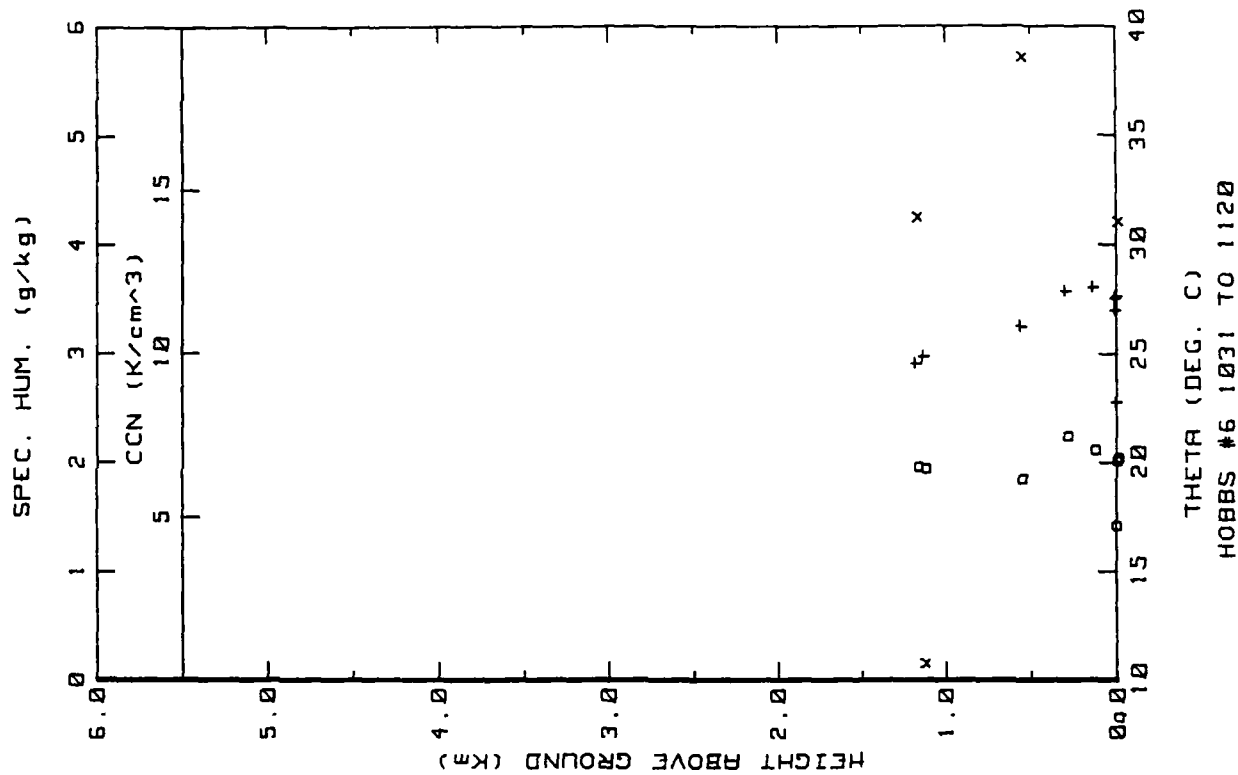


Figure 11d. Hobbs Flight 6 ladder profile (ref. Fig. 5c).

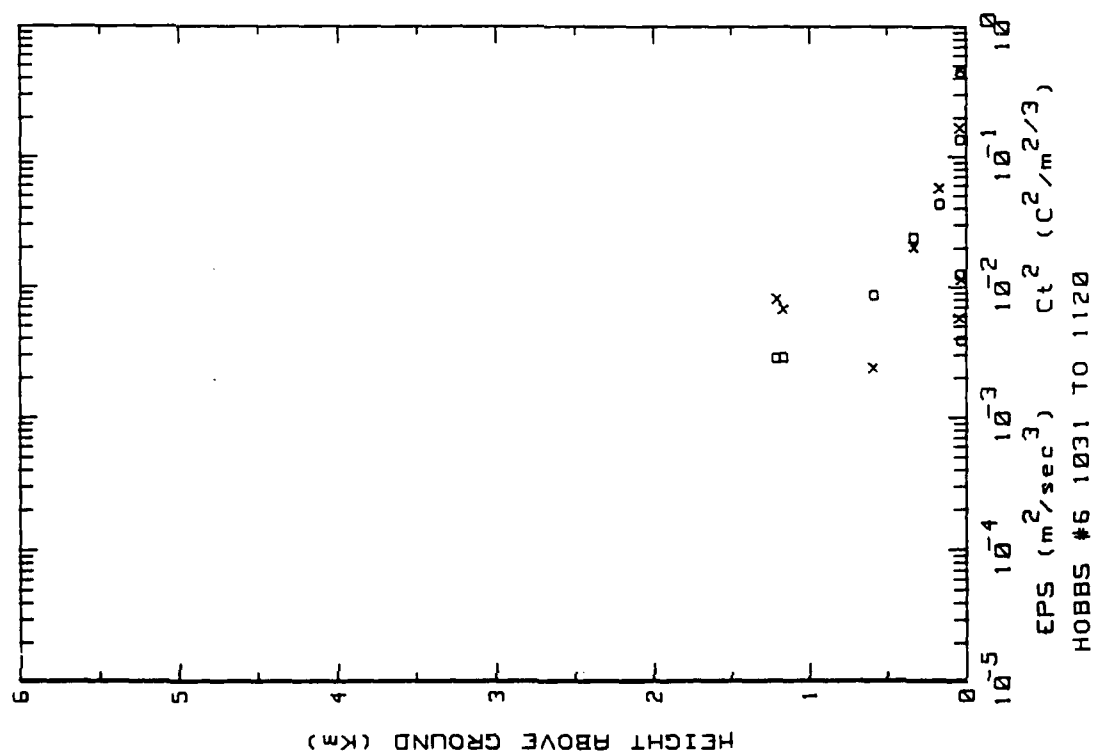


Figure 11c. Hobbs Flight 6 ladder profile (ref. Fig. 5b).

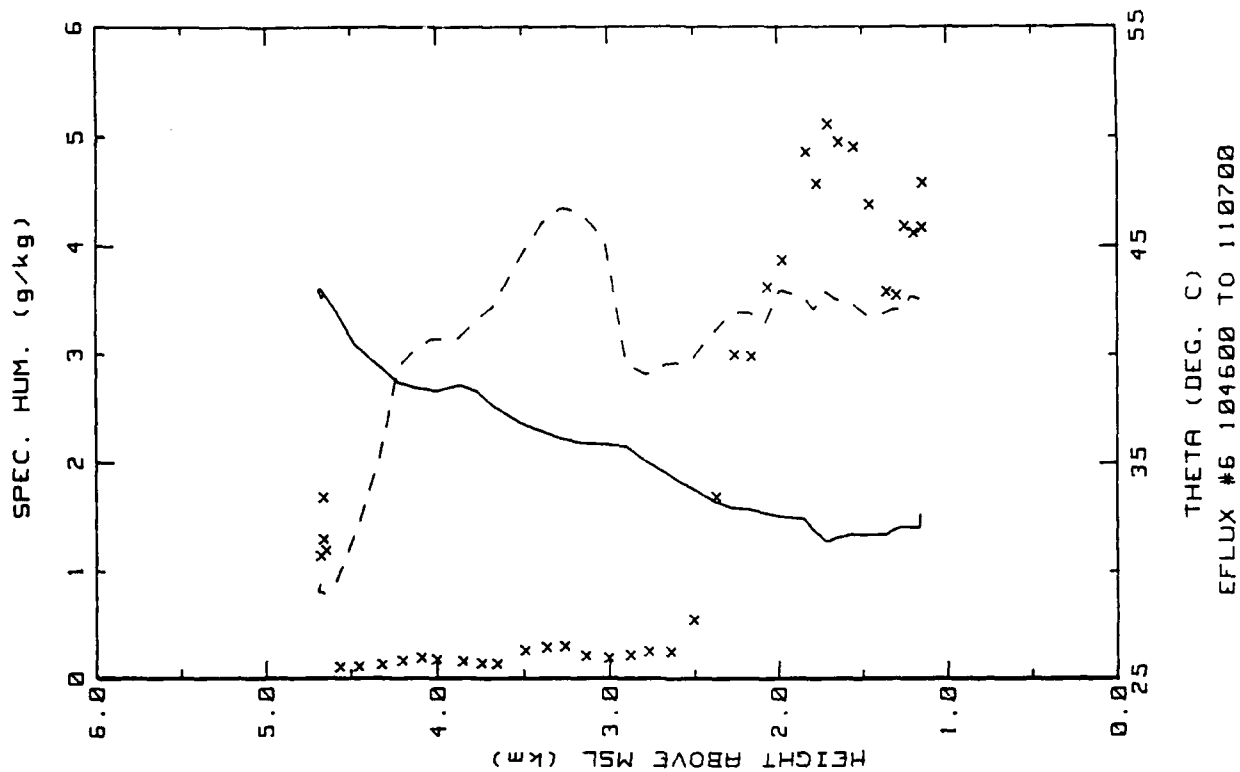


Figure 11f. Hobbs Flight 6 spiral downsonding (ref. Fig. 5h).

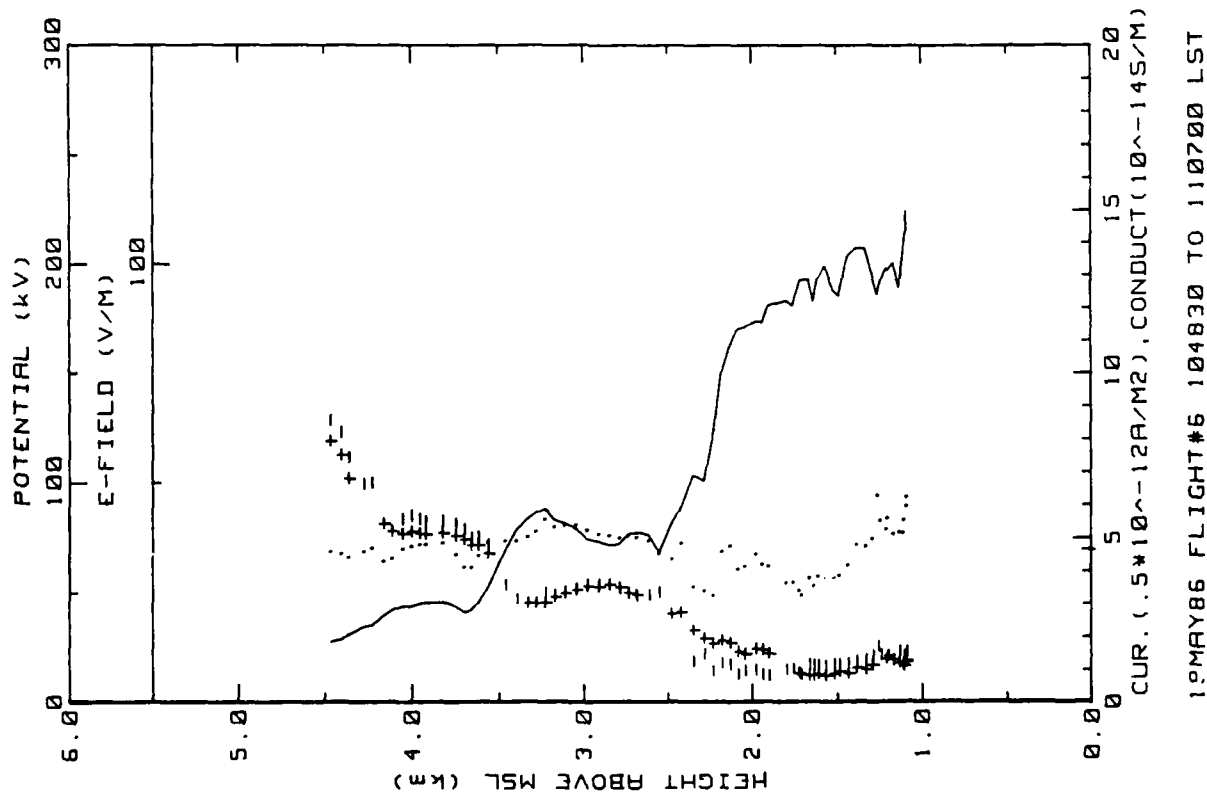


Figure 11e. Hobbs Flight 6 spiral downsonding (ref. Fig. 5e).

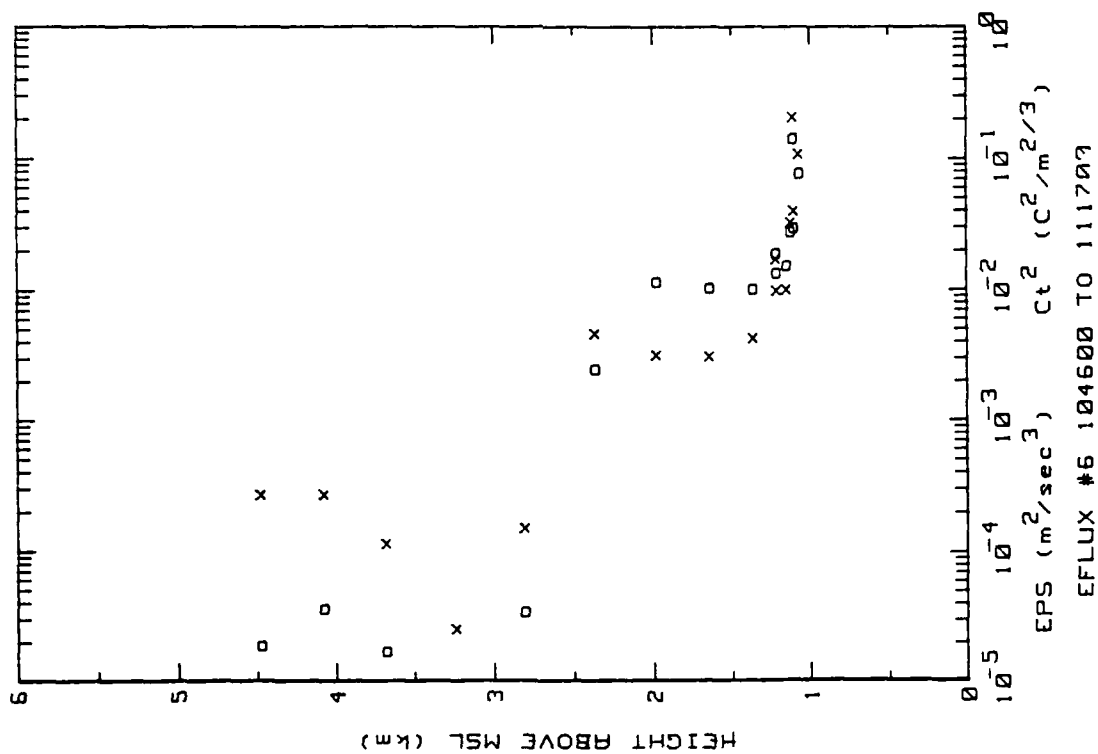


Figure 11g. Hobbs Flight 6 spiral downsonding (ref. Fig. 5b).

Flight: 7

Date: 19 May 1986

Takeoff: 1355 LT from Hobbs

Landed: 1459 at Hobbs

Conditions: Clear skies with SSW winds at 5 m/s. Visibility was reduced because of high aerosol concentrations. A fairly cool day with only moderate convection.

Instruments: Negative conductivity was very noisy on low altitude passes; positive conductivity was somewhat better but still noisy. The computer data acquisition system crashed near the end of the flight losing several minutes of data.

Summary: The flight consisted of a coarse, ascending ladder profile over the ground station at Hobbs followed by a slow spiral descent over the same area. More constant altitude passes were made over the ground station at end of the flight.

Table 5. Hobbs Flight 7 averages and (standard deviations)/averages for constant altitude runs over the ground station. The turbulence data from 1456 LT are not reliable.

AVERAGES FROM LEVEL RUNS

Time HHM	N	Altitude km	Efield1 V/m	Efield2 V/m	+Lam 10 <sup>-14</sup>	-Lam 10 <sup>-14</sup>	Con Cur1 10 <sup>-12</sup>	Con Cur2 10 <sup>-12</sup>	Theta_v C
1400	51	.511	76.08	74.57	1.43	1.53	2.20	2.16	22.8
1409	44	1.830	55.42	53.37	2.03	2.04	2.66	2.57	24.7
1417	34	3.538	18.73	17.70	5.59	8.64	3.44	3.26	34.3
1425	71	2.201	53.10	52.47	2.65	3.01	2.93	2.90	26.2
1440	22	.006	84.67	83.10	1.23	1.17	2.01	1.98	23.3
1442	20	.015	89.38	89.95	1.18	.75	1.65	1.66	22.7
1446	41	.061	90.16	90.07	1.34	.63	1.99	1.99	22.6
1451	46	.151	91.21	91.24	1.15	.85	1.75	1.75	22.8
1453	21	.330	93.49	97.45	.87	.68	1.52	1.51	23.1
1456	10	.006	95.18	94.80	1.09	.84	1.83	1.82	19.6

Time HHM	N	Press mb	Rel Hum %	CGV k/sec	EPS m2/s3	C1 C2/m2/3	Q g/kg	Trose C	T_IR C	T_dew C
1400	51	825	22.8	18.5	1.26E-02	4.56E-03	3.16	16.2	47.7	-5.0
1409	44	705	33.8	4.7	7.38E-03	2.39E-03	3.11	5.2	47.7	-7.3
1417	34	564	29.2	.3	1.20E-05	2.79E-04	1.41	-4.7	46.9	-20.0
1425	71	671	49.4	3.4	1.02E-02	1.02E-02	3.36	2.6	48.4	-7.0
1440	22	887	17.3	24.7	5.61E-01	5.51E-01	3.32	22.6	49.0	-3.4
1442	20	886	17.8	26.6	1.80E-01	2.39E-01	3.29	22.0	49.4	-3.6
1446	41	881	18.1	24.4	4.02E-02	4.68E-02	3.25	21.4	48.7	-3.8
1451	46	872	18.9	27.0	1.80E-02	1.29E-02	3.23	20.7	48.0	-3.8
1453	21	854	20.4	28.0	1.50E-02	6.76E-03	3.31	19.2	48.3	-4.0
1456	10	887	20.4	28.5	<del>1.10E-02</del>	<del>3.33E-03</del>	3.14	19.0	46.8	-4.2

STANDARD DEVIATIONS/MEAN VALUES

Time	Efield1	Efield2	+Lam	-Lam	Concur1	Concur2	CGV	EPS	C12	Q
1400	.153	.155	.103	.196	.124	.134	.526	.578	.830	.016
1409	.038	.036	.087	.154	.100	.101	.172	.451	.513	.027
1417	.027	.043	.046	.015	.034	.076	.125	1.031	.625	.075
1425	.120	.121	.214	.300	.150	.153	.364	.599	.937	.028
1440	.151	.217	.142	.216	.293	.339	.255	.320	.205	.013
1442	.056	.066	.081	.175	.156	.157	.212	.319	.238	.010
1446	.043	.043	.102	.333	.203	.204	.304	.524	.593	.011
1451	.031	.021	.175	.723	.356	.355	.365	.362	.548	.015
1453	.026	.023	.123	.142	.107	.135	.111	.331	.673	.012
1456	.015	.019	.066	.477	.226	.227	.052	.233	.536	.001

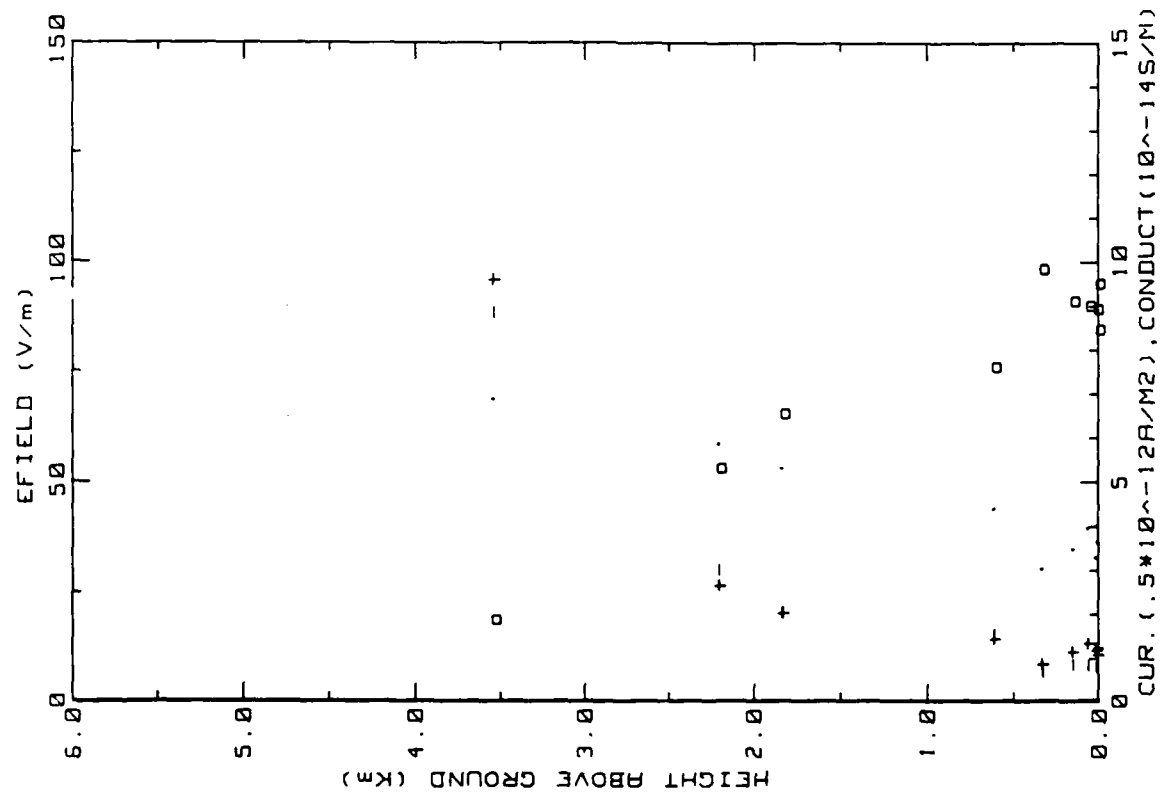


Figure 12a. Hobbs Flight 7 ladder profile (ref. Fig. 5a)

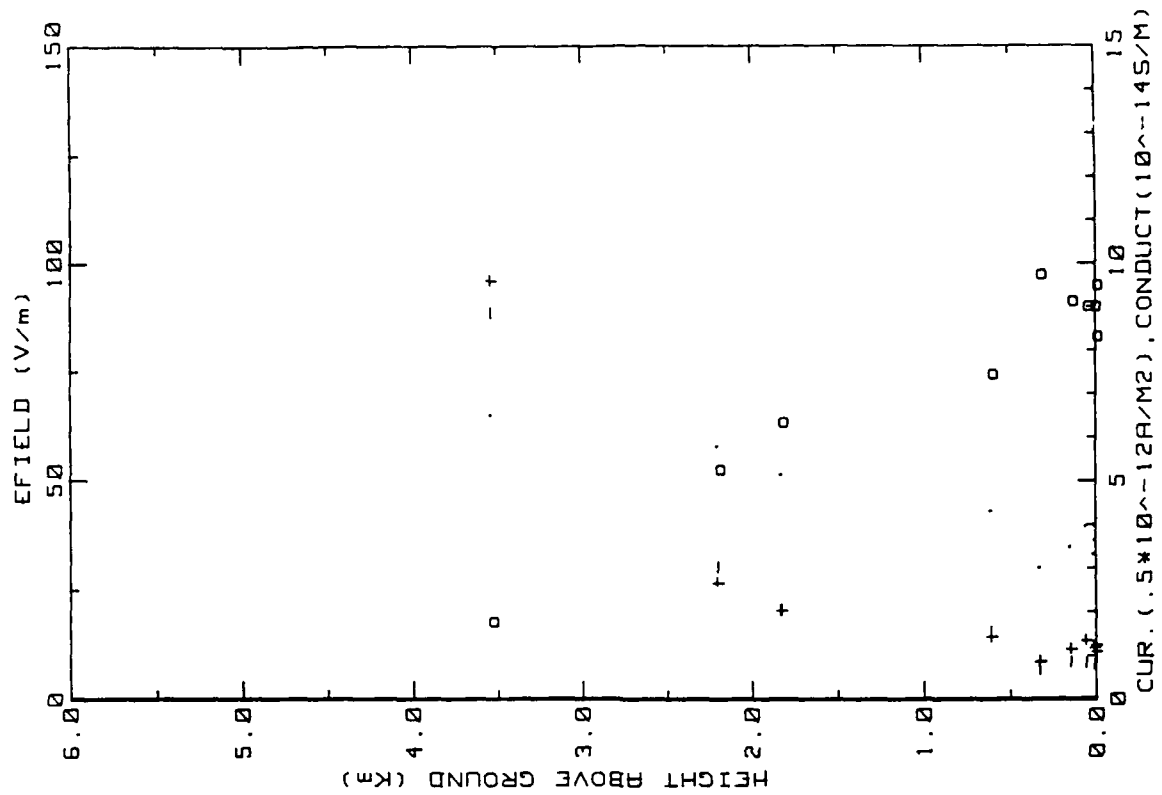


Figure 12b. Similar to 12a, but for inboard E field system.



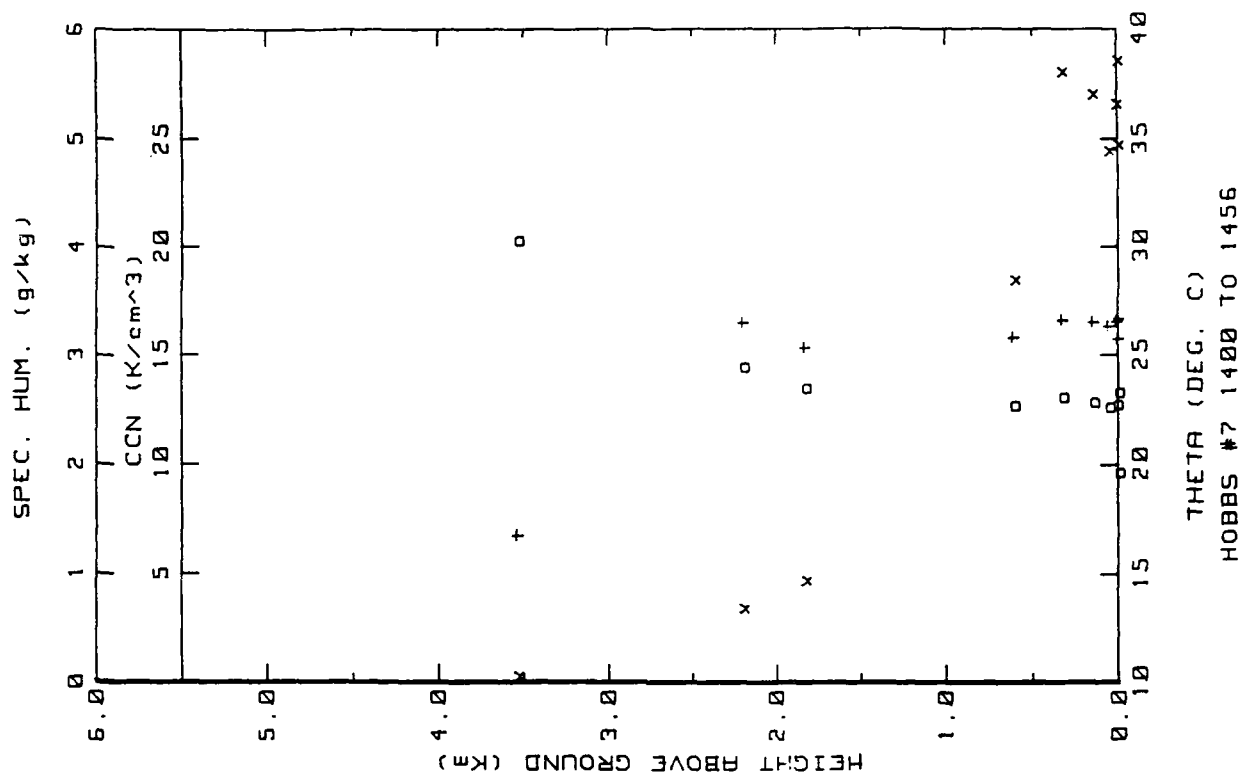


Figure 12c. Hobbs Flight 7 ladder profile (ref. Fig. 5b).

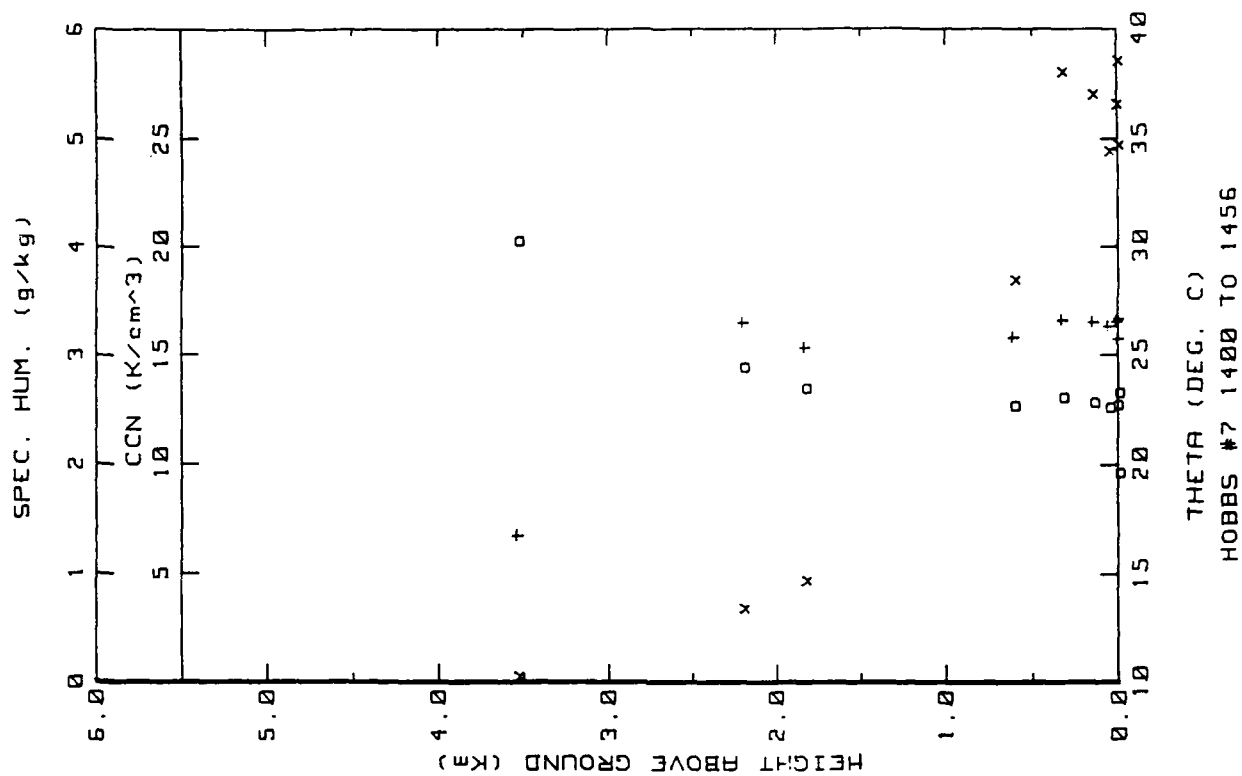


Figure 12d. Hobbs Flight 7 ladder profile (ref. Fig. 5c).

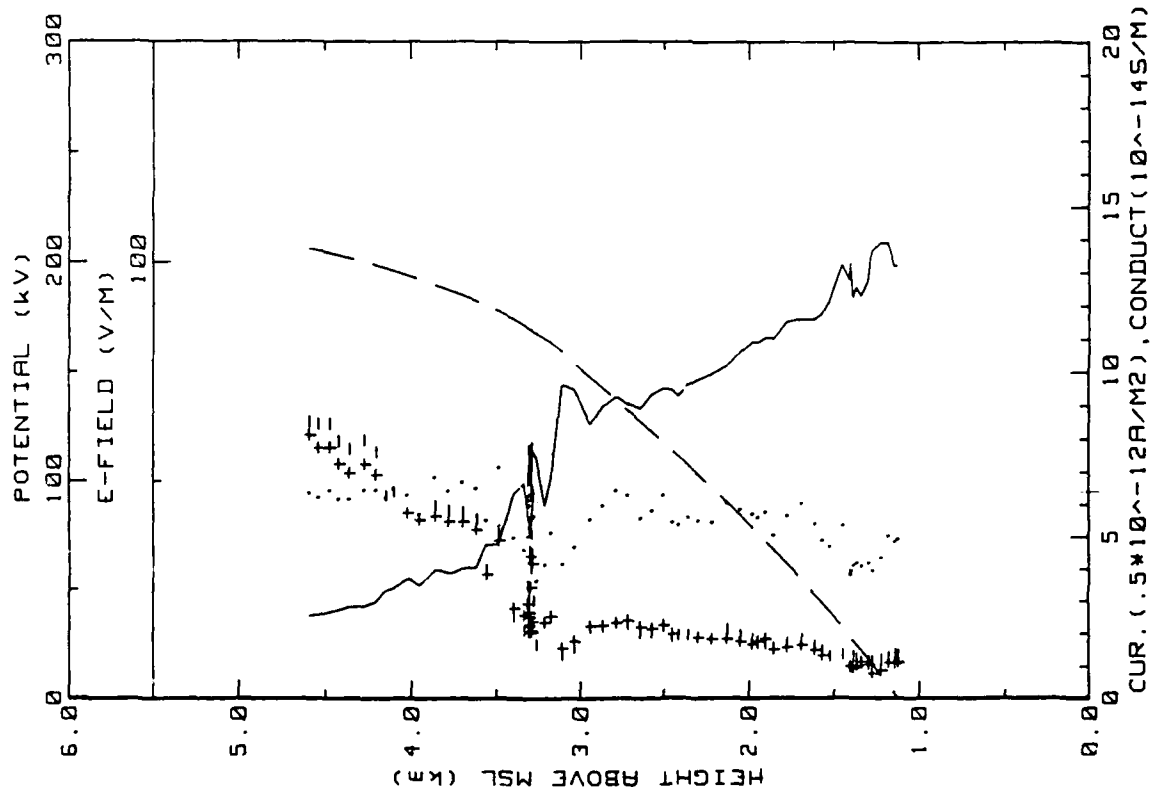


Figure 12e. Hobbs Flight 7 spiral downsonding (ref. Fig. 5e).

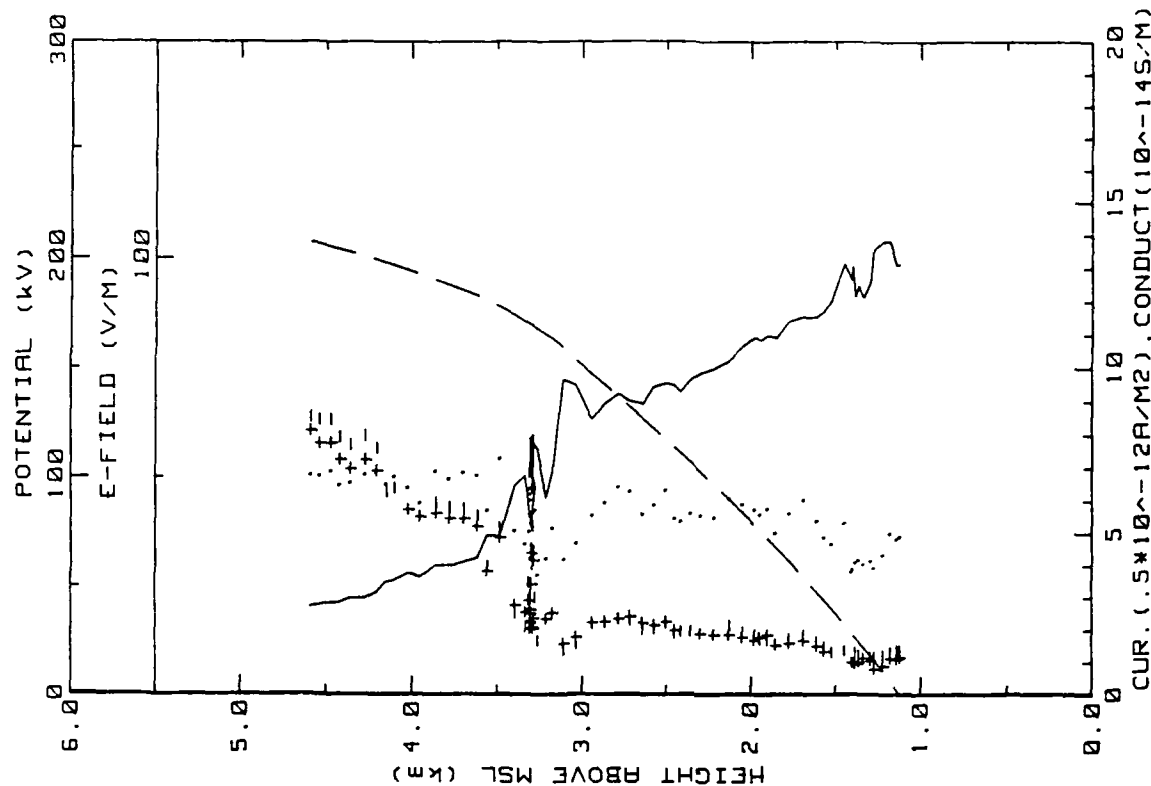


Figure 12f. Same as Fig. 12e but for outboard E<sub>field</sub> system.

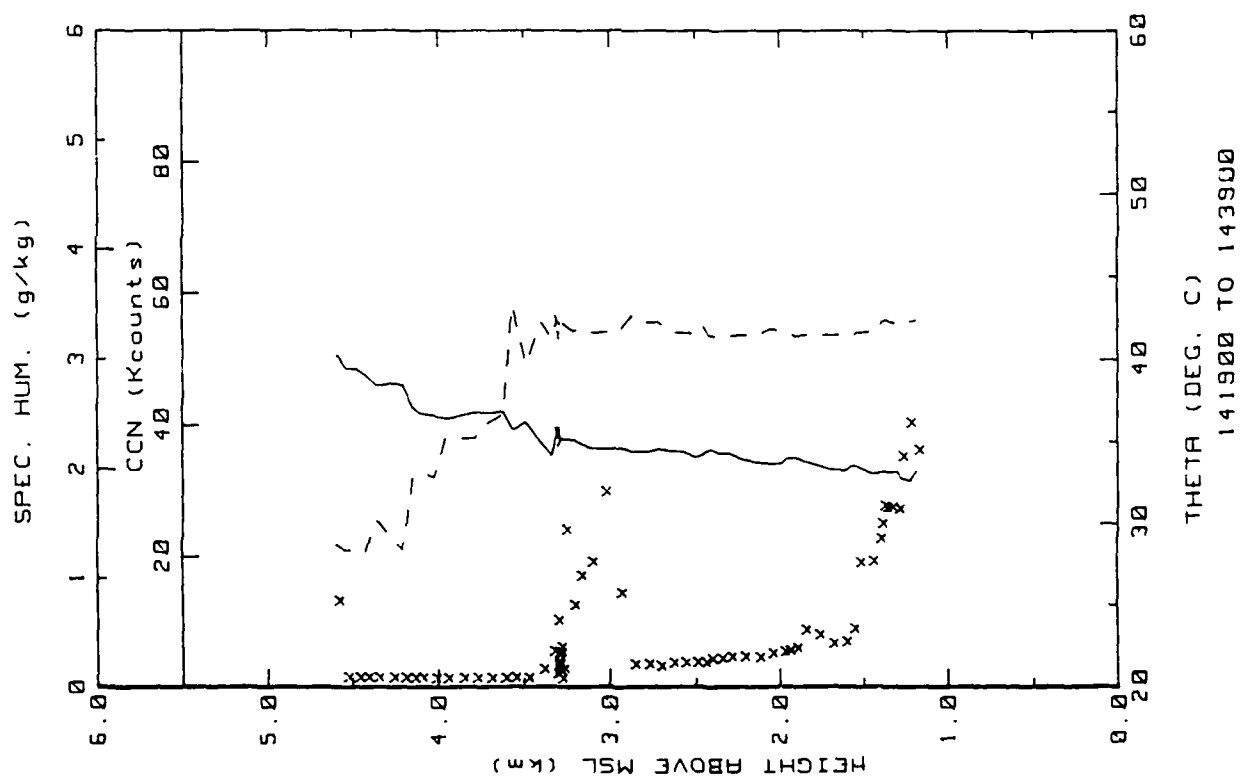


Figure 12g. Hobbs Flight 7 spiral downsound (ref. Fig. 5h).

Flight: 8

Date: 19 May 1986

Takeoff: 1646 LT from Hobbs

Landed: 1800 at Hobbs

Conditions: Bright sunny day with no clouds; gusty winds from the SW. Several dust devils were observed over the burned area adjacent to the airport. The surface layer was somewhat hazy from the presence of aerosols.

Instruments: The negative conductivity tube was very noisy.

Summary: Followed the usual flight procedure, i.e., a ladder profile was obtained over the ground station while climbing to the flight apex of 4.6 km and a downsounding was performed while descending in a slow spiral over the same area.

Table 6a. Hobbs Flight 8 averages for constant altitude runs over the ground station.

AVERAGES FROM LEVEL RUNS

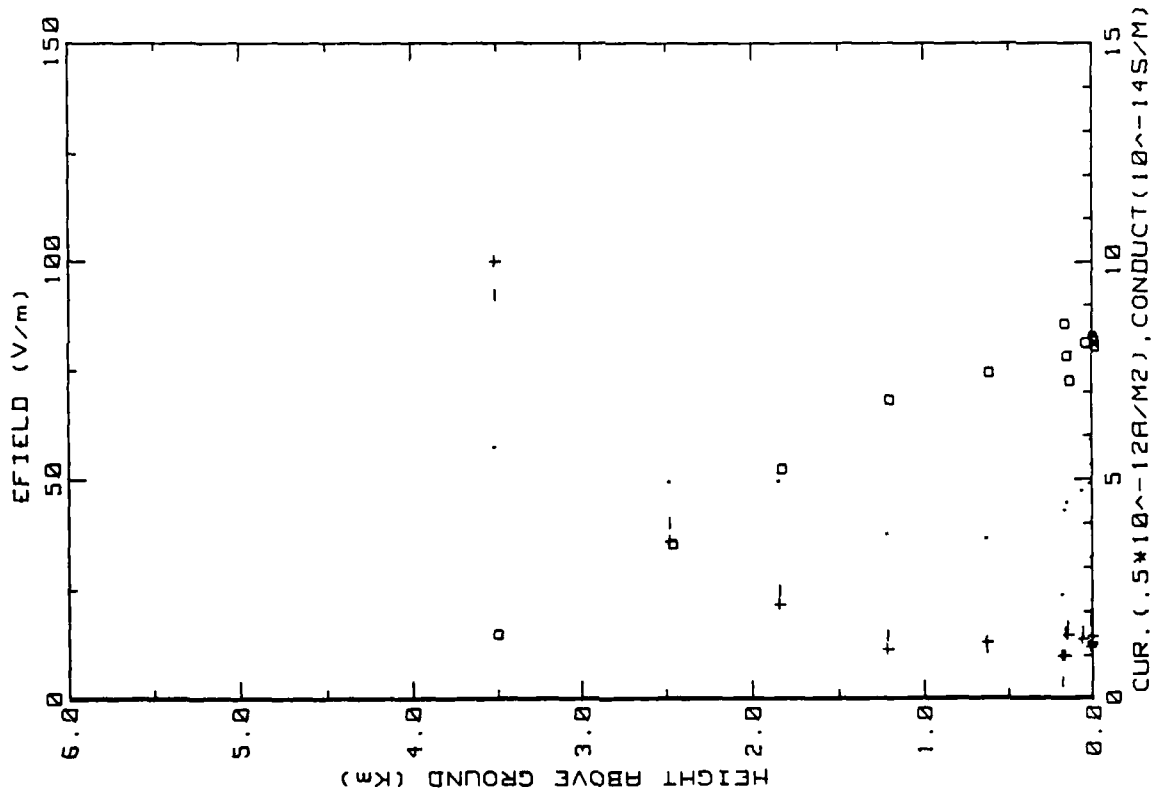
Time HHMM	N	Altitude km	Efield1 V/m	Efield2 V/m	Lam 10 <sup>-14</sup>	-Lam 10 <sup>-14</sup>	Con Cur1 10 <sup>-12</sup>	Con Cur2 10 <sup>-12</sup>	Theta_v C
1650	21	.528	75.75	74.45	1.31	1.15	1.89	1.84	23.9
1652	36	1.214	70.47	68.19	1.15	1.46	1.94	1.88	24.0
1656	36	1.840	54.69	52.38	2.17	2.47	2.59	2.49	25.3
1701	44	2.475	37.27	35.39	3.60	4.00	2.61	2.48	26.6
1707	50	3.512	16.15	14.98	10.00	9.21	3.10	2.87	35.0
1737	9	.006	81.95	81.48	1.25	2.35	2.97	2.95	23.4
1740	14	.006	80.22	80.38	1.31	.41	1.62	1.62	23.6
1741	30	.151	72.72	72.55	1.48	1.66	2.25	2.24	23.3
1744	18	.006	82.56	81.84	1.45	1.81	2.69	2.67	23.6
1748	24	.015	82.61	82.65	1.20	1.77	2.45	2.45	23.1
1749	21	.166	77.81	79.24	.95	1.52	2.14	2.15	23.2
1751	28	.031	81.97	81.25	1.30	1.54	2.40	2.37	23.1
1754	21	.181	86.34	85.52	1.00	.37	1.21	1.19	23.6

Time HHMM	N	Press mB	Rel Hum %	CON k/cc	EPS m2/s3	CT C2/m2/3	g g/kg	Trose C	T_IR C	T_dew C
1650	21	821	21.2	14.6	1.34E-02	2.59E-03	3.13	17.1	37.2	-5.3
1652	36	762	29.4	14.4	4.91E-03	7.49E-04	3.17	11.1	37.5	-6.0
1656	36	702	36.5	5.7	7.70E-03	1.36E-03	2.97	5.8	37.3	-7.9
1701	44	643	41.5	3.7	2.75E-03	3.31E-03	2.46	.0	35.5	-11.5
1707	50	555	23.3	.1	8.82E-06	2.17E-04	1.22	-3.6	35.5	-21.6
1737	9	883	16.8	11.2	1.38E-01	1.48E-01	3.27	22.8	38.5	-3.7
1740	14	883	16.8	11.1	1.18E-01	1.23E-01	3.30	22.9	38.0	-3.6
1741	30	869	17.9	10.0	1.15E-02	7.51E-03	3.23	21.2	38.8	-4.1
1744	18	883	16.5	10.9	7.58E-02	9.12E-02	3.26	23.0	38.2	-3.7
1748	24	862	17.1	10.2	3.07E-02	4.43E-02	3.24	22.3	38.3	-3.8
1749	21	867	18.1	9.5	9.31E-03	4.39E-03	3.21	21.0	38.5	-4.2
1751	28	878	17.3	9.8	2.87E-02	1.39E-02	3.22	21.9	38.5	-4.0
1754	21	866	19.0	15.8	9.75E-03	6.48E-03	3.43	21.2	36.7	-3.3

Table 6b. Hobbs Flight 8 (standard deviations)/averages for  
constant altitude runs over the ground station.

STANDARD DEVIATIONS/MEAN VALUES

Time	Efield1	Efield2	+Lam	-Lam	Concur1	Concur2	CCN	EPS	CT2	Q
1650	.051	.049	.110	.164	.113	.113	.085	.558	.532	.013
1652	.045	.053	.128	.183	.162	.158	.199	.346	.391	.027
1656	.014	.018	.071	.084	.087	.087	.079	.491	.368	.054
1701	.128	.134	.164	.220	.069	.088	.412	.581	.772	.157
1707	.032	.040	.019	.020	.034	.041	.574	.350	.785	.034
1737	.063	.047	.108	.059	.126	.113	.010	.143	.155	.011
1740	.056	.054	.100	1.263	.285	.287	.049	.511	.418	.016
1741	.060	.065	.066	.167	.150	.153	.081	.591	1.083	.012
1744	.063	.058	.077	.032	.068	.065	.053	.514	.422	.012
1748	.057	.057	.093	.140	.117	.117	.152	.398	.349	.012
1749	.063	.056	.140	.119	.179	.172	.101	.483	.575	.029
1751	.029	.030	.104	.491	.267	.263	.063	.245	.197	.015
1754	.028	.029	.088	.357	.161	.158	.031	.569	.744	.011



19MAY86 FLIGHT#8 1650 TO 1754 LST SYS2

Figure 13a. Hobbs Flight 8 ladder profile (ref. Fig. 5a)

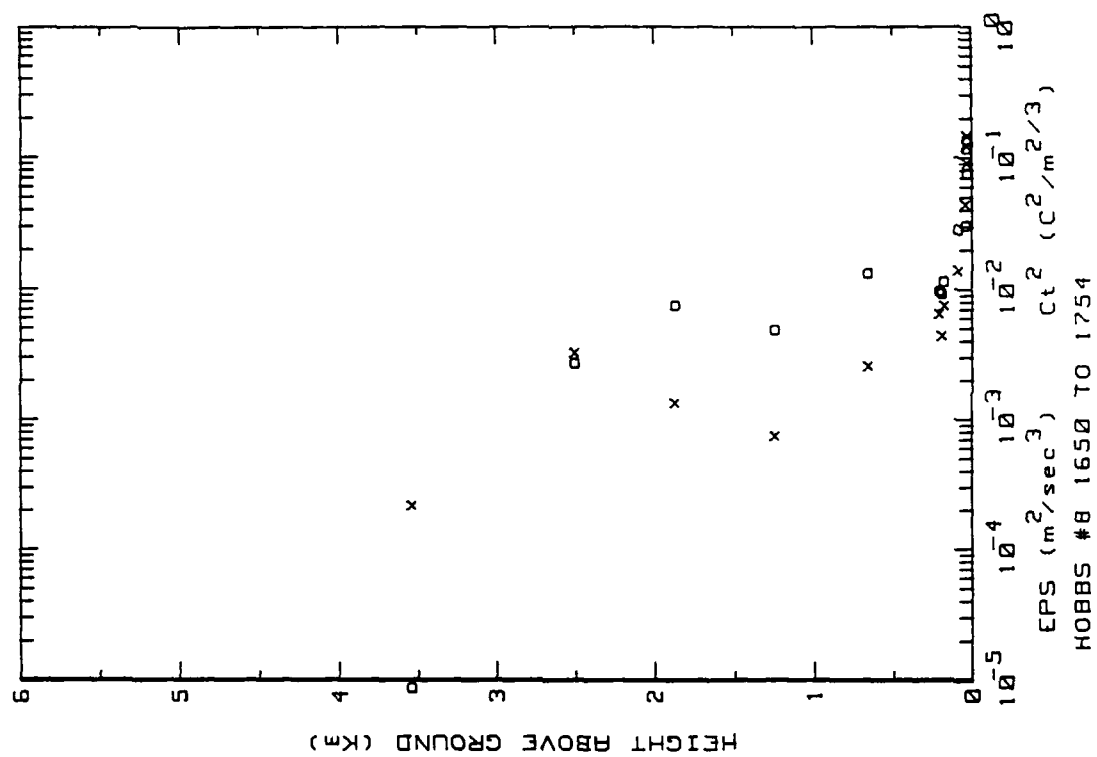


Figure 13b. Hobbs Flight 8 ladder profile (ref. Fig. 5b).

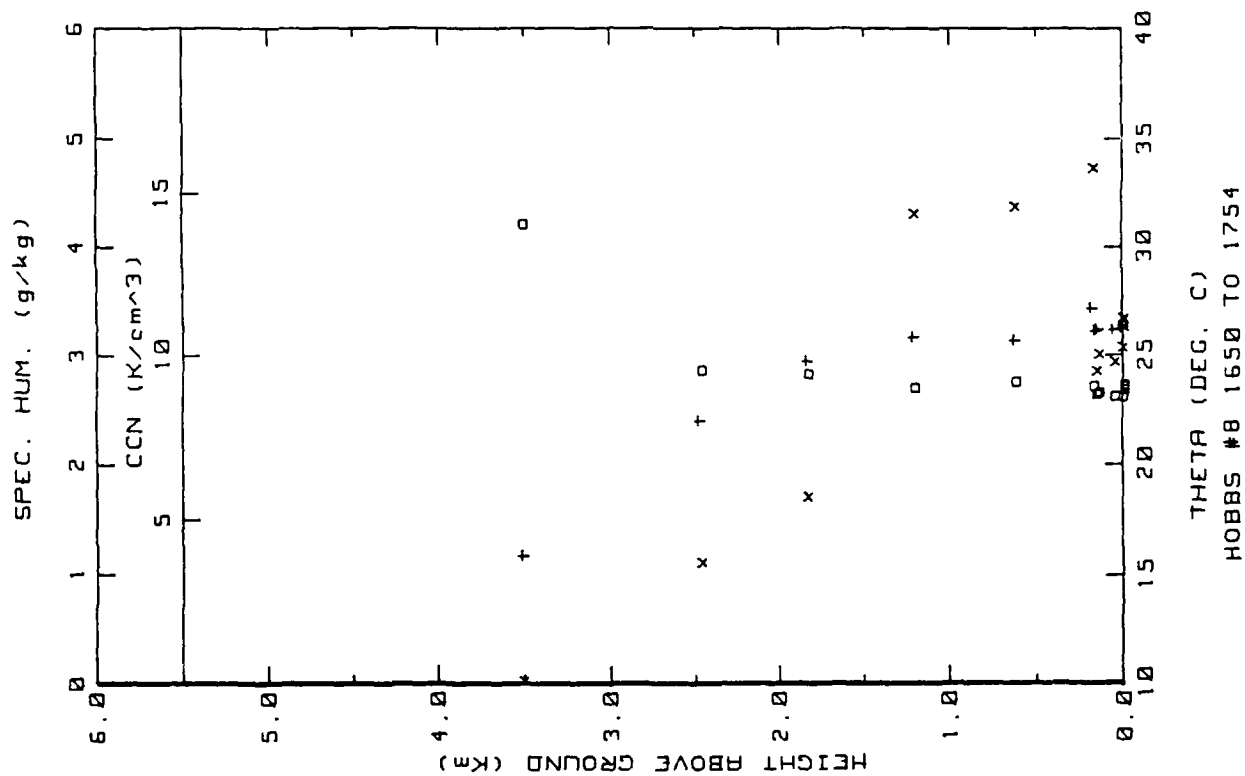
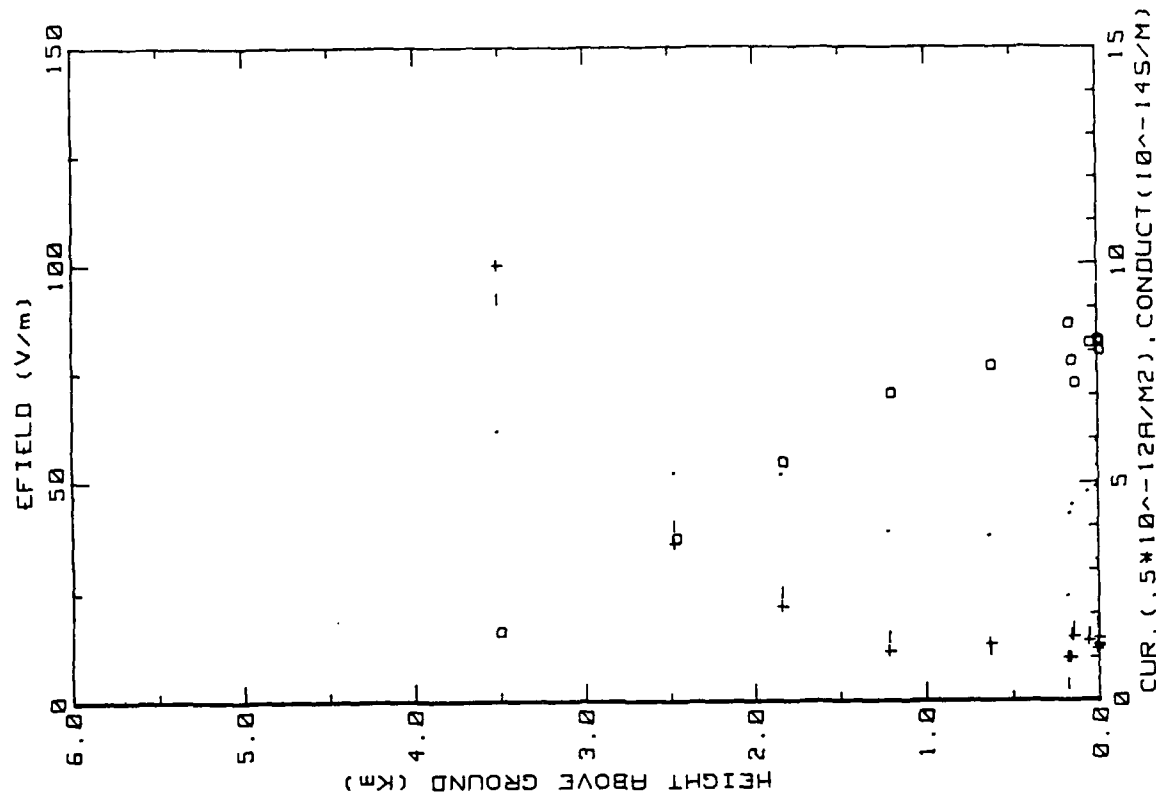


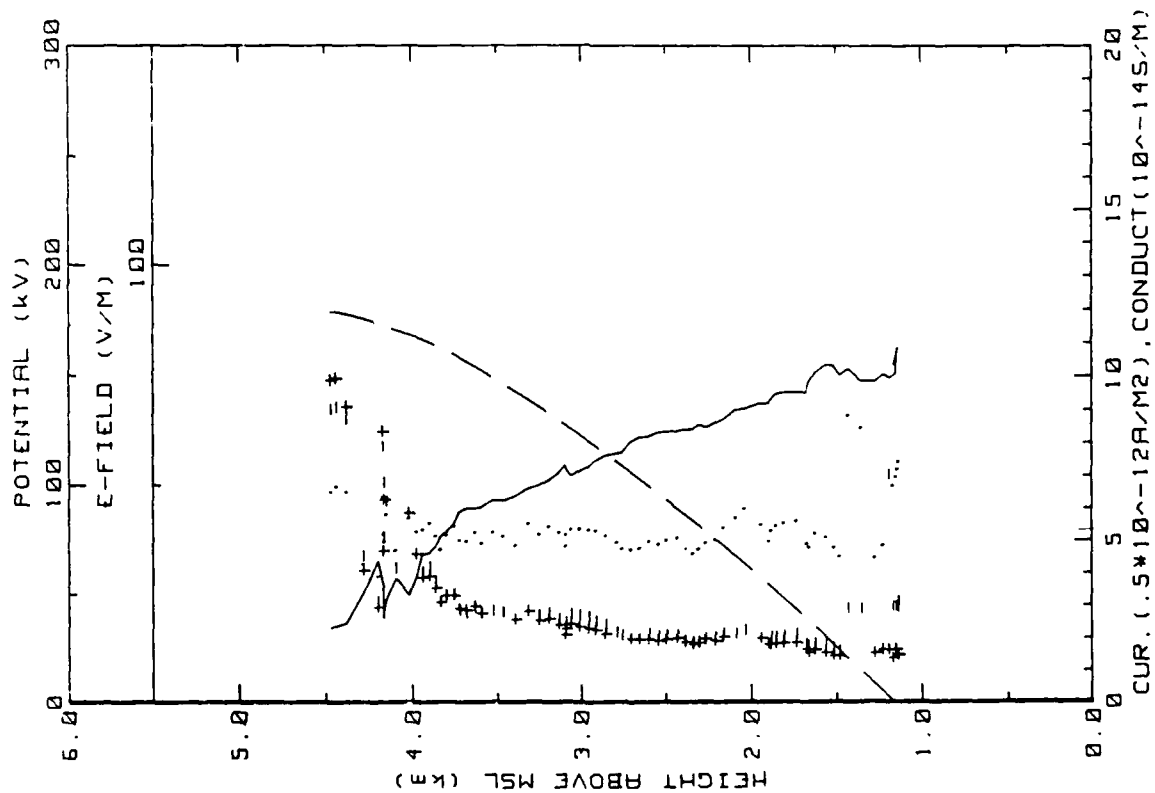
Figure 13c. Hobbs Flight 8 ladder profile (ref. Fig. 5c).



19MAY86 FLIGHT#8 1650 TO 1754 LST

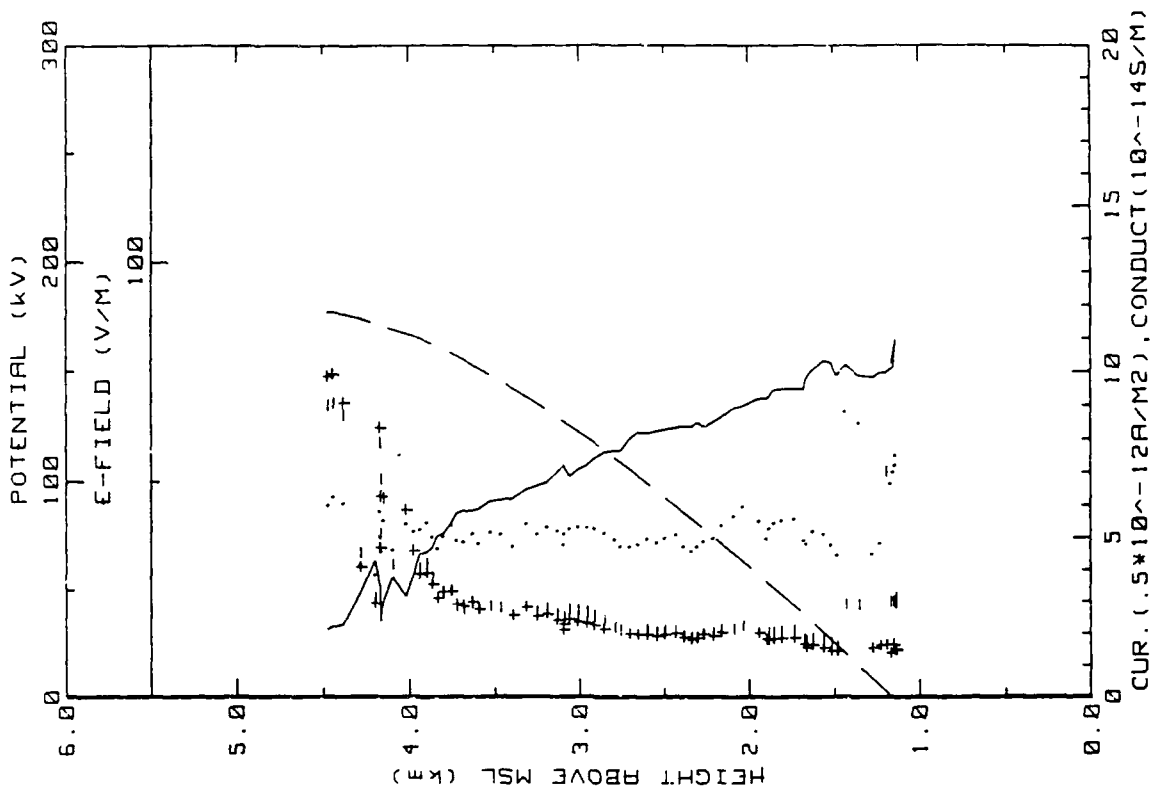
Figure 13d. Similar to 13a, but for outboard E field system.





19MAY86 FLIGHT#8 171000 TO 172900 LST

Figure 13e. Hobbs Flight 8 spiral down-sounding (ref. Fig. 5e).



19MAY86 FLIGHT#8 171000 TO 172900 LST

Figure 13f. Same as Fig. 12e but for inboard E field system.

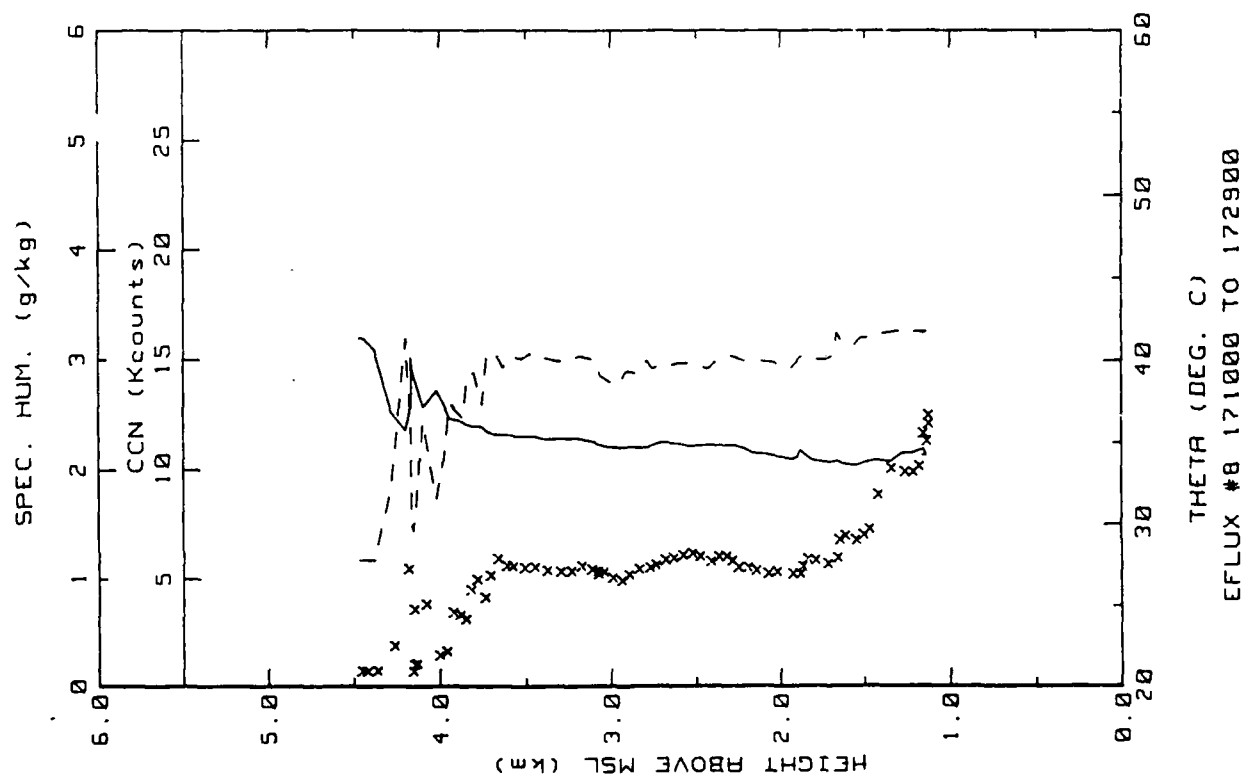


Figure 13g. Hobbs Flight 8 spiral down sounding (ref. Fig. 5h).

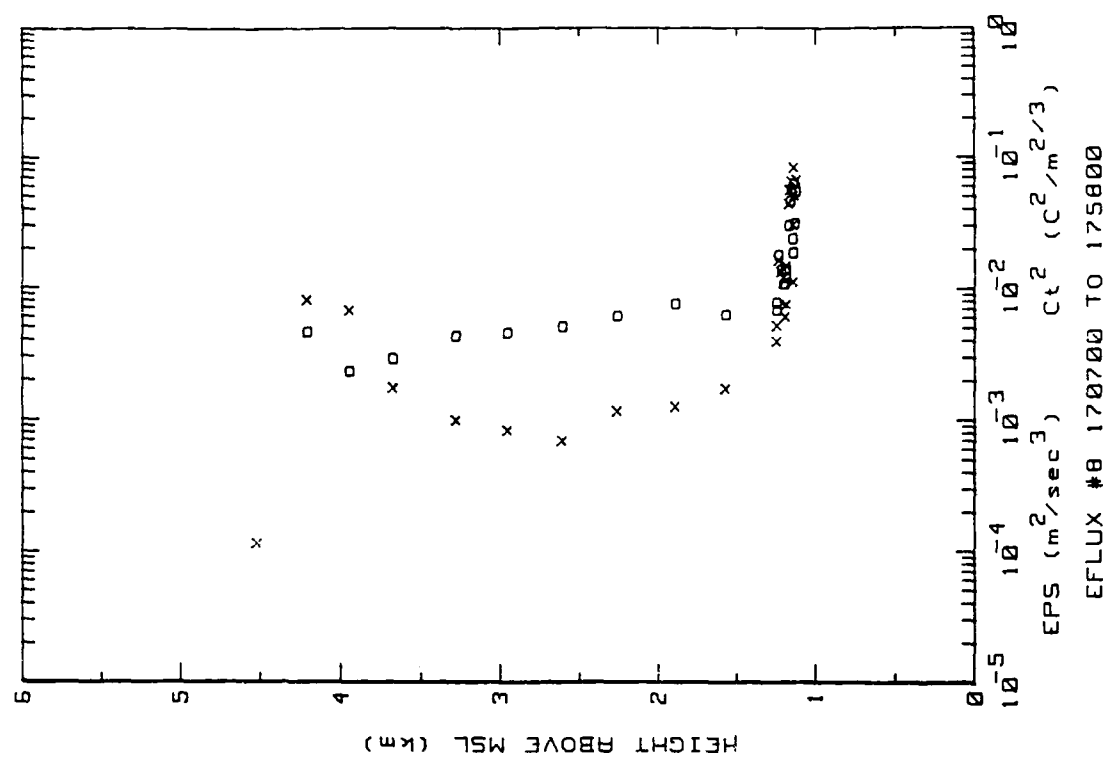


Figure 13h. Hobbs Flight 8 spiral down sounding (ref. Fig. 5g).

Flight: 9

Date: 22 May 1986

Takeoff: 0958 LT from Hobbs

Landed: 1127 at Hobbs

Conditions: Cirrus and scattered cumulus clouds with bases at 5.3 km covered the work area. The PBL looked very hazy viewed from the aircraft. Variable winds mostly from the W at 5-7 m/s.

Instruments: The top and bottom probe inputs were reversed to the outboard electric field system in an attempt to correct the anomalous Air-Earth Conduction Current Densities observed in previous flights.\* All other instruments worked properly.

Summary: A ladder profile was made while ascending 50 km NE of Hobbs under partly cloudy skies. The aircraft was over a solid deck of clouds between 1042 and 1046 LT at 7.2 km altitude. A downsounding was obtained from a spiral descent starting NE of Hobbs and ending over the airport.

Table 7. Hobbs Flight 9 averages and (standard deviations)/averages for constant altitude runs 50 km NE of Hobbs.

AVERAGES FROM LEVEL RUNS

Time HHH	N	Altitude km	Efield1 V/m	Efield2 V/m	+Lam 10 <sup>-14</sup>	-Lam 10 <sup>-14</sup>	Con Cur1 10 <sup>-12</sup>	Con Cur2 10 <sup>-12</sup>	Theta v C
1010	21	.589	50.95	49.11	1.73	1.83	1.81	1.75	27.0
1013	40	1.238	35.91	34.52	2.33	3.01	1.91	1.84	29.1
1018	46	2.168	51.34	50.13	1.91	2.07	2.03	1.94	31.6
1036	85	6.194	5.77	6.94	22.25	20.31	2.46	2.36	54.2
1043	60	6.190	3.50	5.25	22.50	20.59	1.50	2.26	54.2
1118	21	.125	55.50	55.10	2.02	2.40	2.34	2.32	27.1
1120	21	.310	55.79	55.34	1.72	2.05	2.17	2.15	28.1
1124	25	.460	54.62	54.29	1.62	2.14	2.09	2.07	27.6

Time HHH	N	Press mB	Rel Hum %	CCN k/cc	EPS m2/s3	C1 C2/m2/3	Q g/kg	Trose C	T <sub>IR</sub> C	T <sub>rew</sub> C
1010	21	820	17.0	4.9	4.4E-03	1.03E-03	3.11	20.5	22.3	-5.4
1013	40	757	17.8	1.9	2.86E-03	2.27E-03	2.50	15.1	11.8	-9.2
1018	46	671	46.2	1.0	3.33E-05	2.58E-04	4.63	8.1	11.7	-2.7
1036	85	352	54.7	.1	1.92E-04	1.30E-03	1.07	-21.4	11.7	-28.1
1043	60	352	37.2	.1	2.35E-05	5.62E-04	.74	-21.2	17.1	-32.0
1118	21	866	12.5	3.3	2.44E-02	2.13E-02	2.89	25.4	17.1	-5.6
1120	21	848	13.6	5.0	2.13E-02	1.31E-02	3.06	24.5	17.1	-5.1
1124	25	833	14.4	3.1	7.24E-03	2.47E-03	2.93	22.5	17.1	-5.9

STANDARD DEVIATIONS/MEAN VALUES

Time	Efield1	Efield2	+Lam	-Lam	Concur1	Concur2	CCN	EPS	C12	Q
1010	.018	.019	.063	.062	.034	.035	.649	.526	.826	.052
1013	.032	.031	.036	.042	.028	.029	.220	1.150	.800	.064
1018	.034	.033	.027	.032	.031	.031	.045	.239	.239	.027
1036	.038	.065	.021	.020	.039	.090	.123	1.261	.572	.102
1043	.311	.227	.011	.003	.325	.239	.113	.179	.278	.113
1118	.025	.020	.082	.063	.104	.106	.110	.575	.727	.015
1120	.029	.025	.031	.033	.127	.126	.128	1.130	1.574	.041
1124	.022	.019	.060	.050	.067	.066	.114	.483	.718	.026

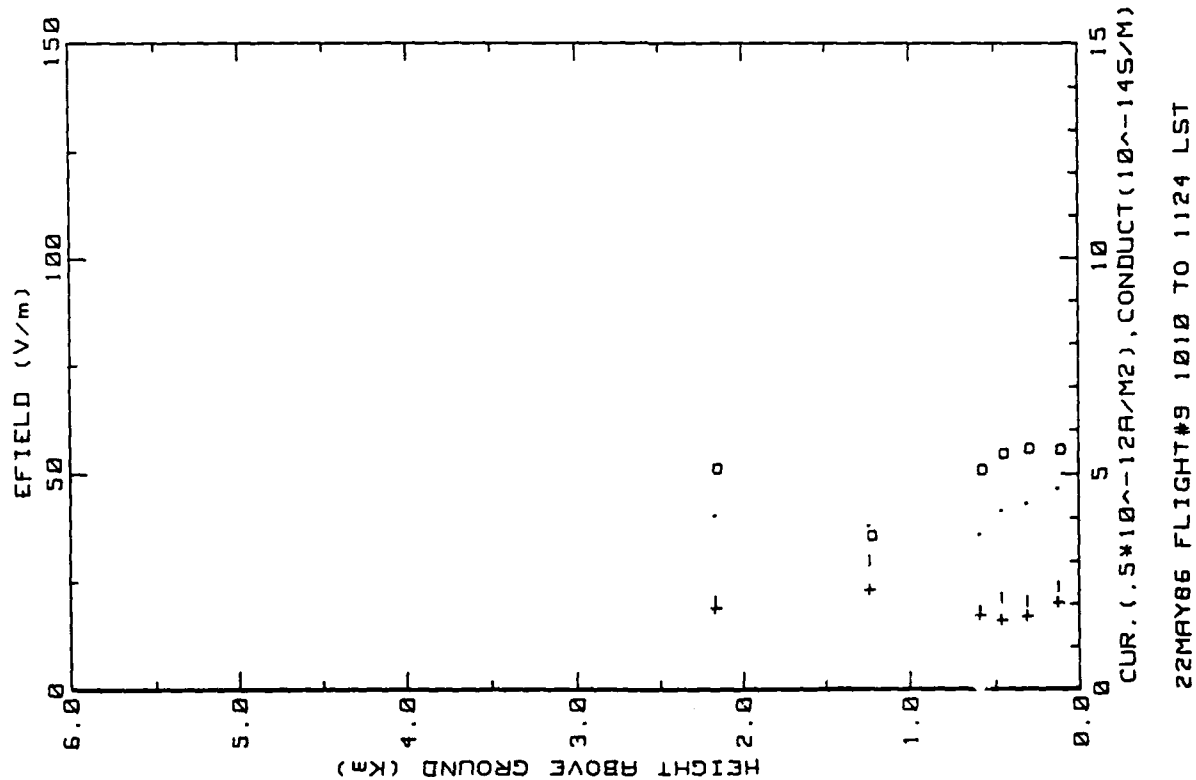


Figure 14a. Hobbs Flight 9 ladder profile (ref. Fig. 5a)

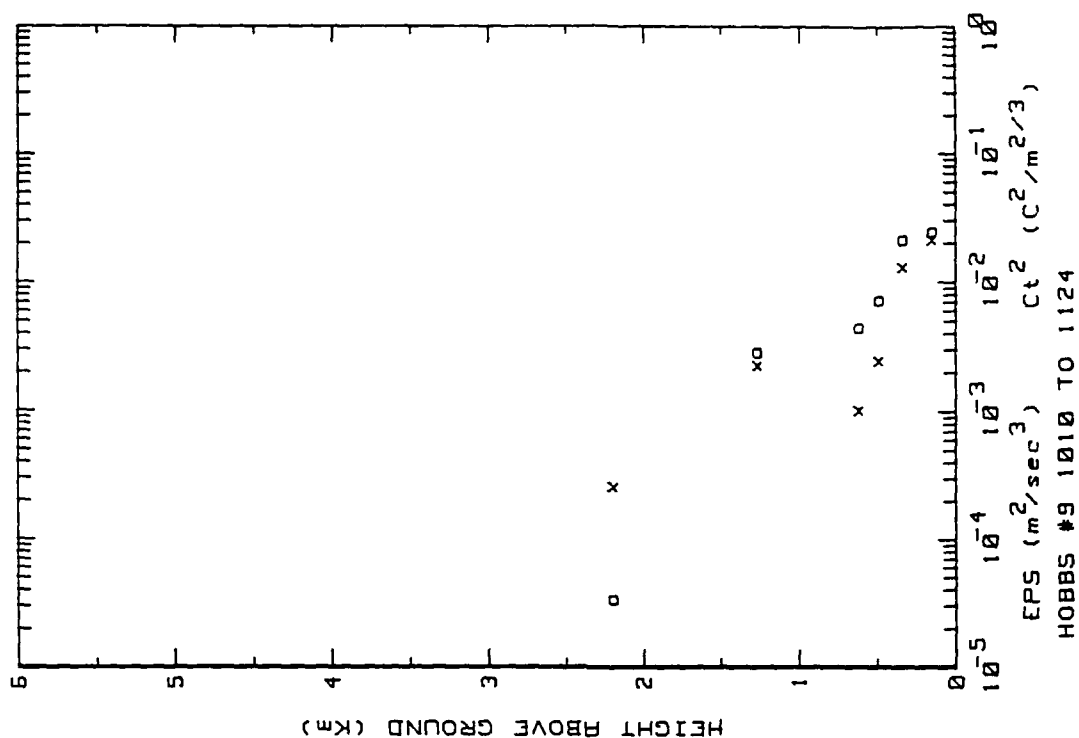


Figure 14b. Hobbs Flight 9 ladder profile (ref. Fig. 5b).

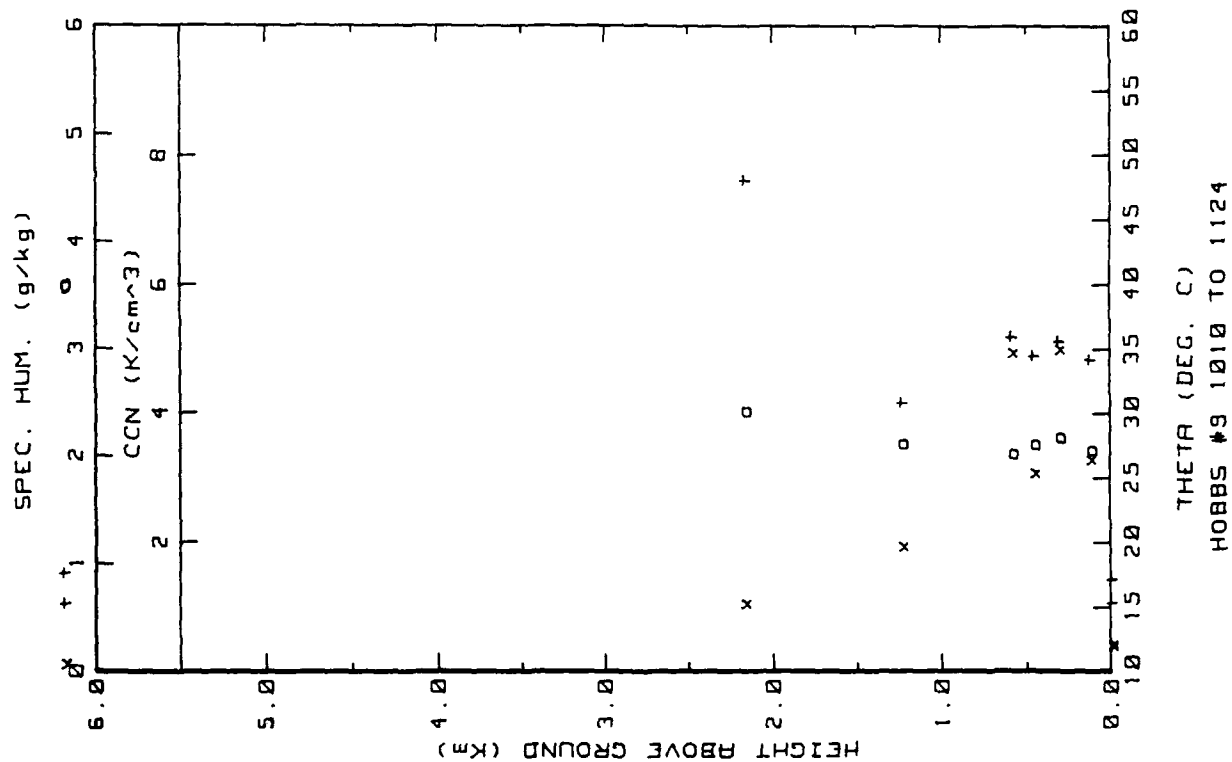


Figure 14c. Hobbs Flight 9 ladder profile (ref. Fig. 5c).

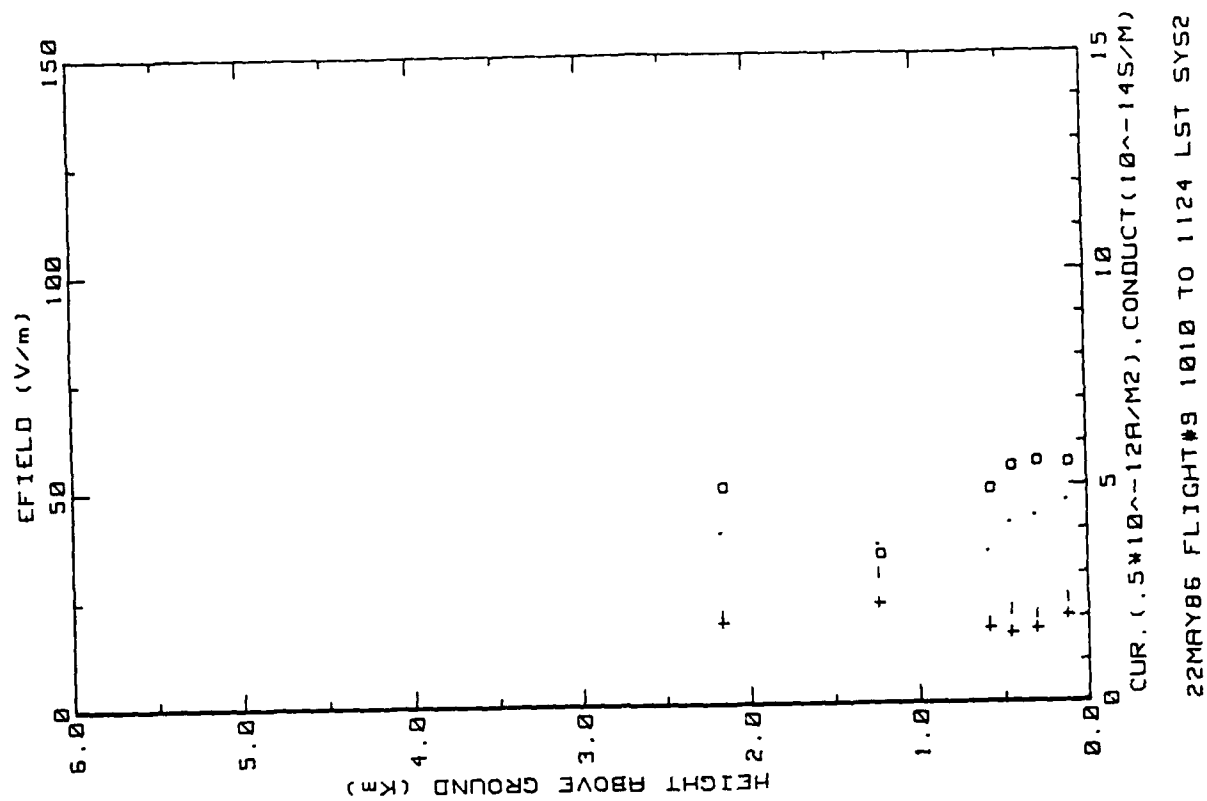
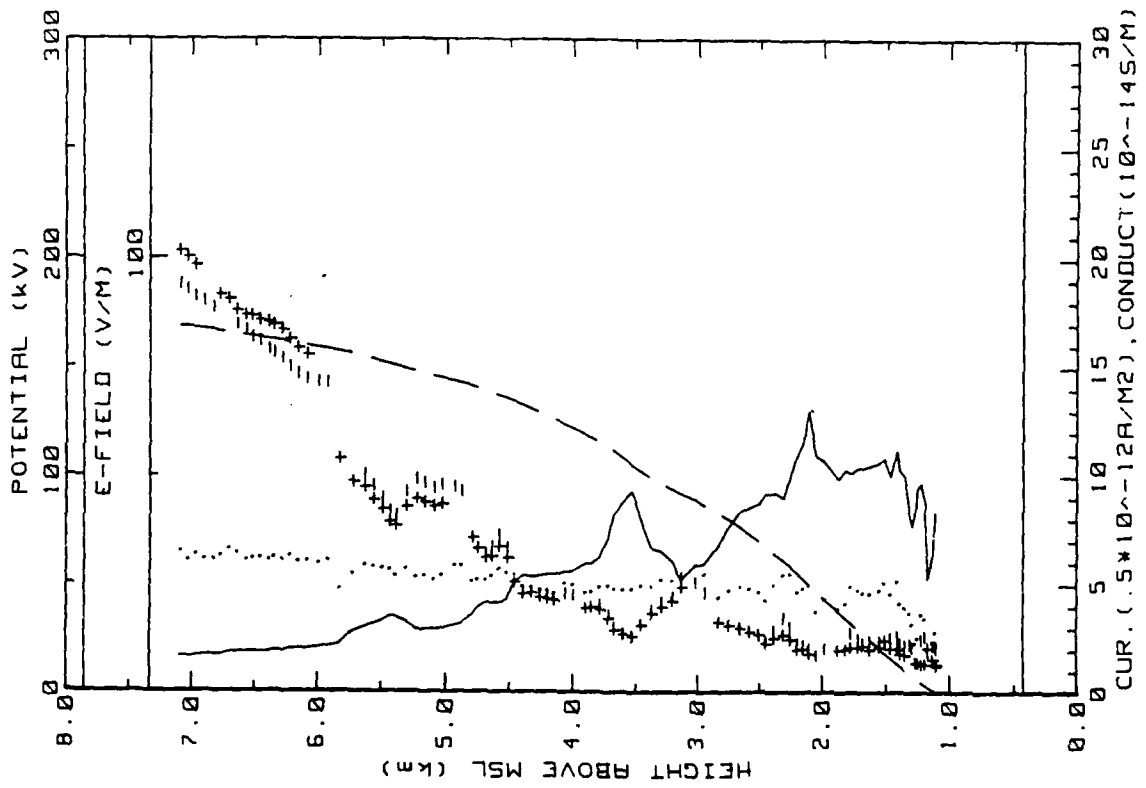
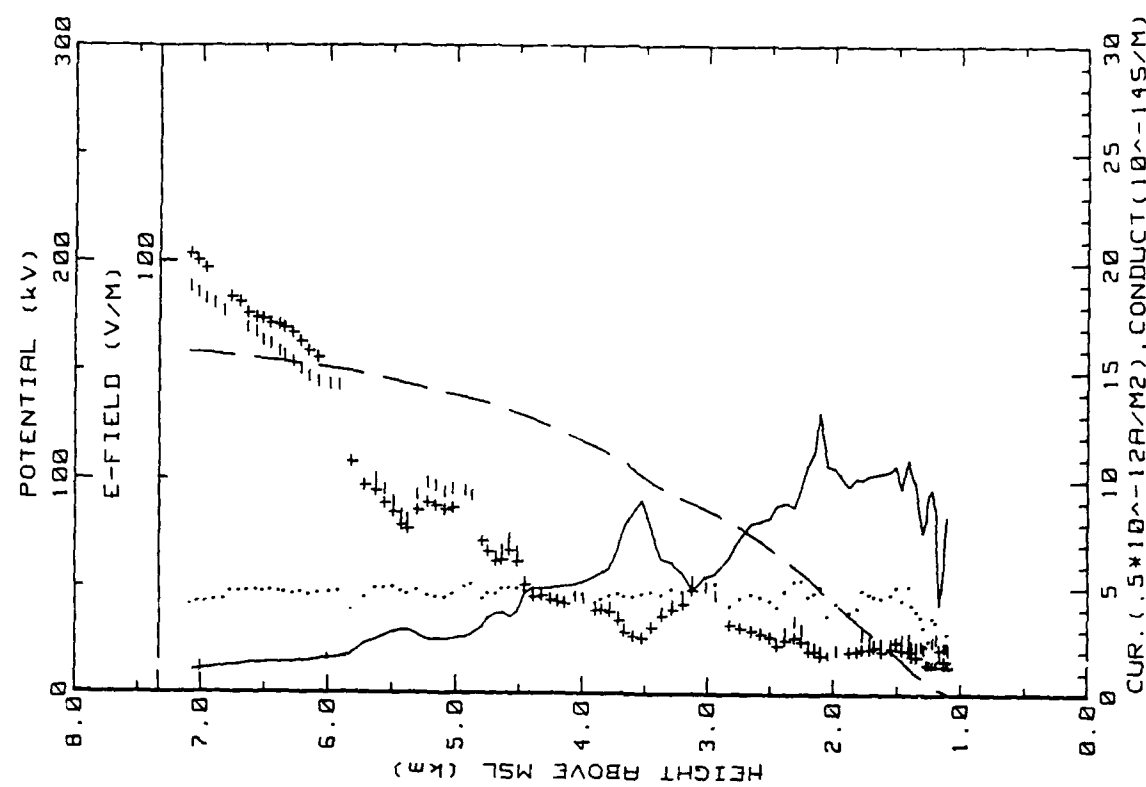


Figure 14d. Similar to 14a, but for inboard E-field system.



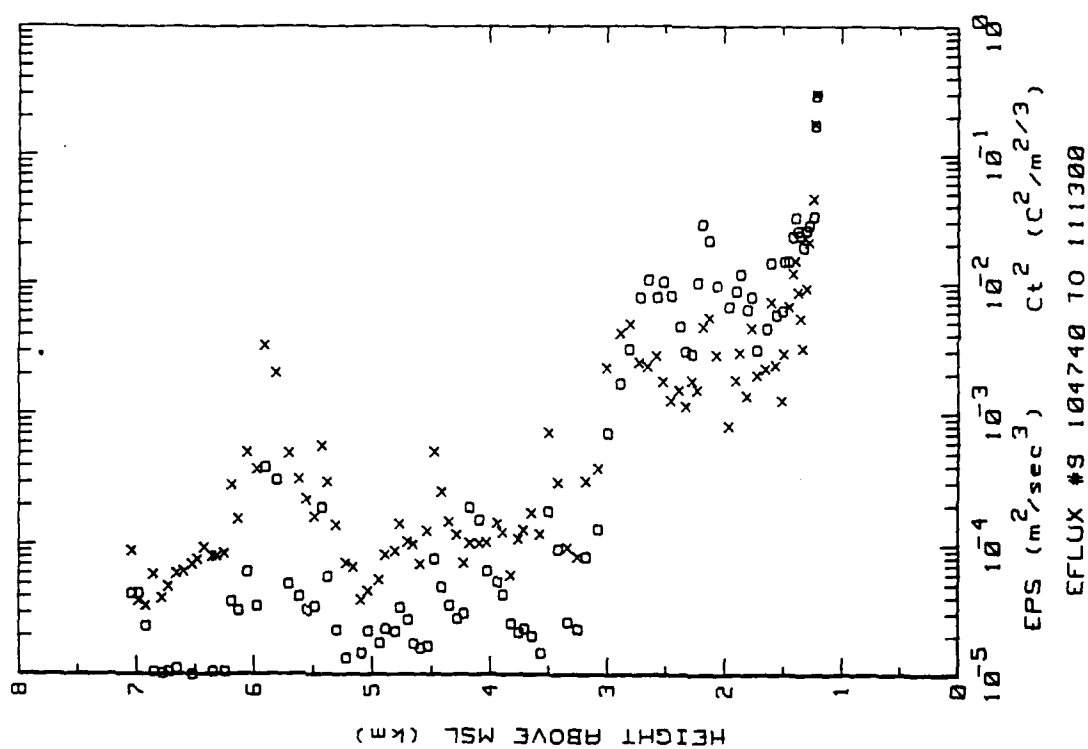
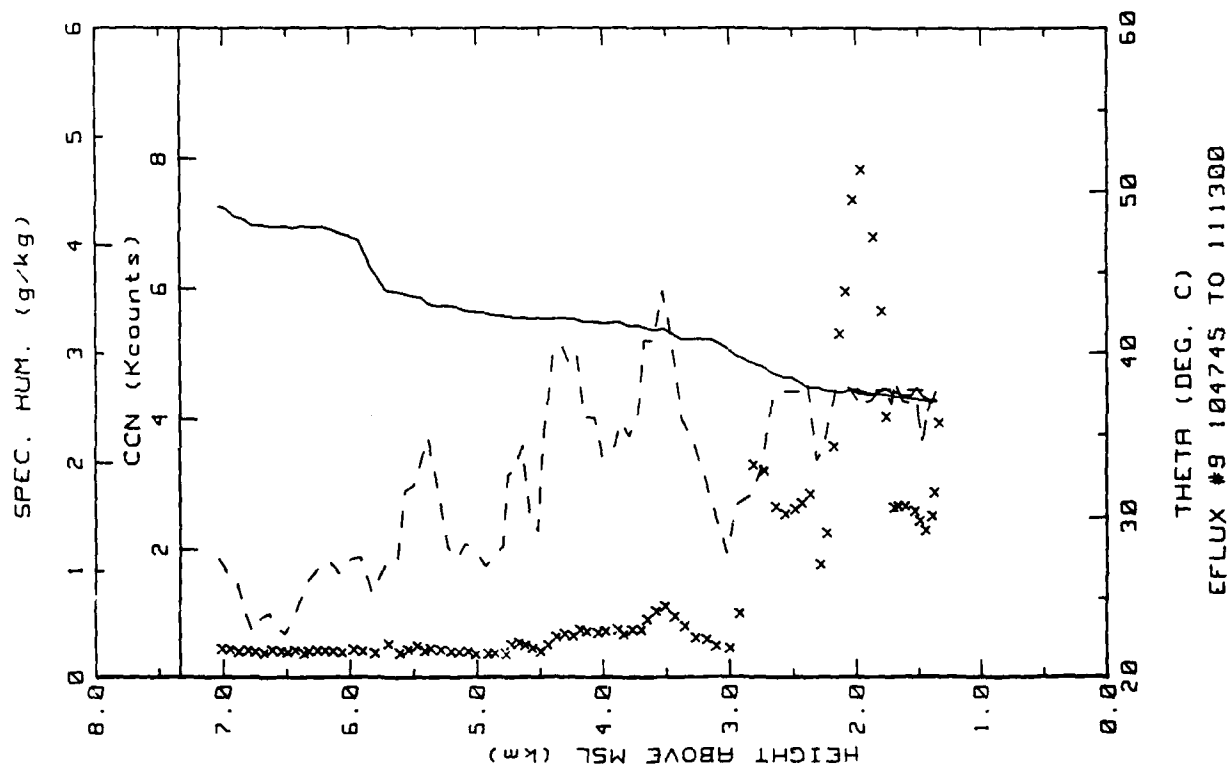
22MAY86 FLIGHT#9 104740 TO 111300 LST

Figure 14e. Hobbs Flight 9 spiral downsonding (ref. Fig. 5e).

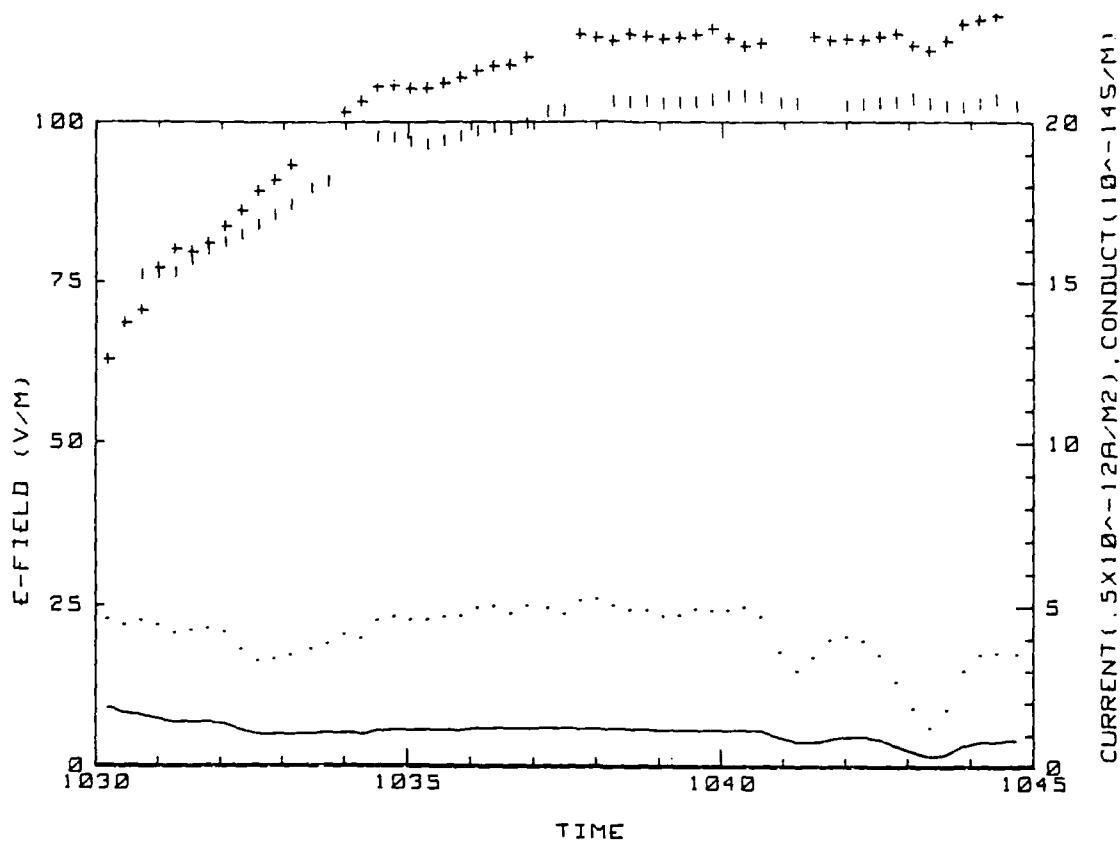


22MAY86 FLIGHT#9 104740 TO 111300 LST

Figure 14f. Same as Fig. 14e but for outboard E-field system.

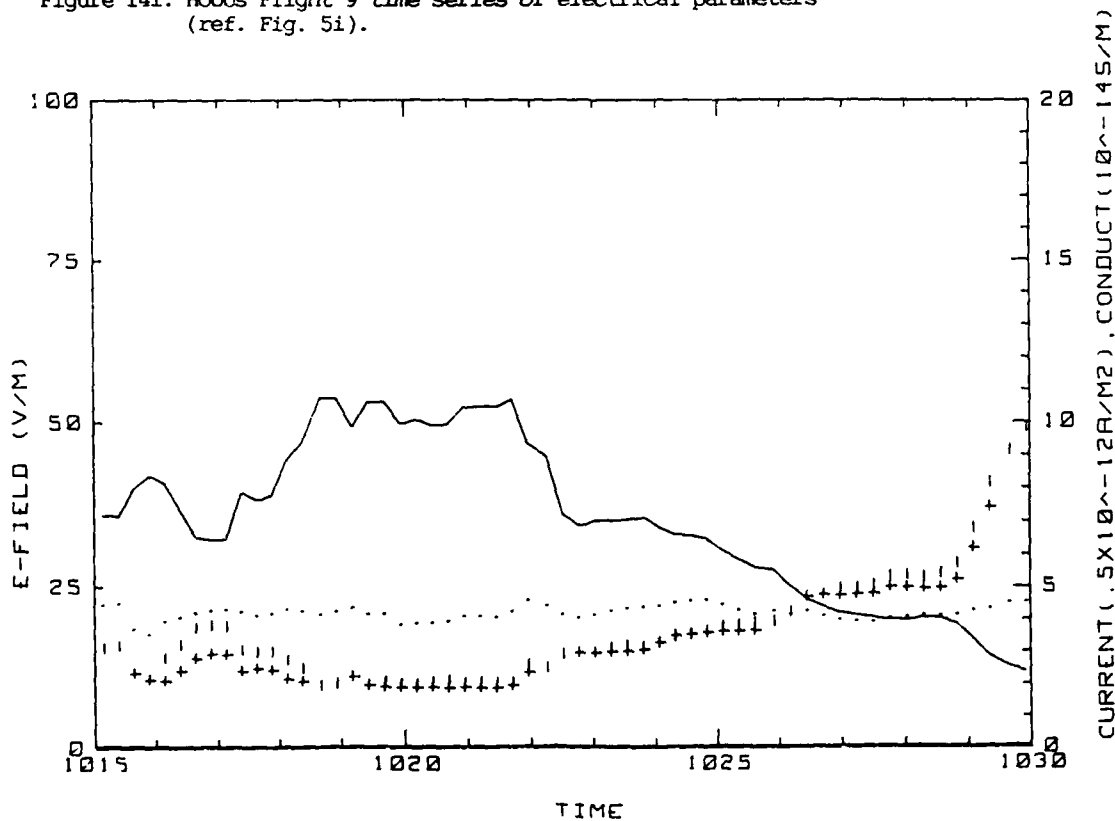






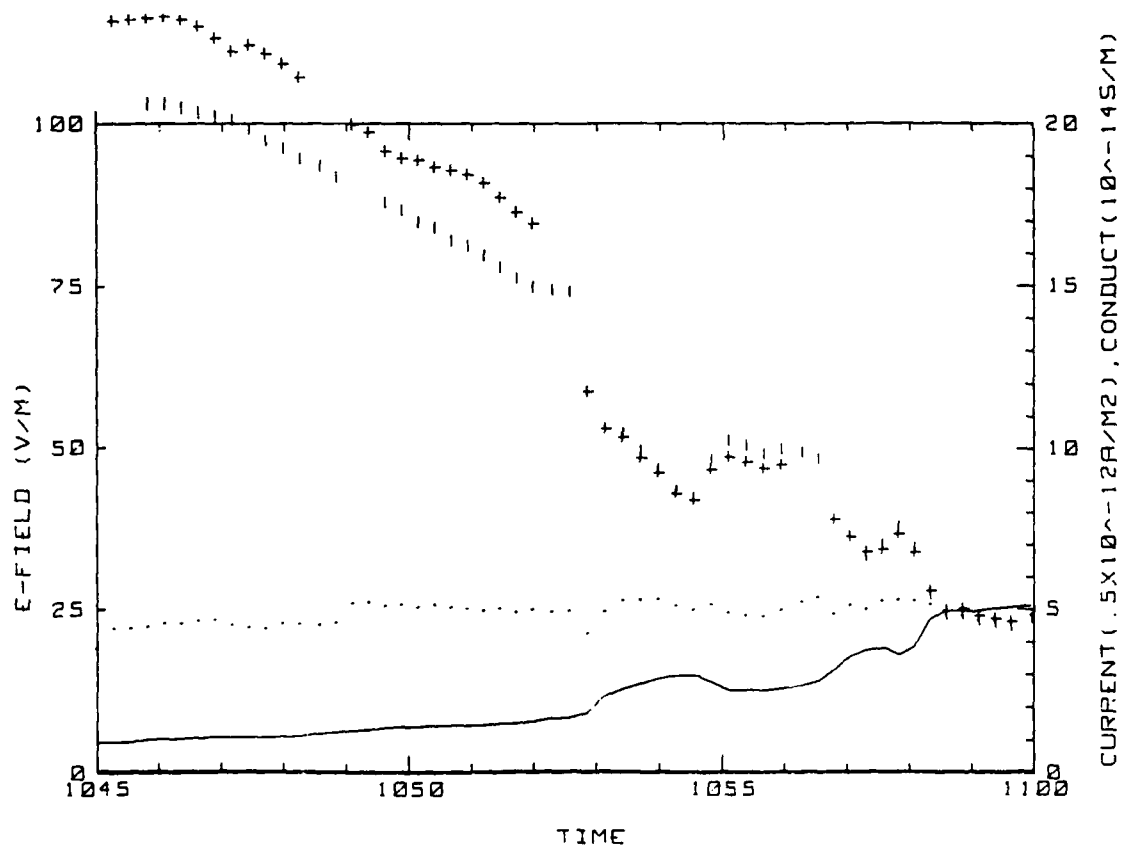
22 MAY 86 FLIGHT#9 103000 TO 104500 LST

Figure 14i. Hobbs Flight 9 time series of electrical parameters (ref. Fig. 5i).



22 MAY 86 FLIGHT#9 101500 TO 103000 LST

Figure 14j. Hobbs Flight 9 time series of electrical parameters. (ref. Fig. 5j)



22 MAY 86 FLIGHT#9 104500 TO 110000 LST

Figure 14k. Hobbs Flight 9 time series of electrical parameters  
(ref. Fig. 5i).

Flight: 10

Date: 23 May 1986

Takeoff: 1009 LT from Hobbs.

Landed: 1025 at Hobbs

Conditions: High cirrus clouds with winds from the N at 5-7 m/s.

Instruments: see below

Summary: The flight was aborted because of an equipment malfunction.

Flight: 11

Date: 24 May 1986

Takeoff: 1042 LT from Hobbs.

Landed: 1217 at Hobbs.

Conditions: High cirrus and altostratus clouds covered about 1/4 of sky. The PBL was hazy and winds were variable but mostly from the E at 3-5 m/s.

Instruments: All worked properly initially. All the wires on the turbulence probes were broken by particle impaction near the apex of the flight when the aircraft passed through a cirrus cloud. The upsounding was interrupted by a computer crash.

Summary: The flight consisted of up- and downsoundings over Hobbs followed by passes over the ground station. No turbulence data was obtained on the spiral descent or the constant altitude runs because of broken probes.

Table 8. Hobbs Flight 11 averages and (standard deviations)/averages for constant altitude runs over the ground station.

AVERAGES FROM LEVEL RUNS

Time HHM	N	Altitude km	Efield1 V/m	Efield2 V/m	+Lam 10 <sup>-14</sup>	-Lam 10 <sup>-14</sup>	Con Cur1 10 <sup>-12</sup>	Con Cur2 10 <sup>-12</sup>	theta_v C
1156	10	.006	92.83	89.63	1.68	1.74	3.17	3.06	27.6
1200	13	.006	98.11	93.91	1.44	1.54	2.93	2.80	27.9
1202	11	.015	108.86	104.37	1.40	1.55	3.21	3.08	28.0
1207	21	.031	104.68	101.29	1.46	1.70	3.30	3.20	27.5
1209	34	.151	98.49	95.32	1.30	1.48	2.70	2.62	27.4
1212	12	.310	116.22	112.25	1.21	1.42	3.06	2.95	27.6

Time HHM	N	Press mb	Rel Hum %	CCN k/cc	EPS m2/s3	CT C2/m2/3	Q g/kg	Trose C	T <sub>IR</sub> C	T <sub>dew</sub> C
1156	10	684	49.1	5.6	2.41E-16	0.00E+00	11.31	25.5	17.1	14.0
1200	13	694	49.1	6.4	1.49E-16	0.00E+00	11.47	25.7	17.1	14.2
1202	11	683	49.2	5.9	1.15E-16	0.00E+00	11.50	25.7	17.1	14.3
1207	21	881	43.3	5.1	8.75E-17	0.00E+00	10.94	25.2	17.1	13.5
1209	34	669	55.8	6.3	6.06E-17	0.00E+00	11.82	23.8	17.1	14.5
1212	12	853	56.4	5.9	5.61E-17	0.00E+00	11.25	22.5	17.1	13.4

STANDARD DEVIATIONS/MEAN VALUES

Time	Efield1	Efield2	+Lam	-Lam	Concur1	Concur2	CCN	EPS	CT2	Q
1156	.057	.067	.080	.062	.053	.072	.003	.084	0.000	.013
1200	.066	.055	.073	.051	.114	.088	.022	.032	0.000	.040
1202	.100	.101	.059	.055	.141	.153	.045	.034	0.000	.018
1207	.063	.062	.089	.054	.086	.086	.058	.205	0.000	.033
1209	.033	.045	.084	.050	.084	.037	.100	.104	0.000	.020
1212	.025	.025	.032	.033	.026	.028	.043	.062	0.000	.034

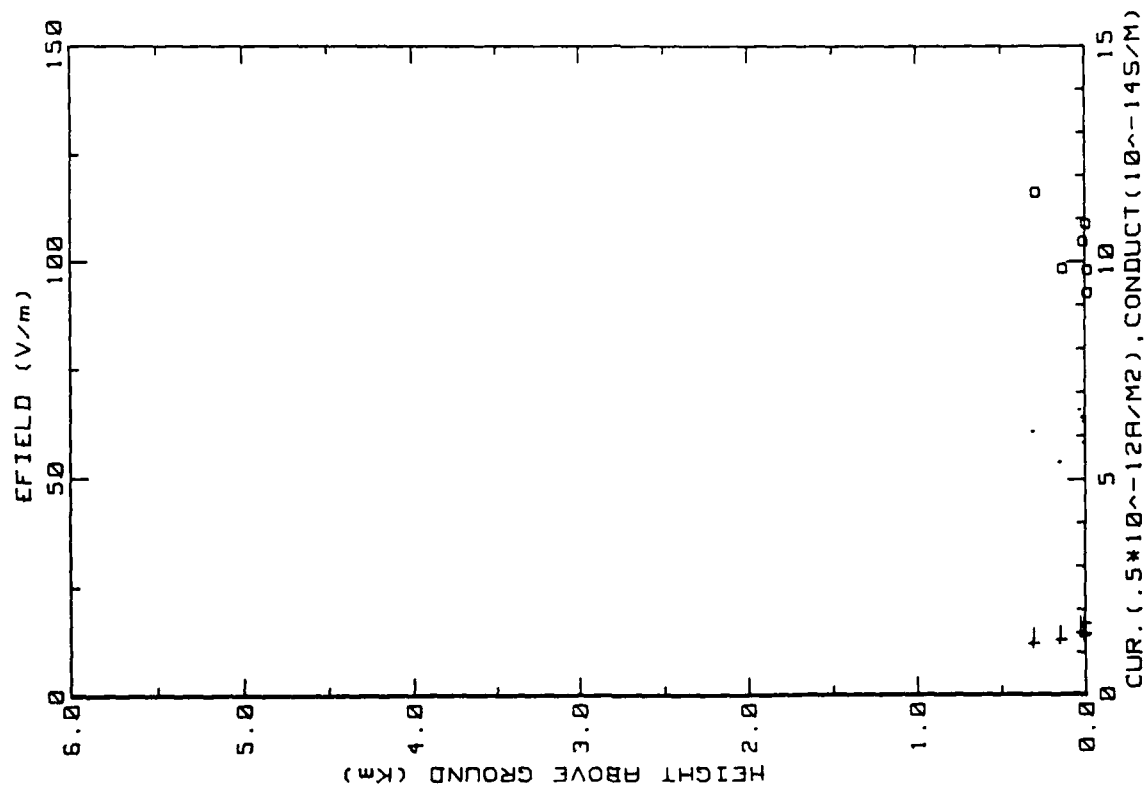


Figure 15a. Hobbs Flight 11 ladder profile (ref. Fig. 5a)

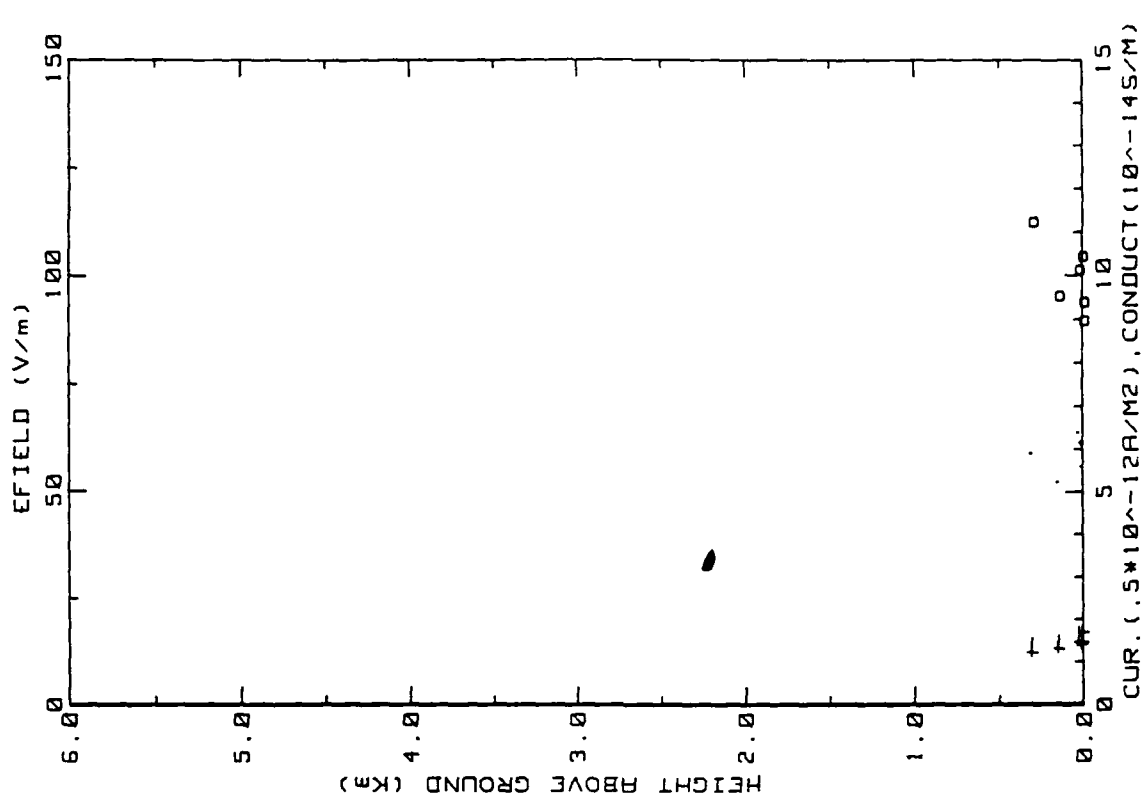
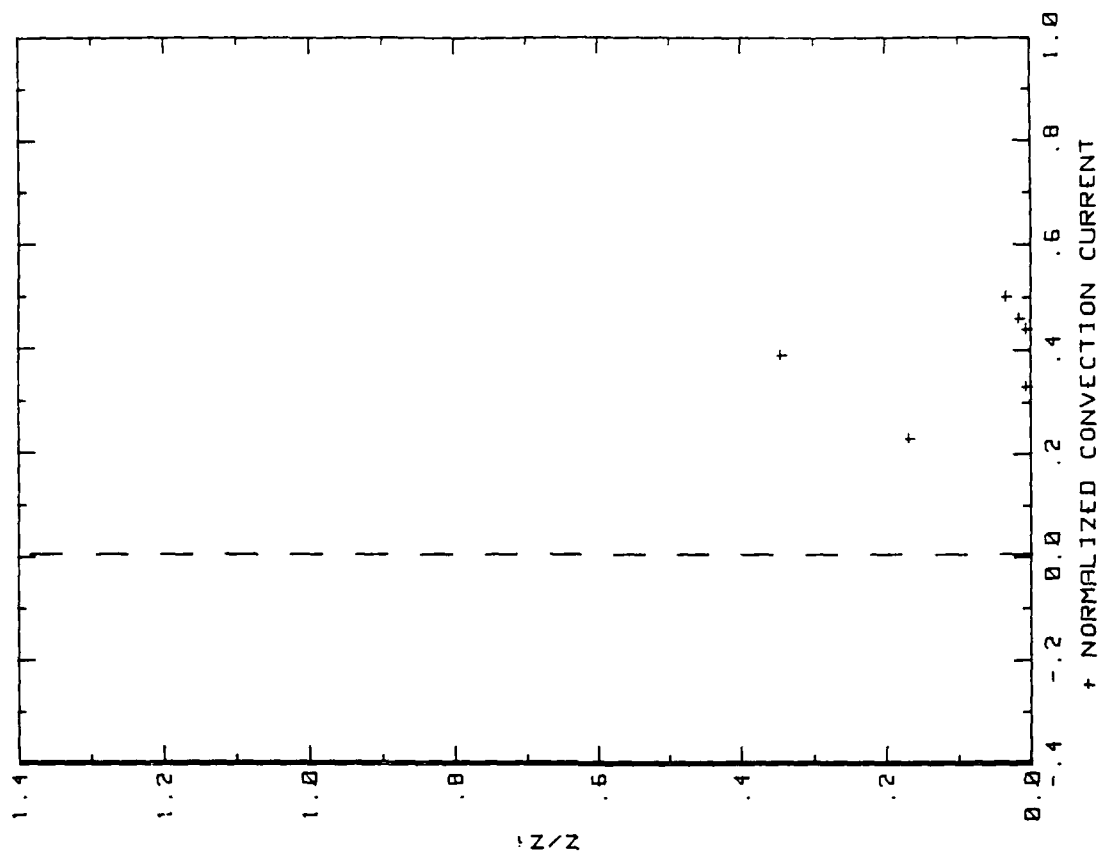


Figure 15b. Similar to 15a. but for inboard E-field system.



24MAY86 FLIGHT#11 1156 TO 1212 LST

Z1=900 Jo=2.25

Figure 15d. Hobbs Flight 11 convection current profile (ref. Fig. 5d)

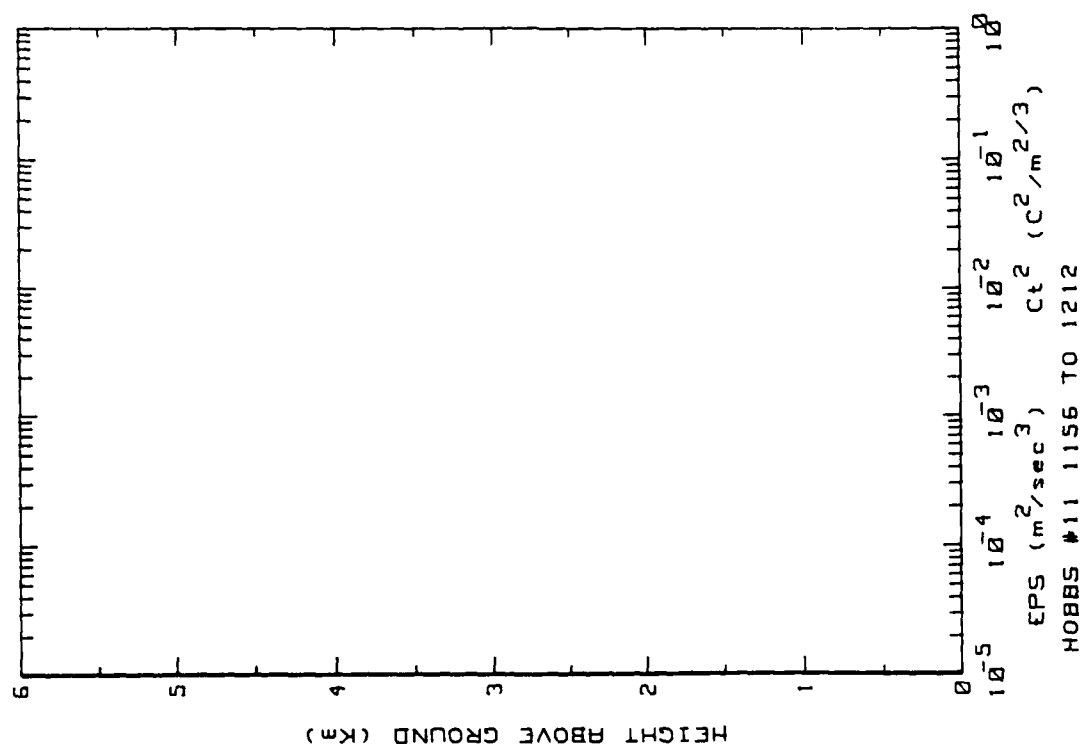


Figure 15c. Hobbs Flight 11 ladder profile (ref. Fig. 5b).

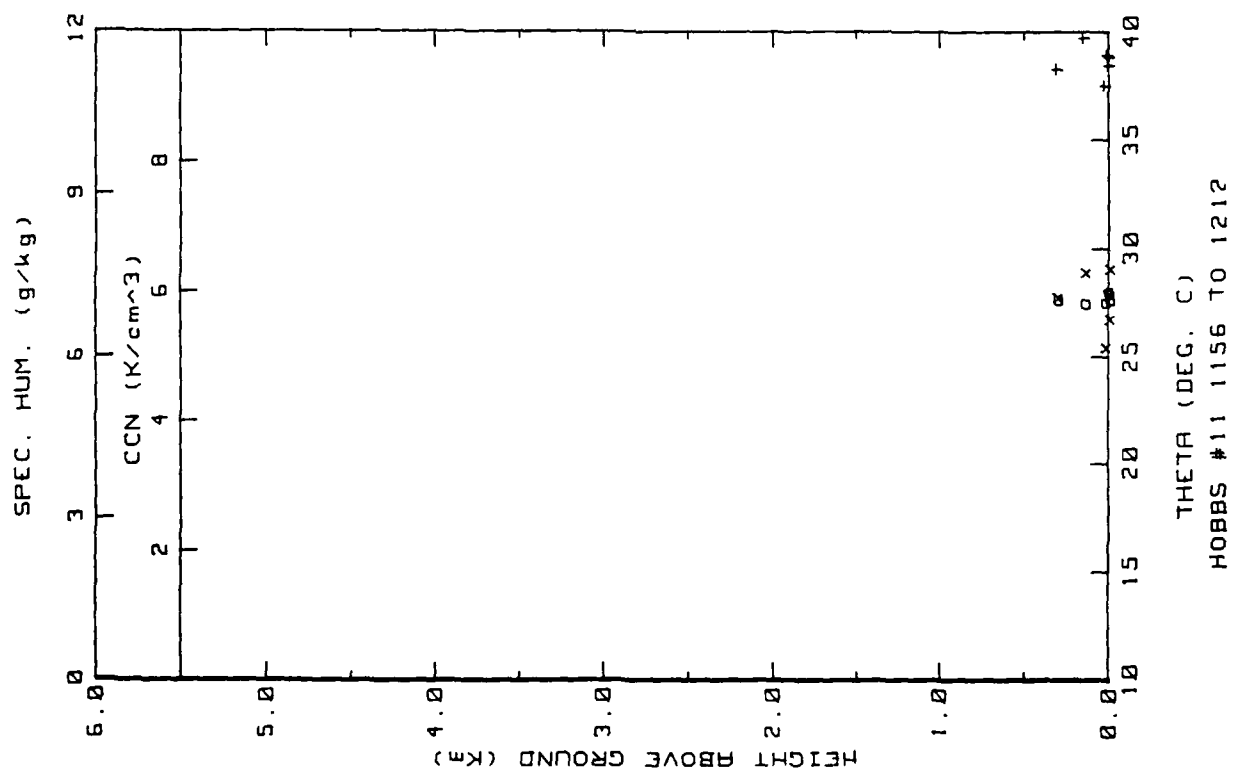


Figure 15e. Hobbs Flight 11 ladder profile (ref. Fig. 5c).



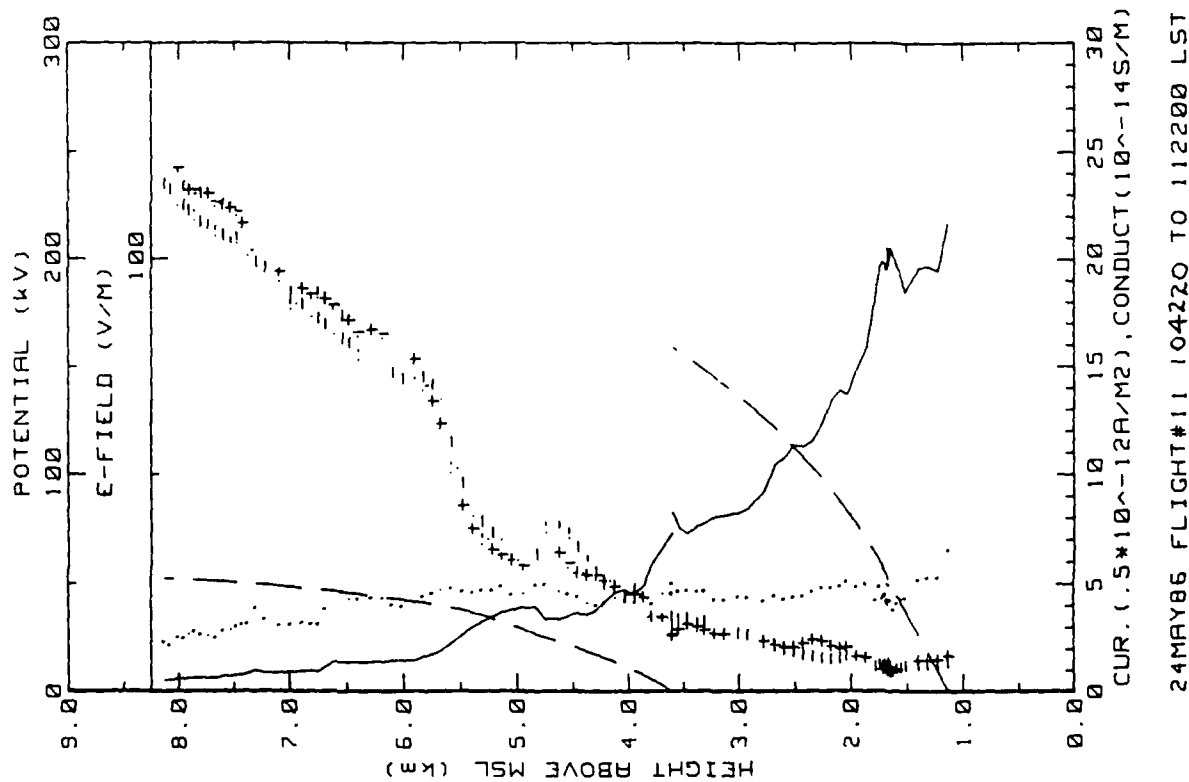


Figure 15f. Hobbs Flight 11 continuous upspounding (ref. Fig. 5e).

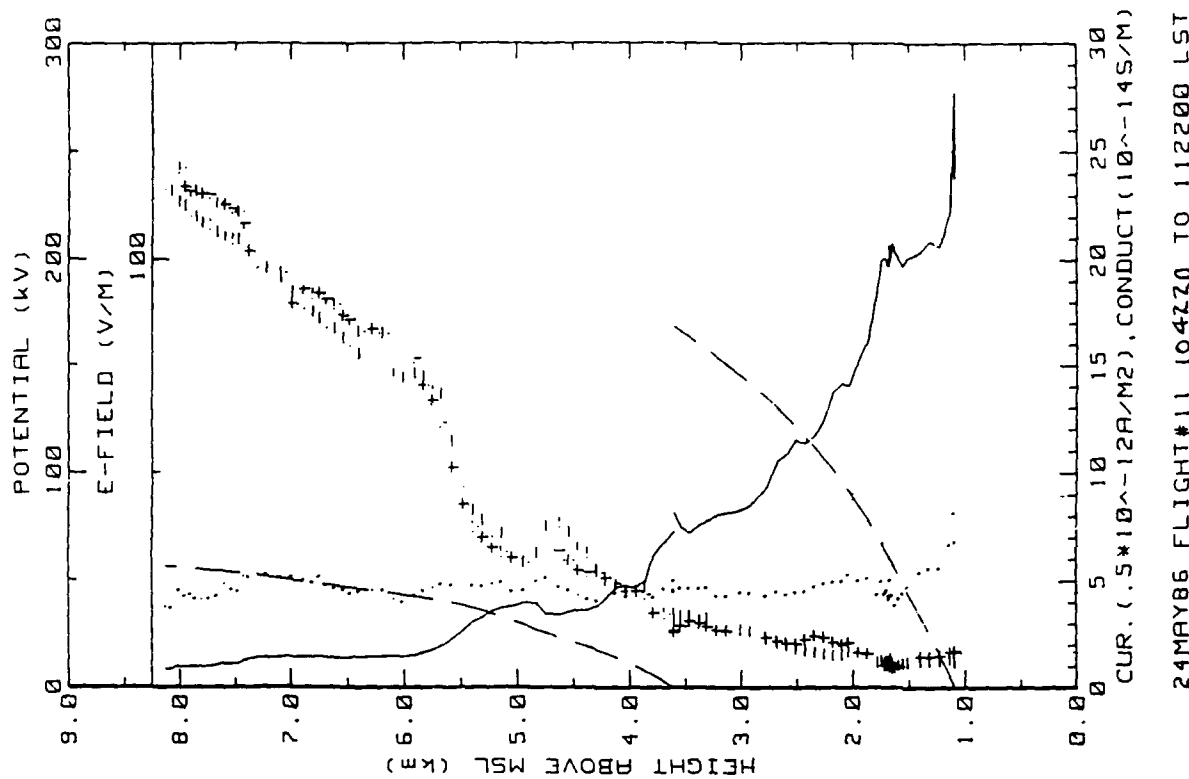


Figure 15g. Same as Fig. 15f but for outboard E-field system.

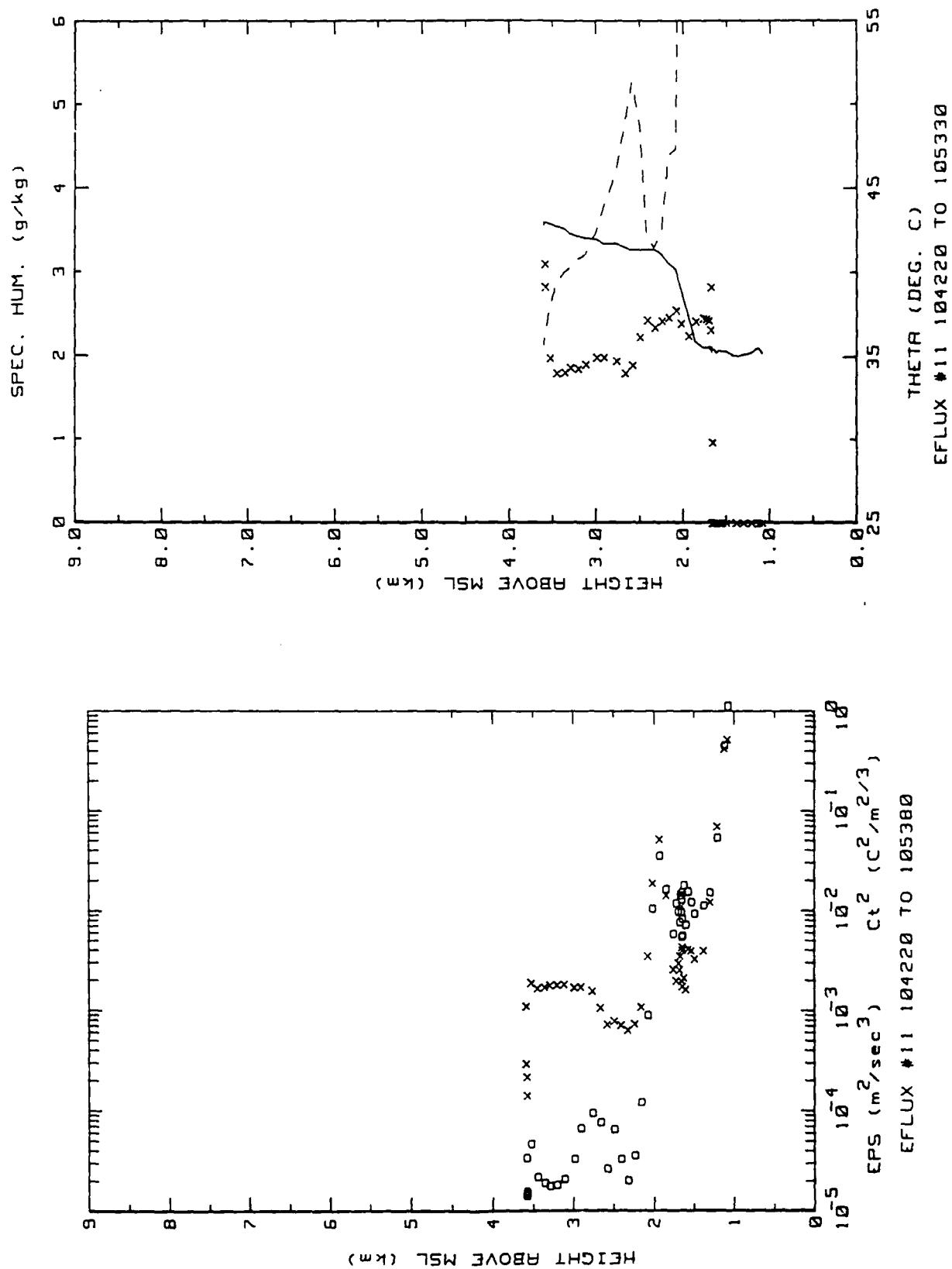


Figure 15h. Hobbs Flight 11 continuous upsonding (ref. Fig. 5b).

Figure 15i. Hobbs Flight 11 continuous upsonding (ref. Fig. 5h).

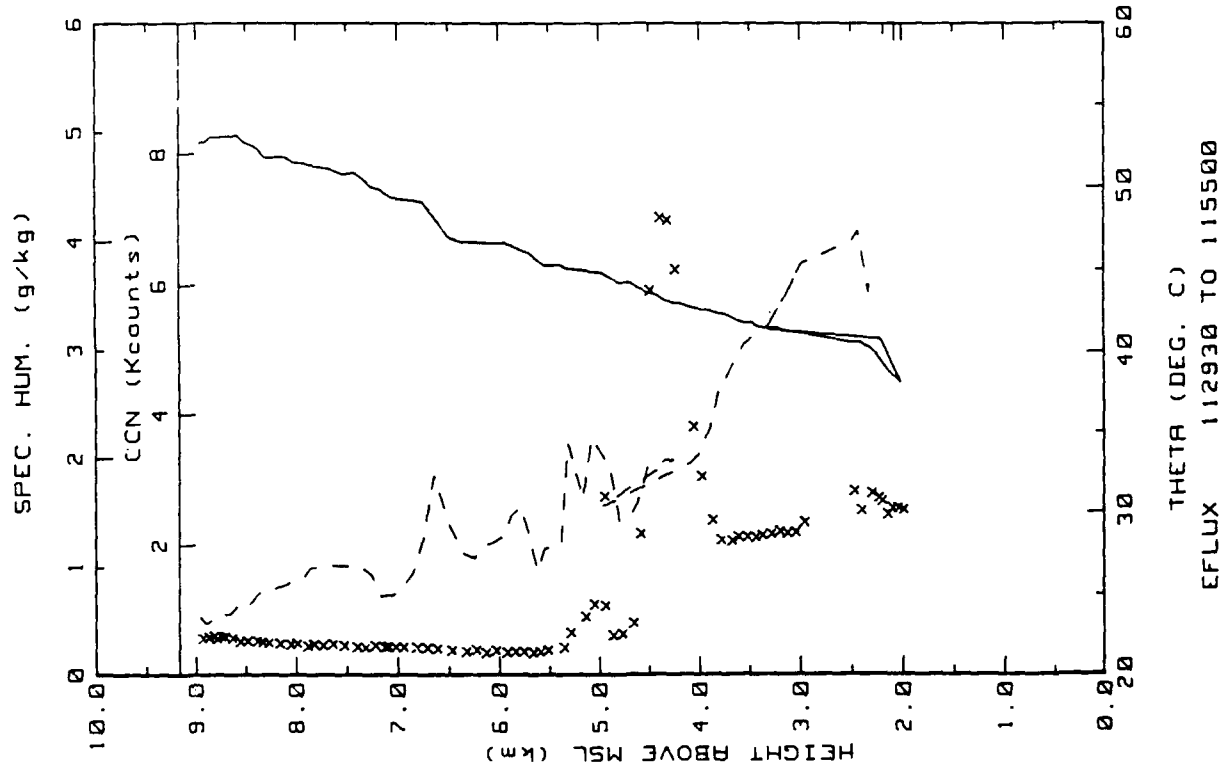


Figure 15j. Hobbs Flight 11 continuous upsonding (ref. Fig. 5h)

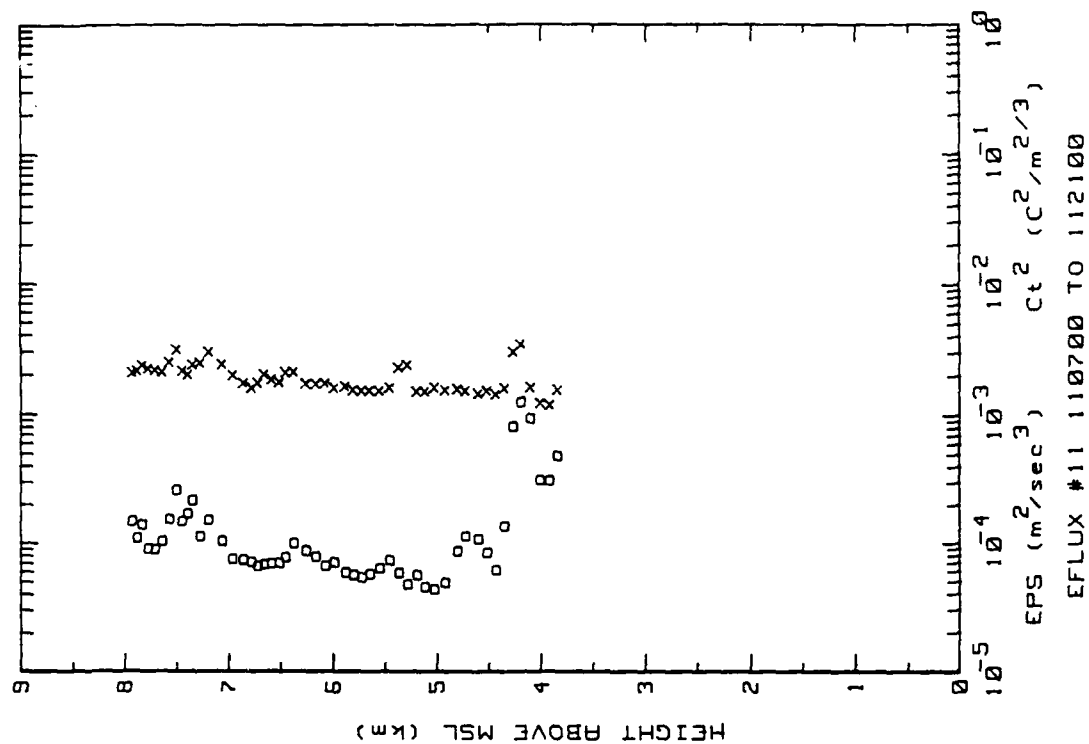
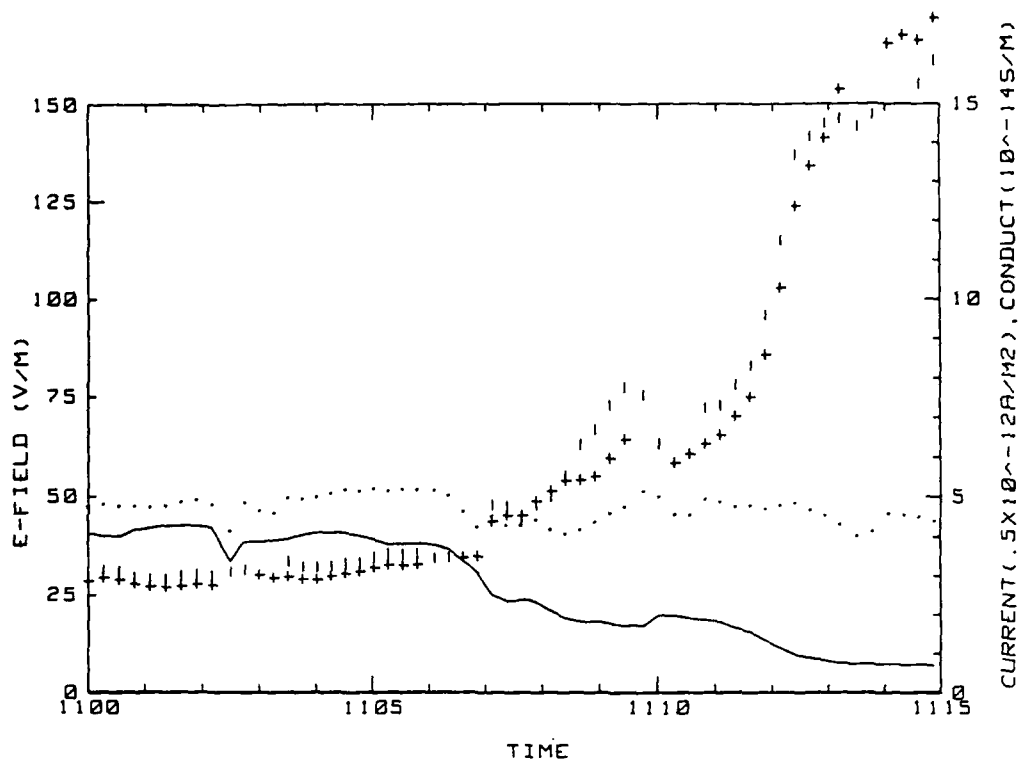
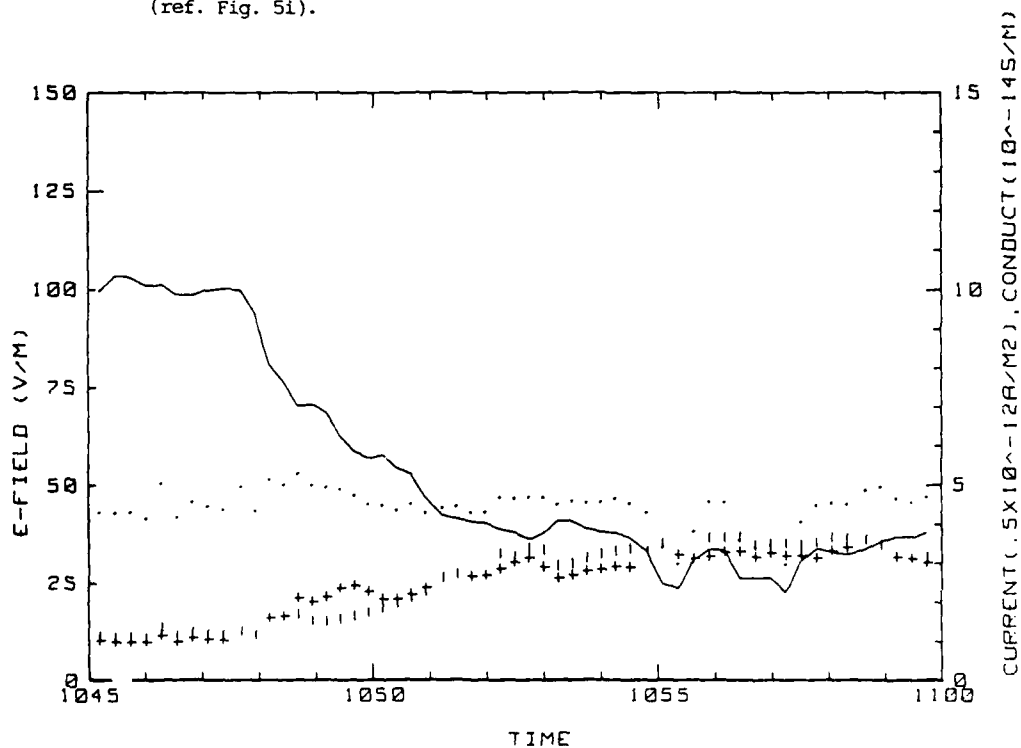


Figure 15k. Hobbs Flight 11 continuous upsonding (ref. Fig. 5b)



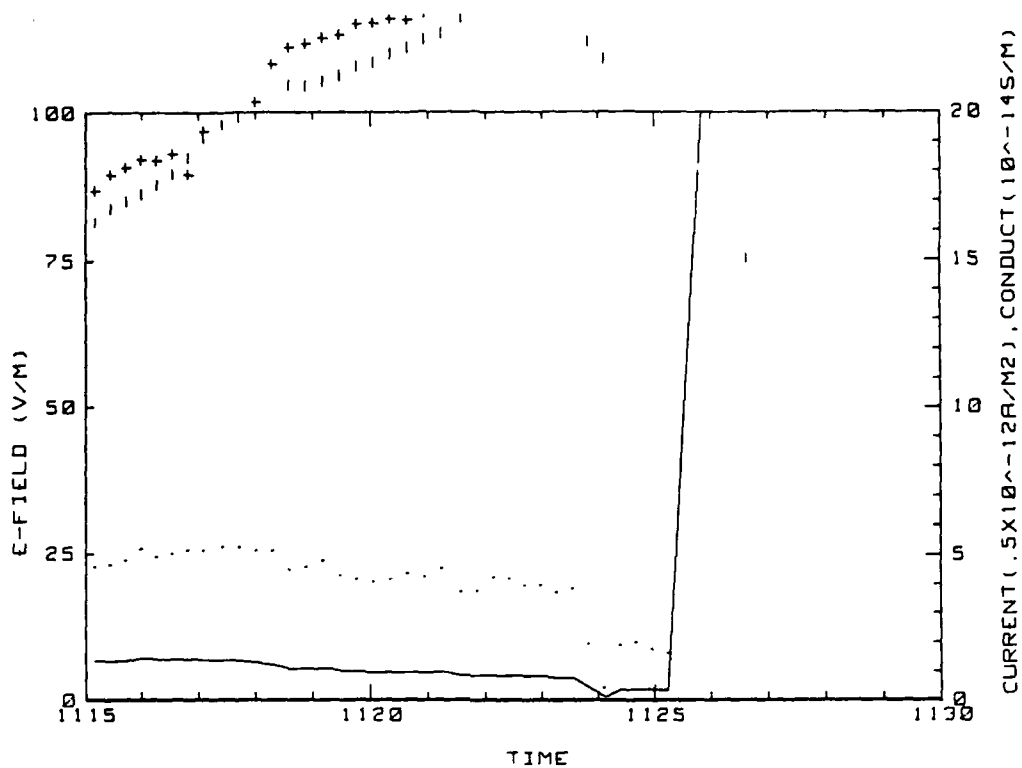
24 MAY 86 FLIGHT#11 110000 TO 111500 LST

Figure 15l. Hobbs Flight 11 time series of electrical parameters  
(ref. Fig. 5i).



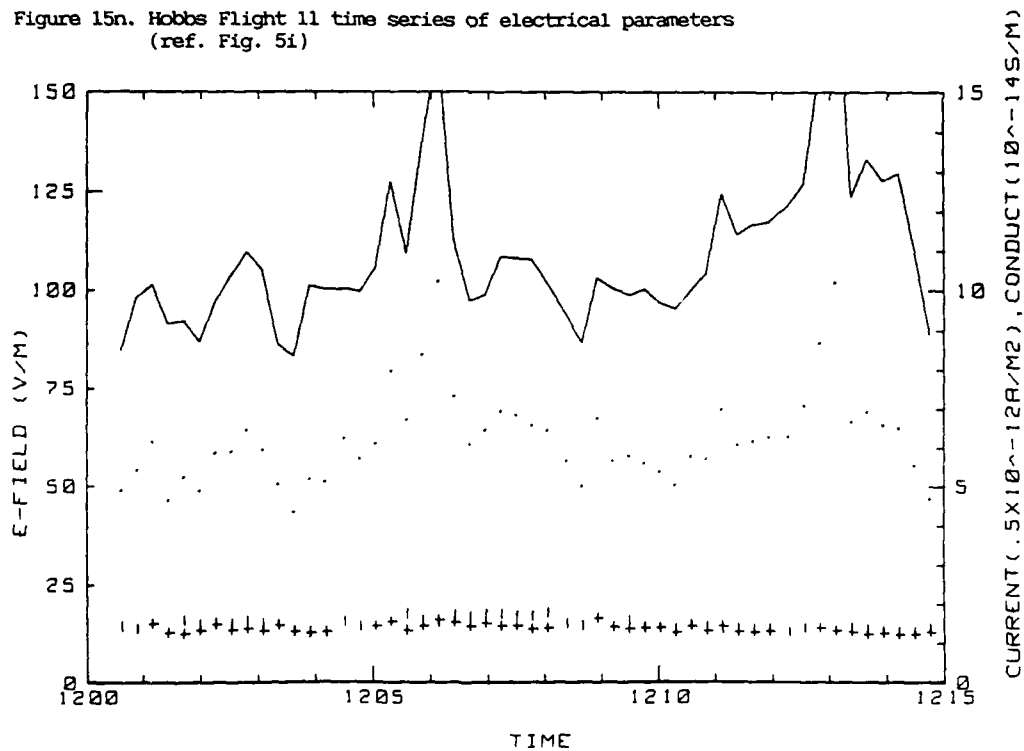
24 MAY 86 FLIGHT#11 104500 TO 110000 LST

Figure 15m. Hobbs Flight 11 time series of electrical parameters  
(ref. Fig. 5i)



24 MAY 86 FLIGHT#11 111500 TO 113000 LST

Figure 15n. Hobbs Flight 11 time series of electrical parameters  
(ref. Fig. 5i)



24 MAY 86 FLIGHT#11 120000 TO 121500 LST

Figure 15o. Hobbs Flight 11 time series of electrical parameters  
(ref. Fig. 5i)

Flight: 12

Date: 27 May 1986

Takeoff: 1457 LT from Hobbs.

Landed: 1717 LT at Lea County Airport.

Conditions: High cirrus with some altocumulus and scattered cumulus. Winds were variable but mostly from the NE at 5 m/s.

Instruments: All worked properly.

Summary: After takeoff, the aircraft ascended enroute to Roswell where a spiral down sounding was performed starting at 1544 and ending at 1605 LT. A linear up sounding was made between Roswell and Hobbs from 1614 to 1636 LT and was followed by a spiral descent from 7 km over the ground station ending at 1701 LT. A partial ladder profile was obtained over the ground station just before landing.

Table 9. Hobbs Flight 12 averages and (standard deviations)/averages for constant altitude runs over the ground station.

AVERAGES FROM LEVEL RUNS

Time HHM	N	Altitude km	Efield1 V/m	Efield2 V/m	+Lam 10 <sup>-14</sup>	-Lam 10 <sup>-14</sup>	Con Cur1 10 <sup>-12</sup>	Con Cur2 10 <sup>-12</sup>	Theta_v C
1701	16	.006	84.75	84.82	2.31	2.53	4.11	4.11	20.5
1702	15	.005	86.76	87.06	2.29	2.53	4.44	4.35	21.3
1704	21	.015	87.99	86.99	2.33	2.54	4.30	4.25	20.9
1706	24	.031	86.97	87.53	2.29	2.61	4.33	4.25	20.7
1709	28	.151	74.08	73.30	2.12	2.44	3.44	3.40	20.3
1711	30	.310	72.44	71.73	2.07	2.29	3.16	3.13	20.3

Time HHM	N	Press mB	Rel Hum %	CCN k/cc	EPS m2/s3	CT C2/m2/3	Q g/kg	Trose C	T_LR C	T_dew C
1701	16	887	55.5	4.5	1.57E-01	1.72E-01	5.52	19.4	32.9	3.8
1702	15	887	54.1	4.9	3.47E-01	3.83E-01	5.65	20.2	33.4	3.9
1704	21	886	54.7	5.5	1.30E-01	1.55E-01	5.60	19.7	32.4	3.7
1706	24	885	55.1	6.2	7.02E-02	8.40E-02	5.57	19.4	31.6	3.6
1709	28	872	57.7	5.8	1.54E-02	9.68E-03	5.49	17.8	31.2	3.2
1711	30	856	41.1	5.3	1.39E-02	4.97E-03	5.53	15.3	31.0	3.1

STANDARD DEVIATIONS/MEAN VALUES

Time	Efield1	Efield2	+Lam	-Lam	Concur1	Concur2	CCN	EPS	CT	Q
1701	.137	.164	.059	.063	.145	.153	.005	1.061	.855	.013
1702	.163	.125	.077	.047	.192	.158	.010	.268	.196	.015
1704	.125	.125	.050	.045	.153	.154	.021	.617	.577	.015
1706	.115	.112	.073	.060	.119	.120	.008	.525	.427	.013
1709	.034	.032	.053	.049	.032	.051	.003	.334	.458	.011
1711	.023	.018	.029	.032	.036	.051	.016	.436	.724	.018

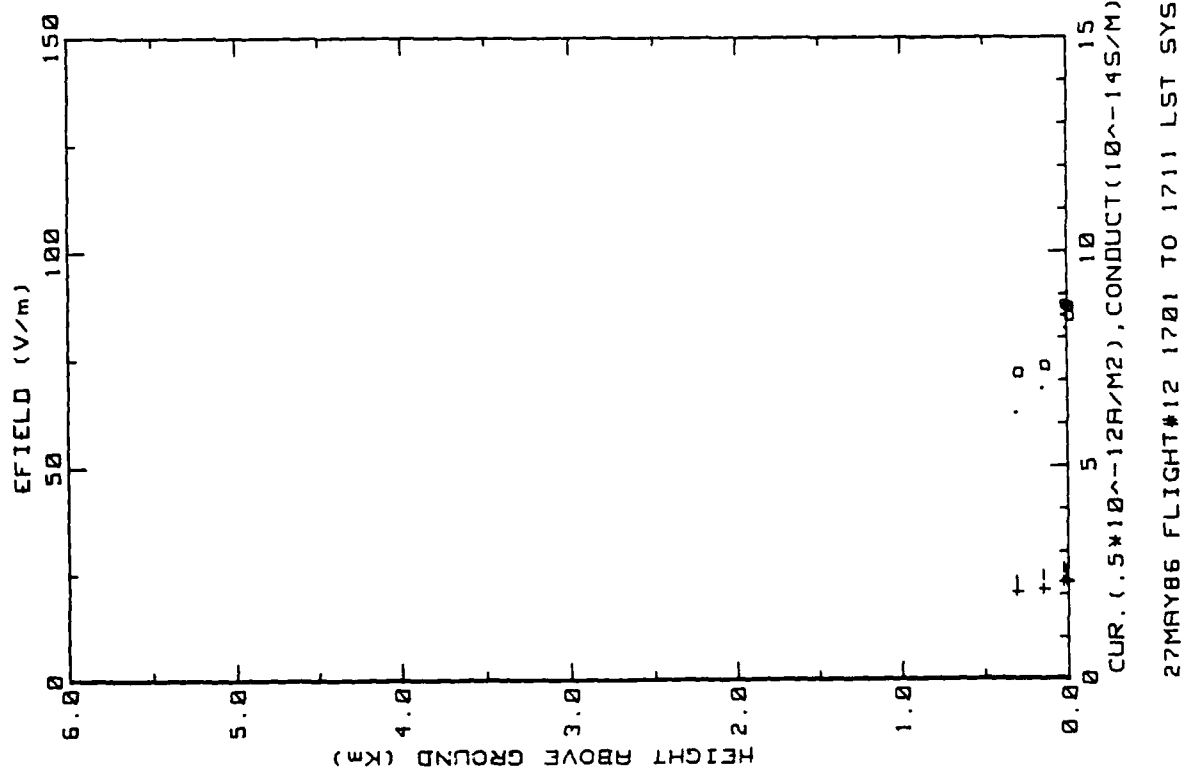


Figure 16a. Hobbs Flight 12 ladder profile (ref. Fig. 5a)

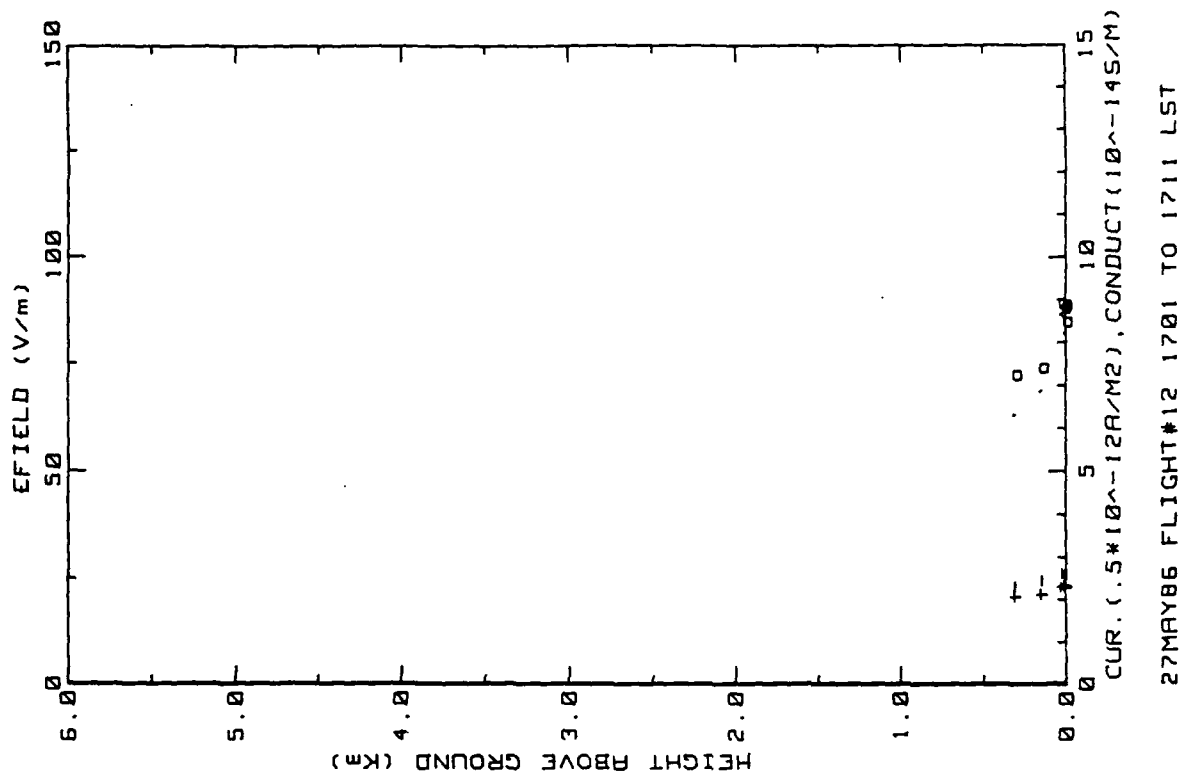


Figure 16b. Similar to 16a. but for outboard E<sub>field</sub> system.



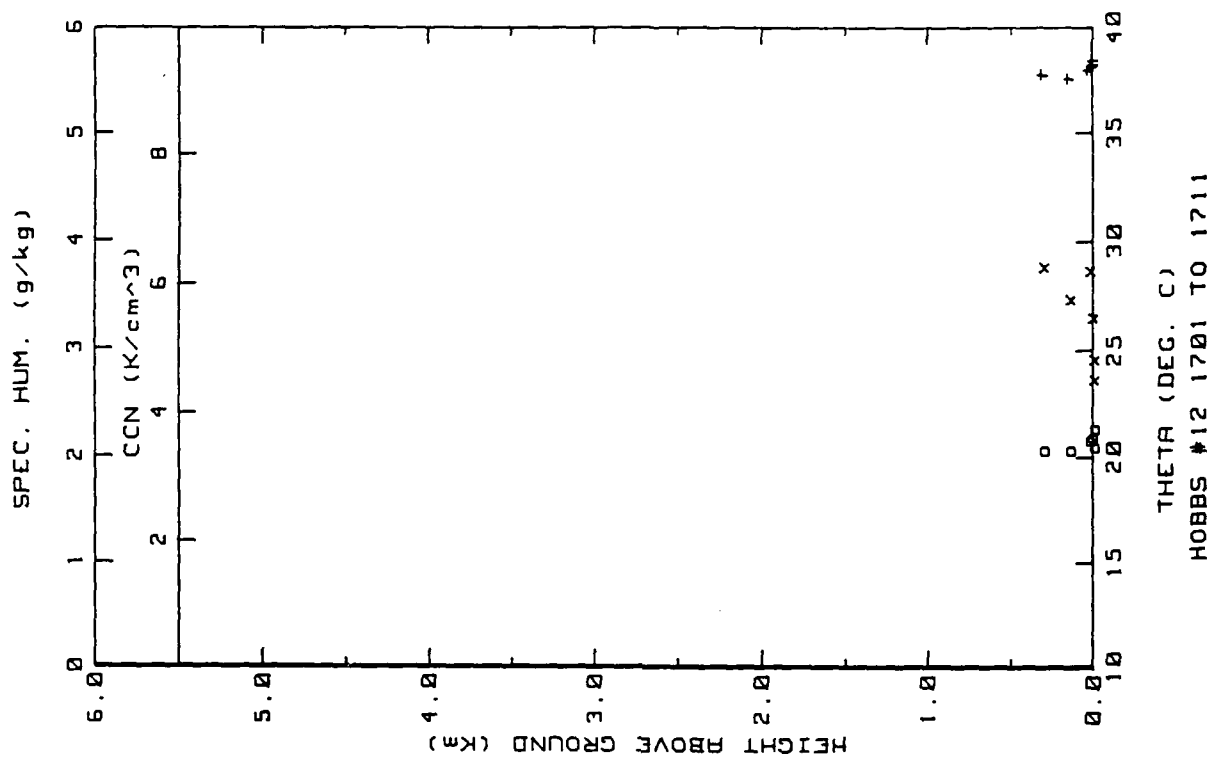


Figure 16d. Hobbs Flight 12 ladder profile (ref. Fig. 5c).

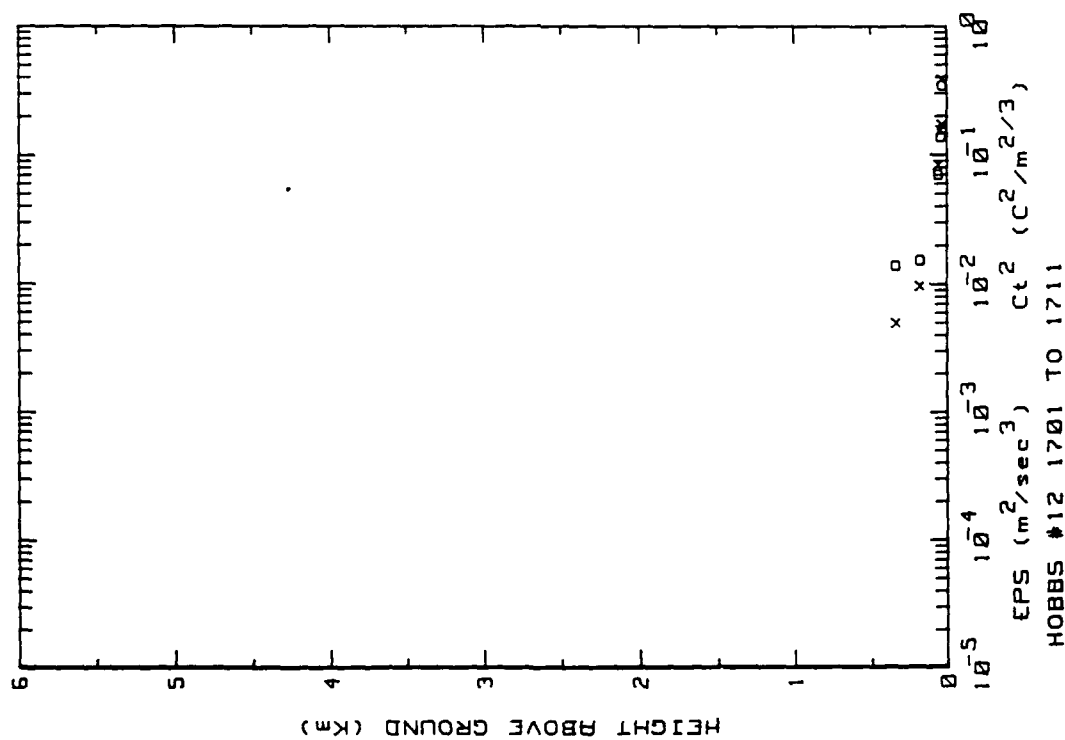
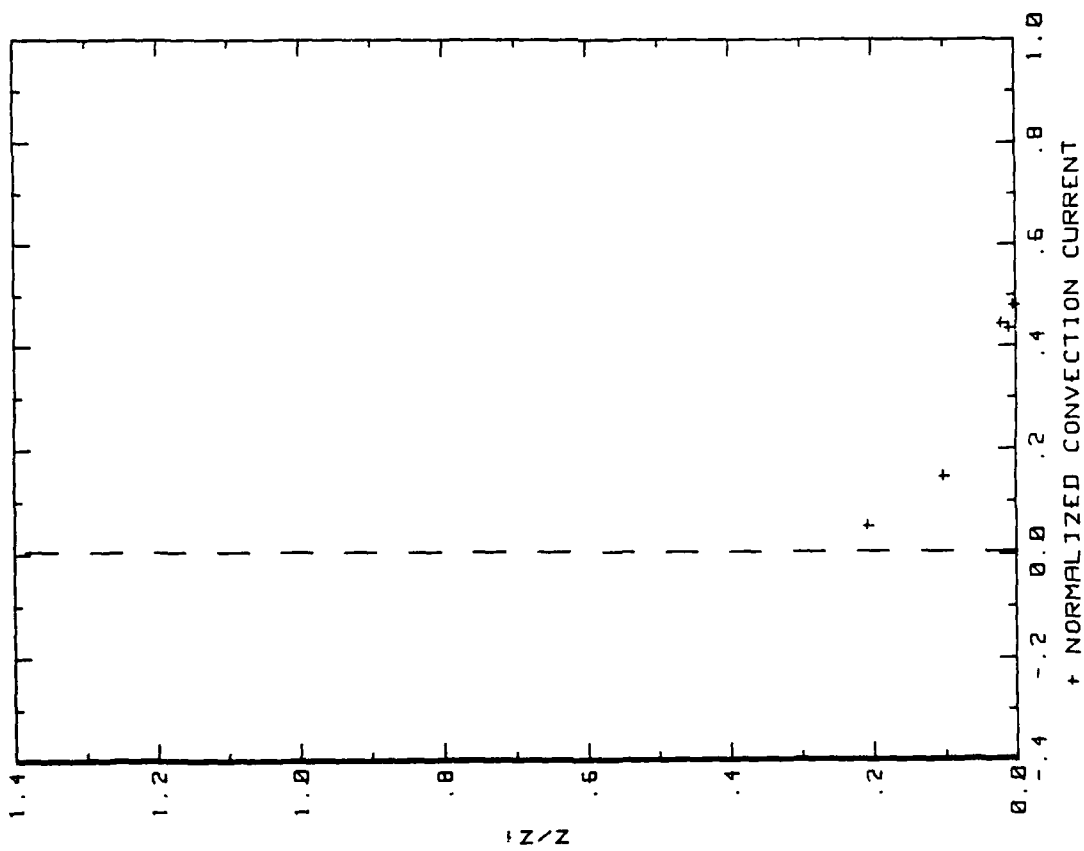


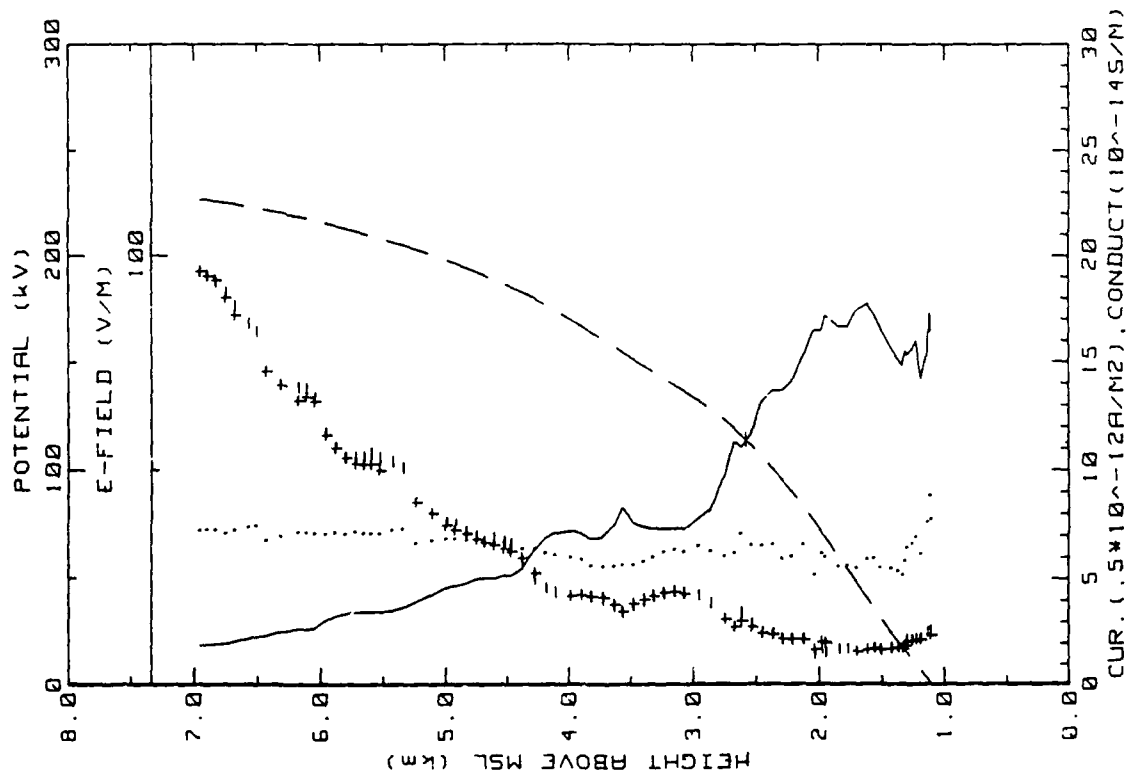
Figure 16c. Hobbs Flight 12 ladder profile (ref. Fig. 5b).



27MAY86 FLIGHT#12 1702 TO 1711 LST

Z1-1500 Jo-3.00

Figure 16e. Hobbs Flight 12 convection current profile  
(ref. Fig. 5d)



27MAY86 FLIGHT#12 154400 TO 160430 LST  
 Figure 16f. Hobbs Flight 12 spiral down sounding near Roswell, NM  
 (ref. Fig. 5e).

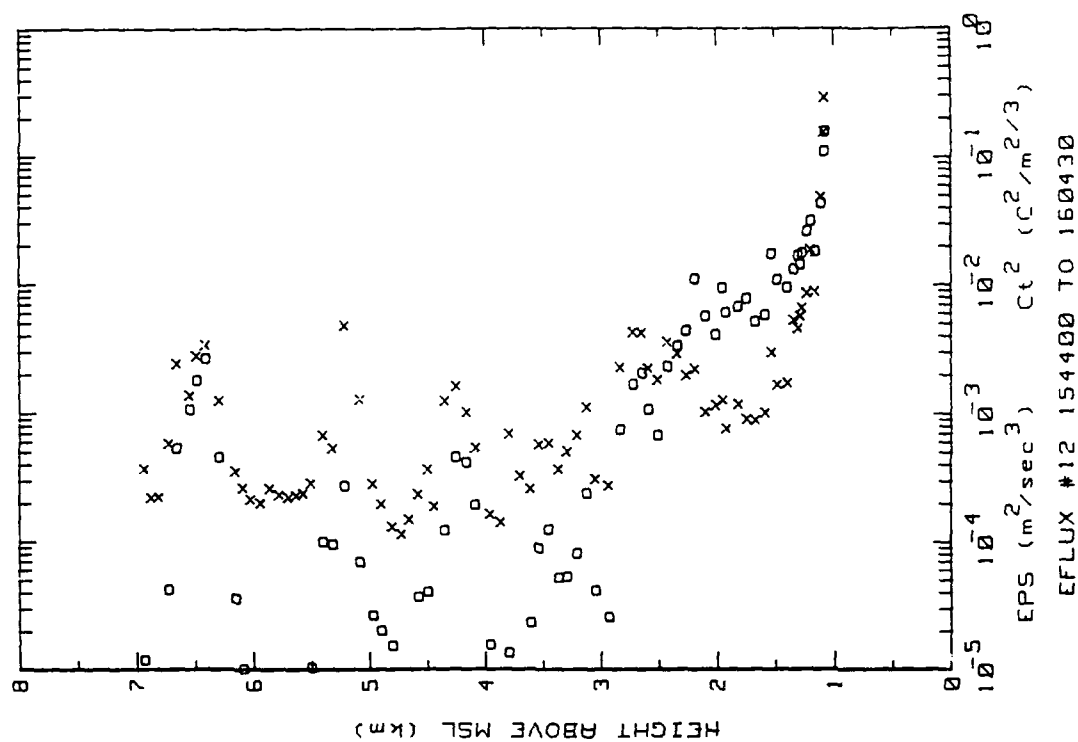
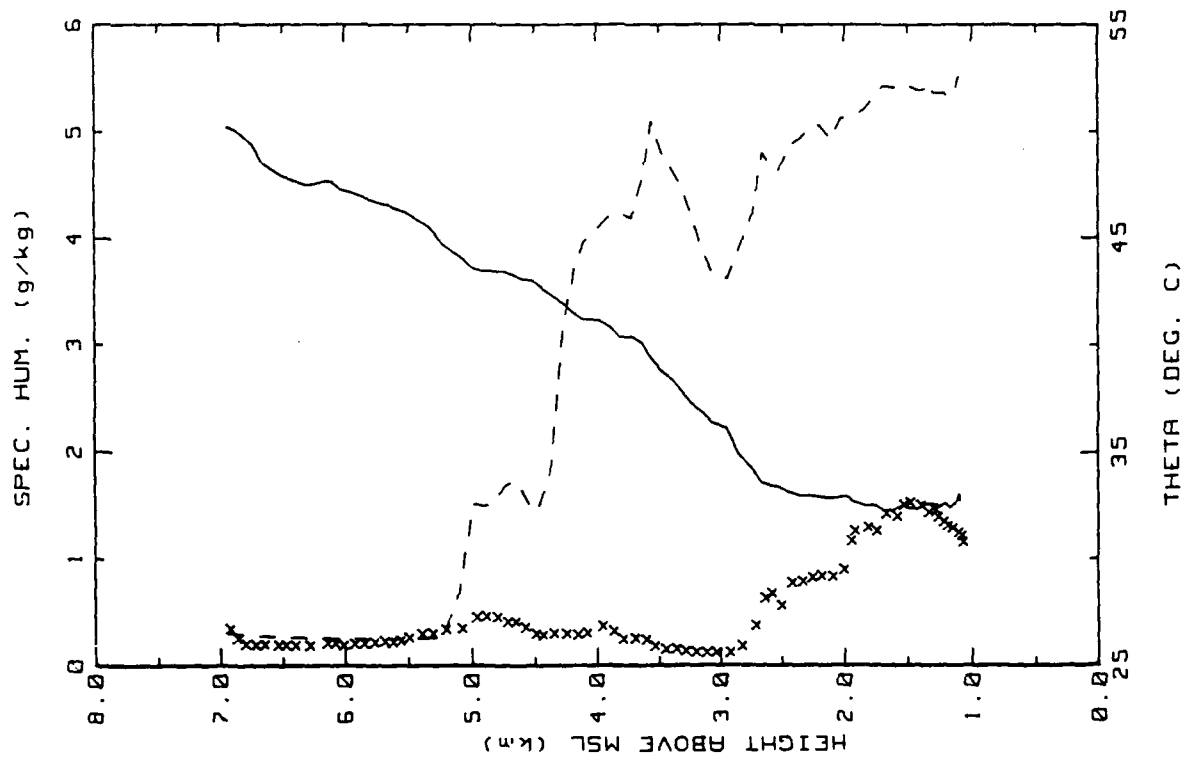
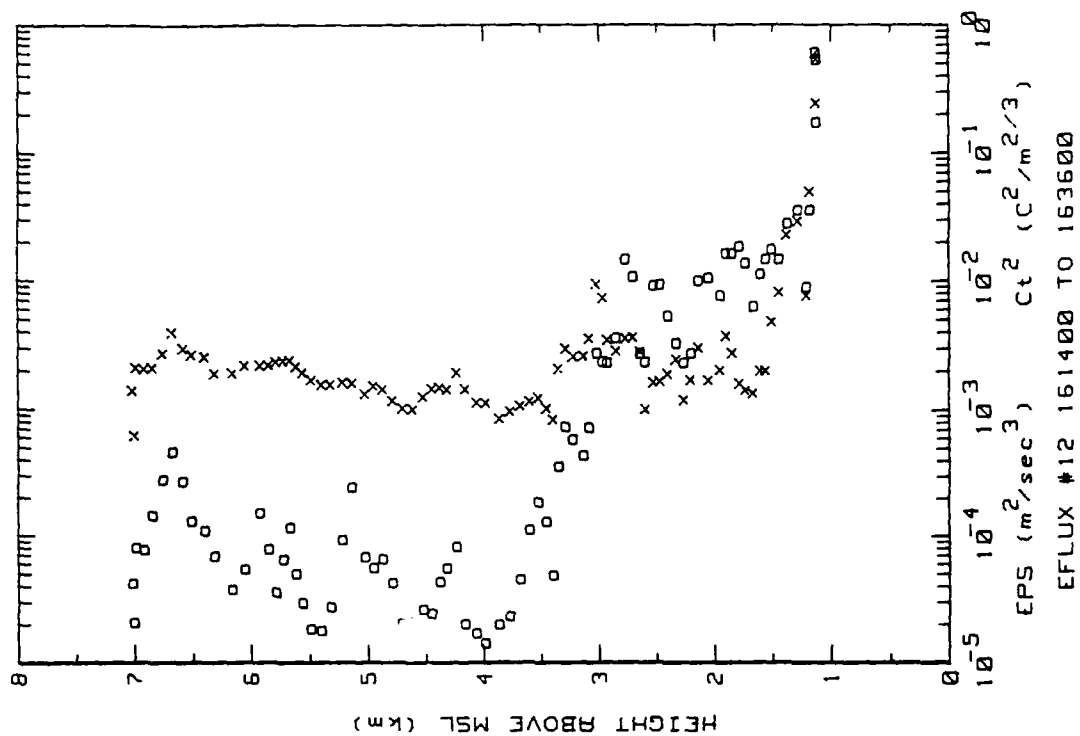


Figure 16g. Hobbs Flight 12 spiral down sounding near Roswell, NM  
 (ref. Fig. 5b).



THETA (DEG. C)

EFLUX #12 154400 TO 160430



EFLUX #12 161400 TO 163600

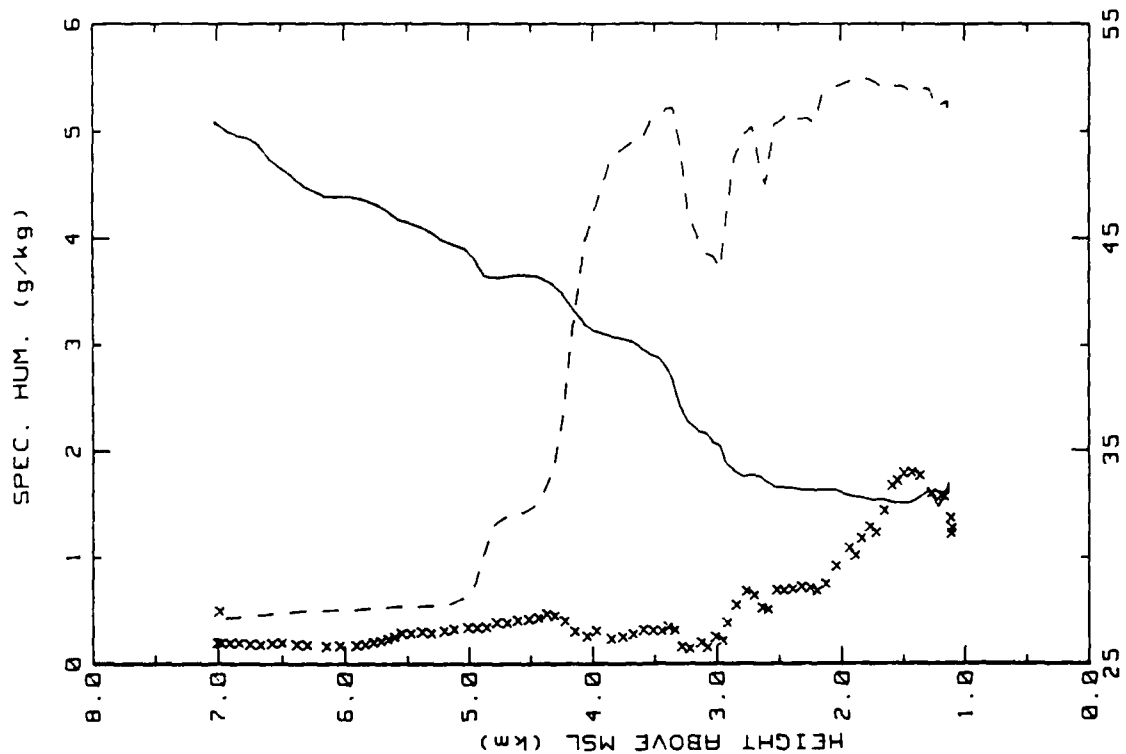


Figure 16j. Hobbs Flight 12 continuous upsonding between Roswell and Hobbs (ref. Fig. 5h)

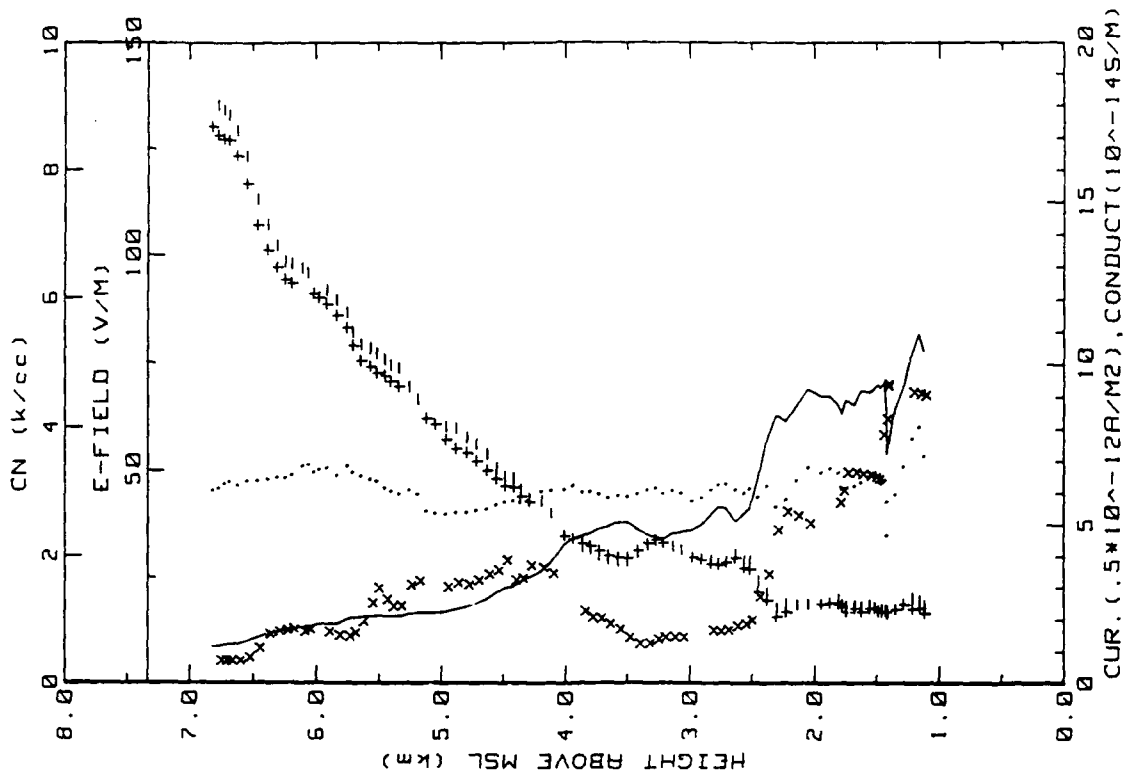


Figure 16k. Hobbs Flight 12 spiral downsonding near Hobbs (ref. Fig. 5f).

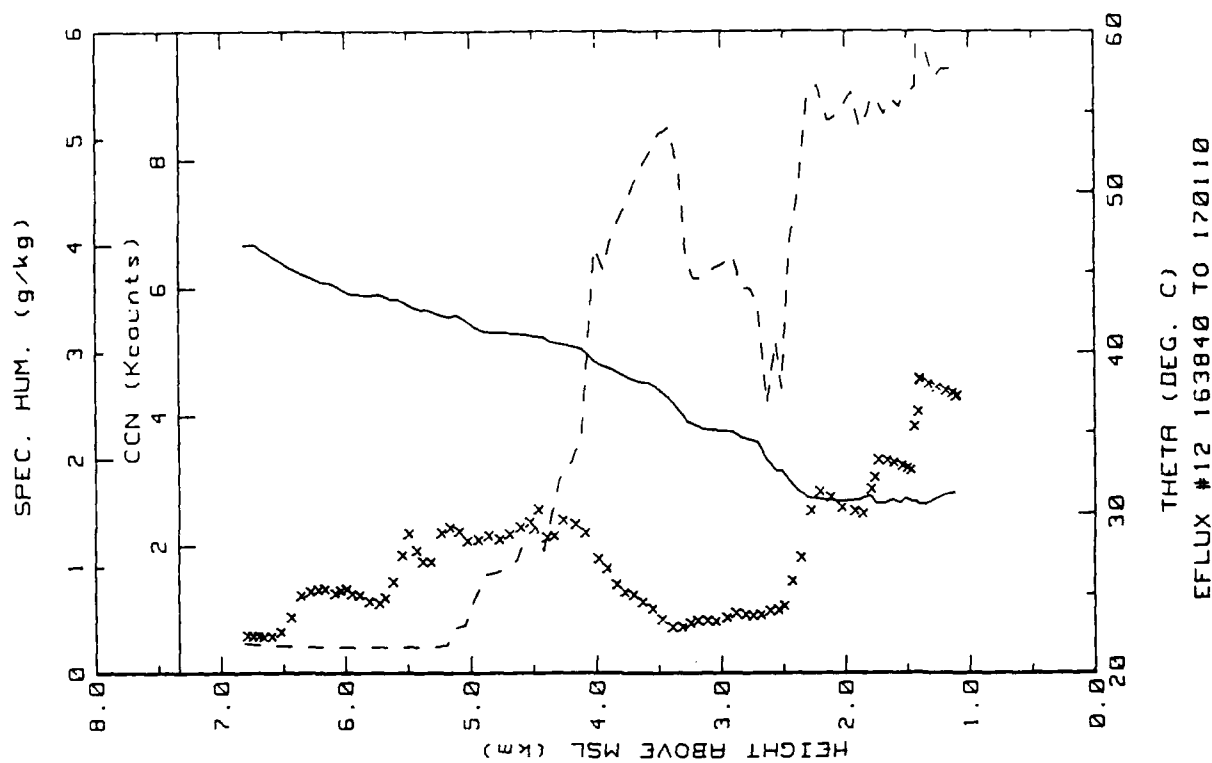


Figure 16n. Hobbs Flight 12 spiral downsonding near Hobbs (ref. Fig. 5h).

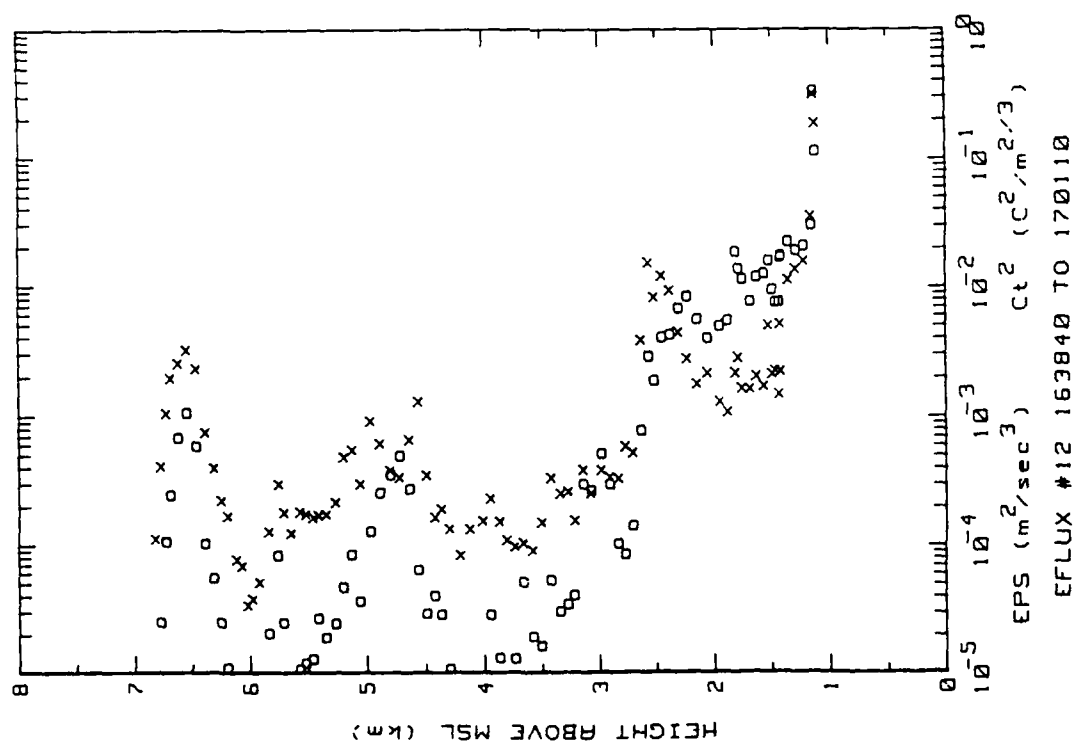
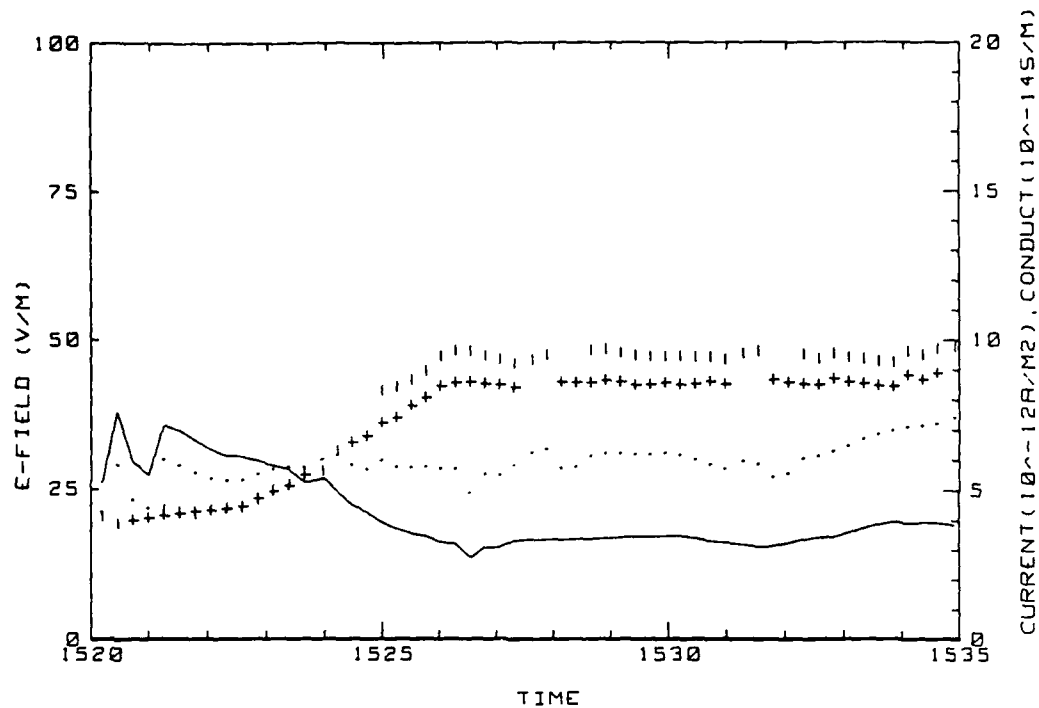
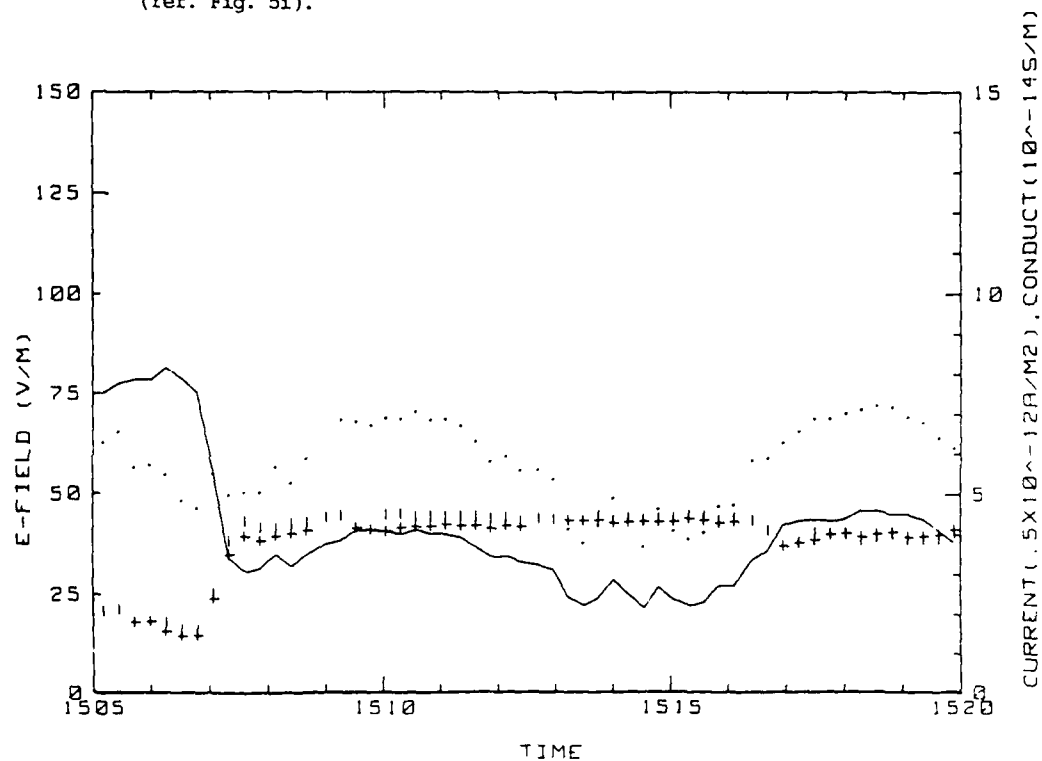


Figure 16l. Hobbs Flight 12 spiral downsonding near Hobbs (ref. Fig. 5b).



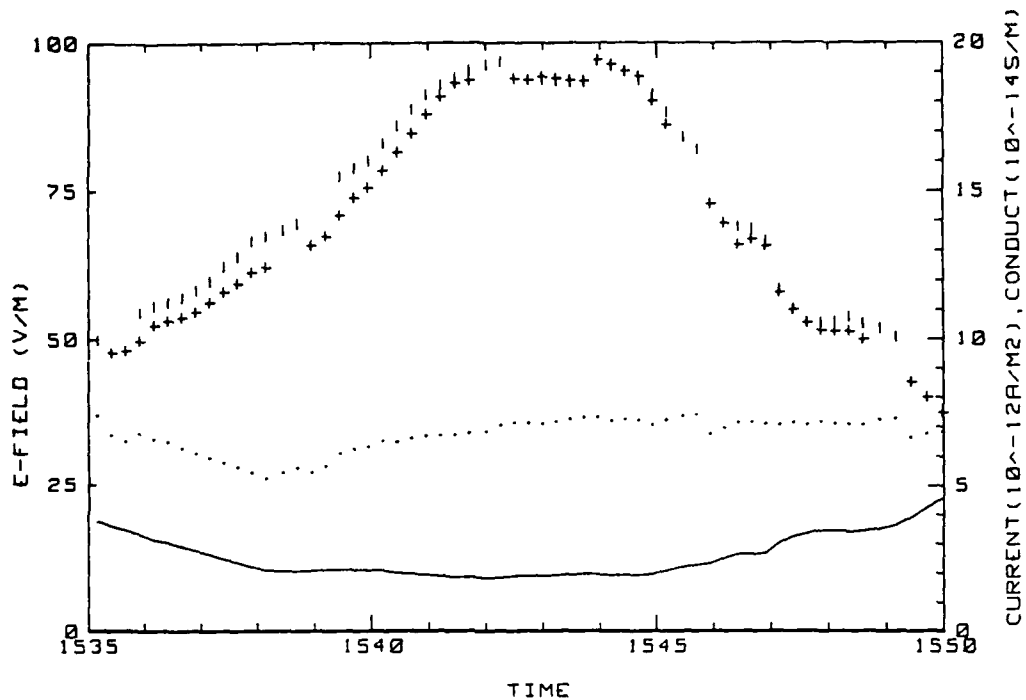
FLIGHT#12 152000 TO 153500 LST

Figure 16n. Hobbs Flight 12 time series of electrical parameters  
(ref. Fig. 5i).



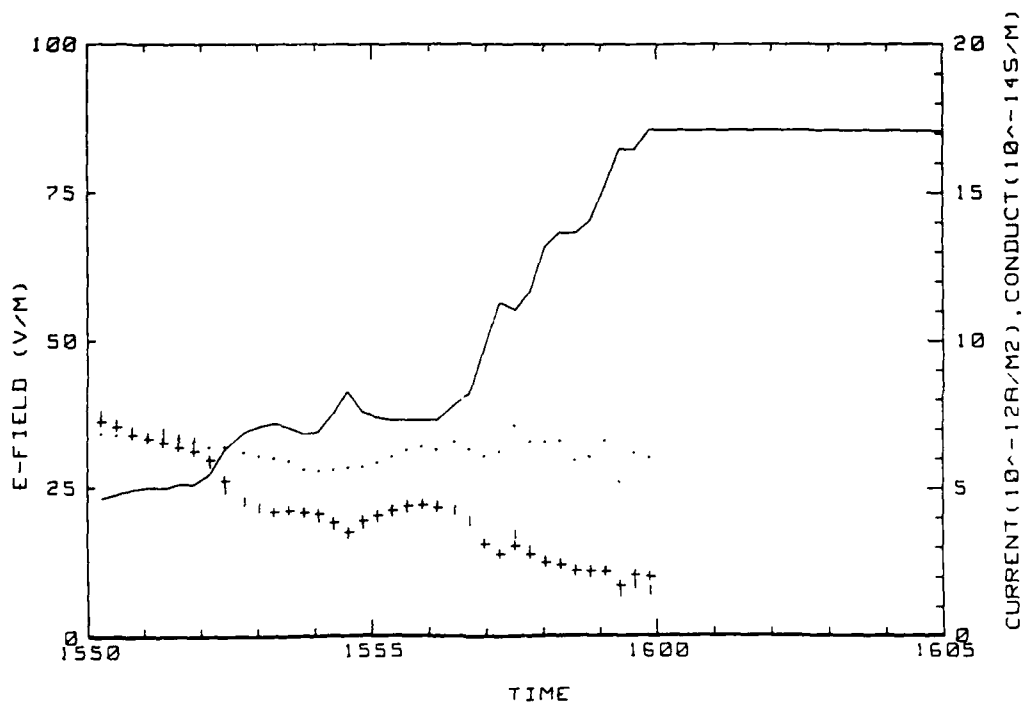
27 MAY 86 FLIGHT#12 150500 TO 152000 LST

Figure 16o. Hobbs Flight 12 time series of electrical parameters  
(ref. Fig. 5i).



FLIGHT#12 153500 TO 155000 LST

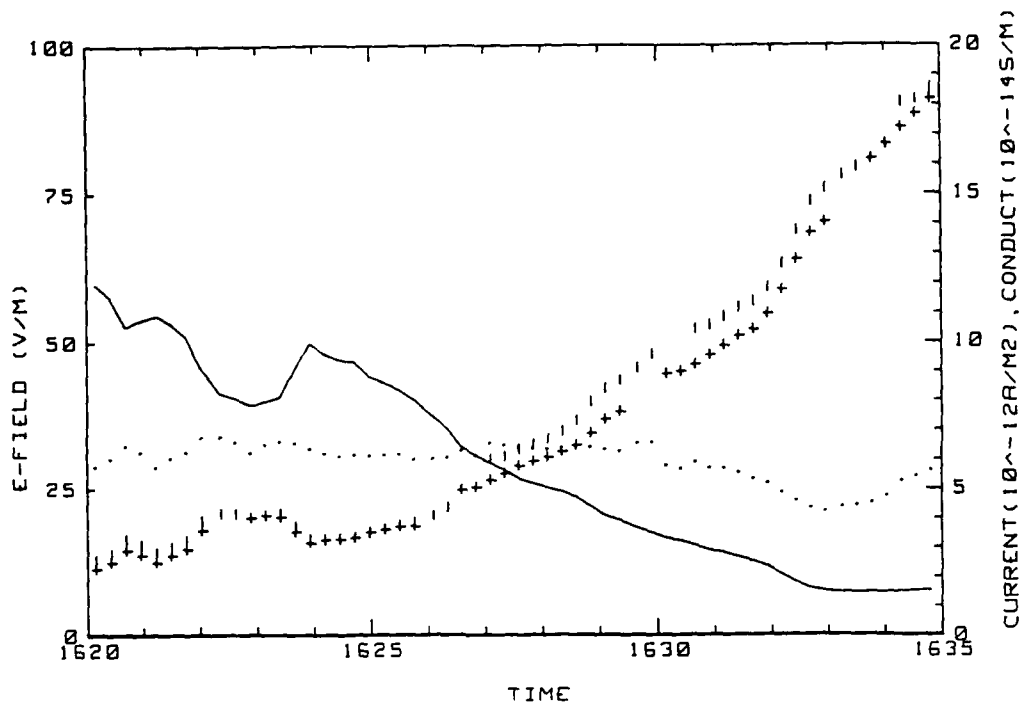
Figure 16p. Hobbs Flight 12 time series of electrical parameters (ref. Fig. 5i).



FLIGHT#12 155000 TO 160500 LST

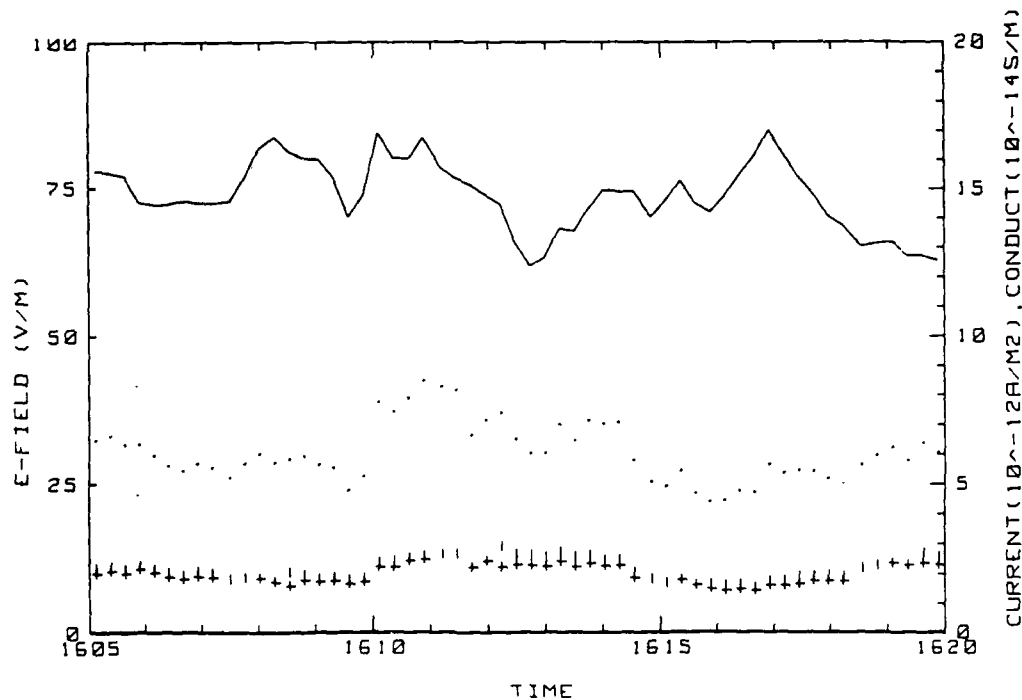
Figure 16q. Hobbs Flight 12 time series of electrical parameters (ref. Fig. 5i).





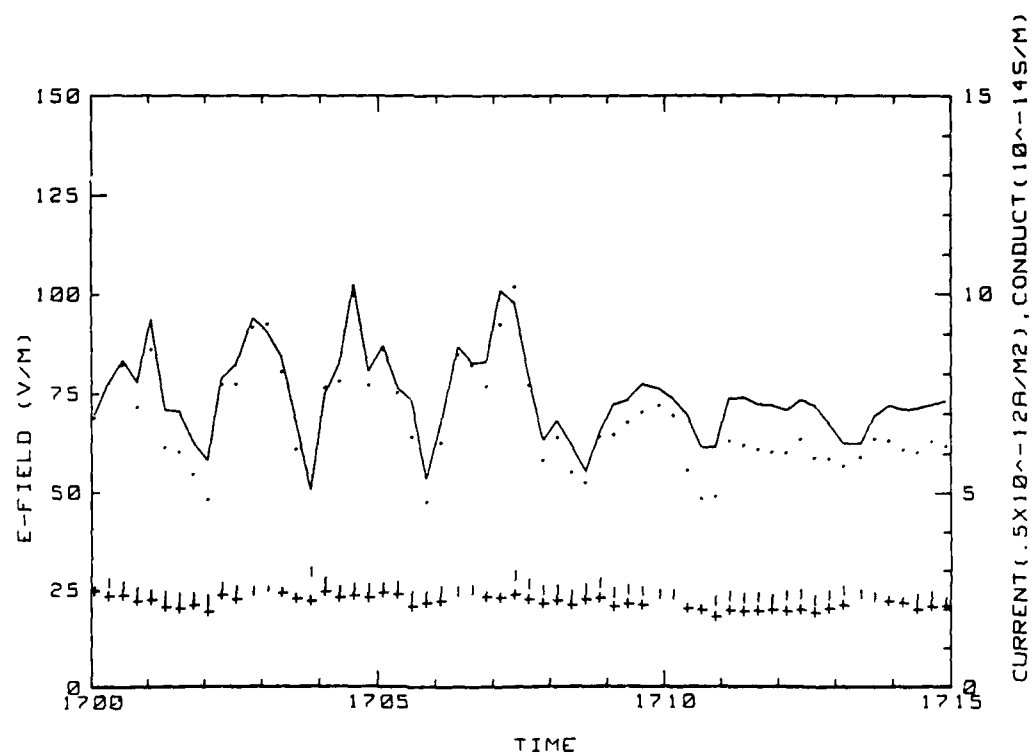
FLIGHT#12 162000 TO 163500 LST

Figure 16r. Hobbs Flight 12 time series of electrical parameters  
(ref. Fig. 5i).



85 FLIGHT#12 160500 TO 162000 LST

Figure 16s. Hobbs Flight 12 time series of electrical parameters  
(ref. Fig. 5i).



27 MAY 86 FLIGHT#12 170000 TO 171500 LST

Figure 16t. Hobbs Flight 12 time series of electrical parameters  
(ref. Fig. 5i).

Flight: 13

Date: 27 May 1986

Takeoff: 1748 LT from Lea County Airport.

Landed: 1919 at Hobbs.

Conditions: High cirrus with some scattered cumulus; mostly clear over the ground station. Winds were from the NE at about 4 m/s and visibility was good. Convection was not as strong as during flight 12 (performed earlier in the day).

Instruments: The positive conductivity tube appeared to be slightly noisy; all other instruments worked properly.

Summary: The flight consisted of a coarse ladder profile over the ground station followed by a slow spiral descent over the same area.

Table 10a. Hobbs Flight 13 averages for constant altitude runs over the ground station.

AVERAGES FROM LEVEL RUNS

Time HHH	N	Altitude km	Efield1 V/m	Efield2 V/m	Lam 10 <sup>-14</sup>	-Lam 10 <sup>-14</sup>	Con Cur1 10 <sup>-12</sup>	Con Cur2 10 <sup>-12</sup>	Theta v C
1750	19	.006	74.60	72.90	2.54	2.65	4.10	4.01	20.0
1753	28	.005	74.03	72.97	2.63	2.85	4.11	4.05	20.1
1755	20	.015	75.75	75.80	2.72	2.99	4.29	4.24	20.2
1758	19	.031	72.96	71.43	2.67	2.90	4.15	4.06	20.1
1800	35	.151	65.15	64.39	2.47	2.71	3.38	3.34	19.7
1803	30	.330	64.13	63.68	2.32	2.47	3.08	3.05	20.3
1806	34	.940	55.94	65.71	2.24	2.41	3.64	3.03	20.9
1810	32	1.568	45.77	45.84	3.26	3.41	3.05	3.06	22.6
1818	45	2.570	35.72	36.01	4.30	4.32	3.07	3.10	31.1
1819	36	2.757	35.26	35.51	4.21	4.32	3.01	3.03	30.0
1821	42	3.392	24.85	25.12	5.96	5.23	3.02	3.06	33.7
1825	41	3.930	17.97	18.27	5.97	8.55	3.00	3.05	35.4
1829	36	4.590	12.24	12.73	12.06	12.53	3.00	3.13	40.5

Time HHH	N	Press mB	Rel Hum %	CON k/cc	SP3 m2/s3	CT C2/m2/3	G g/kg	Urose C	U <sub>IR</sub> C	U <sub>case</sub> C
1750	19	888	38.6	0.0	1.75E-01	1.71E-01	5.90	18.9	17.1	4.5
1753	28	808	38.1	5.9	1.94E-01	2.01E-01	5.86	19.0	17.1	4.4
1755	20	887	37.9	3.4	6.45E-02	8.65E-02	5.85	19.0	17.1	4.4
1758	19	866	38.4	3.5	2.56E-02	3.28E-02	5.83	18.7	17.1	4.3
1800	35	973	41.7	3.1	7.78E-03	2.73E-03	5.82	17.2	17.1	4.1
1803	30	655	44.1	2.7	4.70E-03	1.21E-03	5.82	16.0	17.1	3.8
1806	34	723	58.5	2.8	3.75E-03	7.54E-04	5.81	10.4	17.1	2.7
1810	32	731	50.5	1.2	1.54E-03	4.61E-03	5.97	5.8	17.1	-3.7
1818	45	640	53.3	.7	8.33E-04	2.13E-03	4.69	3.1	33.7	-3.2
1819	36	621	64.5	1.1	3.30E-05	3.00E-04	3.89	1.2	30.1	-5.1
1821	42	508	30.1	1.6	1.37E-05	3.90E-04	1.35	0.5	23.1	-18.5
1825	41	319	13.4	.9	1.55E-04	7.42E-04	.54	-5.0	23.2	-31.3
1829	33	470	15.0	2.0	1.51E-05	7.80E-04	.45	-11.5	22.5	-33.3

Table 10b. Hobbs Flight 13 (standard deviations)/averages for constant altitude runs over the ground station.

STANDARD DEVIATIONS/MEAN VALUES

Time	Efield1	Efield2	+Lam	-Lam	Concur1	Concur2	CCN	EPS	CT2	Q
1750	.146	.143	.055	.034	.150	.152	0.000	.387	.275	.010
1753	.140	.134	.042	.056	.144	.139	.657	.850	.809	.008
1755	.101	.091	.044	.036	.120	.111	.083	.294	.251	.007
1758	.053	.048	.035	.040	.074	.070	.148	.442	.452	.006
1800	.020	.021	.050	.033	.045	.043	.133	.412	.741	.008
1803	.017	.017	.030	.041	.032	.031	.109	.453	.929	.008
1806	.022	.021	.047	.039	.029	.031	.115	.447	.270	.020
1810	.073	.070	.090	.067	.046	.045	.227	.863	.537	.124
1818	.025	.026	.079	.022	.051	.051	.053	.760	.676	.065
1819	.022	.021	.105	.028	.051	.053	.060	.648	.309	.062
1821	.019	.020	.055	.021	.029	.031	.056	.399	.518	.098
1825	.046	.045	.043	.052	.013	.013	.063	1.065	.248	.020
1829	.038	.040	.044	.043	.019	.022	.250	.502	.340	.035

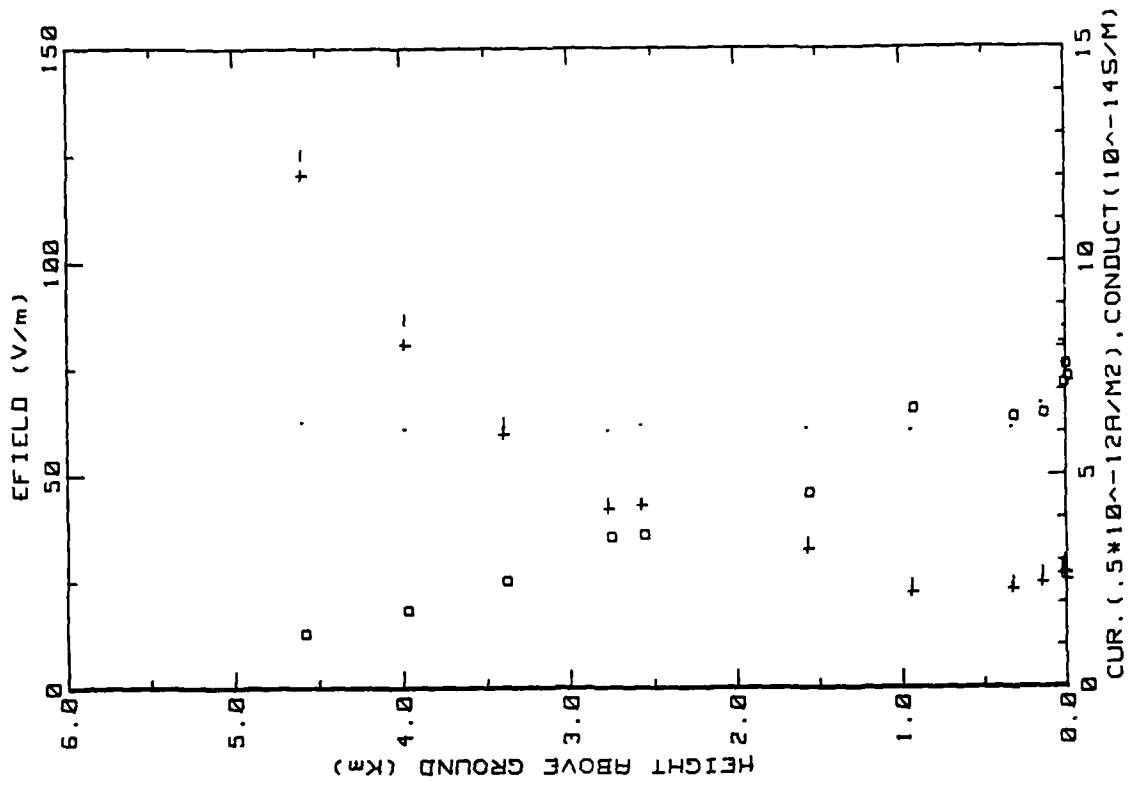


Figure 17a. Hobbs Flight 13 ladder profile (ref. Fig. 5a)

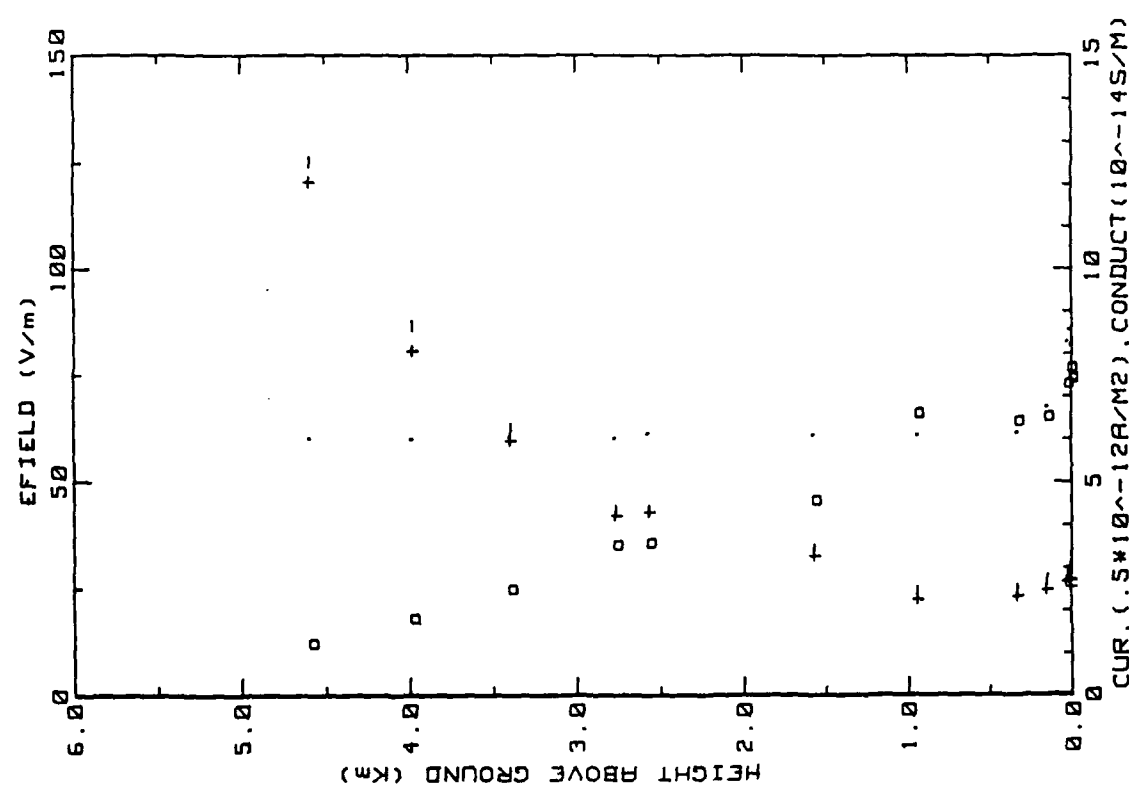


Figure 17b. Similar to 17a. but for inboard E-field system.

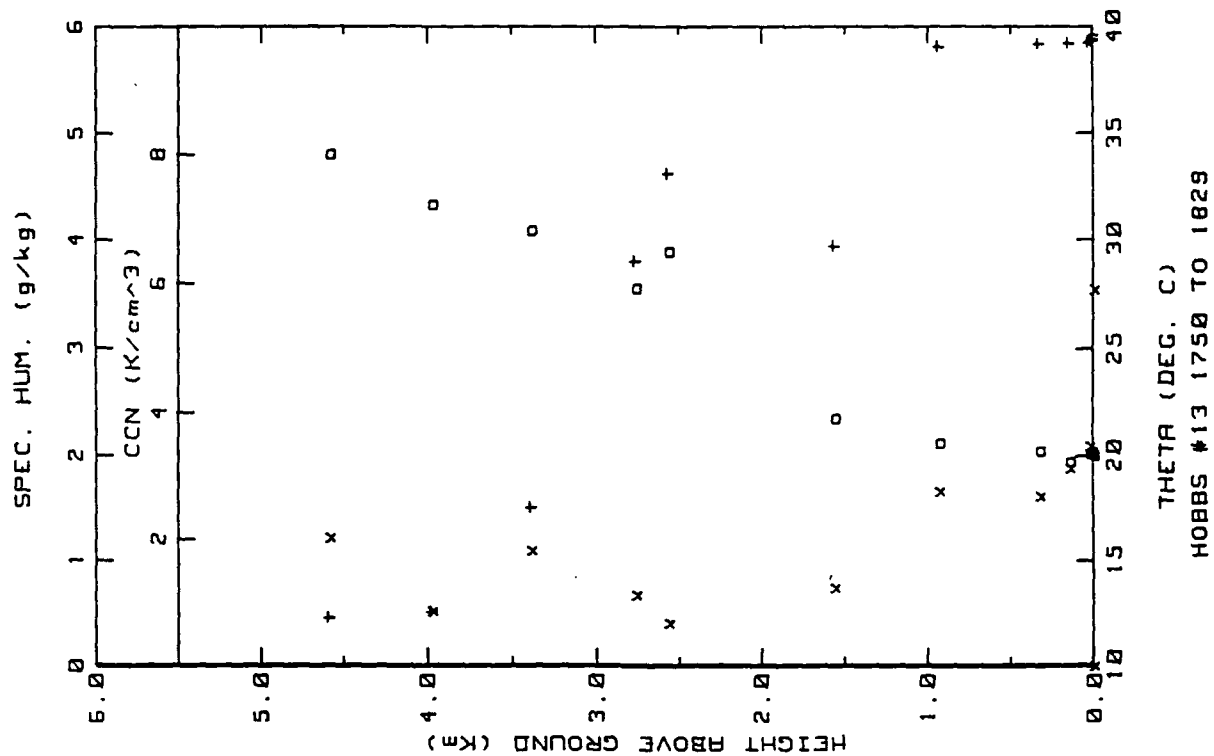


Figure 17c. Hobbs Flight 13 ladder profile (ref. Fig. 5b).

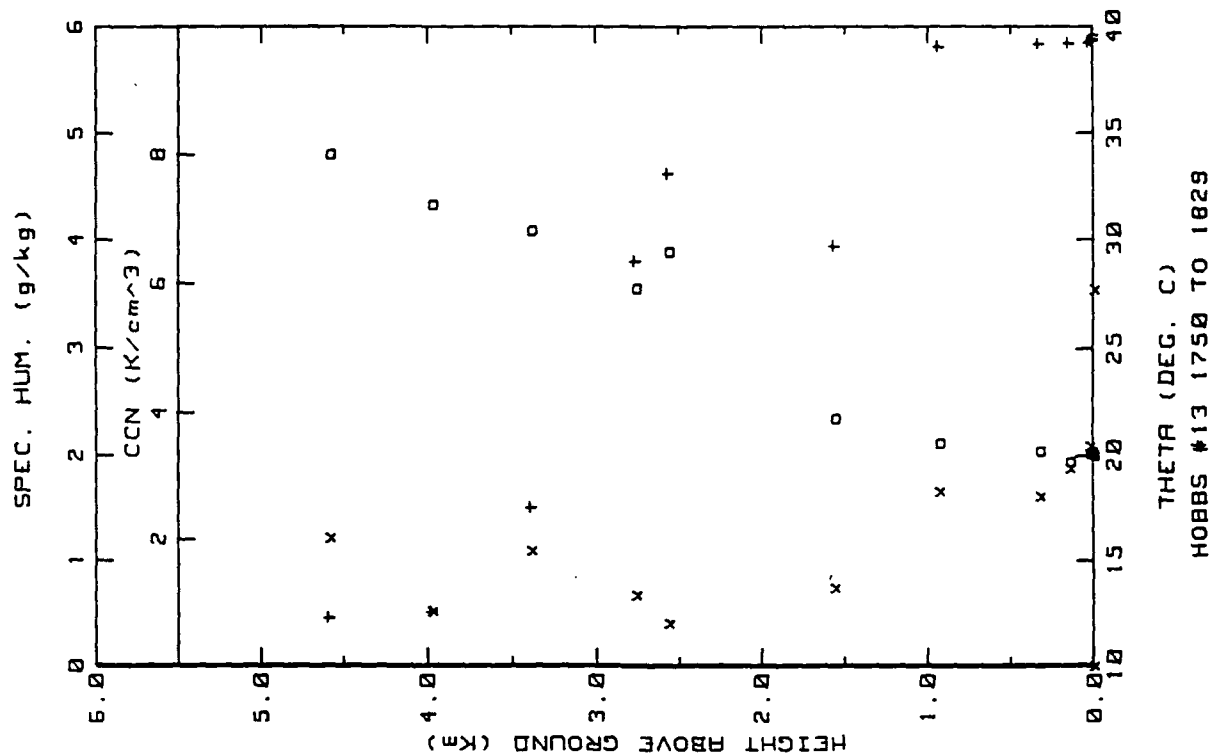
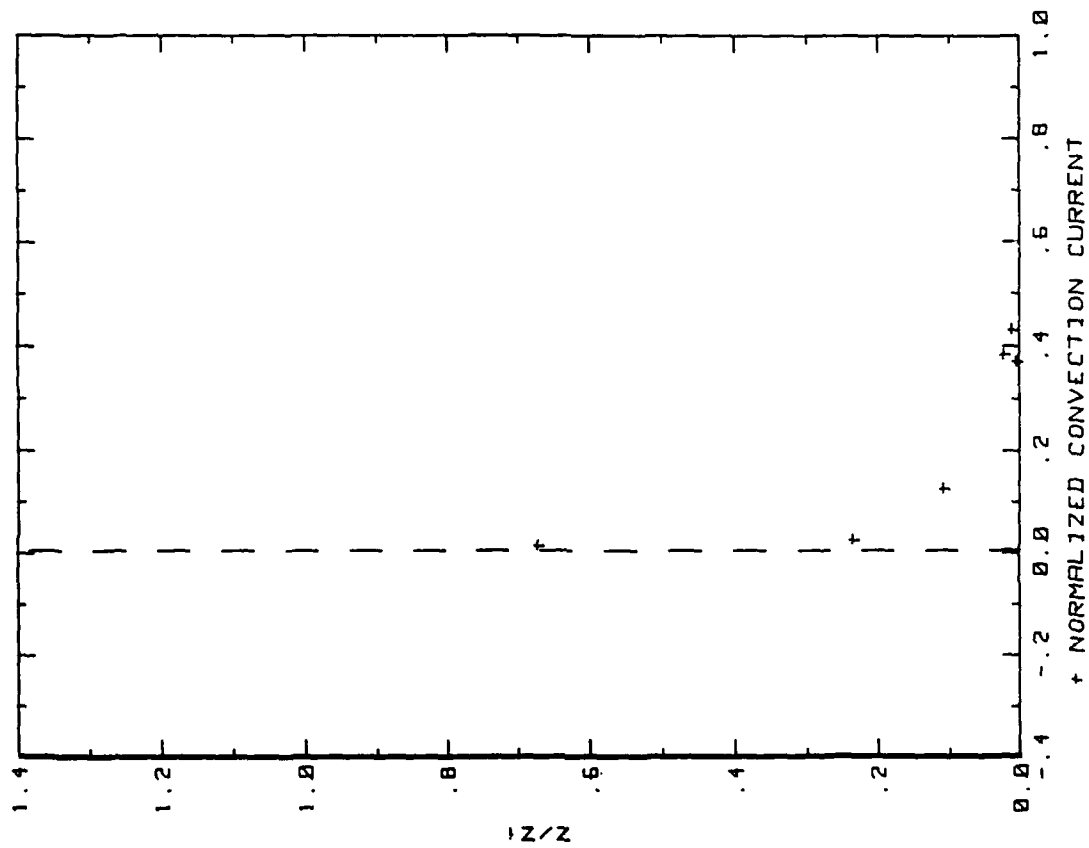


Figure 17d. Hobbs Flight 13 ladder profile (ref. Fig. 5c).



27MAY86 FLIGHT#13 1753 TO 1829 LST

Z1=1400 J0=3.00

Figure 17e. Hobbs Flight 13 convection current profile (ref. Fig. 5d).



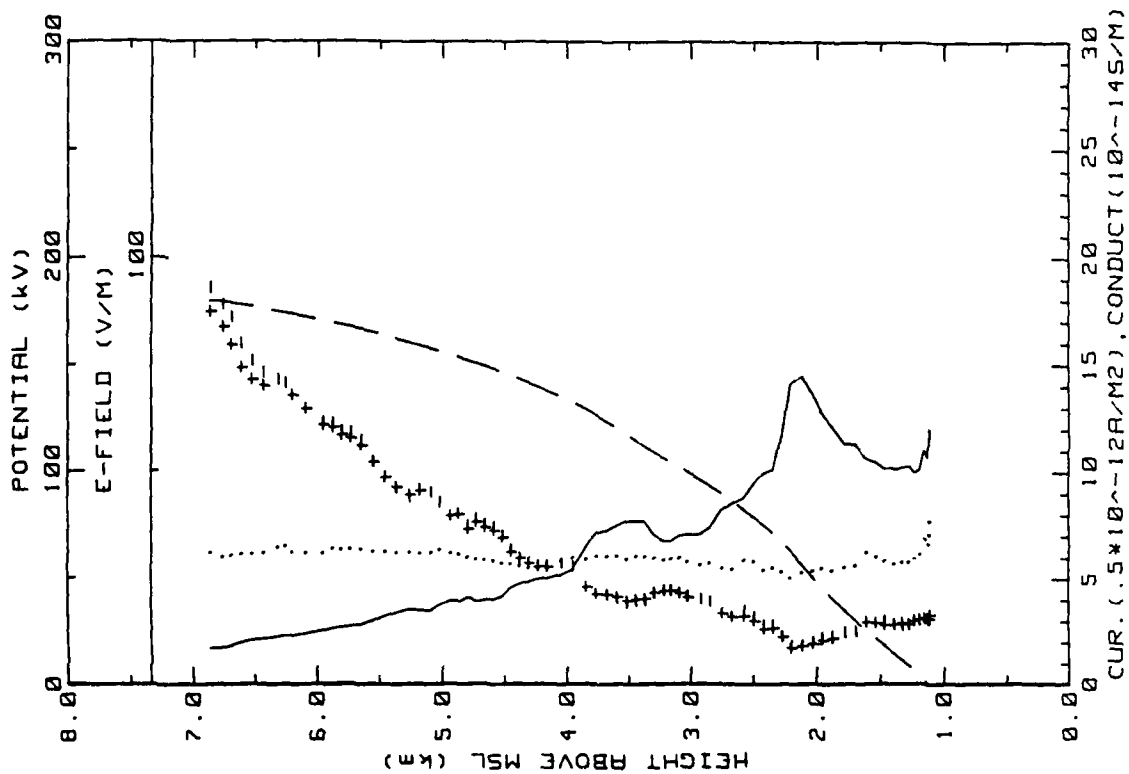


Figure 17f. Hobbs Flight 13 spiral downsonding (ref. Fig. 5e).

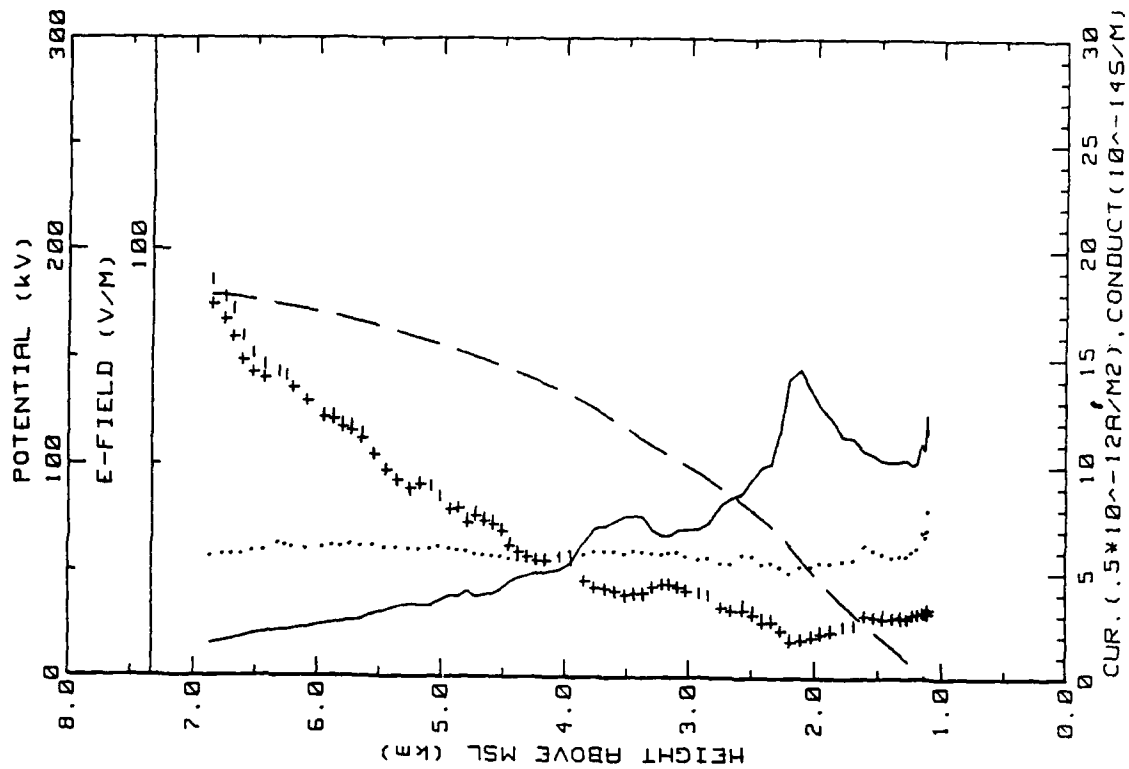


Figure 17g. Same as Fig. 17f but for outboard E<sub>field</sub> system.

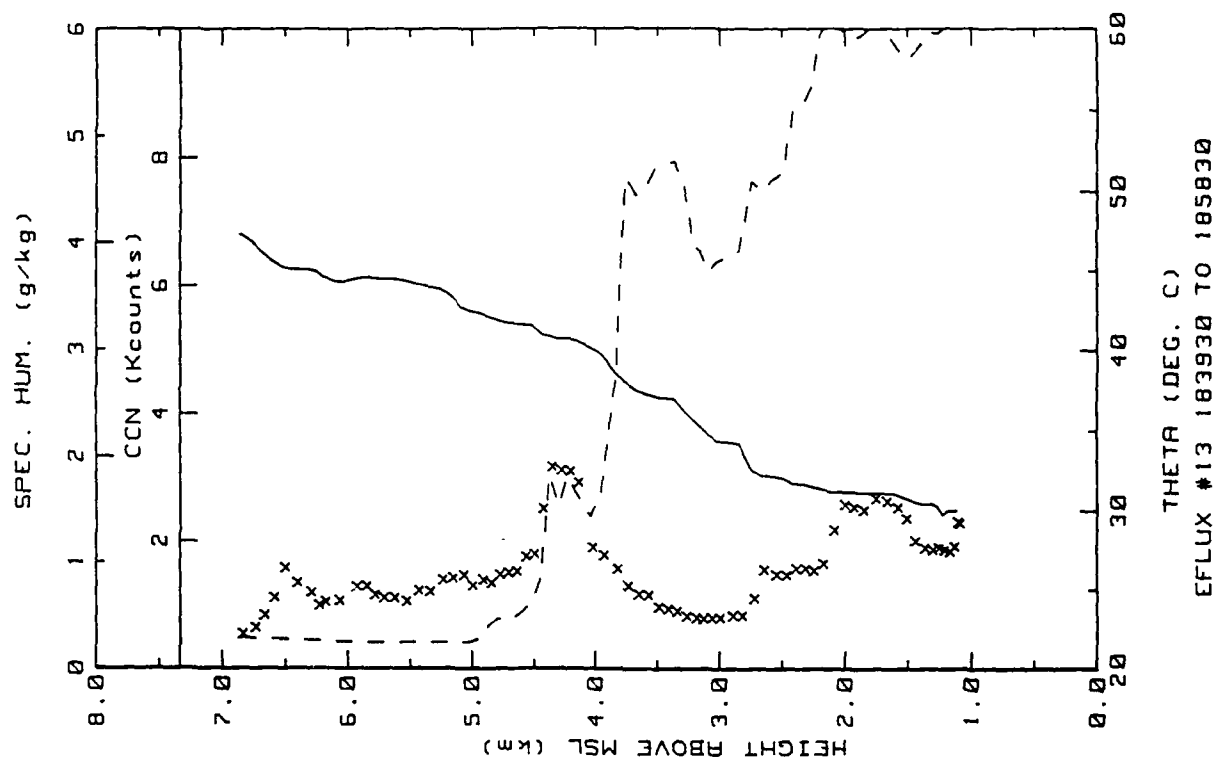


Figure 17h. Hobbs Flight 13 spiral downsonding (ref. Fig. 5g).

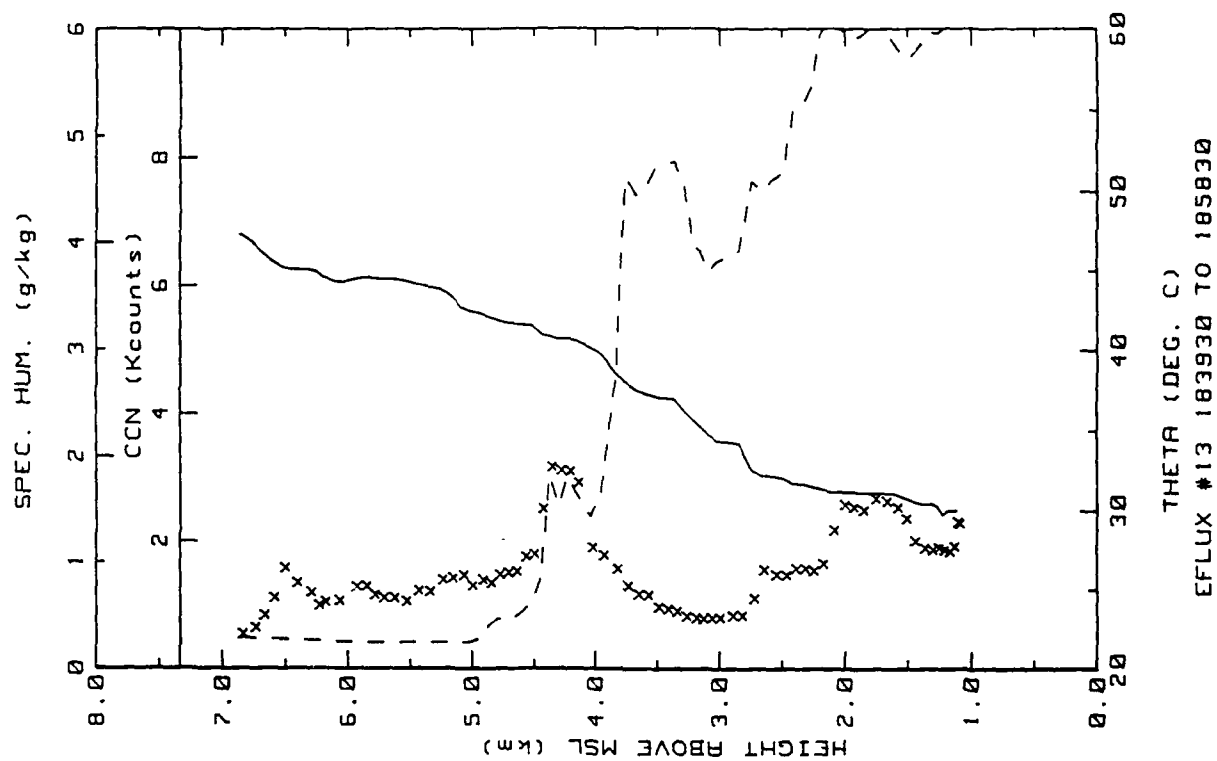
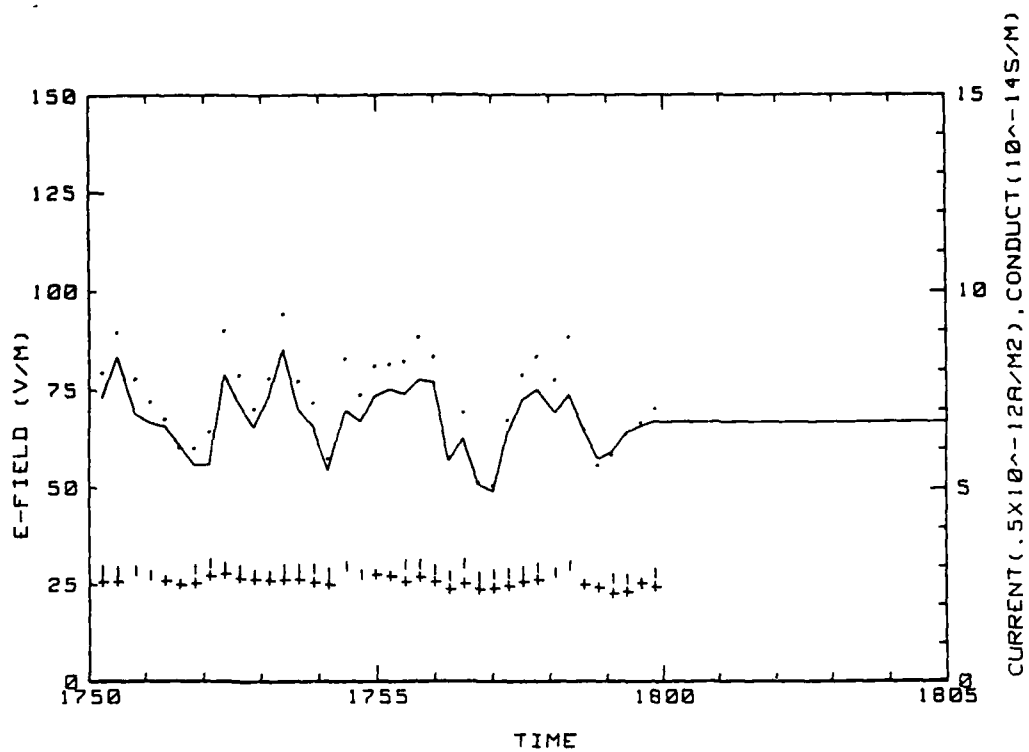
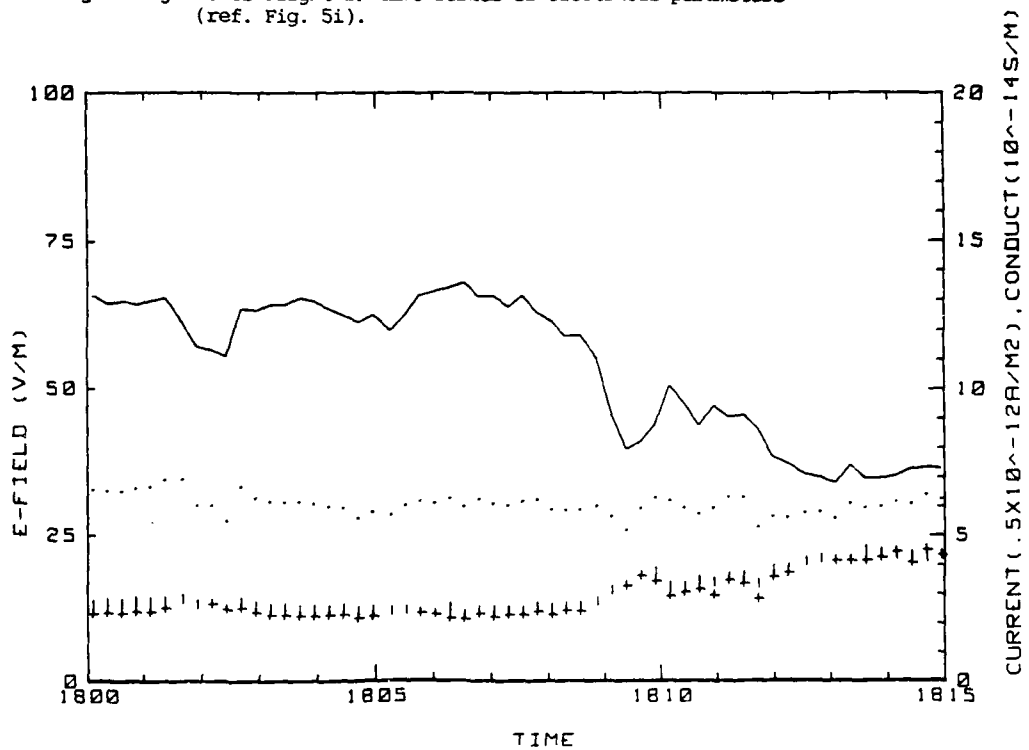


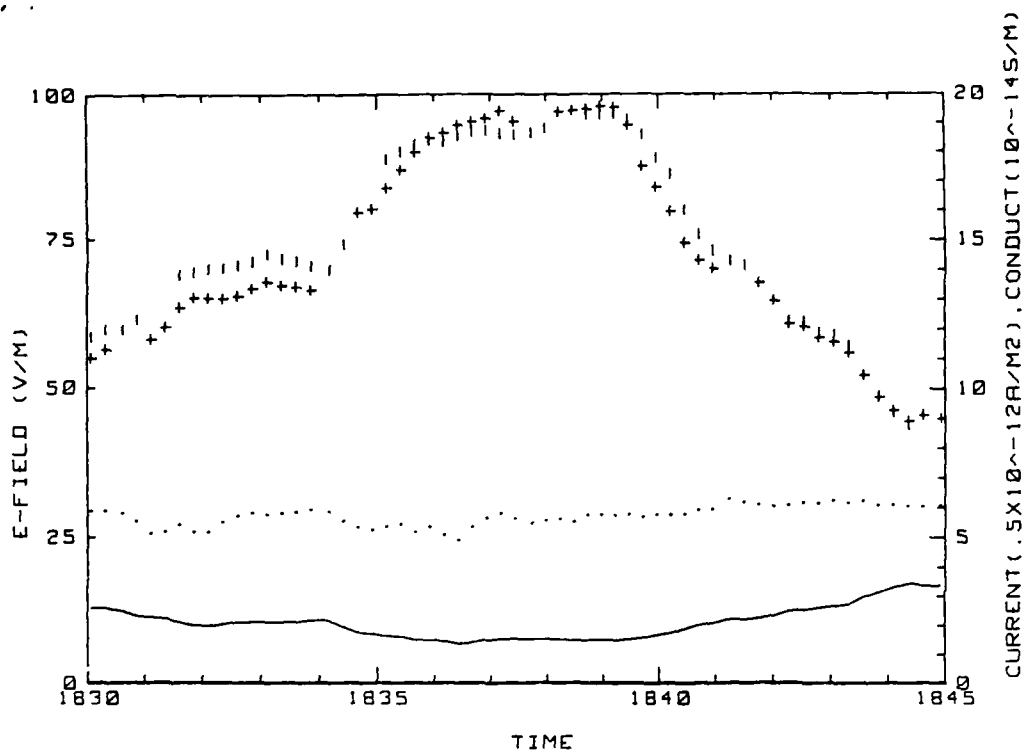
Figure 17i. Hobbs Flight 13 spiral downsonding (ref. Fig. 5h).



27 MAY 86 FLIGHT#13 175000 TO 180500 LST  
Figure 17j. Hobbs Flight 13 time series of electrical parameters  
(ref. Fig. 5i).

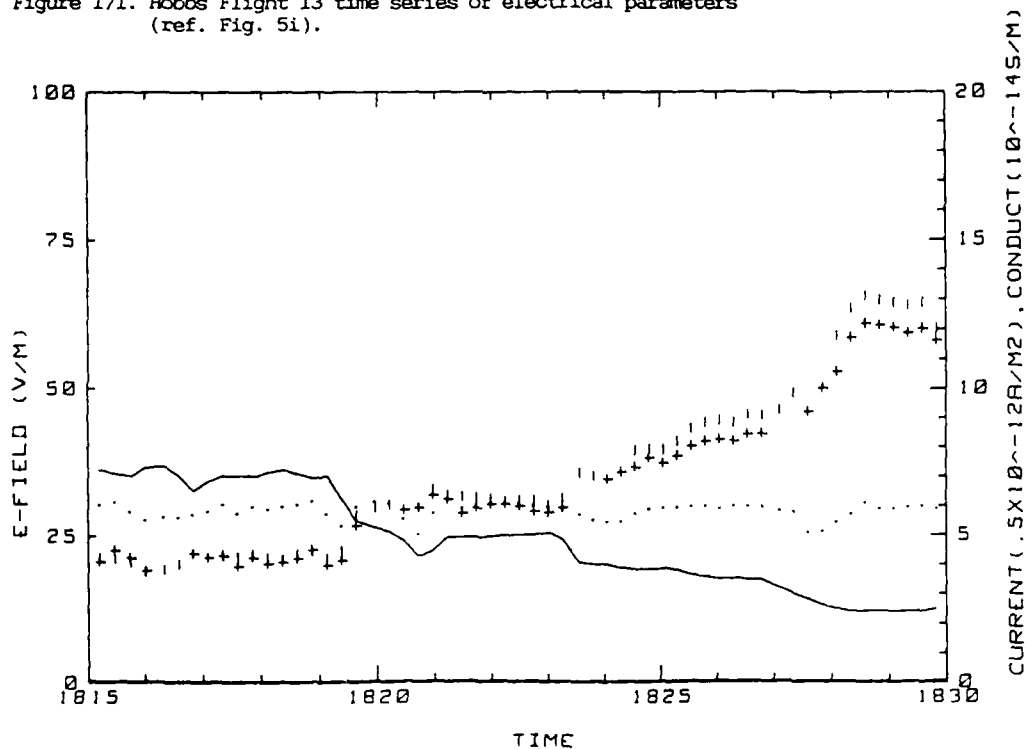


27 MAY 86 FLIGHT#13 180000 TO 181500 LST  
Figure 17k. Hobbs Flight 13 time series of electrical parameters  
(ref. Fig. 5i).



27 MAY 86 FLIGHT#13 183000 TO 184500 LST

Figure 17l. Hobbs Flight 13 time series of electrical parameters (ref. Fig. 5i).



27 MAY 86 FLIGHT#13 181500 TO 183000 LST

Figure 17m. Hobbs Flight 13 time series of electrical parameters (ref. Fig. 5i).

Flight: 14

Date: 28 May 1986

Takeoff: 0950 from Hobbs.

Landed: 1123 at Hobbs.

Conditions: Clear over Hobbs with cumulus clouds on the horizon. Winds were variable from the SE to SW at around 3 m/s. A layer of aerosols was evident at 4-6 km altitude. Convection was fairly intense for a morning flight.

Instrumentation: The positive conductivity tube was noisy during all the low passes.

Summary: A ladder profile was made on the ascent over the airport and was followed by a slow spiral descent into the same area. A series of low passes was executed over the ground station at the end of the flight.

Table 11a. Hobbs Flight 14 averages for constant altitude runs over the ground station. Conduction current densities calculated using only negative conductivity are included.

AVERAGES FROM LEVEL RUNS										Using $\lambda_-$ only	
Time HH:MM	N	Altitude km	Efield1 V/m	Efield2 V/m	$\lambda_{\text{low}}$ $10^{-14}$	$\lambda_{\text{low}}$ $10^{-14}$	Con Cur1 $10^{-12}$	Con Cur2 $10^{-12}$	theta_v C	Con Cur1 $10^{-12}$	Con Cur2 $10^{-12}$
1000	11	.006	107.27	105.99	1.56	1.54	3.32	3.29	21.6	3.32	3.27
1005	8	.015	95.45	93.23	1.56	1.90	3.37	3.25	22.0	3.33	3.33
1007	18	.061	104.99	103.47	1.44	1.38	2.92	2.60	21.1	2.65	2.65
1010	30	.031	92.75	97.77	1.36	1.27	2.60	2.57	19.9	2.51	2.49
1011	36	.151	99.08	92.37	1.24	1.17	2.25	2.23	19.8	2.18	2.15
1017	30	.950	68.48	68.28	1.50	1.40	1.95	1.95	21.9	1.89	1.89
1022	27	1.520	25.55	25.63	4.29	3.68	2.07	2.06	24.9	1.95	2.00
1024	35	2.181	22.97	23.32	5.15	4.65	2.26	2.29	27.7	2.13	2.17
1028	30	2.760	14.04	24.33	4.58	4.68	2.23	2.25	30.8	2.25	2.28
1031	35	3.383	15.83	16.29	6.43	6.82	2.10	2.15	34.1	2.15	2.22
1035	44	3.992	11.69	12.27	8.47	8.90	2.05	2.13	36.8	2.17	2.19
1040	37	5.000	7.79	8.32	13.05	13.74	2.11	2.25	45.4	2.11	2.20
1046	16	5.871	6.52	6.93	16.12	17.19	2.17	2.31	50.5	2.24	2.30
1112	10	.006	95.34	95.94	1.33	1.38	2.78	2.74	22.6	3.24	3.20
1113	25	.031	101.50	100.35	1.28	1.26	2.53	2.57	22.1	2.58	2.55
1116	22	.061	102.49	101.12	1.21	1.26	2.53	2.52	23.2	2.57	2.54
1118	18	.163	99.22	98.56	1.23	1.19	2.39	2.38	22.6	2.36	2.34
1120	31	.324	95.36	94.36	1.16	1.07	2.13	2.11	23.0	2.05	2.00

Time HH:MM	N	Press mB	Rel num %	CCN k/cc	U <sub>1</sub> m2/s2	U <sub>2</sub> m2/s2	Q g/kg	T <sub>rose</sub> C	T <sub>IR</sub> C	T <sub>dev</sub> C
1000	11	888	36.3	8.5	1.01E+00	7.53E-01	6.12	20.5	34.6	5.0
1005	8	883	34.7	8.5	4.11E-01	4.47E-01	5.36	20.8	34.7	4.6
1007	18	880	37.1	9.3	1.92E-02	2.75E-02	5.89	19.4	35.5	4.4
1010	30	886	38.6	9.5	1.22E-02	5.99E-03	5.78	18.5	35.2	4.2
1011	36	872	41.2	10.5	1.05E-02	4.53E-02	5.78	17.3	35.2	4.0
1017	30	792	52.4	7.1	4.95E-01	2.11E-01	5.52	11.3	34.4	1.9
1022	27	731	38.7	7	3.52E-04	5.17E-04	3.55	8.1	35.7	-5.1
1024	35	673	60.7	7	2.31E-04	6.87E-04	4.35	4.1	35.2	-2.6
1028	30	621	64.9	5	5.47E-05	1.71E-04	4.09	4	34.6	-5.4
1031	35	552	55.8	5	1.23E-05	4.23E-04	2.97	-3.3	34.2	-10.7
1035	44	518	52.1	5	1.84E-05	5.16E-04	2.10	-8.0	34.9	-16.6
1040	37	442	37.6	5	5.15E-05	9.39E-04	73	-12.5	34.6	-25.1
1046	16	377	34.3	7	1.24E-05	9.27E-04	70	-20.1	36.7	-31.9
1112	10	835	31.4	20.5	3.83E-01	3.30E-01	5.73	21.7	41.4	4.3
1113	25	816	32.3	20.3	6.41E-02	7.52E-02	5.56	20.8	42.8	3.5
1116	22	801	23.1	25.3	4.12E-02	4.41E-02	5.65	20.5	43.1	3.8
1118	18	770	23.1	25.4	2.70E-02	1.50E-02	5.54	20.2	42.9	3.6
1120	31	655	33.7	24.5	1.57E-02	7.91E-03	5.61	18.9	42.9	3.3

Table 11b. Hobbs Flight 14 (standard deviations)/averages for constant altitude runs over the ground station. Conduction current densities calculated using only negative conductivity are included.

STANDARD DEVIATIONS/MEAN VALUES

Using  
 $\lambda$ - only

Time	Efield1	Efield2	$\lambda_{1am}$	$\lambda_{2am}$	Concur1	Concur2	CCN	EPS	C12	G	Concur1	Concur2
1000	.070	.071	.079	.073	.119	.124	.045	.649	.431	.014	.113	.117
1005	.070	.059	.056	.102	.296	.272	.005	.466	.325	.013	.191	.152
1007	.034	.034	.113	.089	.085	.091	.049	.298	.297	.020	.033	.097
1010	.038	.039	.231	.066	.143	.144	.073	.374	.587	.018	.004	.085
1011	.049	.050	.500	.123	.266	.266	.132	.236	.558	.017	.119	.114
1017	.078	.077	.406	.325	.291	.287	.393	.686	.351	.059	.259	.255
1022	.093	.091	.085	.032	.107	.107	.067	.615	.475	.118	.039	.057
1024	.034	.032	.072	.026	.044	.043	.069	.804	.471	.018	.029	.027
1028	.026	.025	.127	.011	.066	.070	.050	.287	.503	.002	.020	.021
1031	.029	.030	.032	.010	.035	.036	.062	.401	.550	.026	.053	.034
1035	.062	.062	.031	.015	.069	.071	.063	.785	.340	.036	.065	.065
1040	.032	.045	.027	.022	.024	.030	.114	.534	.407	.117	.022	.031
1045	.030	.022	.005	.003	.029	.023	.050	.154	.175	.007	.025	.023
1112	.044	.034	.072	.063	.119	.112	.003	.353	.345	.012	.106	.090
1113	.035	.037	.321	.050	.193	.195	.003	.535	.312	.012	.065	.085
1116	.043	.041	.509	.072	.384	.384	.006	.702	.519	.012	.040	.060
1118	.017	.015	.522	.054	.222	.225	.013	.305	.201	.010	.053	.055
1020	.038	.037	.207	.077	.125	.124	.055	.456	.409	.012	.056	.053

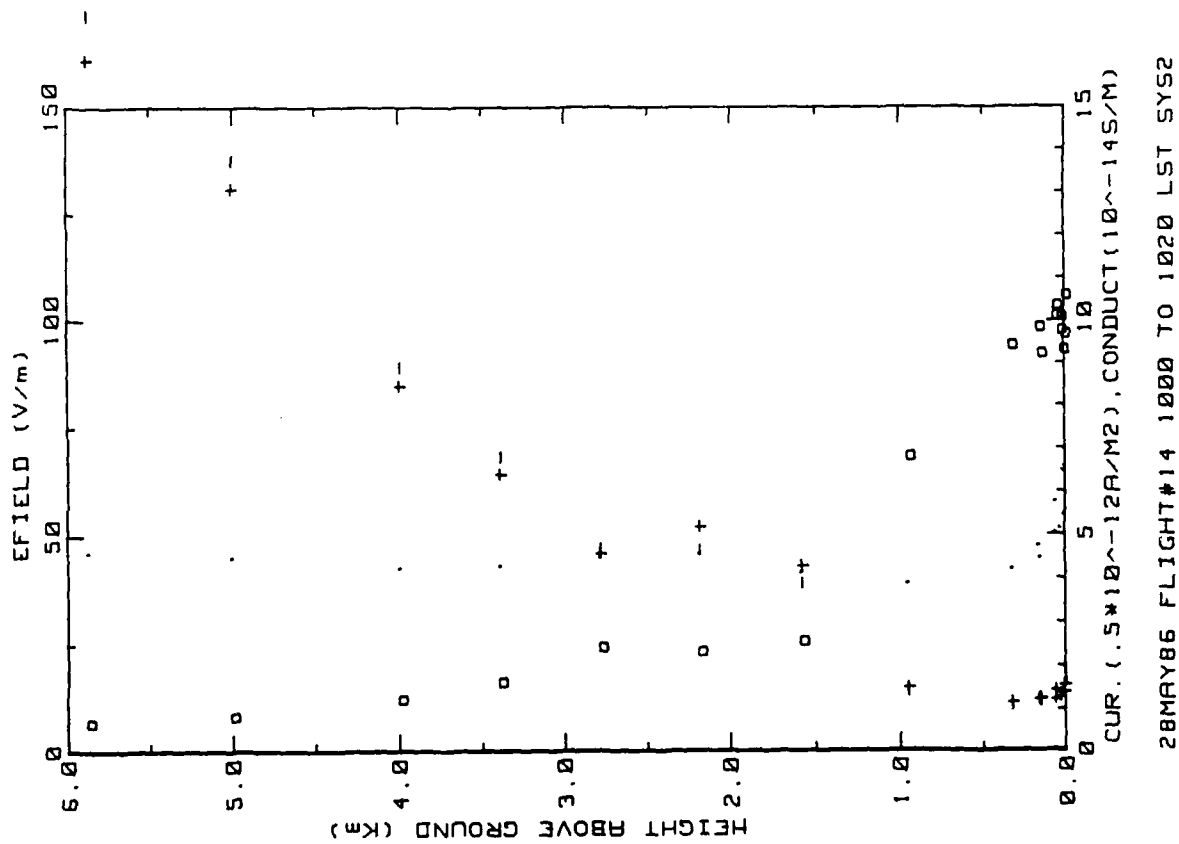


Figure 18a. Hobbs Flight 14 ladder profile (ref. Fig. 5a)

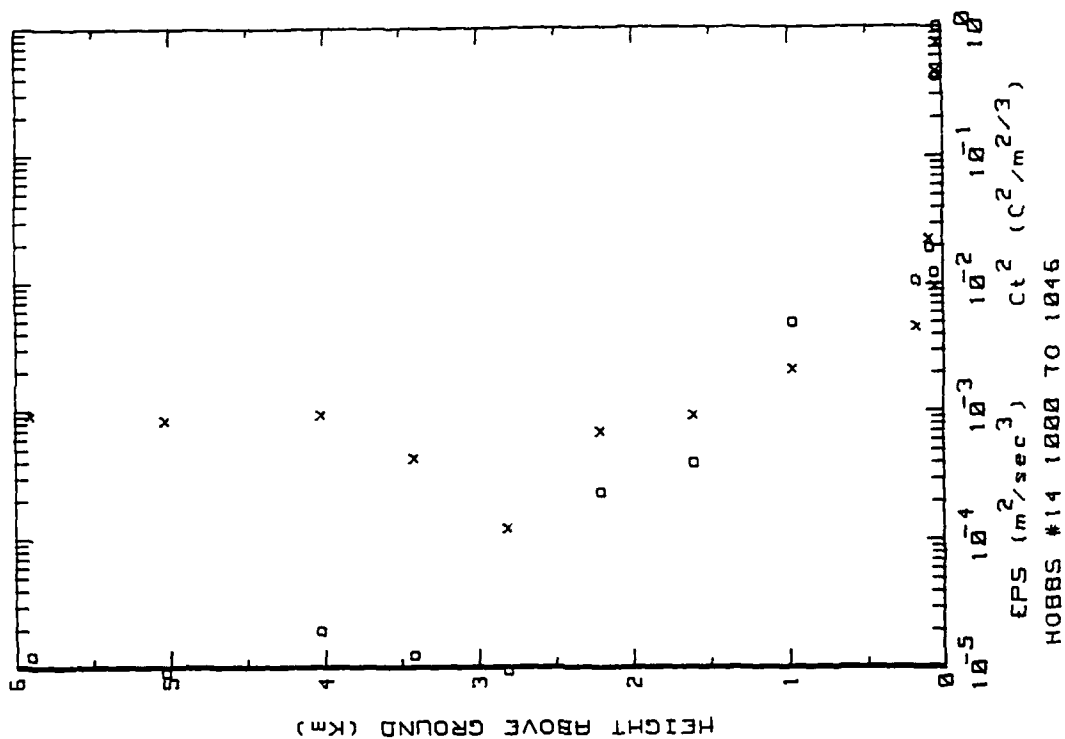


Figure 18b. Hobbs Flight 14 ladder profile (ref. Fig. 5b).



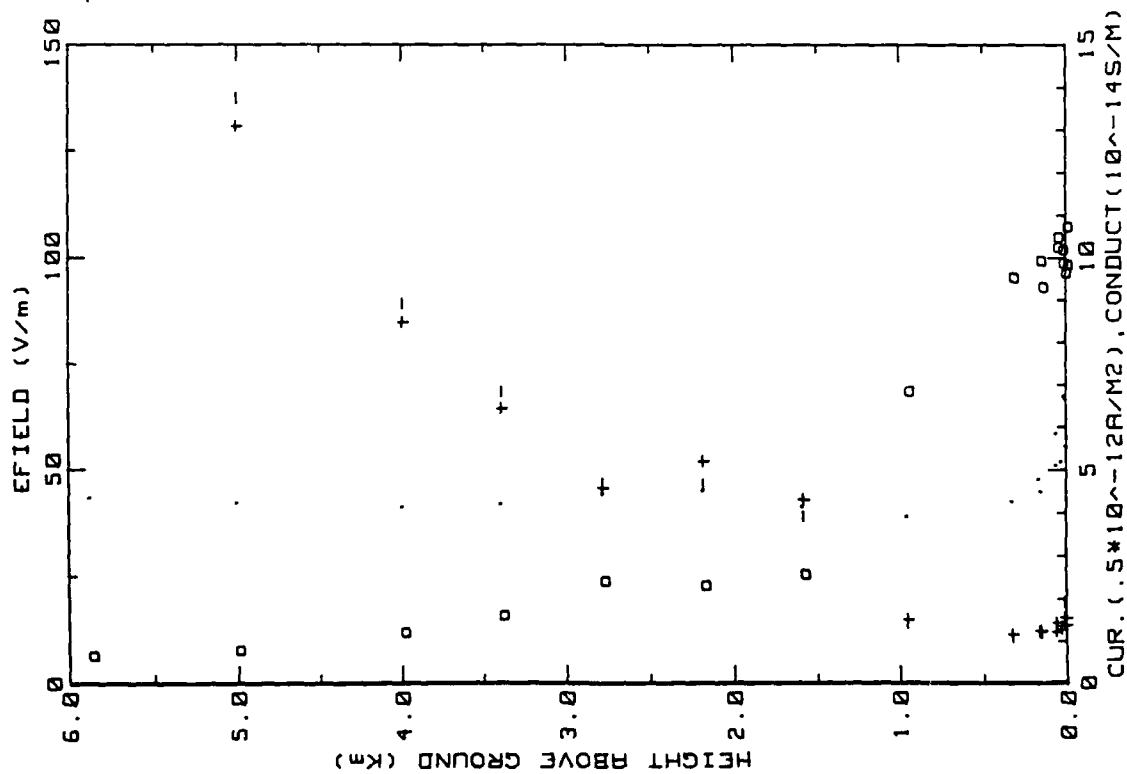


Figure 18c. Similar to 18a. but for outboard E<sub>field</sub> system.

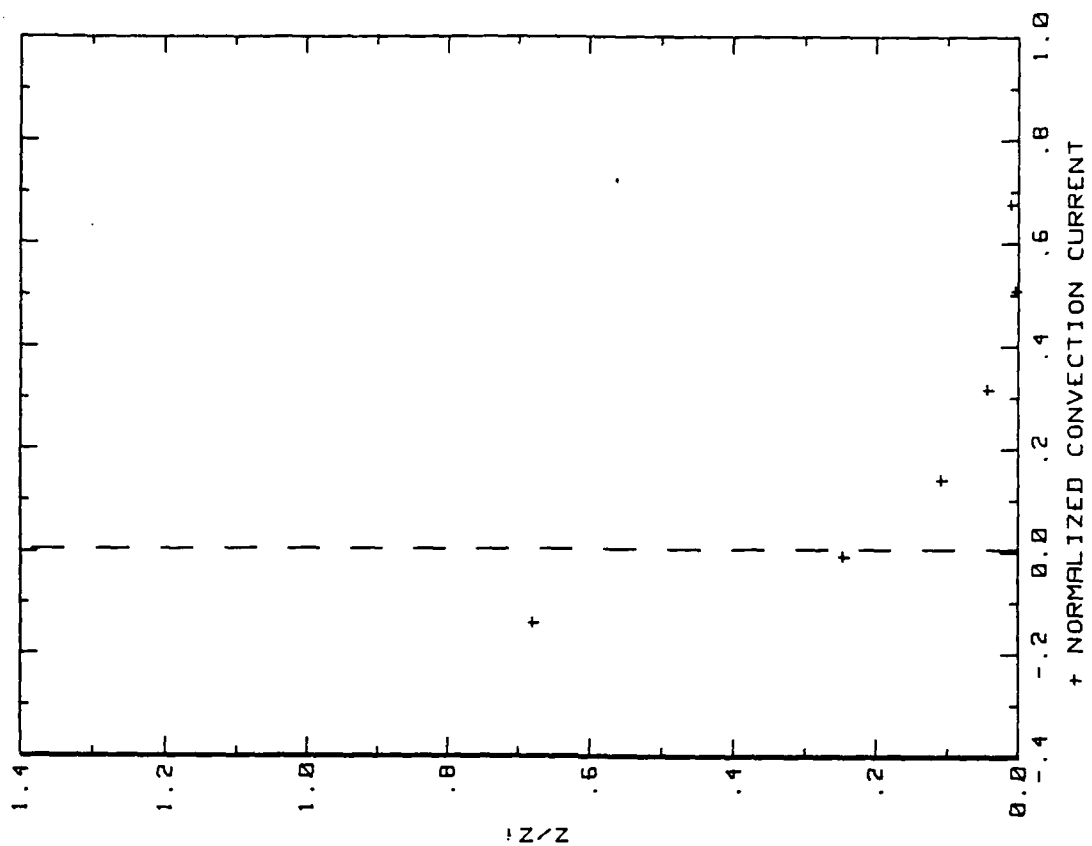


Figure 18d. Hobbs Flight 14 convection current profile (ref. Fig. 5d).

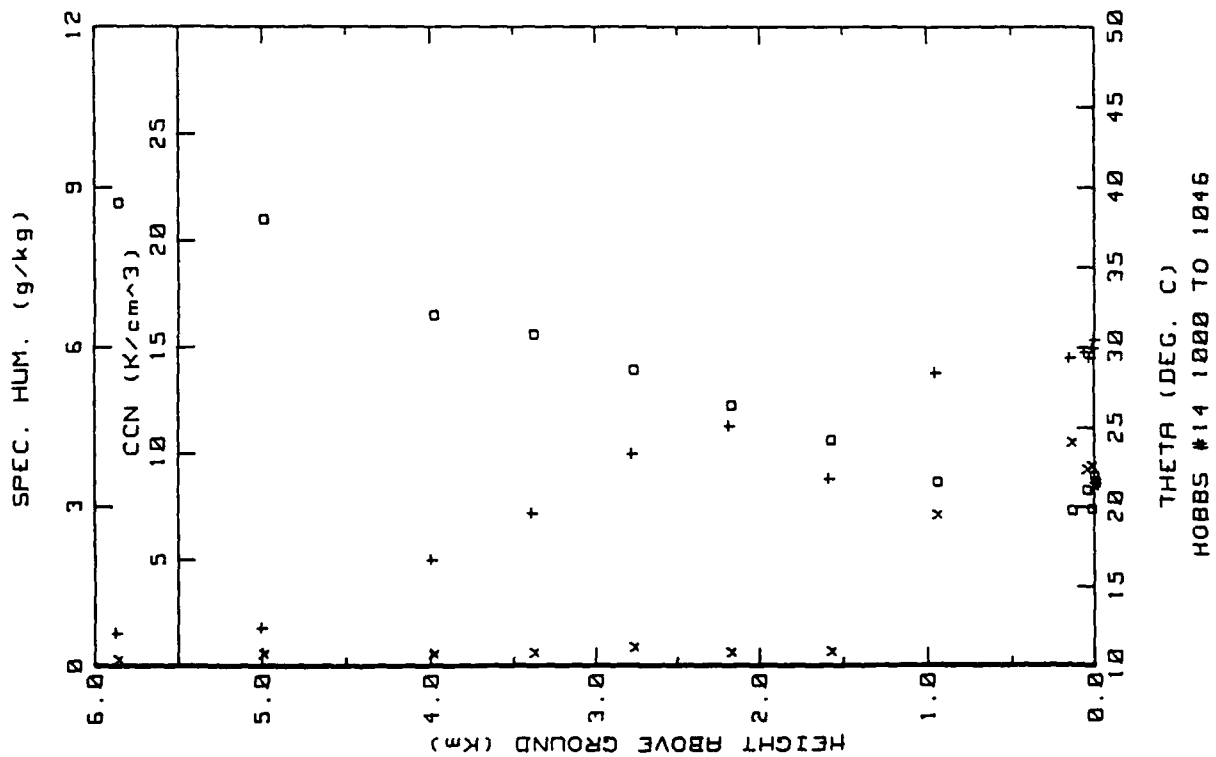


Figure 18a. Hobbs Flight 14 ladder profile (ref. Fig. 5c).

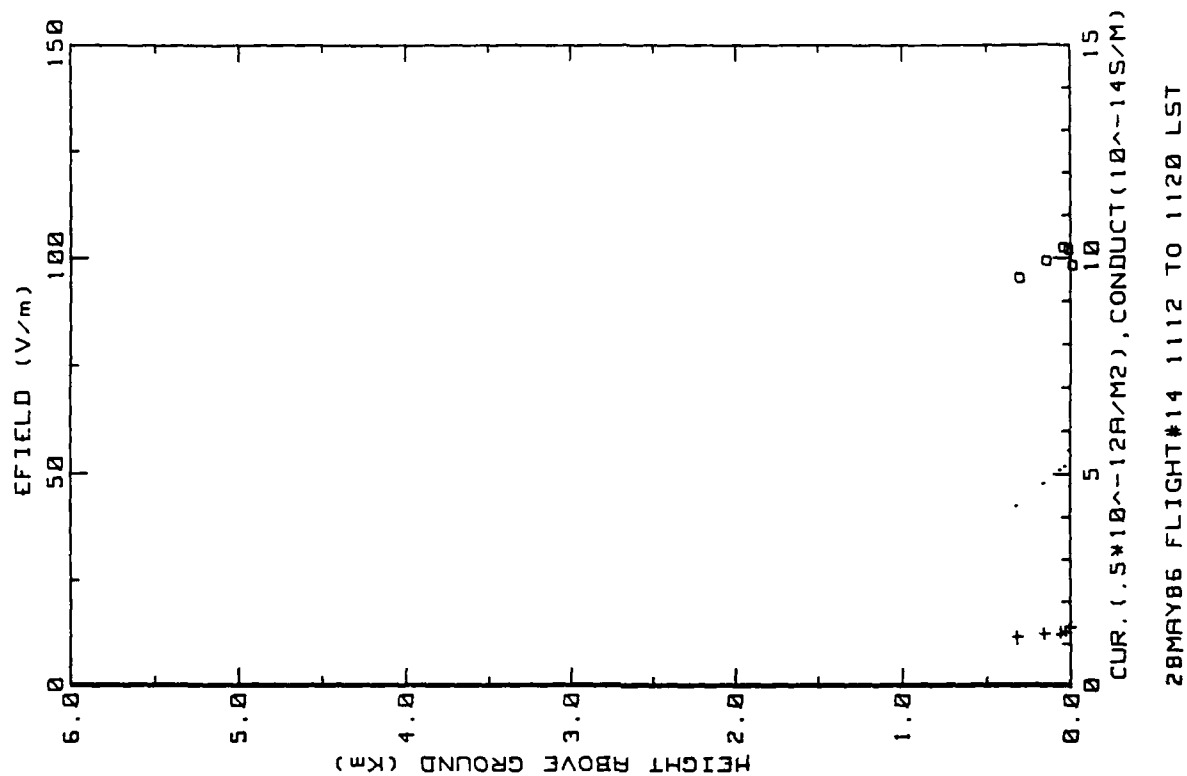
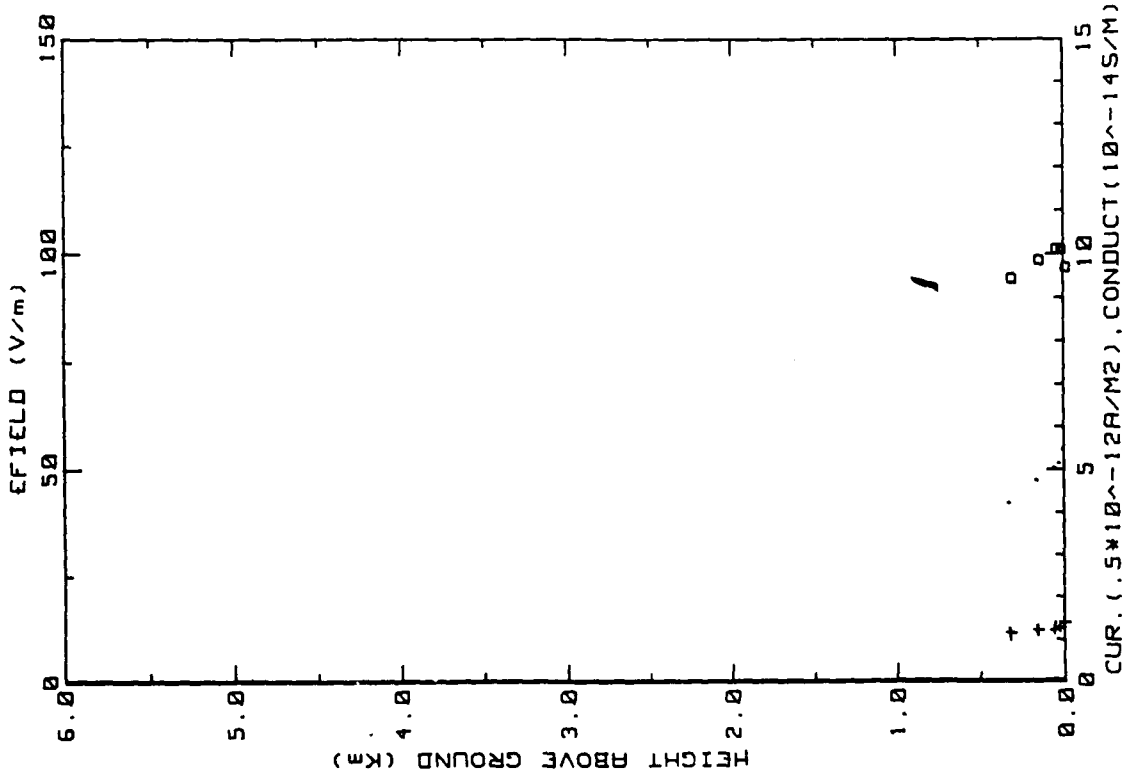


Figure 18f. Hobbs Flight 14 ladder profile (ref. Fig. 5a)



28MAY86 FLIGHT#14 1112 TO 1120 LST SYS2

Figure 18g. Similar to 18f, but for inboard E-field system.

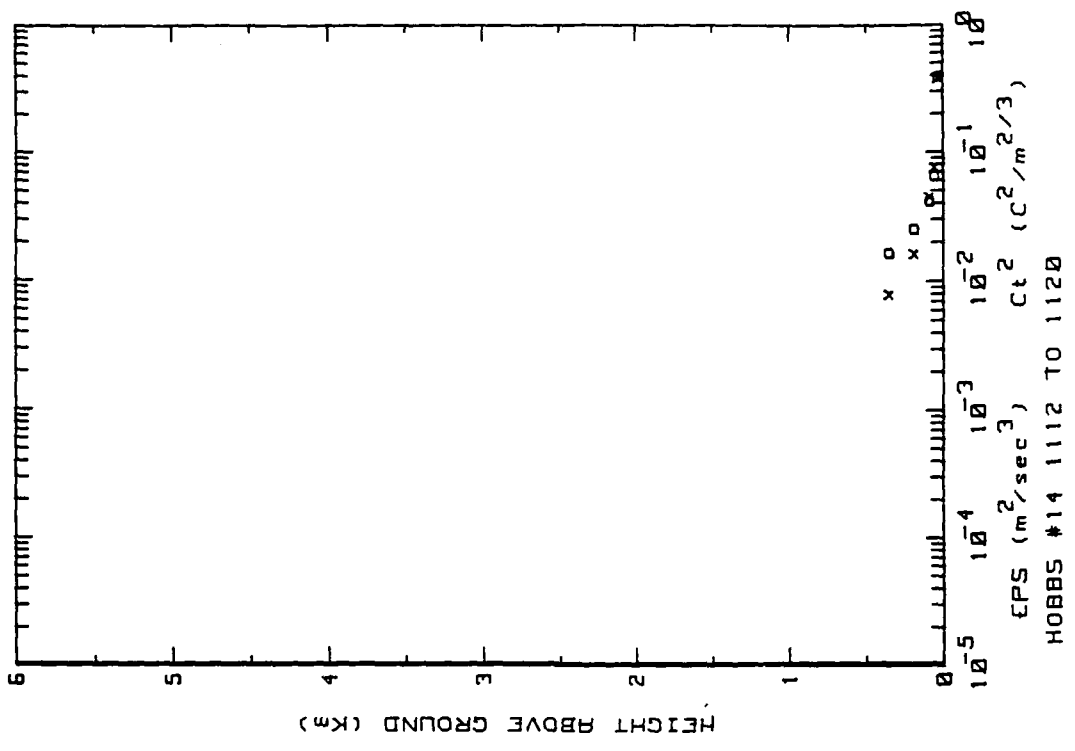


Figure 18h. Hobbs Flight 14 ladder profile (ref. Fig. 5b).

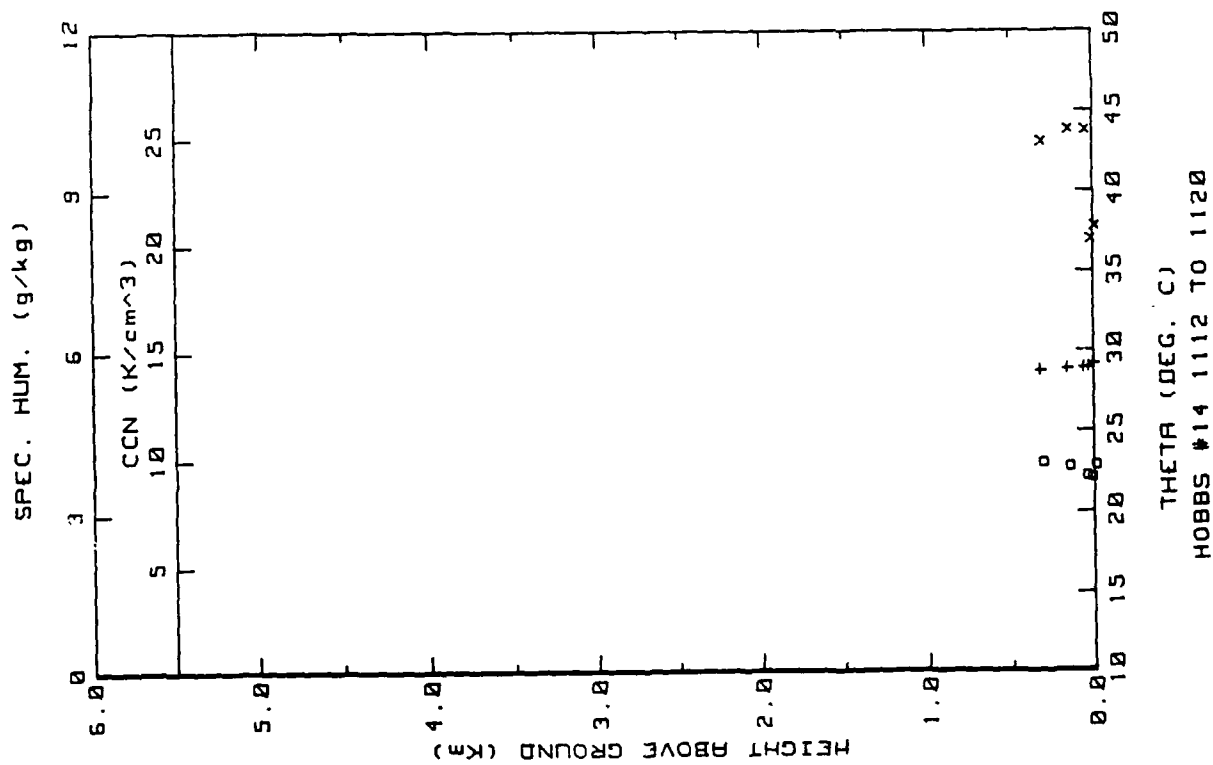


Figure 18i. Hobbs Flight 14 ladder profile (ref. Fig. 5c).

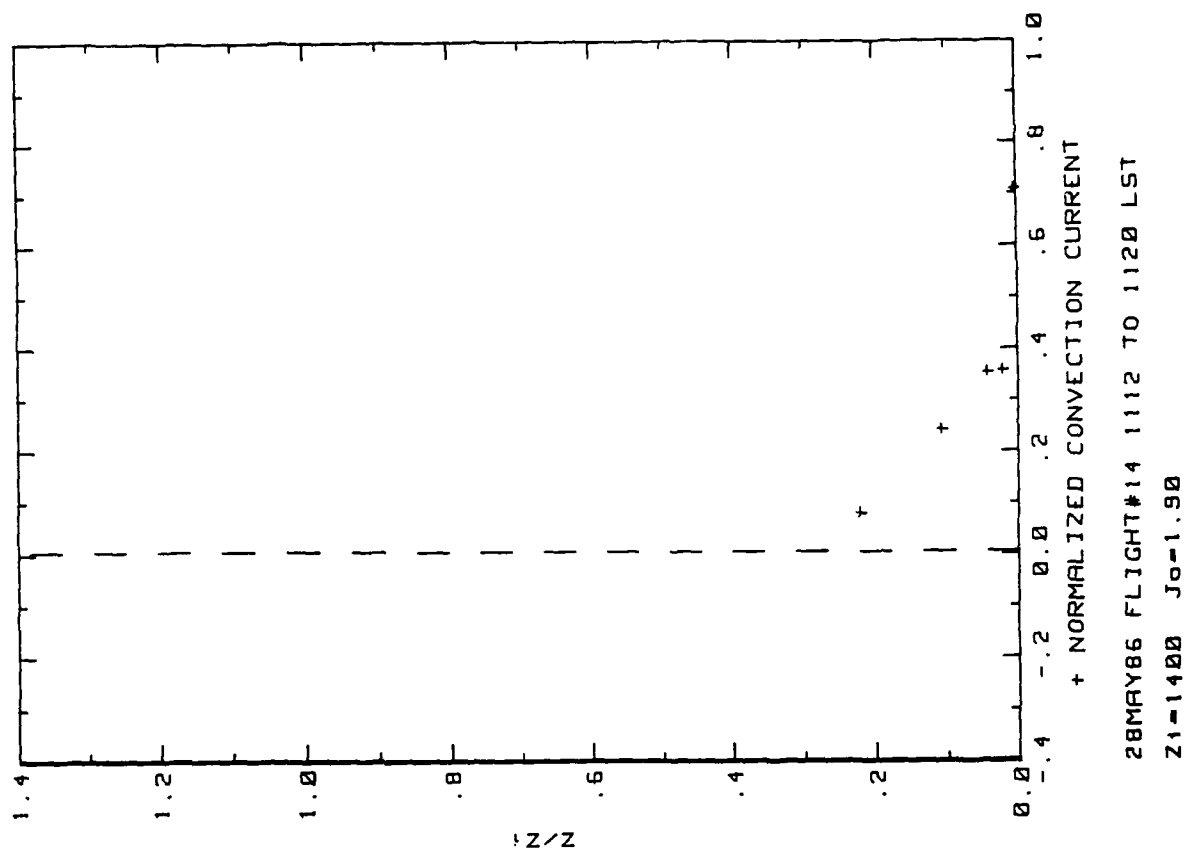


Figure 18j. Hobbs Flight 14 convection current profile (ref. Fig. 5d).

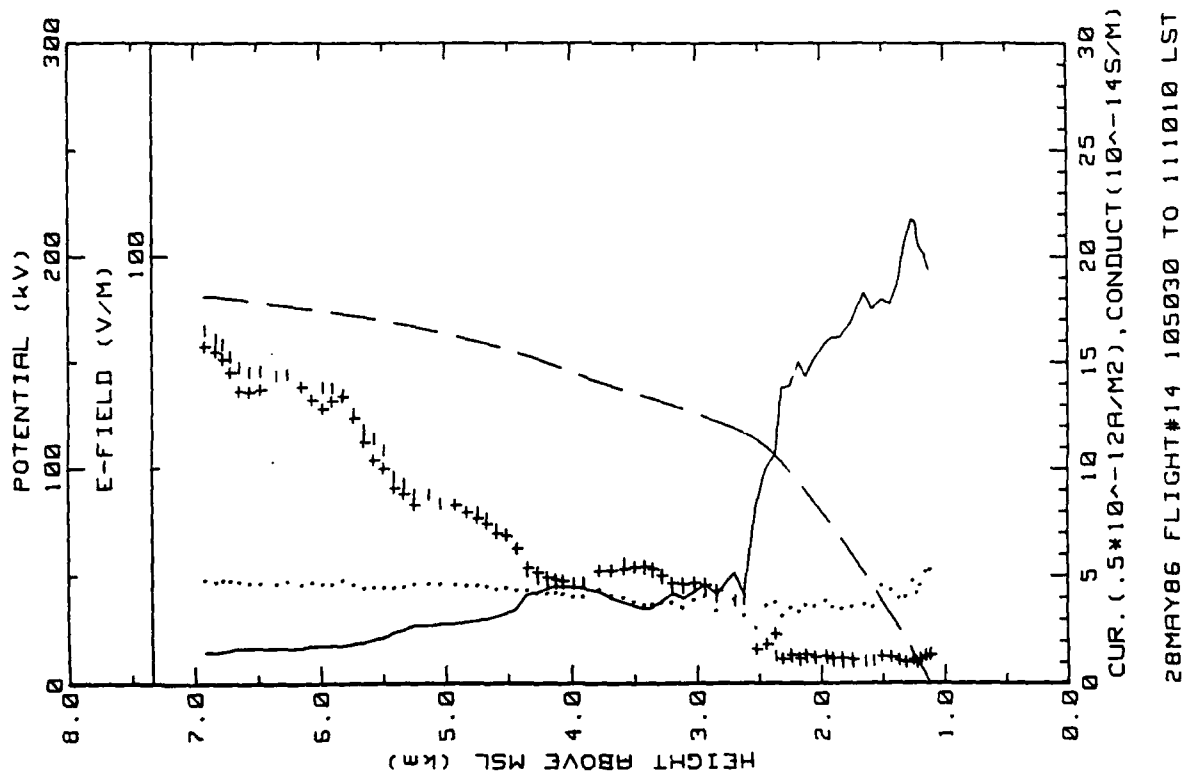


Figure 18k. Hobbs Flight 14 spiral downsonding (ref. Fig. 5e).

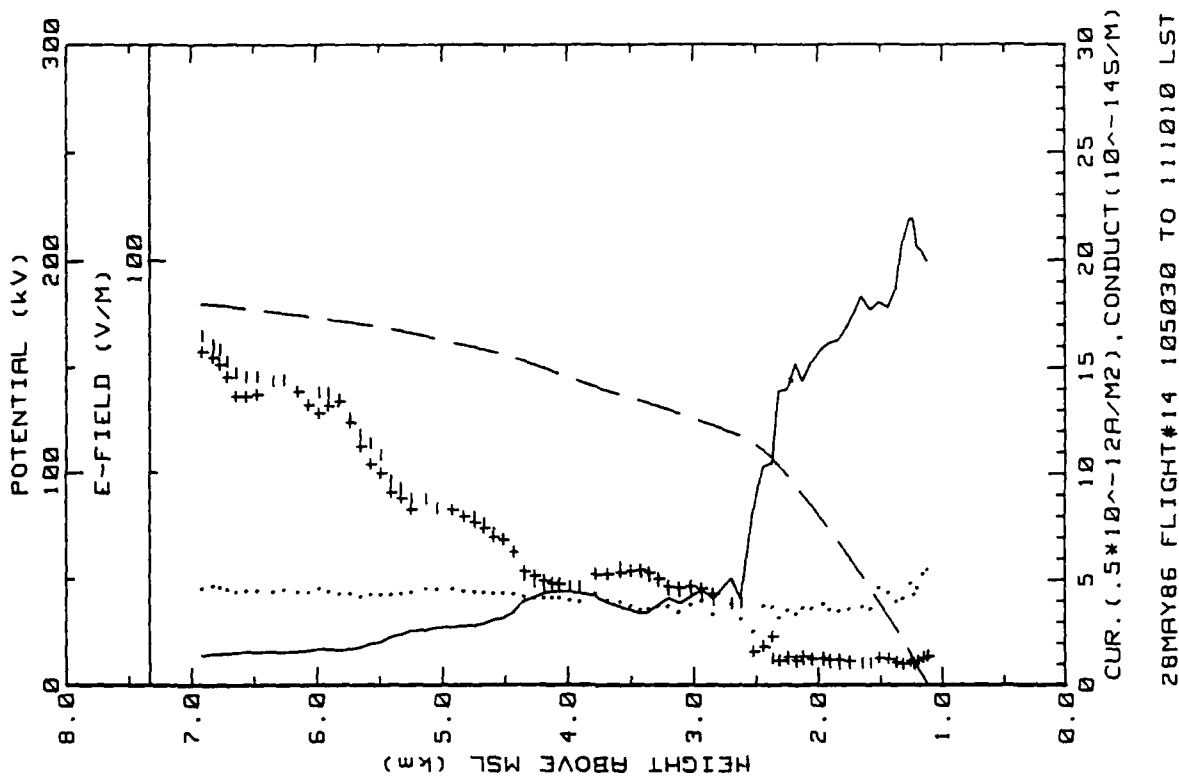


Figure 18l. Same as Fig. 18k but for outboard E-field system.

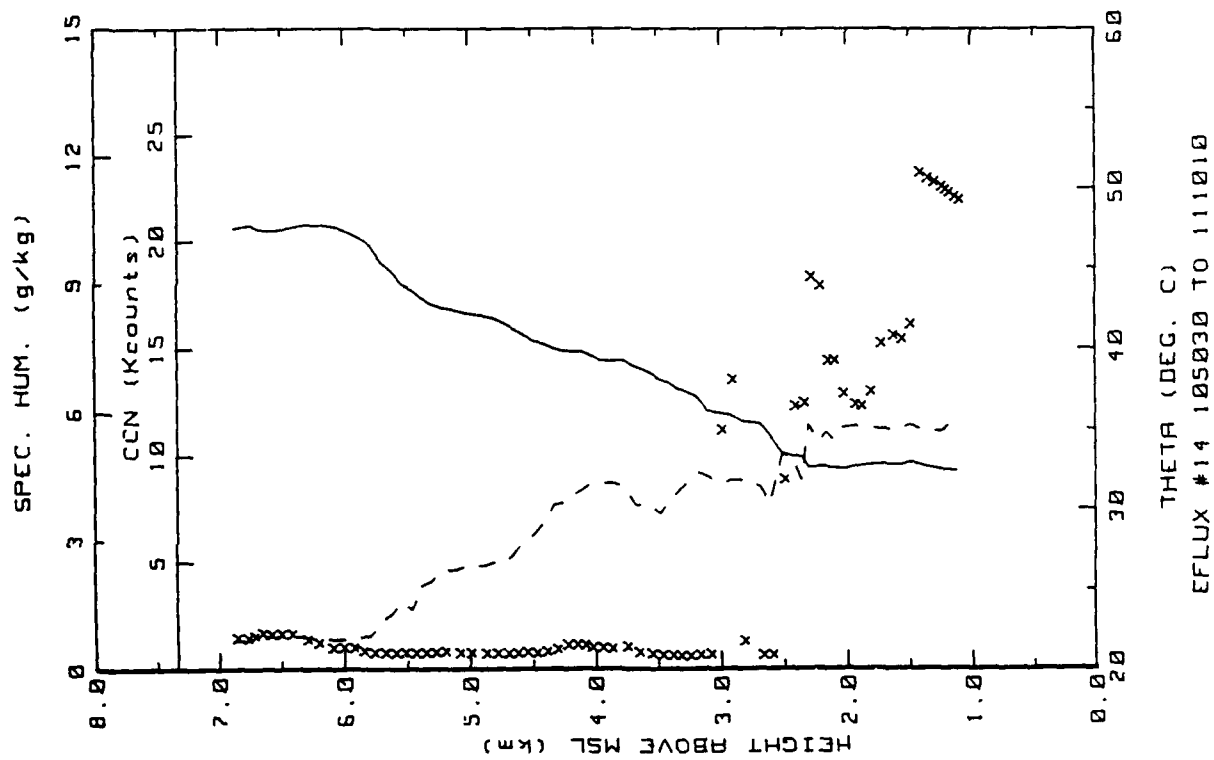


Figure 18m. Hobbs Flight 14 spiral downsonding (ref. Fig. 5h).

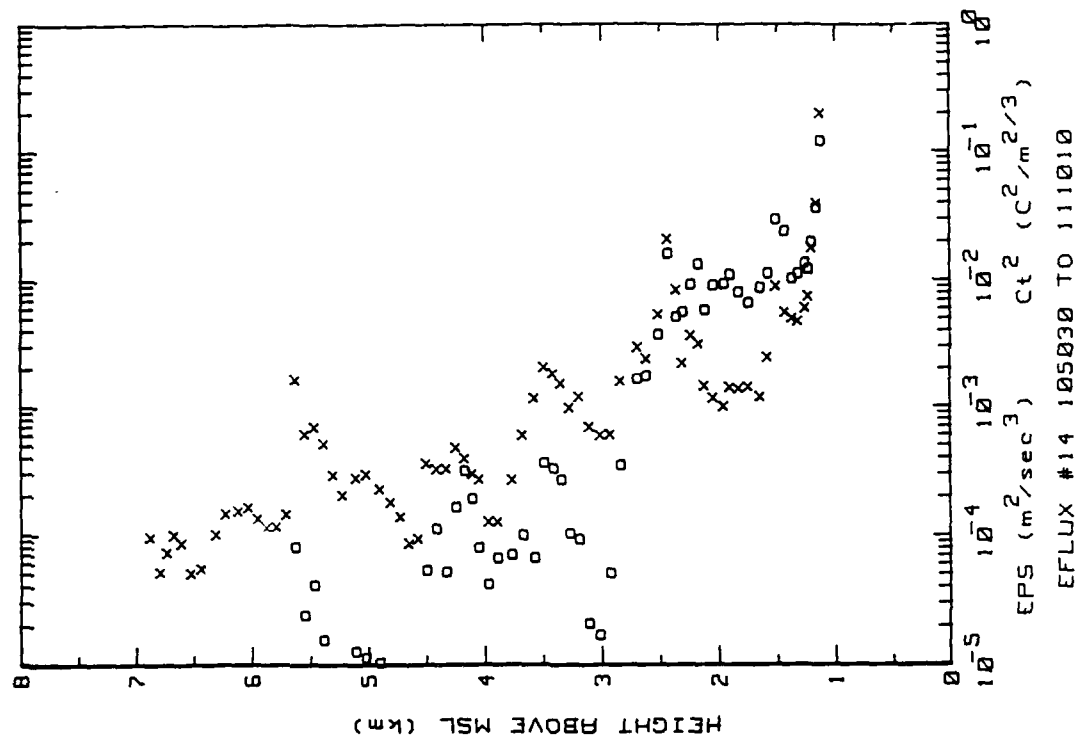


Figure 18n. Hobbs Flight 14 spiral downsonding (ref. Fig. 5b).

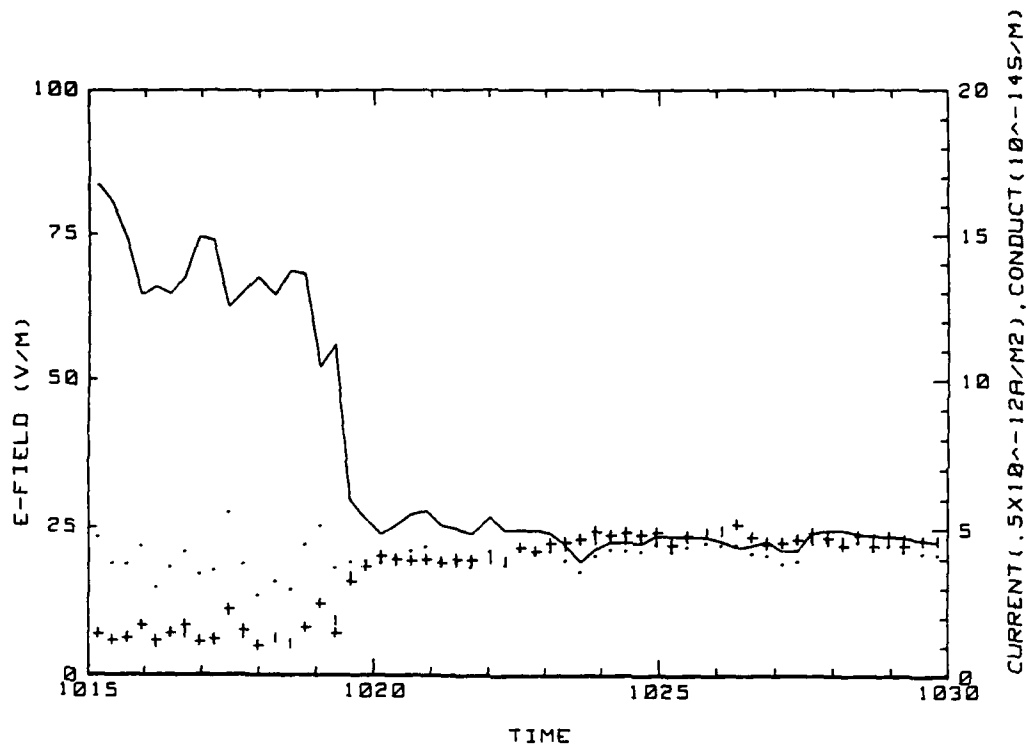


Figure 18o. Hobbs Flight 14 time series of electrical parameters  
(ref. Fig. 5i).

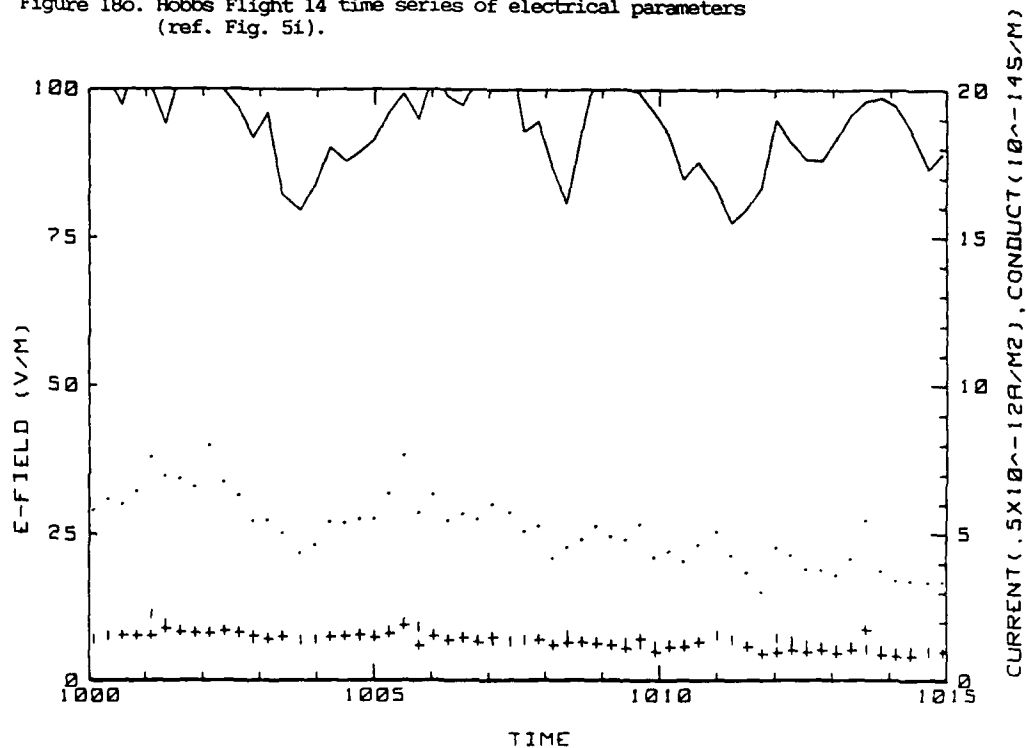
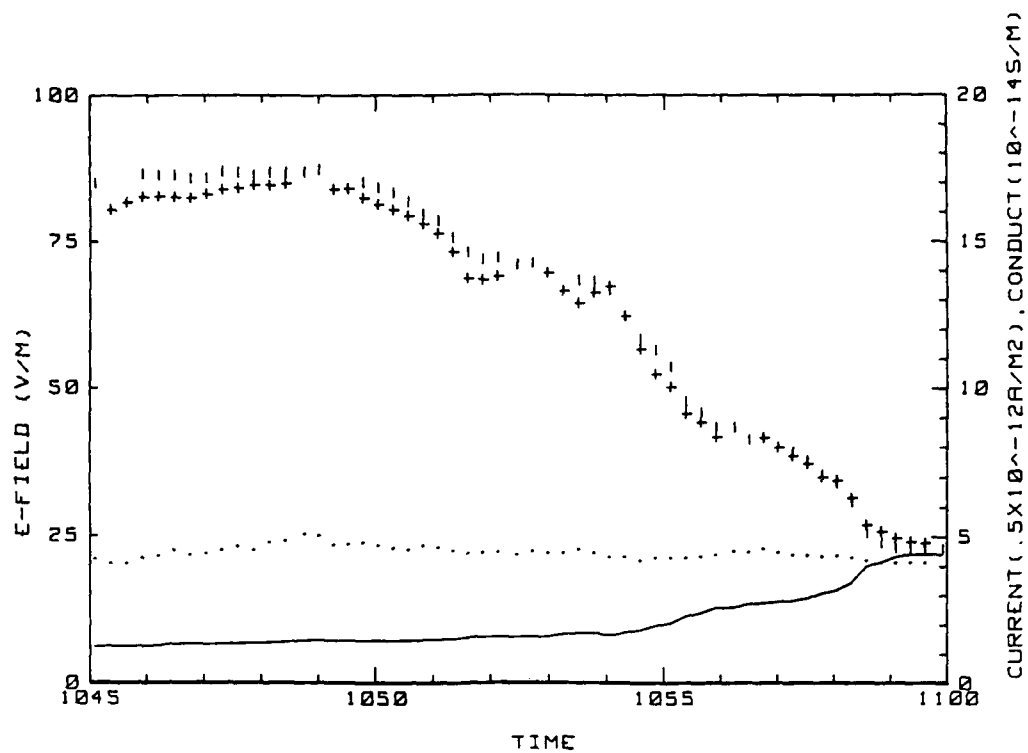
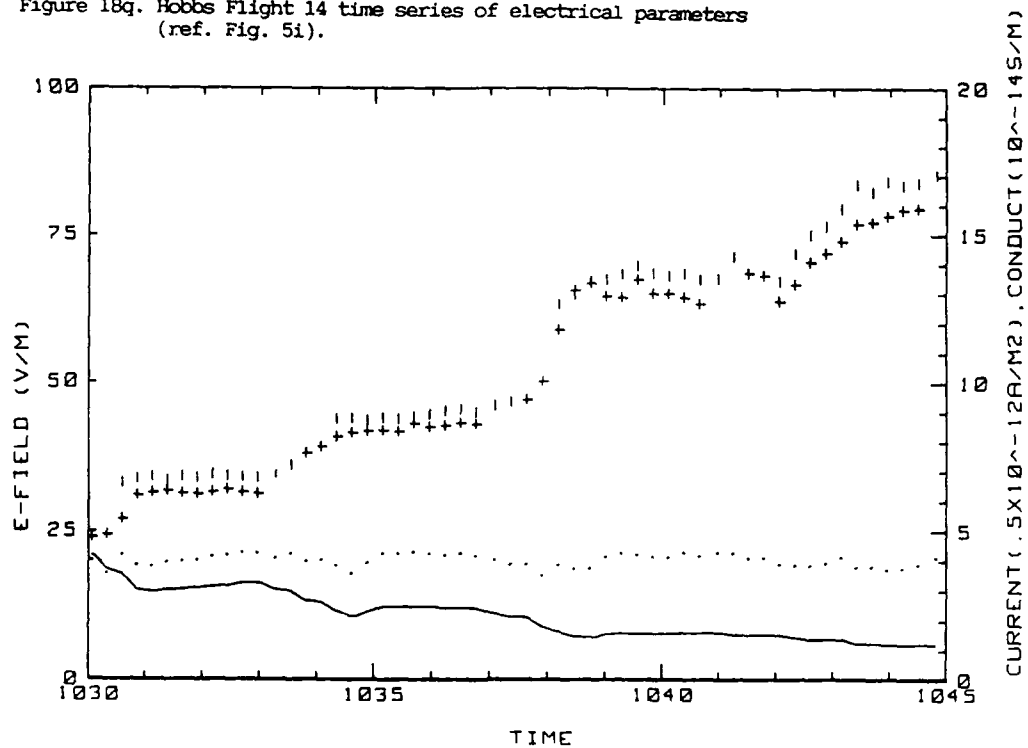


Figure 18p. Hobbs Flight 14 time series of electrical parameters  
(ref. Fig. 5i).



28 MAY 86 FLIGHT#14 104500 TO 110000 LST

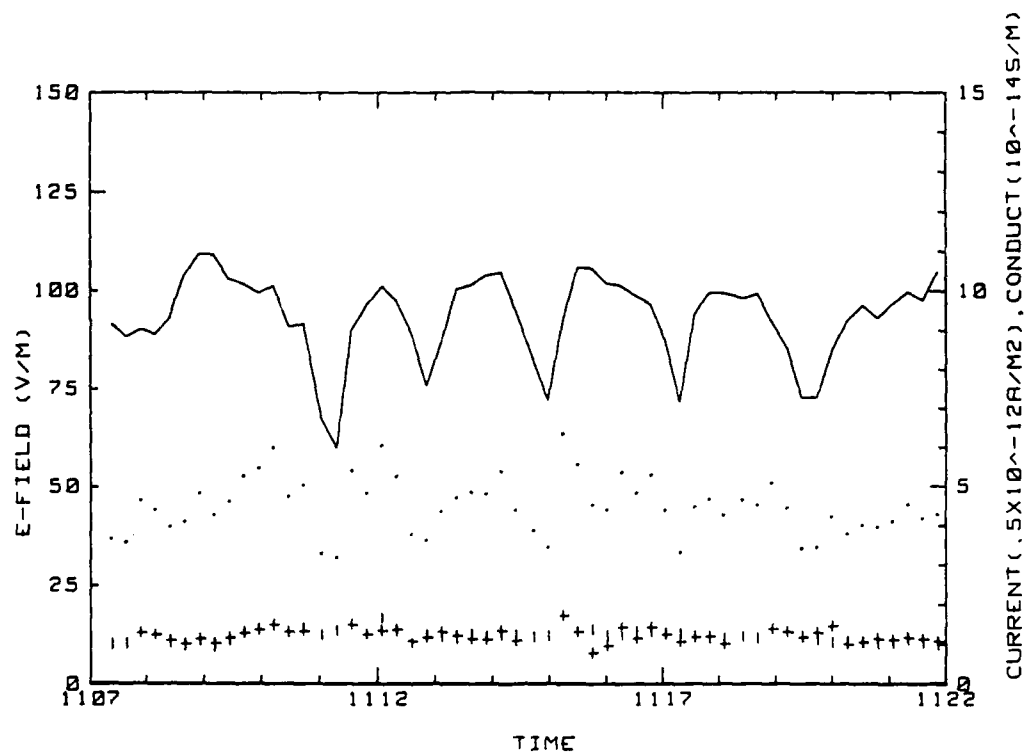
Figure 18q. Hobbs Flight 14 time series of electrical parameters (ref. Fig. 5i).



28 MAY 86 FLIGHT#14 103000 TO 104500 LST

Figure 18r. Hobbs Flight 14 time series of electrical parameters (ref. Fig. 5i).





28 MAY 86 FLIGHT#14 110700 TO 112200 LST

Figure 18s. Hobbs Flight 14 time series of electrical parameters  
(ref. Fig. 5i).

Flight: 15

Date: 28 May 1966

Takeoff: 1428 LT from Hobbs.

Landed: 1603 at Hobbs.

Conditions: Altocumulus covered about 1/4 of the sky N of Hobbs and scattered cumulus with 3.9 km bases and 4.6 km tops were present over Hobbs. Winds were variable from SE-SW at 3-7 m/s; several dust devils formed over the burned area adjacent to runway 21. Visibility was fair.

Instruments: The positive conductivity tube was noisy.

Summary: The flight consisted of low passes over the ground station, a ladder profile to 7 km, a slow spiral descent over the Hobbs airport and more passes over the ground station, in that order. A bumpy ride indicated good convection both near the ground and at the inversion.

Table 12a. Hobbs Flight 15 averages for constant altitude runs over the ground station. Conduction current densities calculated using only negative conductivity are included.

Using  $\lambda$ .  
only

AVERAGES FROM LEVEL RUNS

Time HHMM	N	Altitude km	Efield1 V/m	Efield2 V/m	+Lam 10 <sup>-14</sup>	-Lam 10 <sup>-14</sup>	Con Cur1 10 <sup>-12</sup>	Con Cur2 10 <sup>-12</sup>	Theta_v C	Con Cur1 10 <sup>-12</sup>	Con Cur2 10 <sup>-12</sup>
1431	16	.061	109.33	106.58	.62	.97	1.74	1.69	25.7	2.12	2.07
1435	15	.006	108.40	106.95	.97	.89	2.02	1.93	24.6	1.94	1.91
1437	16	.031	110.59	108.97	1.18	.58	2.58	2.54	24.5	2.19	2.16
1439	16	.195	113.15	111.44	1.11	.77	2.12	2.09	25.1	1.73	1.71
1442	23	.349	109.49	108.15	.92	.88	1.95	1.93	25.1	1.93	1.91
1445	33	.970	101.72	100.18	.73	.63	1.39	1.37	25.0	1.29	1.27
1449	26	1.504	96.03	85.12	.94	.72	1.42	1.40	26.1	1.24	1.22
1453	19	2.228	26.85	26.68	2.35	2.16	1.17	1.16	28.9	1.12	1.11
1458	66	2.955	19.00	19.06	3.38	3.31	1.28	1.28	32.0	1.29	1.30
1504	43	3.877	7.29	7.74	7.85	8.63	1.20	1.28	36.5	1.26	1.34
1511	45	5.090	4.66	5.17	13.96	14.44	1.31	1.46	46.3	1.30	1.45
1547	16	.031	102.72	101.22	.92	.81	1.80	1.79	24.0		
1550	17	.151	103.40	101.25	.92	.66	1.84	1.80	24.7		
1551	20	.236	116.89	114.54	.51	.56	1.23	1.21	25.0		
1554	19	.620	105.49	104.10	.64	.52	1.21	1.19	25.4		
1556	26	.930	103.17	101.64	1.00	.59	1.65	1.62	25.4		

Time HHMM	N	Press mb	Rel Hum %	CCN k/cc	EPS m2/s3	CT C2/m2/3	Q g/kg	Trose C	T <sub>IR</sub> C	T <sub>dew</sub> C
1431	16	880	27.3	17.5	1.16E+00	5.91E-01	5.77	24.0	47.1	4.0
1435	15	805	28.1	16.5	5.69E-01	4.32E-01	5.74	23.5	47.1	4.1
1437	16	803	28.4	17.9	7.00E-02	7.32E-02	5.68	23.2	47.3	3.9
1439	16	863	29.6	18.7	1.89E-02	1.04E-02	5.67	22.1	46.6	3.6
1442	23	350	31.8	19.7	1.22E-02	4.82E-03	5.65	20.7	46.1	3.3
1445	33	789	44.6	17.6	1.12E-02	1.83E-03	5.70	14.2	43.8	2.3
1449	26	725	59.6	21.7	2.12E-02	3.42E-03	5.70	8.6	44.5	1.2
1453	19	632	74.3	4.5	1.86E-02	1.96E-02	5.85	4.6	43.2	.4
1458	66	612	73.5	4.4	1.82E-04	6.25E-04	4.78	.6	41.4	-3.5
1504	43	525	33.0	10.7	8.42E-06	3.52E-04	1.44	-6.7	41.7	-20.3
1511	45	465	28.1	1.8	6.81E-06	5.94E-04	.91	-12.9	39.3	-27.6
1547	16	933	23.7	17.3	1.47E-01	1.16E-01	5.63	22.6	46.8	3.8
1550	17	870	20.1	16.5	2.69E-02	3.16E-02	5.76	22.2	46.6	3.9
1551	20	836	32.6	13.5	1.38E-02	5.15E-03	5.92	21.1	43.0	4.0
1554	19	622	37.5	15.1	1.23E-02	2.17E-03	5.91	18.1	42.3	3.4
1556	26	752	44.5	5.0	1.08E-02	1.07E-03	5.92	15.0	41.4	2.5

Table 12b. Hobbs Flight 15 (standard deviations)/averages for constant altitude runs over the ground station. Conduction current densities calculated using only negative conductivity are included.

STANDARD DEVIATIONS/MEAN VALUES

Time	Efield1	Efield2	+Lam	-Lam	Concur1	Concur2	CON	EPS	C12	D	Using $\lambda$ -only	
											Concur1	Concur2
1431	.074	.085	.104	.093	.098	.101	.095	.830	.782	.020	.098	.097
1435	.014	.015	.252	.114	.145	.144	.007	.815	.572	.013	.115	.119
1437	.016	.015	.079	.084	.099	.097	.058	.263	.262	.008	.100	.095
1439	.026	.027	.412	.088	.235	.235	.008	.361	.373	.004	.092	.092
1442	.019	.019	.530	.100	.280	.280	.012	.512	.886	.006	.103	.103
1445	.033	.025	.523	.210	.416	.415	.021	.441	.566	.011	.233	.233
1449	.036	.036	.671	.244	.424	.423	.019	.704	.836	.002	.231	.231
1453	.157	.153	.271	.243	.154	.143	.504	.409	.405	.016	.142	.132
1458	.137	.135	.211	.098	.151	.153	1.126	.457	.404	.091	.104	.104
1504	.149	.141	.016	.019	.153	.144	.046	.450	.366	.090	.156	.147
1511	.094	.079	.049	.023	.090	.077	.297	.402	.527	.092	.089	.069
1547	.097	.106	.187	.236	.245	.252	.057	1.036	1.016	.015		
1550	.056	.061	.276	.035	.194	.196	.009	.838	.915	.008		
1551	.055	.054	.538	.119	.239	.239	.064	.334	.559	.006		
1554	.054	.054	.635	.114	.325	.323	.009	.317	.575	.004		
1556	.031	.031	.229	.116	.157	.157	.060	.336	.498	.002		

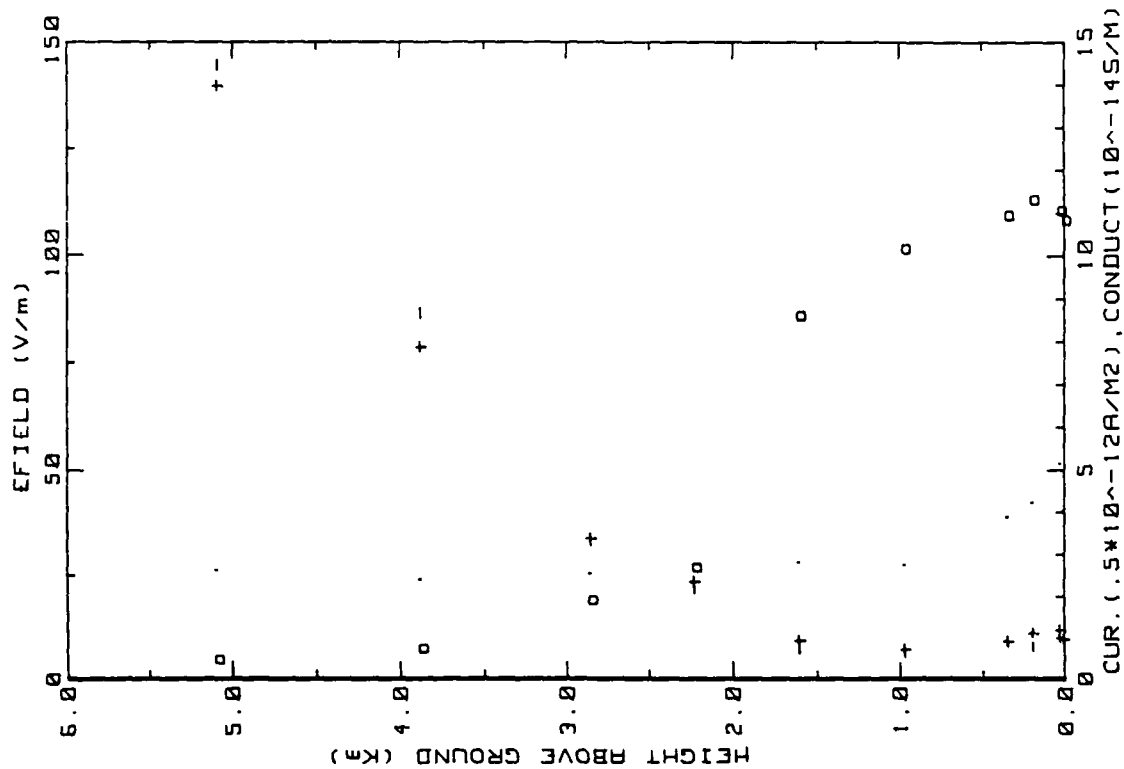


Figure 19a. Hobbs Flight 15 ladder profile (ref. Fig. 5a)

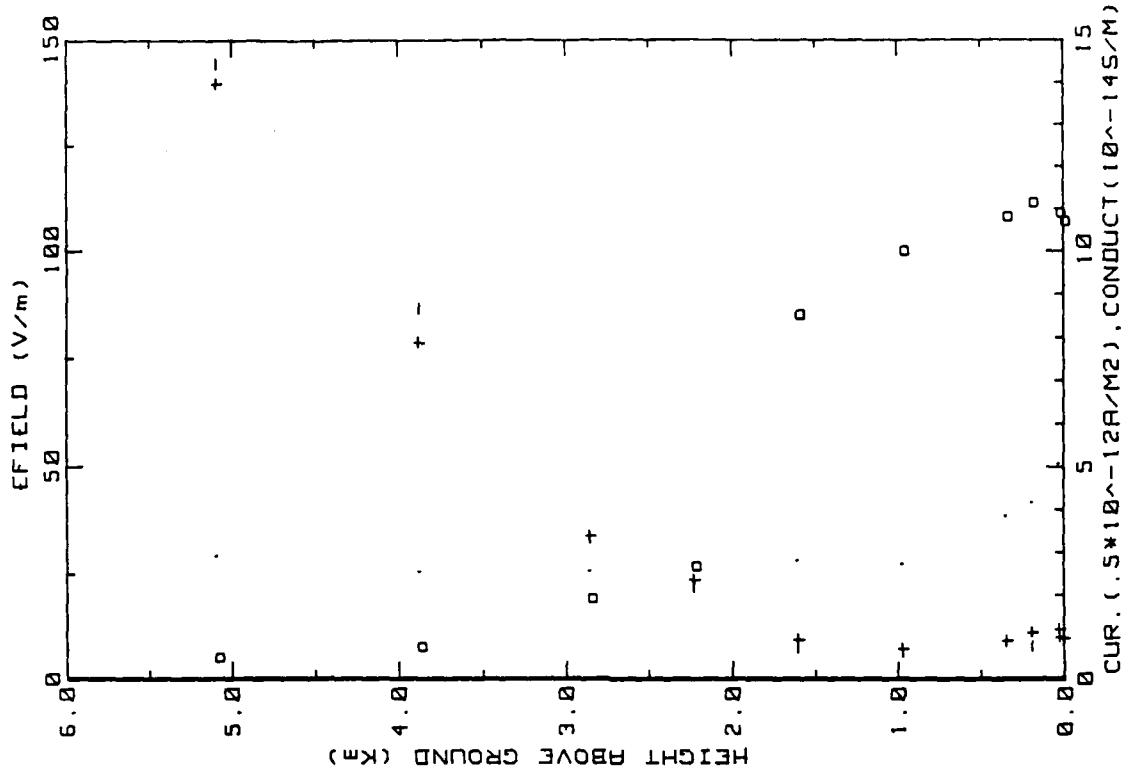


Figure 19b. Similar to 19a. but for inboard E-field system.

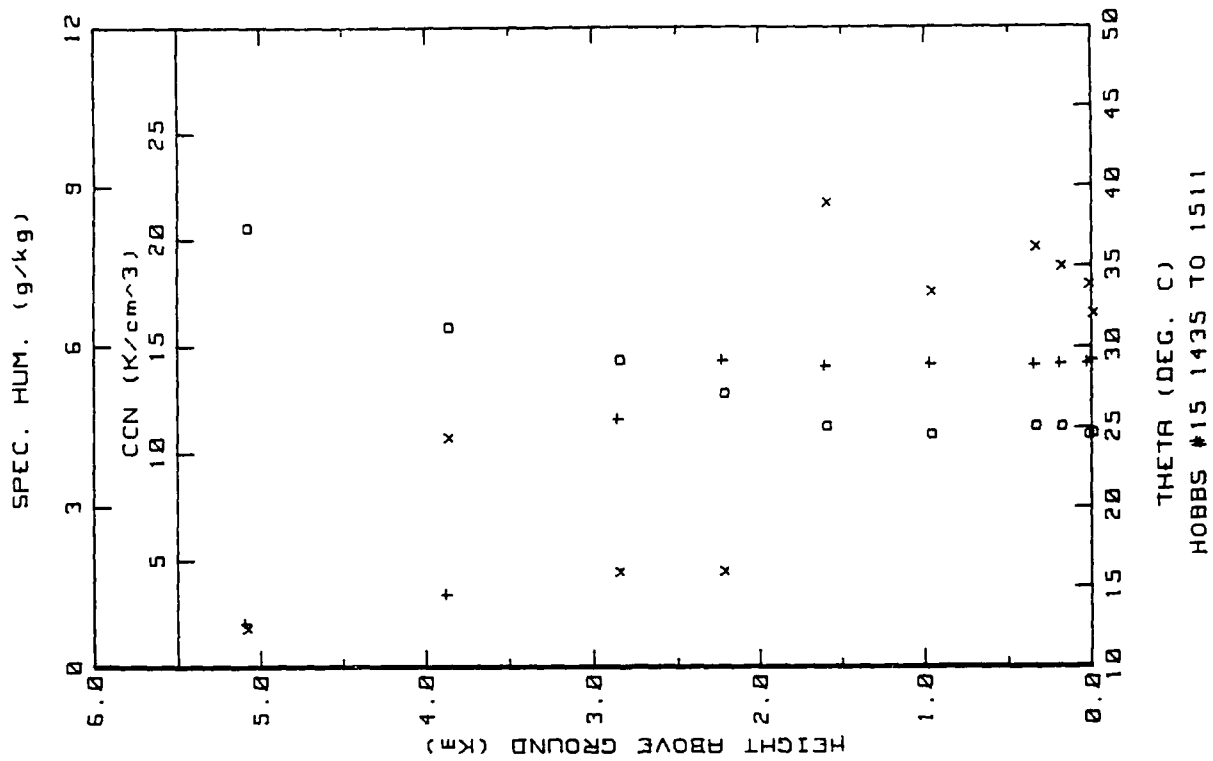


Figure 19c. Hobbs Flight 15 ladder profile (ref. Fig. 5b).

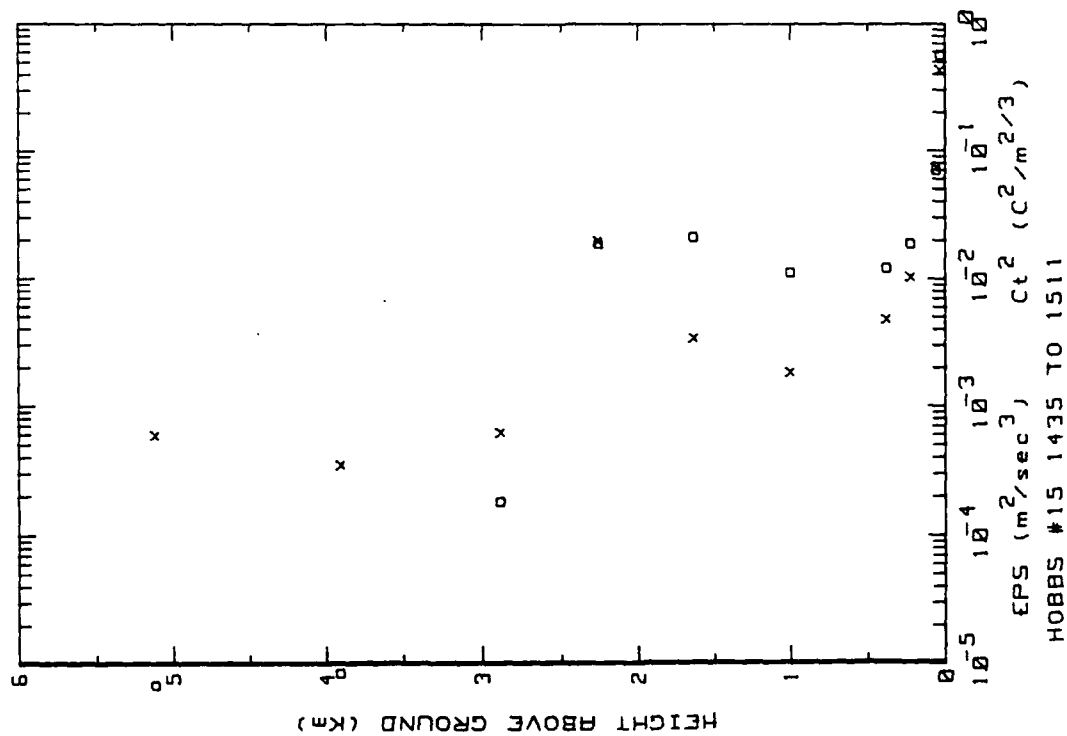
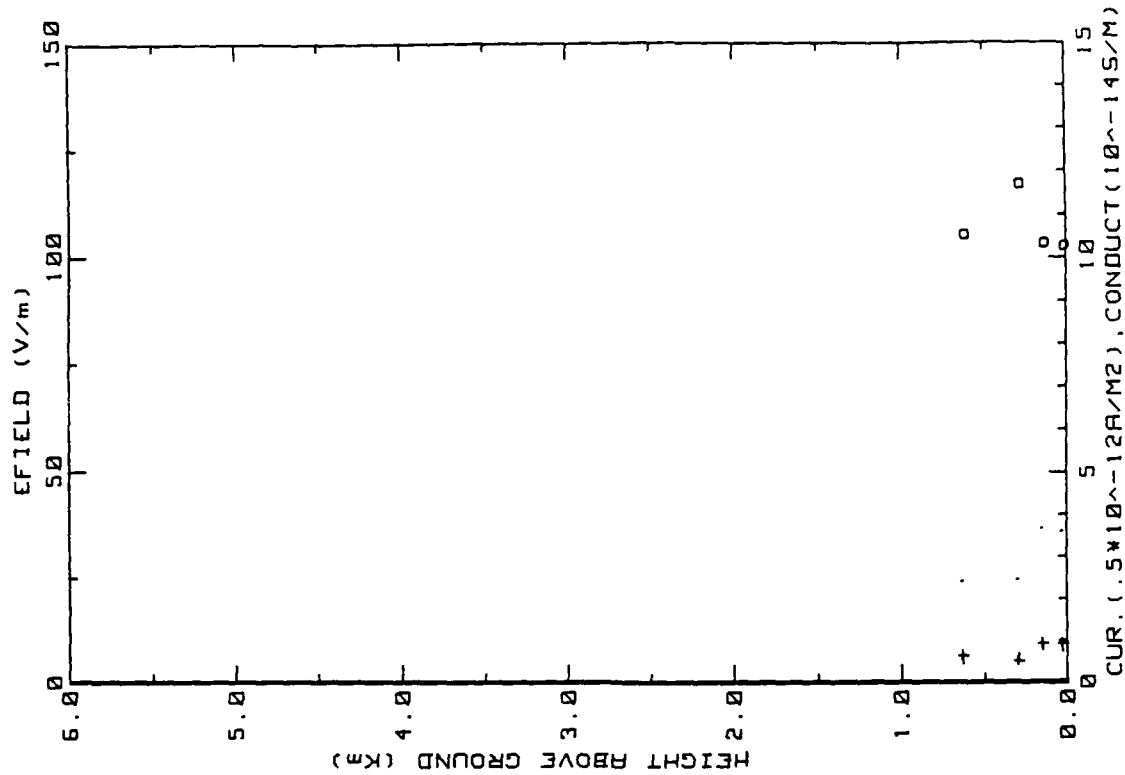
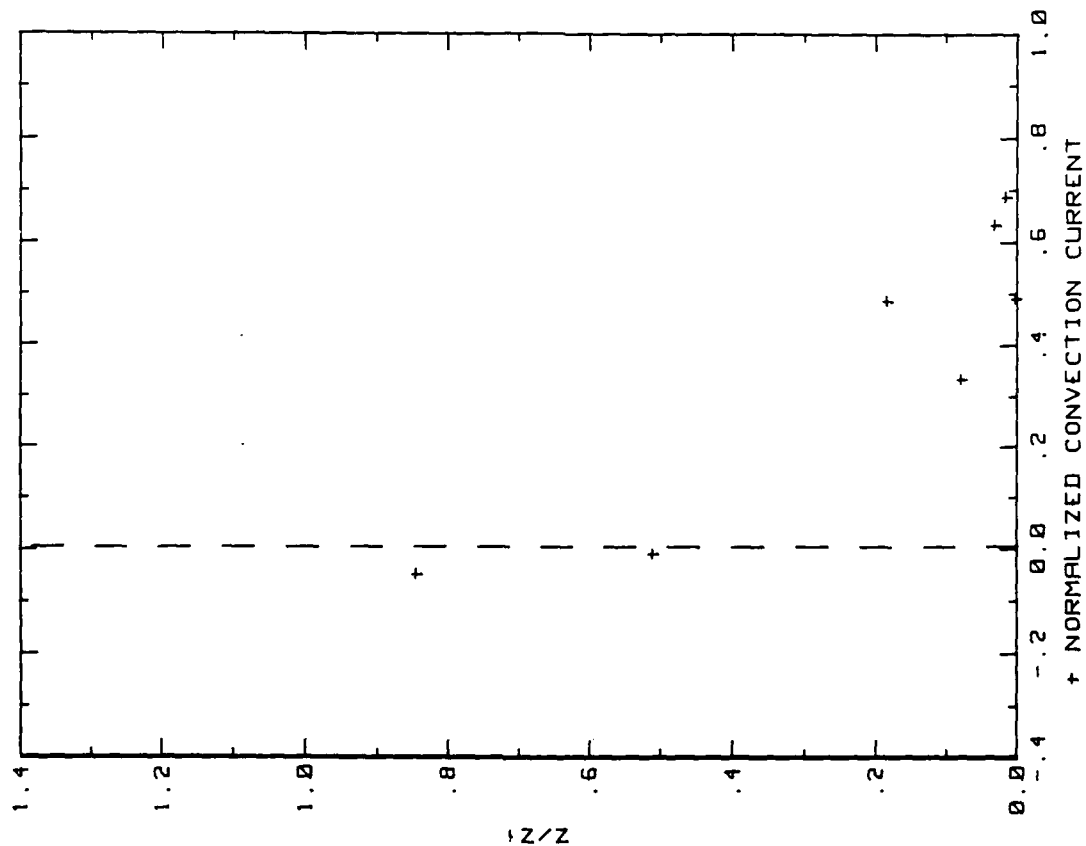


Figure 19d. Hobbs Flight 15 ladder profile (ref. Fig. 5c).



28MAY86 FLIGHT#15 1547 TO 1556 LST

Figure 19f. Hobbs Flight 15 ladder profile (ref. Fig. 5a)



28MAY86 FLIGHT#15 1431 TO 1518 LST

Z1=1900 J0=1.30 using  $\lambda^+ \neq \lambda^-$

Figure 19e. Hobbs Flight 15 convection current profile (ref Fig. 5d).

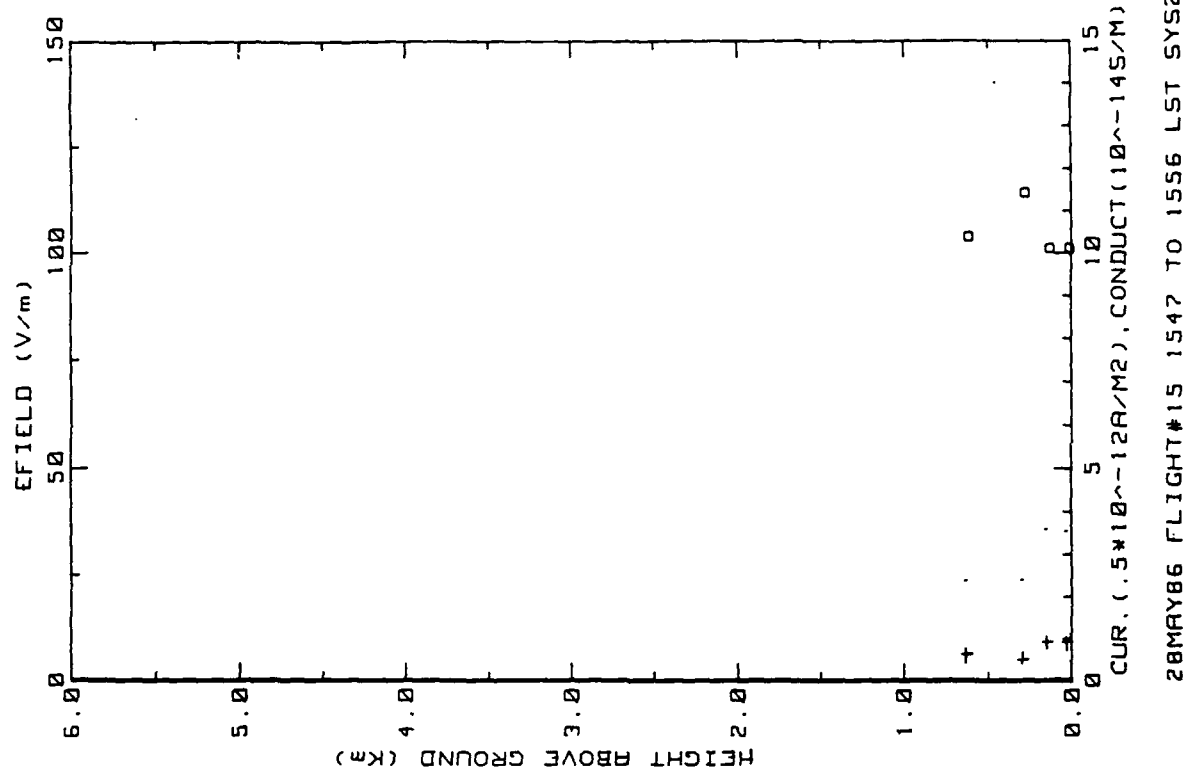


Figure 19h. Hobbs Flight 15 ladder profile (ref. Fig. 5b).

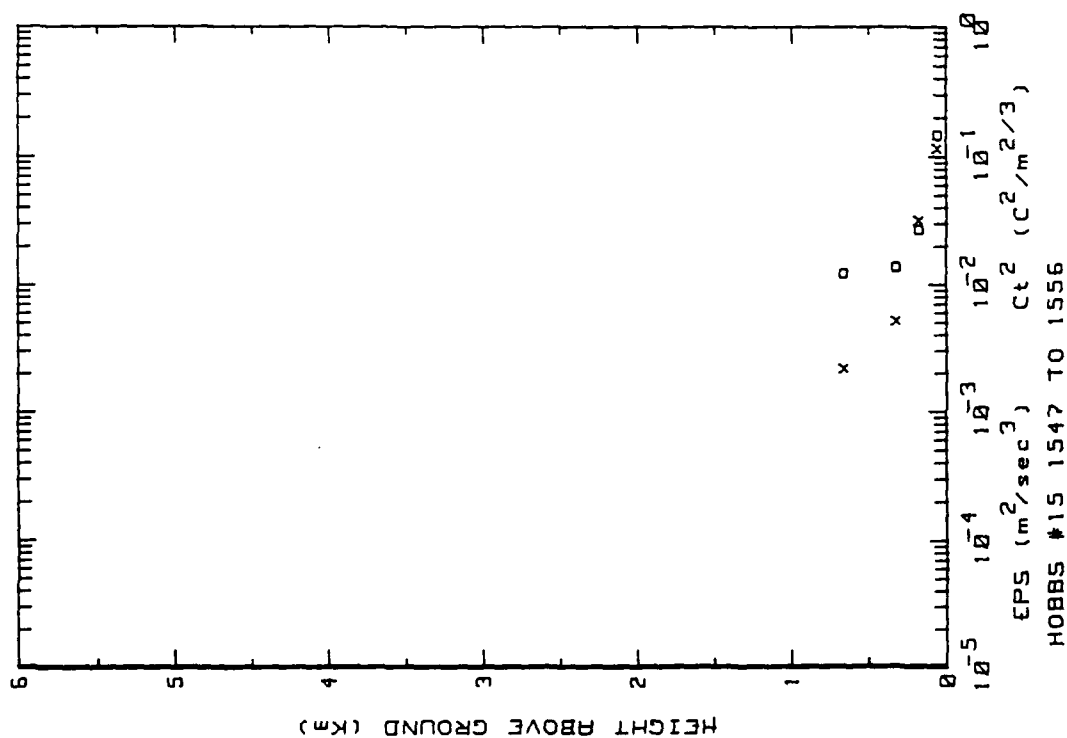


Figure 19g. Similar to 19f, but for inbound E<sub>field</sub> system.



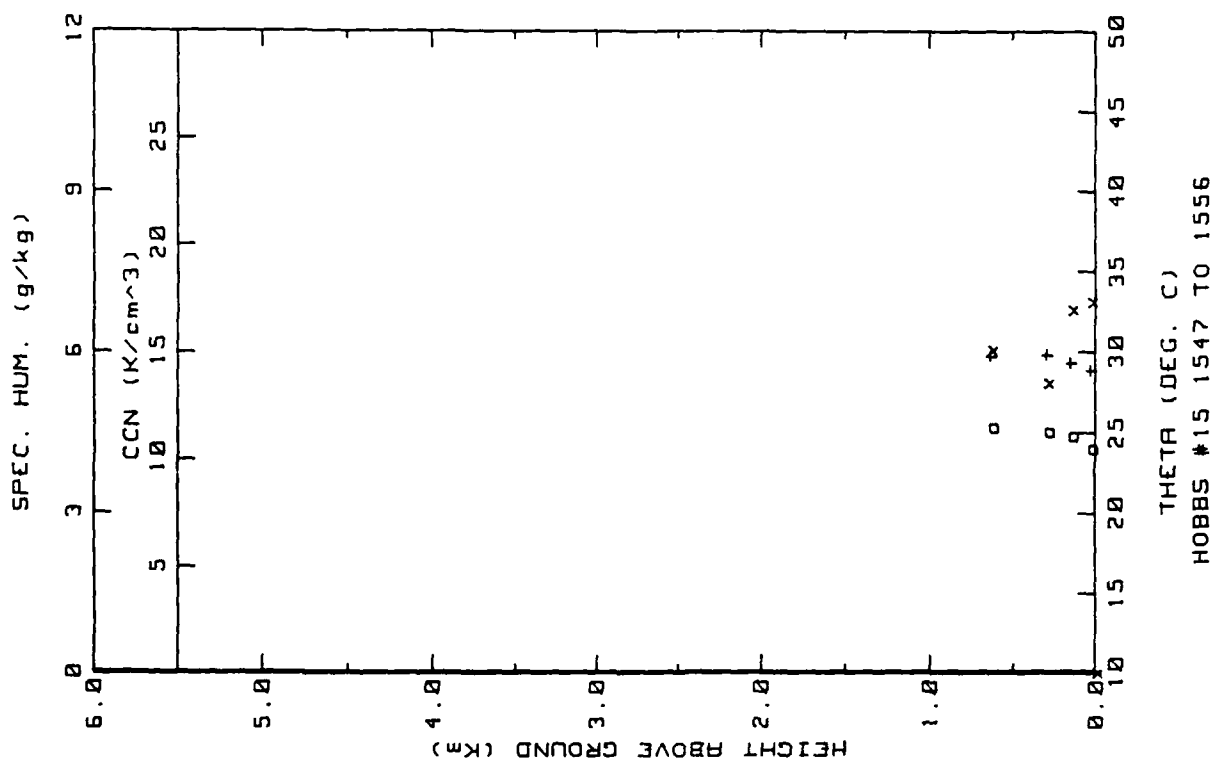
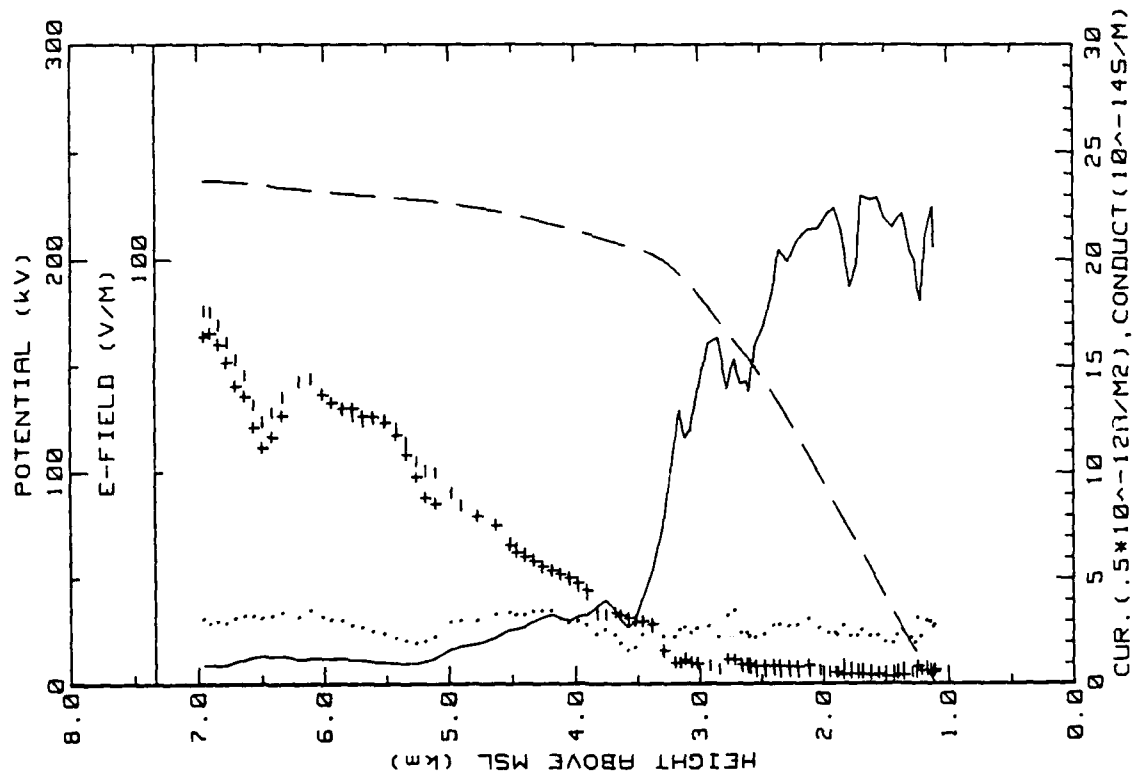
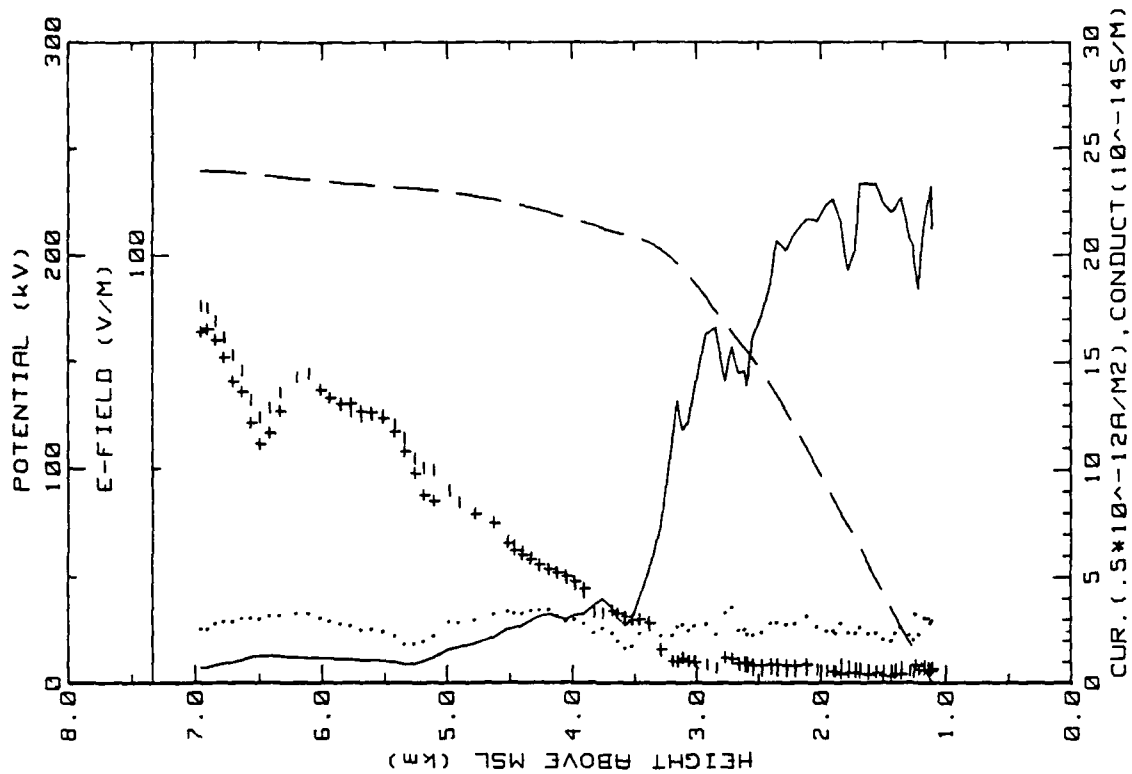


Figure 19i. Hobbs Flight 15 ladder profile (ref. Fig. 5c).



28MAY86 FLIGHT#15 151915 TO 154320 LST

Figure 19j. Hobbs Flight 15 spiral down sounding (ref. Fig. 5e).



28MAY86 FLIGHT#15 151915 TO 154320 LST

Figure 19k. Same as Fig. 19j but for onboard E-field system.

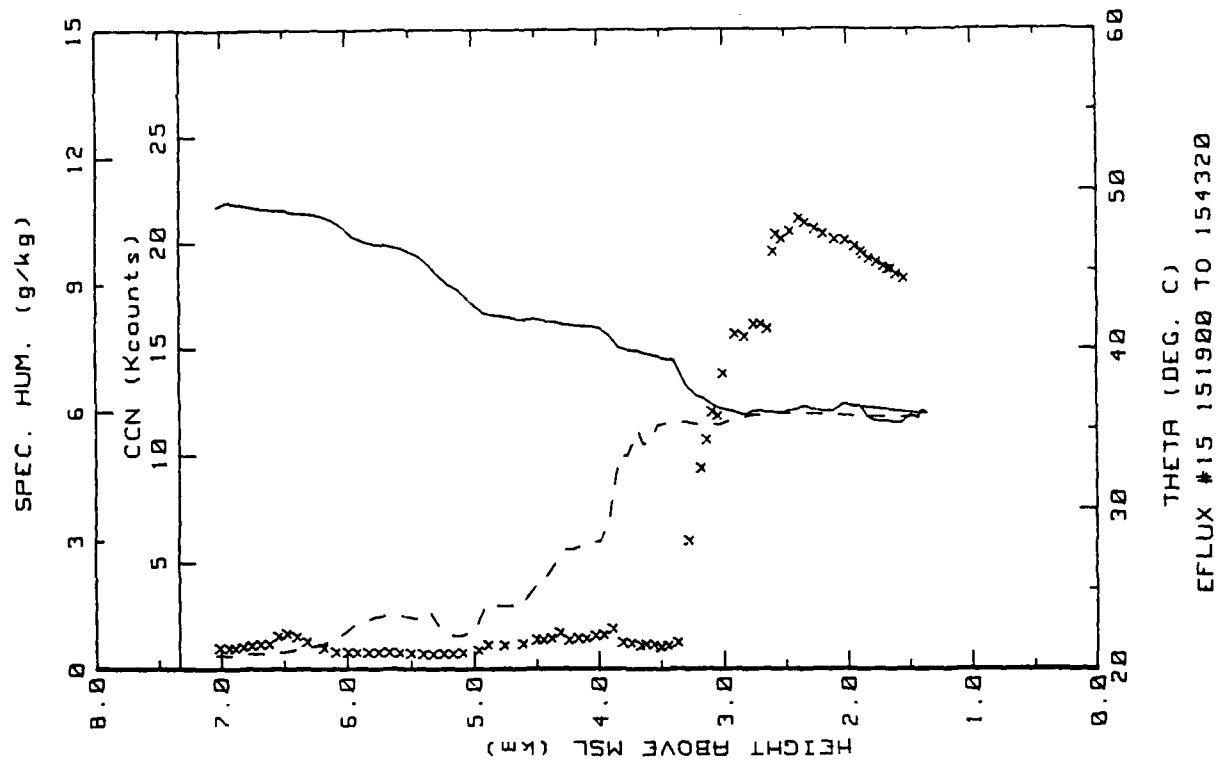


Figure 191. Hobbs Flight 15 spiral down sounding (ref. Fig. 5b).

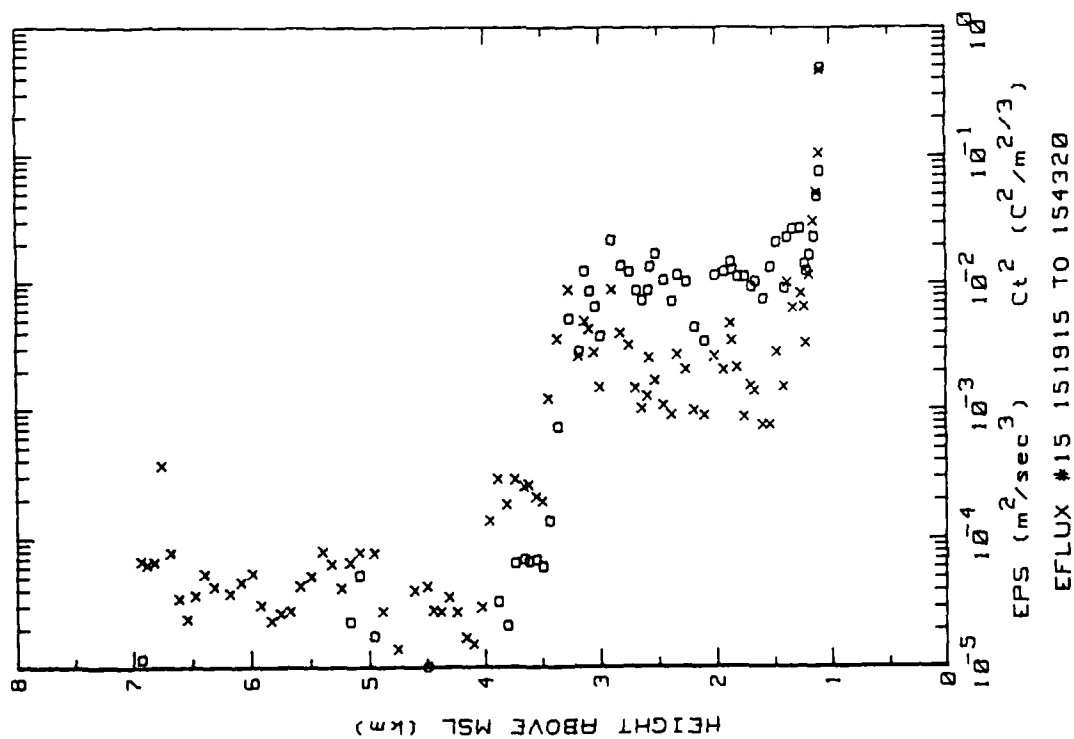
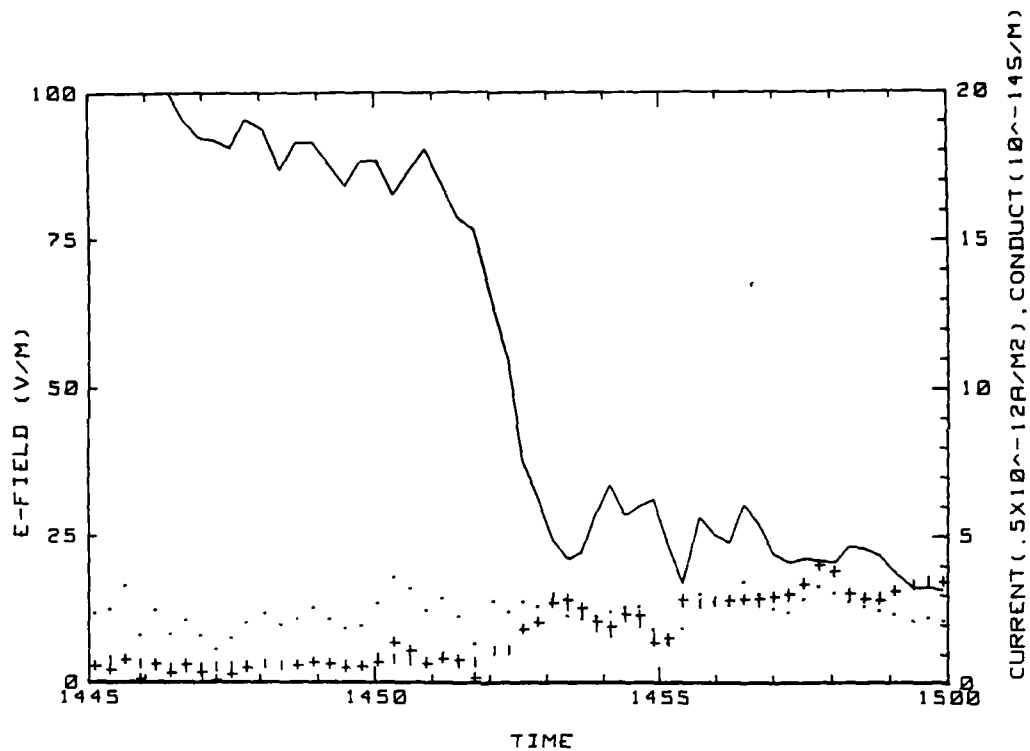
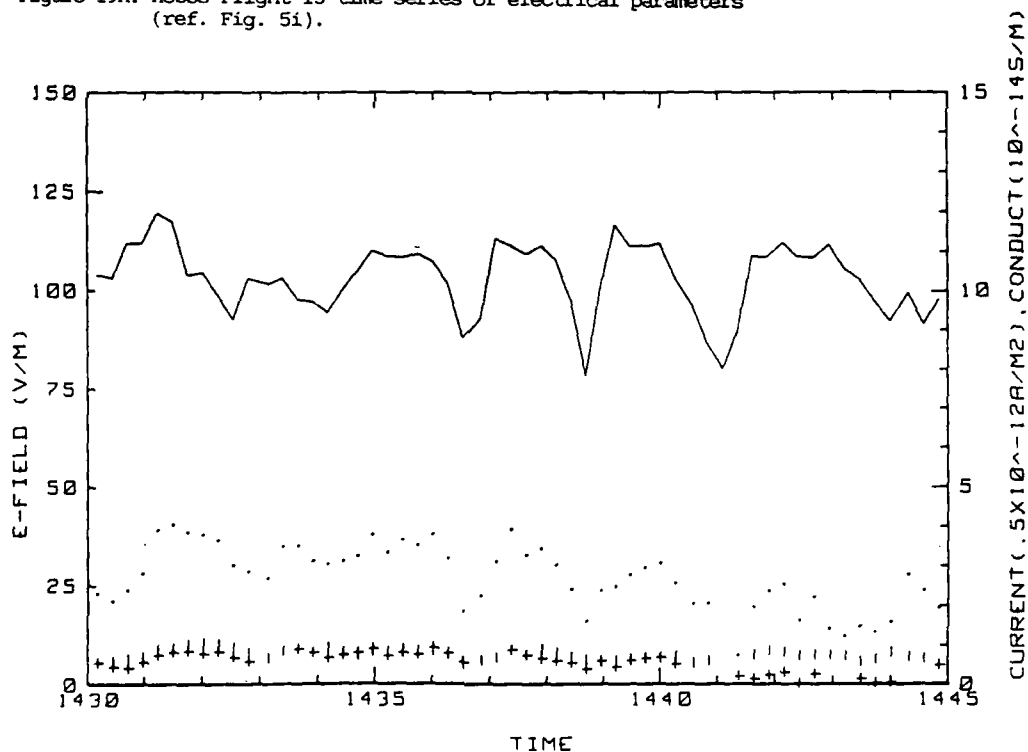


Figure 190. Hobbs Flight 15 spiral down sounding (ref. Fig. 5h).



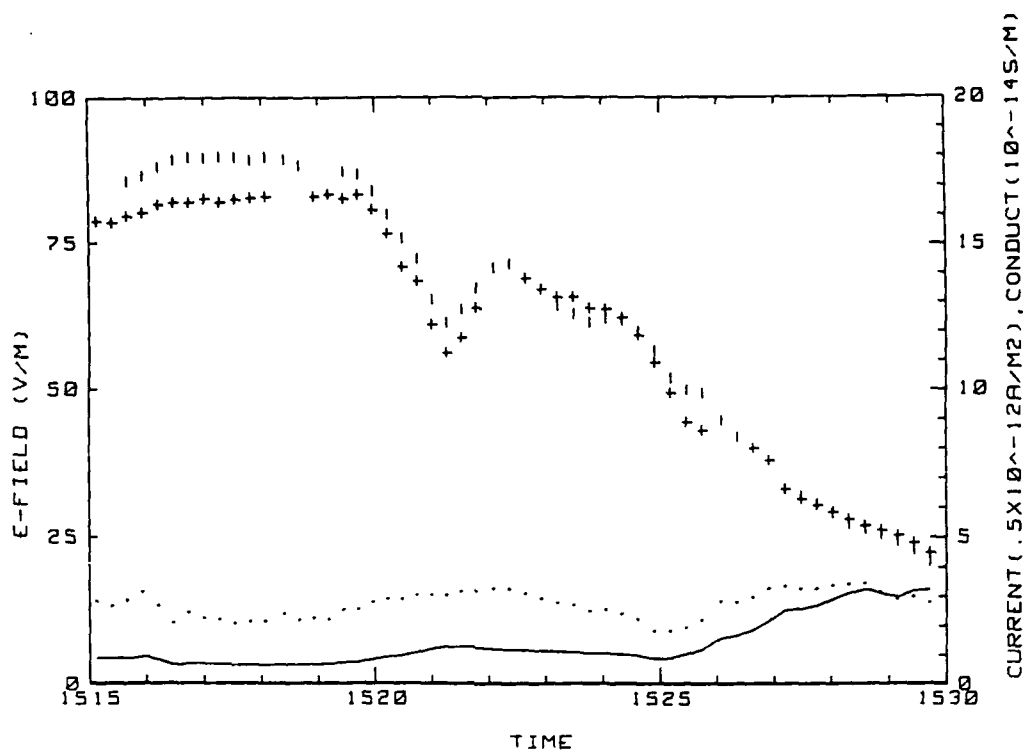
28 MAY 86 FLIGHT#15 144500 TO 150000 LST

Figure 19n. Hobbs Flight 15 time series of electrical parameters  
(ref. Fig. 5i).



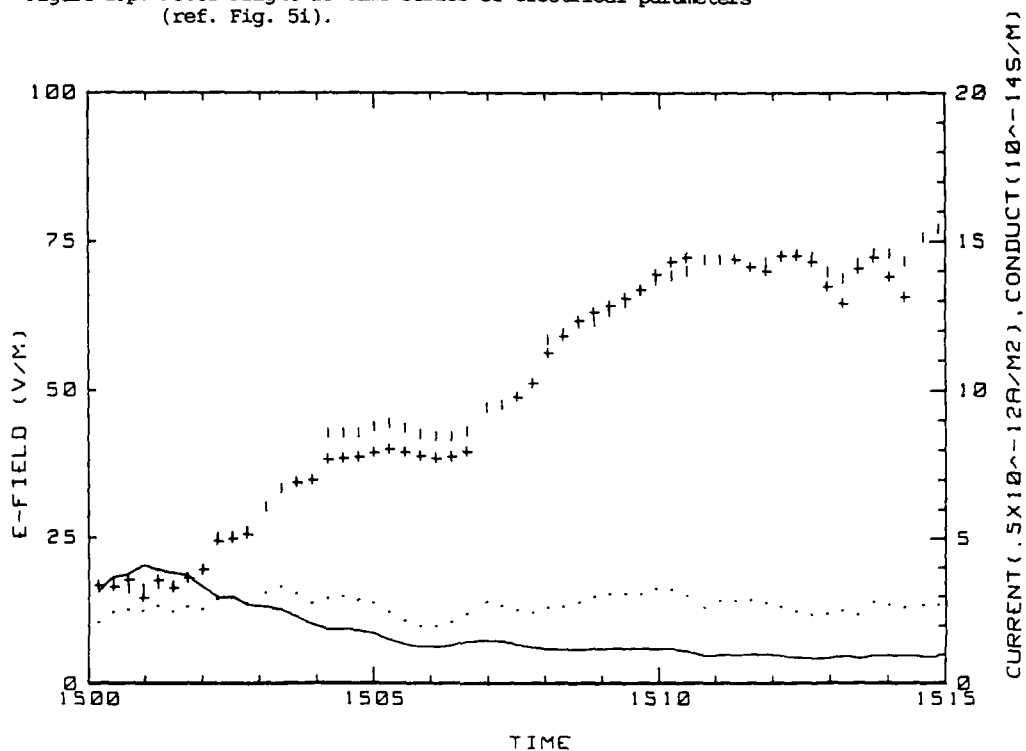
28 MAY 86 FLIGHT#15 143000 TO 144500 LST

Figure 19o. Hobbs Flight 15 time series of electrical parameters  
(ref. Fig. 5i).



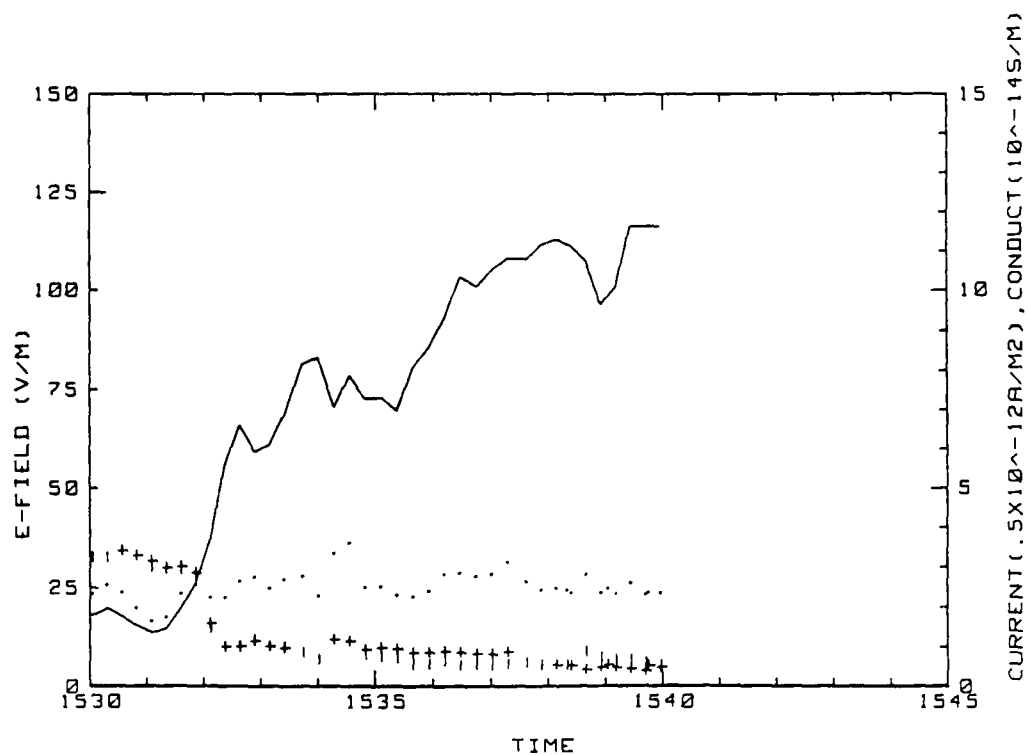
28 MAY 86 FLIGHT#15 151500 TO 153000 LST

Figure 19p. Hobbs Flight 15 time series of electrical parameters  
(ref. Fig. 5i).



28 MAY 86 FLIGHT#15 150000 TO 151500 LST

Figure 19q. Hobbs Flight 15 time series of electrical parameters  
(ref. Fig. 5i).



28 MAY 86 FLIGHT#15 153000 TO 154000 LST

Figure 19r. Hobbs Flight 15 time series of electrical parameters  
(ref. Fig. 5i).

Flight: 16

Date: 29 May 1986

Takeoff: 0519 LT from Hobbs.

Landed: 0655 at Hobbs.

Conditions: Low overcast with higher stratocumulus clouds. Cloud base just after takeoff was < 300 m and gradually lifted during the time of the flight. Winds were from the NE at about 2 m/s and remained fairly steady. Sunrise was approximately 0548 LT.

Instruments: All worked properly.

Summary: The purpose of the flight was to examine the PBL structure prior to the onset of convective mixing to examine the effect of surface radioactivity on the electrical parameters. Five ladder profiles and 2 spiral soundings were performed, mostly within the PBL, to examine the altitude and temporal variation of electric field and conductivity.

Table 13a. Hobbs Flight 16 averages for constant altitude runs over the ground station.

AVERAGES FROM LEVEL RUNS

Time HHMM	N	Altitude m	Efield V/m	Efield2 V/m	Beam 10 <sup>-14</sup>	Beam 10 <sup>-14</sup>	Con Cur1 10 <sup>-12</sup>	Con Cur2 10 <sup>-12</sup>	Theta, v C
0519	8	.003	43.38	43.22	0.00	1.35	1.77	1.74	19.1
0522	32	.151	56.78	55.33	1.37	1.33	1.53	1.49	19.5
0526	14	.031	53.57	52.52	1.64	1.54	1.76	1.74	19.5
0528	8	.015	51.01	50.55	1.81	1.83	1.85	1.84	19.4
0530	13	.003	48.50	47.41	0.00	1.56	1.53	1.88	19.2
0532	10	.003	44.51	44.18	2.04	2.03	1.90	1.79	19.1
0534	25	.061	44.32	43.74	1.70	1.71	1.50	1.48	19.6
0535	16	.061	43.91	43.34	1.62	1.63	1.42	1.41	19.8
0541	36	.257	75.62	73.97	1.29	1.23	1.87	1.83	20.5
0542	31	.183	53.72	52.75	1.40	1.27	1.43	1.40	20.1
0546	16	.125	55.00	54.22	1.42	1.34	1.52	1.50	19.9
0548	16	.061	50.85	50.20	1.55	1.71	1.65	1.64	19.8
0551	13	.031	45.07	44.55	1.73	1.64	1.52	1.50	19.3
0554	15	.003	46.05	44.68	2.07	2.04	1.89	1.84	19.3
0557	11	.003	48.50	48.16	1.97	1.96	1.92	1.91	19.4
0600	25	.006	52.13	51.46	1.83	1.77	1.87	1.84	19.3
0604	11	.031	55.90	55.44	1.61	1.57	2.09	2.08	19.4
0608	21	.152	76.98	75.23	1.25	1.20	1.89	1.85	19.9
0610	38	.236	75.91	74.13	1.29	1.23	1.92	1.87	19.8
0616	16	.531	56.98	56.30	1.87	1.71	2.04	2.02	22.9
0618	19	.532	45.38	44.87	2.19	2.17	1.95	1.94	24.4
0622	25	1.542	31.10	31.06	3.31	3.27	2.05	2.05	26.5
0640	19	.006	66.82	65.94	1.65	1.53	2.11	2.08	19.5
0644	18	.031	72.89	71.87	1.44	1.23	1.93	1.91	19.6
0647	23	.100	52.28	51.08	1.28	1.16	2.01	1.98	19.7
0649	13	.190	74.35	72.92	1.43	1.33	2.02	1.98	19.8
0651	21	.298	107.85	105.86	1.06	.95	2.16	2.12	20.1

Time HHMM	N	Press mD	Rel Hum %	OXN x/cc	EPS m2/s3	CI C2/m2/3	Q g/kg	Trose C	T <sub>DR</sub> C	T <sub>dew</sub> C
0519	8	886	68.7	9.2	2.12E-01	4.47E-03	9.57	17.3	18.1	11.5
0522	32	971	78.4	5.3	5.02E-03	1.21E-03	10.32	16.2	17.1	12.4
0526	14	883	56.7	5.7	5.61E-03	2.03E-03	9.66	17.4	17.5	11.6
0528	8	985	58.0	6.0	7.88E-03	2.26E-03	9.53	17.6	17.4	11.6
0530	13	886	69.0	6.1	1.06E-02	3.79E-03	9.71	17.5	19.1	11.8
0532	10	886	65.8	5.4	1.74E-02	3.05E-03	9.70	17.3	10.2	11.7
0534	25	880	71.3	8.6	1.98E-03	1.37E-03	9.94	17.2	17.9	12.0
0535	16	880	70.1	7.5	1.75E-03	1.63E-03	9.91	17.5	18.1	12.0
0541	36	860	83.5	3.9	6.94E-03	1.76E-03	11.05	16.0	17.4	13.3
0542	31	867	79.0	4.6	3.97E-03	1.21E-03	10.58	16.4	18.2	12.7
0546	16	873	76.2	4.3	1.94E-03	7.67E-04	10.40	15.8	18.5	12.5
0548	16	880	72.0	4.6	1.96E-03	1.57E-03	10.12	17.4	18.3	12.3
0551	13	883	71.0	1.3	4.06E-03	9.72E-04	9.87	17.2	18.3	11.9
0554	15	886	70.9	1.3	9.69E-03	1.26E-03	9.96	17.5	18.4	12.1
0557	11	886	70.5	1.6	8.33E-03	1.59E-03	9.97	17.6	17.6	12.2
0600	25	966	71.3	1.3	5.32E-03	1.02E-03	10.09	17.5	18.2	12.3
0604	11	883	73.6	1.3	6.25E-03	1.21E-03	10.22	17.2	18.1	12.5
0608	21	971	80.1	1.7	5.14E-03	1.13E-03	10.77	16.5	17.8	13.0
0610	38	862	87.1	2.5	4.72E-03	8.49E-04	11.13	15.5	17.8	13.4
0616	16	822	79.1	1.7	1.62E-05	2.05E-05	10.08	14.8	16.9	11.2
0618	19	792	75.5	1.6	4.18E-05	1.27E-04	9.22	13.4	17.6	9.3
0622	25	723	57.5	.9	4.06E-05	2.29E-04	5.80	9.5	16.7	3.8
0640	19	885	77.0	3.5	7.24E-03	5.36E-04	10.85	17.5	18.0	13.4
0644	18	933	79.2	3.0	4.53E-03	3.19E-04	10.95	17.4	16.4	13.5
0647	23	875	81.5	3.3	4.38E-03	4.13E-04	11.10	16.9	18.3	13.6
0649	12	867	84.5	5.1	9.23E-04	4.00E-04	11.35	16.0	18.5	13.8
0651	21	855	91.0	2.6	1.73E-04	1.52E-04	11.43	15.1	18.5	13.7



Table 13b. Hobbs Flight 16 (standard deviations)/averages for  
constant altitude runs over the ground station.

STANDARD DEVIATIONS/MEAN VALUES

Time	Efield1	Efield2	Flam	-Lam	Concur1	Concur2	CCN	EPS	CT2	Q
0519	.052	.033	0.000	.082	.123	.087	.013	1.071	.301	.005
0522	.043	.041	.041	.046	.029	.027	.033	.311	.386	.015
0526	.042	.045	.053	.073	.066	.064	.009	.198	.243	.003
0528	.037	.038	.092	.098	.081	.070	.004	.225	.251	.005
0530	.047	.050	0.000	.080	.094	.098	.012	.227	.363	.004
0532	.073	.081	.118	.130	.101	.111	.006	.305	.320	.005
0534	.051	.051	.065	.165	.089	.088	.029	.140	.244	.012
0535	.053	.052	.051	.057	.049	.047	.012	.403	.191	.009
0541	.106	.106	.097	.191	.065	.067	.065	.241	.381	.012
0542	.184	.184	.025	.037	.164	.165	.028	.211	.230	.010
0546	.078	.076	.025	.025	.065	.063	.106	.203	.314	.008
0548	.131	.132	.036	.246	.227	.225	.020	.126	.222	.011
0551	.063	.059	.058	.067	.058	.058	.015	.116	.411	.005
0554	.054	.057	.067	.066	.077	.087	.168	.179	.503	.009
0557	.165	.177	.033	.100	.097	.112	.012	.223	.267	.009
0600	.186	.191	.055	.062	.171	.177	.127	.139	.314	.003
0604	.069	.068	.042	.054	.052	.054	.012	.257	.340	.007
0608	.074	.075	.032	.055	.065	.085	.023	.142	.329	.007
0610	.099	.100	.028	.047	.091	.093	.050	.257	.340	.011
0616	.057	.058	.040	.044	.041	.040	.023	.345	1.153	.007
0618	.098	.092	.092	.066	.041	.041	.167	.982	.450	.026
0622	.034	.032	.005	.010	.038	.036	.046	.274	.367	.009
0640	.066	.078	.085	.138	.050	.057	.012	.200	.402	.004
0644	.096	.097	.086	.148	.045	.042	.013	.120	.253	.002
0647	.023	.026	.057	.072	.054	.068	.015	.149	.166	.005
0649	.070	.068	.023	.034	.060	.057	.013	.574	.582	.003
0651	.053	.054	.062	.067	.025	.025	.013	.700	.295	.003

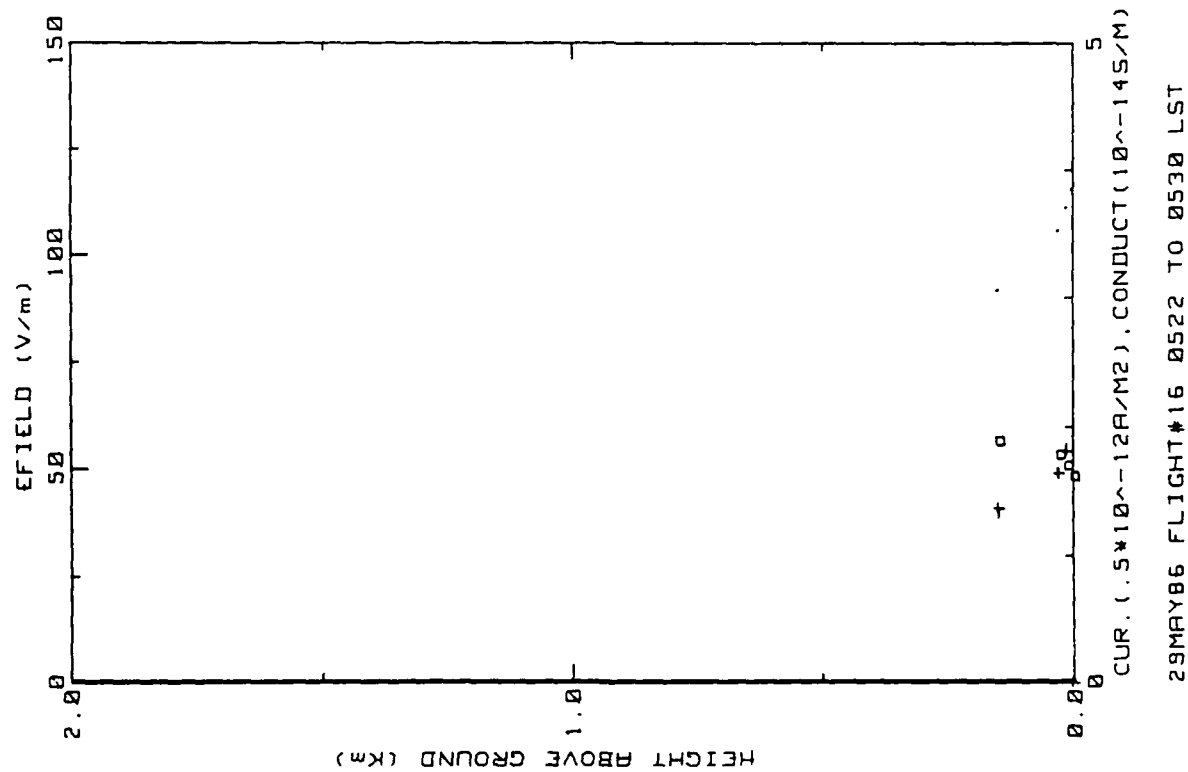


Figure 20a. Hobbs Flight 16 ladder profile (ref. Fig. 5a)

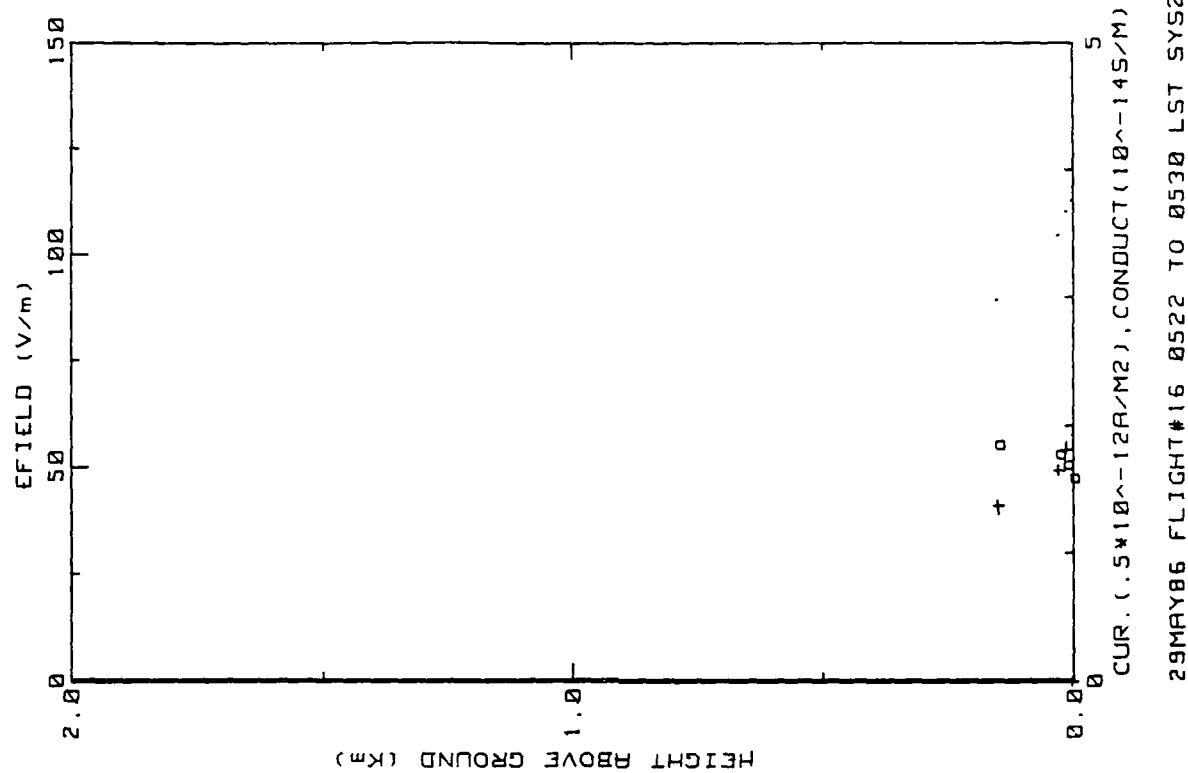


Figure 20b. Similar to 20a. but for inboard E-field system.

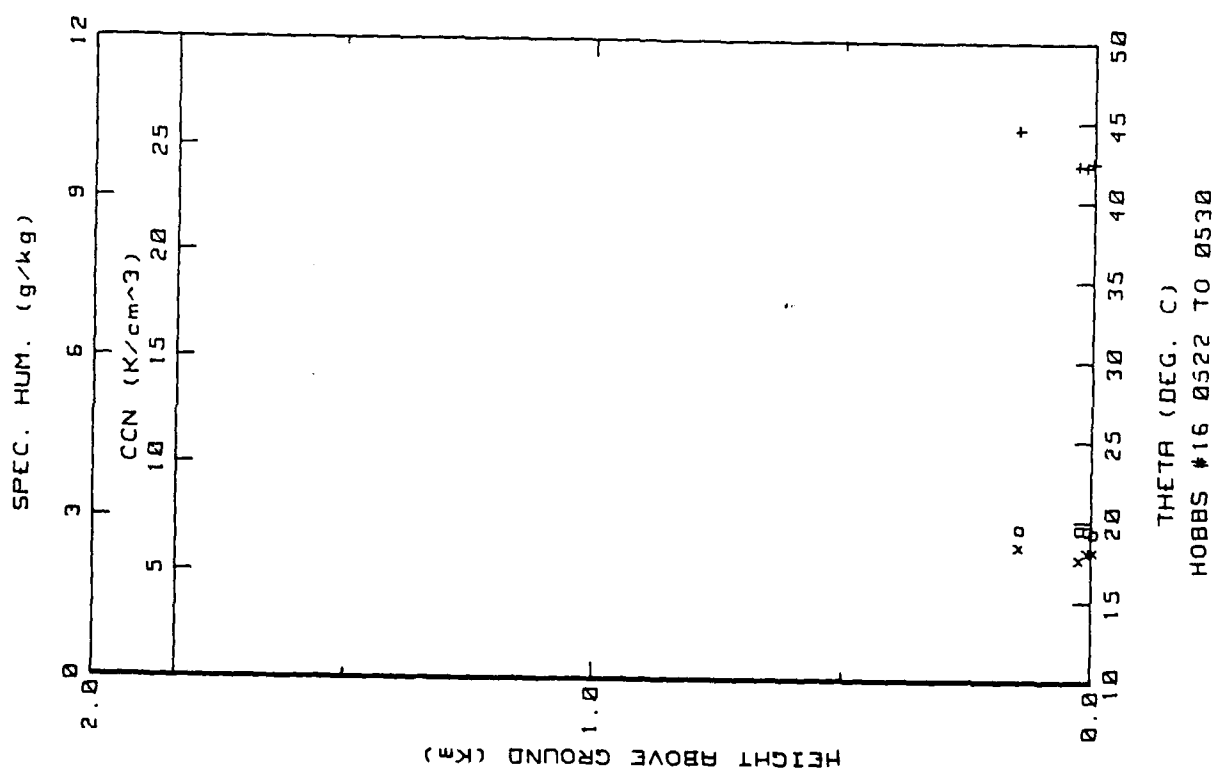


Figure 20c. Hobbs Flight 16 ladder profile (ref. Fig. 5c).

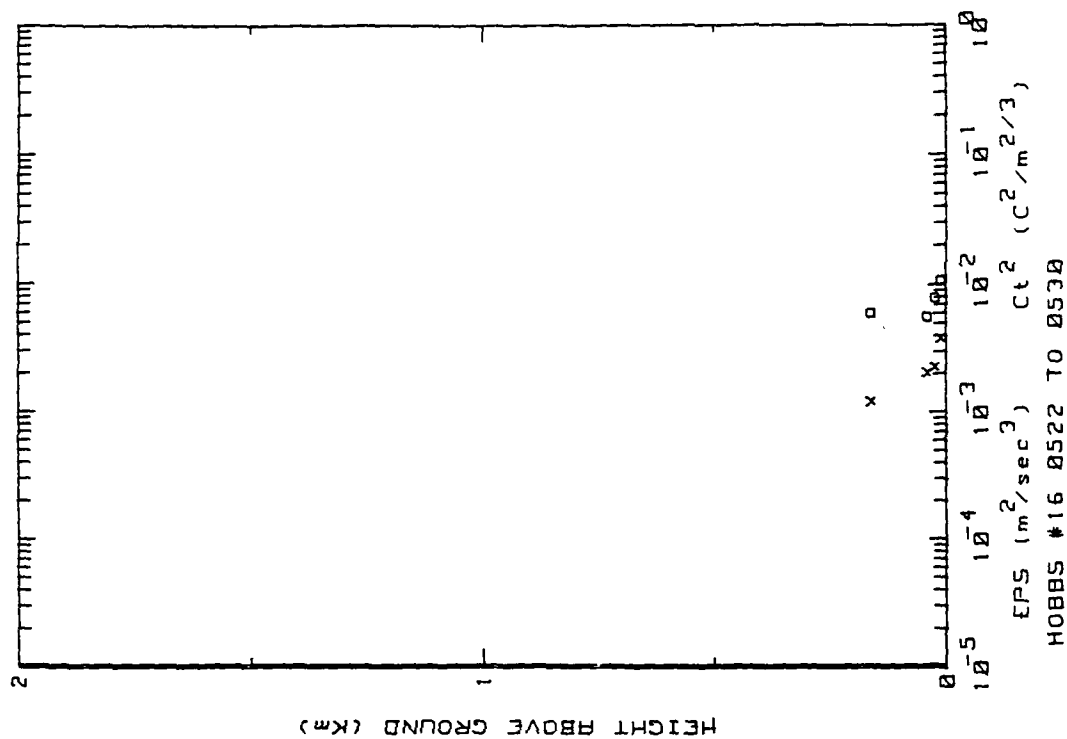


Figure 20d. Hobbs Flight 16 ladder profile (ref. Fig. 5b).

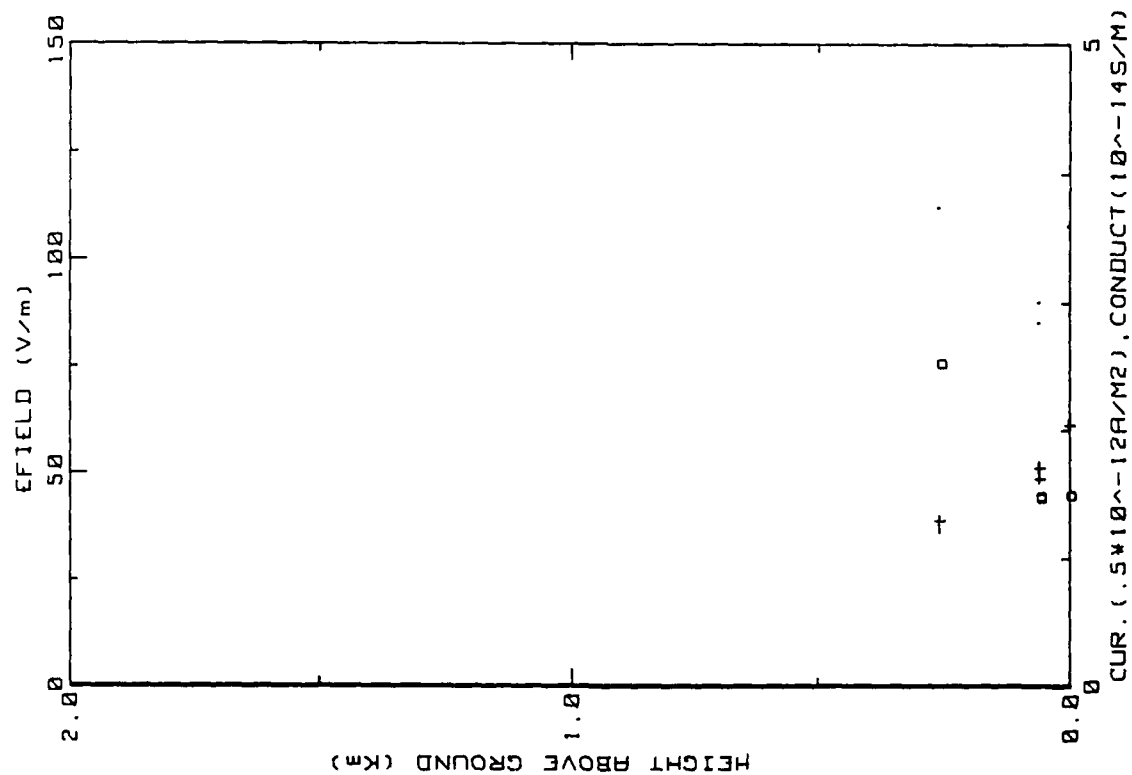


Figure 20e. Hobbs Flight 16 ladder profile (ref. Fig. 5a)

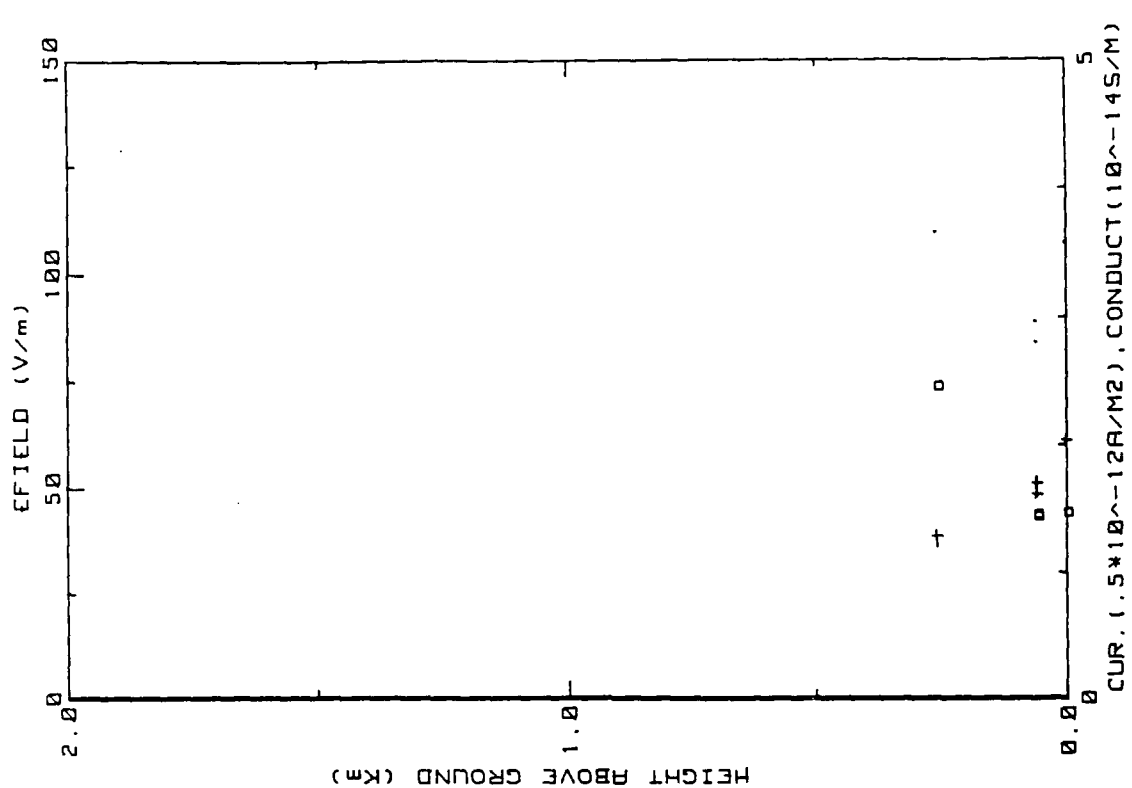


Figure 20f. Similar to 20e. but for inboard E-field system.

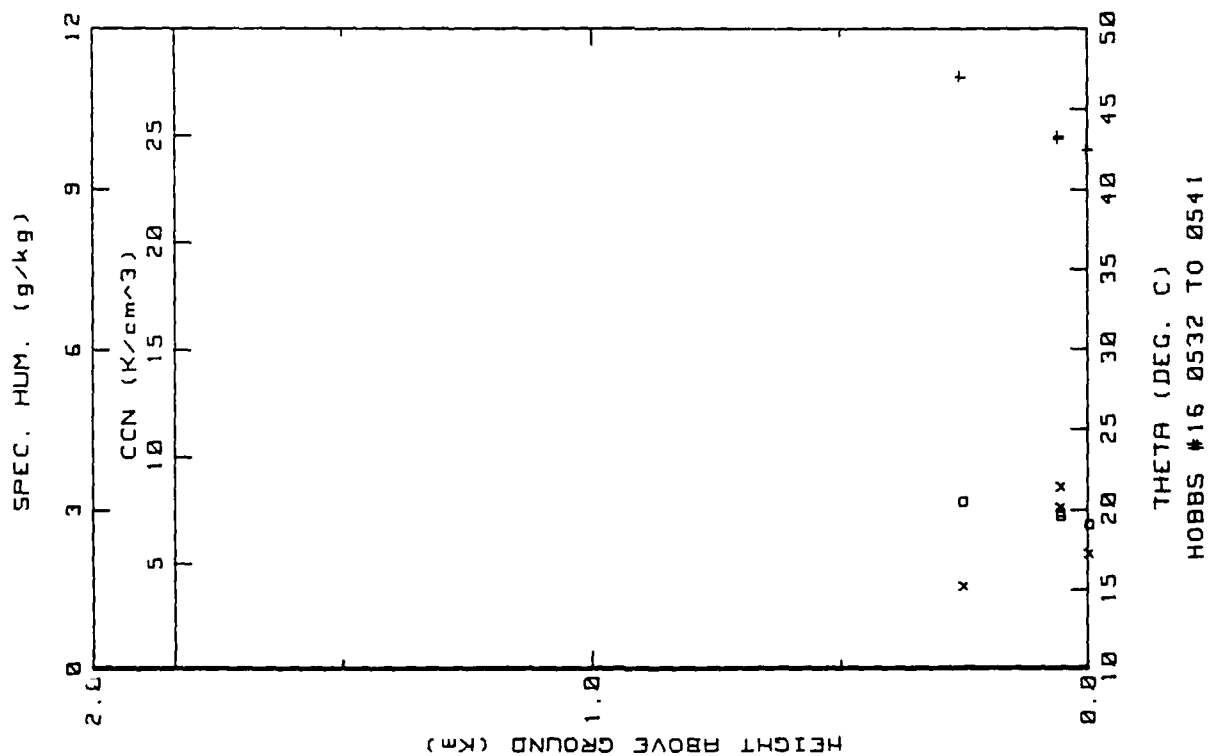


Figure 20g. Hobbs Flight 16 ladder profile (ref. Fig. 5c).

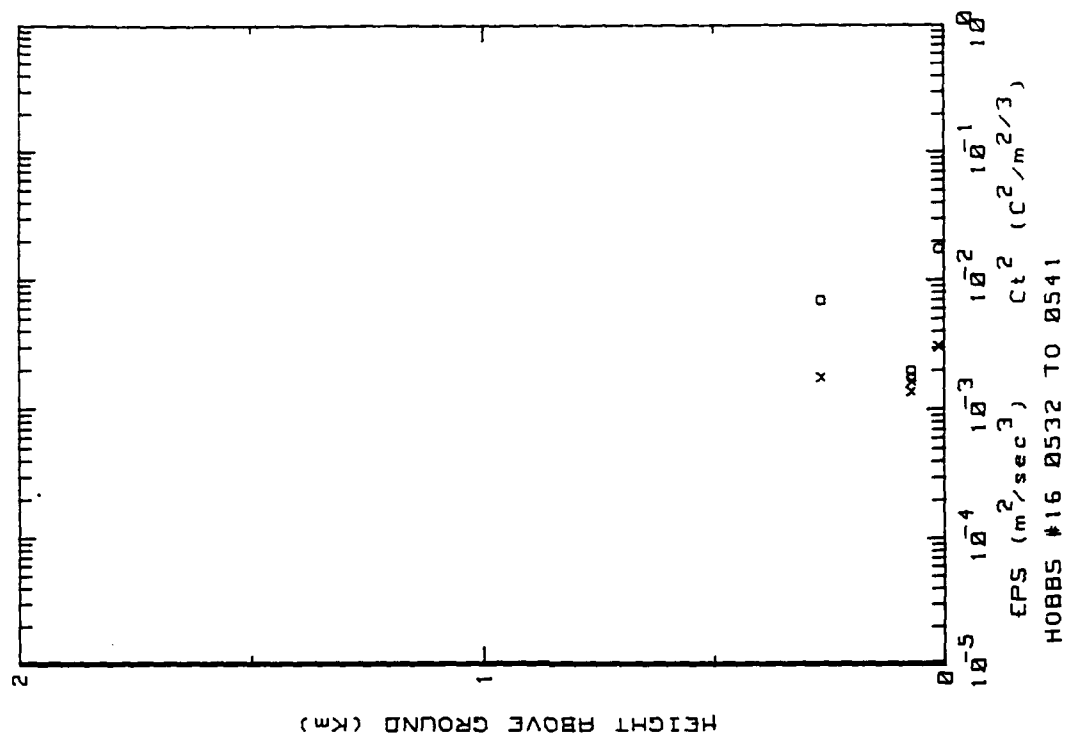


Figure 20h. Hobbs Flight 16 ladder profile (ref. Fig. 5b).

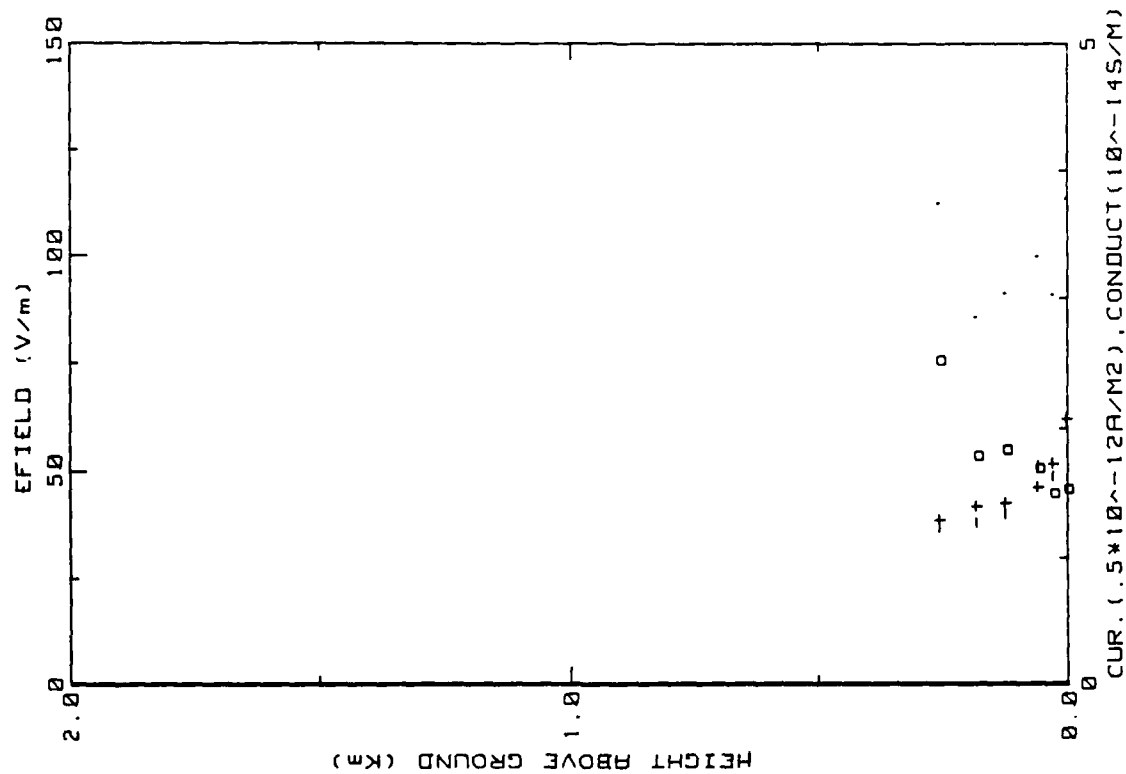


Figure 20i. Hobbs Flight 16 ladder profile (ref. Fig. 5a)

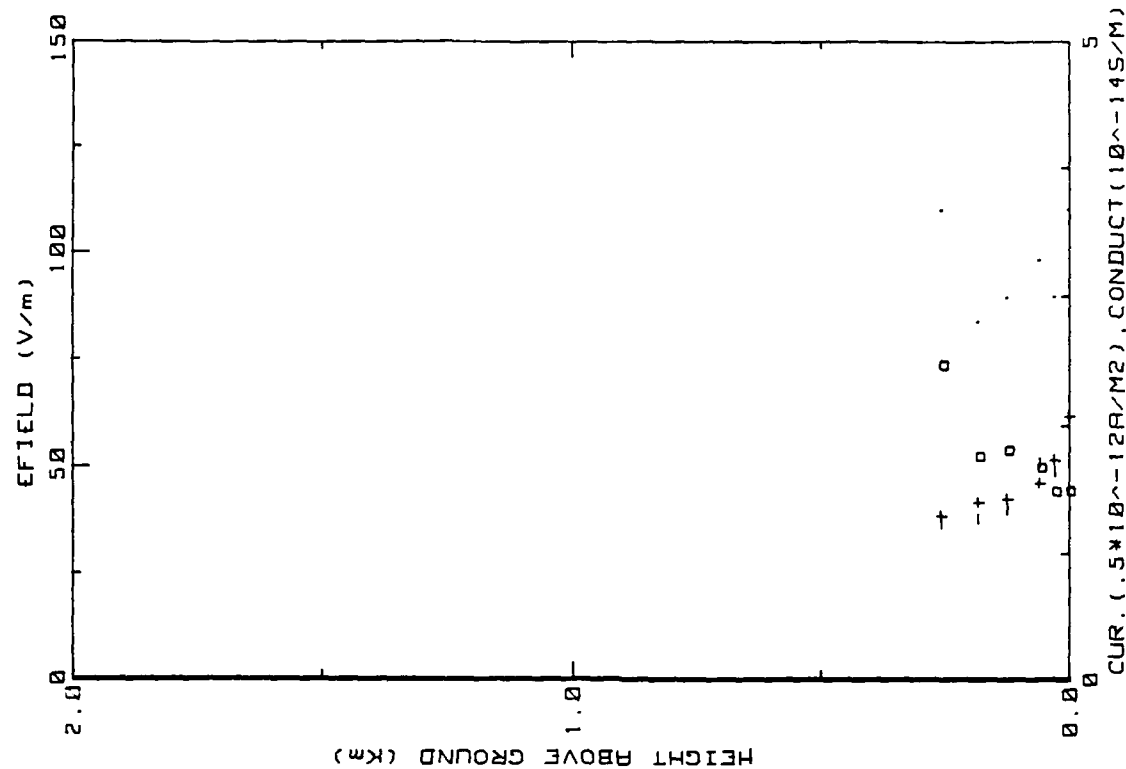


Figure 20j. Similar to 20i. but for inboard E-field system.

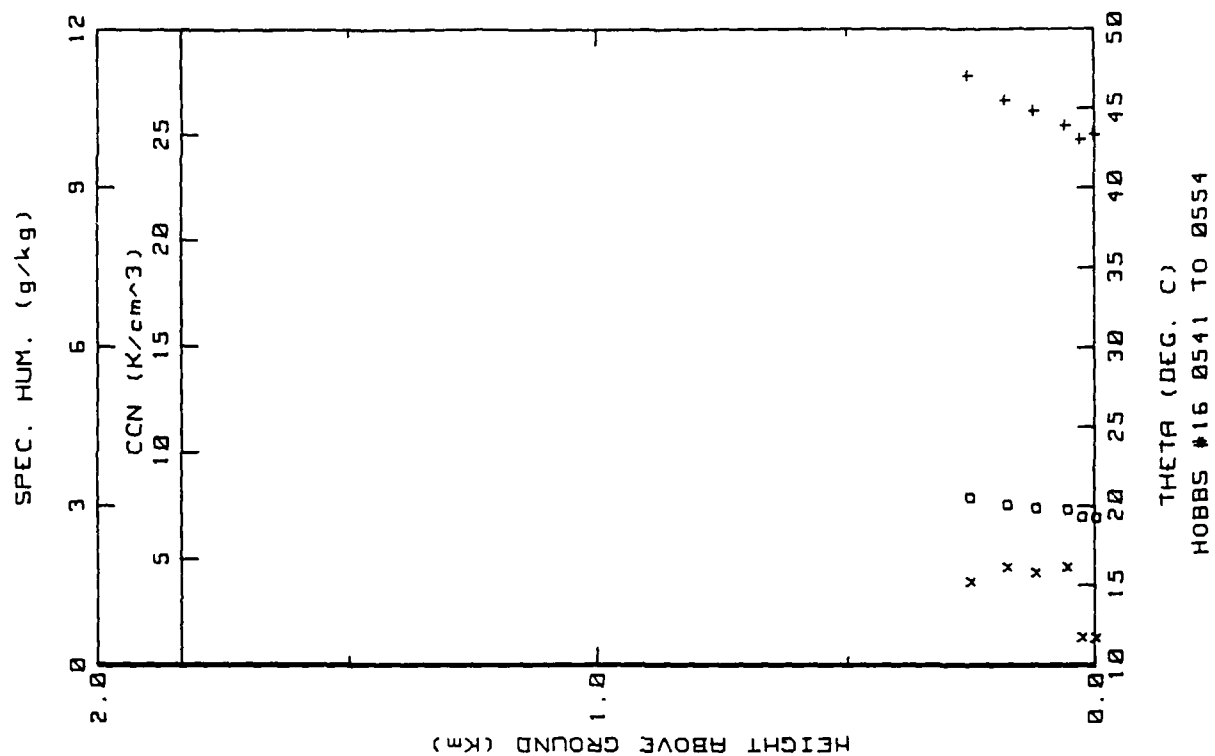


Figure 20k. Hobbs Flight 16 ladder profile (ref. Fig. 5b).

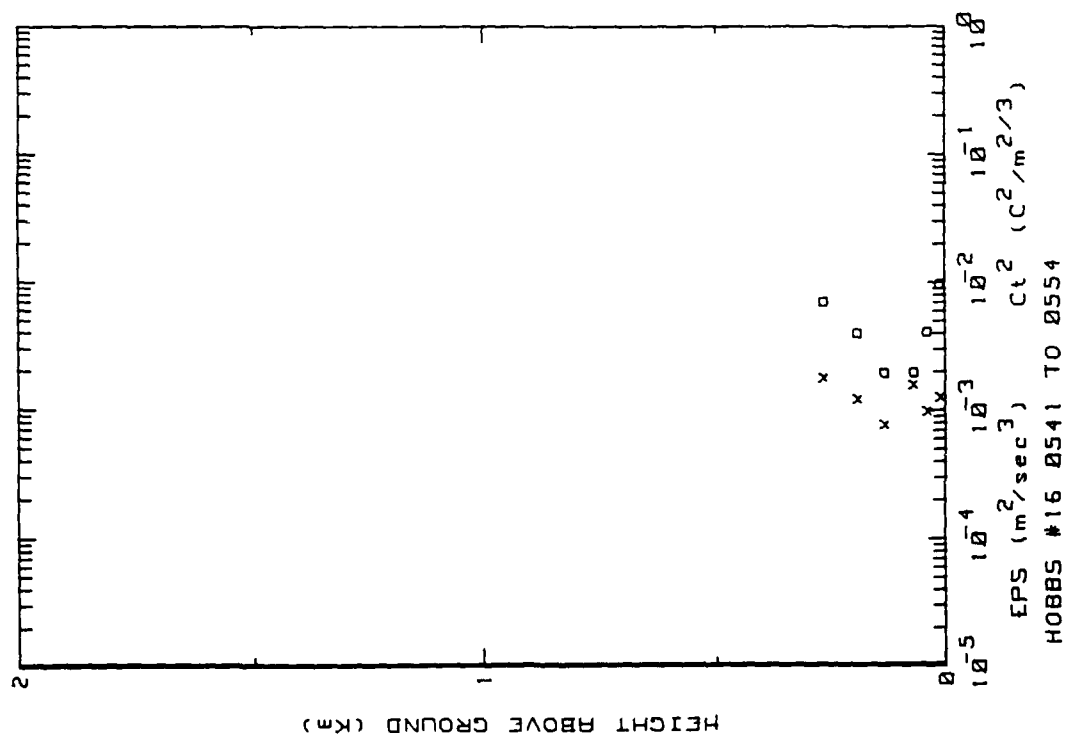
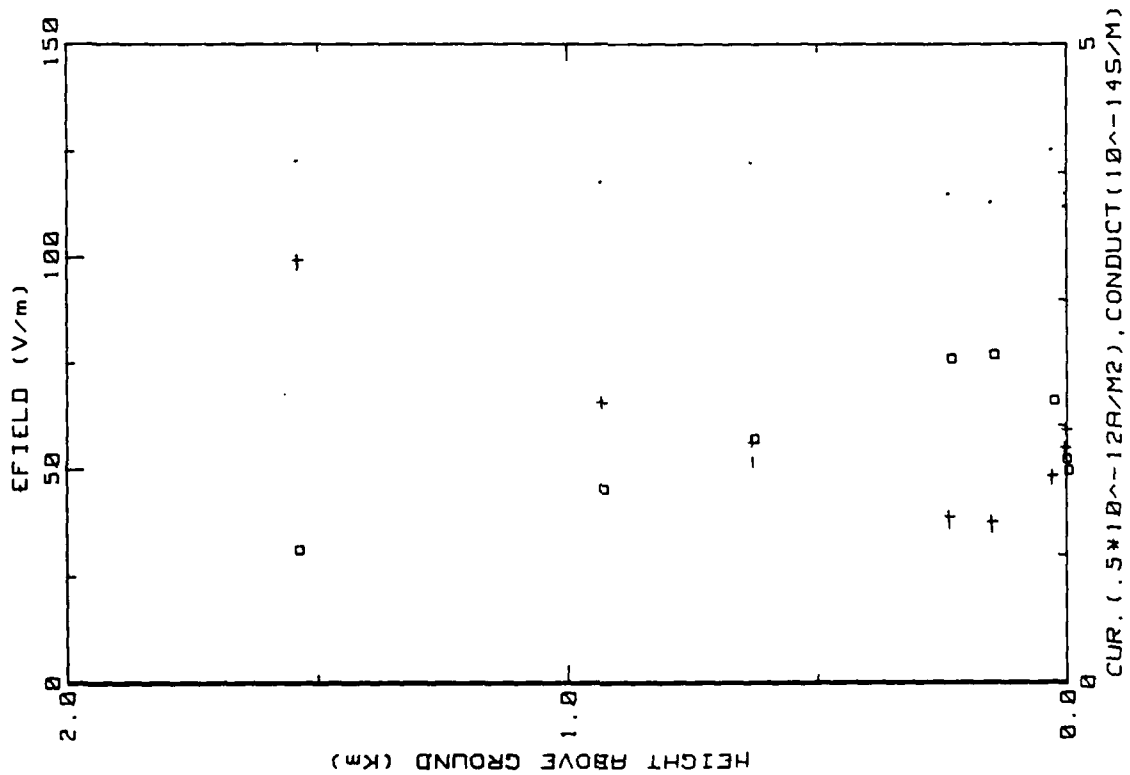
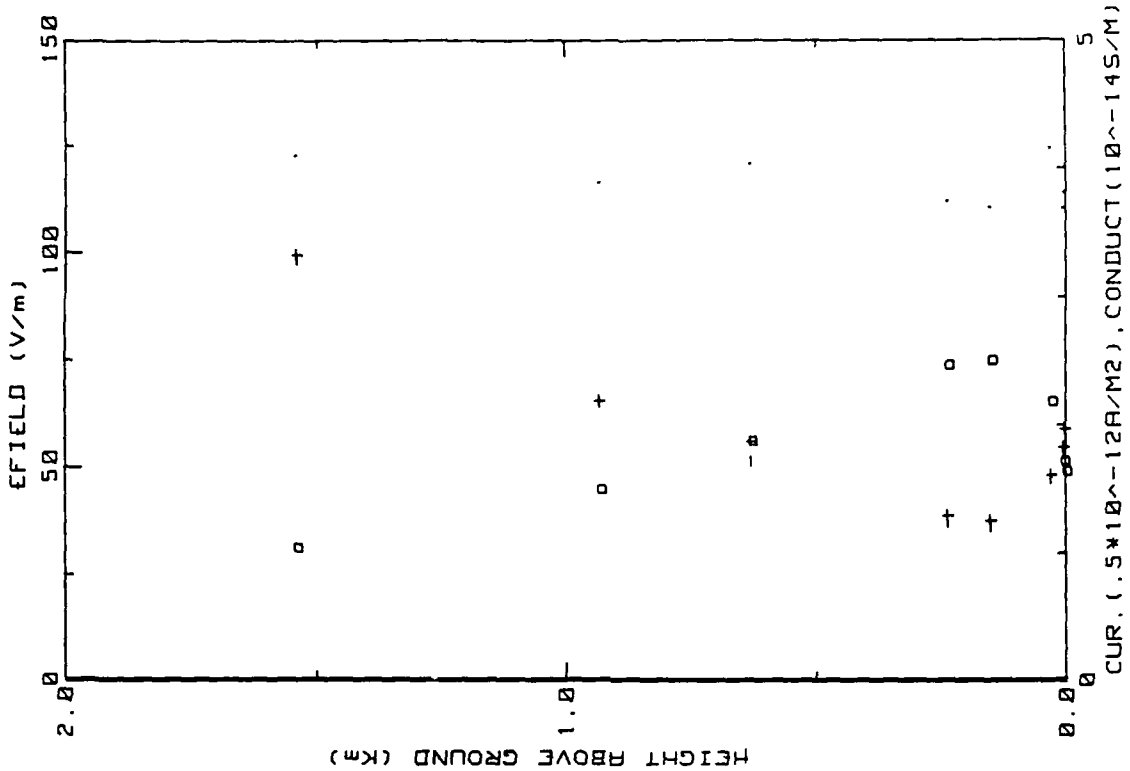


Figure 20l. Hobbs Flight 16 ladder profile (ref. Fig. 5c).



29MAY86 FLIGHT#16 0557 TO 0622 LST

Figure 20a. Hobbs Flight 16 ladder profile (ref. Fig. 5a)



29MAY86 FLIGHT#16 0557 TO 0622 LST SYS2

Figure 20n. Similar to 20m. but for inboard E-field system.



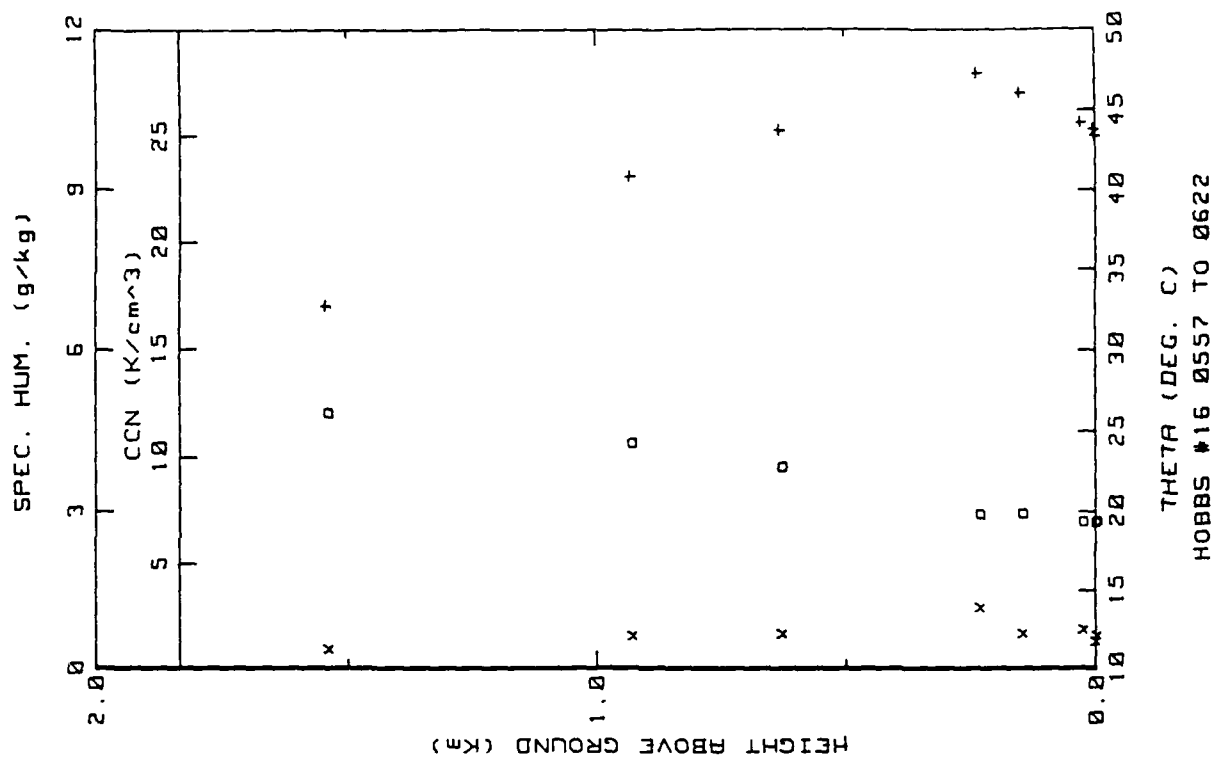


Figure 20p. Hobbs Flight 16 ladder profile (ref. Fig. 5c).

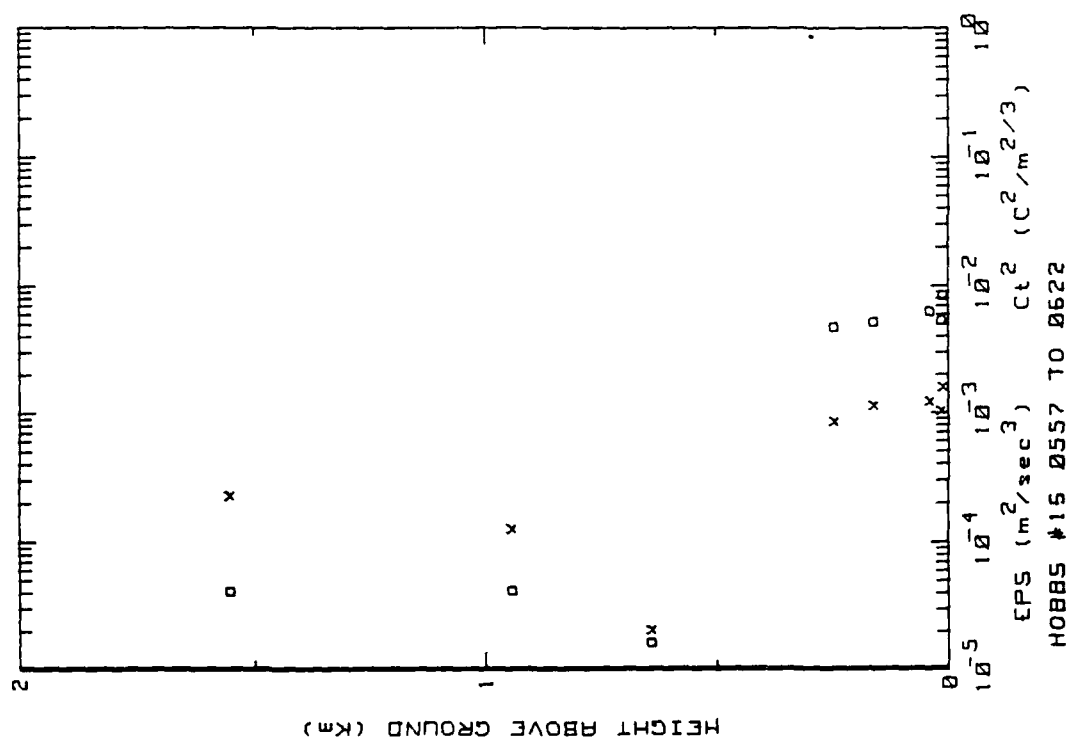


Figure 20o. Hobbs Flight 16 ladder profile (ref. Fig. 5b).

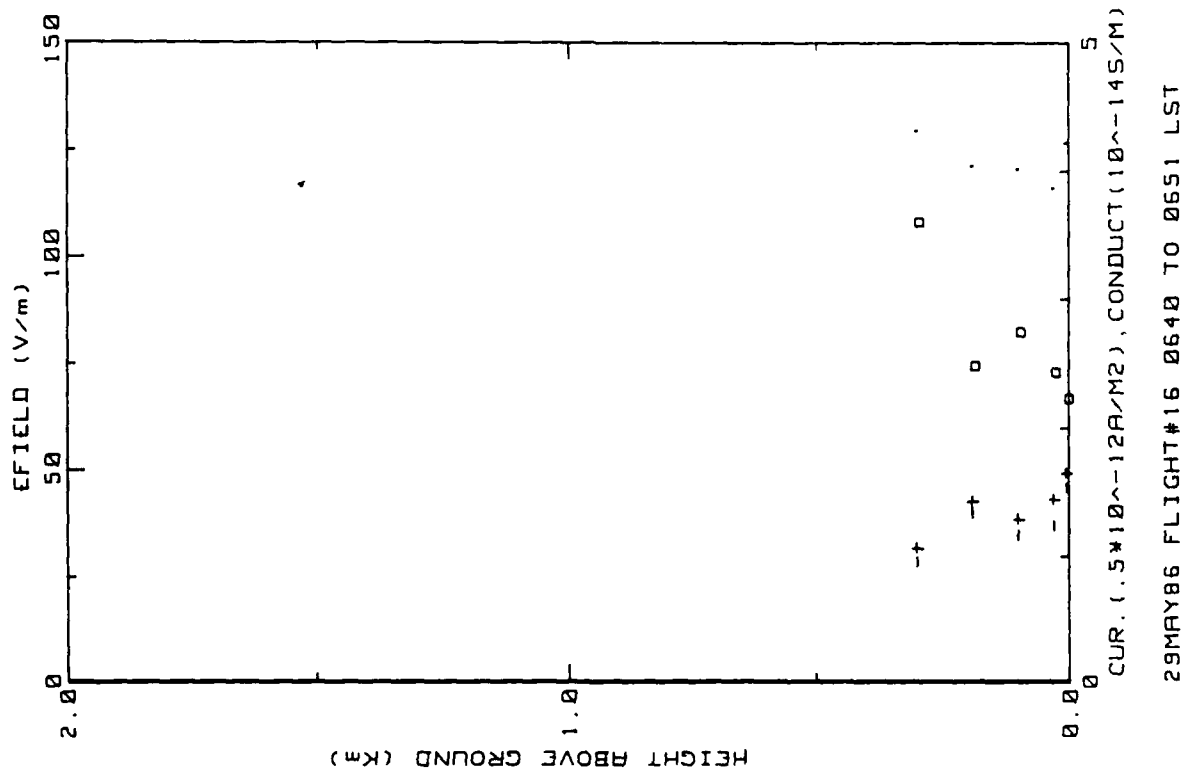


Figure 20q. Hobbs Flight 16 ladder profile (ref. Fig. 5a)

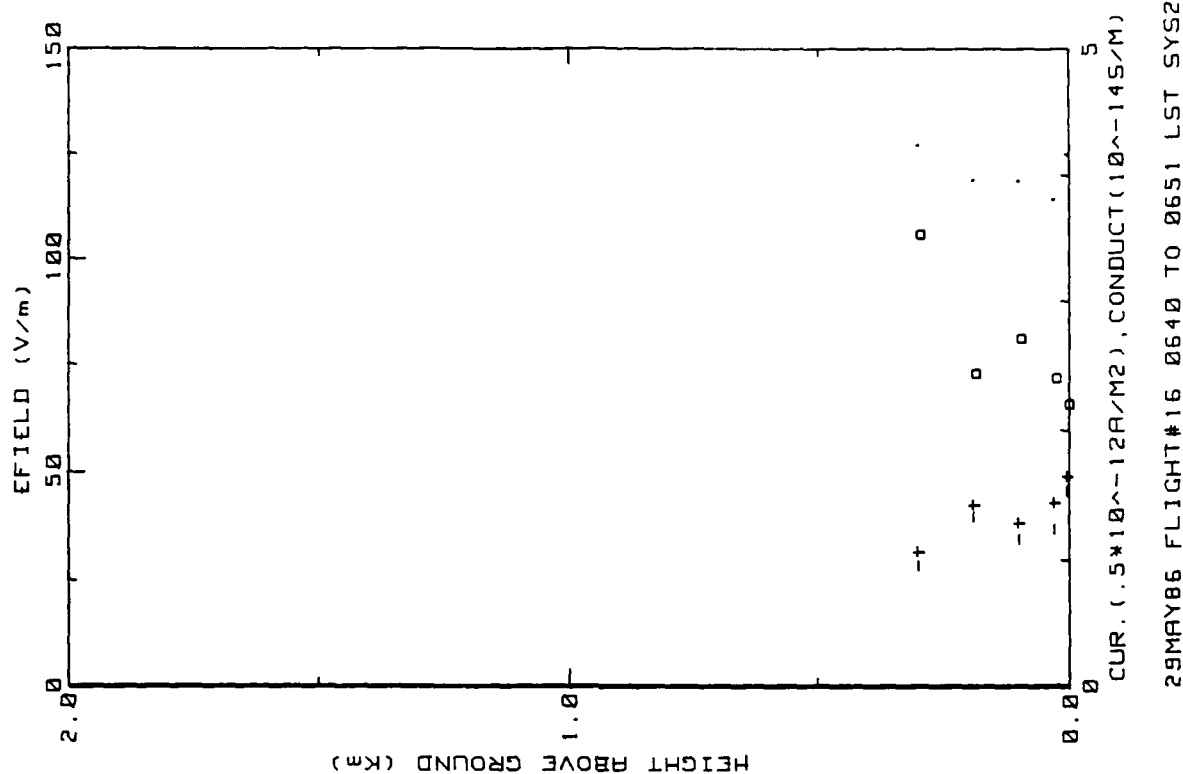


Figure 20r. Similar to 20q, but for inboard E<sub>field</sub> system.

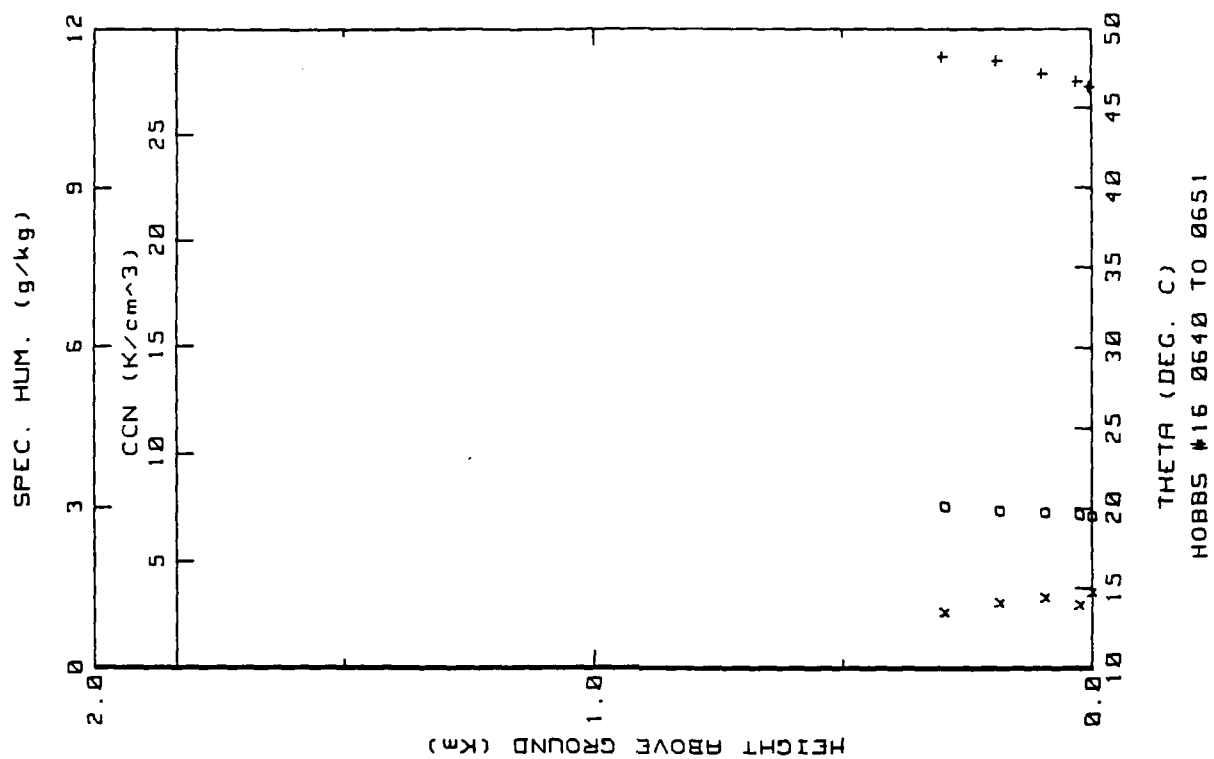


Figure 20t. Hobbs Flight 16 ladder profile (ref. Fig. 5c).

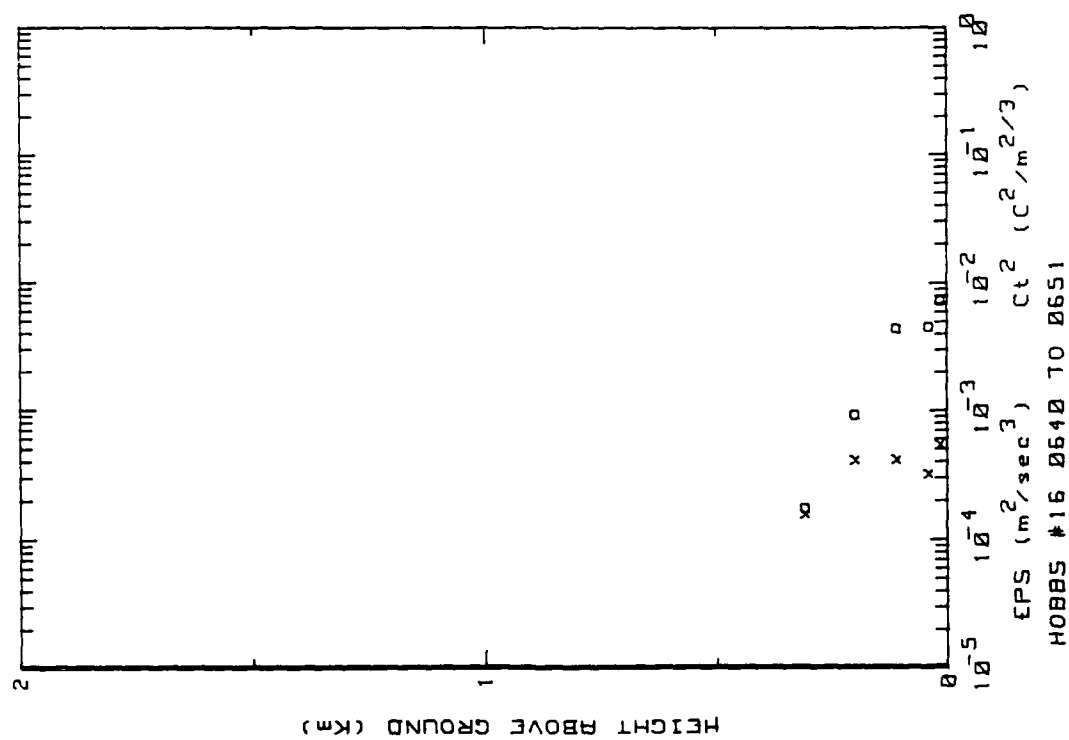
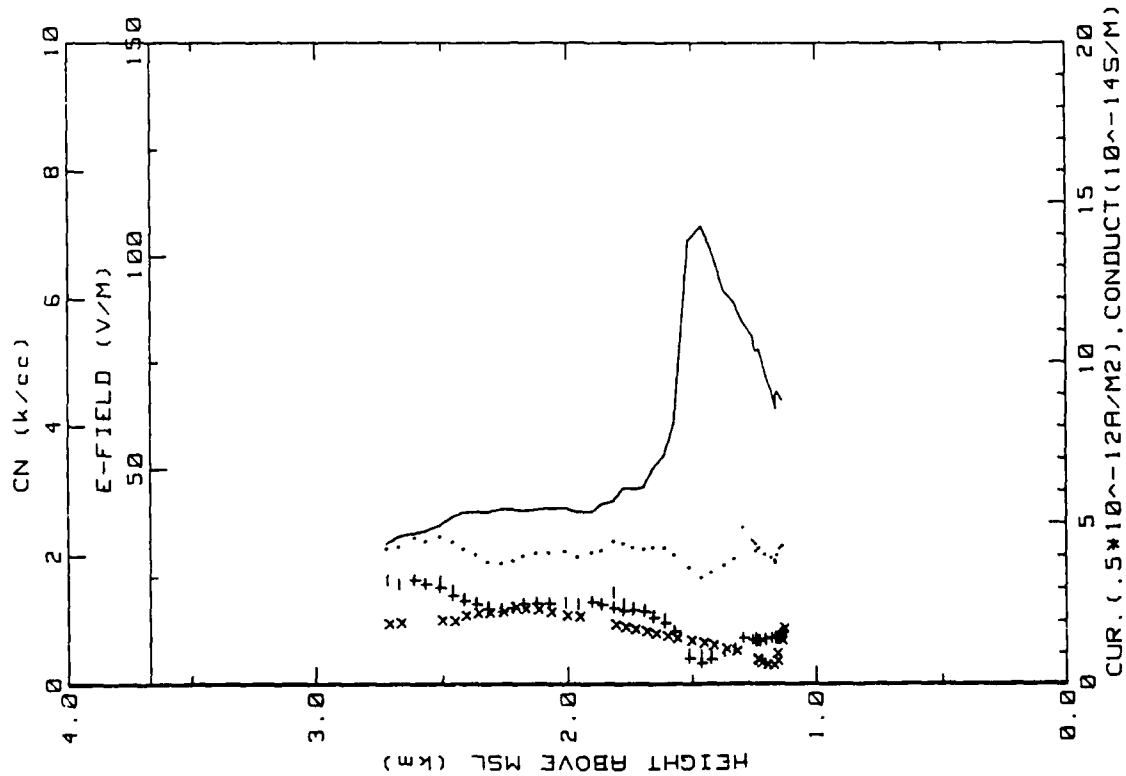
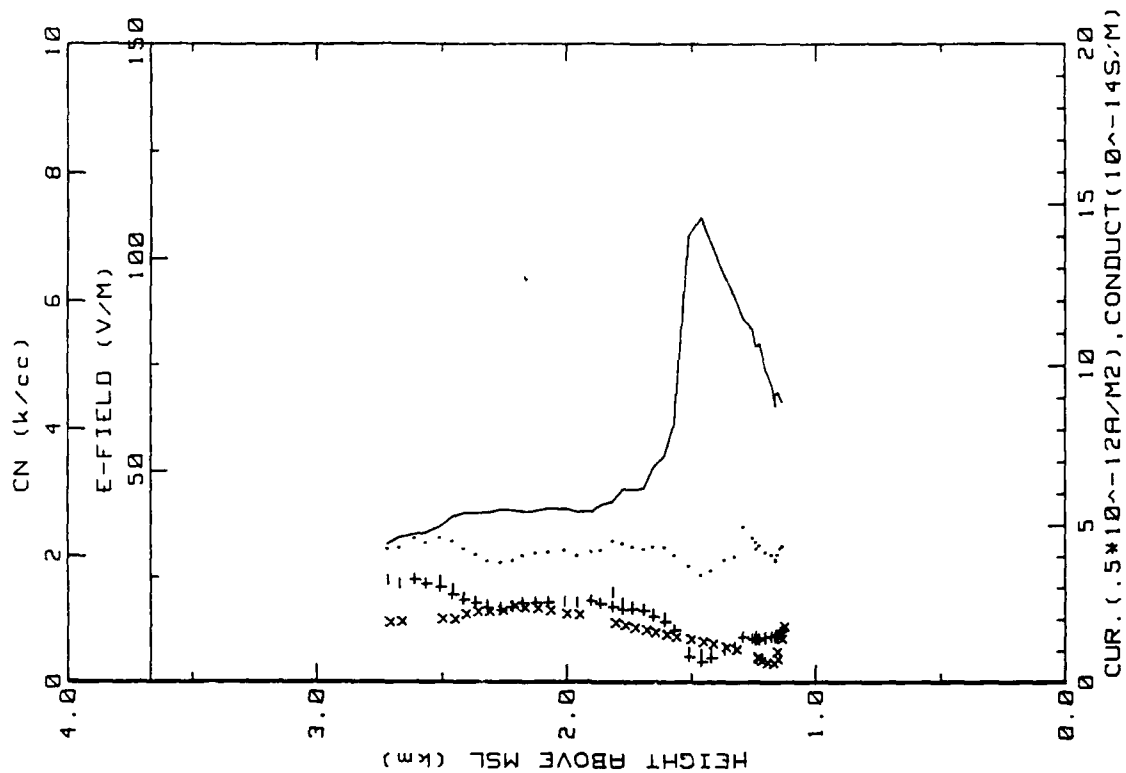


Figure 20s. Hobbs Flight 16 ladder profile (ref. Fig. 5b).



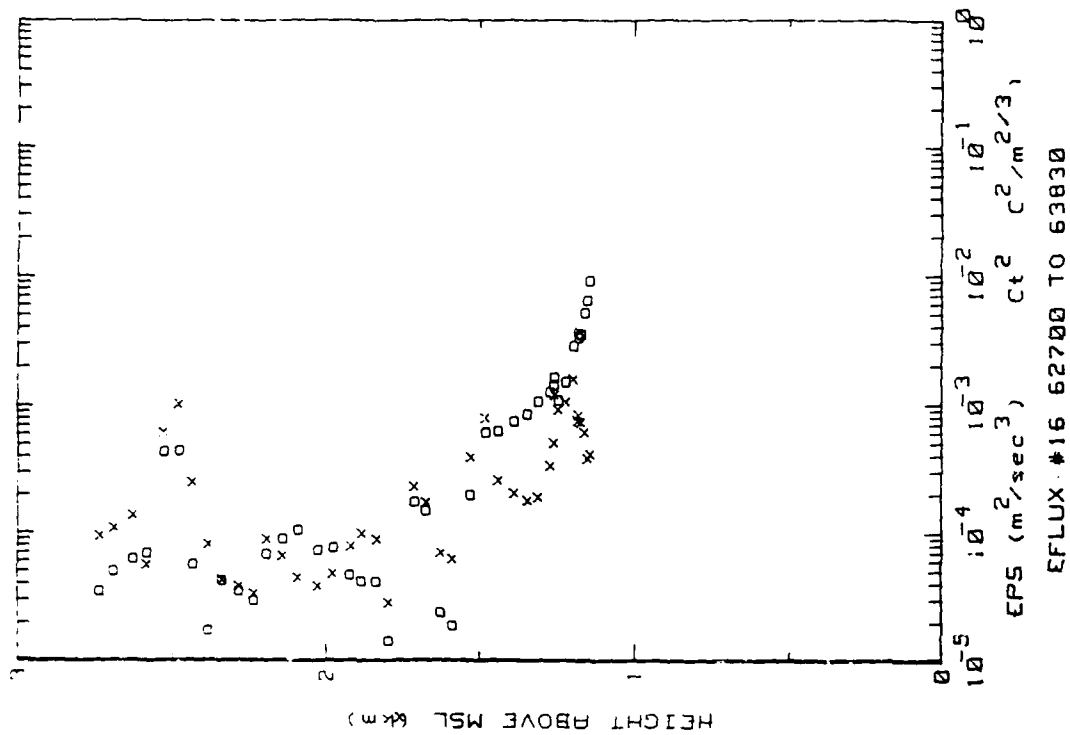
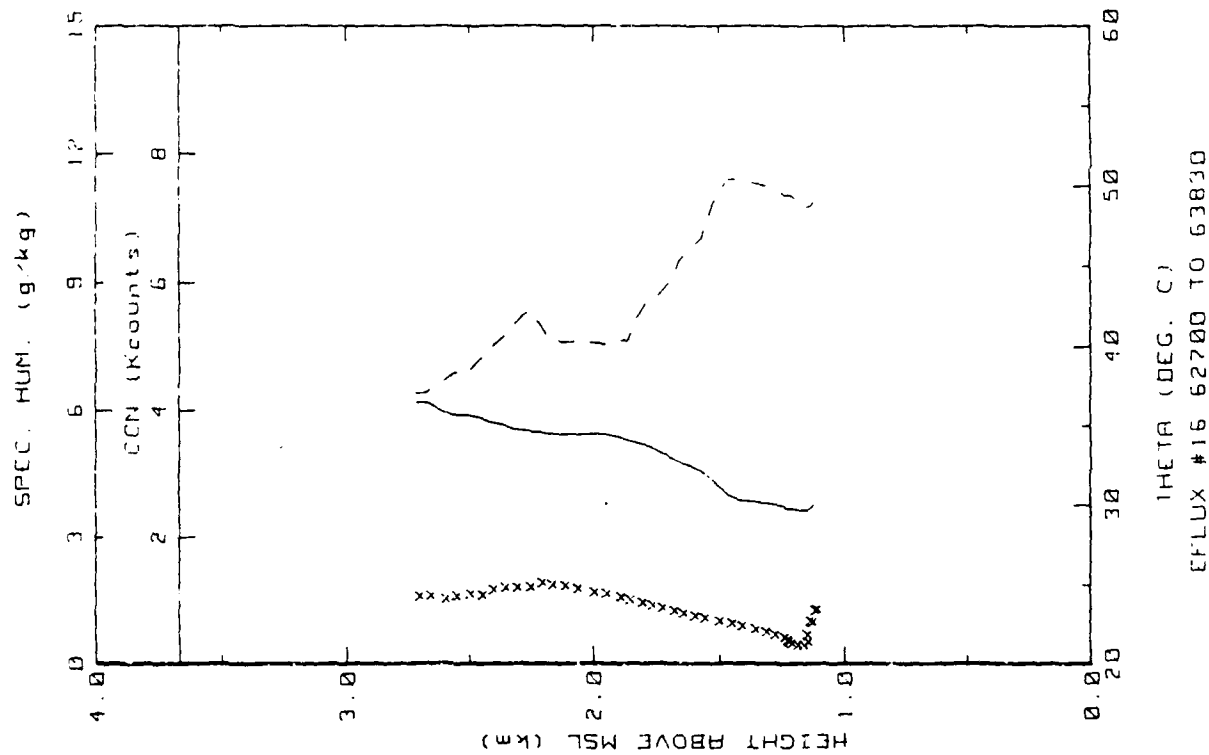
29MAY86 FLIGHT#16 62700 TO 63830 LST

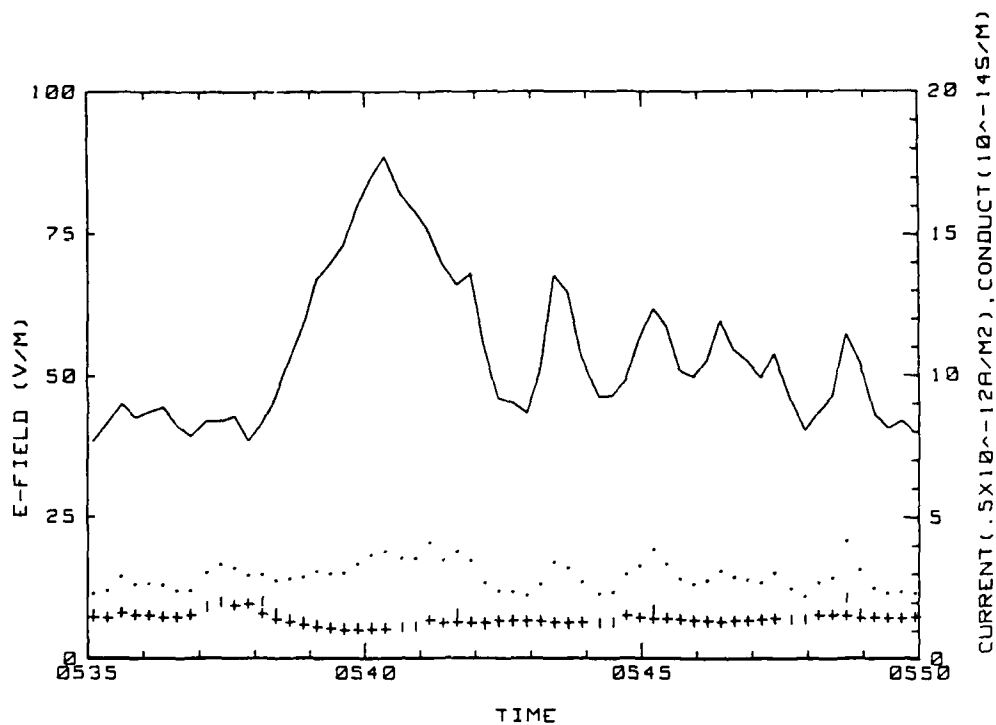
CUR. (.5\*10<sup>-12</sup>R/M<sup>2</sup>), CONDUCT(10<sup>-14</sup>S/M)



29MAY86 FLIGHT#16 62700 TO 63830 LST

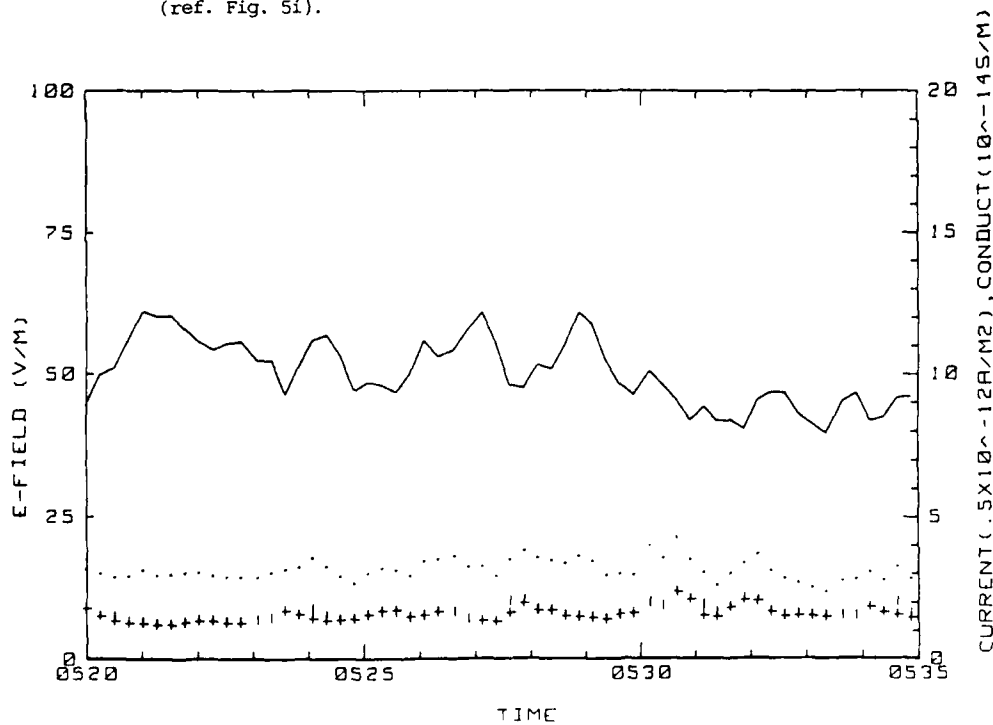
CUR. (.5\*10<sup>-12</sup>R/M<sup>2</sup>), CONDUCT(10<sup>-14</sup>S/M)





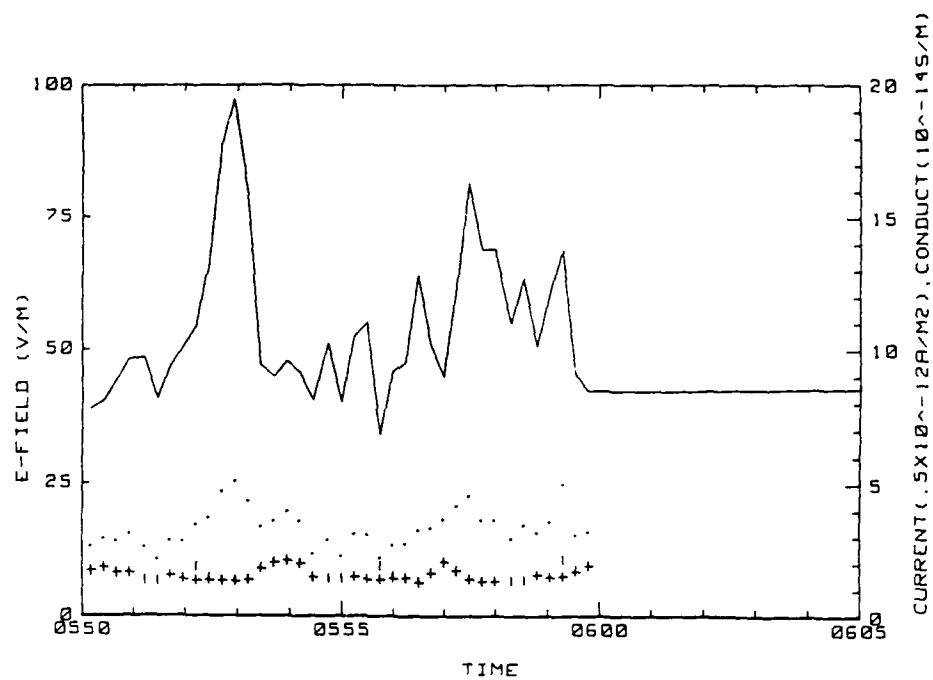
29 MAY 86 FLIGHT#16 053500 TO 055000 LST

Figure 20y. Hobbs Flight 16 time series of electrical parameters  
(ref. Fig. 5i).



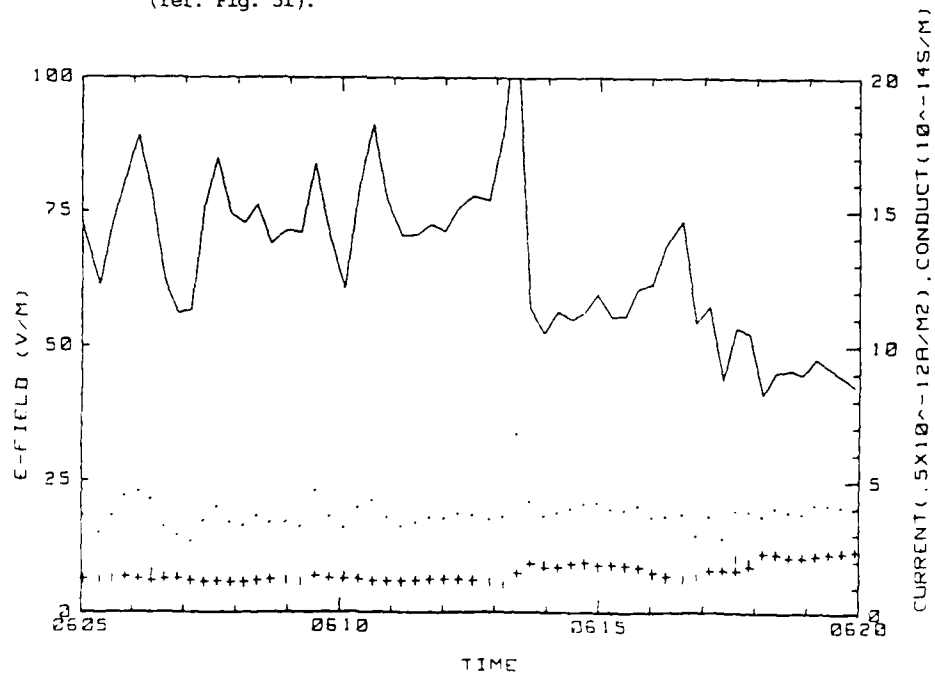
29 MAY 86 FLIGHT#16 052000 TO 053500 LST

Figure 20z. Hobbs Flight 16 time series of electrical parameters  
(ref. Fig. 5i).



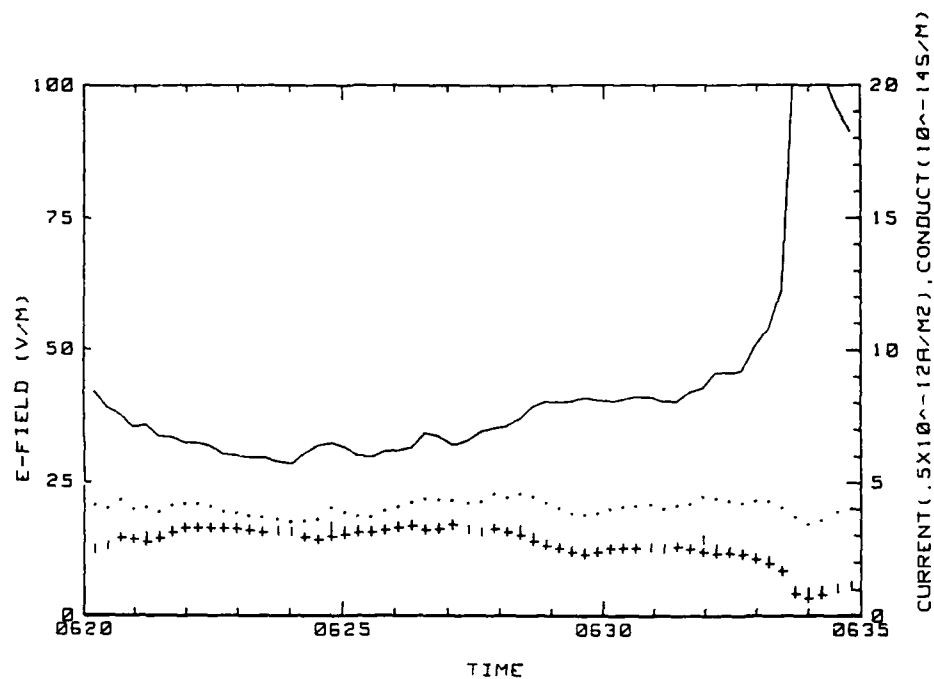
29 MAY 86 FLIGHT#16 055000 TO 060500 LST

Figure 20aa. Hobbs Flight 16 time series of electrical parameters (ref. Fig. 5i).



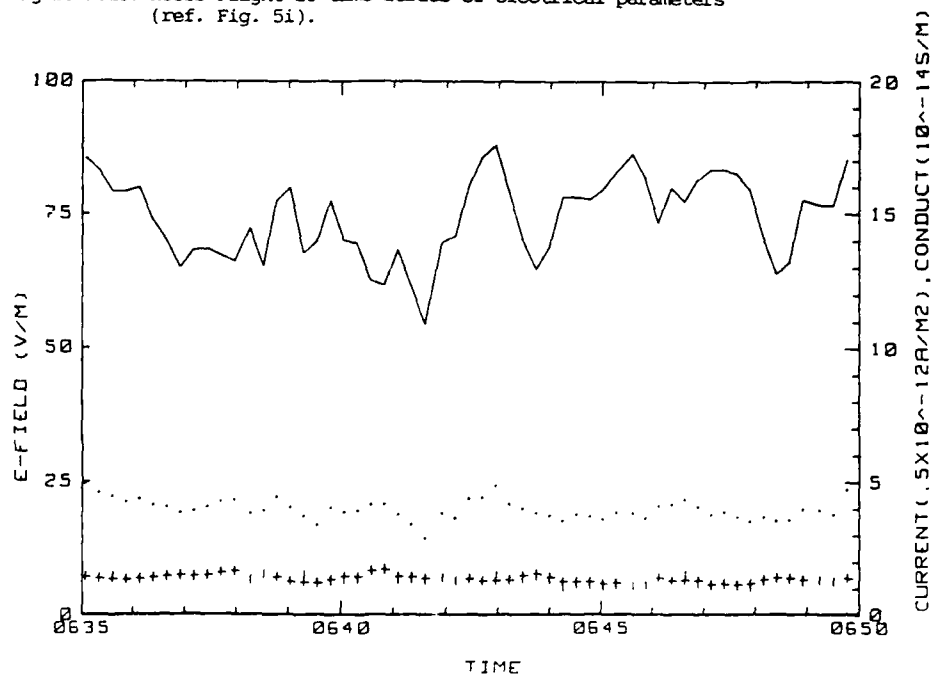
29 MAY 86 FLIGHT#16 060500 TO 062000 LST

Figure 20ab. Hobbs Flight 16 time series of electrical parameters (ref. Fig. 5i).



29 MAY 86 FLIGHT#16 062000 TO 063500 LST

Figure 20ac. Hobbs Flight 16 time series of electrical parameters (ref. Fig. 5i).



29 MAY 86 FLIGHT#16 063500 TO 065000 LST

Figure 20ad. Hobbs Flight 16 time series of electrical parameters (ref. Fig. 5i).



BAHAMAS DATA

Period: 5 March 1987 to 17 March 1987

Flight: 1

Date: 5 March 1987

Takeoff: 1244 (LT) from Nassau

Landed: 1518 at Rock Sound, Eleuthera (RSD)

Conditions: Overcast with 1200 m ceiling. Variable winds mainly from the NE to 10-12 m/s. Lots of whitecaps with 2-3 m swells.

Instruments: The negative conductivity tube, Lyman-alpha hygrometer and the aerosol counter did not work properly.

Summary: Mainly a shakedown flight to test instrumental operation and calibration. Ladder and spiral profiles were obtained enroute to RSD and upwind (NE) of Eleuthera over the deep ocean. Plume structure was noted in the electric field records.

Table 14a. RSD Flight 1 averages for constant altitude runs between Nassau and RSD.

AVERAGES FROM LEVEL RUNS

Time HHMM	N	Altitude km	E_field V/m	+Lam 10 <sup>-14</sup>	-Lam 10 <sup>-14</sup>	Con Curr 10 <sup>-12</sup>	Theta_v °	Rel Hum %	ONN k/cc
1247	197	.750	75.29	1.13	2.07	2.42	23.3	83.1	1.86
1303	41	.005	155.81	1.03	1.40	3.71	22.8	67.1	2.05
1306	52	.015	140.10	1.07	1.23	3.24	22.7	54.8	2.05
1309	31	.031	142.81	1.04	1.16	3.18	22.4	63.7	2.04
1311	36	.061	118.70	1.03	1.25	2.68	22.4	55.2	2.04
1318	40	.151	119.38	.98	1.19	2.60	22.3	67.5	2.01
1320	50	.305	55.52	1.03	1.59	2.48	22.4	71.9	1.97
1322	50	.510	78.38	1.23	2.35	2.79	22.5	80.4	1.89
1323	38	.910	62.37	1.35	2.44	2.30	22.5	81.9	1.82
1325	76	1.280	48.84	1.65	1.61	1.51	24.2	94.1	1.73
1340	51	1.550	56.53	1.48	.02	1.55	26.3	100.0	1.66
1350	20	.006	109.09	1.35	27.85	36.45	22.5	63.8	2.04
1352	14	.091	62.40	1.41	3.60	3.54	22.8	61.0	2.02
1405	56	.005	167.95	.93	1.24	3.74	23.0	63.5	2.04
1410	56	.015	175.58	.99	1.10	3.36	22.6	63.0	2.04
1413	30	.031	166.44	.84	.82	2.77	22.4	65.3	2.04
1416	52	.061	155.44	.83	1.11	2.97	22.2	63.7	2.03
1419	51	.151	123.93	.87	1.05	2.35	21.6	62.2	2.01
1422	54	.310	111.36	.90	1.04	2.15	21.9	67.7	1.96
1426	31	.910	93.08	.95	2.91	3.01	21.9	82.8	1.89
1430	31	.915	78.64	.93	0.00	2.15	22.0	94.9	1.82
1433	40	1.220	41.31	1.32	5.33	2.30	22.9	60.2	1.73
1437	41	1.520	42.40	1.89	1.65	1.58	25.0	94.6	1.67

Time HHMM	N	Altitude km	EPS m2/s3	CT2 C2/m2/3	Q g/kg	Cq2 (g/kg)2m2/3	Press mB	Trose °C	T_IR °C	T_dew °C
1247	197	.750	1.00E-03	7.86E-04	9.0	4.27E-03	926.3	14.2	24.3	11.3
1303	41	.006	3.64E-02	2.40E-02	10.1	8.64E-02	1011.1	20.7	24.5	14.4
1306	52	.015	1.42E-02	1.70E-02	9.7	3.45E-02	1009.8	20.5	24.4	13.7
1309	31	.031	7.23E-03	1.04E-02	9.3	1.85E-02	1008.3	20.2	24.3	13.1
1311	36	.061	3.65E-03	3.29E-03	9.4	1.18E-02	1004.6	19.9	23.6	13.2
1318	40	.151	2.27E-03	2.15E-03	9.3	7.07E-03	995.5	19.1	23.5	12.9
1320	50	.305	1.32E-03	8.55E-04	9.2	4.90E-03	976.6	17.6	23.6	12.4
1322	50	.510	1.41E-05	1.22E-03	9.9	5.02E-03	940.1	14.6	24.6	11.3
1323	38	.910	1.46E-05	9.71E-03	7.8	2.44E-02	906.8	11.8	24.8	8.7
1325	76	1.280	1.20E-05	1.01E-03	9.2	2.22E-03	867.2	9.8	22.8	8.9
1340	51	1.550	5.55E-04	3.44E-04	8.5	1.81E-03	839.2	9.0	21.6	9.0
1350	20	.006	8.36E-04	3.62E-02	9.7	1.10E-01	1010.0	20.8	25.6	13.7
1352	14	.091	9.61E-05	5.10E-03	8.9	2.71E-02	1001.2	20.1	25.5	12.3
1405	56	.006	9.40E-04	3.95E-02	9.7	9.82E-02	1009.7	20.9	24.7	13.6
1410	56	.015	3.18E-03	1.89E-02	9.4	3.57E-02	1003.4	20.5	24.6	13.2
1413	30	.031	7.70E-03	1.31E-02	9.3	3.74E-02	1006.5	20.1	24.6	13.4
1416	52	.061	1.31E-02	6.01E-02	9.1	2.02E-02	1003.8	19.7	24.3	12.6
1419	51	.151	5.20E-03	2.20E-03	8.3	5.88E-03	994.7	18.5	23.9	11.1
1422	54	.310	1.03E-02	1.40E-03	8.4	3.87E-03	974.5	17.1	24.3	11.0
1426	31	.910	1.97E-03	2.93E-03	8.9	3.46E-03	939.6	14.0	24.3	11.1
1430	31	.915	2.47E-03	5.11E-03	9.7	5.75E-03	908.8	11.3	24.3	10.5
1433	40	1.220	8.42E-04	1.81E-03	9.1	5.50E-03	871.1	9.4	23.5	9.0
1437	41	1.520	1.04E-04	2.35E-04	7.5	1.02E-03	841.9	8.3	21.9	7.4

Table 14b. RSD Flight 1 (standard deviations)/averages for  
constant altitude runs between Nassau and RSD.

STANDARD DEVIATIONS/MEAN VALUES

Time	E_Field	+Lam	-Lam	Con Curr	CCN	EPS	CT2	Q	Co2
1247	.093	.071	.297	.305	.004	.445	.563	.032	2.305
1303	.130	.073	.123	.158	.000	.280	.261	.055	1.473
1306	.136	.091	.126	.167	.000	.238	.287	.052	2.373
1309	.155	.062	.074	.165	.001	.371	.309	.043	1.406
1311	.092	.057	.115	.101	.001	.391	.552	.043	1.583
1318	.066	.037	.072	.093	.001	.511	.799	.031	1.083
1320	.064	.071	.130	.119	.002	.553	.505	.033	.683
1322	.122	.112	.122	.191	.002	.465	.702	.048	.561
1323	.063	.201	.499	.288	.002	.509	.955	.139	3.075
1325	.130	.034	.612	.298	.002	1.662	1.409	.024	.389
1340	.215	.182	.417	.296	.005	.950	1.270	.021	.453
1350	.170	.039	.417	.455	.000	.176	.177	.063	1.593
1352	.136	.034	.184	.215	.002	.899	.796	.054	2.588
1405	.162	.080	.306	.231	.000	.263	.191	.068	1.769
1410	.144	.089	.408	.272	.000	.389	.267	.070	2.679
1413	.115	.071	.247	.106	.001	.181	.274	.050	2.263
1416	.106	.085	.133	.102	.001	.145	.363	.045	3.543
1419	.072	.045	.066	.071	.001	.800	.610	.038	2.301
1422	.047	.035	.101	.069	.001	.537	.505	.040	1.023
1426	.051	.054	.143	.299	.002	.341	.550	.031	1.668
1430	.472	.107	0.000	1.505	.002	.493	.558	.045	3.061
1433	.113	.061	.941	.699	.002	1.856	1.096	.134	2.766
1437	.078	.041	.752	.379	.002	.465	1.601	.024	.450

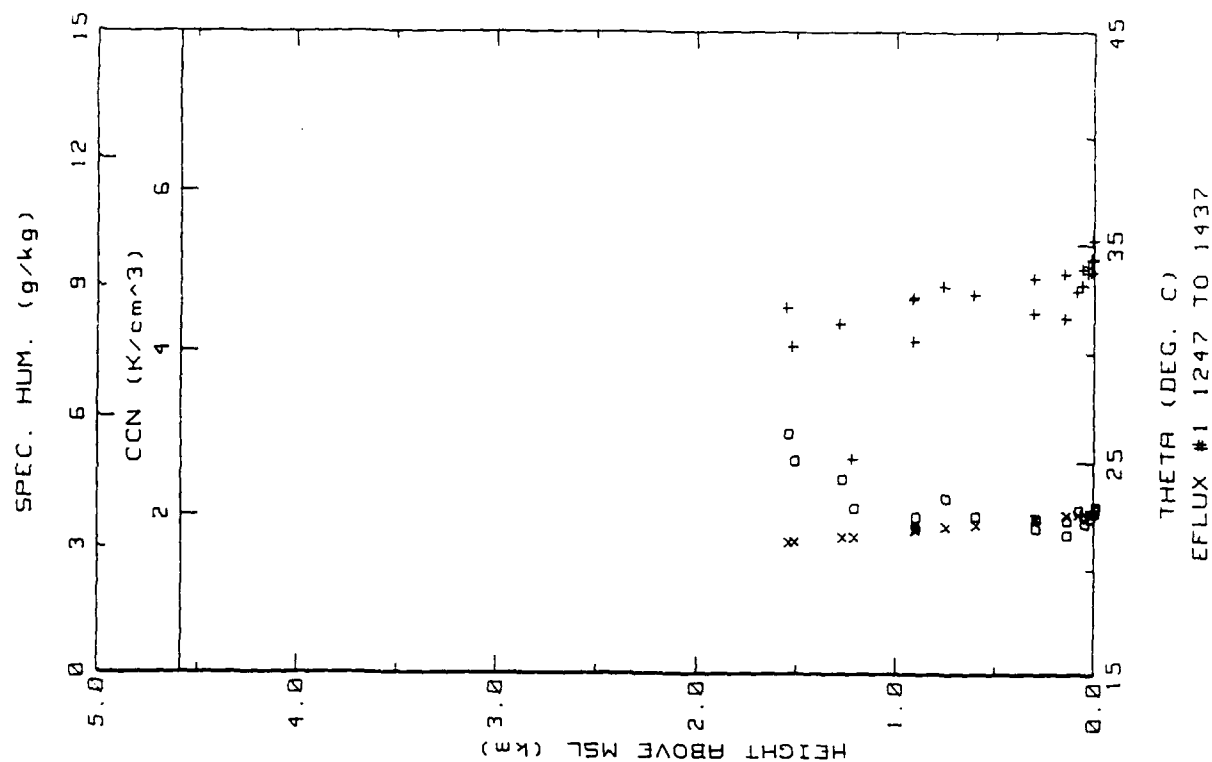


Figure 21b. RSD Flight 1 ladder profile over shallow water between Nassau and RSD. (ref. Fig. 5c).

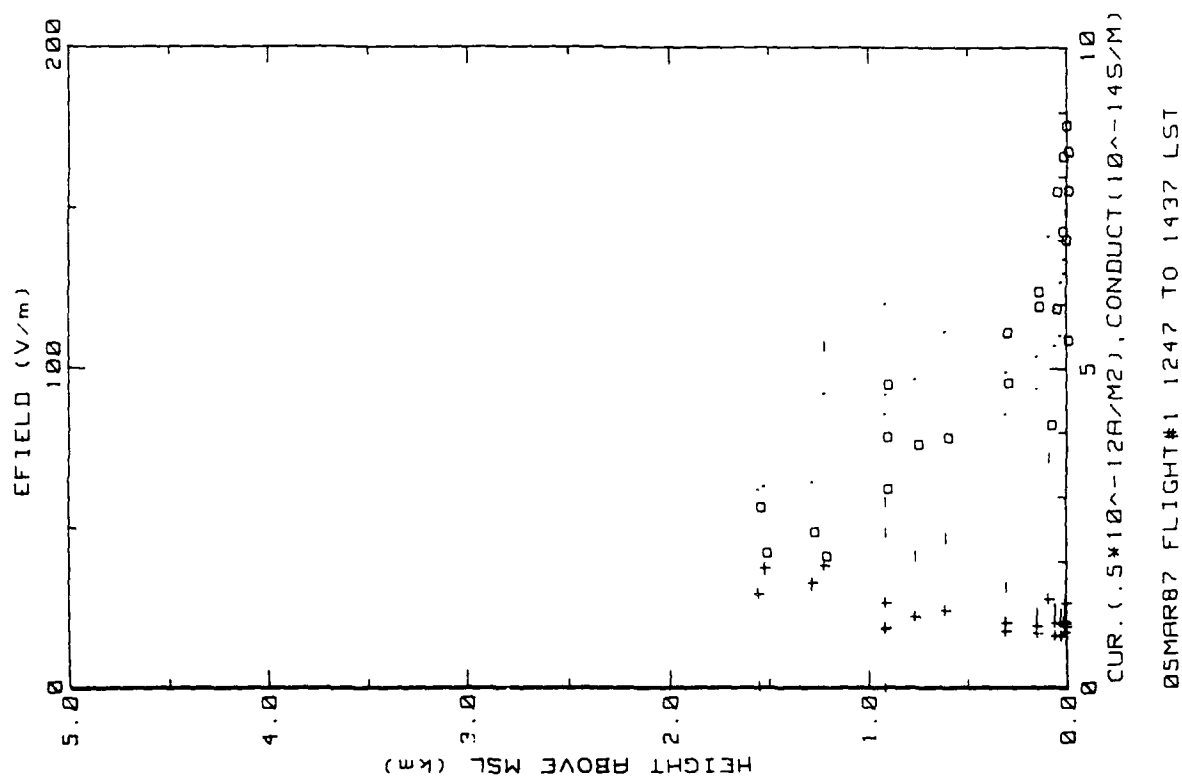


Figure 21a. RSD Flight 1 ladder profile over shallow water between Nassau and RSD. (ref. Fig. 5a).

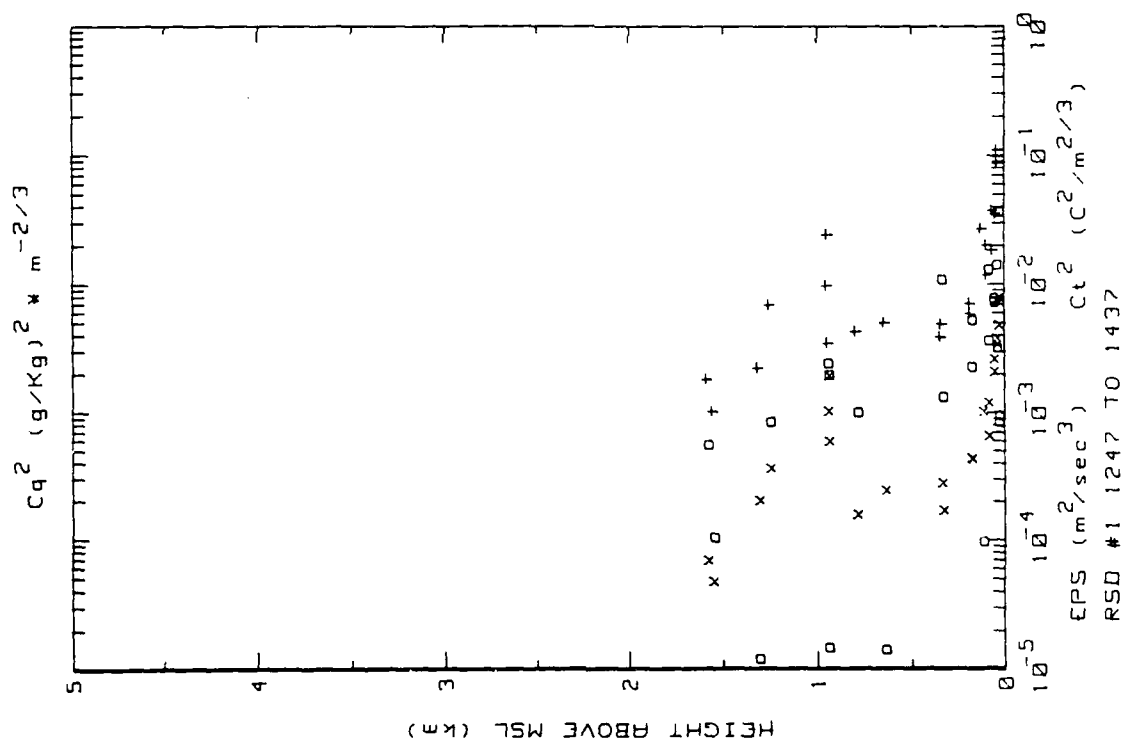


Figure 21c. RSD Flight 1 ladder profile over shallow water between Nassau and RSD. (ref. Fig. 5b).

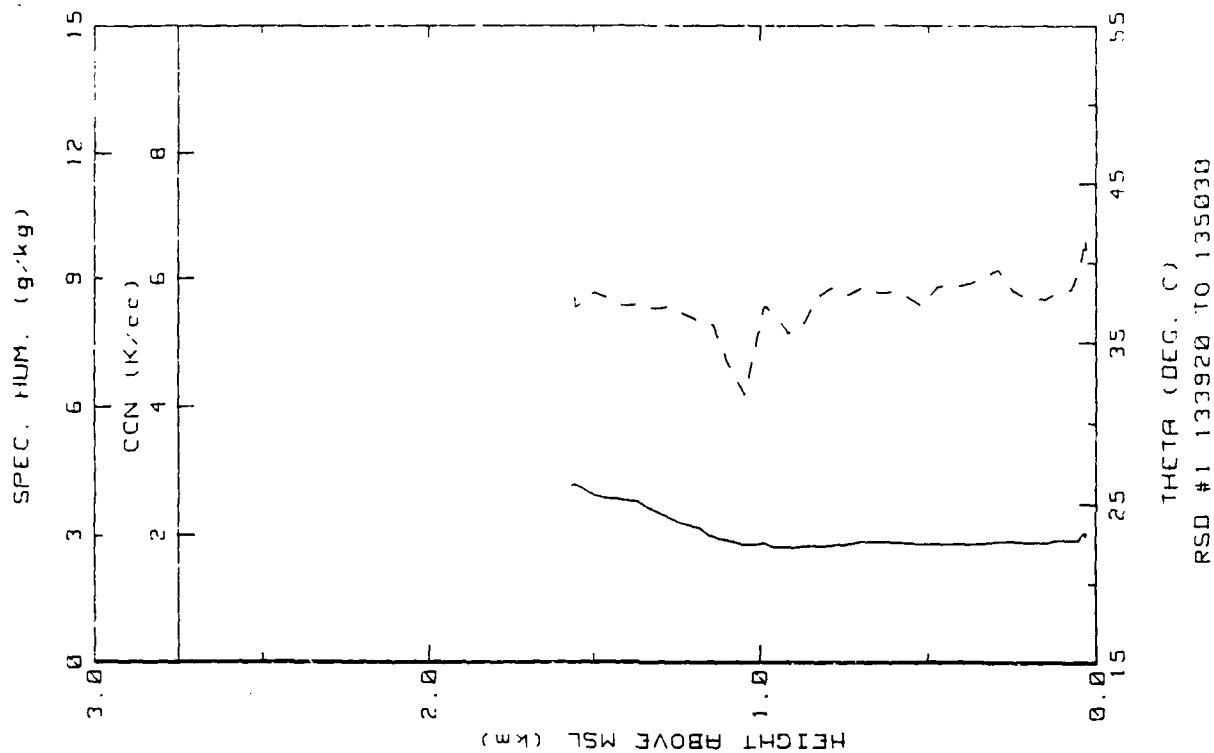


Figure 21e. RSD Flight 1 spiral down-sounding between Nassau and RSD (ref. Fig. 5h).

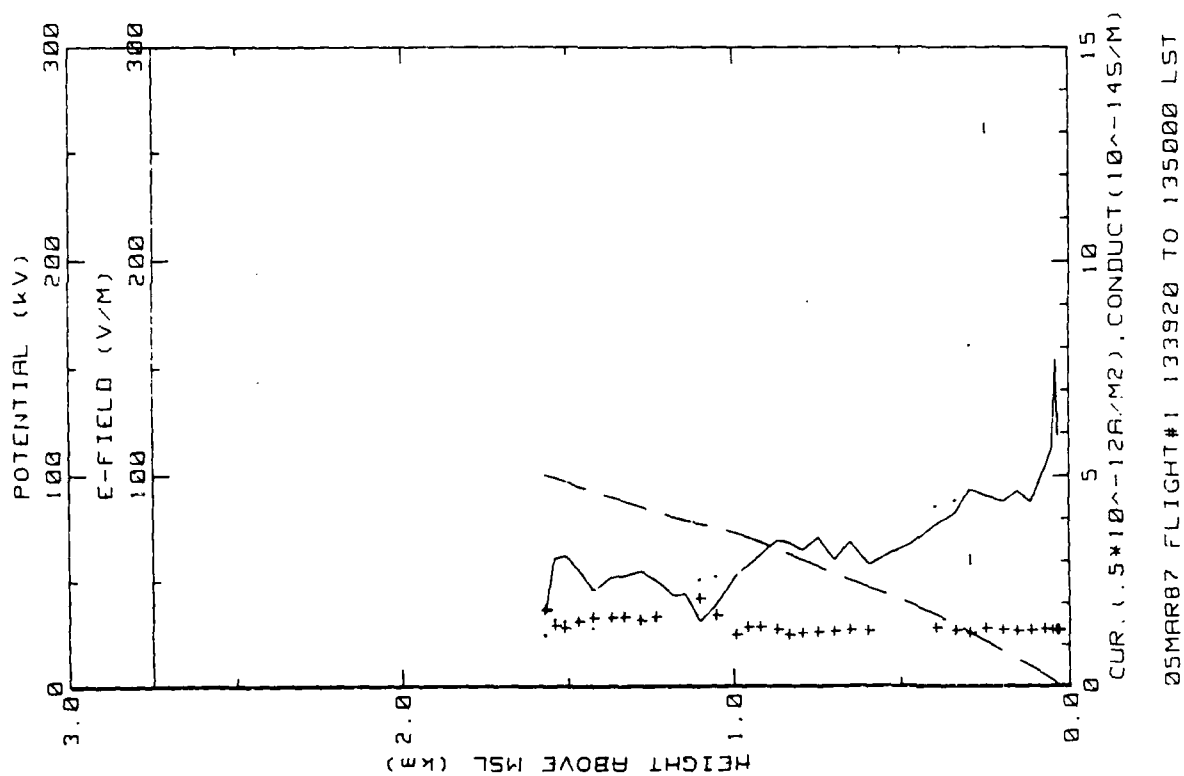


Figure 21d. RSD Flight 1 spiral down-sounding between Nassau and RSD (ref. Fig. 5e).

Flight: 2

Date: 8 March 1987

Takeoff: 1241 (LT) from RSD

Landed: 1624 at RSD

Conditions: Clear skies; light winds (3 m/s) from the west with a layer of haze evident below the trade inversion. Ocean surface calm with very few whitecaps. Scattered cumulus clouds formed to the E of RSD during the last hour of flight.

Instruments: All worked properly.

Summary: Two separate sets of ladder and spiral profiles were obtained; the first were over shallow water about 50 km SW of Rock Sound and the second over deep water 50-100 km E. Aerosol counts were higher and somewhat variable E of RSD denoting a changing air mass. Convection appeared to be organized as evidenced by periodic variations in the electric field records when flying within 50 m of the surface.



Table 15a. RSD Flight 2 averages for constant altitude runs performed SW of RSD over shallow water.

AVERAGES FROM LEVEL RUNS

Time HHH	N	Altitude km	E_field V/m	+Lam 10 <sup>-14</sup>	-Lam 10 <sup>-14</sup>	Con Curr 10 <sup>-12</sup>	Theta_v C	Rel Hum %	CNN k/cc
1303	75	.006	130.58	1.45	1.41	3.70	26.8	71.1	1.43
1307	34	.015	130.81	1.35	1.42	3.55	26.8	72.0	1.43
1311	46	.035	126.62	1.30	1.37	3.40	27.0	72.4	1.60
1312	49	.062	105.35	1.46	1.57	3.19	26.8	70.7	1.49
1315	33	.148	91.11	1.55	1.66	2.90	26.7	74.2	1.38
1317	33	.313	74.30	1.73	1.79	2.63	26.7	70.8	1.16
1322	35	.449	65.68	1.87	1.94	2.54	26.6	71.8	1.07
1325	41	.518	62.58	2.00	2.03	2.48	26.7	70.9	.94
1329	44	.917	74.72	1.60	1.59	2.38	28.9	79.8	.94
1333	52	1.229	56.85	2.04	2.04	2.29	30.2	81.7	.95
1338	62	1.535	32.14	2.68	3.48	2.29	32.2	77.6	.92
1347	54	2.142	34.59	3.58	3.54	2.51	33.4	24.9	.51
1353	22	2.775	25.99	4.56	4.54	2.40	36.6	40.0	.51
1400	61	3.337	18.88	6.22	6.35	2.37	38.9	16.1	.42
1404	58	4.138	13.79	7.63	8.42	2.21	42.8	12.8	.51
1424	43	0.000	138.28	1.41	2.02	4.55	26.5	74.7	1.17
1426	24	.015	134.56	1.41	1.71	3.96	26.3	75.6	1.24
1428	89	.031	119.19	1.20	1.28	2.96	26.6	76.2	1.30

Time HHH	N	Altitude km	EPS m2/s3	CT2 C2/m2/3	O g/kg	Co2 (g/kg)2m-2/3	Press mB	Trose C	T <sub>IR</sub> C	T <sub>deu</sub> C
1303	76	.006	1.60E-03	1.34E-02	13.4	1.86E-02	1005.0	24.3	25.2	18.7
1307	34	.015	7.21E-04	6.56E-03	13.5	1.21E-02	1003.9	24.1	25.0	18.7
1311	46	.035	5.44E-04	3.33E-03	13.6	9.53E-03	1002.1	24.1	25.0	18.8
1312	49	.062	4.30E-04	1.83E-03	13.0	8.45E-03	999.0	23.8	25.0	19.2
1315	33	.148	4.64E-04	1.99E-03	13.0	8.35E-03	989.1	22.8	24.9	18.0
1317	33	.313	5.70E-04	1.61E-02	11.6	1.68E-02	970.5	21.5	25.0	15.9
1322	35	.449	3.46E-04	3.34E-02	11.0	1.58E-02	955.3	20.1	25.0	14.9
1325	41	.518	1.79E-04	5.29E-03	10.2	6.25E-03	936.8	18.8	24.9	13.4
1329	44	.917	6.09E-05	2.16E-04	11.2	6.67E-03	904.5	17.8	24.6	14.0
1333	52	1.229	2.41E-05	1.70E-05	10.7	6.72E-03	872.0	16.1	24.6	13.0
1338	62	1.535	3.67E-05	1.52E-04	9.9	6.98E-03	841.0	15.2	24.5	11.3
1347	54	2.142	9.81E-05	1.33E-05	2.7	2.39E-02	782.0	11.5	24.3	-7.5
1353	22	2.775	7.11E-06	0.00E+00	3.7	2.30E-02	724.2	8.2	24.6	-4.8
1400	61	3.337	4.89E-04	4.25E-03	1.2	4.17E-03	670.9	4.5	24.3	-19.6
1404	58	4.138	5.63E-06	8.36E-05	.9	0.00E+00	511.4	.7	24.1	-20.6
1424	43	0.000	1.72E-03	2.83E-02	13.9	5.32E-02	1007.1	24.1	26.5	19.0
1426	24	.015	5.70E-04	7.87E-03	13.2	2.40E-02	1005.8	23.8	26.9	19.2
1428	89	.031	2.34E-04	2.48E-03	14.6	1.32E-02	1003.2	23.7	24.7	15.3

Table 15b. RSD Flight 2 (standard deviations)/averages for constant altitude runs performed SW of RSD over shallow water.

STANDARD DEVIATIONS/MEAN VALUES

Time	E_Field	+Lam	-Lam	Con Curr	CON	EPS	CT2	Q	Co2
1303	.192	.113	.141	.166	.065	.353	.408	.035	1.015
1307	.162	.024	.050	.155	.051	.257	.390	.025	.398
1311	.188	.029	.044	.177	.062	.358	.284	.029	.371
1312	.098	.050	.053	.078	.065	.353	.468	.028	.481
1315	.056	.037	.047	.063	.130	.217	.393	.029	.629
1317	.069	.091	.089	.082	.067	.263	.269	.090	1.074
1322	.210	.120	.131	.168	.076	.714	.896	.116	1.369
1325	.106	.097	.080	.045	.332	.936	.631	.061	1.073
1329	.041	.018	.012	.046	.075	.585	2.114	.022	.325
1333	.125	.069	.064	.120	.080	.703	4.518	.025	.351
1338	.050	.038	.055	.038	.118	.763	1.804	.025	.484
1347	.060	.052	.012	.065	.400	.929	7.896	.096	.235
1353	.023	.032	.040	.045	.050	.194	0.000	.220	.402
1400	.019	.022	.030	.020	.069	.828	.932	.306	2.163
1404	.020	.004	.005	.026	.225	.242	.561	.021	0.006
1424	.204	.025	.082	.219	.052	.225	.245	.018	.961
1426	.163	.043	.335	.321	.042	.310	.459	.016	.484
1428	.146	.052	.144	.156	.053	.324	.339	.019	.322

Table 15c. RSD Flight 2 averages for constant altitude runs performed E of RSD over deep water.

AVERAGES FROM LEVEL RUNS

Time HHMM	N	Altitude km	E_field V/m	+Lam 10 <sup>-14</sup>	-Lam 10 <sup>-14</sup>	Con Curr 10 <sup>-12</sup>	Theta_v C	Rel Hum %	CNN k/cc
1455	32	.003	133.42	1.37	1.53	3.93	27.1	65.6	.41
1458	26	.006	140.00	1.24	1.50	3.83	26.7	63.2	.61
1459	31	.015	146.27	1.23	1.46	3.93	26.6	67.9	.77
1503	39	.003	177.41	.97	1.12	3.78	25.2	70.9	2.07
1512	38	.015	178.78	1.04	1.20	3.94	26.1	70.6	1.56
1513	38	.031	159.58	.96	1.27	3.57	26.0	78.5	1.77
1518	26	.006	256.60	.58	.94	3.56	26.2	79.8	5.56
1520	36	.015	223.33	.50	.84	3.10	26.1	81.1	6.75
1523	39	.031	255.75	.50	.95	3.03	26.0	82.2	7.12
1525	37	.071	279.90	.54	.95	4.61	26.0	84.1	5.76
1527	31	.170	154.03	.85	1.23	3.14	26.0	87.9	3.14
1525	52	.330	144.35	.75	1.04	2.53	26.1	90.5	3.14
1535	27	.630	59.50	1.57	1.97	2.06	26.3	99.6	1.00
1537	34	.035	51.35	1.33	2.55	2.06	27.1	43.3	1.95
1540	25	1.273	39.31	3.15	3.13	2.47	29.1	12.1	2.50
1544	27	1.873	35.93	3.92	3.78	2.61	30.8	18.0	.45
1547	38	2.494	26.78	4.74	4.59	2.45	34.0	13.2	.22
1550	42	3.038	24.49	5.41	4.93	2.51	36.5	55.9	.22
1554	36	3.683	16.98	7.37	7.91	2.51	39.8	11.7	.25
1557	26	4.132	14.73	8.67	9.33	2.65	41.3	14.0	.14
1614	31	.015	119.12	1.47	1.39	3.42	26.7	68.4	1.66
1616	34	.031	102.91	1.57	1.57	3.42	26.2	63.7	1.36

Time HHMM	N	Altitude km	EPS m2/s3	C12 C2/m2/3	Q g/kg	Cc2 (g/rc)2m-2/3	Press mb	Trose C	T_IR C	T_dew C
1455	32	.003	2.11E-03	1.99E-02	12.7	2.41E-02	1005.6	24.7	24.8	17.8
1458	26	.006	1.29E-03	1.73E-02	12.8	1.49E-02	1005.1	24.2	24.8	18.0
1459	31	.015	6.32E-04	7.46E-03	12.6	1.47E-02	1004.1	24.1	24.6	17.8
1503	39	.003	1.20E-03	1.49E-02	12.9	1.45E-02	1004.7	23.7	24.1	19.1
1512	38	.015	7.66E-04	7.56E-03	12.7	1.20E-02	1004.0	23.5	23.6	17.9
1513	38	.031	5.23E-04	4.87E-03	13.8	9.22E-03	1002.0	23.1	23.7	19.2
1518	26	.006	1.00E-03	1.23E-02	14.2	1.20E-02	1004.4	23.4	23.8	19.7
1520	36	.015	6.03E-04	4.13E-03	14.4	8.43E-03	1003.4	23.2	23.4	19.6
1523	39	.031	3.04E-04	2.32E-03	14.4	9.71E-03	1001.3	22.9	22.5	19.7
1525	37	.071	2.13E-04	1.30E-03	14.5	9.22E-03	998.2	22.7	23.4	19.8
1527	31	.170	1.75E-04	2.28E-03	14.4	9.55E-03	987.0	21.7	25.1	19.6
1525	52	.330	1.25E-04	1.61E-03	13.9	9.83E-03	968.3	20.3	23.5	18.7
1535	27	.630	7.62E-06	3.45E-04	9.8	4.37E-03	935.6	18.3	23.5	12.7
1537	34	.035	1.53E-05	1.06E-04	5.7	2.92E-03	902.6	15.9	23.5	4.2
1540	25	1.273	2.20E-05	0.00E+00	1.6	3.92E-04	867.6	16.2	23.2	-13.7
1544	27	1.873	1.46E-05	1.02E-04	1.5	4.69E-03	807.5	11.0	23.6	-11.9
1547	38	2.494	1.45E-05	1.84E-04	1.3	4.88E-03	749.9	9.0	23.8	-12.9
1550	42	3.038	2.78E-04	6.11E-04	4.3	3.03E-02	695.5	4.8	23.6	-5.3
1554	36	3.683	7.23E-05	9.27E-05	.8	3.27E-02	547.9	2.5	23.5	-24.2
1557	26	4.132	5.47E-05	1.05E-04	.9	3.80E-03	510.1	.3	24.0	-24.5
1614	31	.015	7.24E-04	5.72E-03	12.1	3.51E-02	1004.4	23.3	24.2	17.1
1616	34	.031	7.10E-04	1.46E-03	11.6	2.49E-02	1001.5	23.7	25.0	15.4

Table 15d. RSD Flight 2 (standard deviations)/averages for  
constant altitude runs performed E of RSD over deep  
water.

STANDARD DEVIATIONS/MEAN VALUES

Time	E_Field	+Lam	-Lam	Con Curr	CON	EPS	.012	0	042
1455	.171	.029	.056	.165	.053	.220	.231	.029	1.473
1458	.155	.040	.114	.133	.222	.305	.212	.036	.714
1459	.138	.037	.053	.123	.501	.155	.207	.030	1.236
1508	.139	.042	.080	.129	.196	.201	.204	.024	1.269
1512	.207	.104	.140	.137	.236	.279	.307	.034	.775
1513	.101	.046	.068	.124	.063	.435	.503	.020	.669
1518	.162	.035	.164	.191	.025	.173	.173	.012	.836
1520	.179	.092	.114	.208	.091	.338	.374	.020	.367
1523	.164	.101	.112	.180	.054	.224	.285	.015	.346
1525	.155	.225	.127	.317	.255	.282	.566	.013	.293
1527	.246	.213	.144	.223	.231	.375	.651	.025	.309
1529	.193	.270	.143	.235	.354	.421	.522	.026	.438
1535	.108	.064	.063	.123	.436	.245	1.096	.034	.471
1537	.462	.416	.274	.080	1.109	.500	1.283	.146	1.179
1540	.065	.022	.017	.053	.708	.638	0.000	.025	1.314
1544	.013	.004	.009	.013	.079	.424	1.392	.121	.541
1547	.010	.003	.012	.015	.093	.441	.470	.071	.496
1550	.020	.021	.064	.048	.078	.241	.400	.065	.873
1554	.017	.009	.012	.024	.069	.457	1.045	.013	.147
1557	.010	.010	.010	.009	.402	.068	.513	.015	1.573
1614	.183	.073	.114	.103	.505	.266	.437	.040	1.201
1616	.260	.049	.096	.223	.061	.257	.426	.037	.827

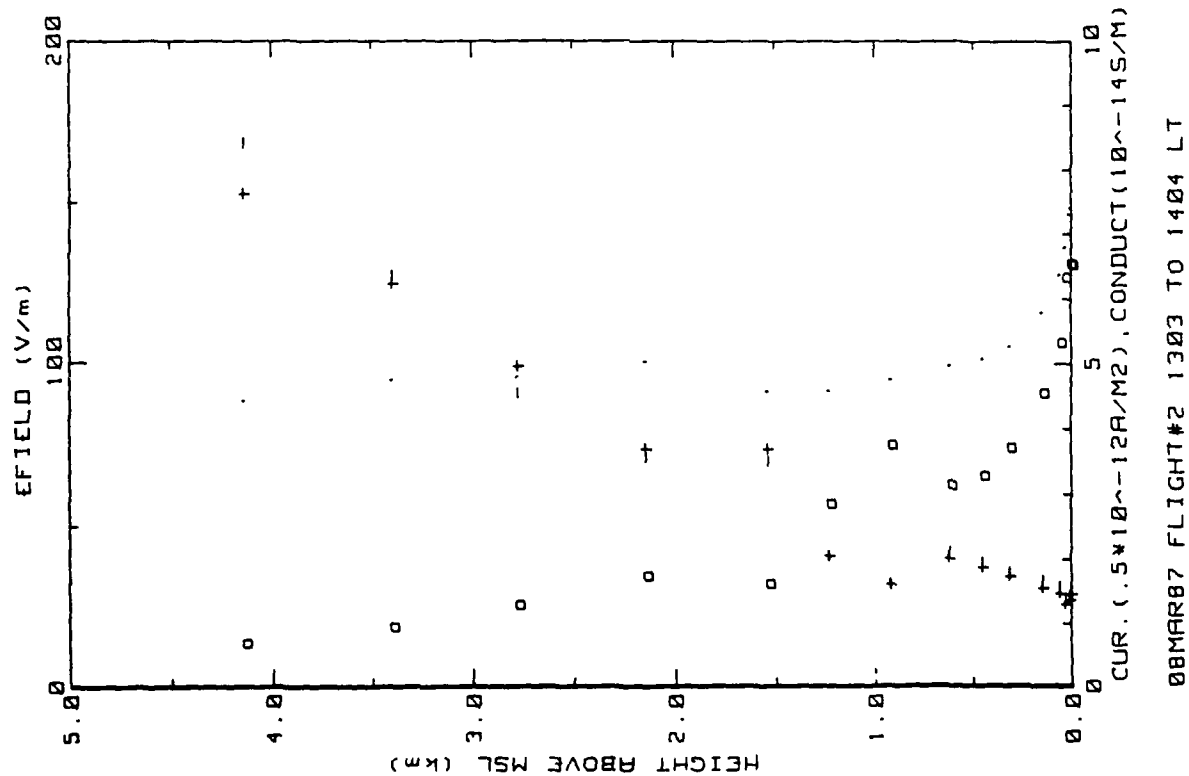


Figure 22a. RSD Flight 2 ladder profile over shallow water SW of RSD. (ref. Fig. 5a).

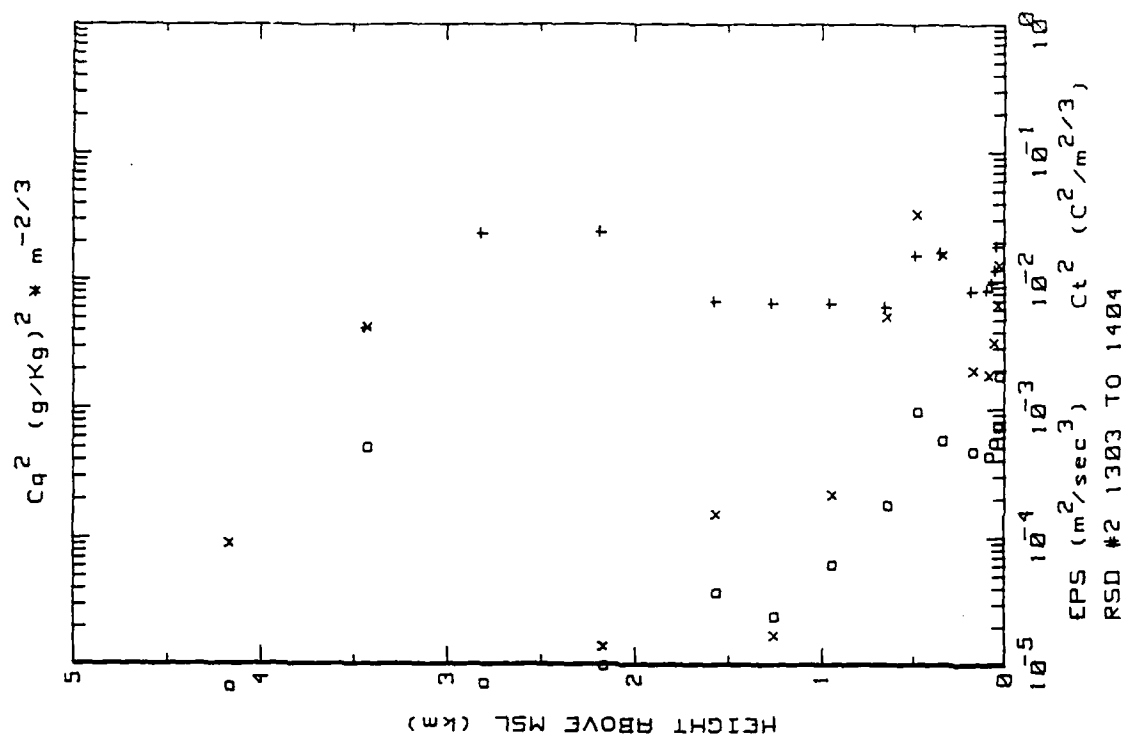


Figure 22b. RSD Flight 2 ladder profile over shallow water SW of RSD. (ref. Fig. 5b).

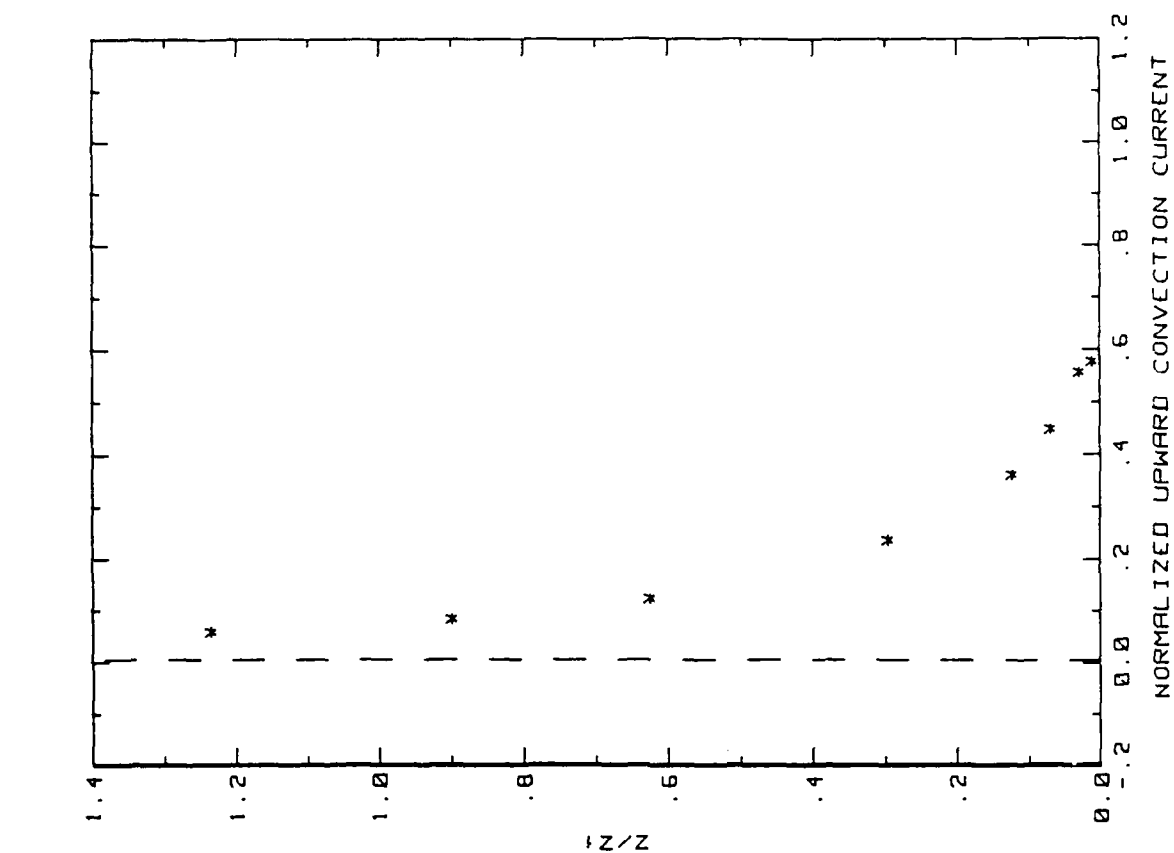
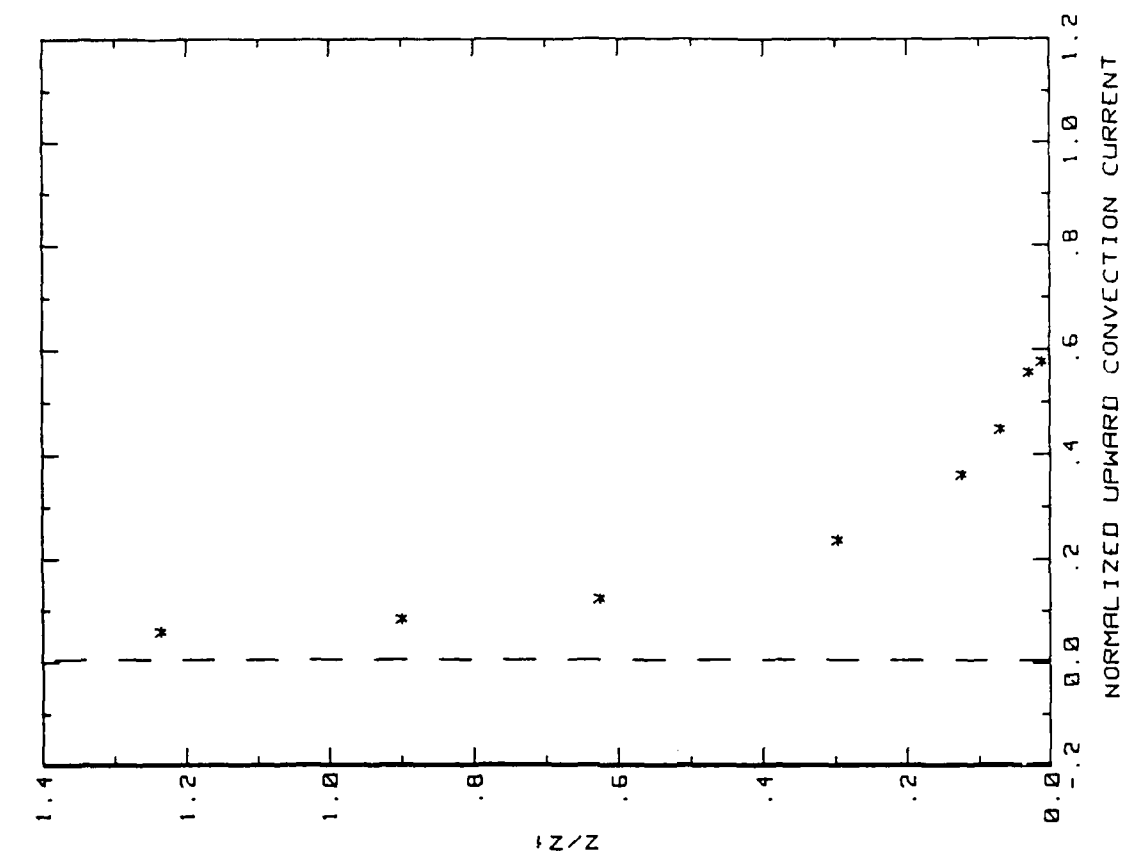


Figure 22c. RSD Flight 2 ladder profile over shallow water SW of RSD. (ref. Fig. 5c).



08MAR87 FLIGHT#2 13:04 TO 14:32 LST  
Z1=500 Jo=2.35

Figure 22d. RSD Flight 2 convection current profile over shallow water SW of RSD

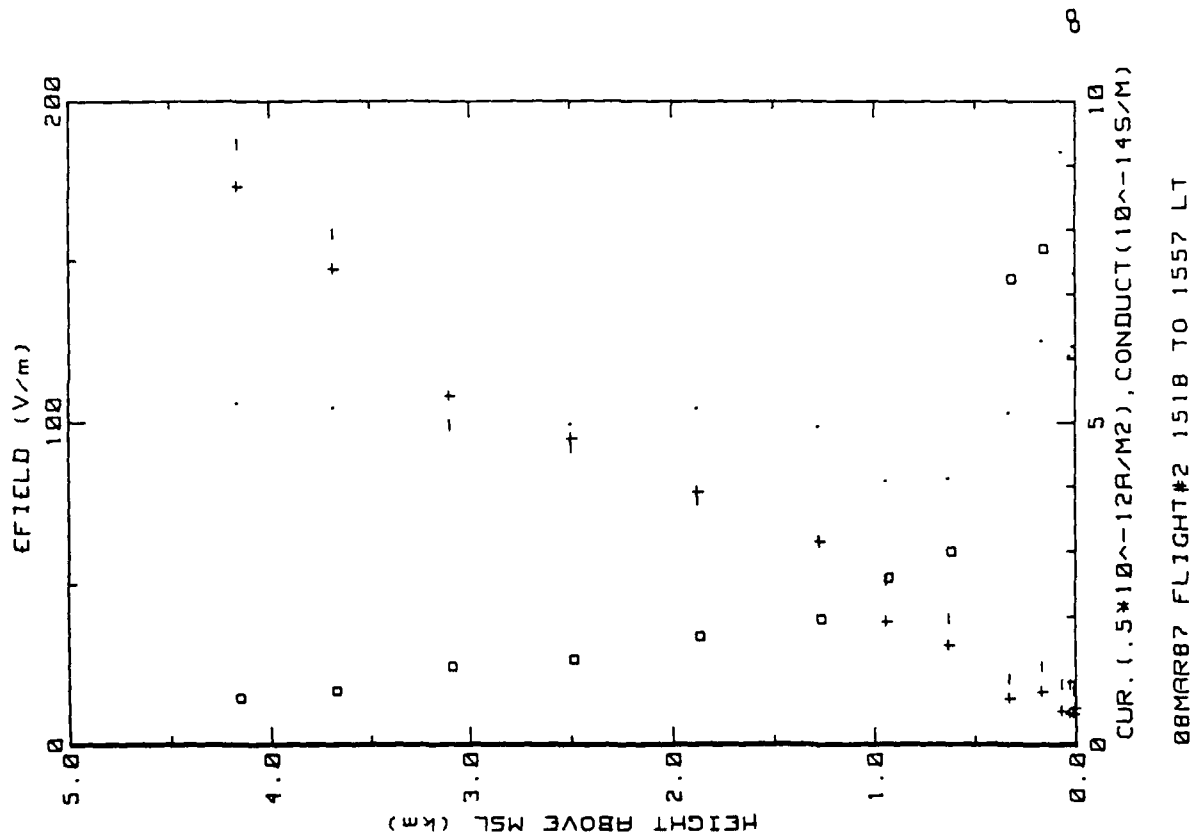


Figure 22e. RSD Flight 2 ladder profile over deep water  
E of RSD. (ref. Fig. 5a).

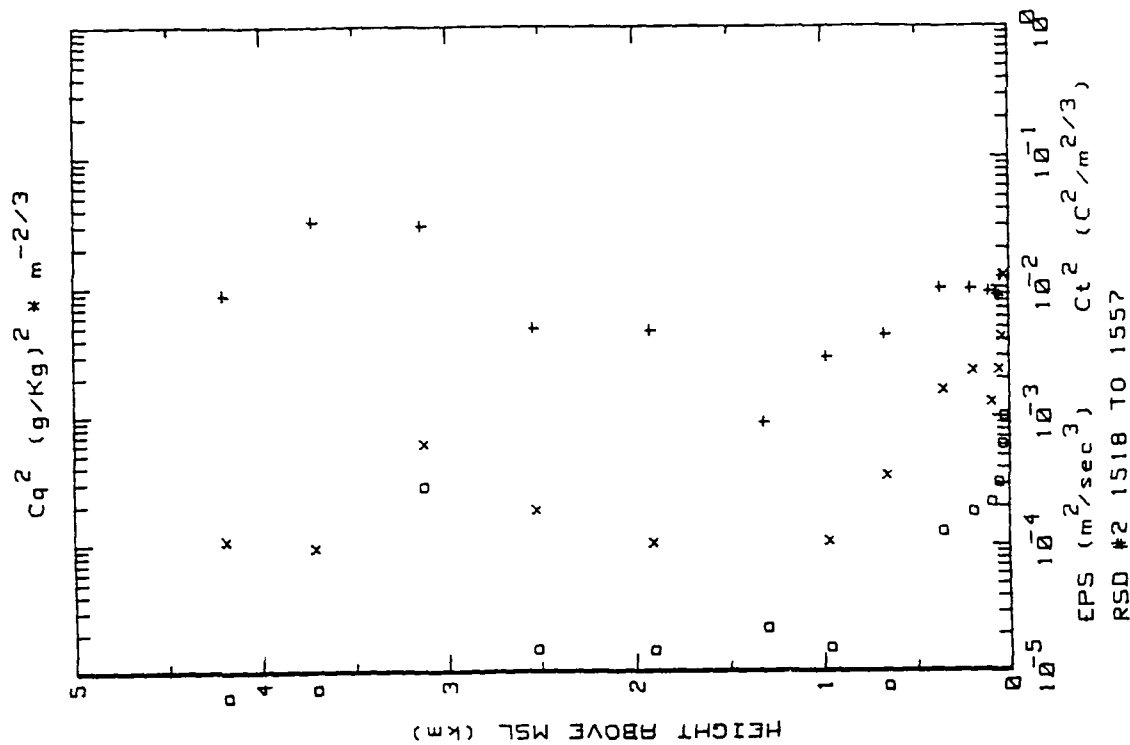


Figure 22f. RSD Flight 2 ladder profile over deep water  
E of RSD. (ref. Fig. 5b).

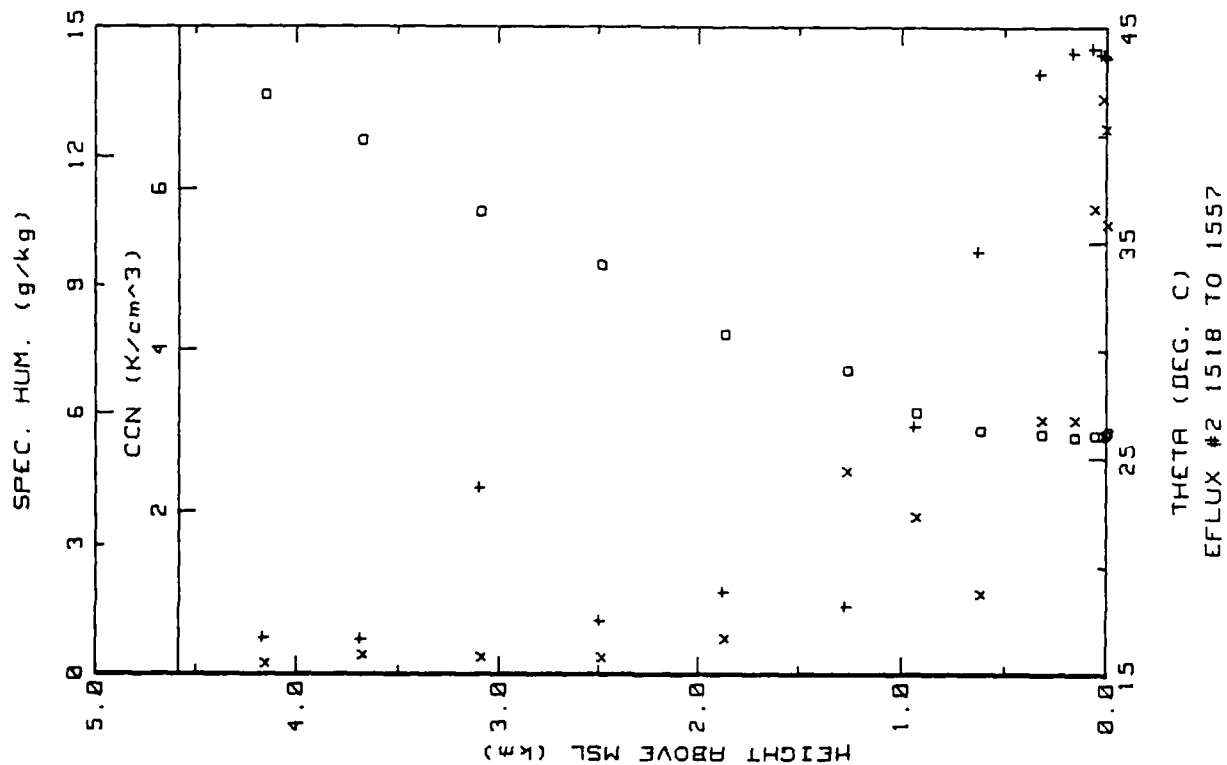
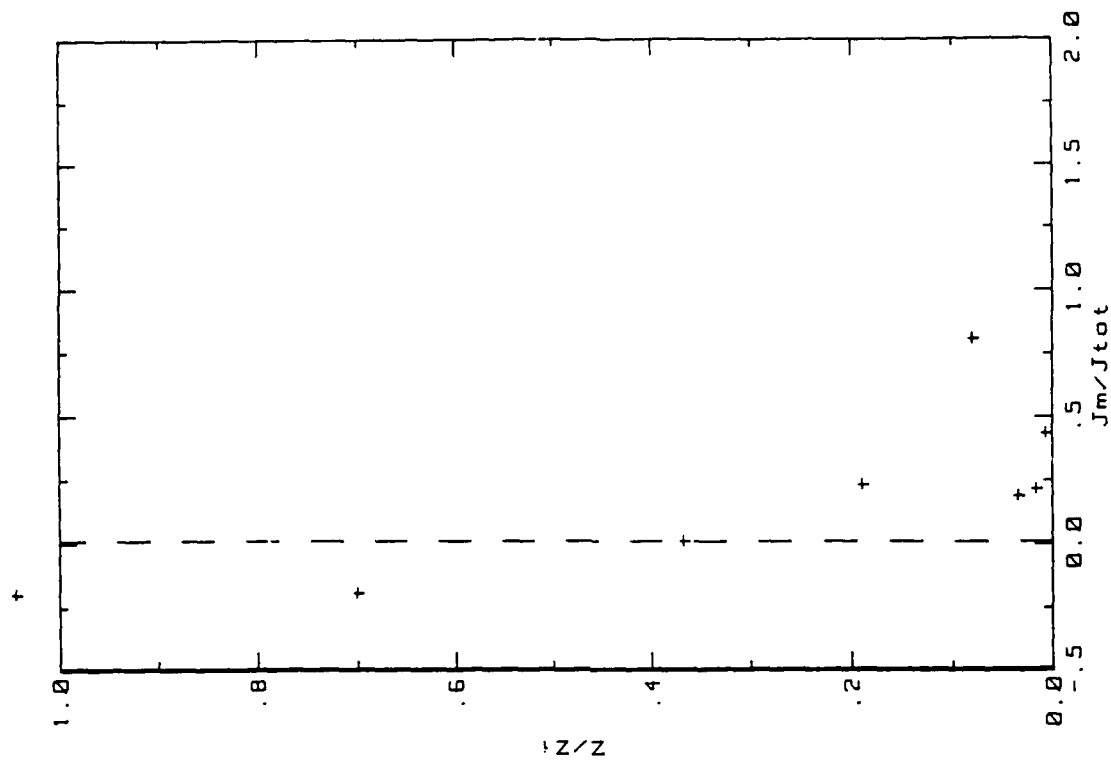


Figure 22g. RSD Flight 2 ladder profile over deep water E of RSD. (ref. Fig. 5c).



08MAR87 FLIGHT#2 14:53 TO 16:18 LST  
Zi=900 Jm/Jtot=3

Figure 22h. RSD Flight 2 convection current profile over deep water E of RSD



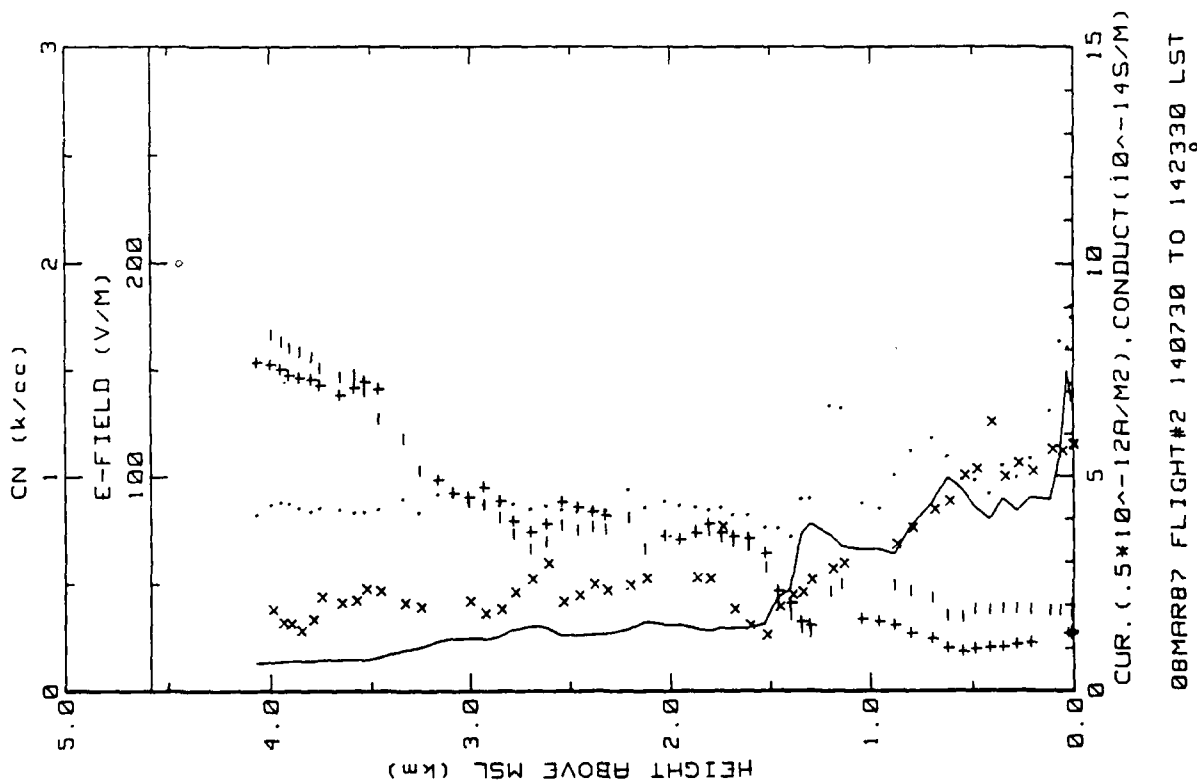


Figure 22f. RSD Flight 2 spiral down-sounding over shallow water SW of RSD (ref. Fig. 5f).

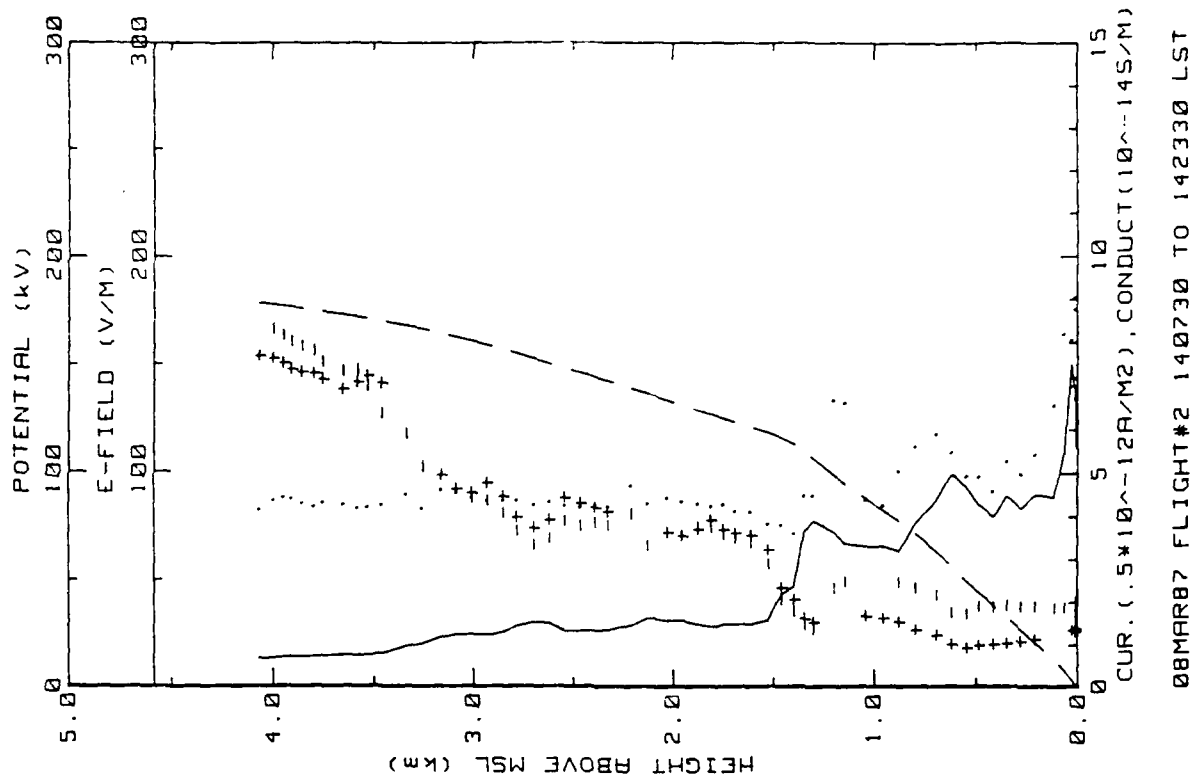


Figure 22j. RSD Flight 2 spiral down-sounding over shallow water SW of RSD (ref. Fig. 5e).

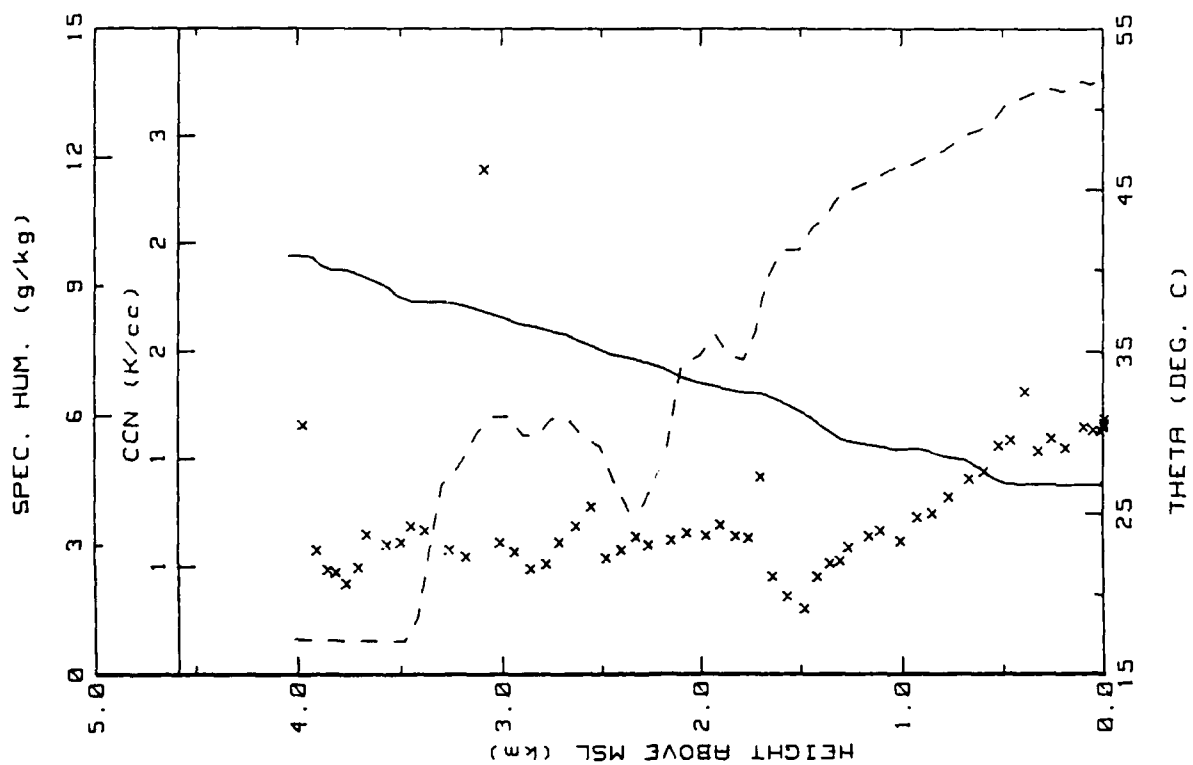


Figure 22k. RSD Flight 2 spiral down-sounding over shallow water SW of RSD (ref. Fig. 5h).

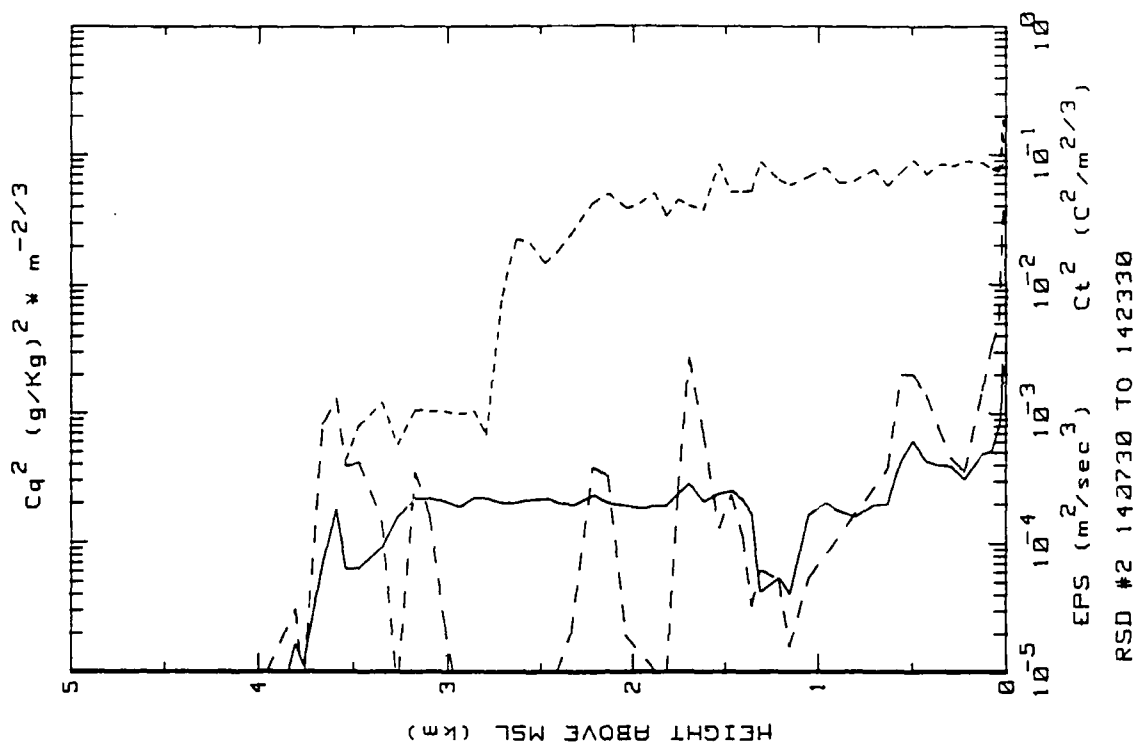


Figure 22l. RSD Flight 2 spiral down-sounding over shallow water SW of RSD (ref. Fig. 5g).

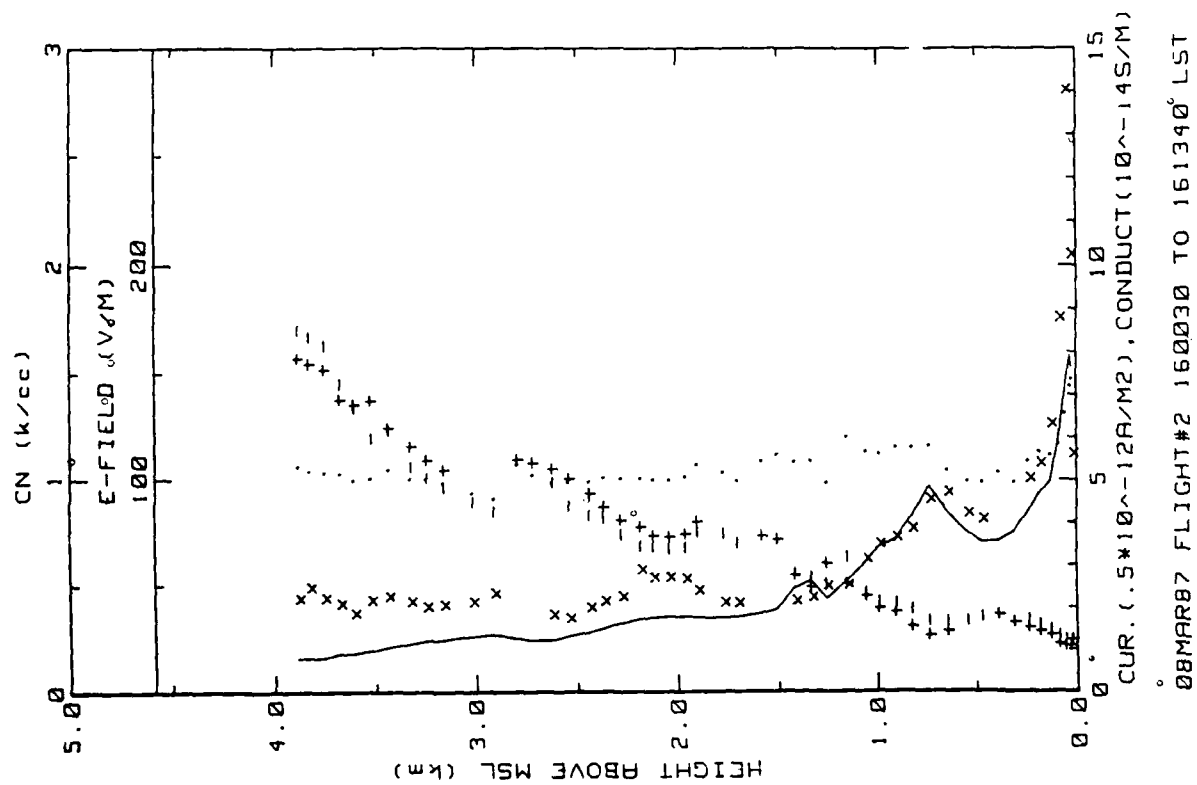


Figure 22n. RSD Flight 2 spiral down-sounding over deep water E of RSD (ref. Fig. 5f).

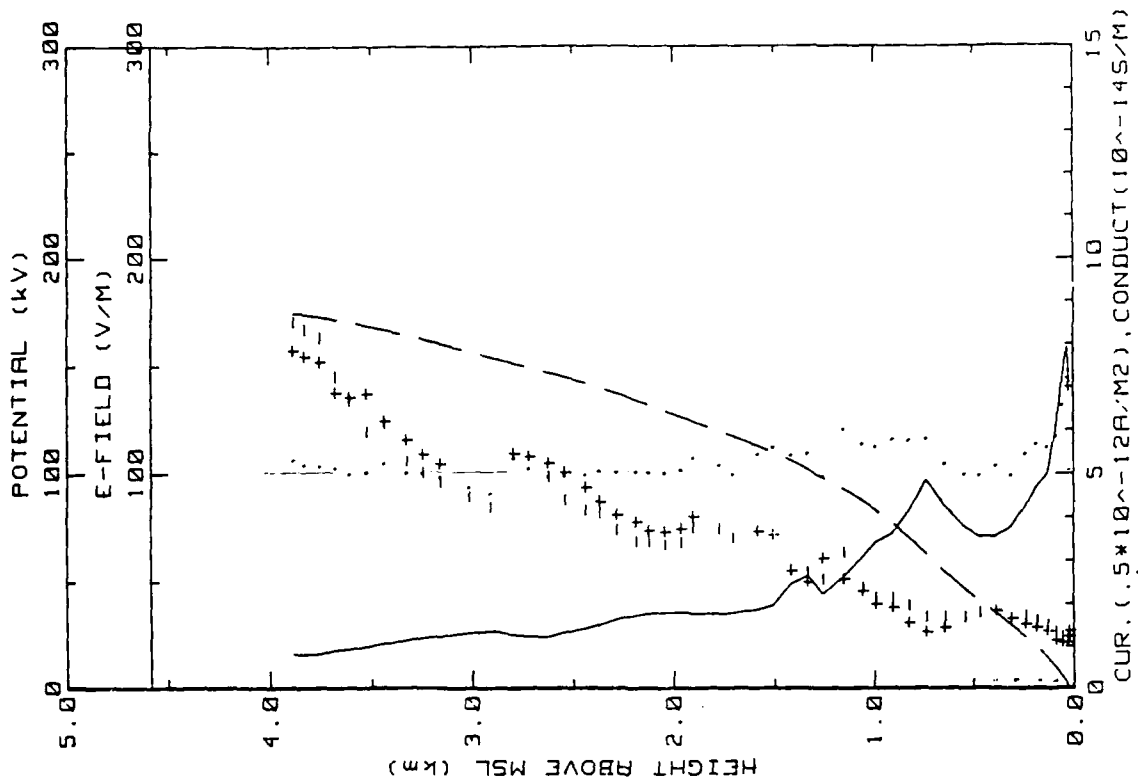


Figure 22n. RSD Flight 2 spiral down-sounding over deep water E of RSD (ref. Fig. 5e).

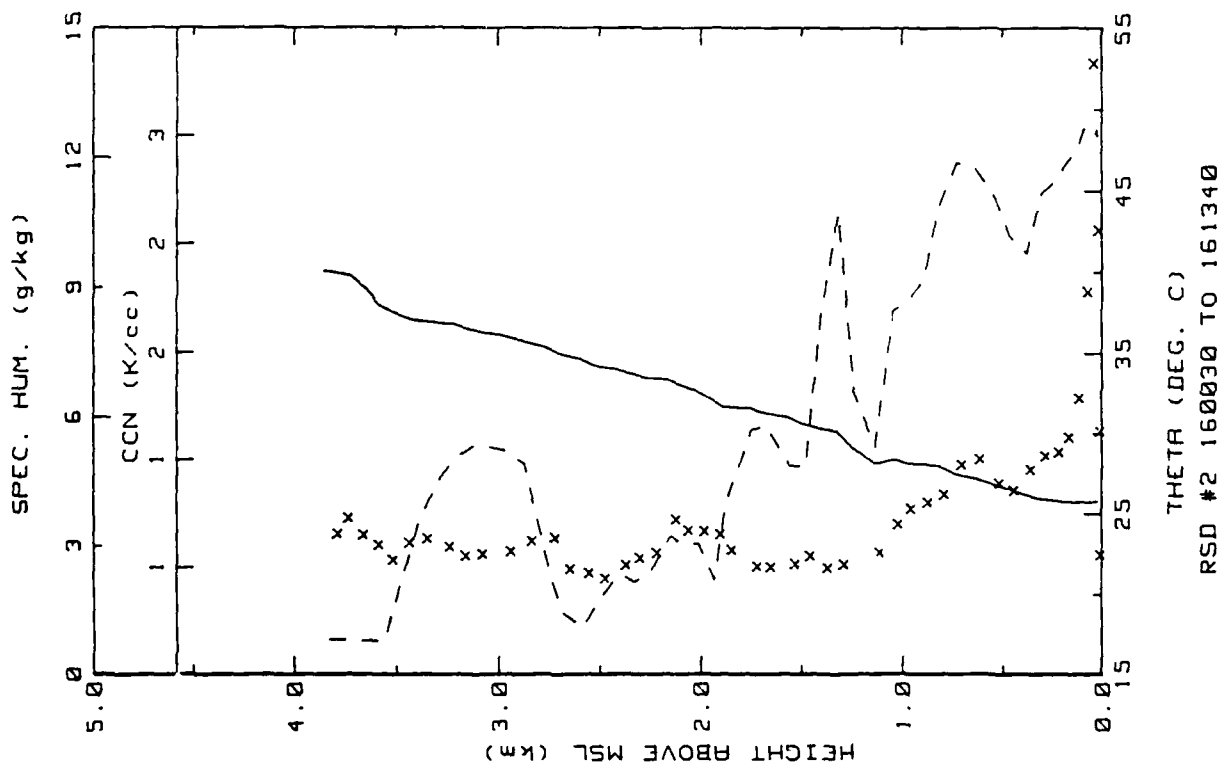


Figure 22o. RSD Flight 2 spiral down sounding over deep water E of RSD (ref. Fig. 5h).

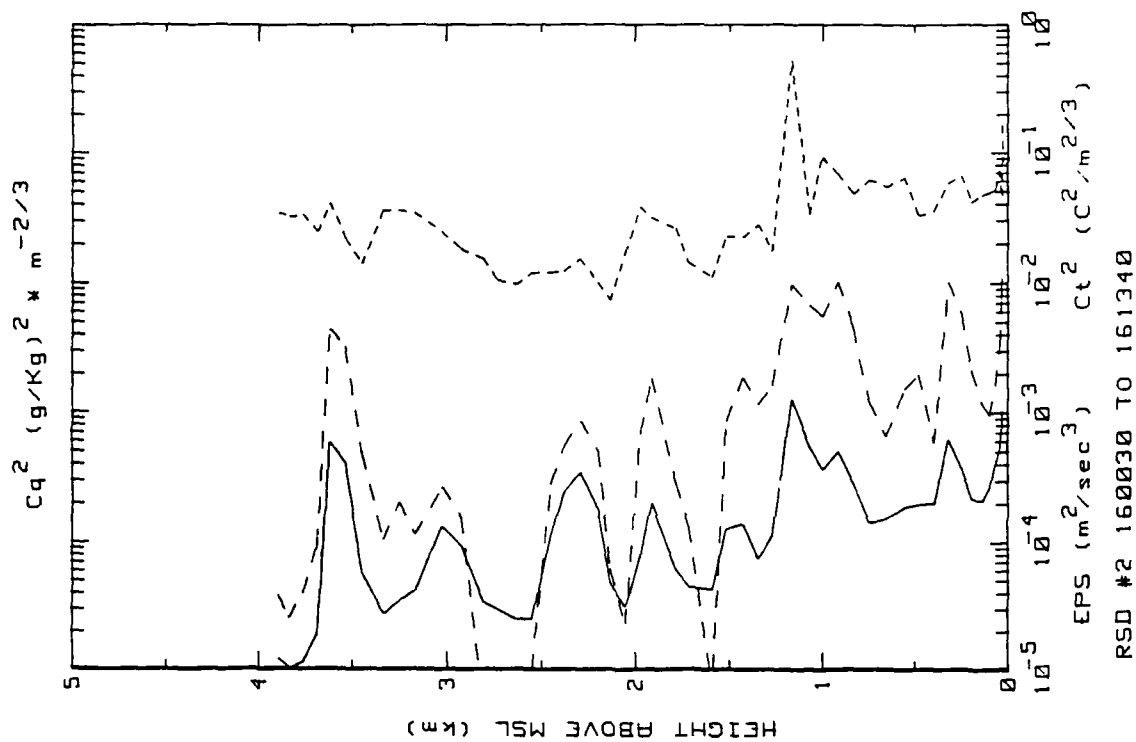


Figure 22p. RSD Flight 2 spiral down sounding over deep water E of RSD (ref. Fig. 5g).

Flight: 3

Date: 9 March 1987

Takeoff: 1030 (LT) from RSD

Landed: 1312 at RSD

Conditions: Clear skies with SW winds at 1-3 m/s. No whitecaps and very little turbulence down low.

Instruments: All worked properly.

Summary: Ladder and spiral profiles were obtained 50-100 km E of RSD over deep ocean. Additional constant altitude passes and a spiral descent from 2 km were performed on the return flight to RSD.

Table 16a. RSD Flight 3 averages for constant altitude runs performed E of RSD over deep water.

AVERAGES FROM LEVEL RUNS

Time HHMM	N	Altitude km	E_field V/m	Flam 10 <sup>-14</sup>	Flam 10 <sup>-14</sup>	Con Curr 10 <sup>-12</sup>	theta_v C	Rel Hum %	SN k/cc
1035	84	.031	122.06	1.20	1.34	3.09	25.0	59.8	1.69
1045	329	.031	122.03	1.22	1.35	3.14	24.9	61.2	1.81
1057	47	.031	128.08	1.23	1.36	3.30	24.9	60.8	1.39
1059	71	.003	141.25	1.21	1.25	3.48	24.9	62.0	1.40
1102	44	.006	136.52	1.20	1.25	3.25	24.9	64.1	1.41
1104	42	.015	141.37	1.19	1.31	3.54	24.8	62.9	1.47
1107	61	.003	149.89	1.13	1.13	3.41	24.9	64.9	1.60
1110	48	.006	144.90	1.14	1.49	3.74	24.8	67.6	1.59
1113	38	.015	135.54	1.16	1.43	3.52	24.8	69.3	1.54
1116	46	.031	127.50	1.16	1.44	3.32	24.9	69.1	1.49
1118	49	.061	116.65	1.17	1.45	3.05	24.7	58.5	2.41
1119	35	.117	118.03	1.16	1.37	2.93	24.7	66.7	1.41
1122	35	.146	108.50	1.22	1.41	2.89	24.7	65.3	1.32
1126	42	.208	98.19	1.23	1.39	2.56	24.7	66.9	1.35
1132	39	.276	94.63	1.17	1.37	2.35	24.7	72.8	1.33
1133	35	.345	88.14	1.22	1.51	2.41	24.5	76.1	1.36
1135	38	.477	81.22	1.24	1.50	2.27	24.8	79.3	1.09
1139	50	.537	74.26	1.33	1.64	2.23	24.9	77.2	1.00
1142	117	.949	55.85	1.83	1.99	2.14	25.4	57.6	.87
1150	31	1.263	43.27	2.31	2.44	2.05	27.1	25.2	.79
1155	36	1.865	39.24	2.59	2.68	2.08	30.0	20.8	.86
1159	41	2.497	19.56	5.44	5.50	2.14	33.9	11.4	.41
1202	57	3.078	47.54	2.33	2.30	2.18	36.1	48.7	1.10
1208	31	3.872	19.63	5.33	5.96	2.14	39.4	20.8	.63
1213	46	4.179	15.02	7.11	7.13	2.15	39.4	30.2	.76

Time HHMM	N	Altitude km	EPS m2/s3	OT2 C2/m2/3	Q g/kg	Ca2 (g/kg)2m/3	Press mB	Trose C	T_IR C	T_dew C
1035	84	.031	3.91E-04	2.01E-03	10.2	1.38E-02	1004.5	22.7	24.3	14.4
1045	329	.061	3.87E-04	2.24E-03	10.3	9.96E-03	1001.1	22.5	24.3	14.5
1057	47	.031	3.85E-04	5.04E-03	10.3	1.50E-02	1003.1	22.4	24.3	14.5
1059	71	.003	9.98E-04	2.25E-02	10.6	3.26E-02	1005.6	22.7	24.4	15.0
1102	44	.006	1.08E-03	1.54E-02	10.9	2.85E-02	1005.3	22.5	24.0	15.4
1104	42	.015	9.09E-04	9.03E-03	10.5	2.28E-02	1004.0	22.4	23.8	15.0
1107	61	.003	1.69E-03	2.55E-02	11.0	3.94E-02	1005.4	22.6	23.9	15.6
1110	48	.006	9.65E-04	1.19E-02	11.4	1.69E-02	1004.8	22.4	23.5	16.1
1113	38	.015	5.87E-04	6.96E-03	11.5	1.41E-02	1004.1	22.2	23.2	16.3
1116	46	.031	5.26E-04	4.49E-03	11.4	1.11E-02	1002.6	22.1	23.0	16.2
1119	49	.061	3.37E-04	2.82E-03	11.2	1.01E-02	995.2	21.8	23.3	15.7
1119	35	.117	3.79E-04	1.56E-03	10.8	7.85E-03	995.8	21.6	23.5	15.1
1122	35	.146	3.01E-04	1.47E-03	10.4	7.21E-03	992.4	21.3	23.6	14.6
1126	42	.208	2.12E-04	9.60E-04	10.4	7.38E-03	985.4	20.8	23.8	14.4
1132	39	.276	1.70E-04	6.35E-04	10.9	6.27E-02	977.7	20.0	23.6	15.0
1133	35	.345	1.63E-04	6.44E-04	11.1	7.50E-03	969.9	19.1	23.4	15.2
1135	38	.477	3.85E-04	2.81E-03	10.8	8.79E-03	955.1	18.2	23.3	14.5
1139	50	.537	2.06E-04	5.15E-03	9.3	1.07E-02	937.6	16.9	23.8	12.9
1142	117	.949	8.35E-05	3.39E-04	6.7	4.50E-03	904.0	15.0	24.2	6.7
1150	31	1.263	9.94E-06	4.45E-05	2.9	6.37E-04	871.1	14.2	24.3	-5.5
1155	36	1.865	7.83E-06	1.99E-05	2.1	2.61E-04	810.9	11.3	24.3	-10.4
1159	41	2.497	5.49E-06	7.62E-05	1.1	0.00E+00	751.3	8.9	23.8	-19.6
1202	57	3.078	9.42E-06	2.14E-04	3.7	3.04E-03	699.8	4.7	23.9	-5.3
1208	31	3.872	2.07E-04	4.83E-04	1.6	6.02E-03	634.0	.6	24.4	-16.5
1213	46	4.179	9.05E-05	8.29E-04	1.5	7.73E-03	609.8	-2.8	24.8	-18.0

Table 16b. RSD Flight 3 (standard deviations)/averages for  
constant altitude runs performed E of RSD over deep  
water.

STANDARD DEVIATIONS/MEAN VALUES

Time	E_Field	1Lam	1Lam	Con Curr	CON	LPS	012	0	042
1035	.126	.041	.123	.140	.102	.265	.468	.034	1.386
1045	.126	.036	.110	.134	.125	.424	.833	.024	1.479
1057	.086	.033	.094	.092	.050	.201	.336	.026	1.646
1059	.149	.032	.185	.157	.055	.332	.453	.028	1.425
1102	.147	.033	.185	.122	.033	.255	.254	.029	1.030
1104	.161	.040	.159	.141	.046	.538	.476	.032	1.292
1107	.186	.055	.191	.153	.120	.331	.365	.035	1.259
1110	.176	.030	.147	.167	.050	.282	.314	.022	.919
1113	.152	.029	.087	.148	.156	.424	.319	.020	.828
1116	.121	.026	.074	.138	.062	.436	.290	.020	.525
1118	.074	.015	.085	.093	.523	.267	.488	.017	.767
1119	.075	.046	.084	.094	.201	.405	.443	.017	.499
1122	.067	.020	.047	.078	.137	.299	.321	.021	.474
1126	.041	.034	.052	.053	.245	.503	.717	.018	.475
1132	.033	.054	.061	.067	.142	.328	.600	.015	2.166
1133	.029	.026	.195	.101	.512	.360	.472	.012	.324
1135	.055	.031	.102	.131	.052	.316	.414	.022	.571
1139	.068	.122	.147	.109	.068	.518	.702	.021	1.049
1142	.037	.029	.041	.035	.050	.795	.875	.051	1.331
1150	.061	.032	.034	.021	.068	.696	1.692	.059	1.204
1155	.023	.027	.025	.005	.077	.714	1.495	.025	1.423
1159	.019	.014	.009	.018	.062	.601	.516	.013	0.000
1202	.043	.053	.068	.043	.051	.520	1.715	.088	1.317
1208	.069	.067	.081	.039	.101	.358	.163	.039	.734
1213	.043	.051	.041	.036	.102	.890	.706	.100	.541

Table 16c. RSD Flight 3 averages and standard deviations for constant altitude runs performed just E of RSD on returning from the experiment area.

AVERAGES FROM LEVEL RUNS

Time HHMM	N	Altitude km	E_Field V/m	+Lam $10^{-14}$	-Lam $10^{-14}$	Con Curr $10^{-12}$	theta_v C	Rel Hum %	CW x/cc
1239	52	.006	127.77	1.23	1.56	3.57	24.8	62.6	1.39
1242	38	.015	134.39	1.18	1.36	3.35	24.8	62.1	1.31
1243	38	.031	119.57	1.18	1.35	3.04	24.7	61.6	1.41
1245	120	.078	110.75	1.21	1.39	2.90	24.6	61.0	1.29
1251	30	.122	99.75	1.16	1.37	2.48	24.5	65.2	1.33
1253	37	.176	89.48	1.15	1.31	2.20	24.5	66.9	1.35
1256	35	.283	84.26	1.08	1.25	2.01	24.9	69.3	1.41

Time HHMM	N	Altitude km	EPS m2/s3	Cl2 m2/s3	G g/kg	Co2 (g/kg)2m-2/3	Press mb	Trose C	T_IR C	T_dew C
1239	52	.006	1.03E-03	2.33E-02	10.6	6.14E-02	1006.0	22.6	25.6	15.1
1242	38	.015	7.13E-04	1.24E-02	10.5	2.37E-02	1005.0	22.5	25.4	14.9
1243	38	.031	4.41E-04	4.43E-03	10.3	1.24E-02	1003.3	22.3	25.2	14.6
1245	120	.078	4.58E-04	3.21E-03	10.1	1.10E-02	1000.3	22.0	25.1	14.2
1251	30	.122	5.19E-04	1.91E-03	10.4	1.13E-02	995.2	21.4	25.0	14.6
1253	37	.176	4.49E-04	8.42E-04	10.4	8.85E-03	989.0	20.9	25.0	14.5
1256	35	.283	4.24E-04	1.68E-02	10.5	7.93E-03	976.9	20.2	25.0	14.4

STANDARD DEVIATIONS/MEAN VALUES

Time	E_Field	+Lam	-Lam	Con Curr	CW	EPS	Cl2	G	Co2
1239	.144	.026	.100	.154	.039	.244	.307	.023	2.790
1242	.167	.030	.111	.151	.039	.260	.477	.027	1.260
1243	.100	.027	.056	.111	.034	.278	.351	.026	.399
1245	.091	.043	.087	.098	.057	.442	.514	.032	.729
1251	.111	.023	.047	.102	.039	.515	.667	.015	.814
1253	.060	.020	.056	.085	.062	.456	.773	.014	.330
1256	.075	.018	.023	.057	.043	.434	2.216	.019	.372



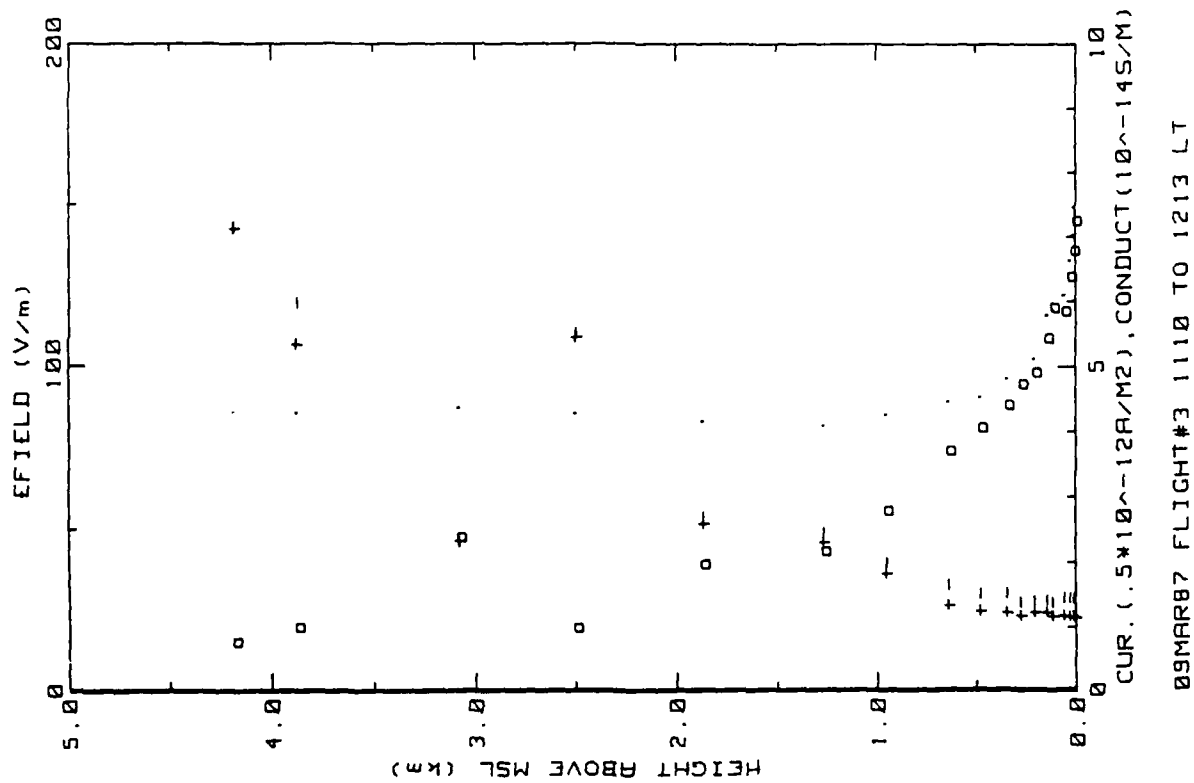


Figure 23a. RSD Flight 3 ladder profile over deep water  
E of RSD. (ref. Fig. 5a).

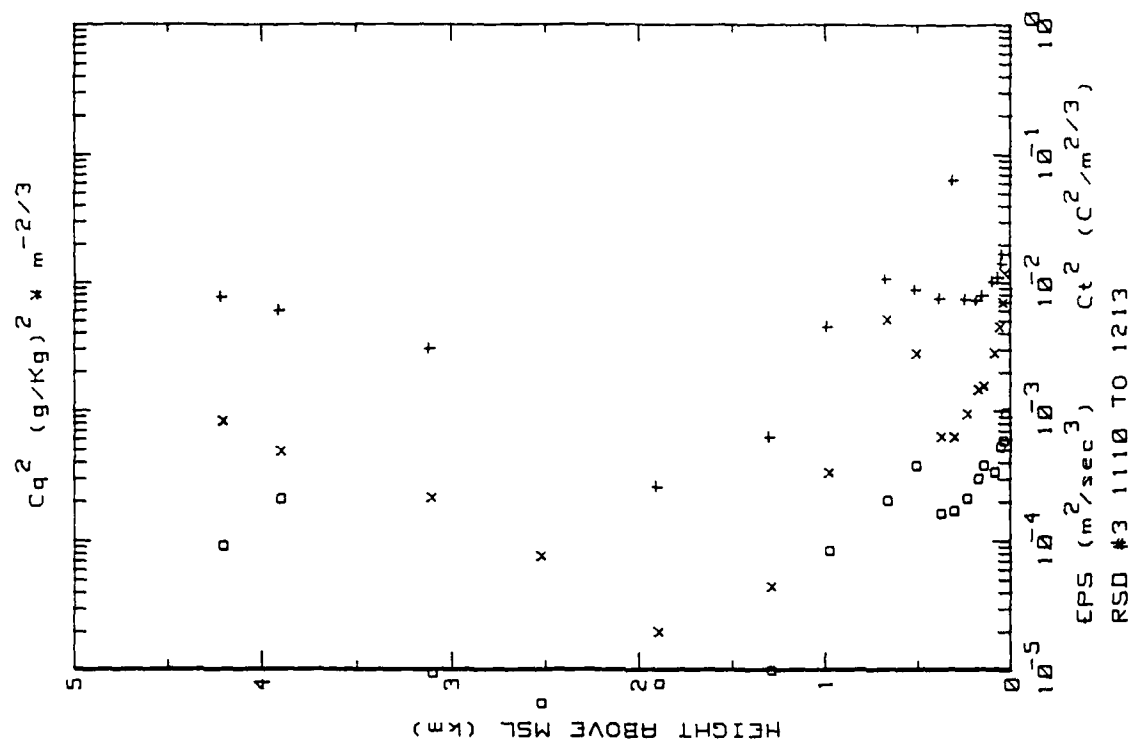


Figure 23b. RSD Flight 3 ladder profile over deep water  
E of RSD. (ref. Fig. 5b).

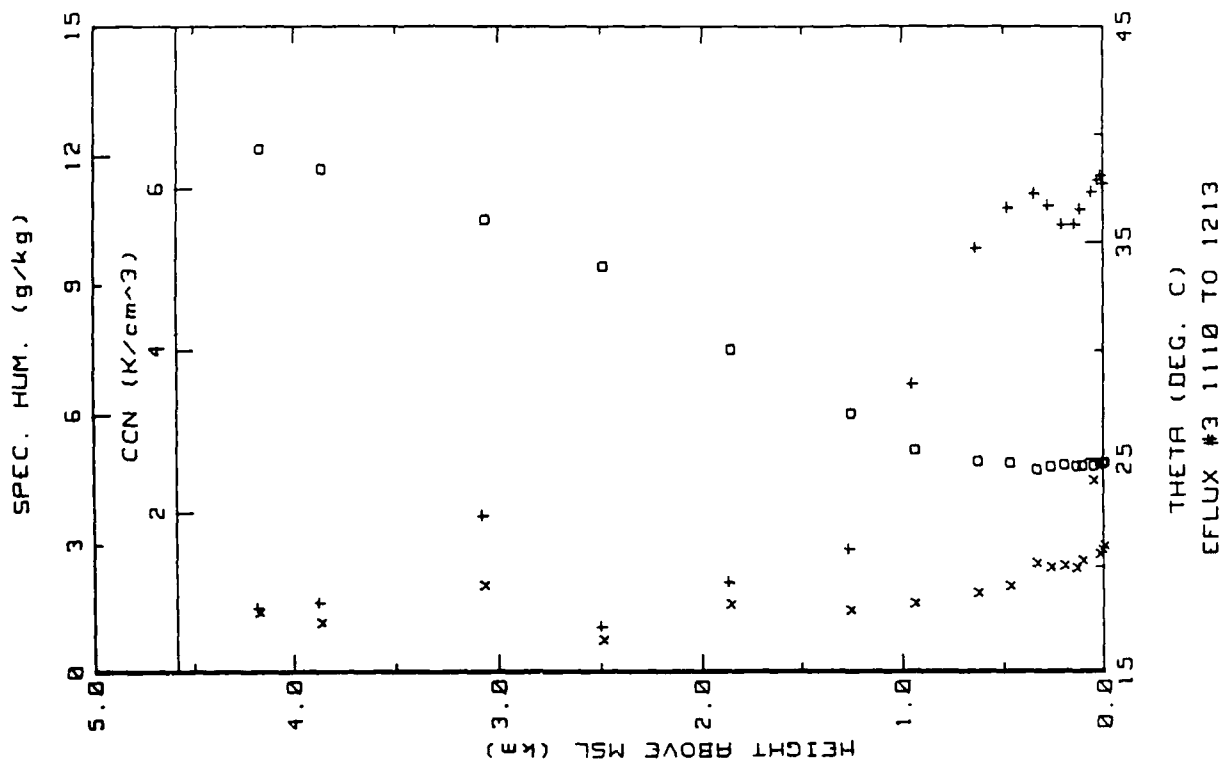
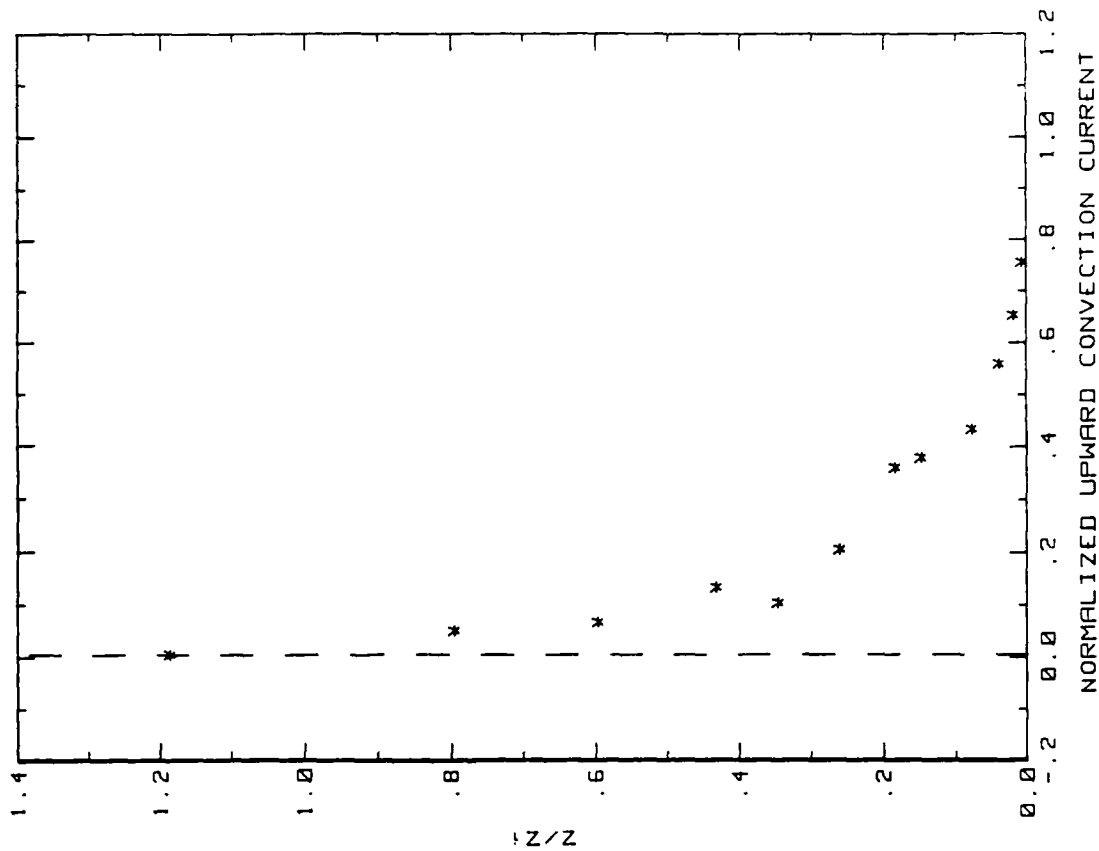


Figure 23c. RSD Flight 3 ladder profile over deep water  
E of RSD. (ref. Fig. 5c).



09MAR87 FLIGHT#3 10:34 TO 12:14 LST  
Z1=800 Jo=2.13 To=1110

Figure 23d. RSD Flight 2 convection current profile over  
deep water E of RSD (ref. Fig. 5d).

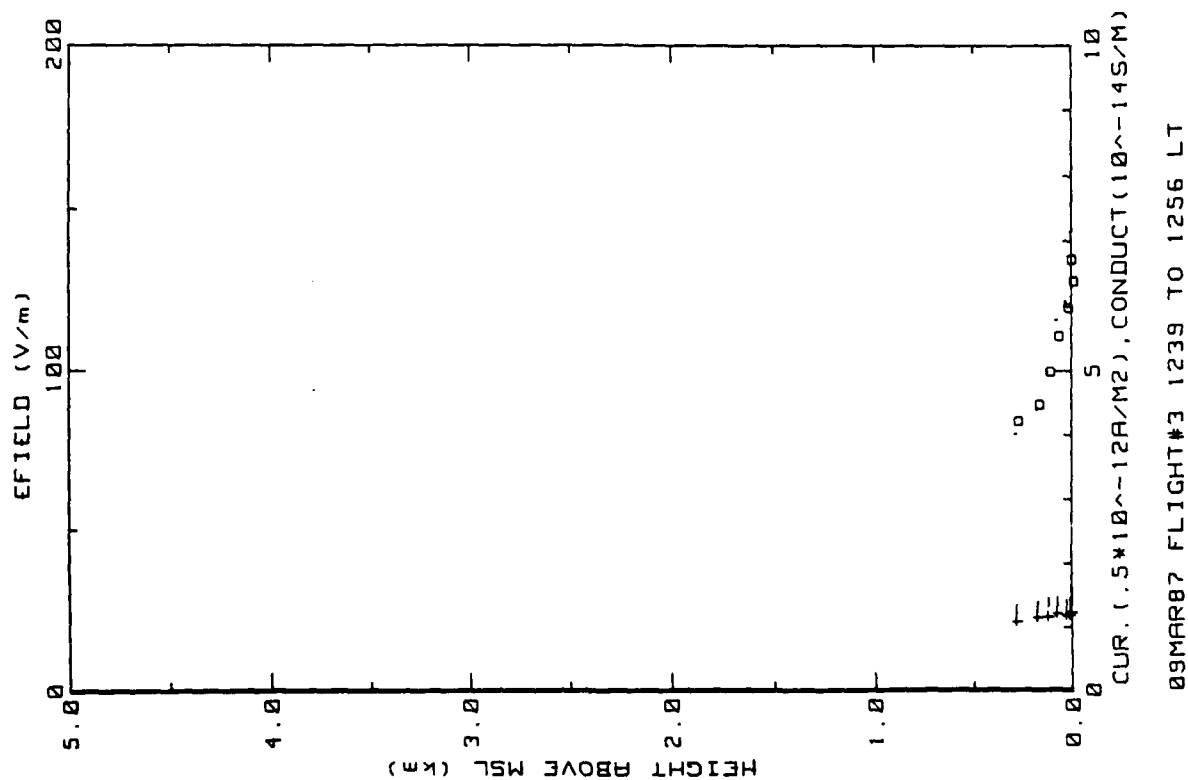


Figure 23e. RSD Flight 3 ladder profile over ocean returning to RSD. (ref. Fig. 5a).

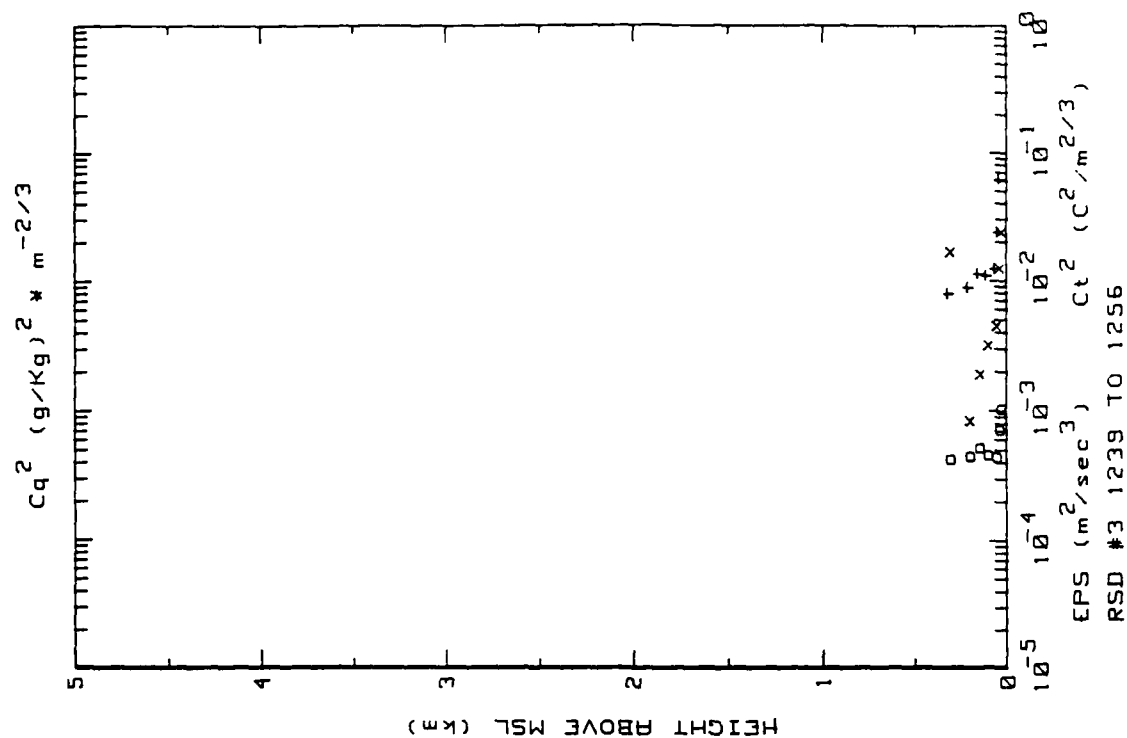


Figure 23f. RSD Flight 3 ladder profile over ocean returning to RSD. (ref. Fig. 5b).

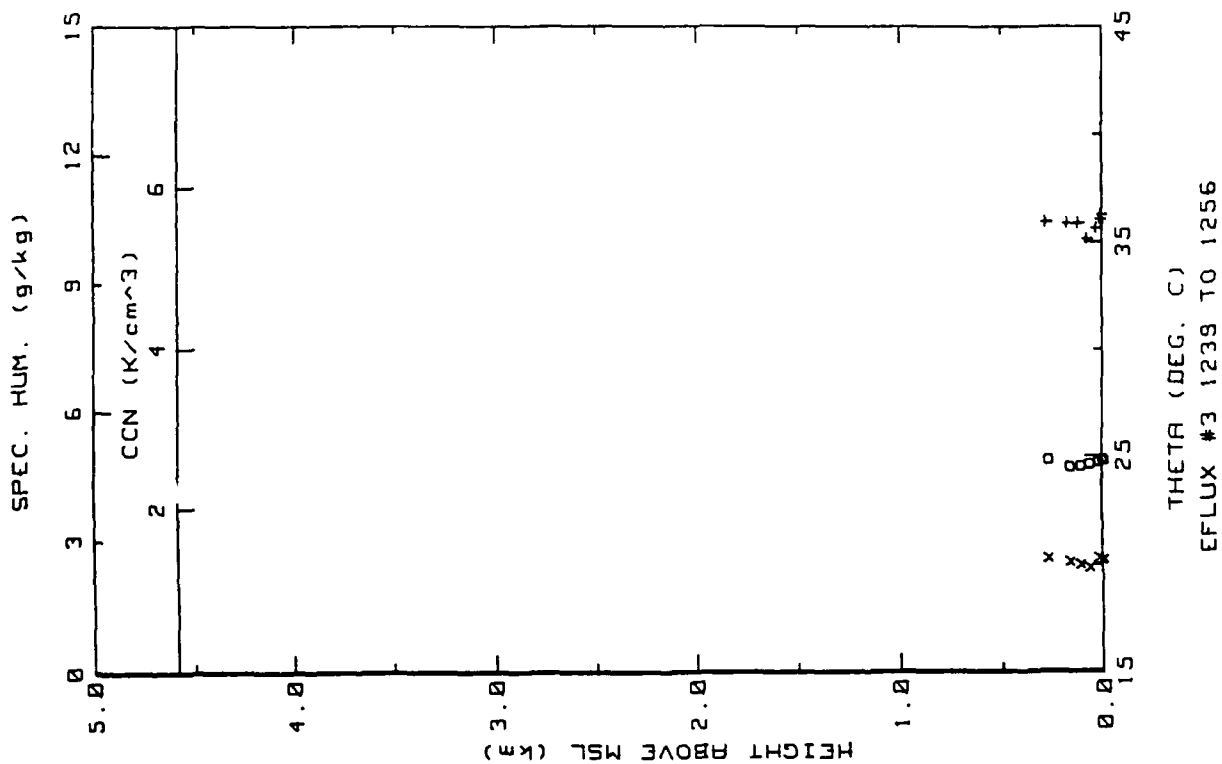


Figure 23g. RSD Flight 3 ladder profile over ocean returning to RSD. (ref. Fig. 5c).

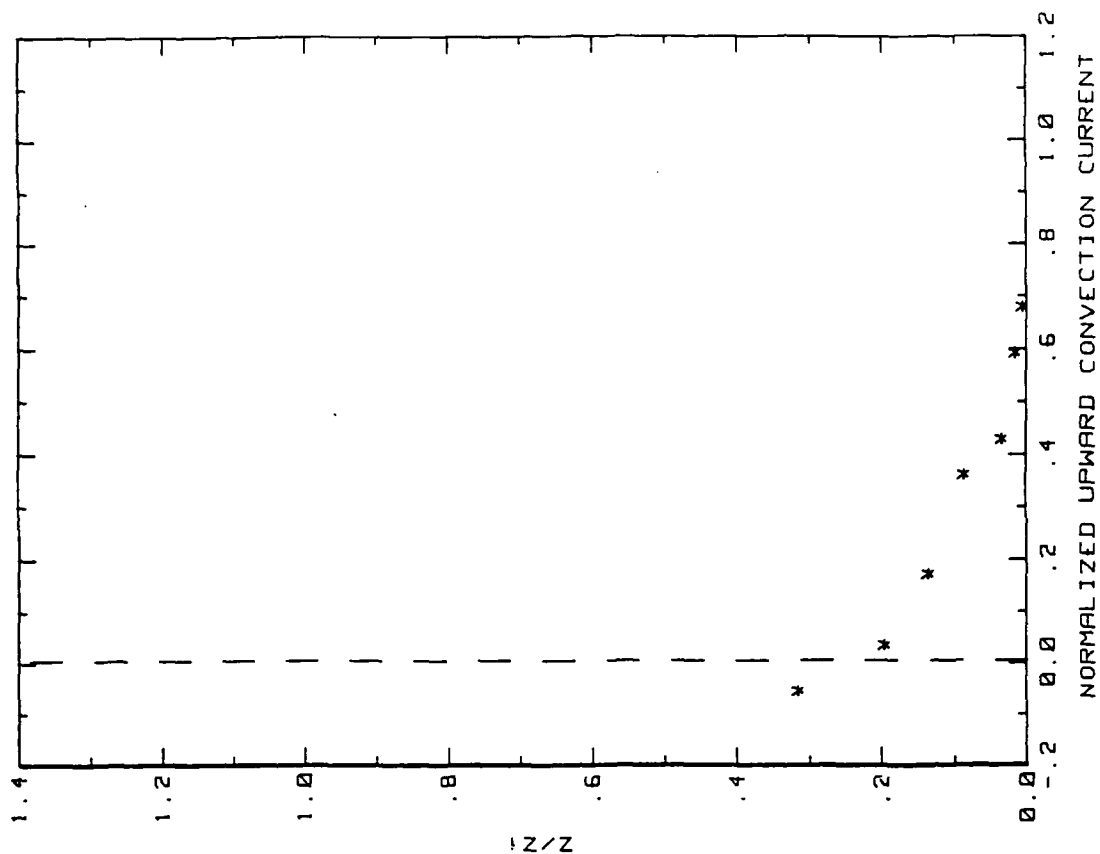


Figure 23h. RSD Flight 3 convection current profile over ocean returning to RSD (ref. Fig. 5d).

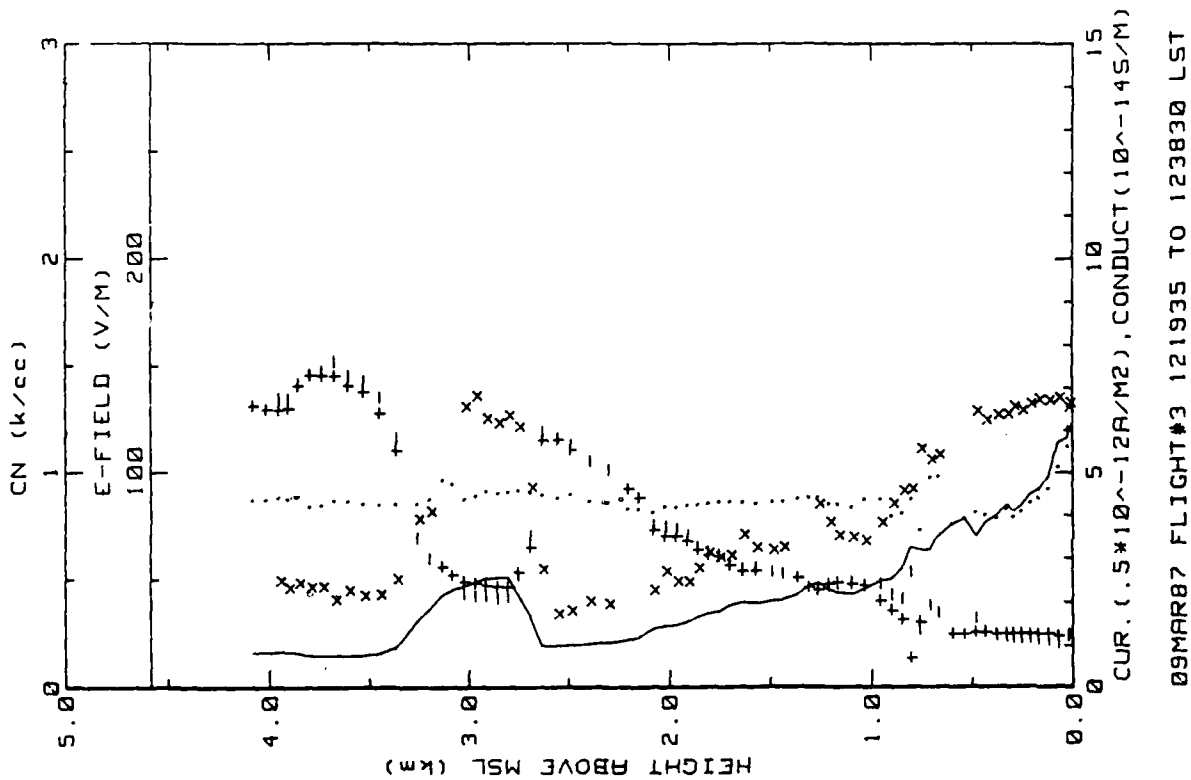


Figure 23i. RSD Flight 3 spiral down sounding over deep water E of RSD (ref. Fig. 5f).

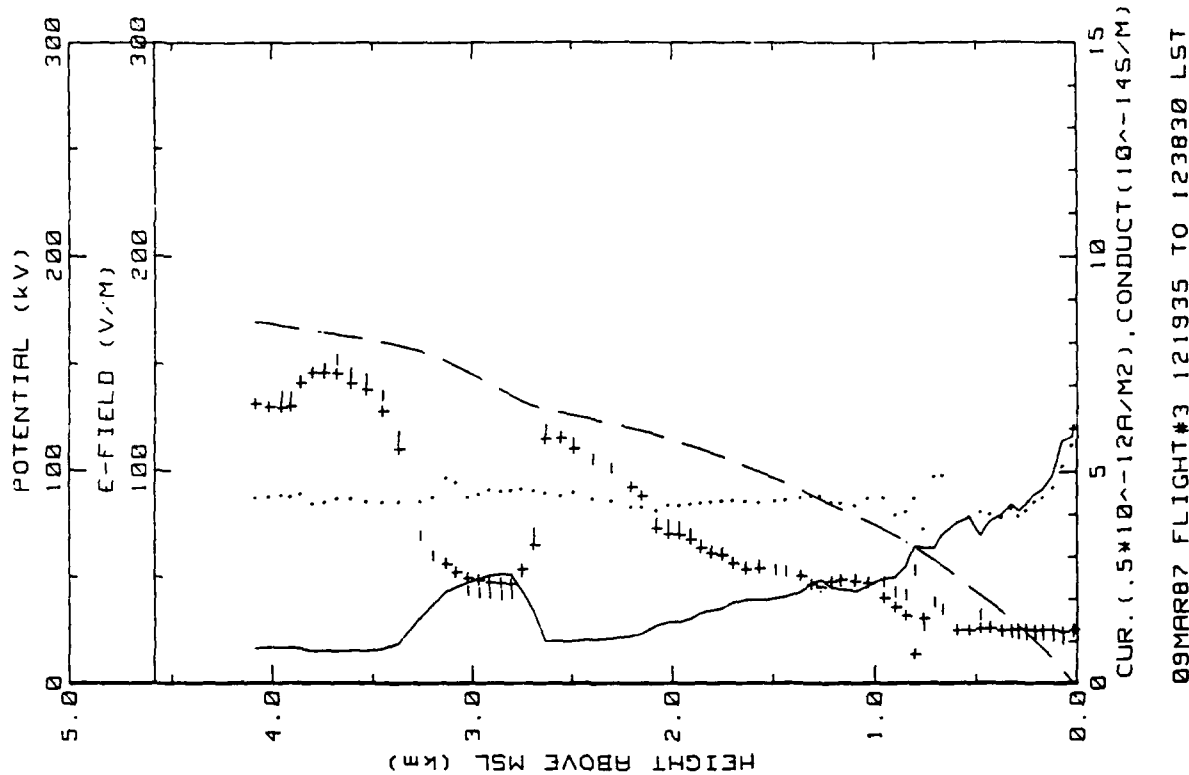


Figure 23j. RSD Flight 3 spiral down sounding over deep water E of RSD (ref. Fig. 5e).

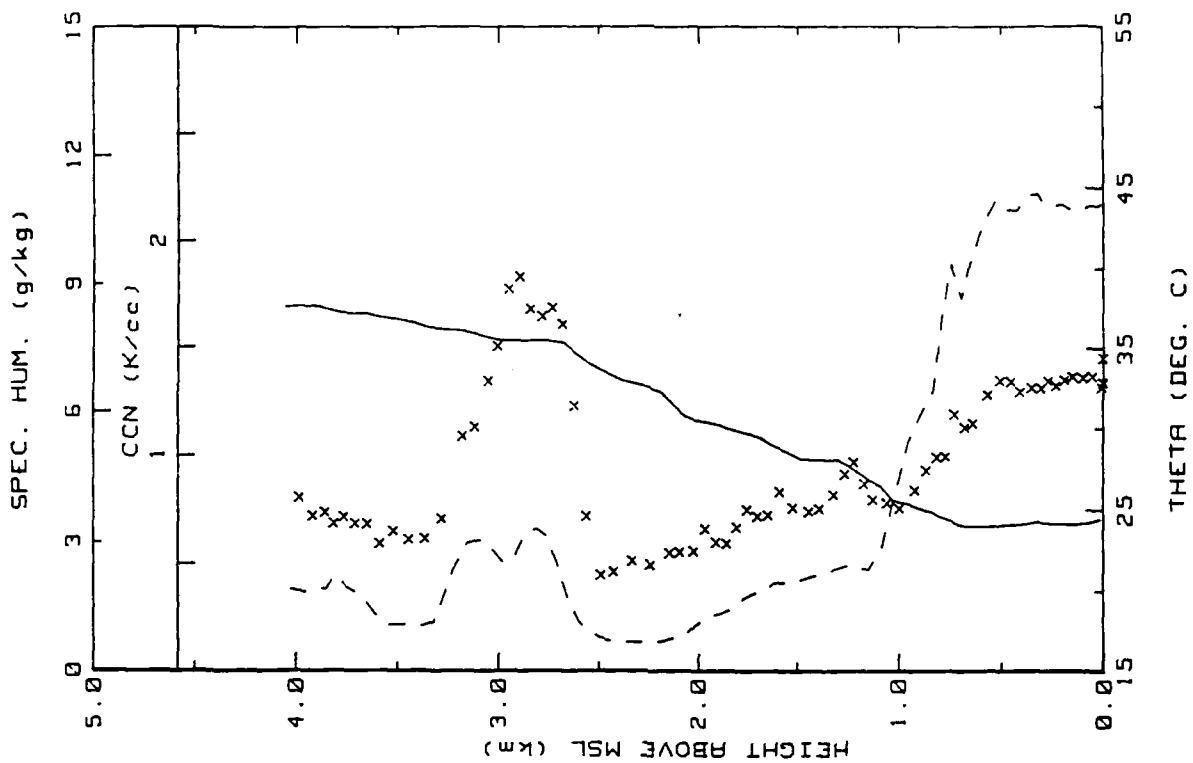


Figure 23l. RSD Flight 3 spiral down sounding over deep water E of RSD (ref. Fig. 5h).

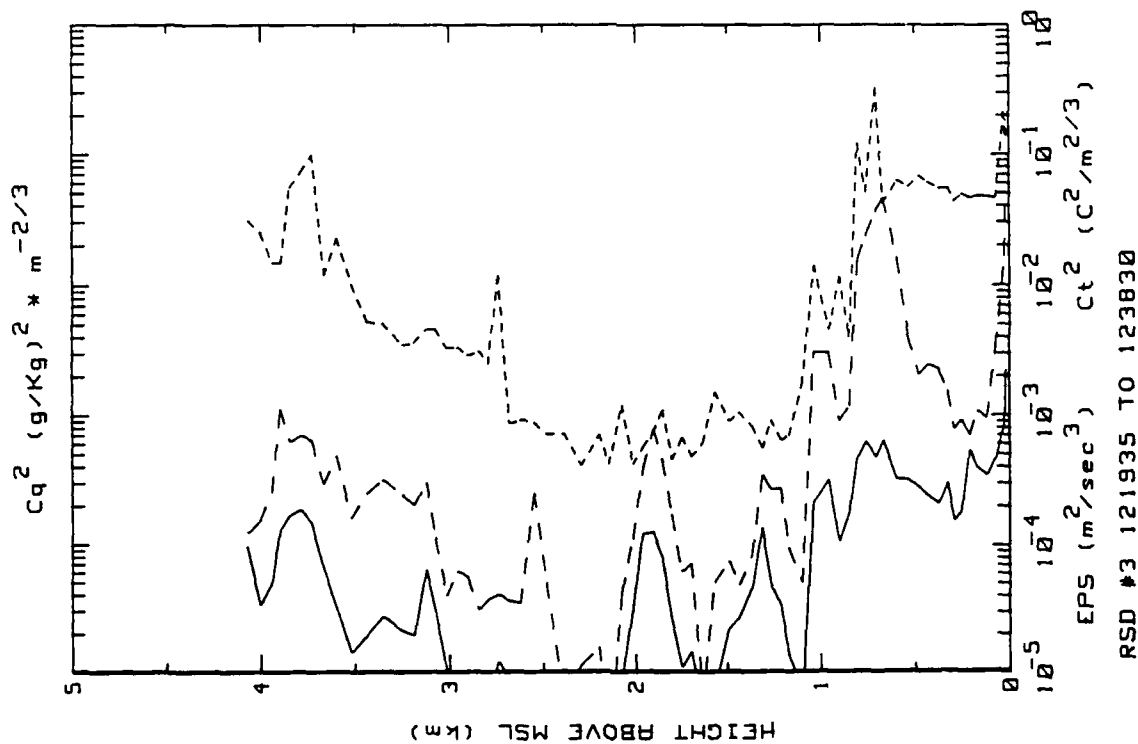
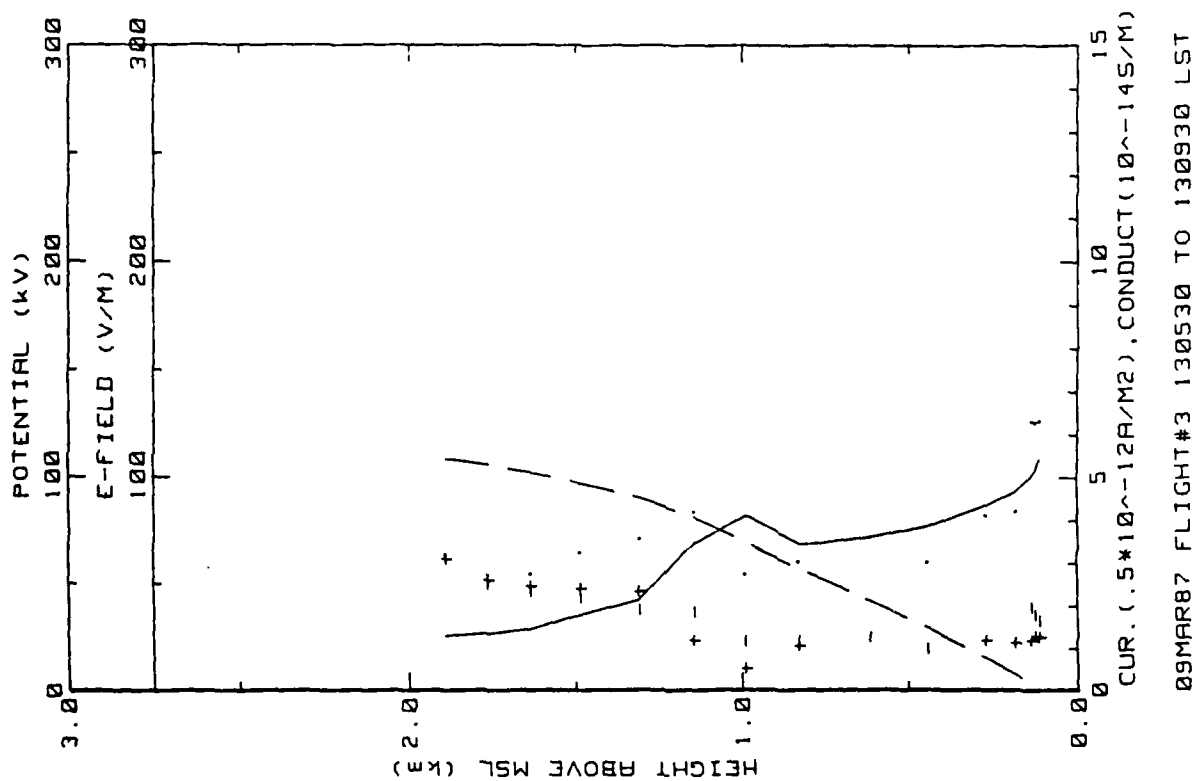
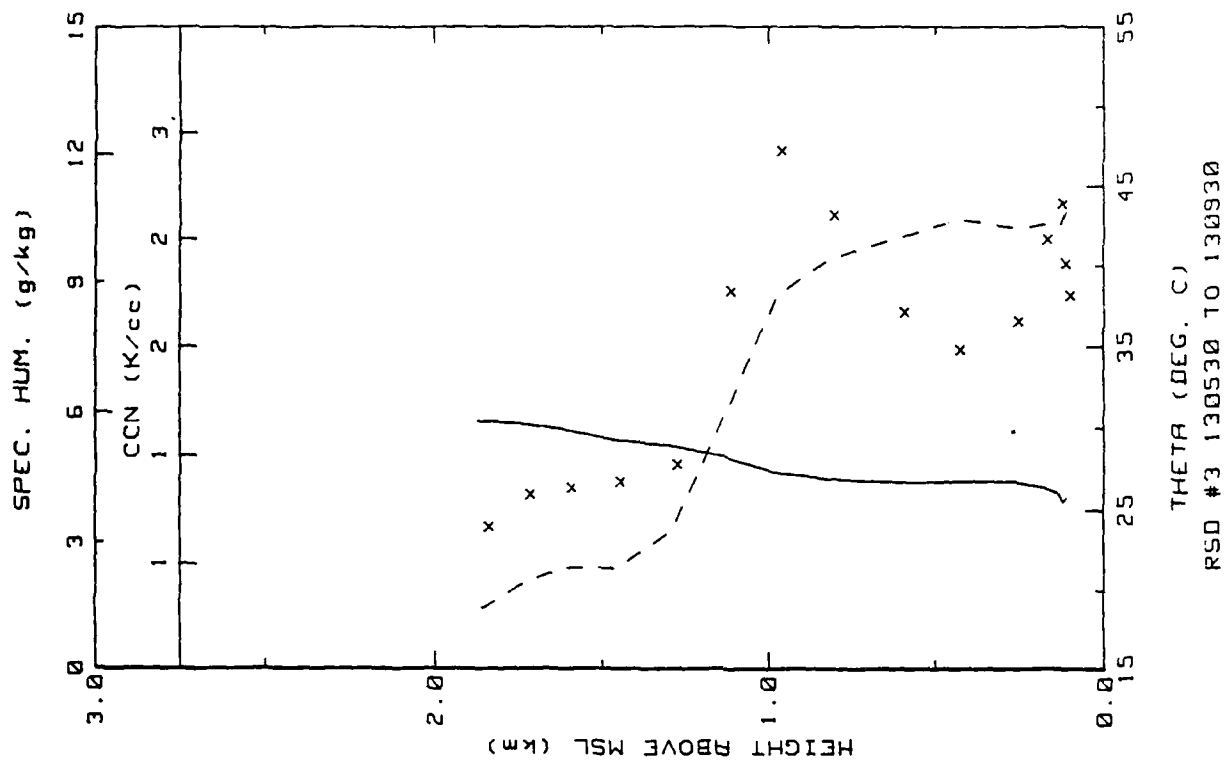


Figure 23k. RSD Flight 3 spiral down sounding over deep water E of RSD (ref. Fig. 5g).



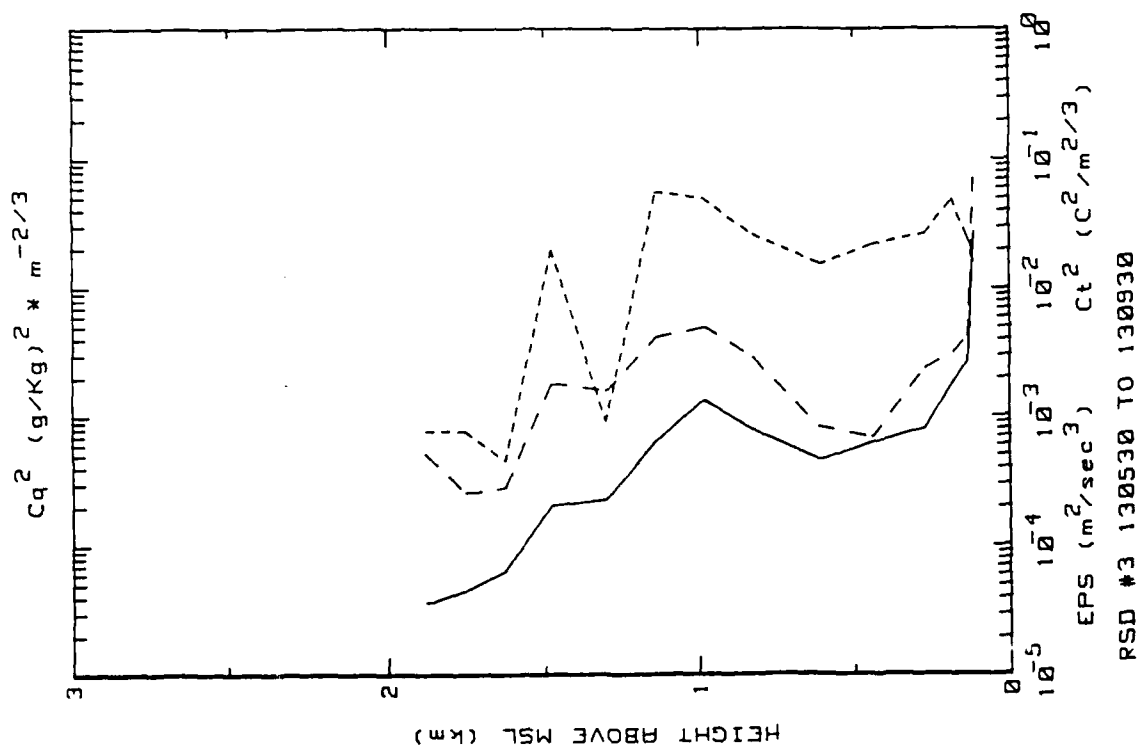


Figure 23b. RSD Flight 3 spiral downounding over ocean near RSD (ref. Fig. 5g).



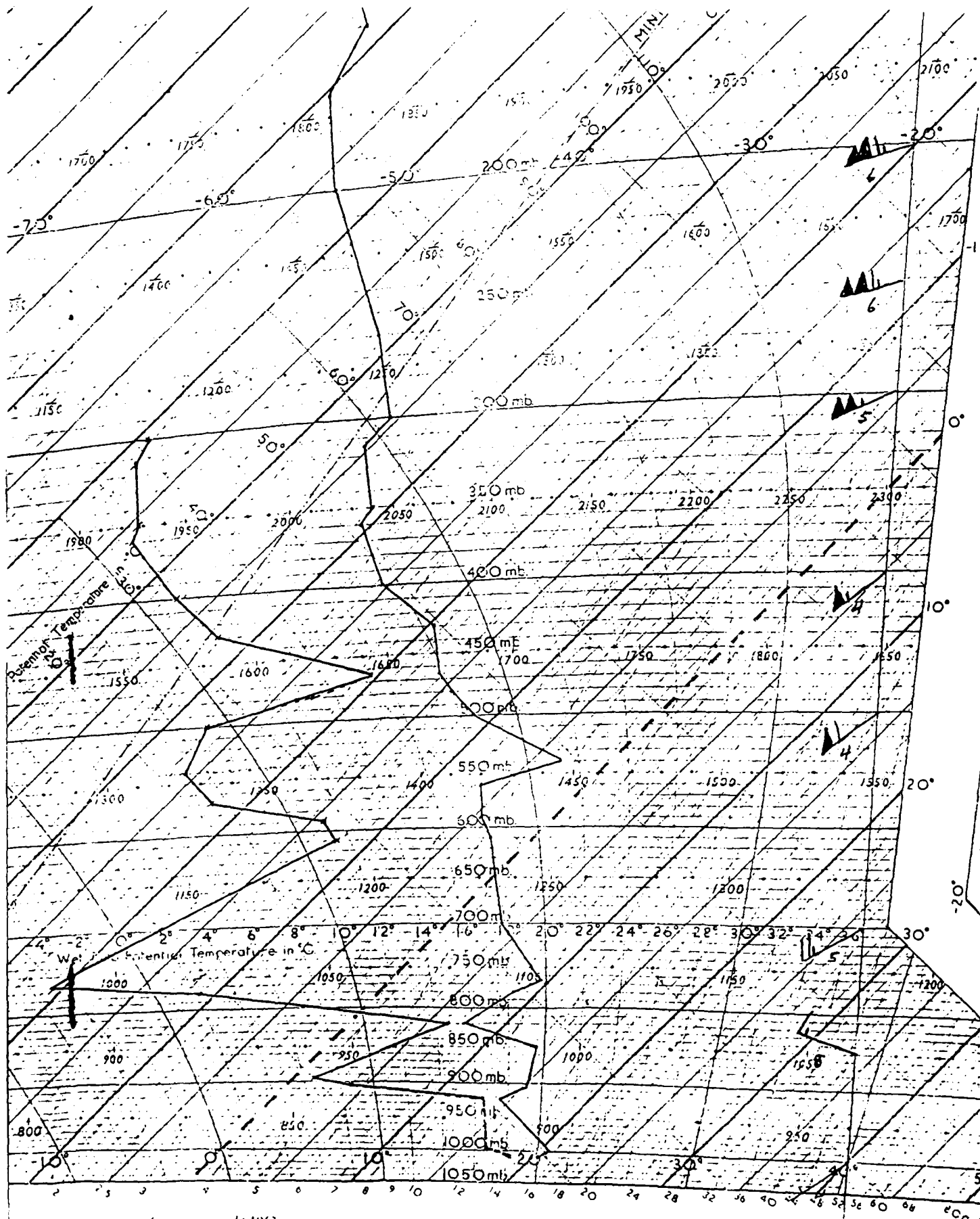


Figure 23p. Meteorological sounding from Nassau, Bahamas, taken on the day of Flight 3 (9 March 1987).

Flight: 4

Date: 10 March 87

Takeoff: 1040 (LT) from RSD

Landed: 1400 at RSD

Conditions: Clouds streets (2/10 cover) with bases at 1.2 km were evident; winds were NNW at 10 m/s. Lots of whitecaps with ocean swells of 1-2 m.

Instruments: Both polar conductivity tubes were noisy and the  $C_q^2$  RMS unit was malfunctioning. Were unable to obtain simultaneous  $C_q^2$  and  $C_T^2$  data.

Summary: Performed ladder and spiral profiles 50-120 km NE of RSD. Got both  $C_q^2$  and  $C_T^2$  data in constant altitude runs by switching signals to a single RMS unit. Only  $C_T^2$  was measured during spiral descent from 4.1 km.

Table 17a. RSD Flight 4 averages for constant altitude runs performed NE of RSD over deep water.

AVERAGES FROM LEVEL RUNS

Time HHMM	N	Altitude km	E_field V/m	+Lam 10 <sup>-14</sup>	-Lam 10 <sup>-14</sup>	Con Curr 10 <sup>-12</sup>	Theta_v C	Rel Hum %	CNN k/cc
1045	89	.005	236.83	.42	.64	2.41	23.4	62.5	4.89
1047	84	.015	224.94	.43	.57	2.27	23.4	50.6	5.10
1054	85	.031	201.55	.40	.50	1.77	23.2	58.5	5.79
1059	62	.112	198.55	.36	.48	1.71	23.0	60.7	5.87
1105	68	.006	199.31	.38	.53	1.74	23.0	65.2	5.45
1108	70	.015	212.71	.40	.46	1.85	22.5	65.1	5.59
1114	117	.031	195.57	.40	.54	1.82	22.1	63.5	5.60
1119	88	.061	198.37	.41	.49	1.77	22.3	62.5	5.46
1127	105	.125	179.68	.41	.55	1.75	22.1	64.0	5.38
1131	96	.191	170.82	.43	.54	1.67	21.6	63.1	4.93
1140	106	.320	160.56	.43	.54	1.55	21.6	65.2	5.07
1146	79	.636	142.46	.48	.58	1.50	21.7	74.1	4.54
1152	33	.943	181.87	.39	.31	1.27	21.9	89.3	4.38
1200	84	1.816	20.16	2.62	2.46	.93	25.1	34.0	.85
1205	68	2.525	9.72	5.14	5.36	1.02	29.9	13.7	.13
1209	37	3.151	8.99	5.31	6.16	1.07	31.5	25.6	.15
1214	12	4.245	7.25	5.24	8.69	1.15	37.5	13.5	.14

Time HHMM	N	Altitude km	EPS m2/s3	CT2 C2/m2/3	Q g/kg	Co2 (g/kg)2m-2/3	Press mB	Trose C	T_DR C	T_dew C
1045	89	.005	1.57E-02	5.40E-02	9.7	7.41E-02	1004.1	21.1	24.2	13.6
1047	84	.015	9.51E-03	3.67E-02	9.4	5.58E-02	1002.9	21.0	24.0	13.1
1054	85	.031	5.28E-03	1.89E-02	8.9	3.66E-02	1001.4	20.8	24.3	12.4
1059	62	.112	2.80E-03	9.60E-03	9.0	2.39E-02	998.1	20.3	23.6	12.4
1105	68	.006	2.84E-02	9.50E-02	9.8	9.34E-02	1003.4	20.5	24.0	13.8
1108	70	.015	1.14E-02	3.05E-02	9.5	5.17E-02	1002.8	20.1	23.9	13.3
1114	117	.031	4.83E-03	2.10E-02	9.2	2.69E-02	1006.6	20.0	23.9	12.9
1119	88	.061	2.27E-03	7.00E-03	9.1	1.80E-02	1003.9	20.1	23.7	12.6
1127	105	.125	1.73E-03	3.85E-03	8.9	1.34E-02	996.7	19.3	23.9	12.3
1131	96	.191	1.25E-03	2.20E-03	8.4	1.45E-02	989.1	18.5	24.0	11.3
1140	106	.320	1.10E-03	1.75E-03	8.1	1.12E-02	974.5	17.1	24.2	10.5
1146	79	.636	1.30E-03	2.80E-03	7.9	1.37E-02	939.4	14.1	24.4	9.6
1152	33	.943	1.02E-03	1.90E-03	8.3	0.00E+00	906.3	11.4	24.3	9.7
1200	84	1.816	6.24E-04	7.00E-03	2.6	9.57E-03	817.5	7.1	22.1	8.0
1205	68	2.525	1.37E-05	3.60E-03	1.0	5.12E-04	750.6	5.0	22.5	-20.7
1209	37	3.151	5.46E-05	7.00E-05	1.5	0.00E+00	694.4	.3	22.2	-16.7
1214	12	4.245	2.23E-04	1.70E-04	.6	0.00E+00	606.5	-4.9	22.8	-28.7

Table 17b. RSD Flight 4 (standard deviations)/averages for  
constant altitude runs performed NE of RSD over deep  
water.

STANDARD DEVIATIONS/MEAN VALUES

Time	E_Field	+Lam	-Lam	Con Curr	CON	EPS	.012	Q	Co2
1045	.119	.258	.670	.499	.031	.390	.477	.051	2.579
1047	.121	.322	.587	.578	.102	.448	.378	.049	1.644
1054	.113	.417	.548	.450	.032	.389	.333	.051	1.246
1059	.164	.406	.514	.478	.032	.371	.386	.053	1.100
1105	.132	.232	.567	.495	.209	1.163	.455	.044	4.100
1108	.076	.225	.563	.382	.024	.527	.419	.040	1.658
1114	.106	.216	.444	.358	.077	.433	.446	.035	2.236
1119	.108	.180	.423	.298	.038	.396	.417	.046	.931
1127	.135	.174	.307	.322	.042	.466	.326	.051	.552
1131	.076	.150	.281	.235	.031	.482	.559	.032	.539
1140	.060	.122	.199	.166	.039	.621	.600	.039	.494
1146	.041	.233	.198	.221	.046	.515	.474	.053	.563
1152	.275	.346	.595	.557	.045	.386	.771	.034	0.000
1200	.240	.138	.256	.279	.215	2.195	2.385	.213	.814
1205	.115	.014	.009	.114	.260	.172	.919	.198	.915
1209	.086	.005	.010	.081	.198	.021	2.795	.046	0.000
1214	.033	.008	.032	.082	.205	1.544	2.743	.000	0.000

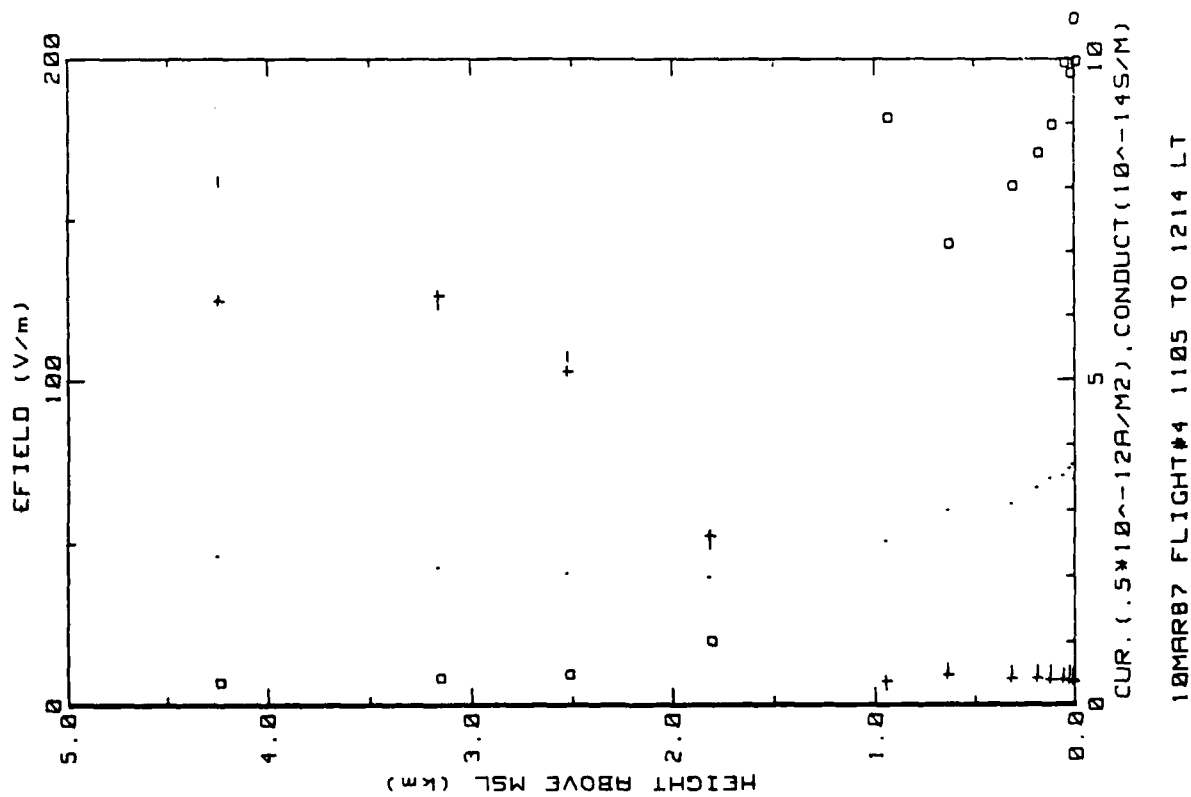


Figure 24a. RSD Flight 4 ladder profile over deep water  
NE of RSD. (ref. Fig. 5a).

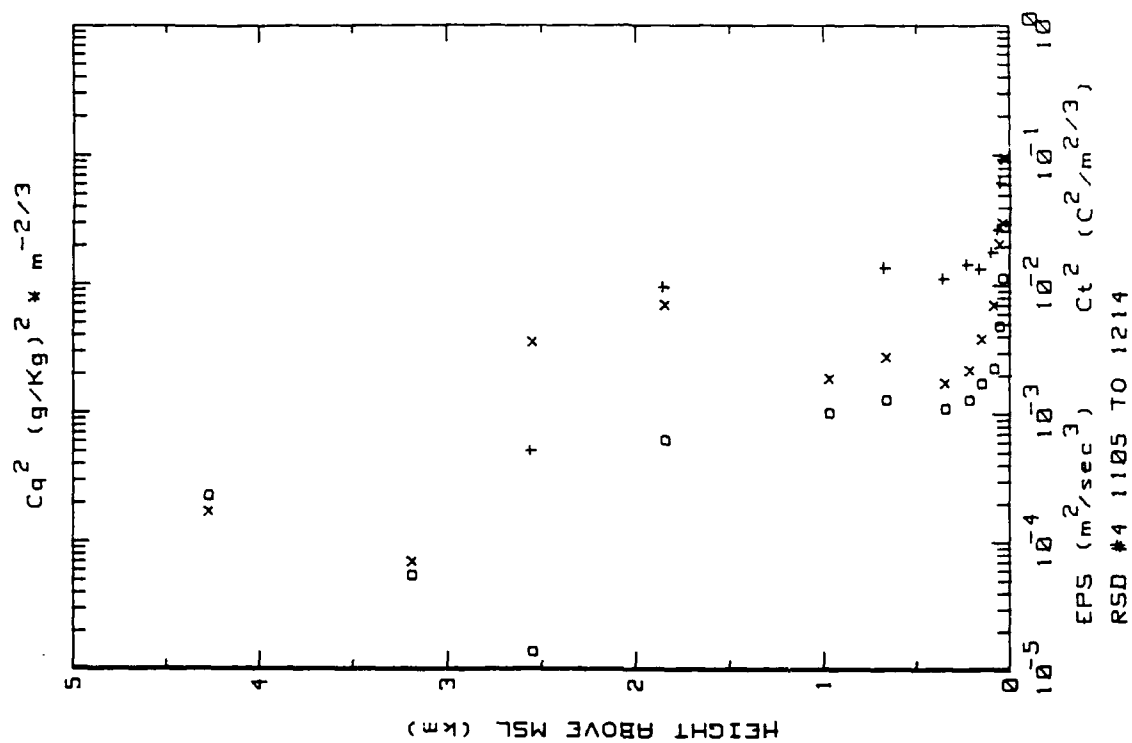


Figure 24b. RSD Flight 4 ladder profile over deep water  
NE of RSD. (ref. Fig. 5b).

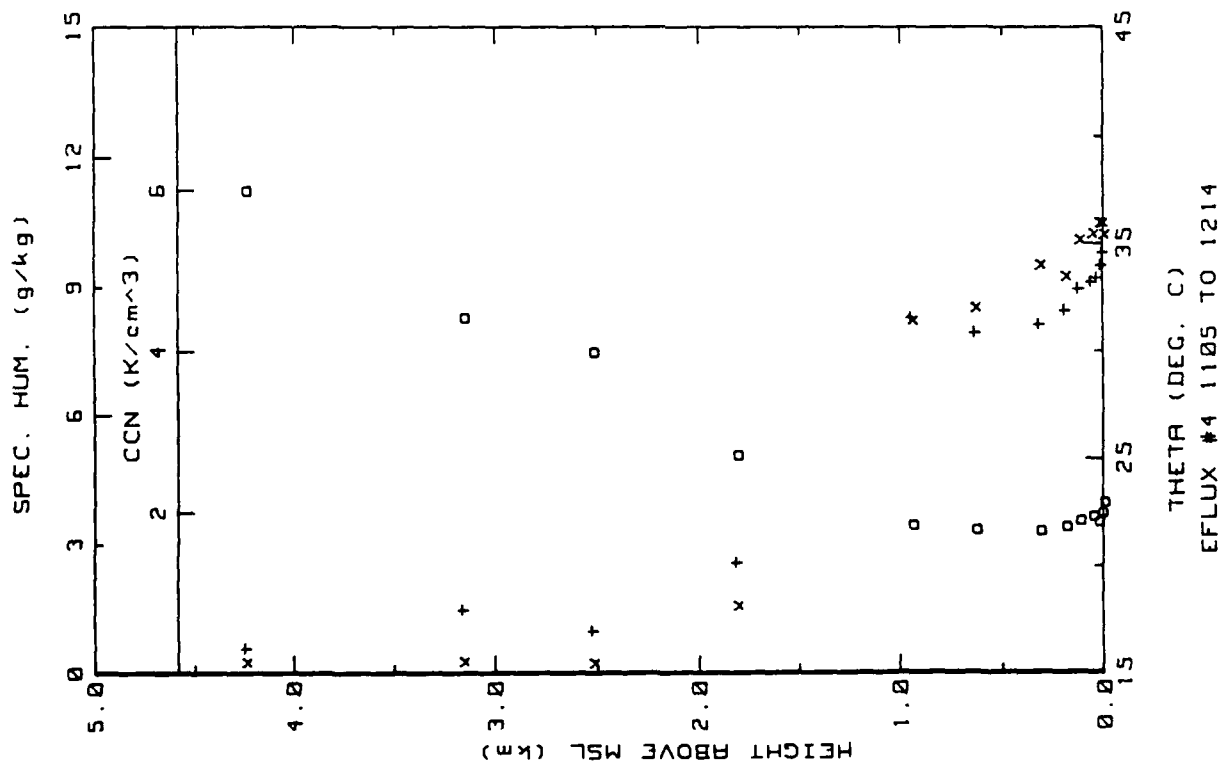
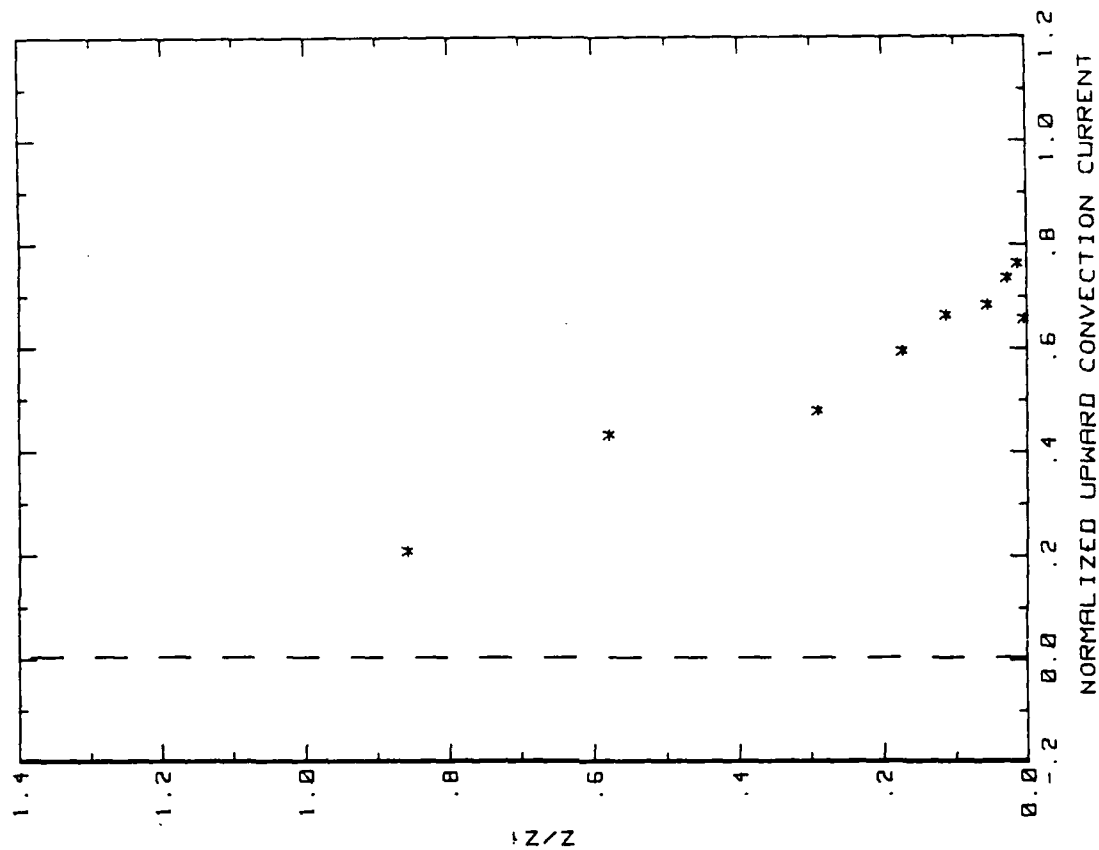


Figure 24c. RSD Flight 4 ladder profile over deep water NE of RSD. (ref. Fig. 5c).



10MAR87 FLIGHT#4 10:46 TO 12:16 LST

Figure 24d. RSD Flight 4 convection current profile over deep water NE of RSD (ref. Fig. 5d). The start time should be 1106 LT. ( $z_1 = 1100$ ,  $J_0 = 1.05$ )

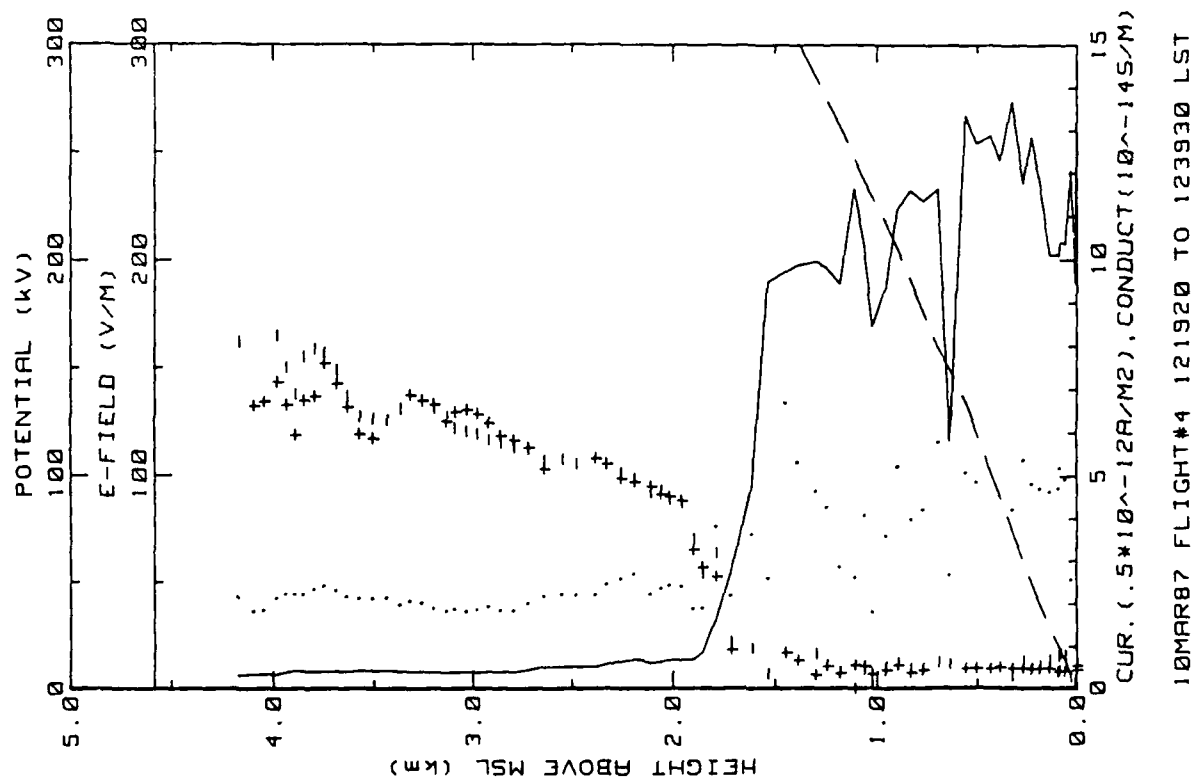


Figure 24e. RSD Flight 4 spiral down sounding over deep water NE of RSD (ref. Fig. 5e).

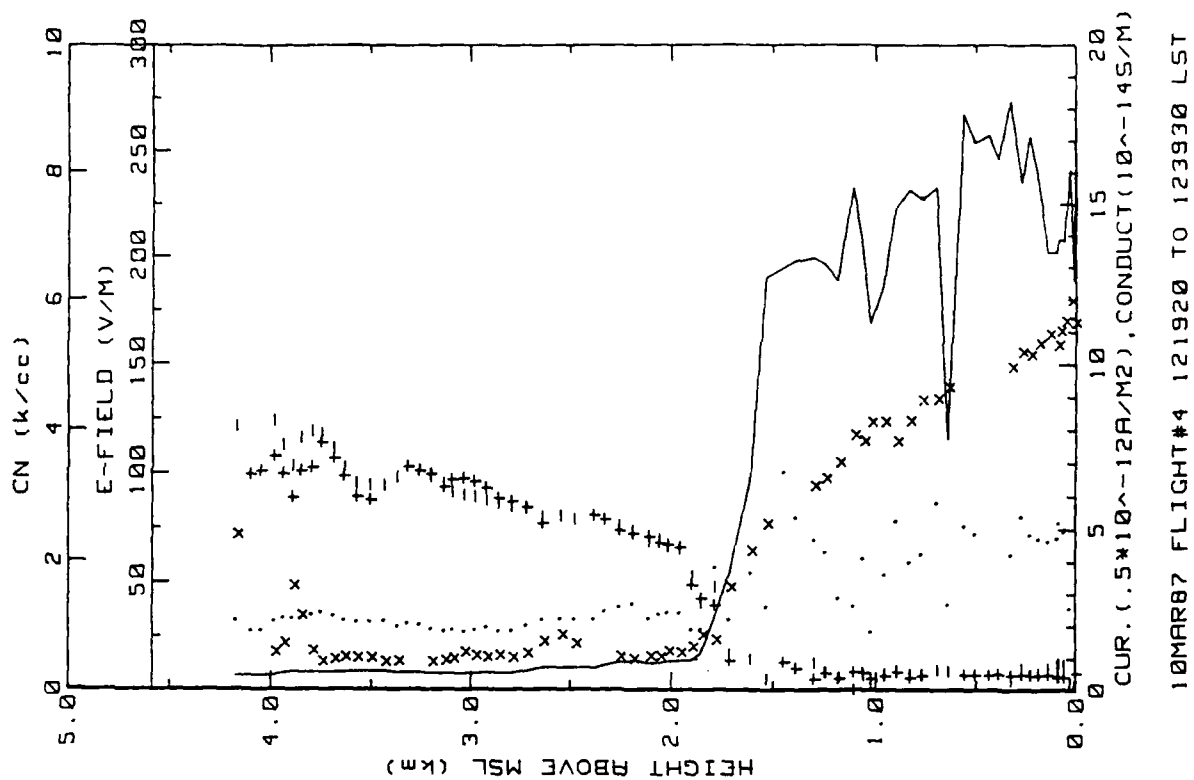


Figure 24f. RSD Flight 4 spiral down sounding over deep water NE of RSD (ref. Fig. 5f).

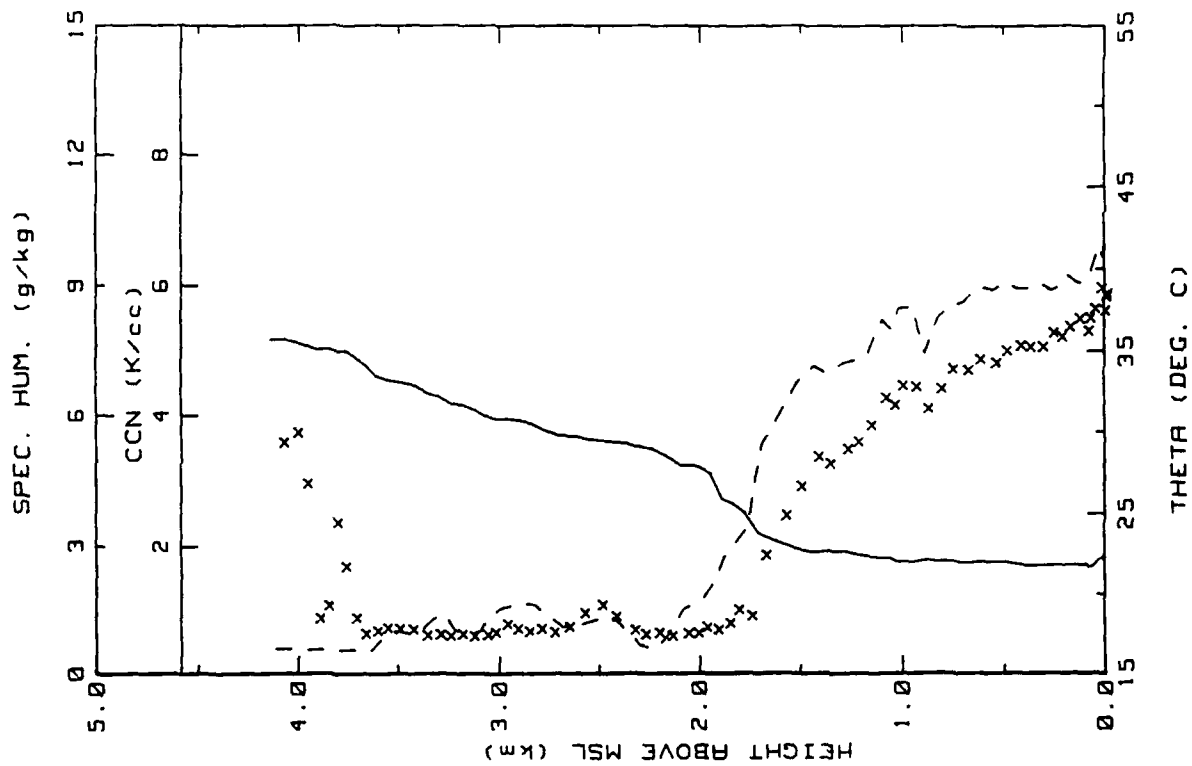


Figure 24g. RSD Flight 4 spiral down sounding over deep water NE of RSD (ref. Fig. 5h).

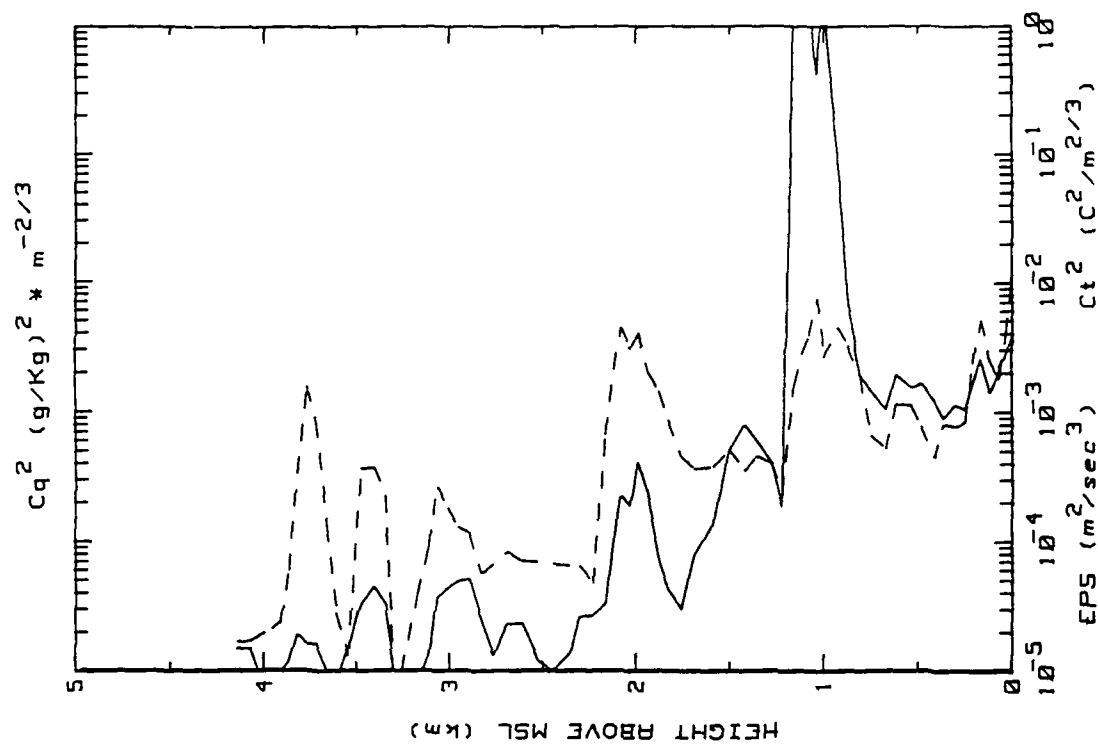


Figure 24h. RSD Flight 4 spiral down sounding over deep water NE of RSD (ref. Fig. 5g). See Fig. 24g for times;  $C_p^2$  is not plotted.



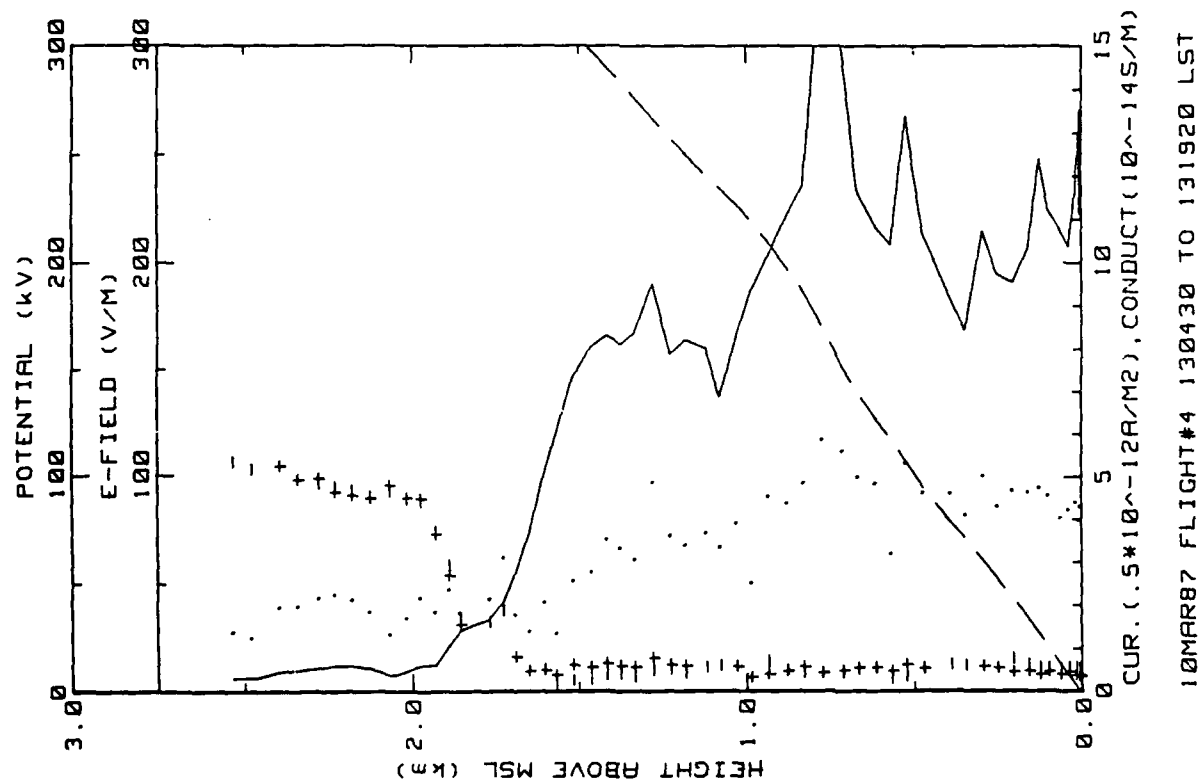


Figure 24i. RSD Flight 4 spiral descending over ocean near RSD (ref. Fig. 5e).

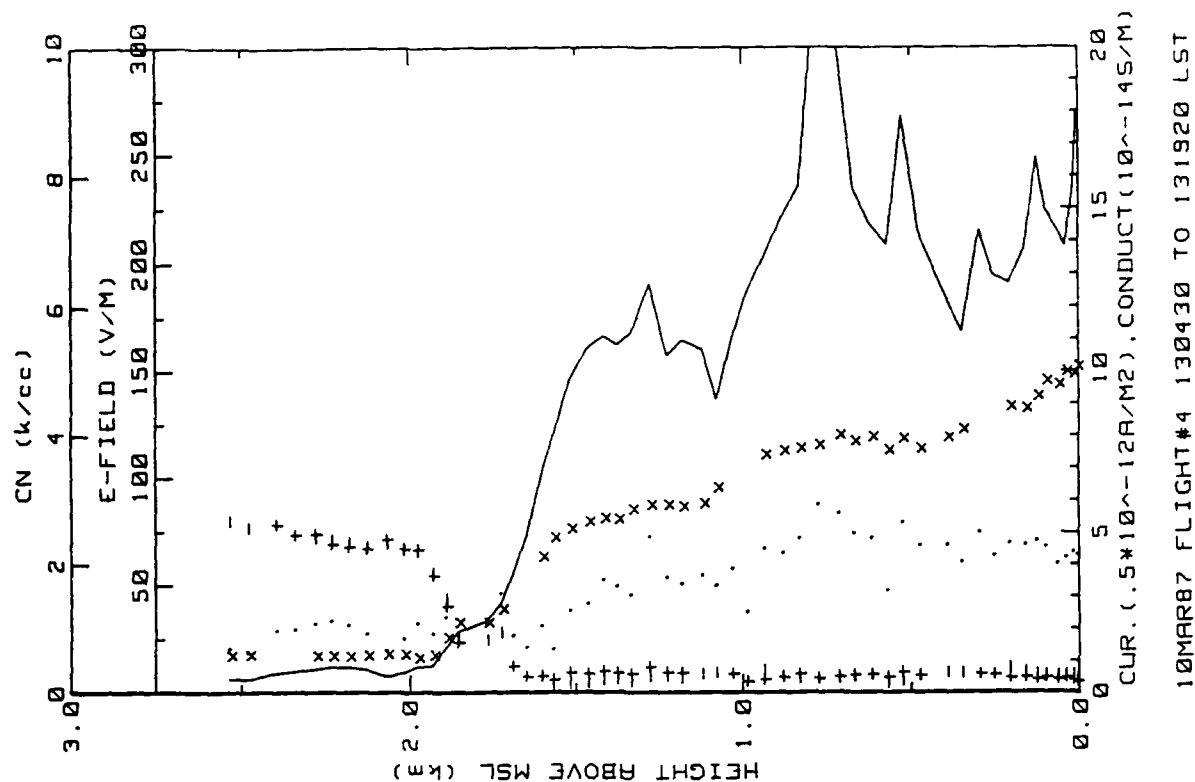


Figure 24j. RSD Flight 4 spiral descending over ocean near RSD (ref. Fig. 5f).

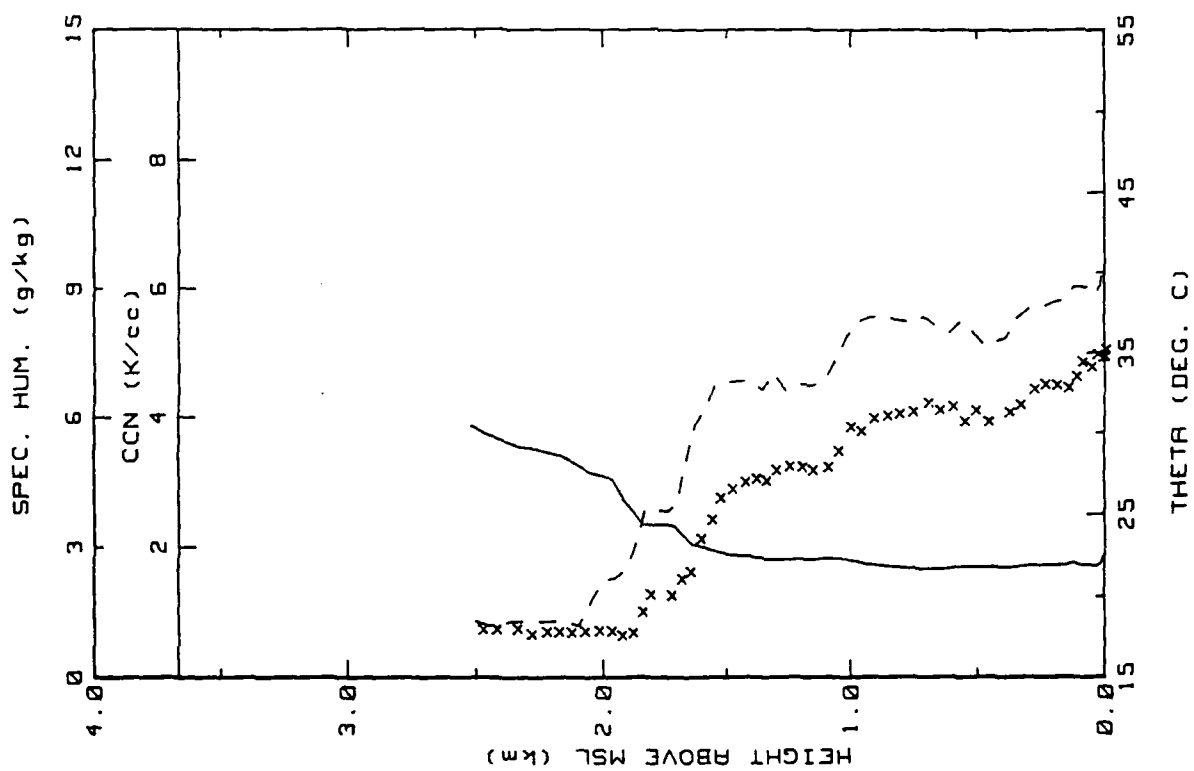


Figure 24k. RSD Flight 4 spiral downounding over ocean near RSD (ref. Fig. 5h).

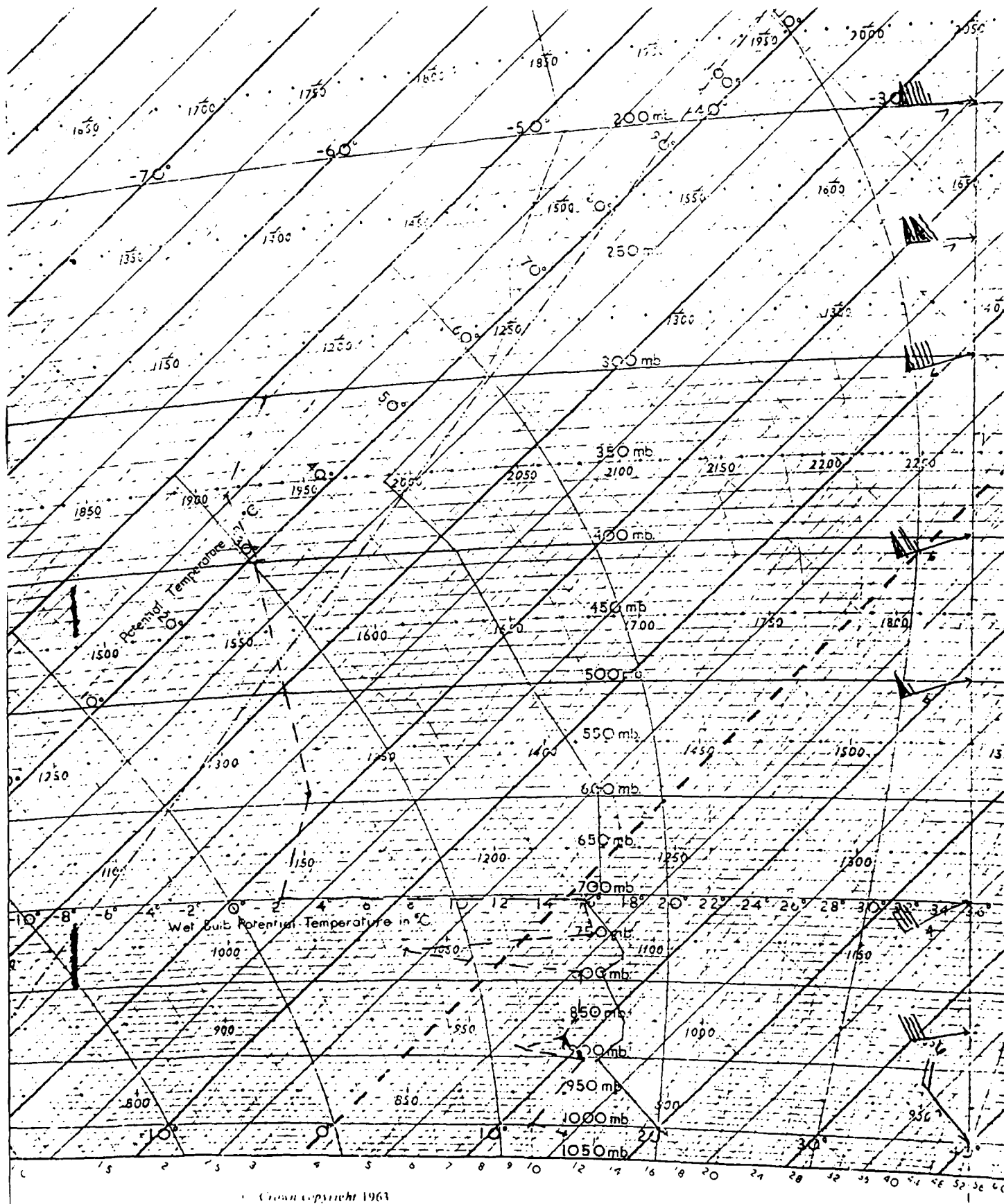


Figure 241. Meteorological sounding from Nassau, Bahamas, taken on the day of Flight 4 (10 March 1987).

Flight: 5

Date: 11 March 1987

Takeoff: 1120 (LT) from RSD

Landed: 1343 at RSD

Conditions: Scattered low cumulus clouds (1-2/10 cover) with bases near 1.0 km and tops at 2.0 km. Surface winds were variable but mostly from the N at 5-10 m/s. Lots of whitecaps and big swells.

Instruments: All worked properly.

Summary: Ladder and spiral profiles were performed 40-100 km NE of RSD. Several closely spaced (in altitude) crosswind constant altitude passes were made to examine the plume structure evident in the electric field records. These were compared with up and downwind passes. A spiral descent was made from 7.6 km to measure ionospheric potential; all other soundings during the deployment were from 4.1 km.

Table 18a. RSD Flight 5 averages for constant altitude runs performed NE of RSD over deep water.

AVERAGES FROM LEVEL RUNS

Time HHH	N	Altitude km	L (field) V/m	+Lam 10 <sup>-14</sup>	-Lam 10 <sup>-14</sup>	Con Curr 10 <sup>-12</sup>	Theta_v C	Rel Hum %	CNN k/cc
1118	46	.003	159.40	.73	.83	2.53	21.6	54.6	2.20
1121	44	.005	158.00	.74	.75	2.48	21.5	54.3	2.17
1124	47	.015	159.87	.78	.80	2.90	21.7	53.5	2.09
1133	42	.031	160.54	.78	.83	2.68	21.6	51.2	2.06
1138	104	.075	158.65	.81	.91	2.75	21.5	57.6	2.03
1140	51	.135	150.78	.85	.96	2.77	21.4	58.9	1.90
1144	54	.231	134.48	.95	1.06	2.73	21.6	58.9	1.70
1148	84	.006	194.46	1.02	1.02	3.95	22.0	57.2	1.61
1153	66	.015	169.17	.98	1.10	3.59	21.7	58.8	1.58
1157	32	.031	150.84	1.02	1.17	3.23	21.5	59.1	1.40
1201	86	.323	107.77	1.18	1.34	2.71	21.5	53.9	1.30
1205	43	.666	85.77	1.24	1.36	2.33	21.5	75.0	1.19
1211	73	.953	87.03	1.33	1.39	2.42	21.5	63.4	1.15
1215	57	2.061	25.22	2.02	2.32	1.03	24.3	53.1	1.11
1222	26	2.503	22.19	4.66	4.79	2.10	30.7	15.4	.36
1229	50	3.166	18.21	5.04	5.56	1.92	35.0	10.7	.36
1233	40	4.230	11.97	8.82	8.13	2.02	39.8	16.0	.18

Time HHH	N	Altitude km	EPS m2/s3	CT2 C2/m2/3	G g/kg	Cu2 (g/kg)2m-2/3	Press mb	Trose C	T_OR C	T_dev C
1118	46	.003	7.11E-03	4.54E-02	9.1	9.32E-02	1016.1	19.8	24.1	12.5
1121	44	.006	4.25E-03	3.17E-02	9.0	6.32E-02	1015.6	19.7	23.9	12.7
1124	47	.015	2.30E-03	1.69E-02	8.9	3.45E-02	1014.1	19.7	24.0	12.6
1133	42	.031	1.92E-03	9.95E-03	8.6	2.35E-02	1012.9	19.6	23.9	11.9
1138	104	.075	1.30E-03	5.28E-03	8.0	1.85E-02	1009.7	19.3	23.8	10.7
1140	51	.135	1.12E-03	2.46E-03	7.9	1.12E-02	1002.8	18.7	24.2	10.5
1144	54	.231	9.24E-04	1.86E-03	7.7	9.69E-03	991.7	18.0	24.2	9.9
1148	84	.006	8.30E-03	3.81E-02	8.3	1.10E-01	1014.1	20.1	24.0	11.4
1153	66	.015	3.13E-03	1.90E-02	8.3	4.74E-02	1013.3	19.7	23.8	11.4
1157	32	.031	1.73E-03	8.54E-03	8.2	2.13E-02	1011.2	19.4	23.5	11.2
1201	86	.323	5.10E-04	9.11E-04	7.8	7.20E-03	981.1	17.0	23.5	10.1
1205	43	.666	5.39E-04	1.87E-03	7.8	5.58E-03	942.5	13.9	23.7	9.4
1211	73	.953	4.92E-04	5.16E-02	7.4	1.84E-02	911.2	10.9	23.6	9.2
1215	57	2.061	1.42E-03	6.08E-03	3.3	1.09E-02	798.0	3.7	22.2	-5.2
1222	26	2.503	1.34E-04	6.13E-05	1.2	1.49E-02	736.1	5.7	22.8	-18.7
1229	50	3.166	3.55E-04	1.37E-04	.7	1.48E-02	696.7	3.2	23.3	-24.8
1233	40	4.230	4.00E-04	1.32E-03	.8	1.49E-03	603.3	-3.1	24.4	-25.4

Table 18b. RSD Flight 5 (standard deviations)/averages for  
constant altitude runs performed NE of RSD over deep  
water.

STANDARD DEVIATIONS/MEAN VALUES

Time	E_Field	+Lam	-Lam	Con Curr	CCN	EPS	• C12	G	Co2
1118	.149	.274	.281	.223	.032	.337	.235	.037	.420
1121	.189	.285	.257	.278	.044	.296	.182	.036	.380
1124	.166	.293	.210	.242	.044	.358	.293	.043	.446
1133	.146	.261	.183	.221	.043	.327	.307	.037	.489
1138	.142	.193	.179	.214	.047	.433	.402	.040	.565
1140	.097	.180	.131	.194	.060	.395	.475	.039	.667
1144	.085	.158	.129	.171	.062	.454	.733	.040	.711
1148	.177	.235	.258	.287	.057	.389	.438	.070	.675
1153	.156	.212	.186	.234	.038	.461	.476	.051	.683
1157	.113	.157	.103	.193	.050	.476	.347	.040	.565
1201	.055	.078	.070	.083	.052	.530	.588	.041	.373
1205	.051	.082	.045	.082	.057	.427	.341	.025	.323
1211	.198	.304	.074	.360	.094	.542	.719	.062	1.255
1215	1.401	.208	.288	1.745	.055	1.615	1.501	.162	1.787
1222	.025	.033	.017	.013	.228	.119	1.186	.022	.044
1228	.035	.027	.030	.042	.151	.319	.572	.027	.052
1233	.017	.011	.011	.044	.105	.549	.371	.033	.057

Table 18c. RSD Flight 5 averages and standard deviations for constant altitude runs performed E of RSD following downsounding.

AVERAGES FROM LEVEL RUNS

Time HHH	N	Altitude km	E_Field V/m	+Lam 10 <sup>-14</sup>	-Lam 10 <sup>-14</sup>	Con Curr 10 <sup>-12</sup>	Theta_v C	Rel Hum %	CCN k/cc
1319	54	.006	174.59	1.06	1.06	3.68	21.4	59.4	1.32
1323	51	.015	0.00	1.02	1.04	0.00	21.7	59.5	1.28
1327	37	.059	158.65	1.00	1.09	3.29	21.4	57.9	1.30
1330	37	.118	143.73	.94	1.03	2.79	21.3	60.7	1.48
1333	42	.212	125.94	.92	1.02	2.43	21.4	60.6	1.38
1336	35	.314	113.63	.92	1.03	2.20	21.7	63.6	1.35
1339	59	.377	119.50	.88	.96	2.20	22.3	66.3	1.29

Time HHH	N	Altitude cm	EPS m2/s3	CT2 C2/m2/3	G g/kg	Ca2 (g/kg)2m-2/3	Press mb	Trose C	T_IR C	T_dew C
1319	54	.006	7.47E-03	4.14E-02	8.4	1.02E-01	1019.5	19.8	26.3	11.7
1323	51	.015	7.32E-03	1.28E-02	8.4	1.11E+01	1012.0	19.6	25.4	11.5
1327	37	.059	8.82E-04	4.19E-03	8.0	1.70E-02	1011.7	19.4	25.3	10.9
1330	37	.118	6.52E-04	2.30E-03	8.1	1.10E-02	1004.8	18.7	25.2	10.9
1333	42	.212	5.42E-04	1.33E-03	7.9	9.86E-03	993.8	17.9	25.1	10.2
1336	35	.314	4.10E-04	1.03E-03	7.9	9.40E-03	982.1	17.2	25.1	10.2
1339	59	.377	8.48E-04	1.32E-03	6.2	1.14E-02	974.9	17.1	19.4	10.7

STANDARD DEVIATIONS/MEAN VALUES

Time	E_Field	+Lam	-Lam	Con Curr	CCN	EPS	CT2	G	Ca2
1319	.215	.415	.201	.362	.055	.288	.231	.053	.509
1323	0.000	.474	.296	0.000	.041	.352	.361	.064	7.785
1327	.192	.290	.123	.253	.050	.434	.448	.035	.534
1330	.133	.131	.091	.169	.084	.448	.523	.032	.519
1333	.099	.156	.030	.143	.065	.515	.928	.040	.540
1336	.110	.113	.059	.107	.061	.439	.754	.033	.591
1339	.127	.171	.081	.146	.065	.367	.591	.046	.916

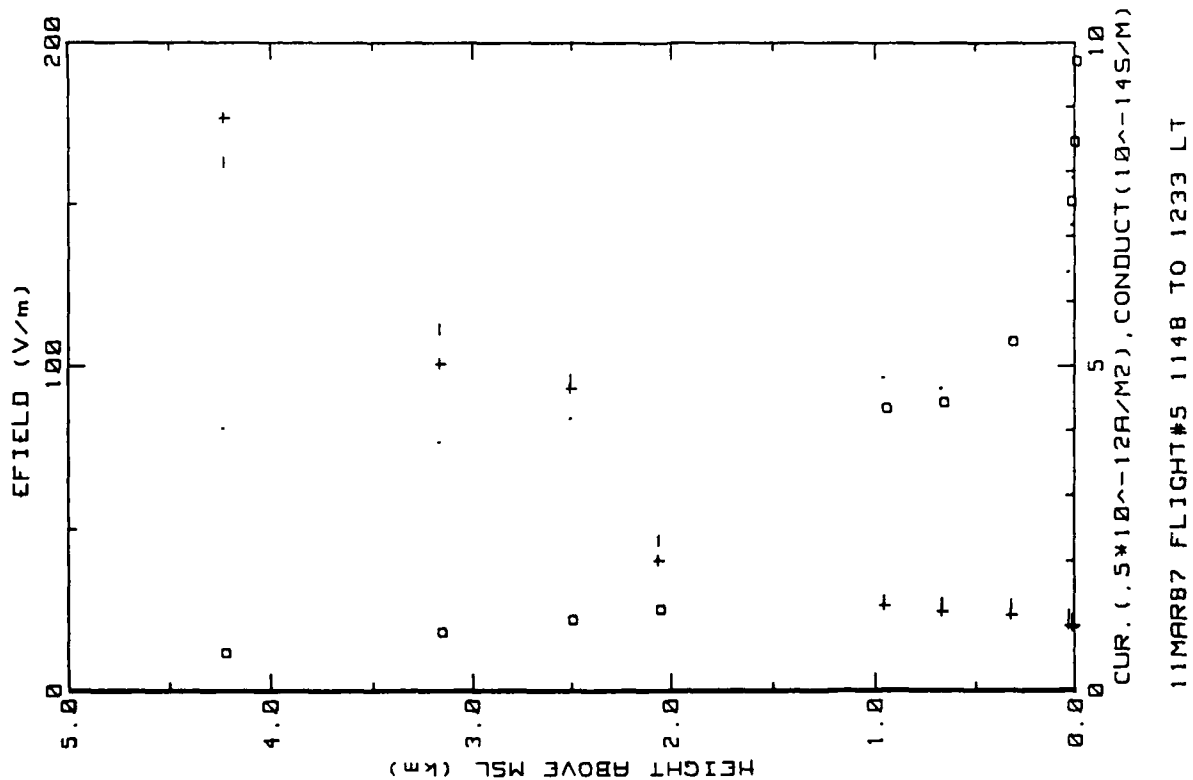


Figure 25a. RSD Flight 5 ladder profile over deep water NE of RSD. (ref. Fig. 5a).

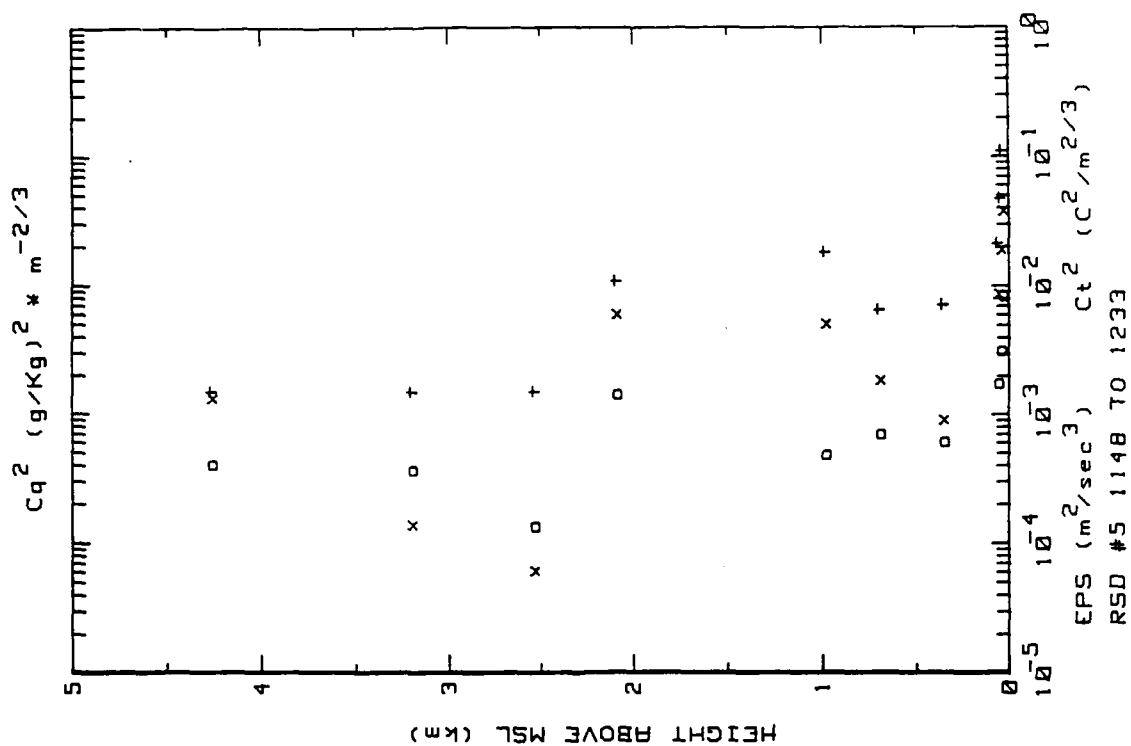


Figure 25b. RSD Flight 5 ladder profile over deep water NE of RSD. (ref. Fig. 5b).



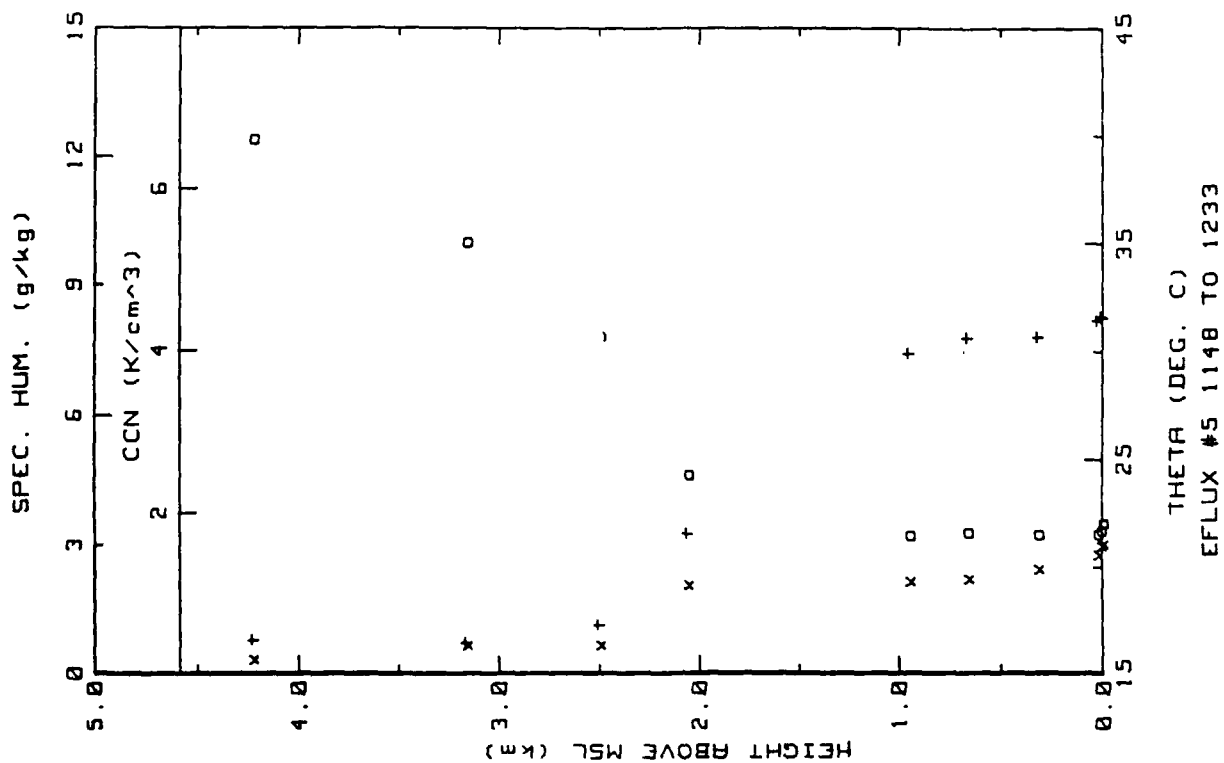


Figure 25c. RSD Flight 5 ladder profile over deep water NE of RSD. (ref. Fig. 5c).

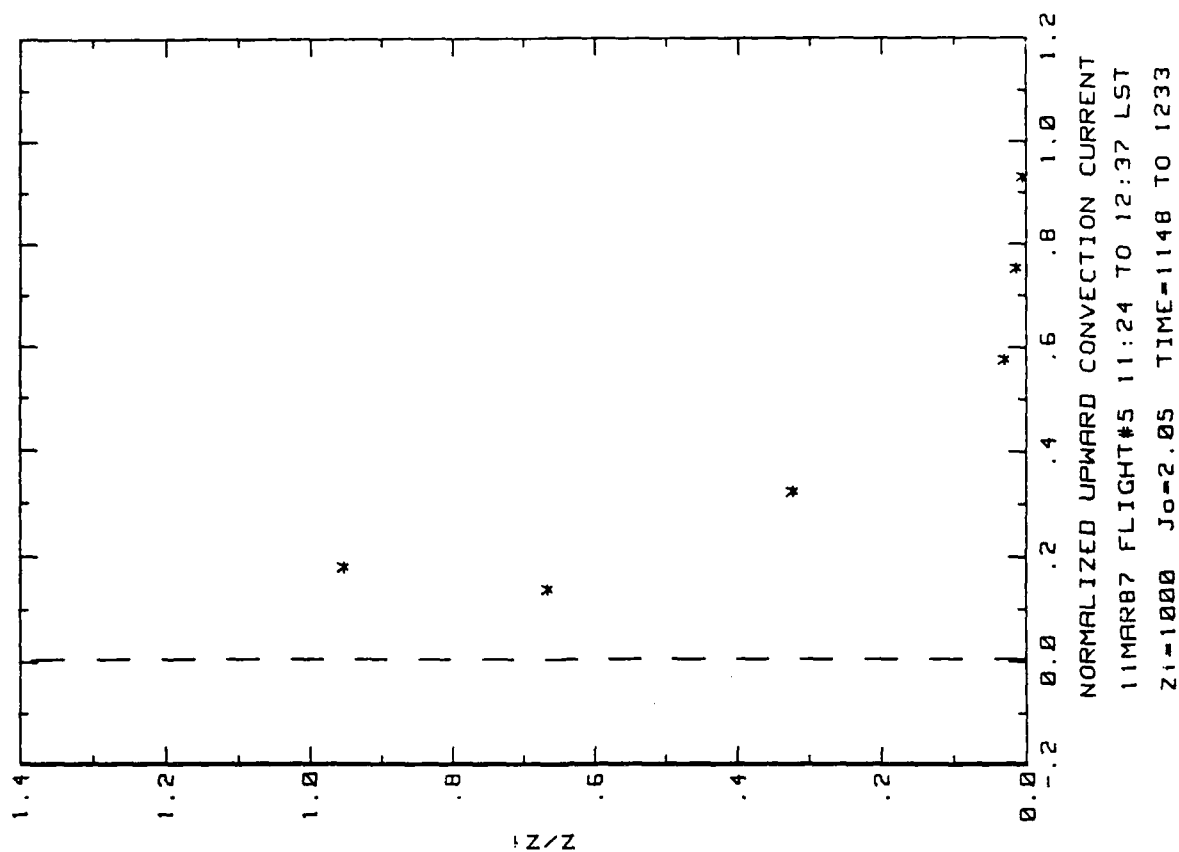


Figure 25d. RSD Flight 5 convection current profile over deep water NE of RSD (ref. Fig. 5d).

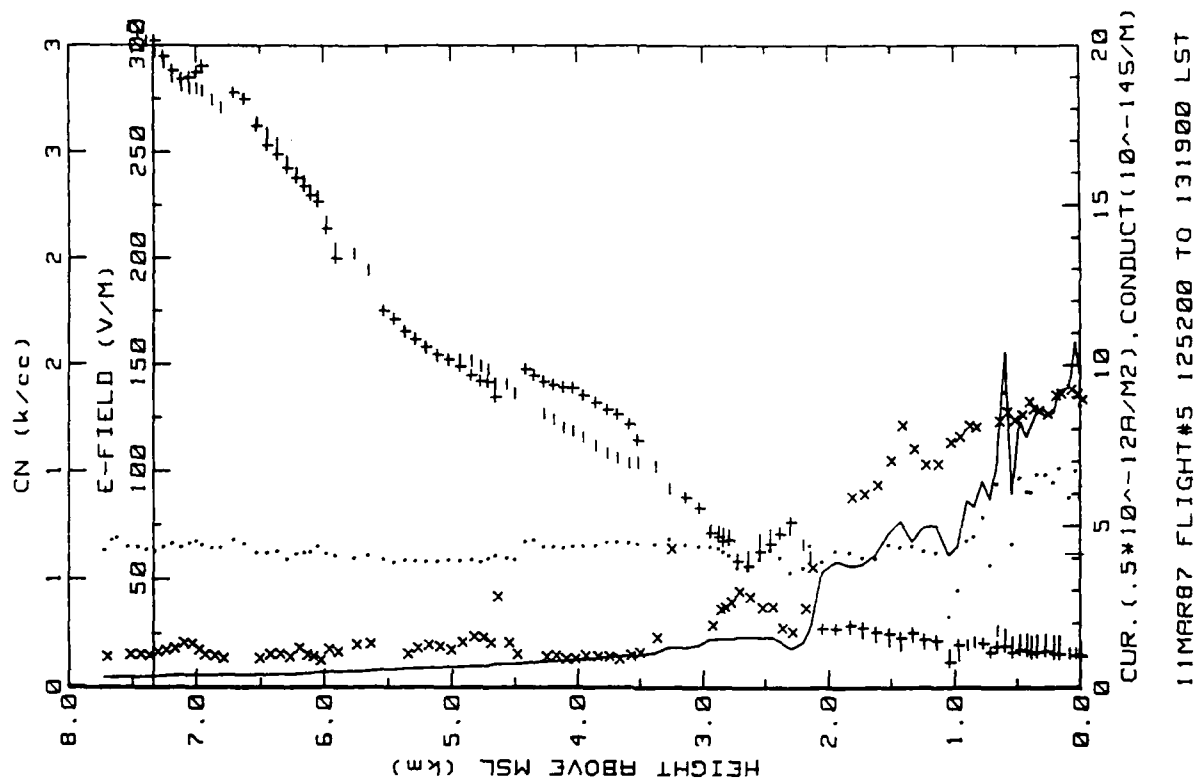


Figure 25f. RSD Flight 5 spiral down sounding over deep water NE of RSD (ref. Fig. 5f).

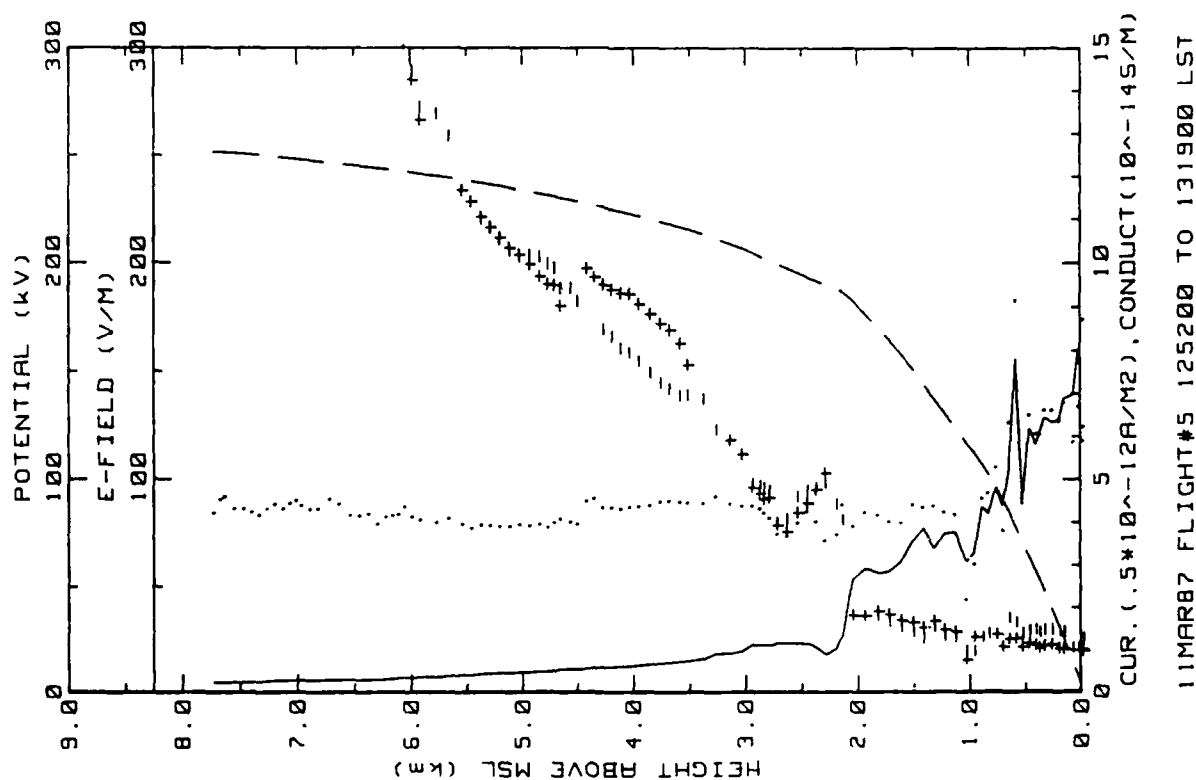


Figure 25e. RSD Flight 5 spiral down sounding over deep water NE of RSD (ref. Fig. 5e).

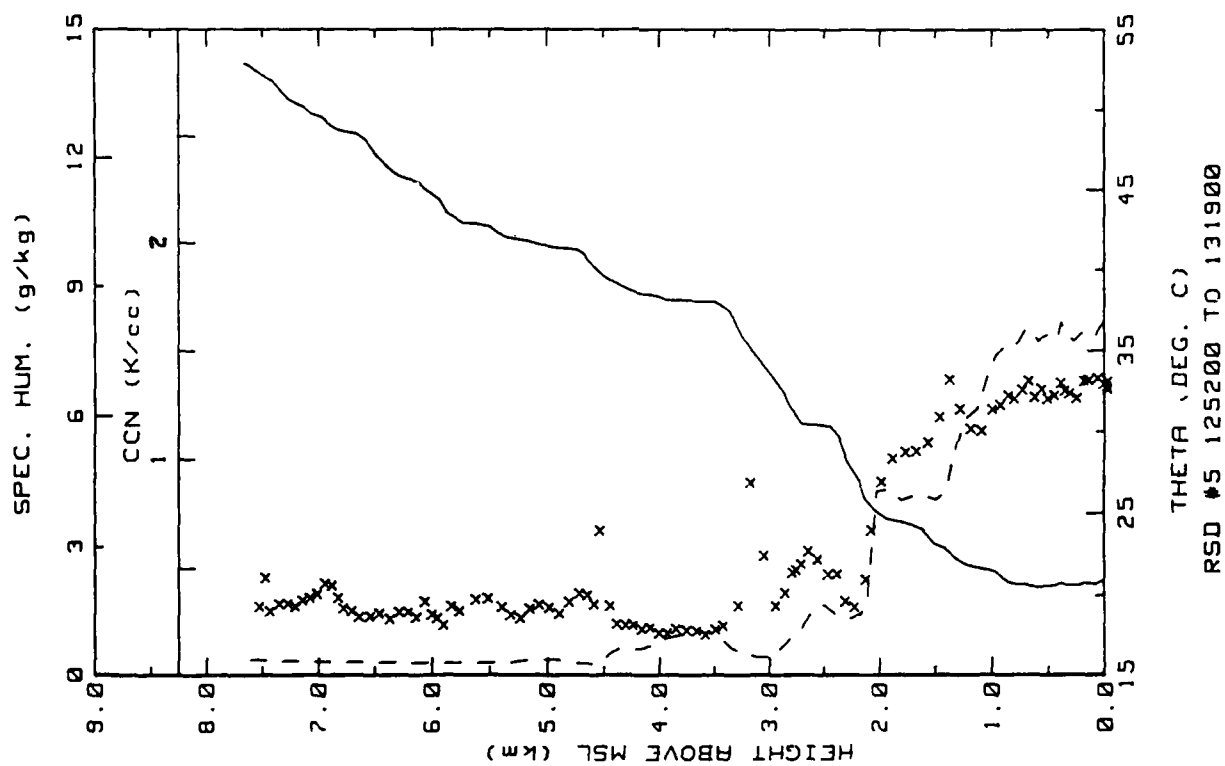


Figure 25g. RSD Flight 5 spiral down sounding over deep water NE of RSD (ref. Fig. 5h).

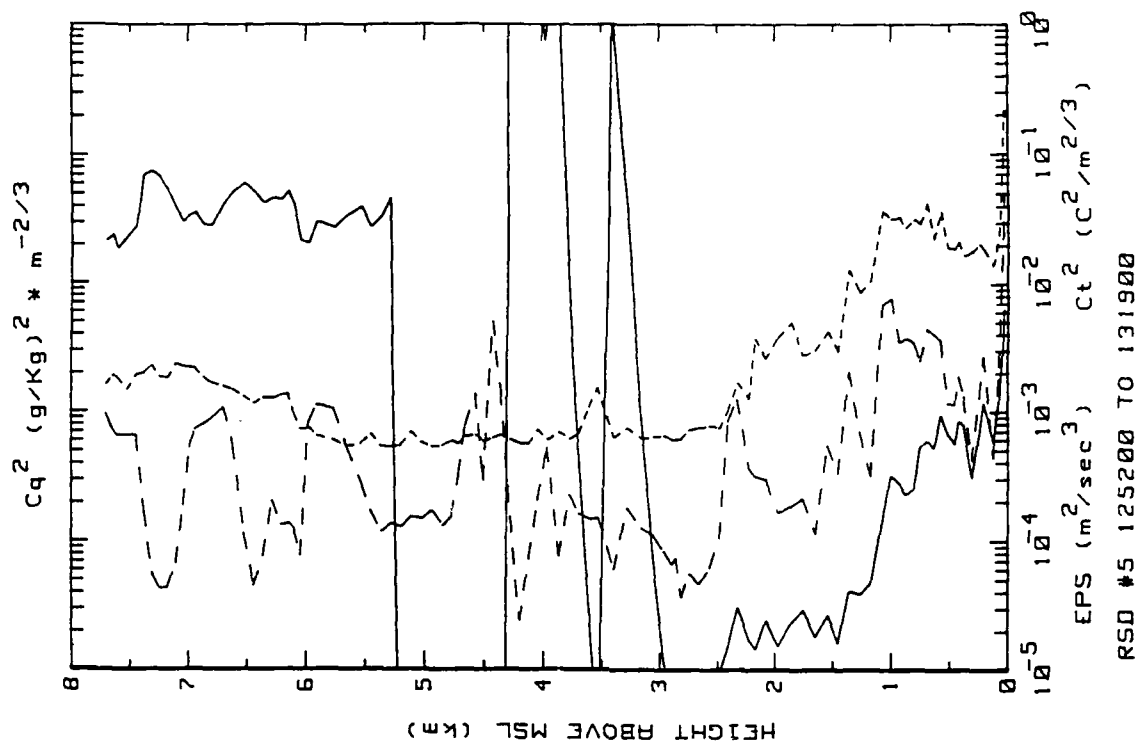


Figure 25h. RSD Flight 5 spiral down sounding over deep water NE of RSD (ref. Fig. 5g).

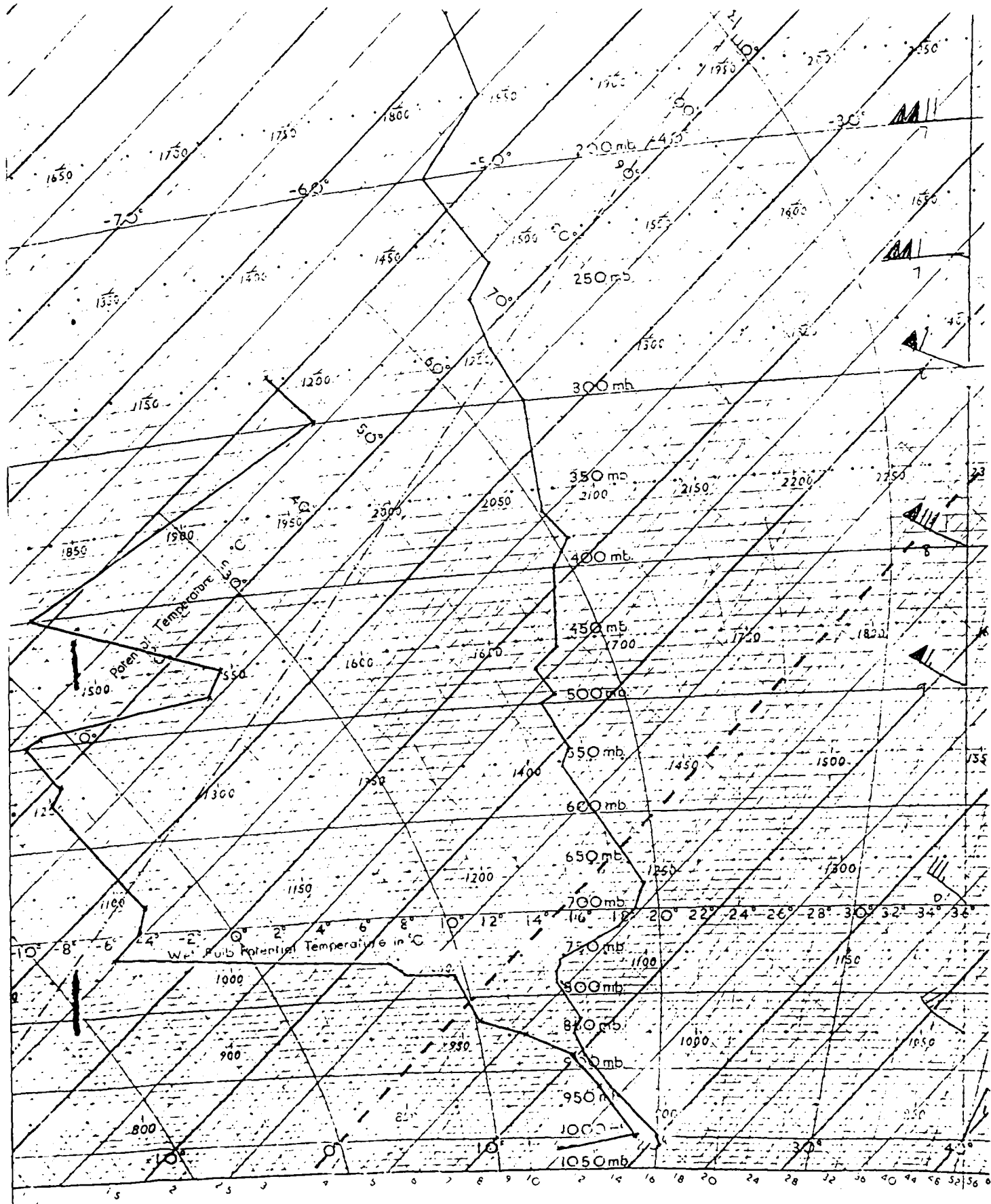


Figure 25i. Meteorological sounding from Nassau, Bahamas, taken on the day of Flight 5 (11 March 1987).

Flight: 6

Date: 12 March 1987

Takeoff: 1156 (LT) from RSD

Landed: 1400 at RSD

Conditions: High overcast and low scattered cumulus with bases near 1.2 km; light precipitation at times during flight. Winds were from WNW at 2 to 4 m/s with no whitecaps and 1m swells.

Instruments: All worked properly.

Summary: Soundings were obtained 40-80 km E of RSD; were unable to ascend above 1.8 km because of clouds. Ended spiral sounding 20 km NE of Cat Island.

Table 19a. RSD Flight 6 averages for constant altitude runs performed E of RSD over deep water.

AVERAGES FROM LEVEL RUNS

line HHH	N	Altitude km	E field V/m	+Lam 10 <sup>-14</sup>	-Lam 10 <sup>-14</sup>	Corr Curr 10 <sup>-12</sup>	theta_v C	Rel Hum %	CNN k/cc
1202	52	.003	130.24	1.47	1.53	3.84	22.1	59.9	1.24
1205	50	.005	120.40	1.50	1.55	3.94	22.0	70.2	.94
1208	50	.006	132.24	1.56	1.65	4.21	22.2	67.7	.97
1211	50	.015	119.57	1.57	1.63	3.94	22.1	60.5	.71
1214	49	.031	106.37	1.55	1.71	3.46	22.0	54.4	.84
1217	53	.061	88.02	1.66	1.81	3.05	22.0	69.8	.93
1220	62	.107	74.95	1.71	1.88	2.70	22.0	67.5	1.03
1224	38	.140	71.81	1.73	1.91	2.61	22.3	65.6	1.02
1227	34	.170	73.66	1.68	1.84	2.58	22.0	70.9	.95
1230	40	.234	70.01	1.55	1.82	2.45	22.1	74.9	.88
1233	34	.339	75.27	1.57	1.72	2.50	22.1	75.2	.82
1235	37	.488	58.13	1.63	1.90	2.37	22.1	82.1	.75
1240	38	.562	52.27	1.58	1.79	2.18	22.2	68.0	.81
1244	43	.970	47.81	2.43	2.61	2.37	23.2	60.8	.59
1247	34	1.287	44.02	2.71	2.65	2.44	24.5	51.8	.42
1250	29	1.604	39.83	2.92	3.05	2.35	25.7	53.7	.41

line HHH	N	Altitude km	EPS m2/s3	CT2 C2/m2/3	Q g/kg	Qc2 (g/kg)2m-2/3	Press mb	rose C	T_IR C	T_dew C
1202	52	.003	1.93E-03	1.91E-02	10.1	5.08E-02	1017.6	20.1	24.4	14.5
1205	50	.005	1.43E-03	1.37E-02	10.0	3.54E-02	1017.0	20.0	24.2	14.4
1208	50	.006	9.85E-04	8.95E-03	9.8	2.67E-02	1016.5	20.2	24.1	14.0
1211	50	.015	5.66E-04	3.54E-03	8.8	2.00E-02	1015.4	20.2	24.1	12.2
1214	49	.031	3.75E-04	1.63E-03	9.2	1.14E-02	1013.8	19.9	24.1	12.9
1217	53	.061	4.59E-04	1.24E-03	9.7	9.70E-03	1010.4	19.4	24.4	13.8
1220	62	.107	4.26E-04	1.03E-03	9.4	9.15E-03	1007.2	19.3	24.4	13.1
1224	38	.140	4.75E-04	5.46E-04	9.3	8.80E-03	1003.4	19.3	24.6	13.0
1227	34	.170	4.66E-04	6.87E-04	9.5	8.54E-03	999.9	18.6	24.5	13.2
1230	40	.234	4.00E-04	2.74E-04	9.7	8.21E-03	992.5	18.1	24.5	13.5
1233	34	.339	3.37E-04	3.41E-04	9.4	7.89E-03	980.6	17.2	24.3	12.7
1236	37	.488	2.31E-04	4.08E-04	9.5	8.44E-03	963.7	15.7	24.3	12.6
1240	38	.562	1.95E-04	1.53E-03	9.3	1.39E-02	944.3	14.1	24.3	12.1
1244	48	.970	9.01E-05	2.24E-03	6.1	5.44E-03	910.7	12.7	24.2	5.2
1247	34	1.287	1.24E-05	1.93E-05	4.9	2.67E-03	877.2	11.1	24.1	1.6
1250	29	1.604	3.58E-05	3.83E-04	4.6	5.72E-03	844.7	9.2	24.0	.3

Table 19b. RSD Flight 6 (standard deviations)/averages for  
constant altitude runs performed E of RSD over deep  
water.

STANDARD DEVIATIONS/MEAN VALUES

Time	E_Field	+Lam	-Lam	Con Curr	CCN	EPS	CT2	Q	Q2
1202	.183	.094	.086	.187	.304	.401	.271	.026	.443
1205	.211	.034	.077	.184	.075	.333	.325	.026	.453
1208	.195	.035	.074	.177	.079	.460	.457	.039	.588
1211	.141	.114	.062	.165	.188	.260	.315	.042	.489
1214	.103	.075	.067	.125	.071	.389	.686	.045	.461
1217	.116	.028	.035	.111	.061	.364	.482	.015	.210
1220	.078	.050	.034	.078	.075	.307	.487	.016	.240
1224	.065	.039	.023	.074	.057	3.304	.504	.015	.152
1227	.081	.026	.020	.076	.057	.418	.562	.019	.162
1230	.053	.037	.047	.065	.062	.488	.905	.012	.123
1233	.066	.082	.027	.083	.075	.430	.641	.027	.170
1236	.068	.051	.018	.086	.113	.306	.605	.016	.107
1240	.121	.154	.058	.195	.145	.458	.635	.044	.400
1244	.154	.097	.128	.101	.126	2.558	2.861	.130	1.601
1247	.038	.033	.030	.048	.169	1.013	4.488	.019	.173
1250	.091	.081	.092	.078	.158	.792	.836	.046	.945

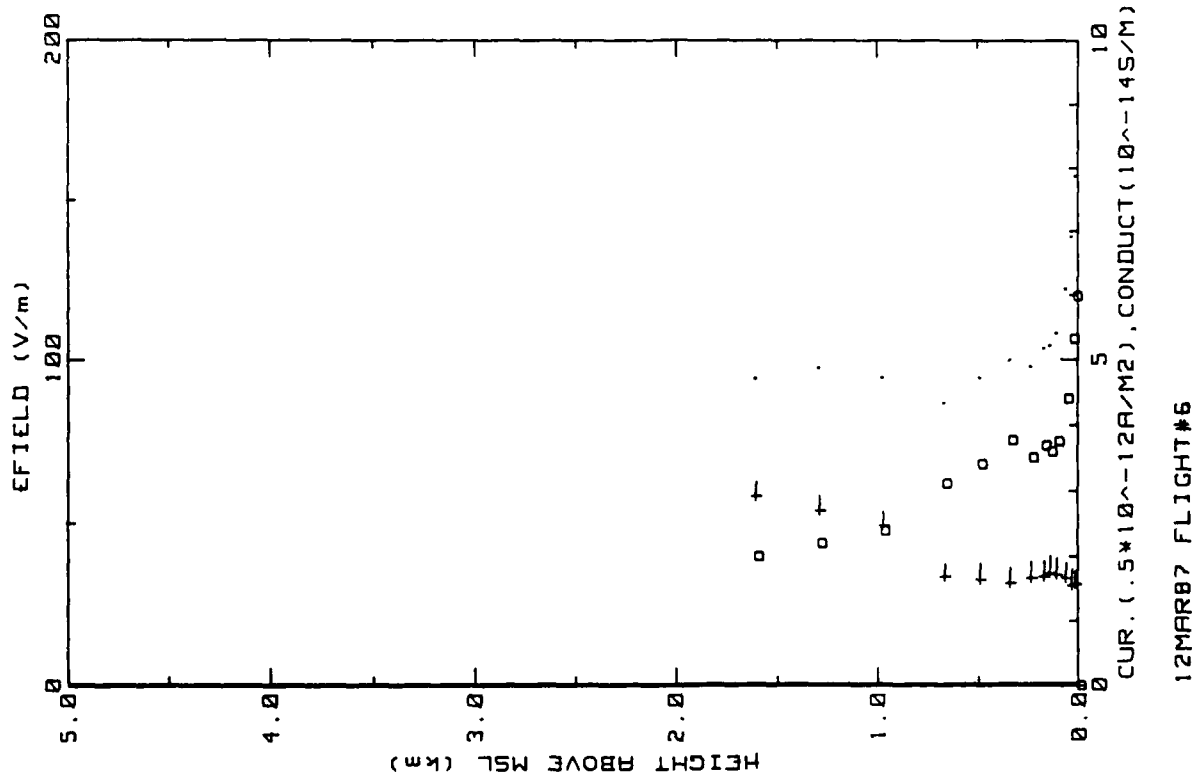


Figure 26a. RSD Flight 6 ladder profile over deep water  
E of RSD. (ref. Fig. 5a). The time interval  
should be 1211 to 1250 LT.

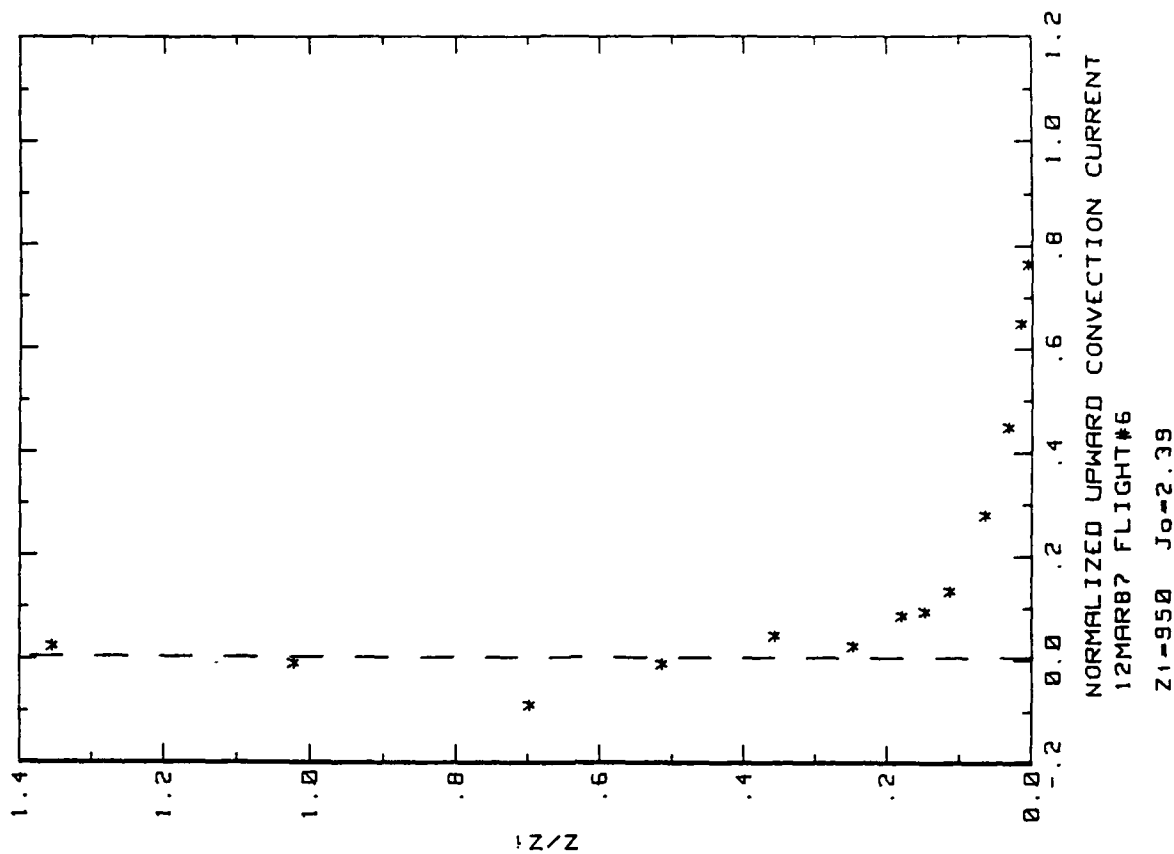


Figure 26b. RSD Flight 6 convection current profile over  
deep water E of RSD (ref. Fig. 5d). The  
appropriate time interval is 1211 to 1250 LT.



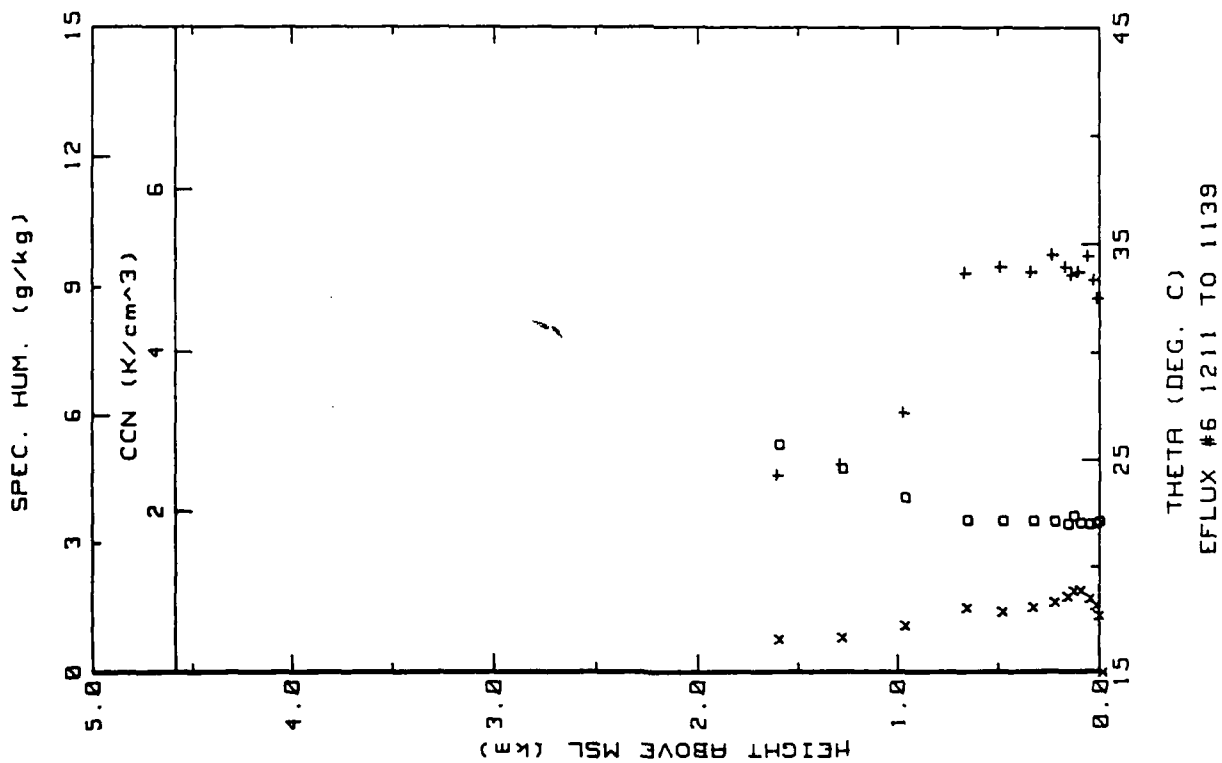


Figure 26c. RSD Flight 6 ladder profile over deep water  
E of RSD. (ref. Fig. 5c). The time interval  
should be 1211 to 1250 LT.

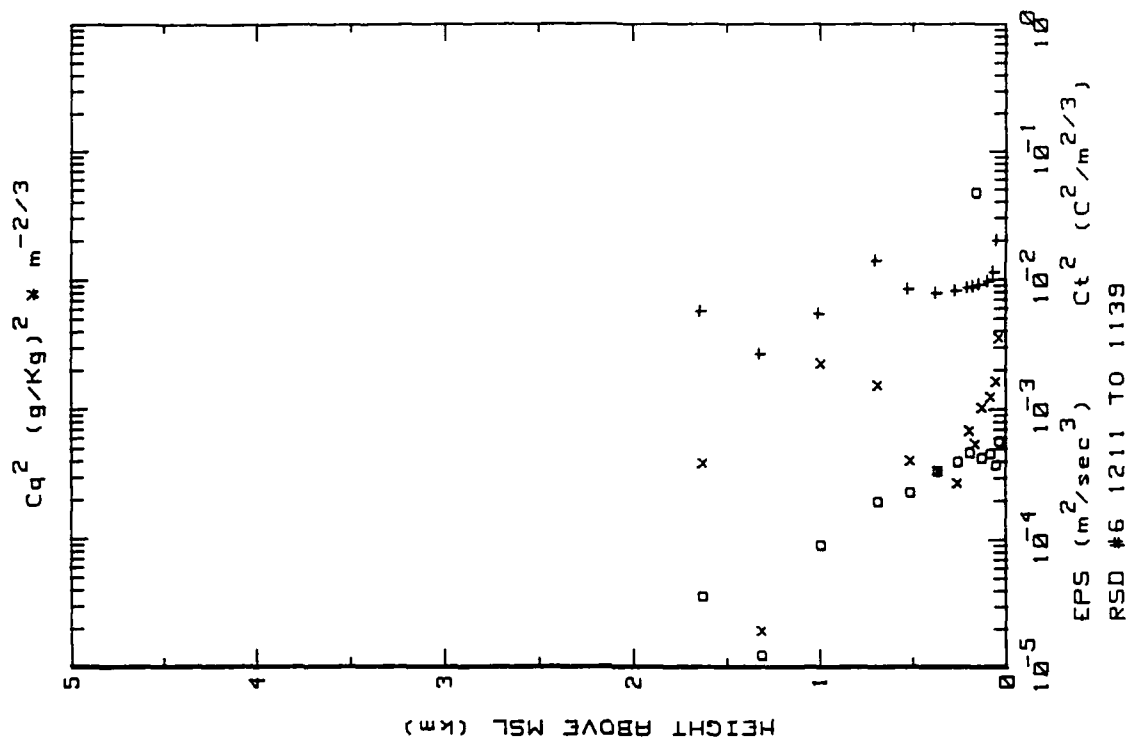


Figure 26d. RSD Flight 6 ladder profile over deep water  
E of RSD. (ref. Fig. 5b). The time interval  
should be 1211 to 1250 LT.

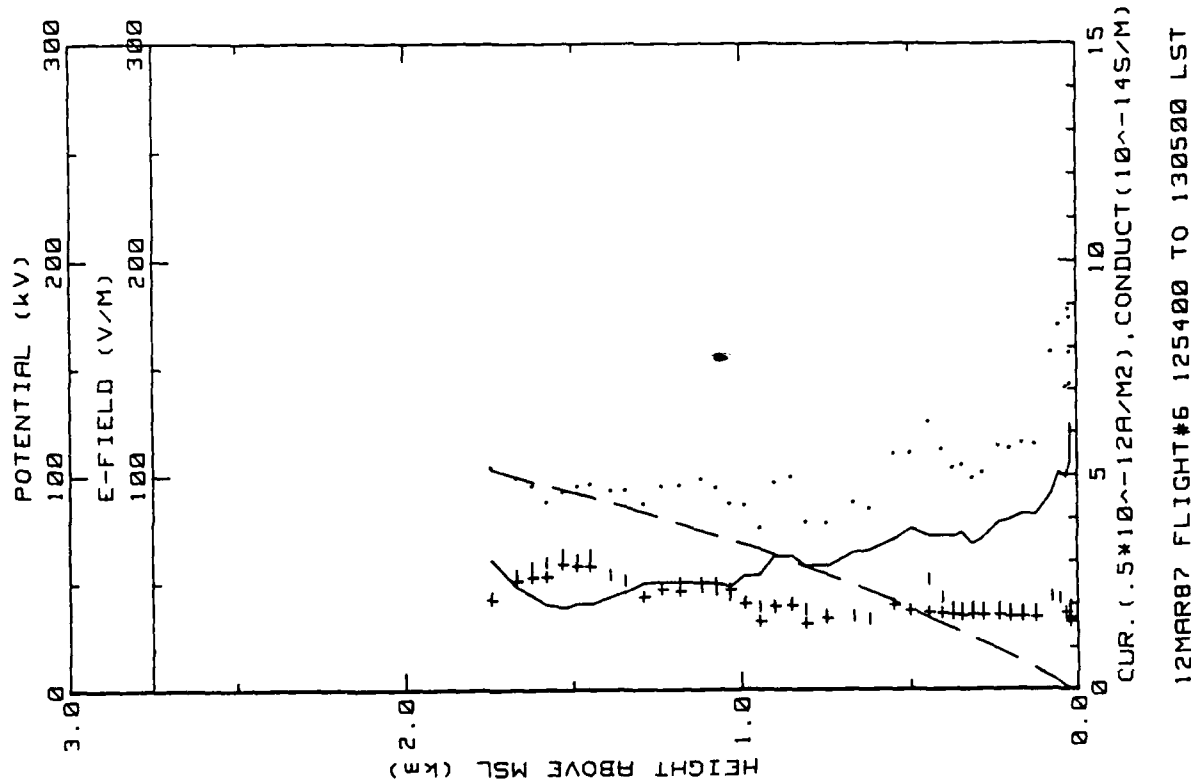


Figure 26e. RSD Flight 6 spiral down-sounding over deep water E of RSD (ref. Fig. 5e).

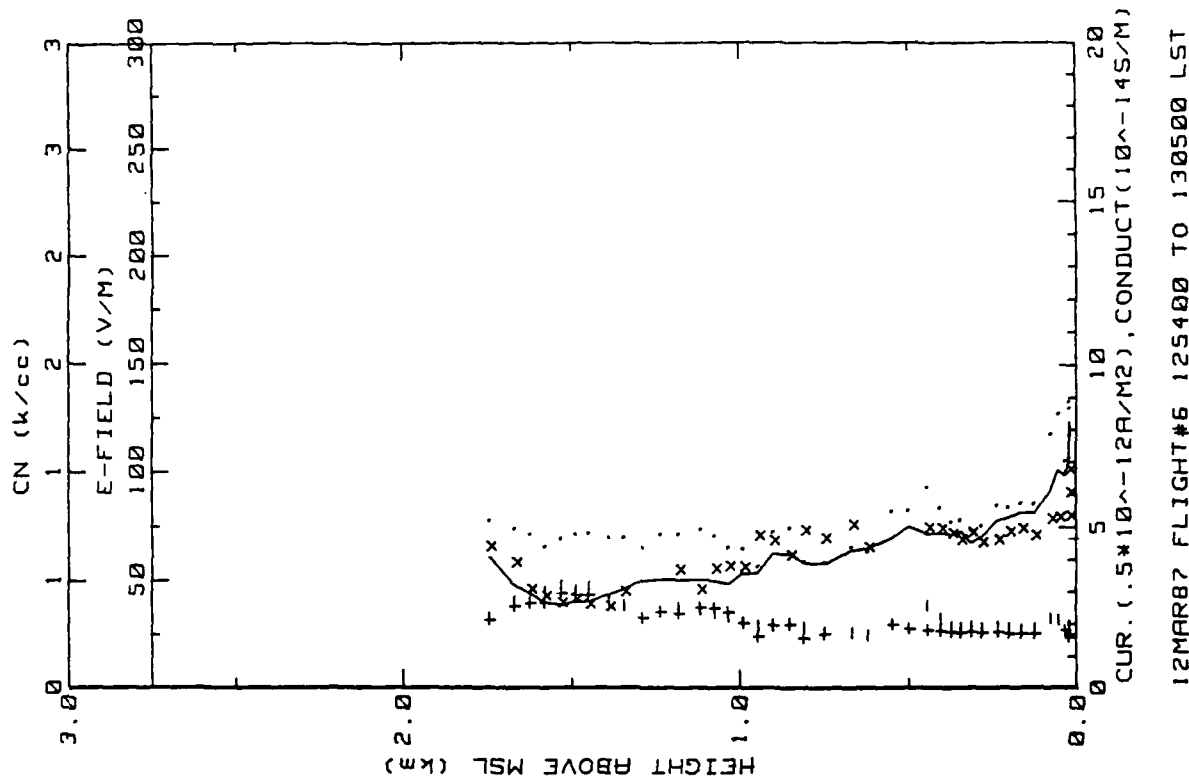


Figure 26f. RSD Flight 6 spiral down-sounding over deep water E of RSD (ref. Fig. 5f).

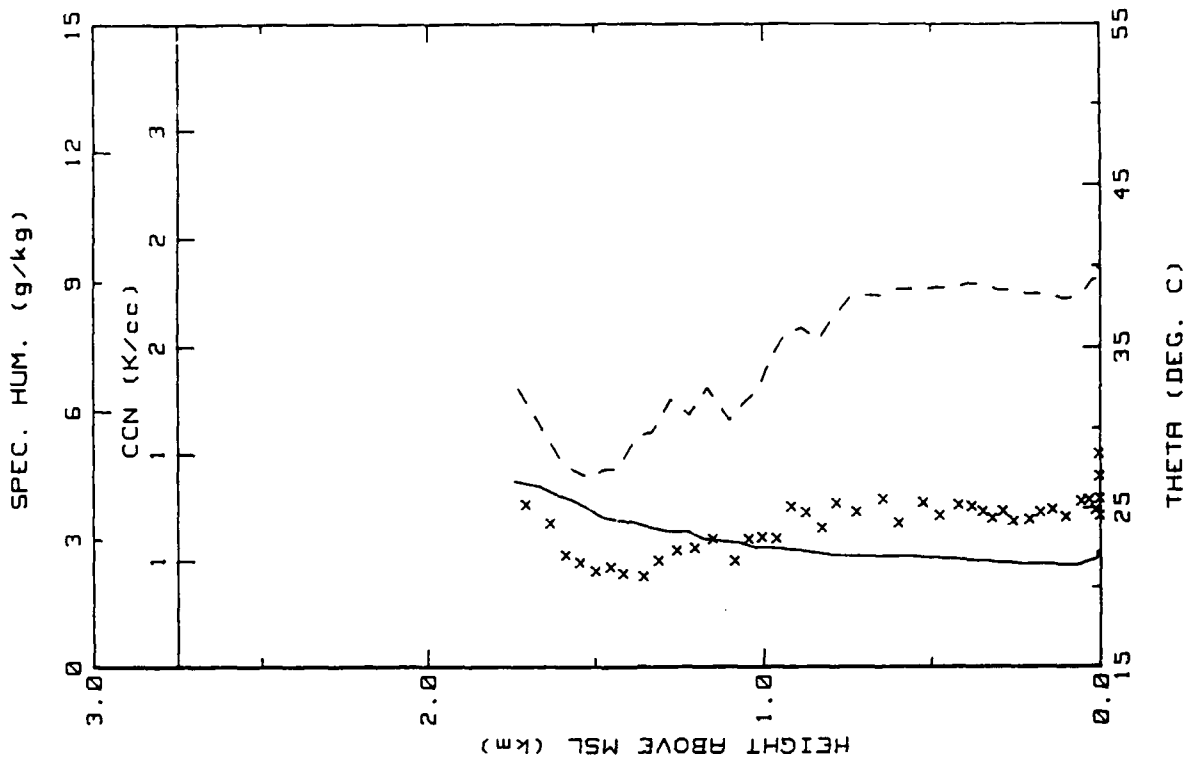


Figure 26h. RSD Flight 6 spiral down sounding over deep water E of RSD (ref. Fig. 5h).

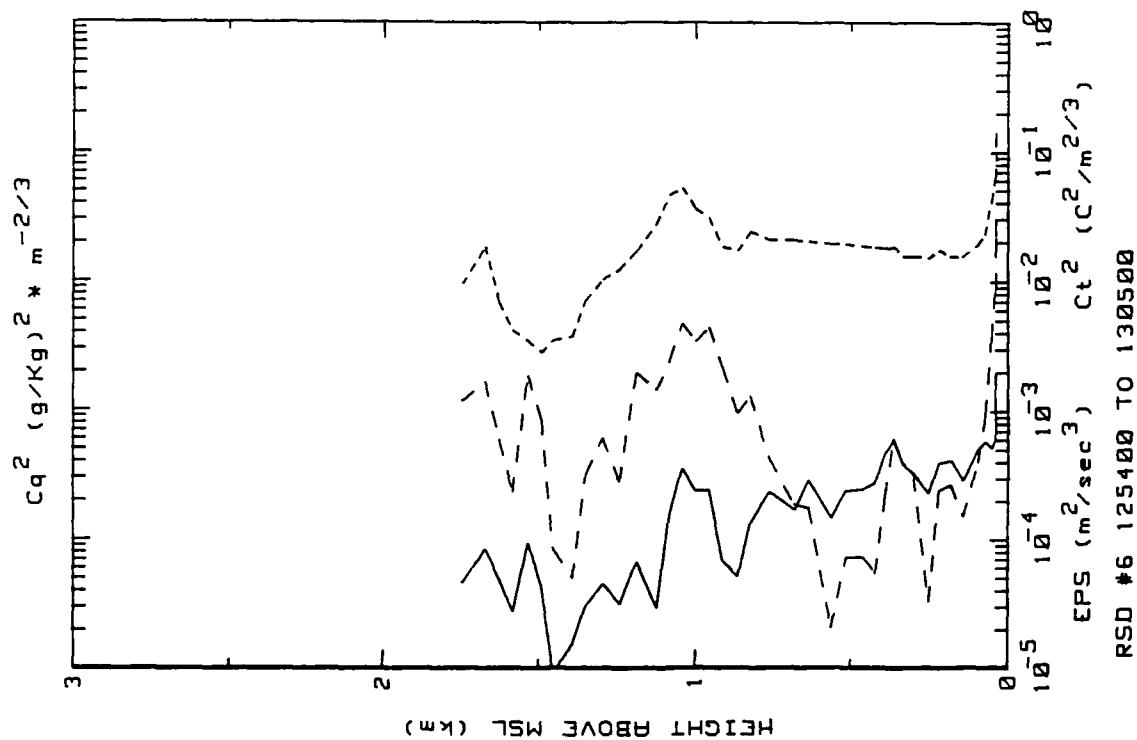


Figure 26g. RSD Flight 6 spiral down sounding over deep water E of RSD (ref. Fig. 5g).

Flight: 7

Date: 13 March 1987

Takeoff: 1320 (LT) from RSD

Landed: 1600 at RSD

Conditions: Clear skies initially; encountered scattered cumulus with bases at 1.4 km and 1.8 km tops during spiral down sounding. Winds were from the NNE at 4 m/s at takeoff and appeared to increase during the flight. Few whitecaps and swells were <1 m.

Instruments: Positive conductivity tube was noisy.

Summary: Made soundings 50-80 km NE of RSD over deep ocean. The ladder and spiral profiles were obtained in slightly different regimes as the latter was performed in a region of scattered cumulus clouds. The aircraft was in a 7° left bank during the spiral descent.

Table 20a. RSD Flight 7 averages for constant altitude runs performed NE of RSD.

13 MAR 1987

AVERAGES FROM LEVEL RUNS

Time HHMM	N	Altitude km	E. field V/m	+Lam 10 <sup>-14</sup>	-Lam 10 <sup>-14</sup>	Corr Curr 10 <sup>-12</sup>	Theta v C	Rel Hum %	CNN k/cc
1326	55	.015	144.52	1.21	1.21	3.51	21.3	62.5	2.21
1330	111	.015	130.27	1.23	1.29	3.26	21.1	59.5	1.85
1336	40	.006	125.69	1.35	1.37	3.35	21.0	56.3	2.08
1340	63	.005	134.18	1.22	1.28	3.23	21.1	56.5	1.69
1342	48	.015	120.50	1.25	1.38	3.15	20.9	56.6	1.54
1344	36	.031	116.30	1.34	1.35	3.11	20.9	58.8	1.50
1346	49	.061	109.21	1.28	1.42	2.93	20.8	57.1	1.13
1351	40	.133	95.37	1.36	1.47	2.83	20.7	55.9	1.01
1353	37	.224	82.54	1.42	1.50	2.41	20.7	57.1	.96
1356	37	.344	75.07	1.42	1.50	2.20	20.8	50.6	.95
1358	34	.543	70.03	1.42	1.49	2.04	20.8	58.8	1.11
1400	33	.959	52.41	1.55	1.55	1.92	20.9	75.2	1.15
1406	135	1.277	59.75	1.51	1.54	1.86	20.8	68.1	.80
1415	65	1.890	41.05	2.47	2.47	2.01	22.5	58.0	.81
1420	42	2.361	21.47	4.27	4.56	1.90	25.1	15.5	.44
1425	54	3.144	18.23	4.93	5.31	1.87	29.5	23.3	.59
1430	113	3.775	15.76	5.90	5.57	1.96	33.6	11.5	.85
1440	41	4.215	12.36	7.61	8.38	1.97	34.7	13.0	.52
1508	50	.006	129.38	1.33	1.36	3.42	20.6	54.6	1.17
1512	70	.031	112.38	1.31	1.37	3.01	20.5	54.3	1.25

Time HHMM	N	Altitude km	EPS m2/s3	C12 C2/m2/3	O g/kg	Co2 (g/kg)2m-2/3	Press mb	Trose C	T_IR C	T_dew C
1326	55	.015	2.52E-03	1.30E-02	8.7	3.42E-02	1011.5	19.5	24.3	12.2
1330	111	.015	1.77E-03	8.67E-03	8.2	3.14E-02	1011.1	19.3	23.9	11.3
1336	40	.006	3.51E-03	1.95E-02	7.8	5.13E-02	1012.3	19.4	24.0	10.5
1340	63	.005	3.32E-03	3.86E-02	7.9	1.21E-01	1012.6	19.5	24.2	10.6
1342	48	.015	2.56E-03	1.45E-02	7.8	4.58E-02	1011.2	19.2	23.9	10.4
1344	36	.031	2.51E-03	9.04E-03	8.0	2.77E-02	1009.1	19.0	24.0	10.8
1346	49	.061	1.94E-03	4.00E-03	7.6	1.07E-02	1005.9	18.7	23.9	10.1
1351	40	.133	1.25E-03	1.93E-03	7.3	1.08E-02	999.1	18.1	23.8	9.2
1353	37	.224	9.29E-04	9.09E-04	7.1	7.92E-03	988.5	17.2	24.1	8.7
1356	37	.344	1.04E-03	1.05E-03	7.1	7.68E-03	974.9	16.2	24.2	8.6
1358	34	.543	5.00E-04	3.19E-04	7.0	5.42E-03	941.6	13.4	24.1	7.7
1400	33	.959	7.13E-04	1.11E-03	6.9	7.21E-03	907.3	10.5	24.0	7.0
1406	135	1.277	6.14E-04	5.62E-03	6.4	1.68E-02	873.9	7.4	24.2	5.5
1415	65	1.890	3.07E-04	1.25E-03	3.5	1.29E-02	812.2	3.7	23.3	-3.9
1420	42	2.361	7.77E-06	1.22E-04	1.0	1.03E-03	767.2	2.9	24.2	-20.1
1425	54	3.144	4.11E-05	5.21E-04	1.1	7.38E-04	693.3	-1.5	23.9	-20.2
1430	113	3.775	1.00E-05	9.32E-04	.5	3.79E-04	544.2	-3.8	24.4	-29.6
1440	41	4.215	2.27E-05	3.30E-04	.5	4.99E-04	609.3	-7.1	22.2	-30.9
1508	50	.006	7.02E-03	2.70E-02	7.5	1.20E-01	1013.5	19.2	25.5	9.9
1512	70	.031	1.51E-03	4.95E-03	7.4	2.37E-02	1011.7	18.1	25.0	5.8

Table 20b. RSD Flight 7 (standard deviations)/averages for  
constant altitude runs performed NE of RSD.

STANDARD DEVIATIONS/MEAN VALUES

Time	E_Field	+Lam	-Lam	Con Curr	CCN	EPS	CT2	Q	Co2
1326	.169	.330	.074	.201	.089	.317	.365	.042	.643
1330	.166	.252	.066	.197	.147	.505	.466	.041	.573
1336	.122	.299	.075	.214	.168	.391	.413	.045	.543
1340	.192	.374	.056	.237	.120	.289	.459	.054	.539
1342	.146	.297	.081	.218	.121	.198	.274	.046	.452
1344	.171	.205	.101	.180	.142	.320	.322	.040	.477
1346	.131	.183	.051	.174	.162	.408	.642	.038	.773
1351	.093	.141	.038	.120	.076	.368	.547	.025	.407
1353	.044	.078	.027	.074	.047	.519	1.091	.028	.667
1356	.048	.107	.036	.087	.073	.242	.622	.023	.375
1358	.037	.071	.058	.082	.089	.697	1.073	.022	.190
1400	.044	.104	.121	.074	.501	.294	.341	.032	.579
1406	.231	.287	.068	.278	.092	.531	1.112	.054	1.595
1415	.200	.168	.125	.182	.105	.696	.561	.124	.913
1420	.054	.029	.023	.047	.155	.597	.252	.107	.861
1425	.047	.073	.049	.042	.146	1.222	.922	.225	.343
1430	.030	.019	.017	.035	.265	1.686	1.197	.007	.285
1440	.034	.015	.008	.033	.077	.605	.383	.008	.700
1508	.143	.333	.077	.271	.103	.535	.457	.047	.702
1512	.136	.271	.066	.177	.099	.396	.317	.039	.581

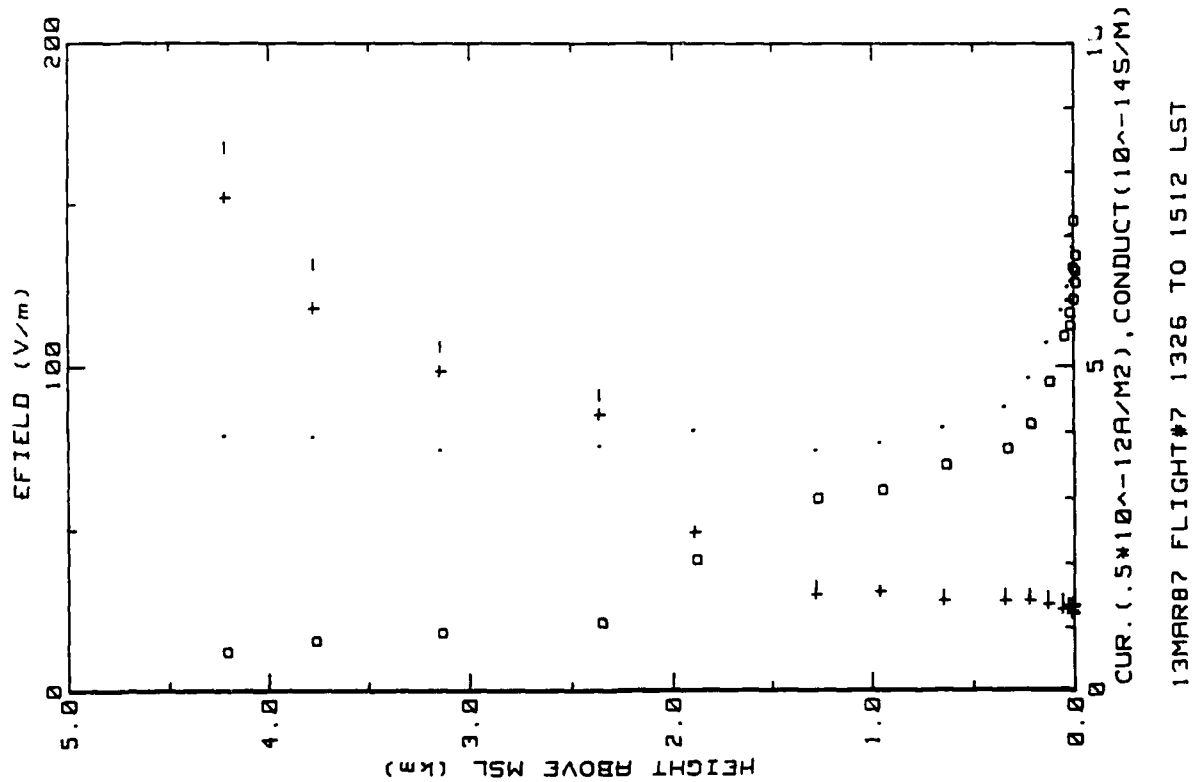


Figure 27a. RSD Flight 7 ladder profile over deep water  
NE of RSD. (ref. Fig. 5a).

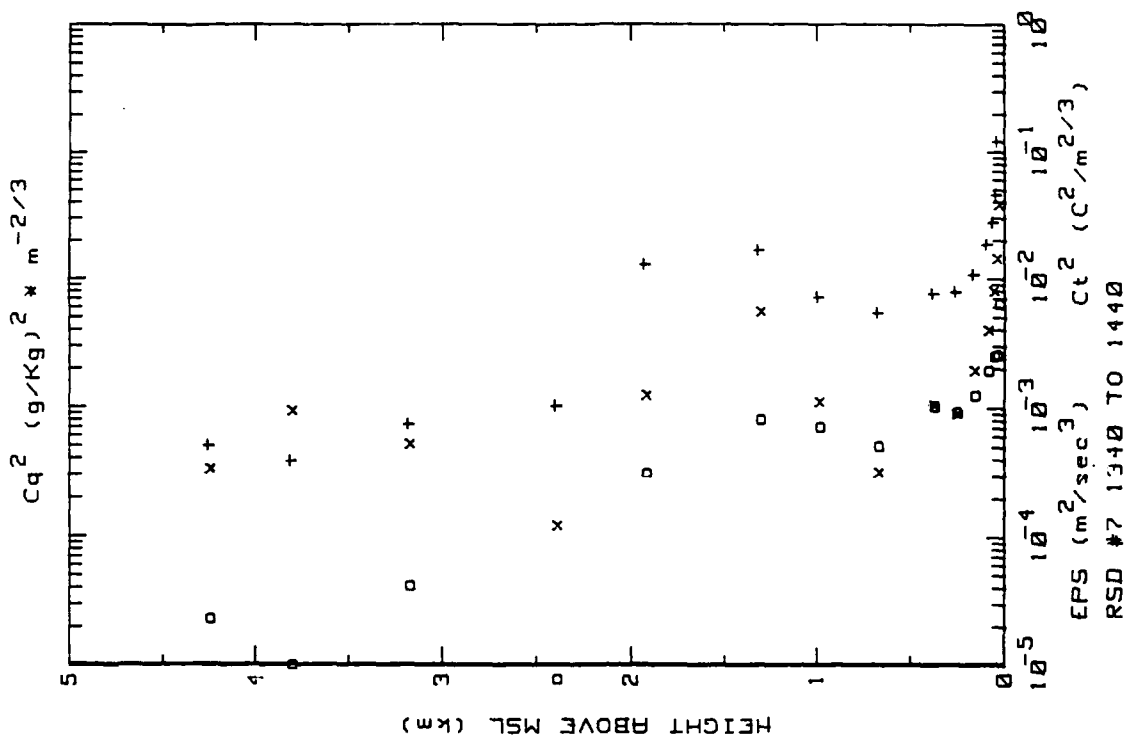


Figure 27b. RSD Flight 7 ladder profile over deep water  
NE of RSD. (ref. Fig. 5b).

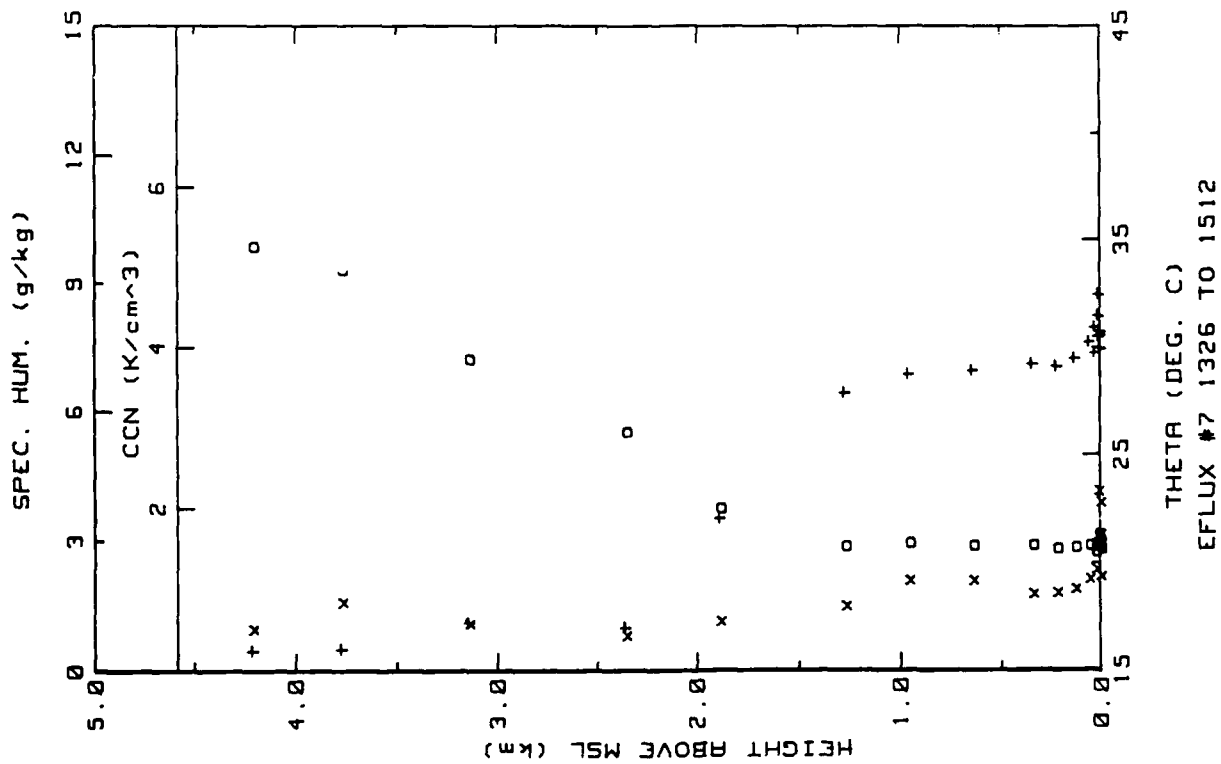


Figure 27c. RSD Flight 7 ladder profile over deep water NE of RSD. (ref. Fig. 5c).

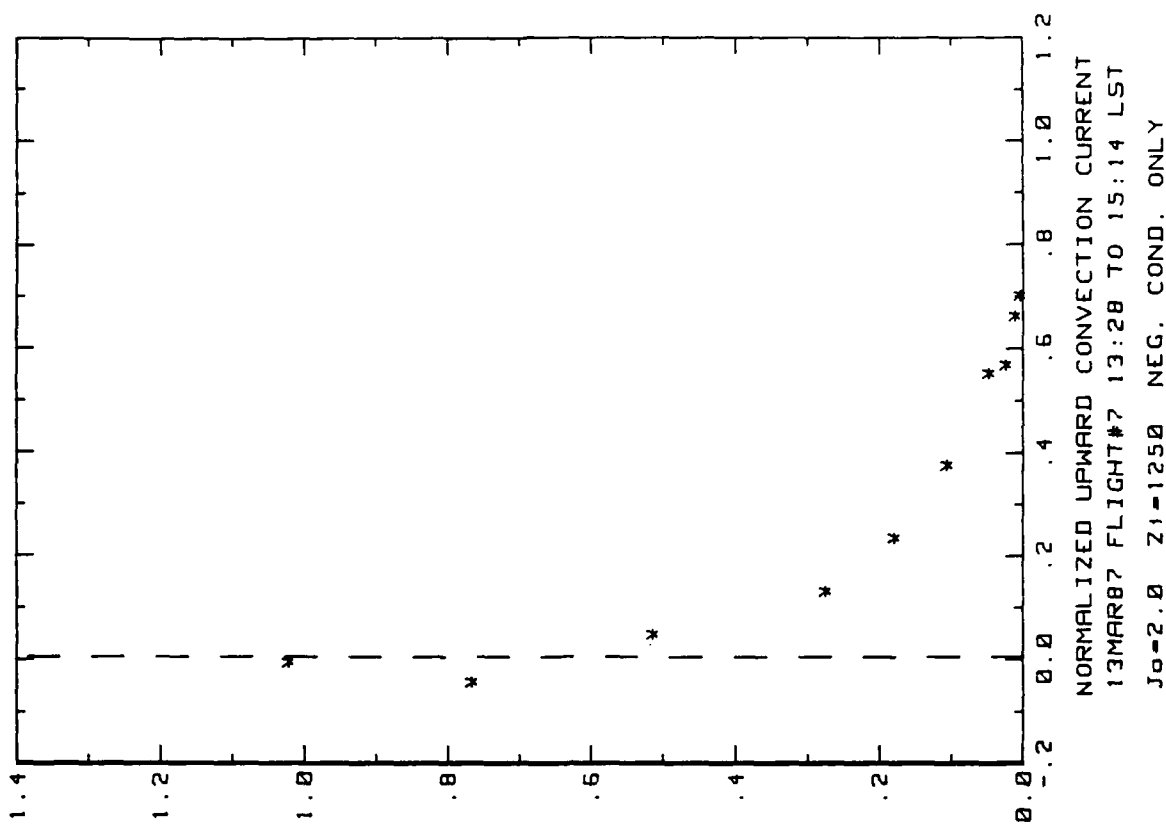


Figure 27d. RSD Flight 7 convection current profile over deep water NE of RSD (ref. Fig. 5d). The conduction and convection currents were calculated using only negative conductivity data and the time interval should be 1340 to 1440.



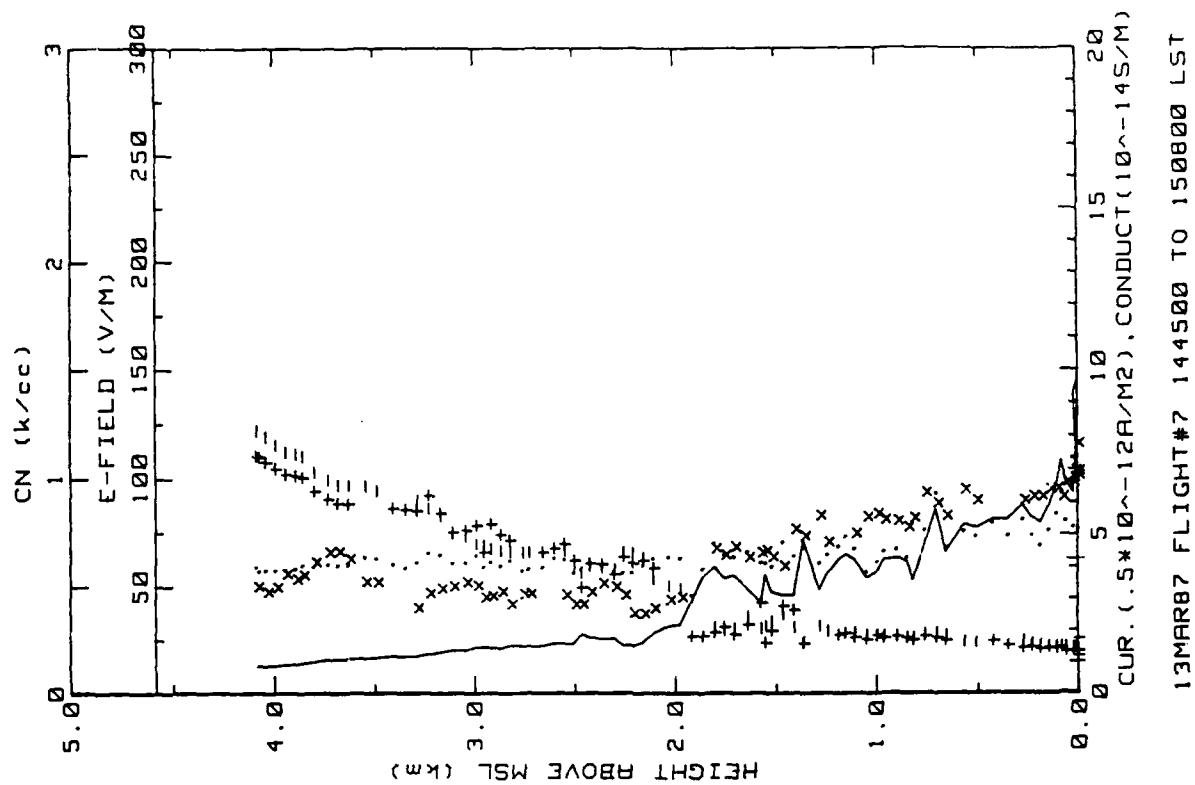


Figure 27f. RSD Flight 7 spiral down sounding over deep water NE of RSD (ref. Fig. 5f).

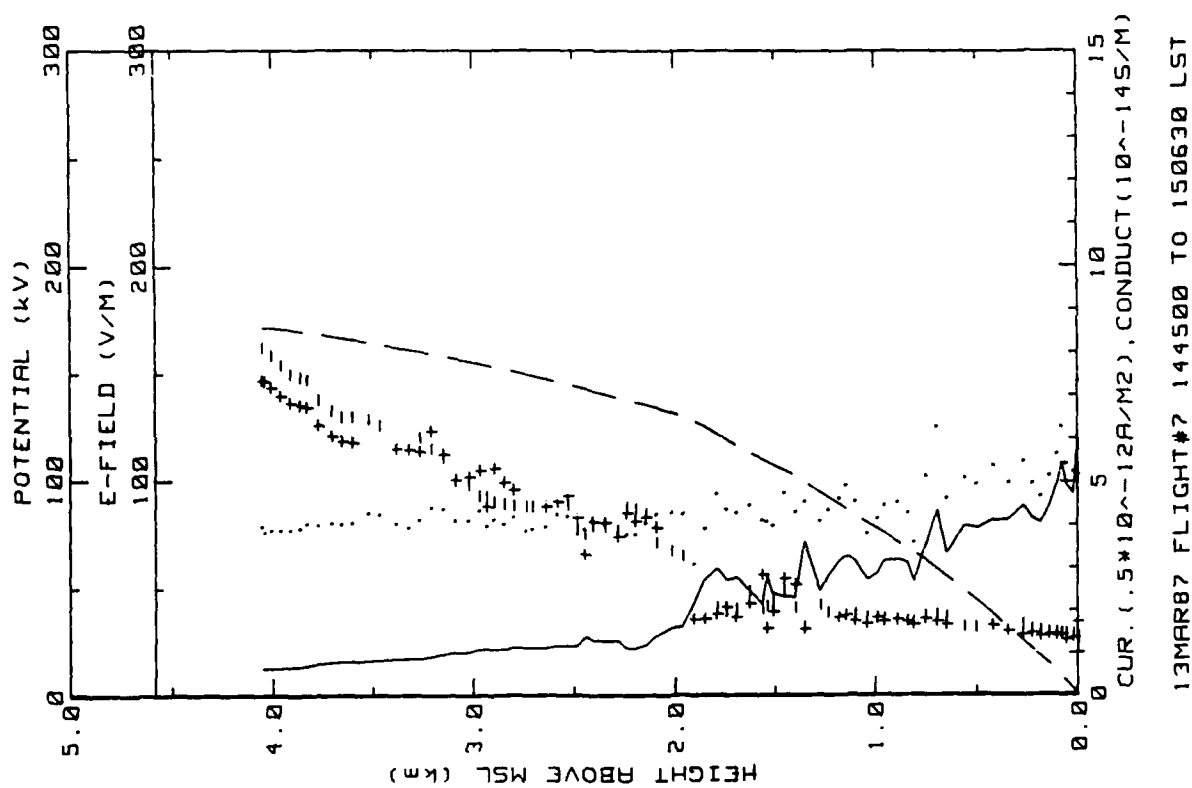


Figure 27e. RSD Flight 7 spiral down sounding over deep water NE of RSD (ref. Fig. 5e).

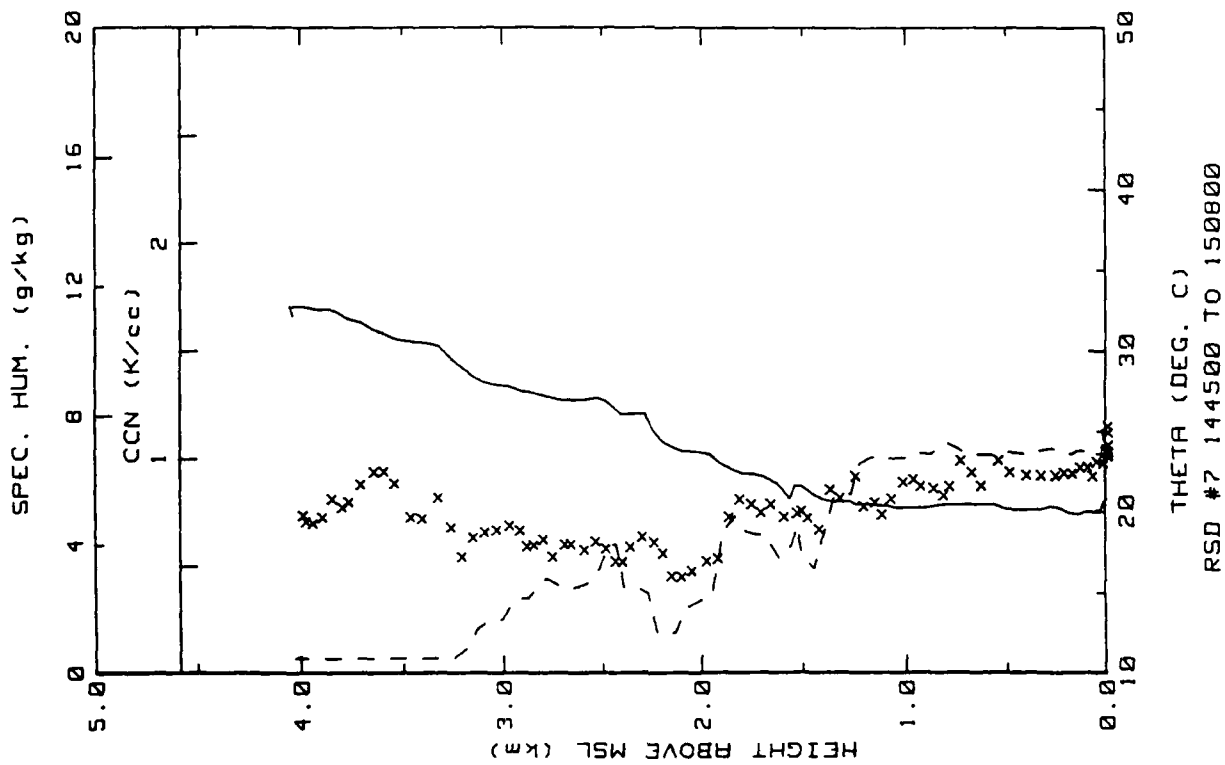


Figure 27g. RSD Flight 7 spiral down sounding over deep water NE of RSD (ref. Fig. 5h).

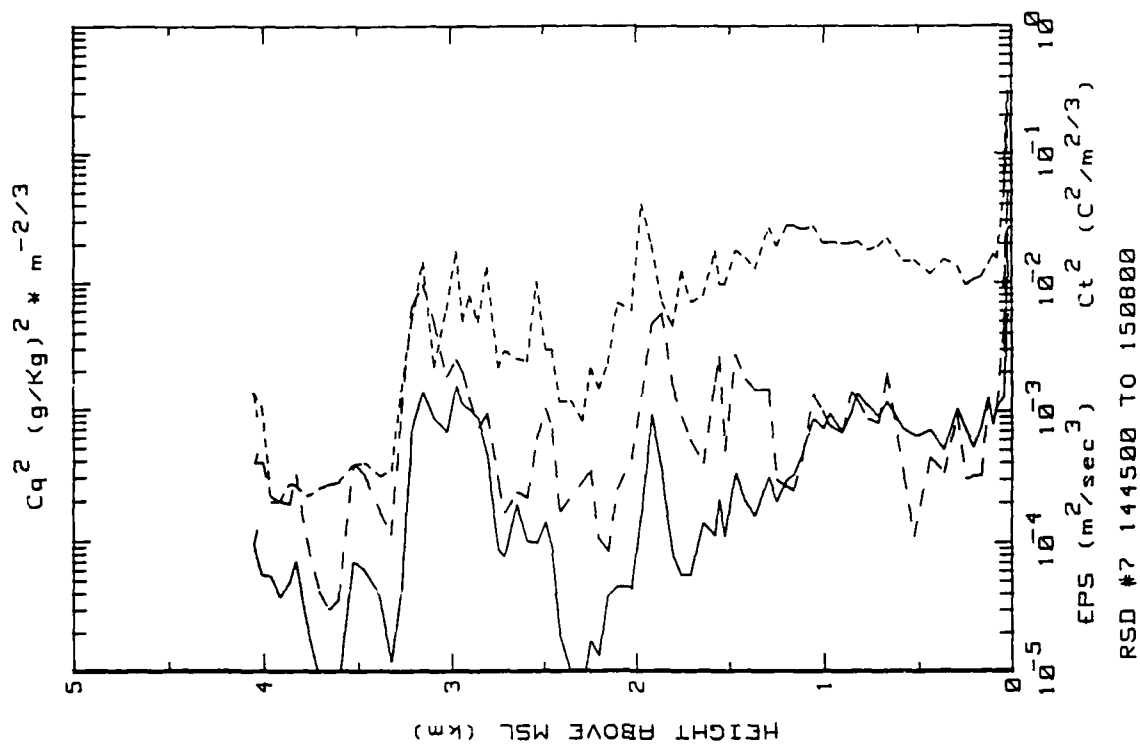


Figure 27h. RSD Flight 7 spiral down sounding over deep water NE of RSD (ref. Fig. 5g).

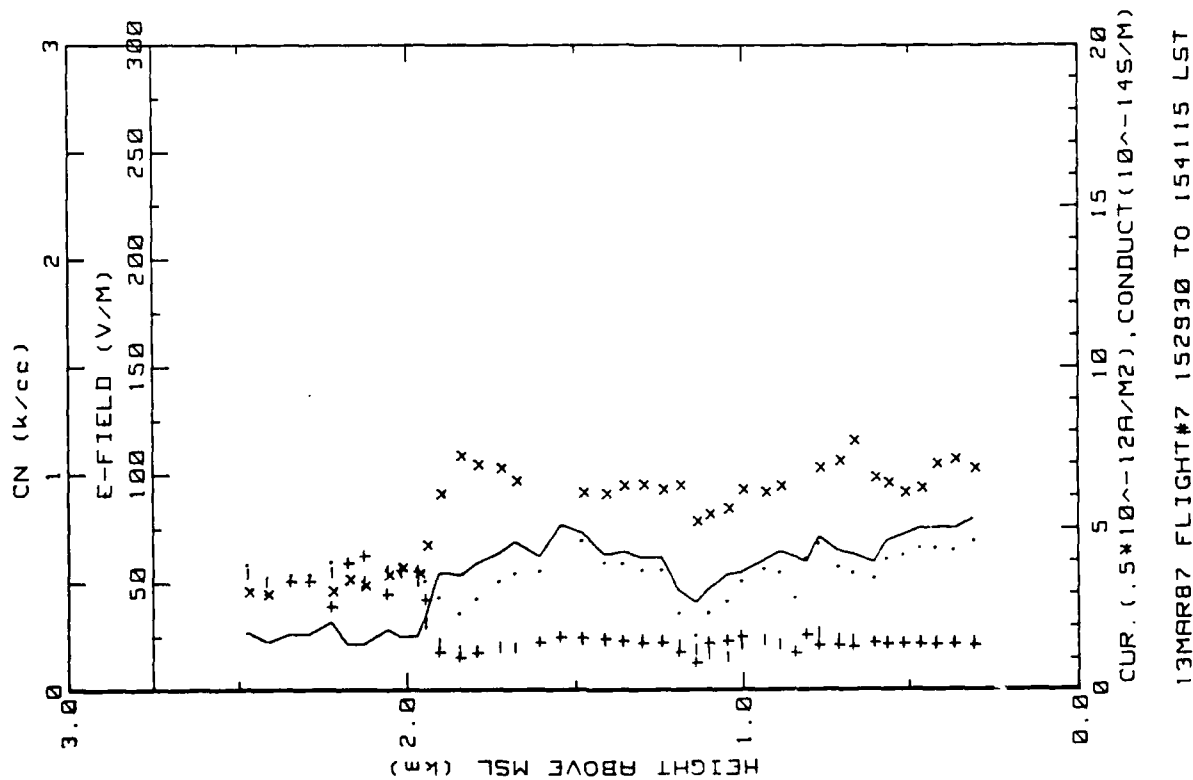


Figure 27i. RSD Flight 7 spiral down sounding over ocean near RSD (ref. Fig. 5f).

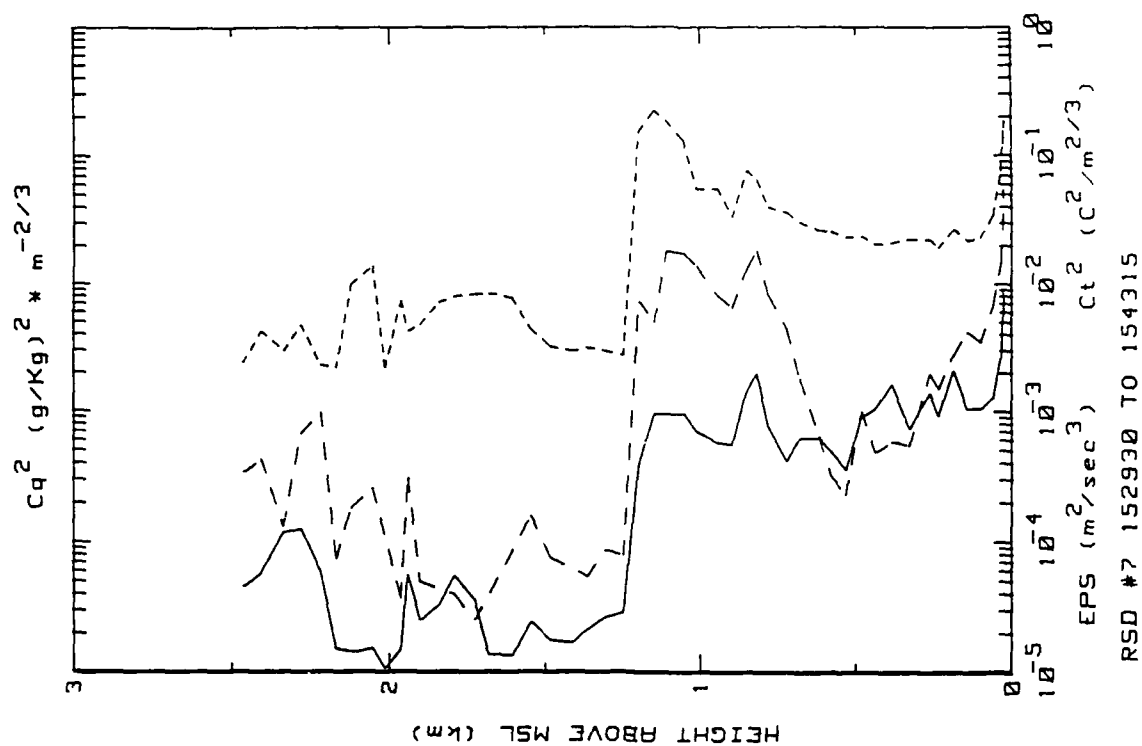


Figure 27j. RSD Flight 7 spiral down sounding over ocean near RSD (ref. Fig. 5g).

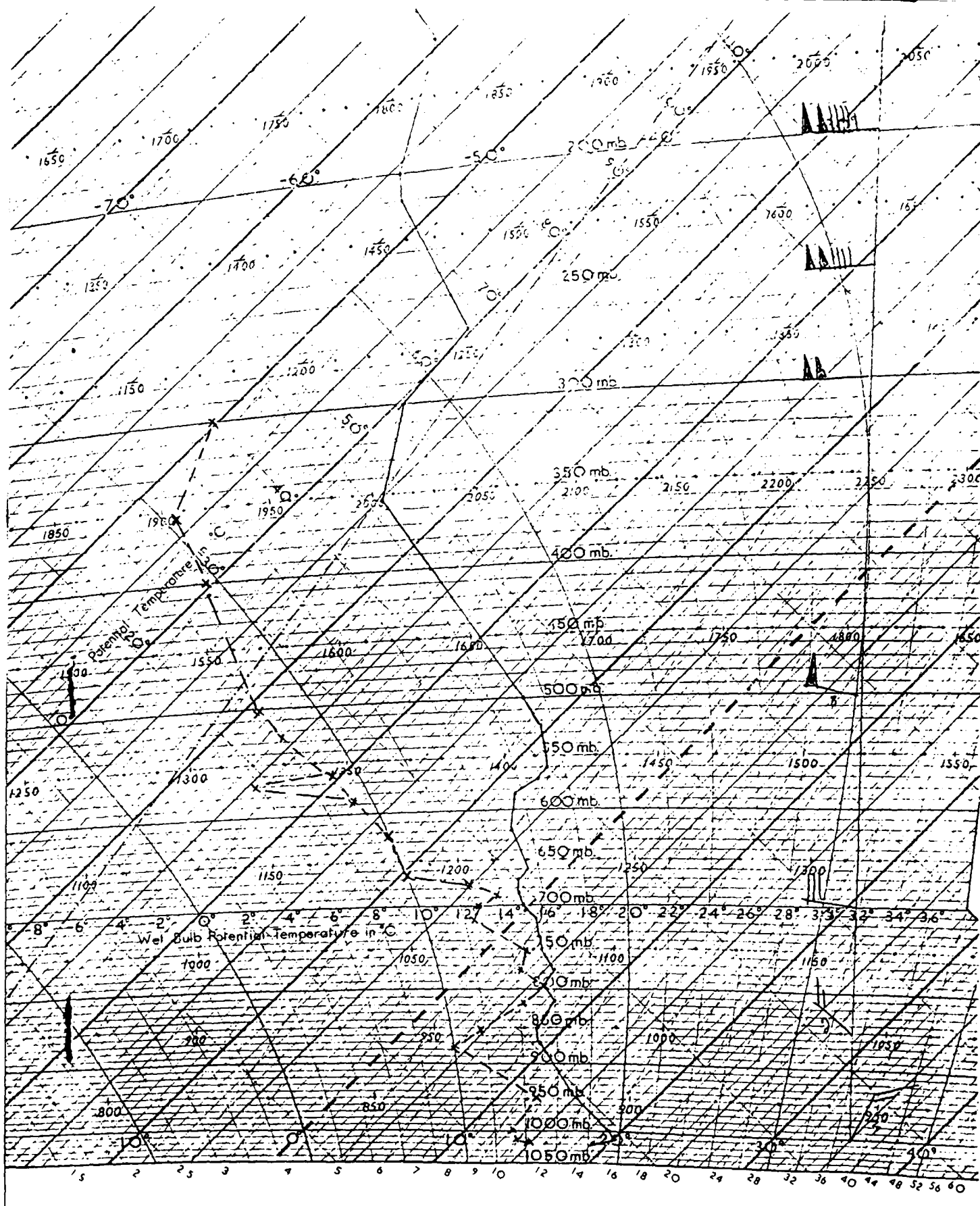


Figure 27k. Meteorological sounding from Nassau, Bahamas, taken on the day of Flight 7 (13 March 1987).

Flight: 8

Date: 14 March 1987

Takeoff: 1421 (LT) from RSD

Landed: 1554 at North Eleuthera

Takeoff: 1632 from North Eleuthera

Landed: 1728 at RSD

Conditions: Low scattered cumulus (<1/10 cover) with bases at 1.4 km; lowered visibility because of haze in mixed layer. Winds at RSD were from the NE gusting to 12 m/s. Lots of whitecaps.

Instruments: Both conductivity tubes were noisy; had added a high and low pass filter to the Lyman-alpha output to record fast fluctuations of humidity on the strip chart.

Summary: A ladder profile and a spiral descent were made over deep water E of Eleuthera enroute to the North Eleuthera airport. Up- and downsoundings were obtained upwind of the island on the return flight to RSD. Electric field records showed plume structure below 50 m altitude.

Table 21a. RSD Flight 8 averages for constant altitude runs performed NE of RSD over deep water.

AVERAGES FROM LEVEL RUNS

Time HHMM	N	Altitude km	E_field V/m	+Lam 10 <sup>-14</sup>	-Lam 10 <sup>-14</sup>	Con Curr 10 <sup>-12</sup>	Theta_v C	Rel Hum %	CHN k/cc
1428	40	.006	214.26	.71	.44	2.06	19.5	55.9	2.40
1431	113	.015	177.76	.13	.14	.49	19.1	54.4	5.66
1439	56	.031	184.31	.27	.05	.80	18.9	52.5	2.62
1443	44	.061	176.51	.55	.63	2.11	18.9	51.1	2.53
1446	47	.127	170.34	.57	.65	2.06	19.5	48.0	2.55
1448	22	.213	156.60	.59	.88	2.00	19.0	50.1	2.49
1450	30	.305	150.51	.61	.71	1.99	18.9	53.0	2.38
1451	33	.601	124.52	.60	.70	1.65	18.8	62.7	2.25
1454	31	.976	103.79	.57	.67	1.29	18.6	62.5	2.22
1455	20	1.281	87.46	.95	.79	1.60	18.7	83.9	2.09
1458	28	1.890	50.77	1.29	1.22	1.18	20.0	74.4	.42
1504	35	2.437	12.42	4.77	4.97	1.21	27.5	9.4	.53
1507	26	3.030	9.78	5.95	6.09	1.18	31.1	13.2	.85
1511	27	3.634	7.70	7.24	7.15	1.11	33.5	14.7	.56
1514	20	4.068	6.01	8.84	8.37	1.03	34.7	15.4	.33

Time HHMM	N	Altitude km	EP3 m2/s3	CT2 C2/m2/3	G g/kg	Cq2 (g/kg)2m-2/3	Press mB	Trose C	T_IR C	T_dew C
1428	40	.006	7.85E-03	3.16E-02	7.2	1.37E-01	1008.4	18.2	24.6	9.2
1431	113	.015	4.06E-03	1.40E-02	6.8	5.41E-02	1007.2	17.7	24.1	8.4
1439	56	.031	3.29E-03	6.74E-03	6.5	2.92E-02	1005.1	17.4	24.0	7.6
1443	44	.061	2.17E-03	5.13E-03	6.2	2.08E-02	1001.6	17.1	24.3	6.9
1446	47	.127	1.61E-03	2.43E-03	5.9	1.76E-02	994.2	17.2	24.4	6.0
1448	22	.213	1.12E-03	7.65E-04	5.7	7.14E-03	984.2	15.9	24.3	5.5
1450	30	.305	1.48E-03	1.01E-03	5.8	1.13E-02	973.6	14.9	24.1	5.6
1451	33	.601	5.47E-04	1.64E-03	5.8	5.58E-03	940.2	12.0	23.8	5.1
1454	31	.976	7.92E-04	1.54E-03	6.2	8.38E-03	899.3	8.1	23.7	5.3
1456	20	1.281	5.77E-04	9.83E-03	5.4	2.30E-02	867.0	5.4	23.5	2.8
1458	28	1.890	3.75E-04	2.20E-03	3.8	5.80E-03	805.5	1.1	22.2	-3.1
1504	35	2.437	5.85E-06	1.27E-04	.6	5.35E-04	753.2	3.3	23.4	-26.2
1507	26	3.030	4.58E-06	1.28E-04	.8	4.17E-04	699.7	.7	23.4	-24.4
1511	27	3.634	4.22E-06	2.29E-04	.7	4.53E-04	648.4	-3.1	23.4	-26.3
1514	20	4.068	7.28E-06	9.32E-05	.6	1.37E-03	613.5	-6.2	23.5	-28.4

Table 21b. RSD Flight 8 (standard deviations)/averages for  
constant altitude runs performed NE of RSD over deep  
water.

STANDARD DEVIATIONS/MEAN VALUES

Time	E_Field	+Lam	-Lam	Con Curr	CON	EPS	CT2	Q	Co2
1428	.103	1.110	.548	.864	.038	.276	.185	.069	.343
1431	.093	.562	.506	.510	.496	.368	.422	.059	.464
1439	.103	2.258	.801	2.780	.048	.660	.438	.047	.436
1443	.142	.254	.095	.232	.035	.499	.771	.054	.571
1446	.066	.237	.135	.186	.068	.418	.431	.055	.576
1448	.033	.120	.076	.078	.045	.502	.515	.035	.290
1450	.051	.216	.105	.165	.041	.498	.651	.057	.468
1451	.025	.072	.082	.075	.043	.498	2.000	.044	.209
1454	.222	.394	.188	.265	.046	.205	.488	.030	.513
1456	.145	.469	.310	.400	.063	.786	.703	.093	.663
1458	.127	.307	.210	.104	.318	.797	1.342	.139	.835
1504	.079	.010	.009	.096	.222	.353	.311	.049	.036
1507	.037	.005	.025	.041	.178	.224	1.090	.013	.047
1511	.029	.008	.018	.035	.124	.055	.284	.030	.080
1514	.045	.005	.003	.068	.120	.187	.344	.024	.064

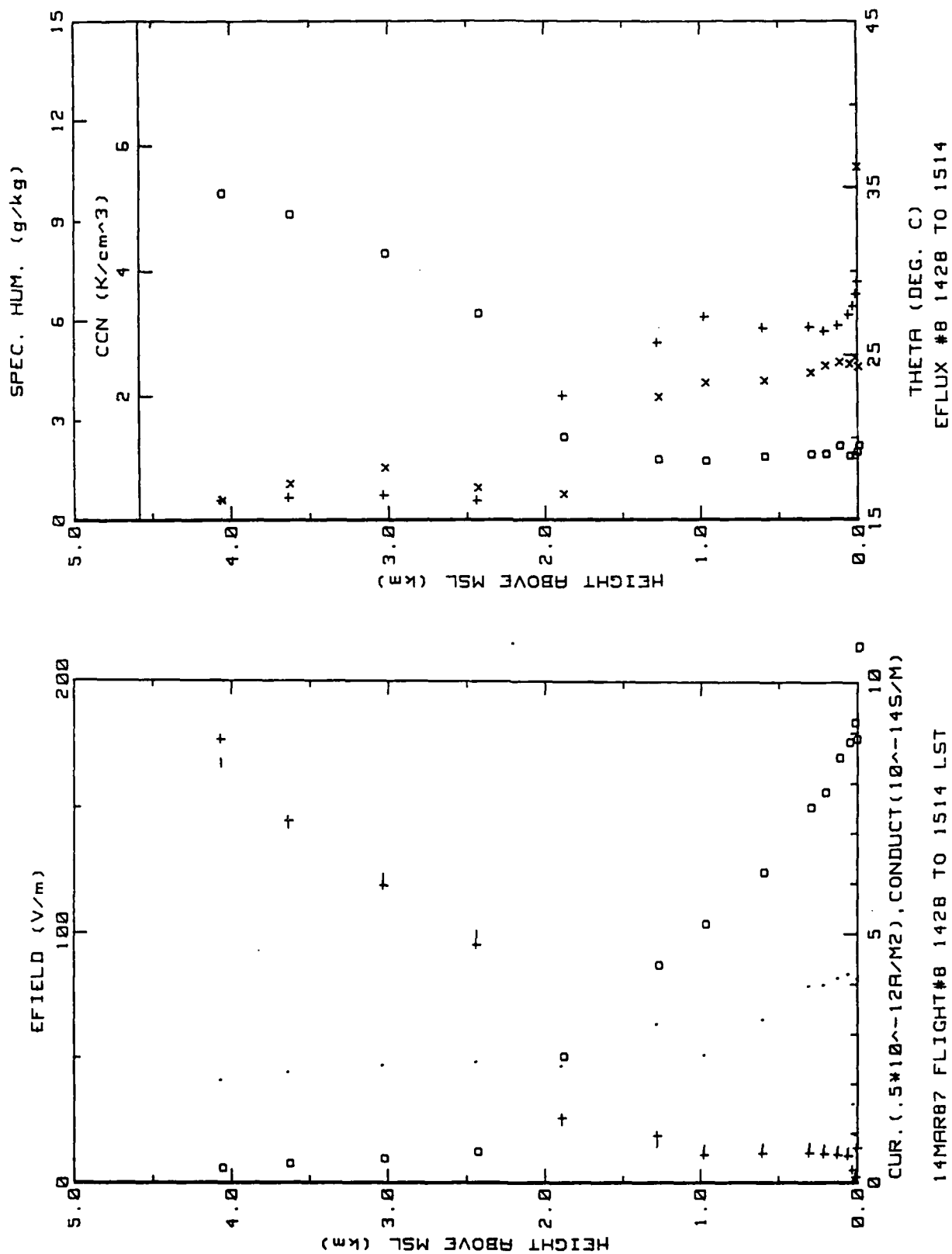


Figure 28a. RSD Flight 8 ladder profile over deep water E of N. Eleuthera. (ref. Fig. 5a).

Figure 28b. RSD Flight 8 ladder profile over deep water E of N. Eleuthera. (ref. Fig. 5c).



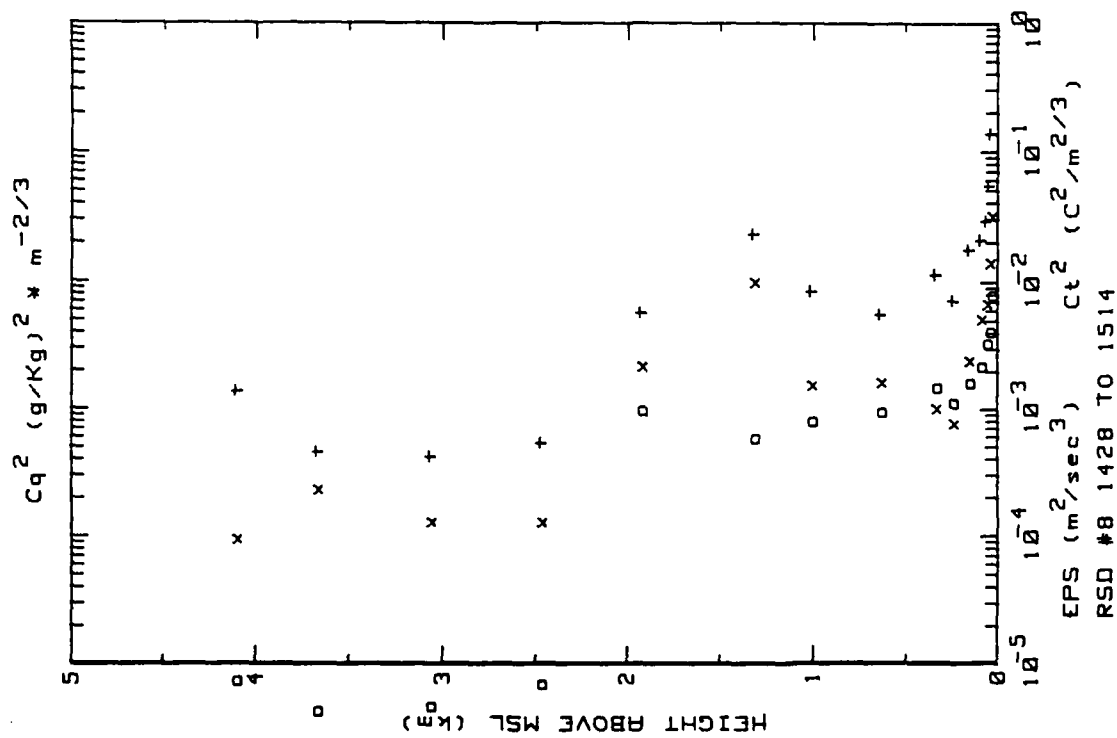


Figure 28c. RSD Flight 8 ladder profile over deep water E of N. Eleuthera. (ref. Fig. 5b).

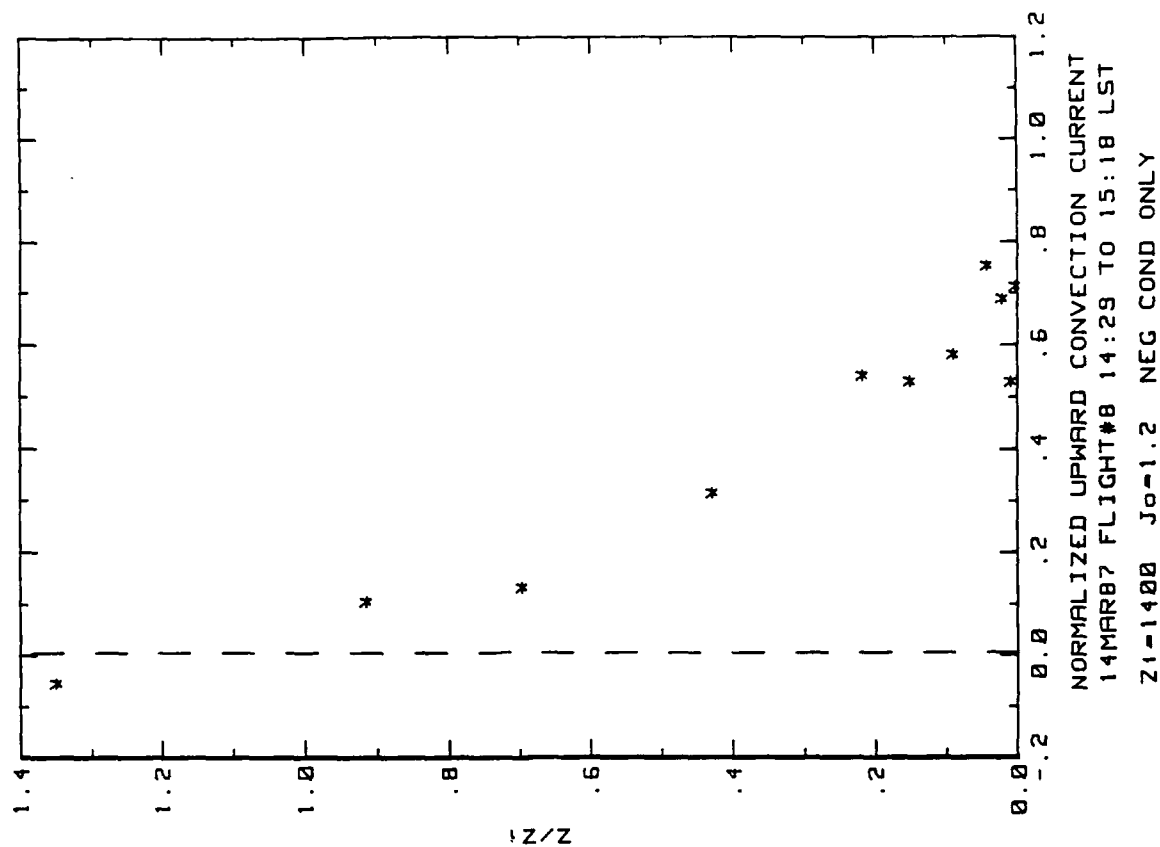


Figure 28d. RSD Flight 8 convection current profile over deep water E of N. Eleuthera (ref. Fig. 5d). The conduction and convection currents were calculated using only negative conductivity data.

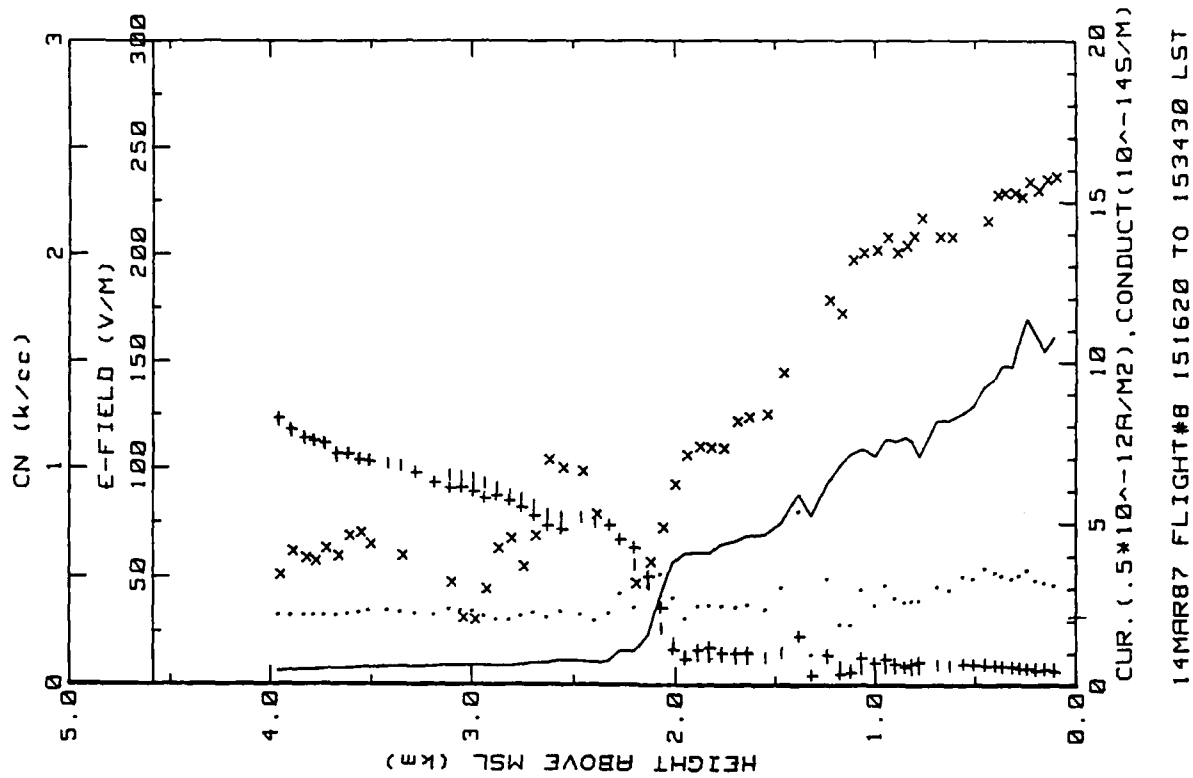


Figure 28f. RSD Flight 8 spiral down sounding over deep water E of N. Eleuthera (ref. Fig. 5f).

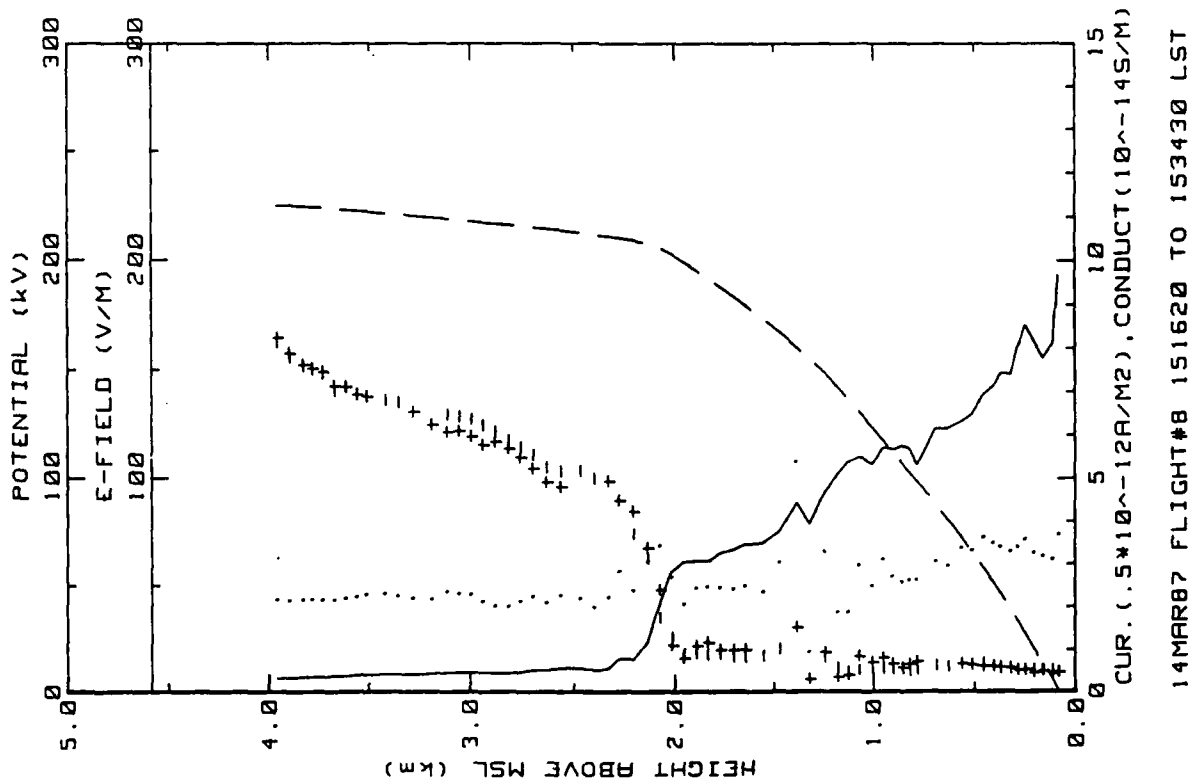


Figure 28e. RSD Flight 8 spiral down sounding over deep water E of N. Eleuthera (ref. Fig. 5e).

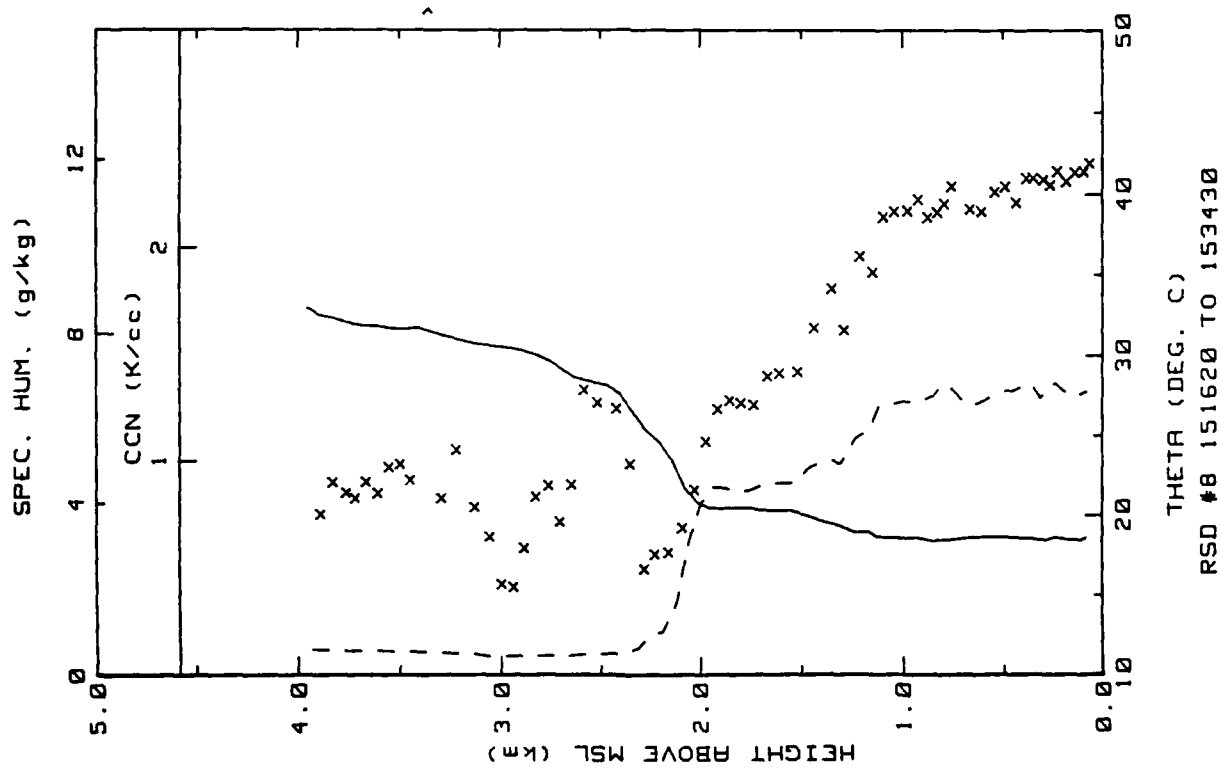


Figure 28g. RSD Flight 8 spiral down sounding over deep water E of N. Eleuthera (ref. Fig. 5h).

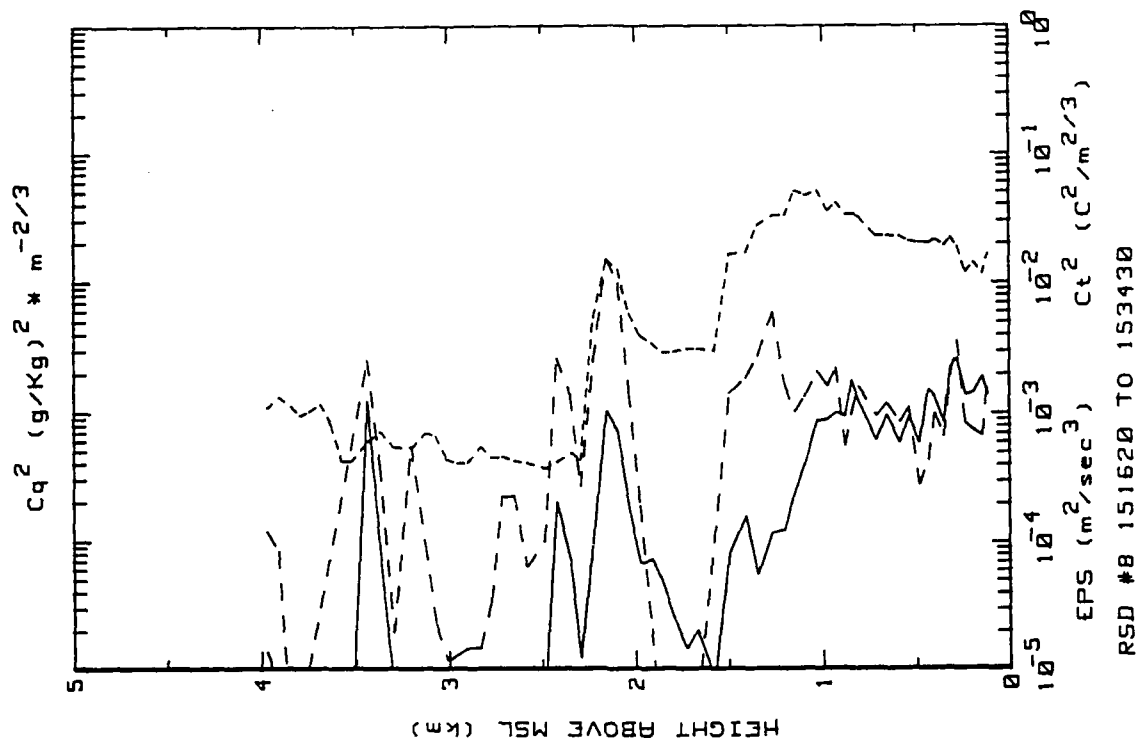


Figure 28h. RSD Flight 8 spiral down sounding over deep water E of N. Eleuthera (ref. Fig. 5g).

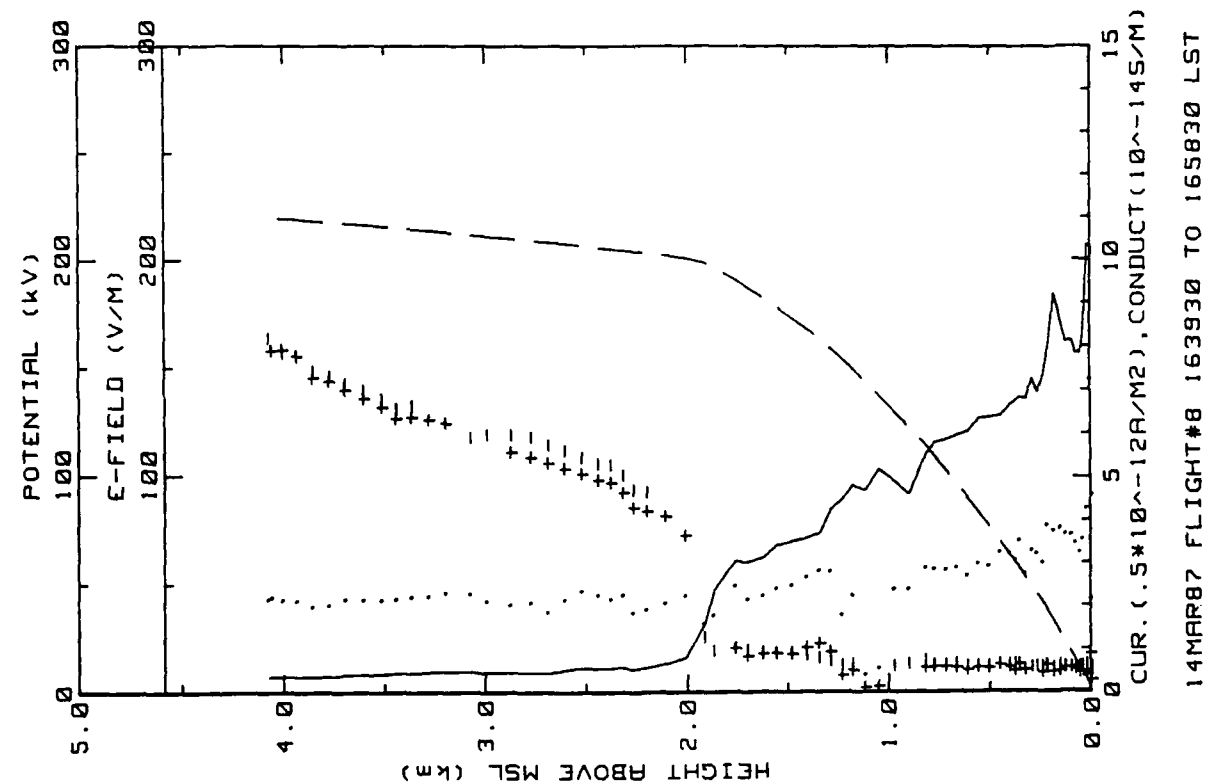


Figure 28i. RSD Flight 8 continuous upsoundings over deep water NE of RSD. (ref. Fig. 5e).

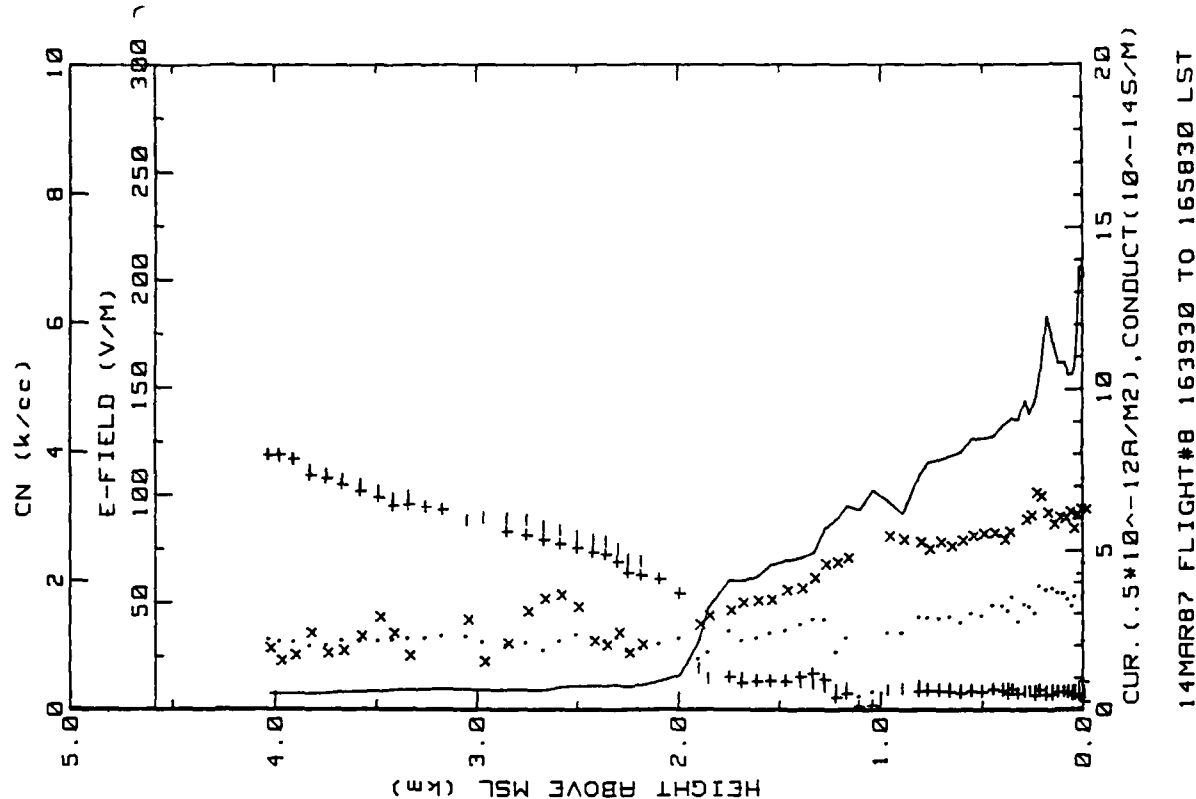
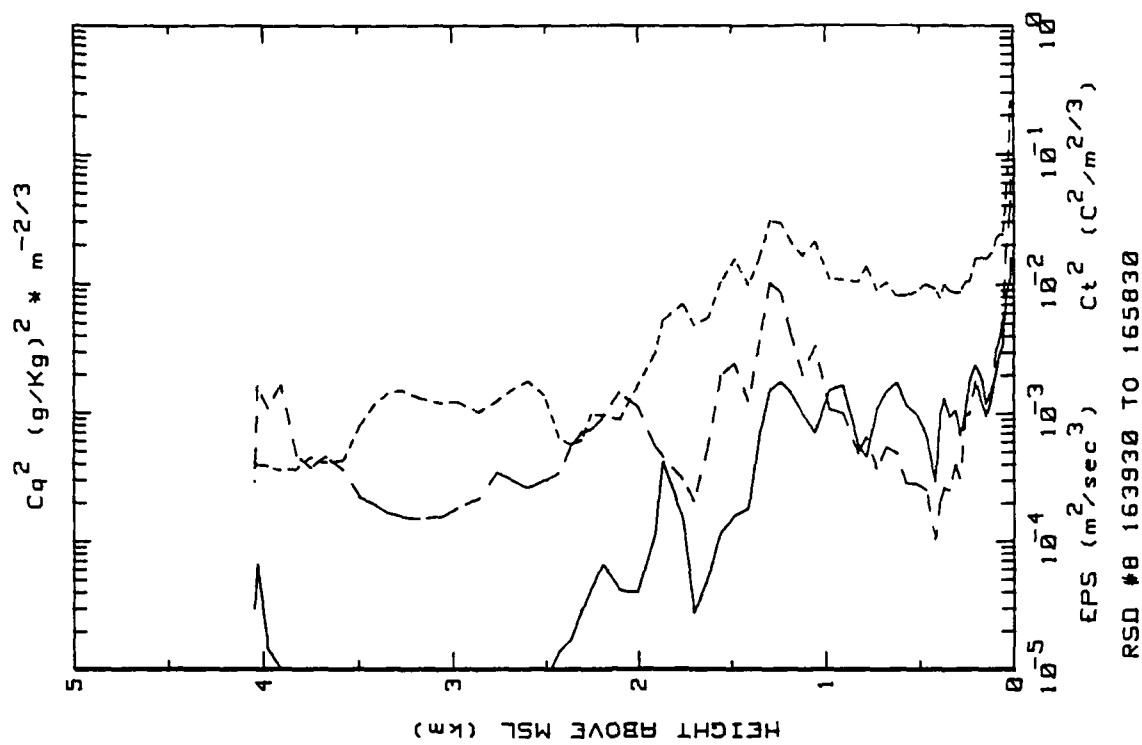
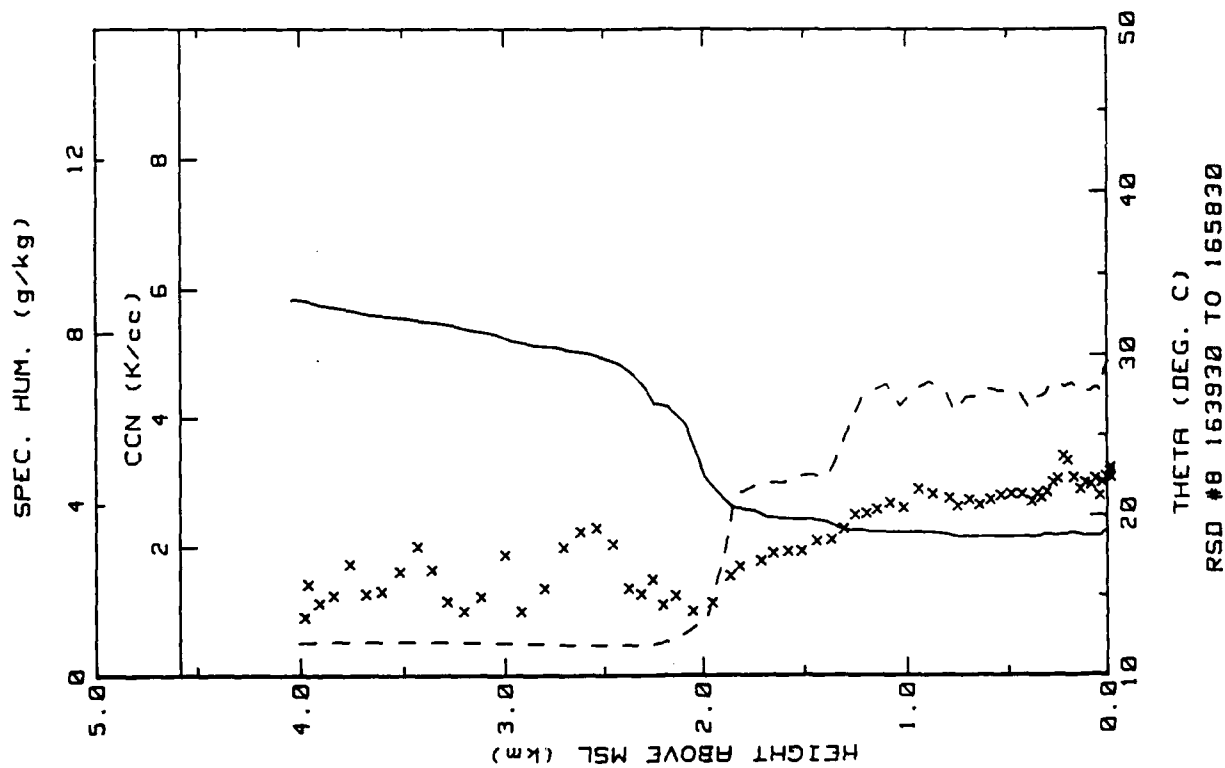
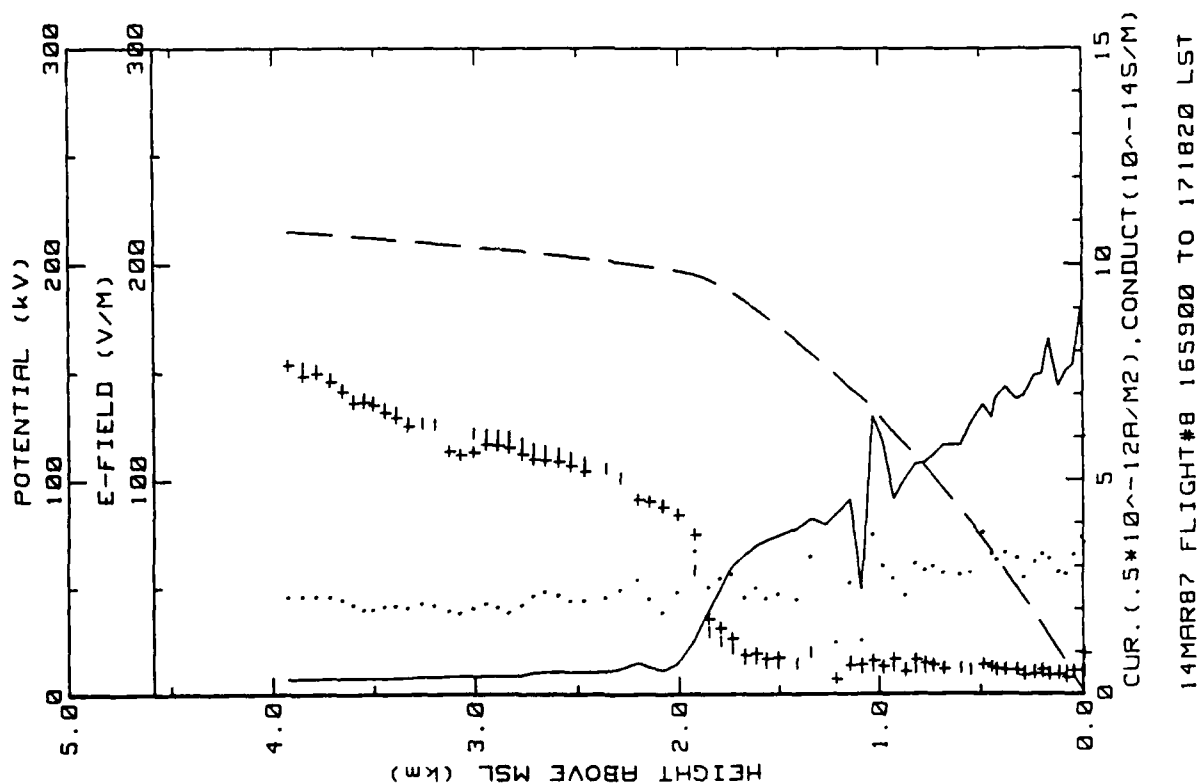
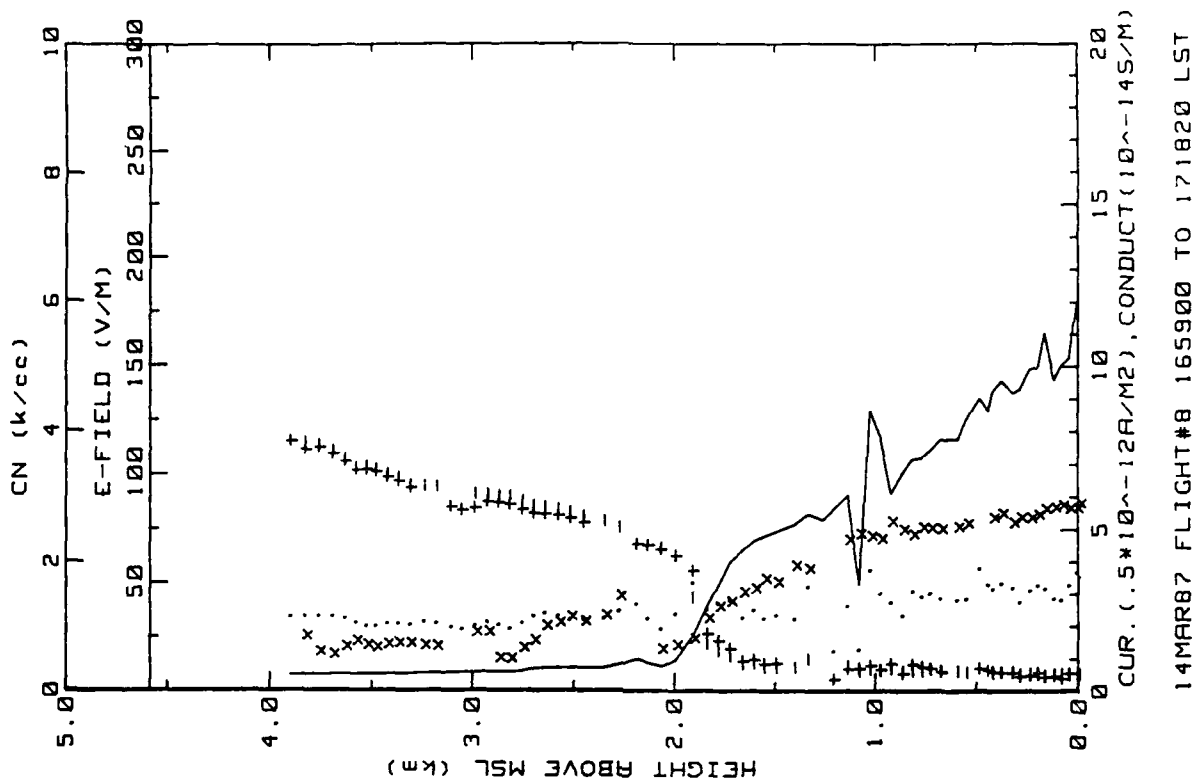


Figure 28j. RSD Flight 8 continuous upsoundings over deep water NE of RSD. (ref. Fig. 5f).





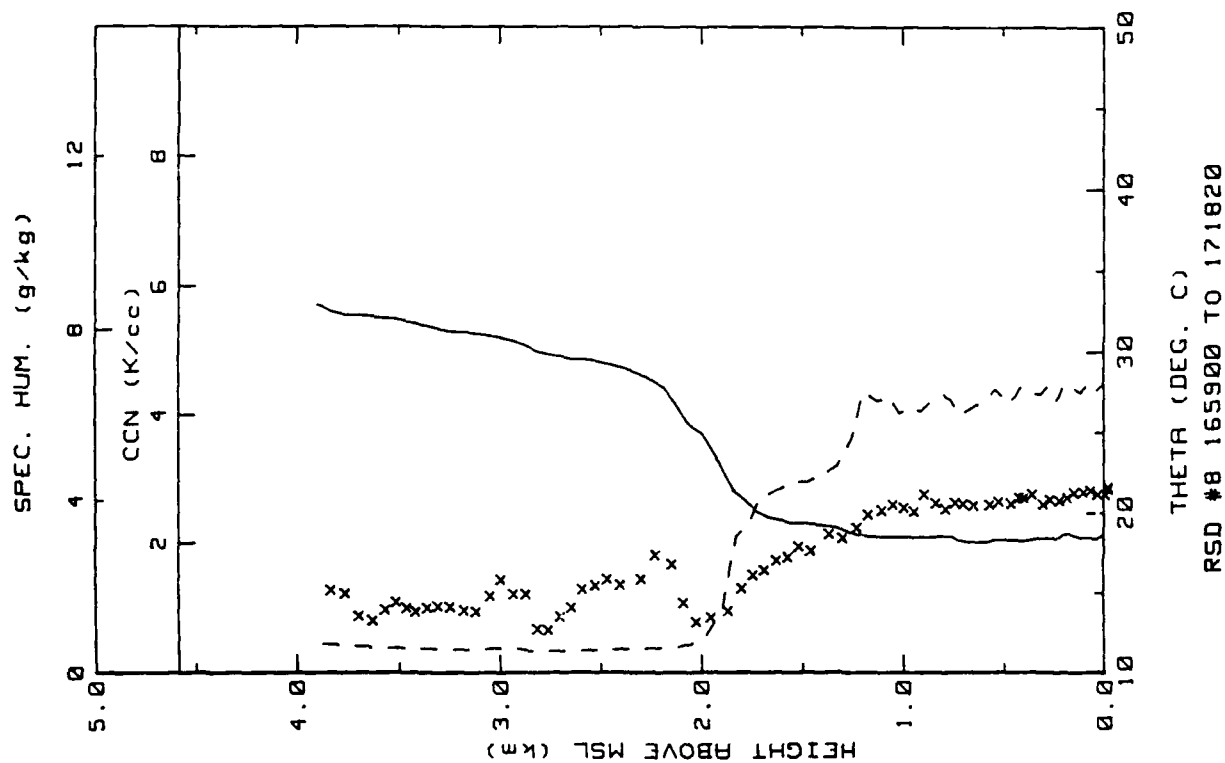


Figure 28o. RSD Flight 8 spiral down sounding over deep water NE of RSD (ref. Fig. 5h).

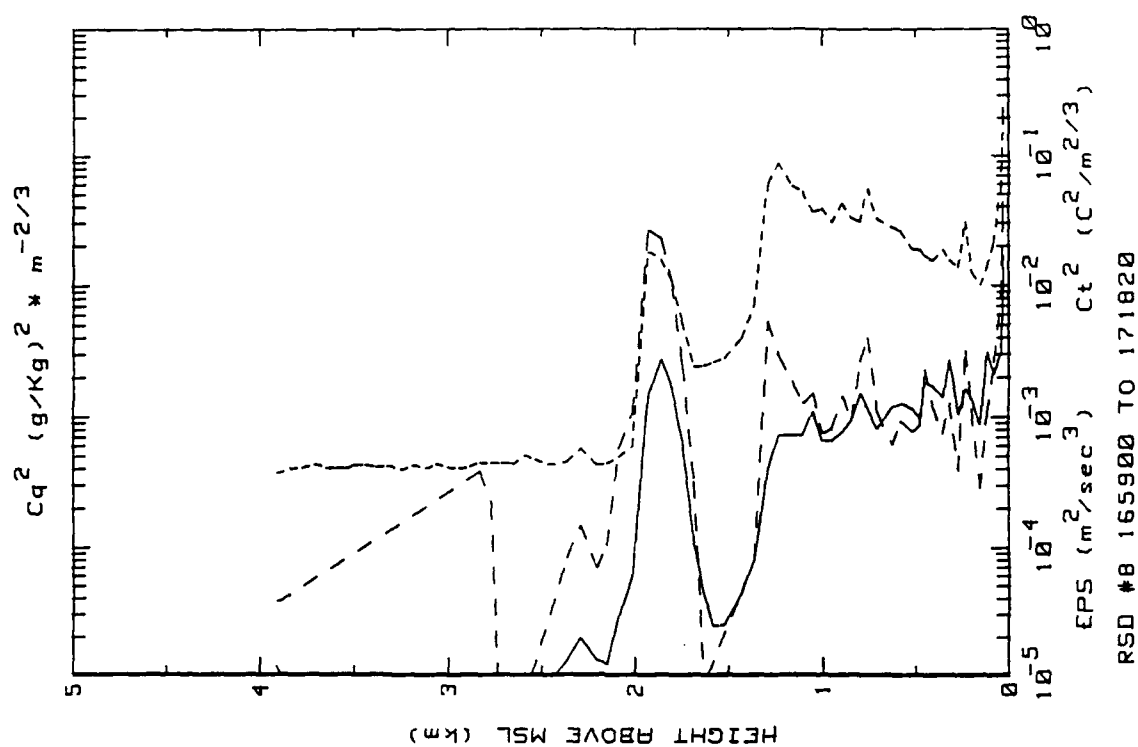


Figure 28p. RSD Flight 8 spiral down sounding over deep water NE of RSD (ref. Fig. 5g).

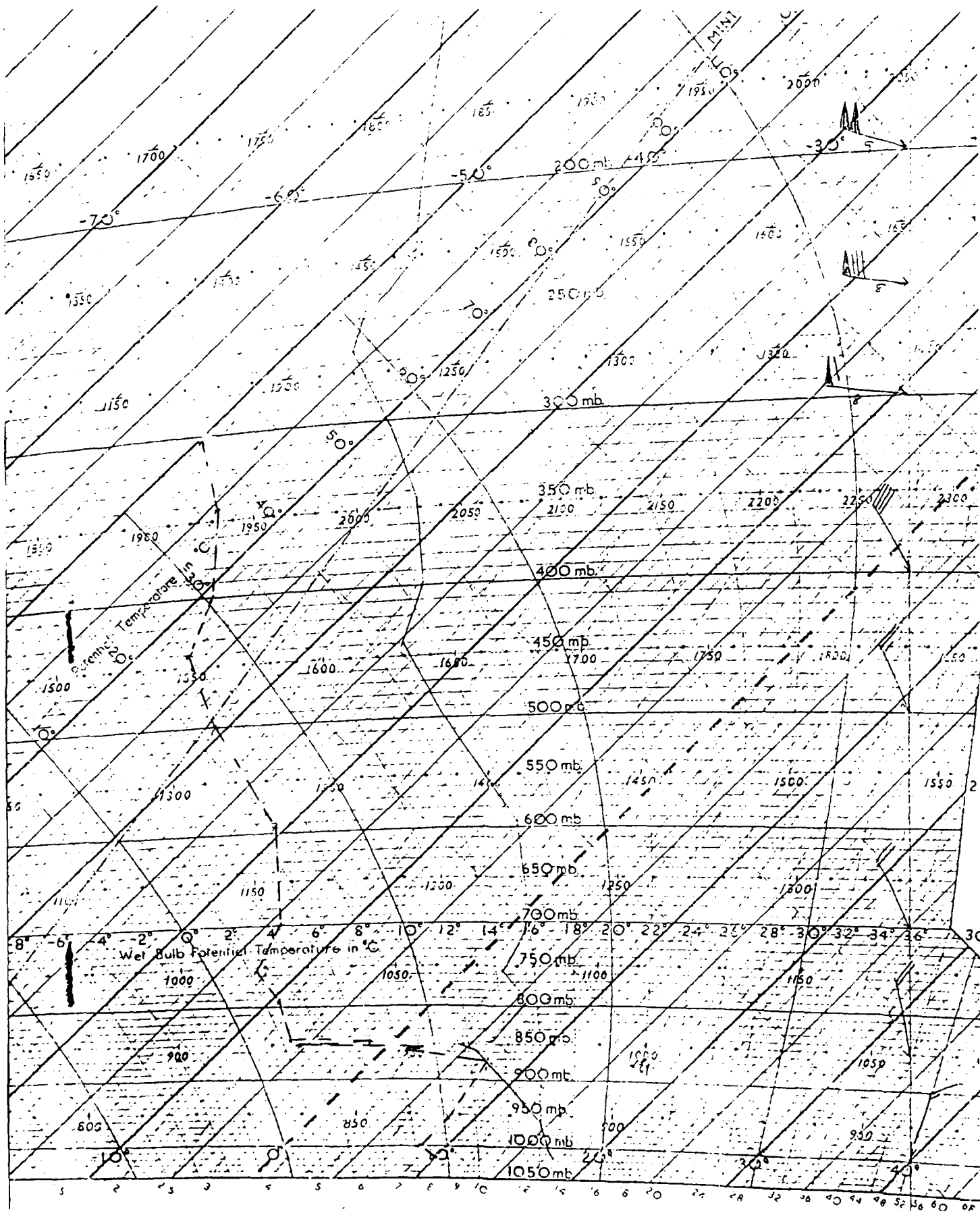


Figure 28q. Meteorological sounding from Nassau, Bahamas, taken on the day of Flight 8 (14 March 1987).



Flight: 9

Date: 16 March 1987

Takeoff: 1006 (LT) from RSD

Landed: 1510 at Nassau

Conditions: Scattered cumulus clouds throughout the flight; bases were at 1.1 km over the Gulf Stream (after 1245 LT). Winds were light and from the E at takeoff from RSD; the direction shifted to NE later in the flight and gained velocity to an estimated 5 m/s. No white caps initially but began to see a few on nearing Bimini.

Instruments:  $C_T^2$  bridge #2 began to give intermittent output so was replaced by #1 bridge at about 1130 LT. The computer sampling rate was increased for several low constant altitude passes to record simultaneous humidity fluctuations and electric field variations for later spectral analysis.

Summary: The purpose of the flight was to obtain data over the Gulf Stream where warmer water temperatures would cause stronger convection than in the Eleutheran waters. Constant altitude runs and one spiral descent was performed over shallow water between RSD and Bimini between 1014 and 1220 LT. A complete ladder profile and continuous downsoundings from 4.1 km were made over the Gulf Stream between Bimini and Florida from 1300 to 1413 LT followed by linear up- (to 2.9 km) and down-soundings enroute to Nassau.

Table 22a. RSD Flight 9 averages and standard deviations for constant altitude runs performed between RSD and Bimini over shallow water.

AVERAGES FROM LEVEL RUNS

Time HHMM	N	Altitude km	E_Field V/m	$\mu_{\text{Lam}}$ $10^{-14}$	$\sigma_{\text{Lam}}$ $10^{-14}$	Con Curr $10^{-12}$	Theta_v °C	Rel Hum %	ONN k/cc
1014	49	.006	171.45	.88	.83	2.95	21.7	57.7	2.33
1017	68	.015	153.84	.85	.84	2.65	21.4	57.6	1.42
1020	41	.031	123.58	.88	.91	2.21	21.3	54.8	1.28
1025	61	.006	188.92	.87	.84	2.92	21.7	58.6	2.25
1029	52	.031	158.91	.86	.84	2.70	21.5	56.8	1.37
1114	21	2.576	15.37	5.37	6.31	1.72	31.0	11.5	.46
1227	9	.006	201.90	.77	.78	3.12	21.3	75.6	2.37
1230	59	.031	193.65	.78	.77	3.00	21.5	71.6	2.87
1232	27	.006	136.15	.60	.72	3.01	21.6	72.3	3.12
1235	121	.059	154.51	.83	.81	2.55	21.5	72.3	1.87
1237	27	.128	136.23	.81	.79	2.16	21.3	74.6	1.52

Time HHMM	N	Altitude km	EPS m2/s3	CT2 (2/m2/3)	G g/kg	Gc2 (g/kg)2m2/3	Press mB	Trose °C	T_DR °C	T_Dew °C
1014	43	.006	1.36E-03	5.73E-03	8.3	7.42E-02	1012.7	20.1	23.0	11.4
1017	68	.015	6.98E-04	1.48E-03	8.2	4.29E-02	1011.3	19.7	22.0	11.1
1020	41	.031	4.14E-04	1.17E-03	7.7	4.28E-02	1008.9	19.5	21.7	10.1
1025	61	.006	1.85E-03	7.45E-03	9.4	7.11E-02	1012.5	20.0	22.6	11.6
1029	52	.031	1.64E-03	6.71E-03	8.1	3.98E-02	1011.6	19.9	23.3	11.1
1114	21	2.576	3.41E-06	4.96E-02	.9	4.10E-04	745.1	5.3	23.8	-22.3
1227	9	.006	6.25E-04	1.53E-02	10.6	3.97E-02	1013.1	19.3	22.9	15.1
1230	59	.031	4.02E-04	5.01E-03	10.0	2.15E-02	1010.8	19.4	22.4	14.2
1232	27	.006	5.54E-04	1.04E-02	10.2	3.81E-02	1012.7	19.6	22.3	14.5
1235	121	.059	1.60E-04	1.20E-02	9.9	1.55E-02	1007.1	19.1	22.2	14.0
1237	27	.128	1.76E-04	2.11E-02	9.8	1.33E-02	998.9	18.3	22.0	13.7

STANDARD DEVIATIONS/MEAN VALUES

Time	E_Field	$\mu_{\text{Lam}}$	$\sigma_{\text{Lam}}$	Con Curr	CON	EPS	CT2	G	Gc2
1014	.147	.033	.035	.134	.017	.194	.527	.042	.247
1017	.135	.041	.107	.152	.075	.277	.661	.048	.392
1020	.033	.029	.005	.067	.033	.209	.405	.035	.373
1025	.144	.039	.055	.141	.105	.419	.477	.052	.343
1029	.122	.031	.025	.140	.031	.337	.414	.052	.366
1114	.008	.013	.007	.006	.079	.072	.506	.005	.253
1227	.105	.031	.070	.113	.027	.197	.213	.027	.173
1230	.123	.042	.074	.127	.050	.342	.323	.053	.247
1232	.093	.035	.032	.103	.113	.437	.317	.031	.381
1235	.050	.064	.057	.100	.051	.350	1.441	.025	.246
1237	.047	.021	.032	.047	.054	.354	.751	.023	.114

Table 22b. RSD Flight 9 averages for constant altitude runs performed over the Gulf Stream between Bimini and Florida.

AVERAGES FROM LEVEL RUNS

Time HHMM	N	Altitude km	C <sub>field</sub> V/m	+Lam 10 <sup>-14</sup>	-Lam 10 <sup>-14</sup>	Corr Curr 10 <sup>-12</sup>	Theta_v C	Rel Hum %	CNV k/cc
1242	125	.061	173.75	.84	1.56	4.83	21.9	63.1	2.73
1248	54	.006	190.34	.80	.75	2.96	21.8	63.8	1.82
1250	50	.015	185.12	.80	.78	2.95	21.9	63.3	2.08
1254	60	.031	174.83	.80	.78	2.75	21.8	64.0	2.01
1256	21	.061	148.20	.80	.77	2.52	21.8	64.9	1.65
1300	63	.006	184.40	.77	.72	2.76	22.0	65.3	2.56
1303	50	.015	192.36	.81	.73	3.00	21.9	67.6	2.61
1307	46	.031	189.84	.79	.72	2.73	21.8	68.4	2.12
1310	46	.061	169.29	.77	.74	2.55	21.8	68.1	1.92
1312	35	.134	146.65	.79	.77	2.34	21.7	67.0	1.58
1314	32	.229	138.78	.85	.90	2.34	21.9	69.9	1.92
1317	51	.330	132.31	.82	.78	2.11	21.8	76.0	1.61
1321	51	.462	122.47	.83	.76	1.99	21.8	82.0	1.65
1324	46	.633	117.42	.84	.76	1.85	22.1	85.3	1.64
1328	59	.895	89.06	.87	.92	1.59	22.5	90.1	1.62
1330	21	1.320	64.77	1.07	1.16	1.44	23.0	86.2	.96
1333	41	1.510	55.56	1.45	1.39	1.55	24.0	85.6	.96
1336	36	1.839	42.10	2.00	1.91	1.53	25.5	78.3	.78
1340	32	2.452	31.04	2.81	2.68	1.72	27.9	53.1	.86
1343	35	3.062	14.89	5.03	5.57	1.57	33.6	9.6	.85
1347	37	3.655	13.70	6.08	6.70	1.74	34.8	13.6	.65
1350	29	4.093	10.95	7.87	8.11	1.74	37.3	13.6	.60

Time HHMM	N	Altitude km	EPS m2/s3	CT2 C2/m2/3	Q g/kg	Co2 (g/kg)2m-2/3	Press mB	Trose C	T <sub>IR</sub> C	T <sub>dew</sub> C
1242	125	.061	7.33E-04	7.05E-03	8.9	2.07E-02	1006.5	19.6	25.6	12.4
1248	54	.006	2.78E-03	3.64E-02	9.2	5.13E-02	1012.1	20.0	26.1	12.5
1250	50	.015	2.35E-03	2.19E-02	9.1	3.55E-02	1010.8	20.0	25.9	12.8
1254	60	.031	1.22E-03	9.54E-03	9.1	1.65E-02	1009.1	19.7	25.9	12.7
1256	21	.061	8.58E-04	3.74E-03	9.1	8.85E-03	1005.3	19.4	25.8	12.5
1300	63	.006	2.93E-03	3.67E-02	9.5	4.43E-02	1011.3	20.1	25.9	13.4
1303	50	.015	2.07E-03	1.84E-02	9.7	2.61E-02	1009.9	19.8	25.9	13.7
1307	46	.031	1.35E-03	1.14E-02	9.6	1.55E-02	1008.0	19.6	25.8	13.6
1310	46	.061	1.17E-03	6.10E-03	9.5	1.13E-02	1004.5	19.3	25.8	13.3
1312	35	.134	1.25E-03	3.80E-03	9.1	1.02E-02	999.3	18.8	25.7	12.5
1314	32	.229	7.21E-04	2.50E-03	9.1	7.30E-03	987.2	18.0	25.6	12.4
1317	51	.330	7.59E-04	3.18E-03	9.4	8.43E-03	975.7	16.9	25.7	12.7
1321	51	.462	6.06E-04	5.08E-03	9.4	9.71E-03	960.7	15.6	25.5	12.5
1324	46	.633	5.59E-04	5.58E-03	9.3	1.06E-02	941.1	14.2	25.4	11.9
1328	59	.895	4.30E-04	7.70E-03	8.5	1.33E-02	902.7	11.3	24.9	9.7
1330	21	1.320	2.30E-04	3.02E-03	7.0	1.07E-02	867.9	3.9	24.1	6.7
1333	41	1.510	5.66E-05	5.41E-03	5.4	8.50E-03	838.2	7.2	23.2	4.9
1336	36	1.839	7.29E-05	2.71E-03	5.7	4.46E-03	813.4	6.3	23.8	3.8
1340	32	2.452	5.05E-04	2.78E-03	5.7	5.02E-03	756.6	2.7	24.1	1.7
1343	35	3.062	1.73E-04	3.06E-03	.6	6.56E-04	701.6	2.9	20.6	-25.2
1347	37	3.655	9.04E-05	2.17E-03	.7	1.79E-04	551.4	-1.9	29.9	-25.2
1350	29	4.093	1.39E-04	1.87E-03	.5	6.94E-05	416.1	-4.0	24.6	-27.9

Table 22c. RSD Flight 9 (standard deviations)/averages for  
constant altitude runs performed over the Gulf  
Stream between Bimini and Florida.

Time	E_Field	+Lam	-Lam	Con Curr	CCN	EPS	C12	Q	Cq2
1242	.069	.050	3.615	3.424	.128	.394	.552	.078	.647
1248	.098	.059	.082	.102	.158	.316	.268	.036	.314
1250	.090	.065	.092	.122	.110	.257	.292	.042	.345
1254	.090	.070	.076	.096	.163	.416	.466	.032	.427
1256	.095	.030	.041	.084	.072	.306	.317	.020	.179
1300	.123	.065	.086	.129	.075	.228	.243	.032	.241
1303	.109	.061	.067	.174	.187	.305	.252	.037	.245
1307	.100	.081	.101	.115	.070	.286	.355	.033	.221
1310	.069	.026	.058	.075	.122	.404	.372	.034	.244
1312	.064	.046	.086	.068	.116	.307	.343	.028	.289
1314	.053	.067	.059	.071	.154	.454	.385	.023	.158
1317	.056	.054	.075	.093	.133	.314	.303	.027	.126
1321	.044	.128	.092	.118	.122	.348	.399	.022	.161
1324	.156	.103	.071	.182	.074	.349	.495	.020	.115
1328	.063	.170	.343	.227	.220	.702	.762	.086	.325
1330	.032	.025	.051	.049	.052	.716	.473	.012	.127
1333	.053	.029	.057	.075	.109	.704	.573	.037	.185
1336	.079	.051	.065	.061	.202	.538	.159	.035	.083
1340	.082	.091	.026	.105	.444	1.237	.296	.031	.315
1343	.027	.011	.027	.056	.655	.443	.879	.022	.468
1347	.017	.005	.010	.025	.107	.595	.144	.031	.263
1350	.040	.007	.019	.045	.088	.579	.074	.023	.141

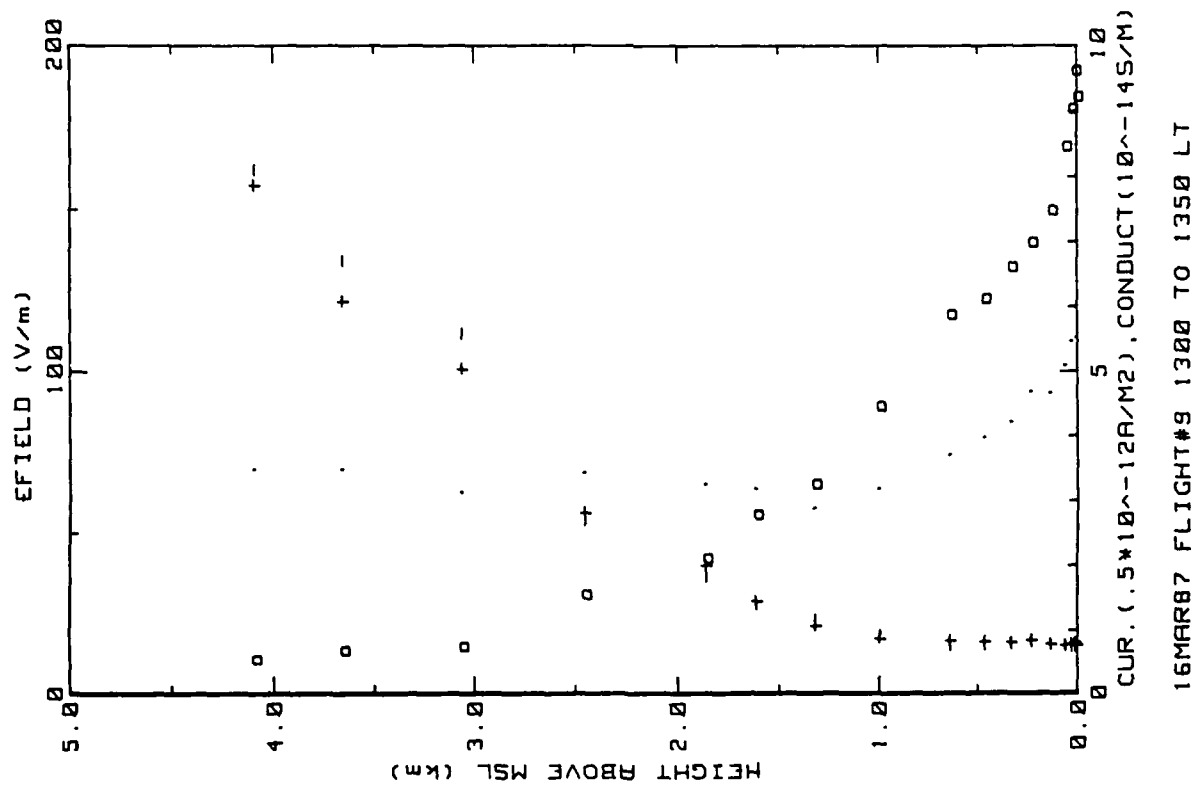


Figure 2a. RSD Flight 9 ladder profile the Gulf Stream E of Bimini. (ref. Fig. 5a).

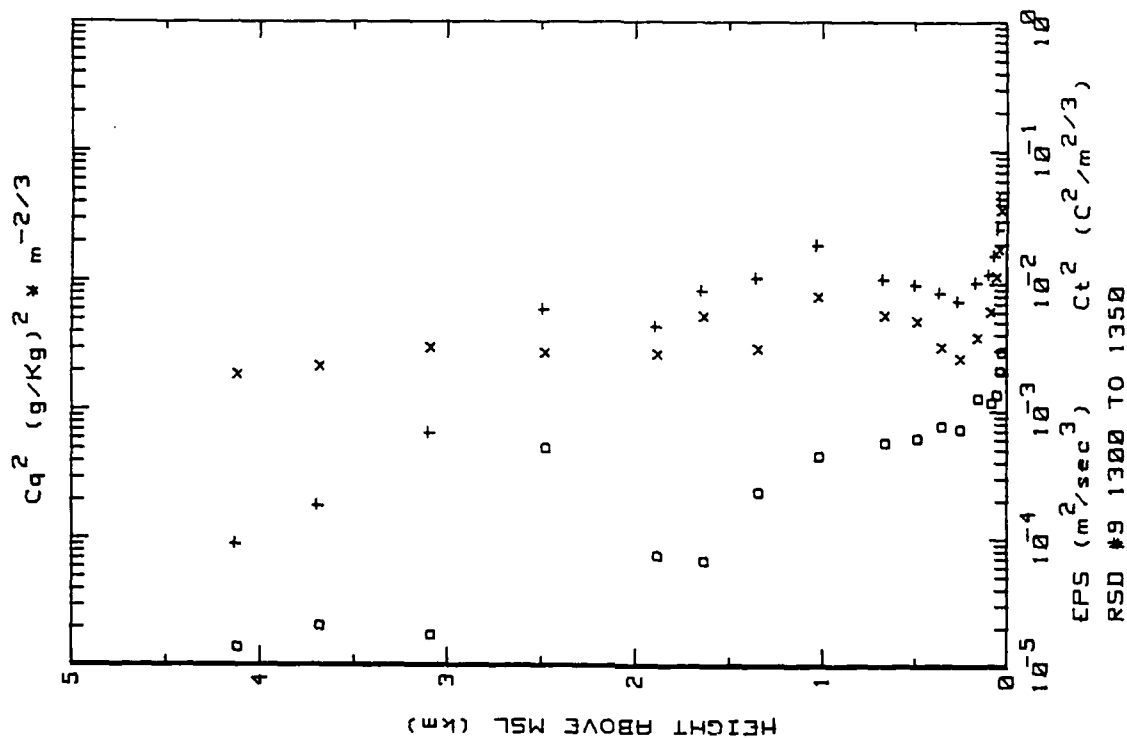


Figure 2b. RSD Flight 9 ladder profile the Gulf Stream E of Bimini. (ref. Fig. 5b).

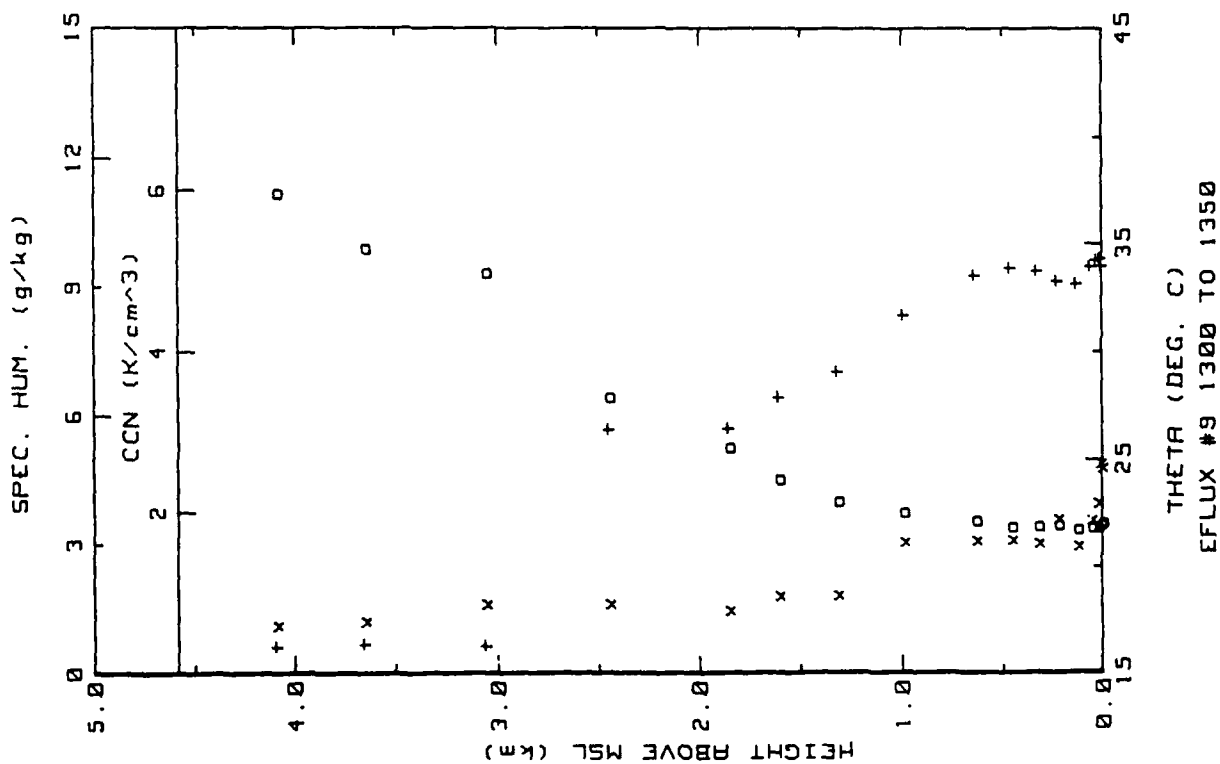


Figure 29c. RSD Flight 9 ladder profile the Gulf Stream E of Bimini. (ref. Fig. 5c).

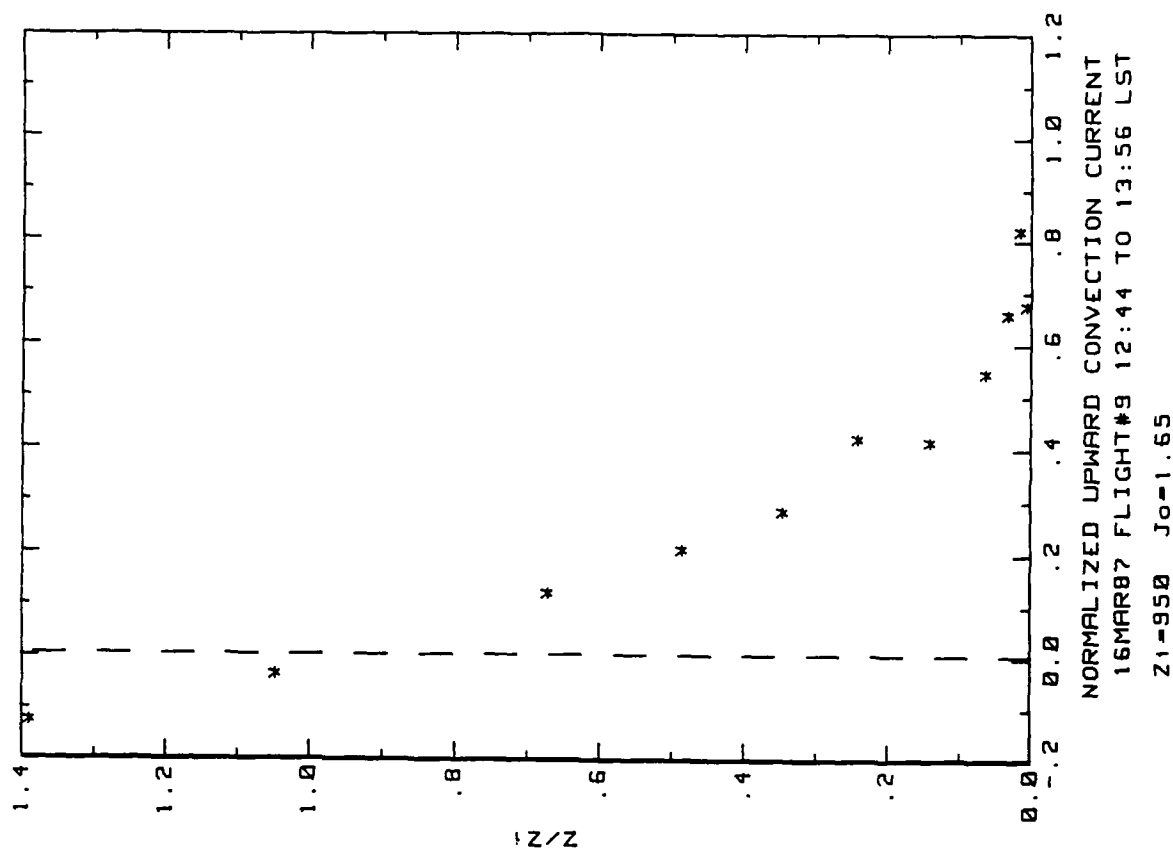


Figure 29d. RSD Flight 9 convection current profile over the Gulf Stream E of Bimini (ref. Fig. 5d). The actual times are 1300 to 1350 LT.

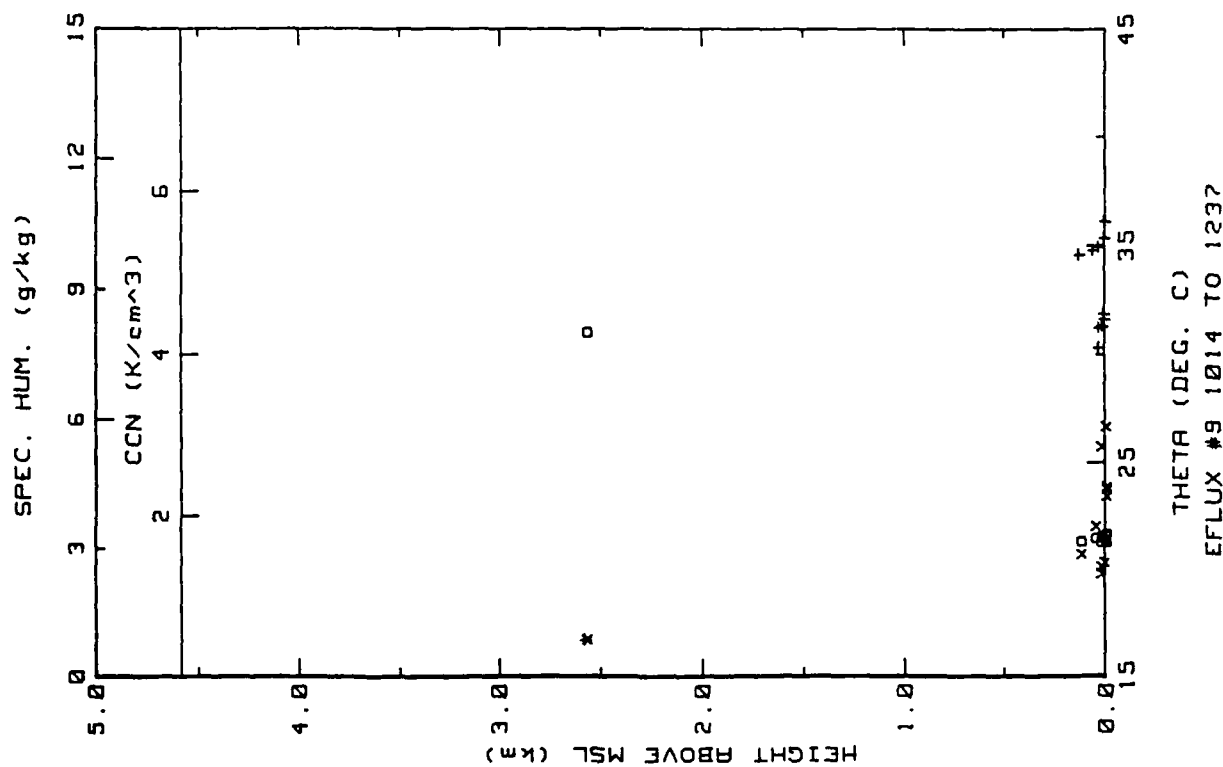


Figure 29e. RSD Flight 9 ladder profile over shallow water between RSD and Bimini. (ref Fig. 5c).

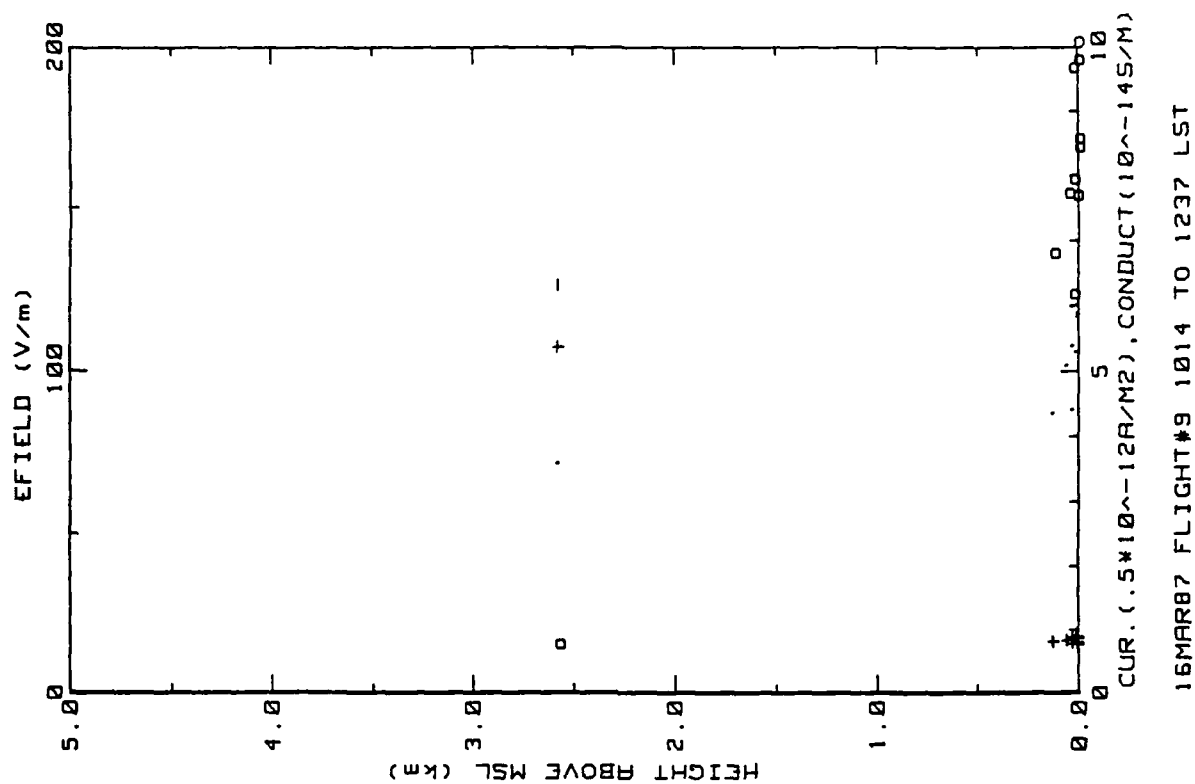


Figure 29f. RSD Flight 9 ladder profile over shallow water between RSD and Bimini. (ref Fig. 5a).

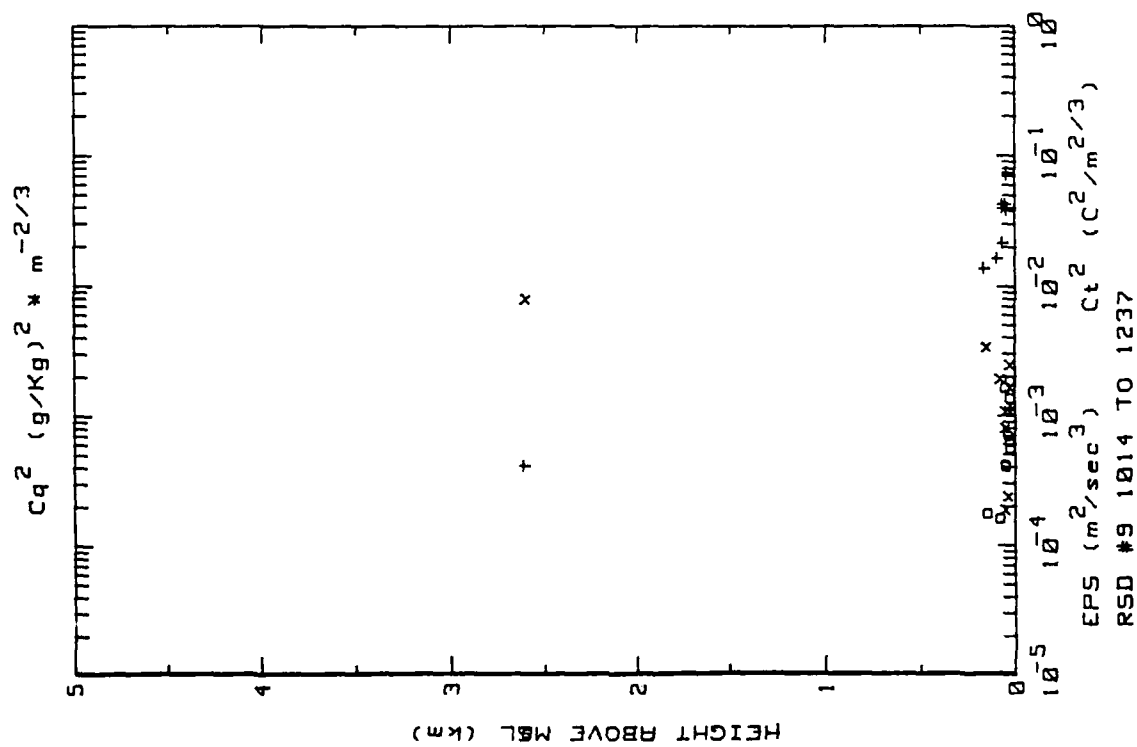


Figure 29g. RSD Flight 9 ladder profile over shallow water between RSD and Bimini. (ref Fig. 5b).



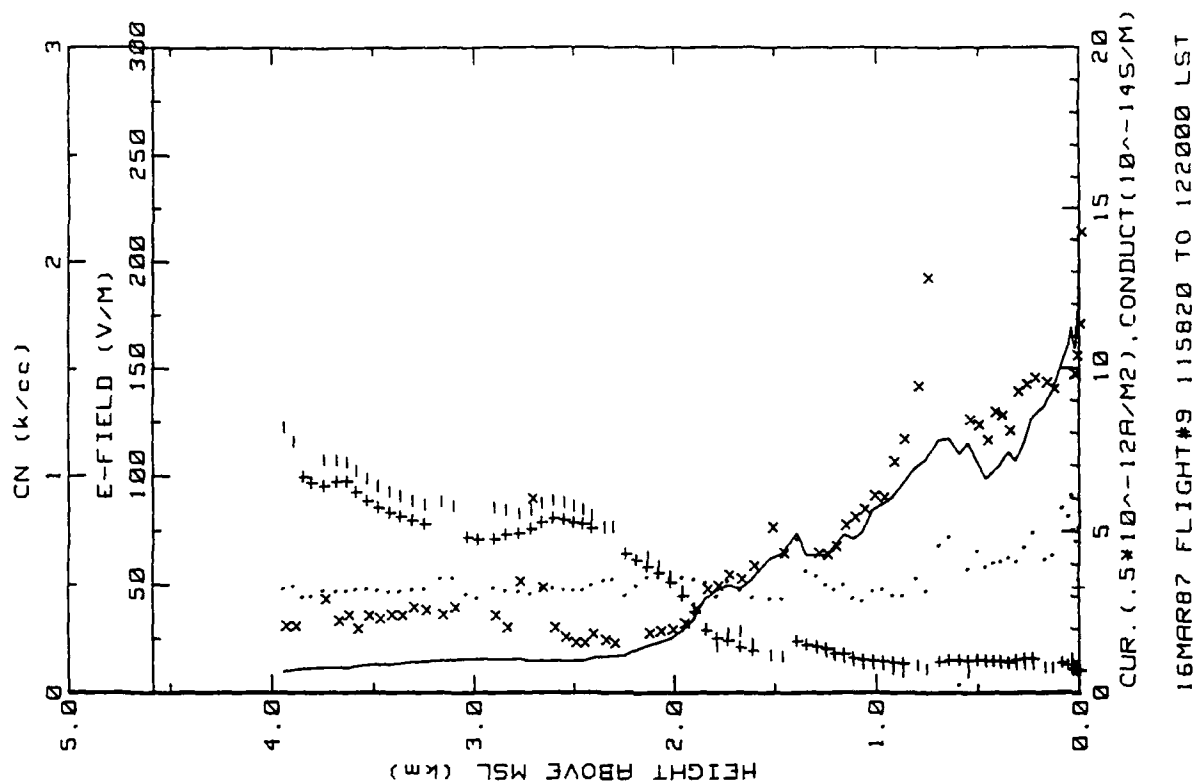


Figure 29h. RSD Flight 9 spiral down sounding over shallow water E of Bimini (ref. Fig. 5e).

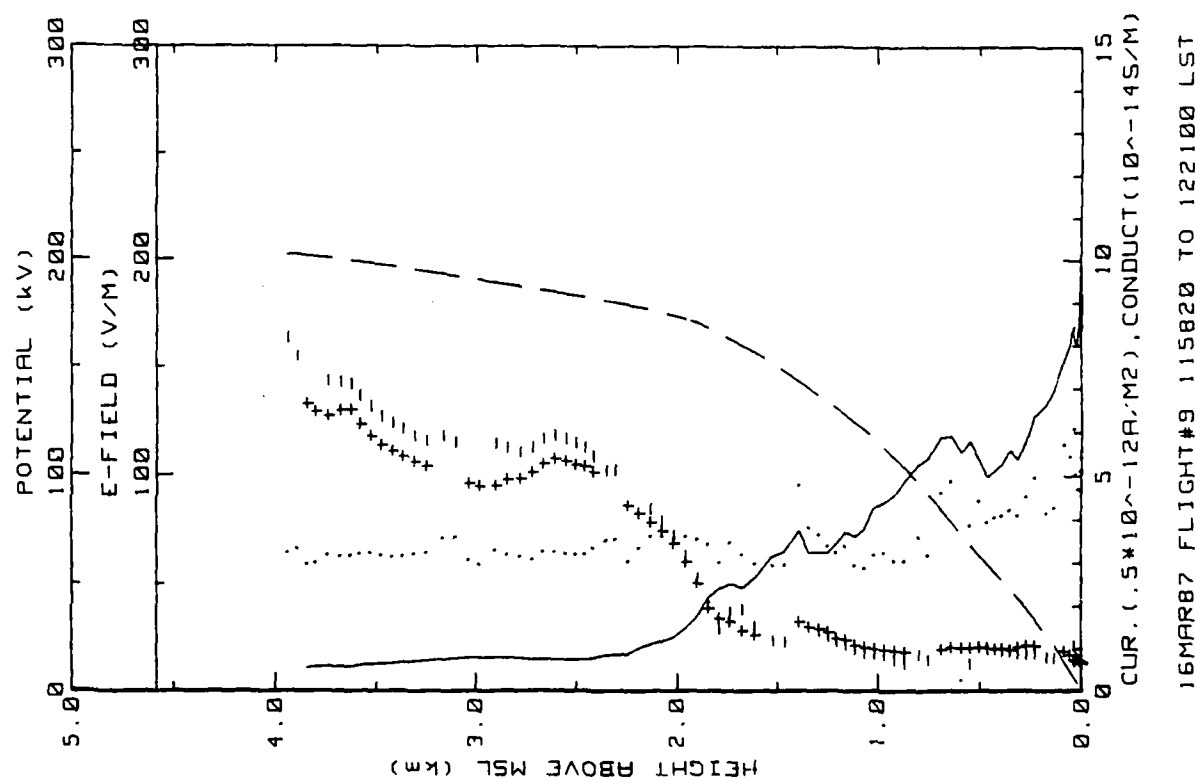


Figure 29i. RSD Flight 9 spiral down sounding over shallow water E of Bimini (ref. Fig. 5f).

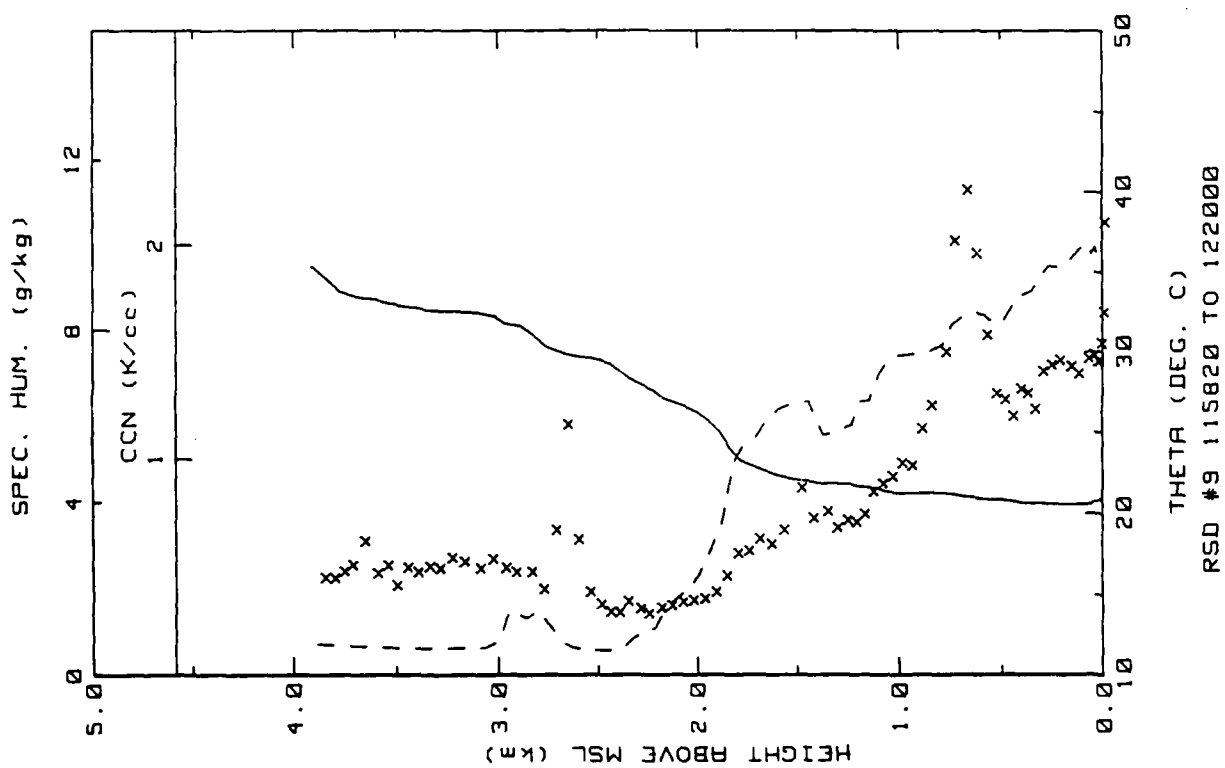


Figure 29j. RSD Flight 9 spiral down sounding over shallow water E of Bimini (ref. Fig. 5h).

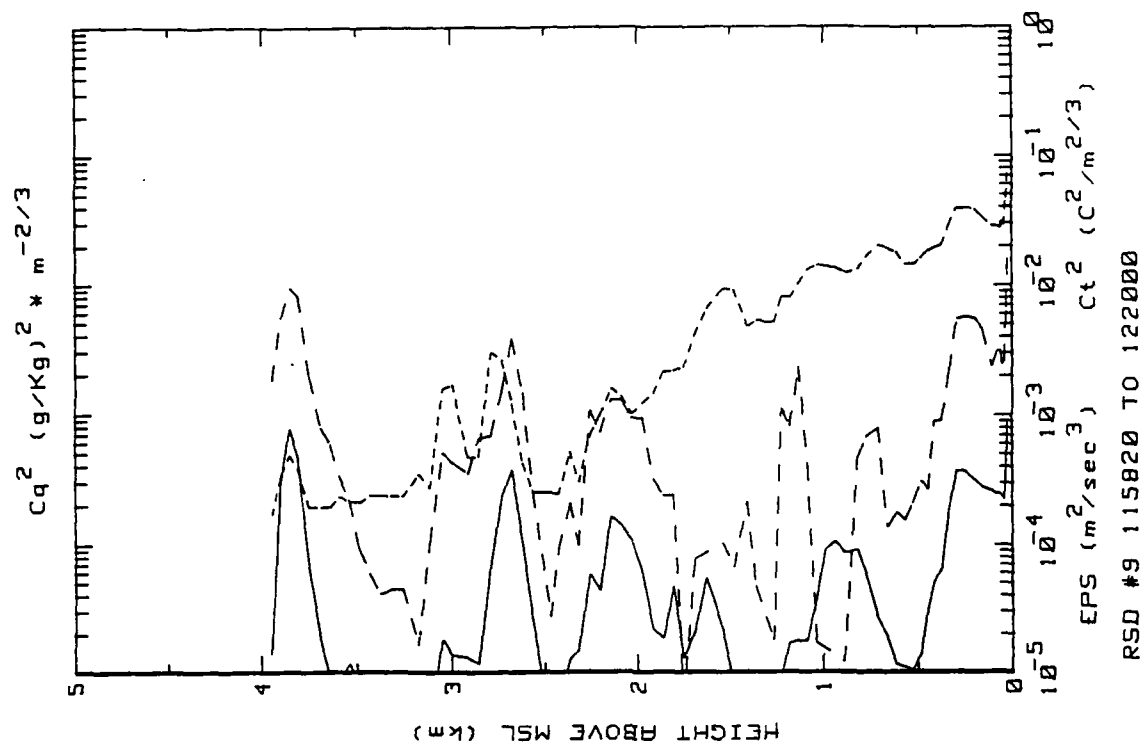


Figure 29k. RSD Flight 9 spiral down sounding over shallow water E of Bimini (ref. Fig. 5g).

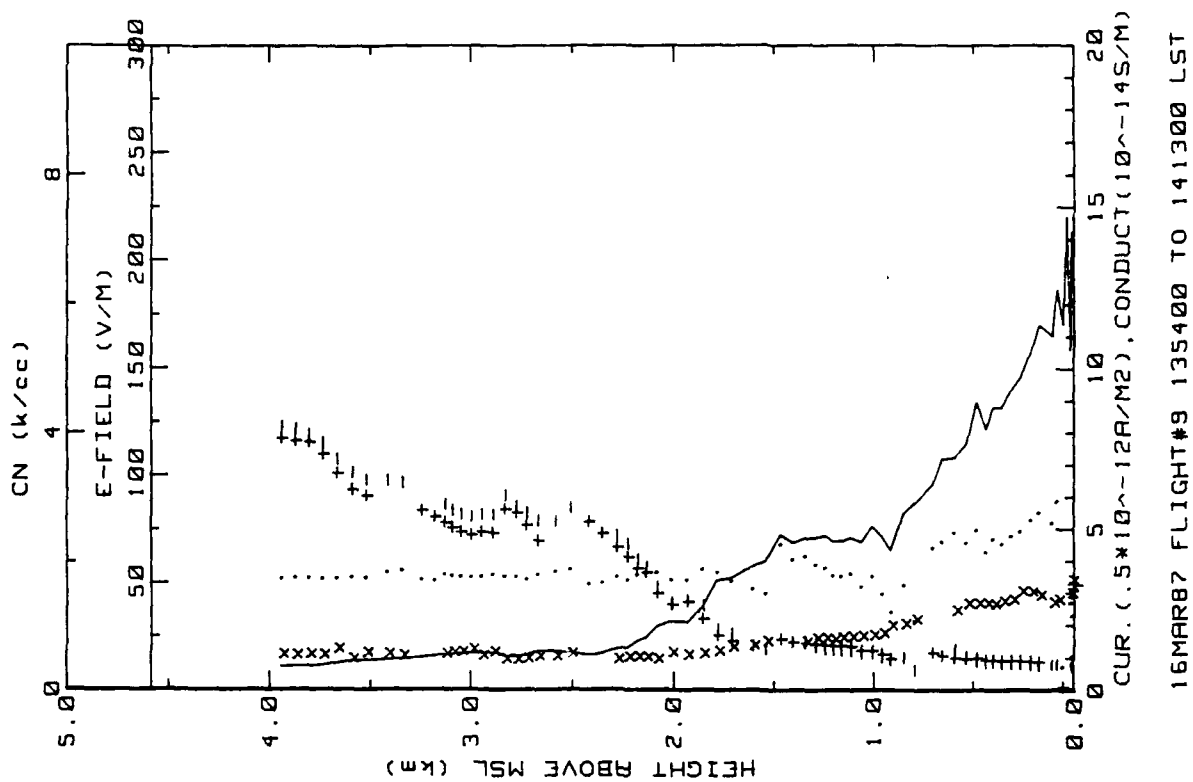


Figure 29m. RSD Flight 9 spiral down sounding over the Gulf Stream W of Bimini (ref. Fig. 5f).

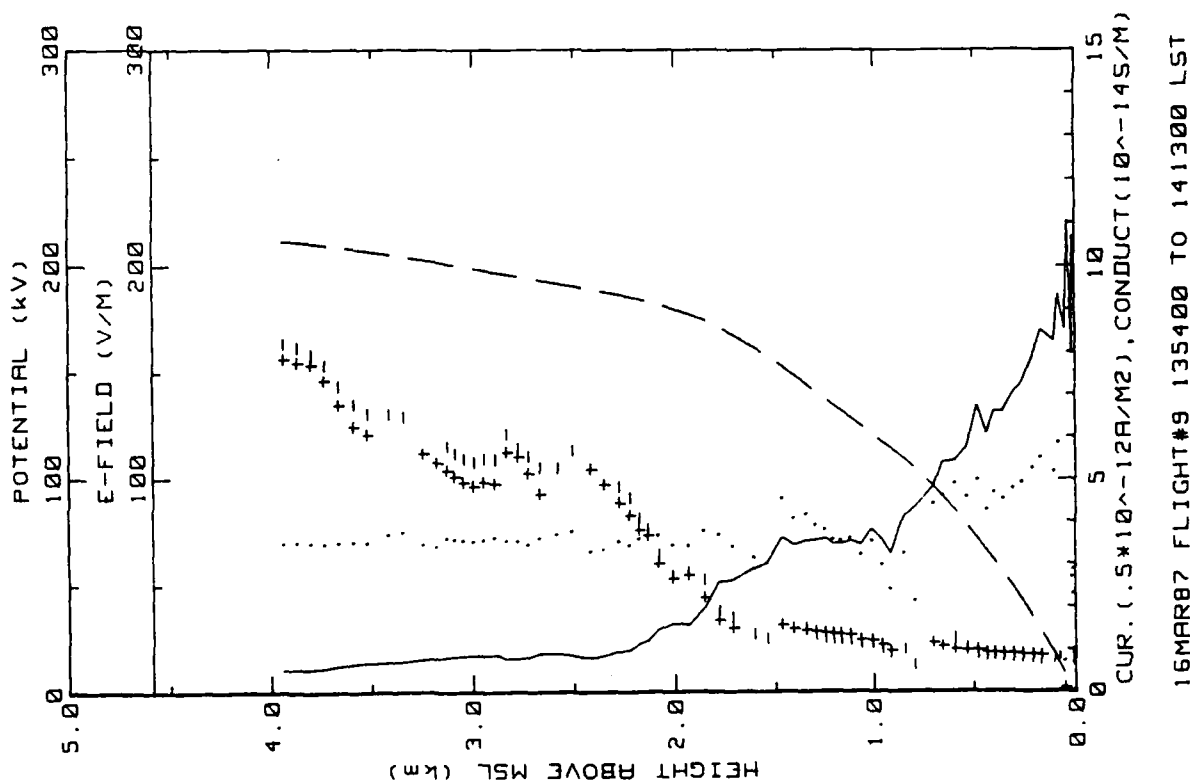


Figure 29l. RSD Flight 9 spiral down sounding over the Gulf Stream W of Bimini (ref. Fig. 5e).

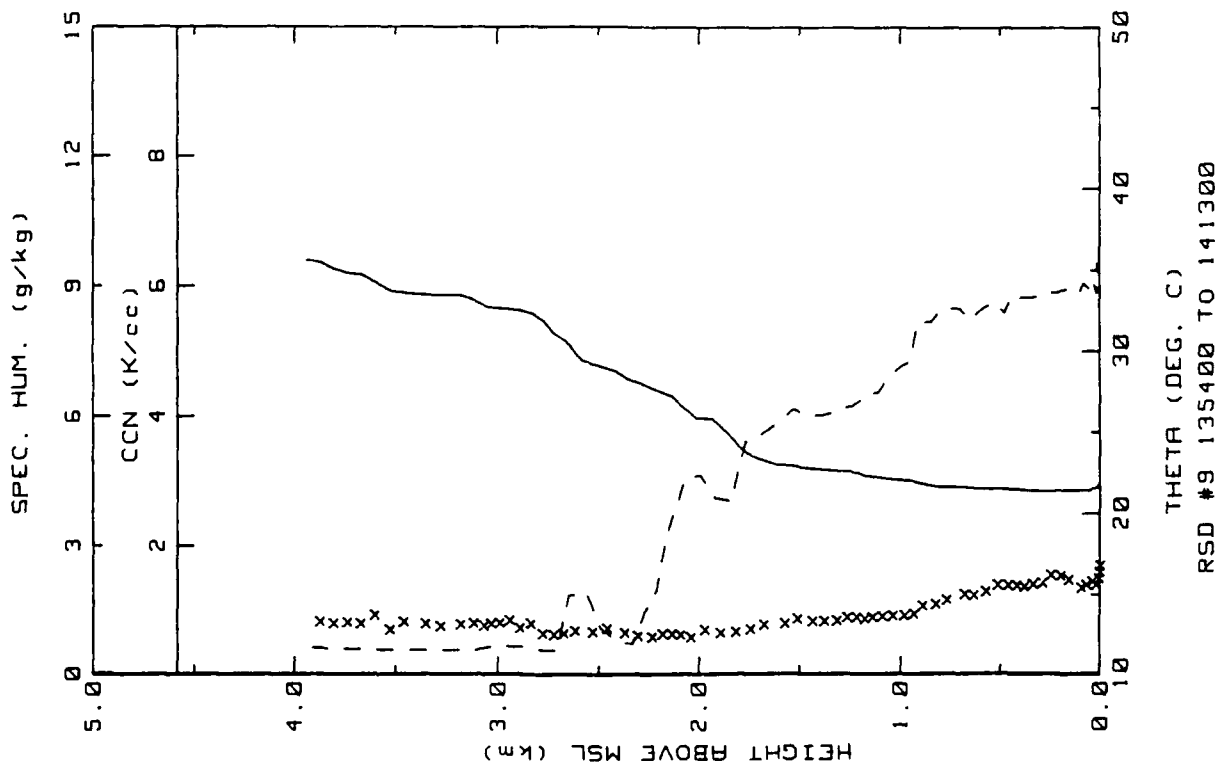


Figure 29n. RSD Flight 9 spiral down-sounding over the Gulf Stream W of Bimini (ref. Fig. 5h).

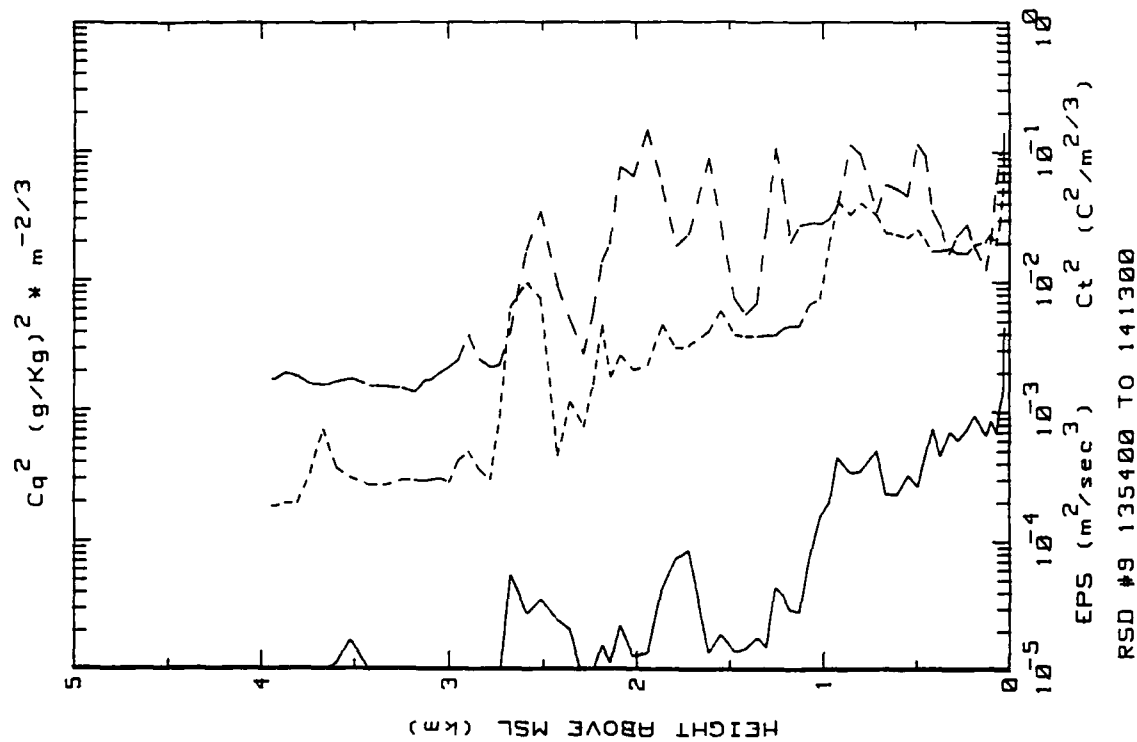


Figure 29o. RSD Flight 9 spiral down-sounding over the Gulf Stream W of Bimini (ref. Fig. 5g).

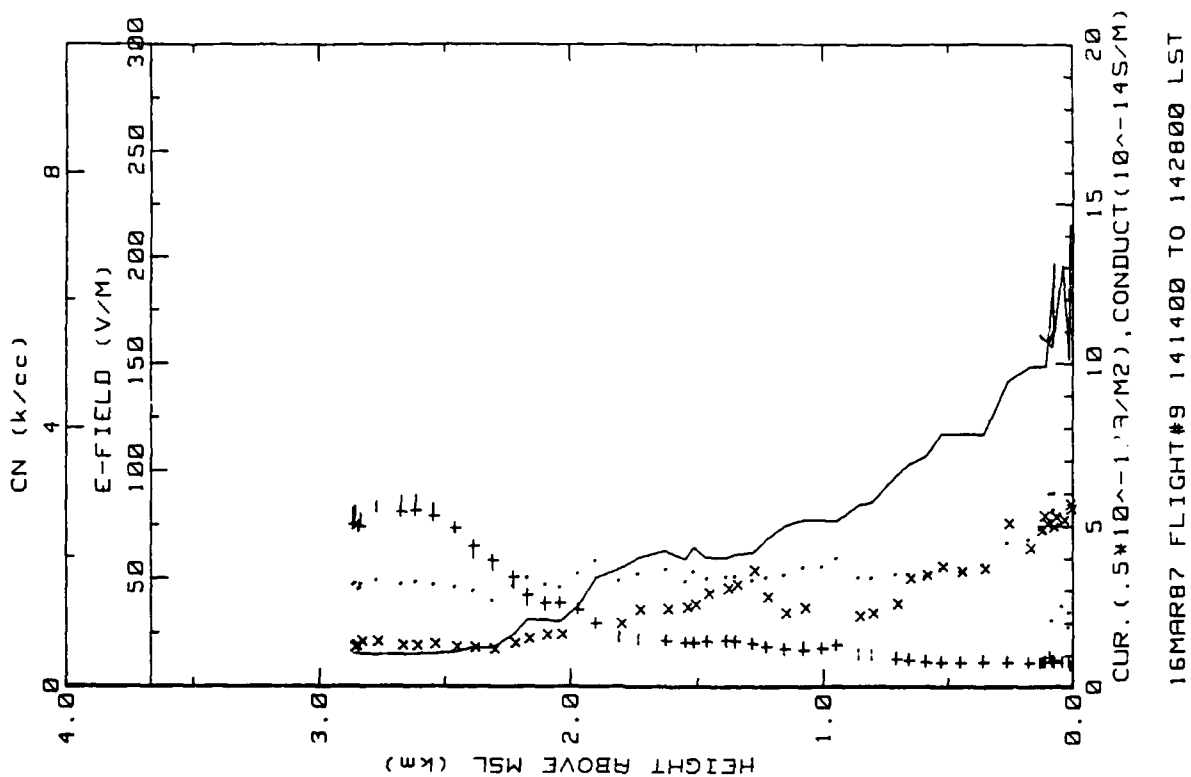


Figure 29p. RSD Flight 9 continuous up sounding between the Gulf Stream and Nassau (ref. Fig. 5e).

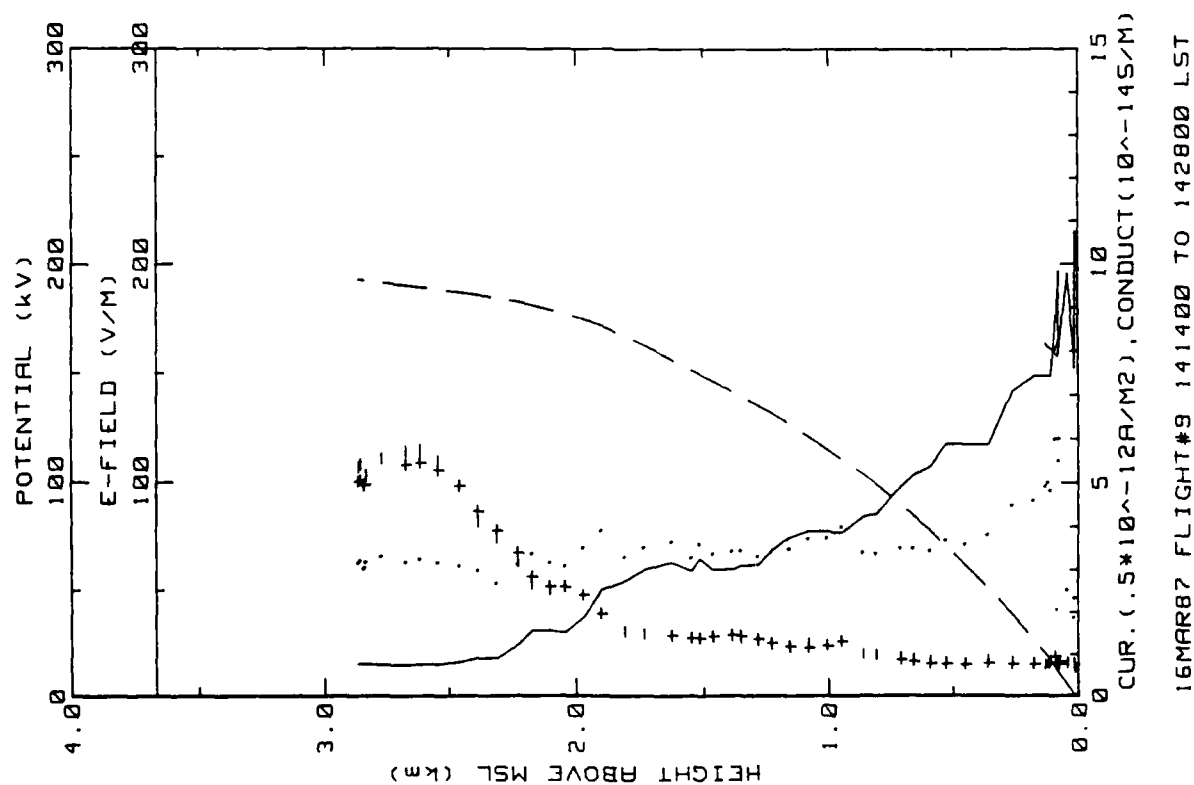


Figure 29q. RSD Flight 9 continuous up sounding between the Gulf Stream and Nassau (ref. Fig. 5f).

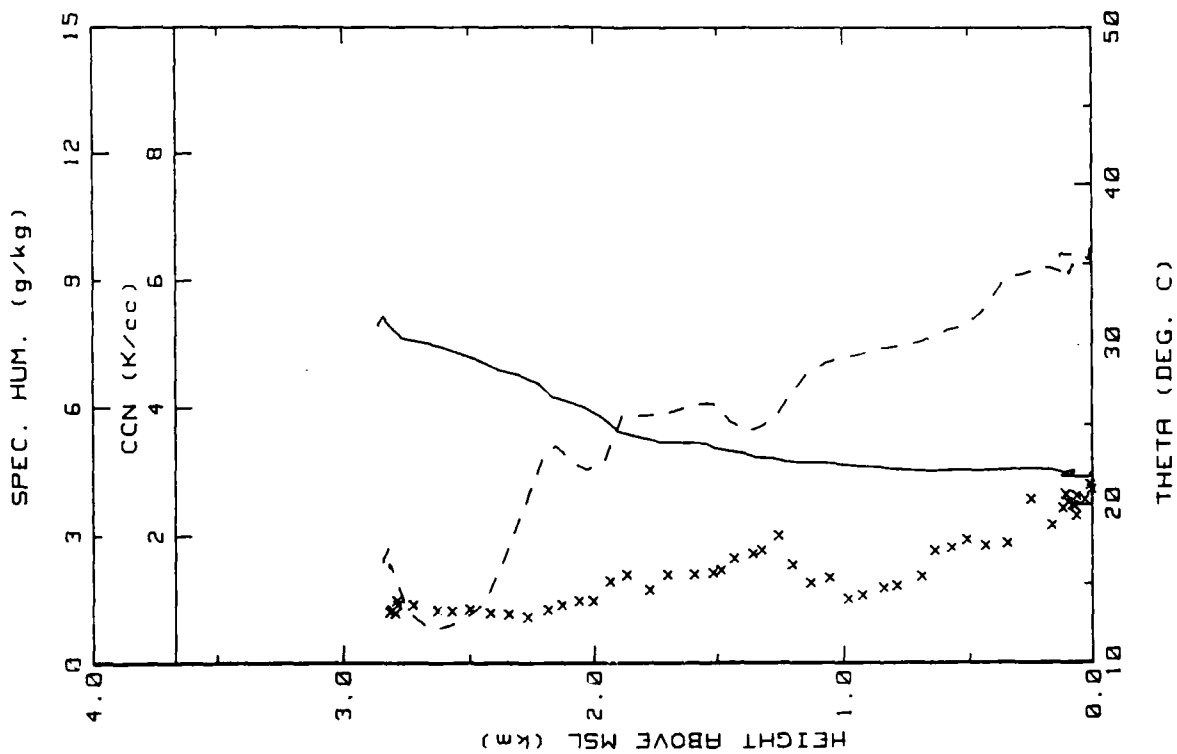


Figure 29r. RSD Flight 9 continuous upsounding between the Gulf Stream and Nassau (ref. Fig. 5h).

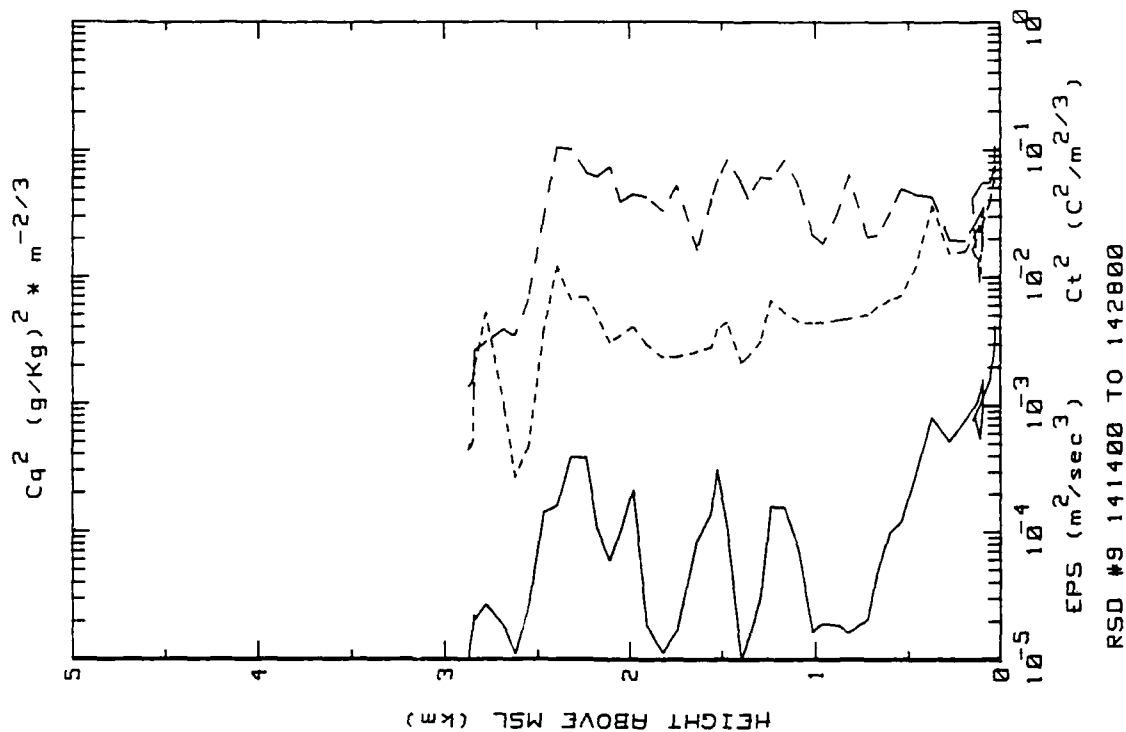


Figure 29s. RSD Flight 9 continuous upsounding between the Gulf Stream and Nassau (ref. Fig. 5g).

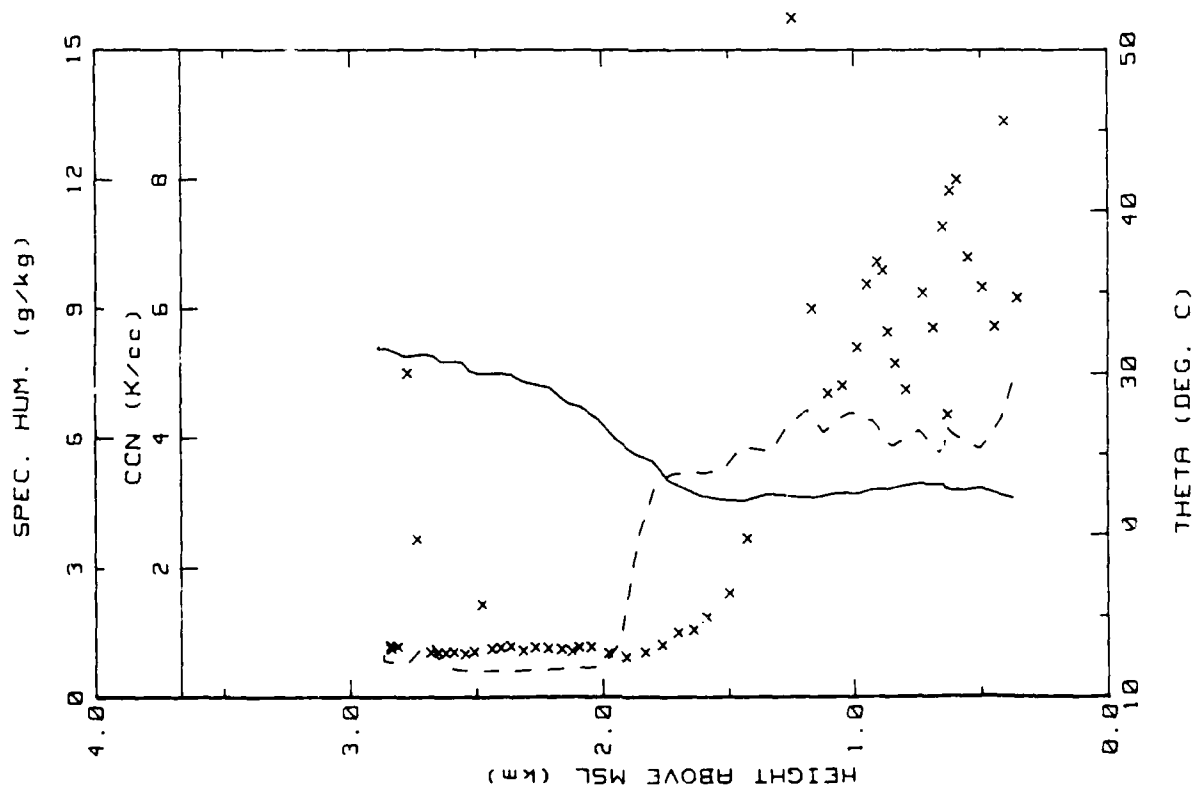


Figure 29t. RSD Flight #9 linear descent into Nassau for landing (ref. Fig. 5h).

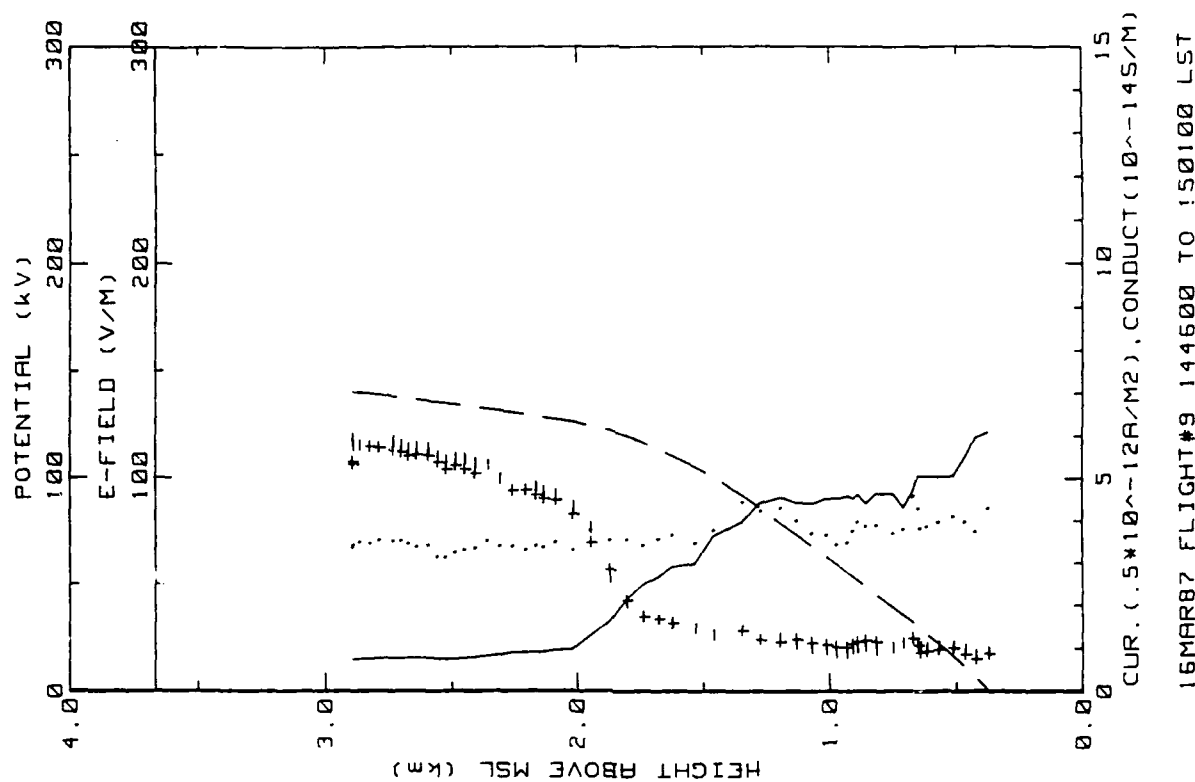


Figure 29u. RSD Flight #9 linear descent into Nassau for landing (ref. Fig. 5e).

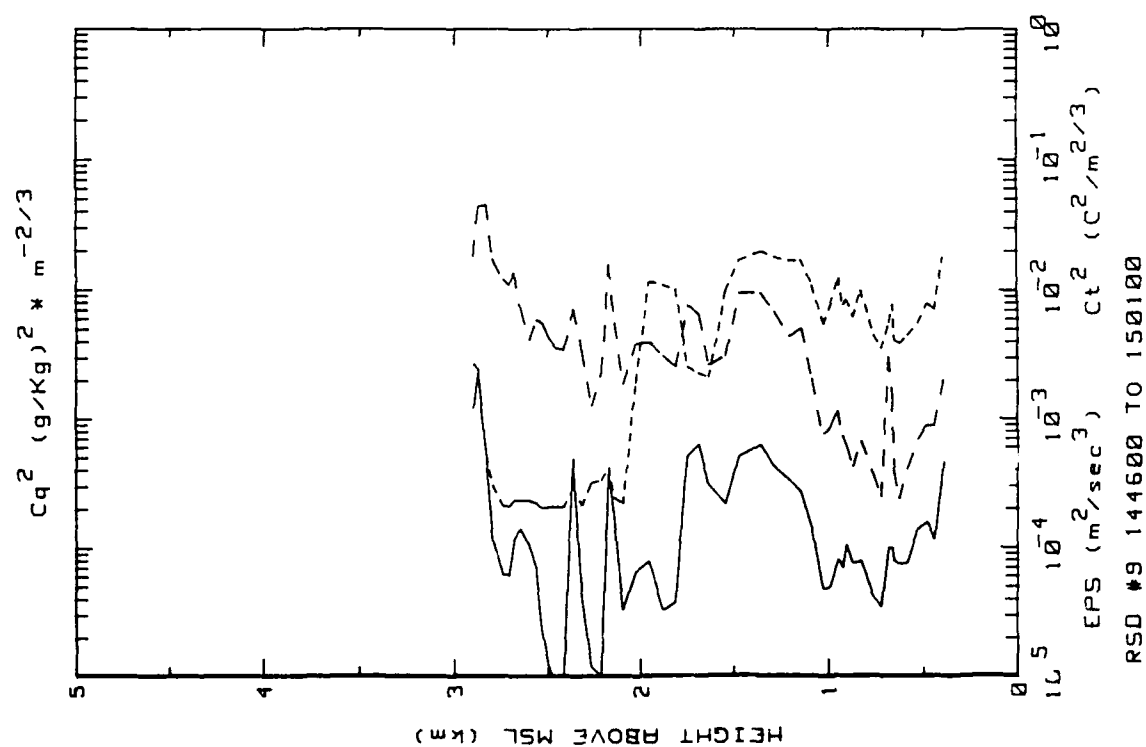


Figure 29v. RSD Flight 9 linear descent into Nassau for landing (ref. Fig. 5g).



THIS PAGE INTENTIONALLY LEFT BLANK

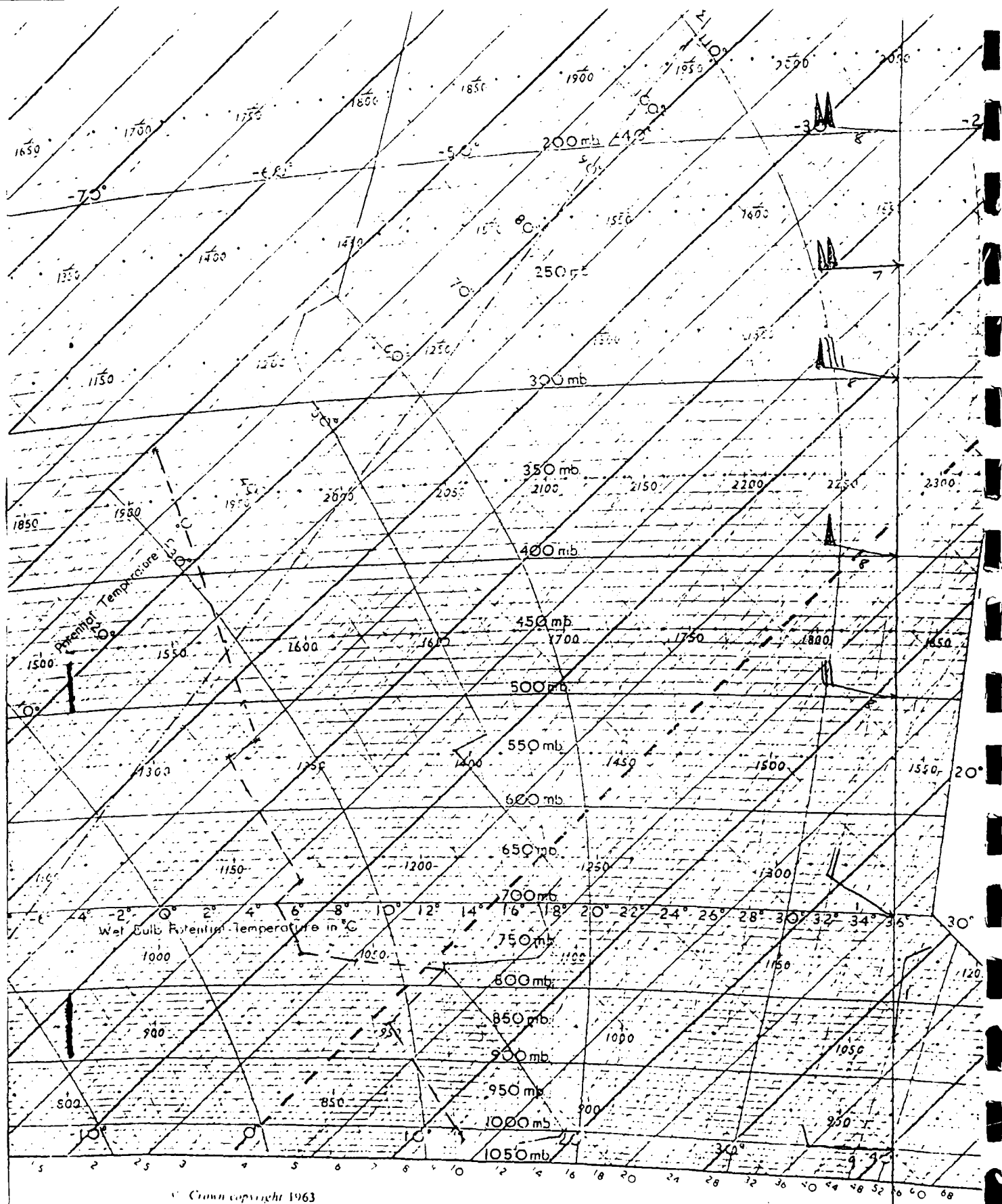


Figure 29w. Meteorological sounding from Nassau, Bahamas, taken on the day of Flight 9 (16 March 1987).

Flight: 10

Date: 16 March 1987

Takeoff: 1615 from Nassau

Landed: 1750 at RSD

Conditions: Clear skies overhead with scattered cumulus to the N and S of the flight path. Winds were from the NE at an estimated 5 m/s. Very few white caps.

Instruments: All worked properly.

Summary: Soundings were obtained on a linear ascent between Nassau and Governors Harbor over shallow water and a spiral descent from 4.1 km E of Eleuthera over deep ocean.

Table 23. RSD Flight 10 averages and standard deviations for constant altitude runs performed just E of RSD.

AVERAGES FROM LEVEL RUNS

Time HH:MM	N	Altitude km	E_field V/m	+Lam 10 <sup>-14</sup>	-Lam 10 <sup>-14</sup>	Con Curr 10 <sup>-12</sup>	Theta_v C	Rel Hum %	CNN k/cc
1706	37	.006	157.93	1.03	.95	2.96	20.9	62.5	1.36
1709	36	.015	160.12	.93	.87	2.93	20.8	62.4	1.15
1712	48	.031	140.26	.99	.91	2.67	20.9	62.4	1.10

Time HH:MM	N	Altitude km	EP3 m2/s3	CT2 C2/m2/3	O g/kg	Co2 (g/kg)2m-2/3	Press mb	Trose C	T_IR C	T_dew C
1706	37	.006	3.83E-03	6.07E-02	8.5	8.37E-02	1011.2	19.3	25.3	11.9
1709	36	.015	1.90E-03	2.30E-02	8.5	4.01E-02	1010.2	19.1	25.0	11.7
1712	48	.031	1.31E-03	8.90E-03	8.5	2.23E-02	1008.2	19.0	24.8	11.6

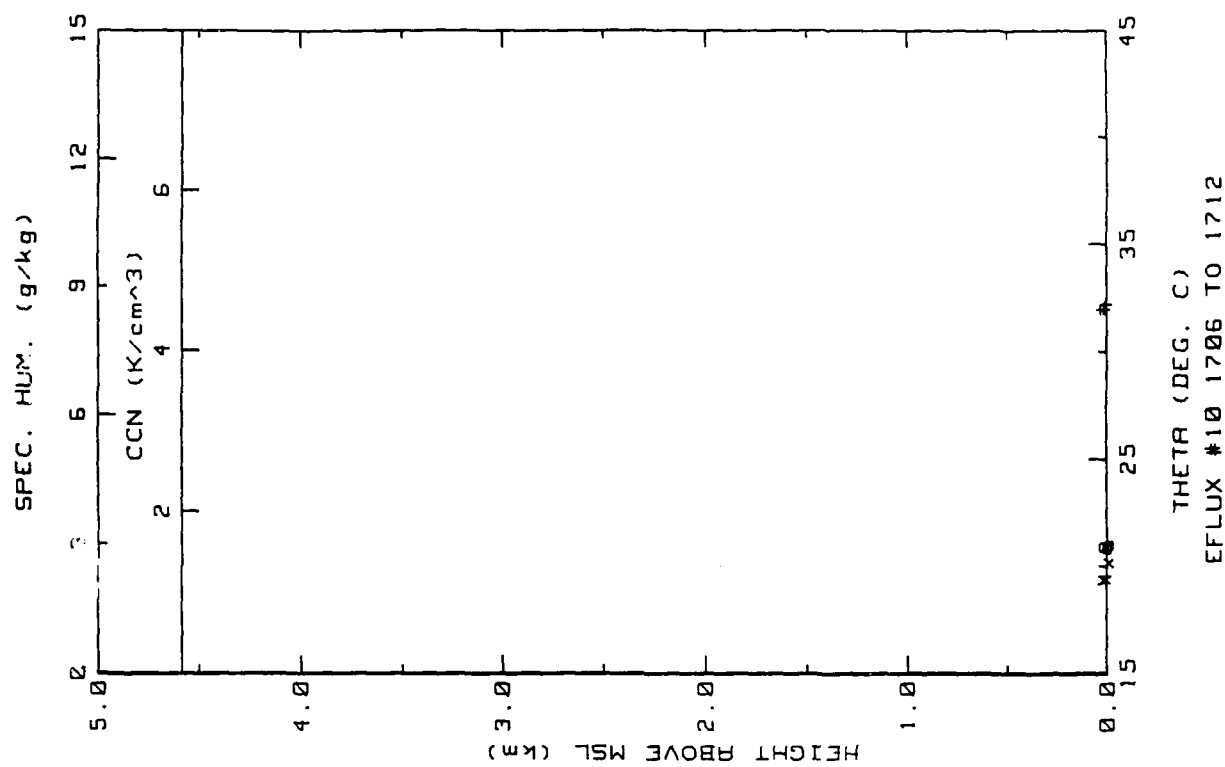


Figure 30a. RSD Flight 10 plot of level runs performed just E of RSD (ref. Fig. 5b).

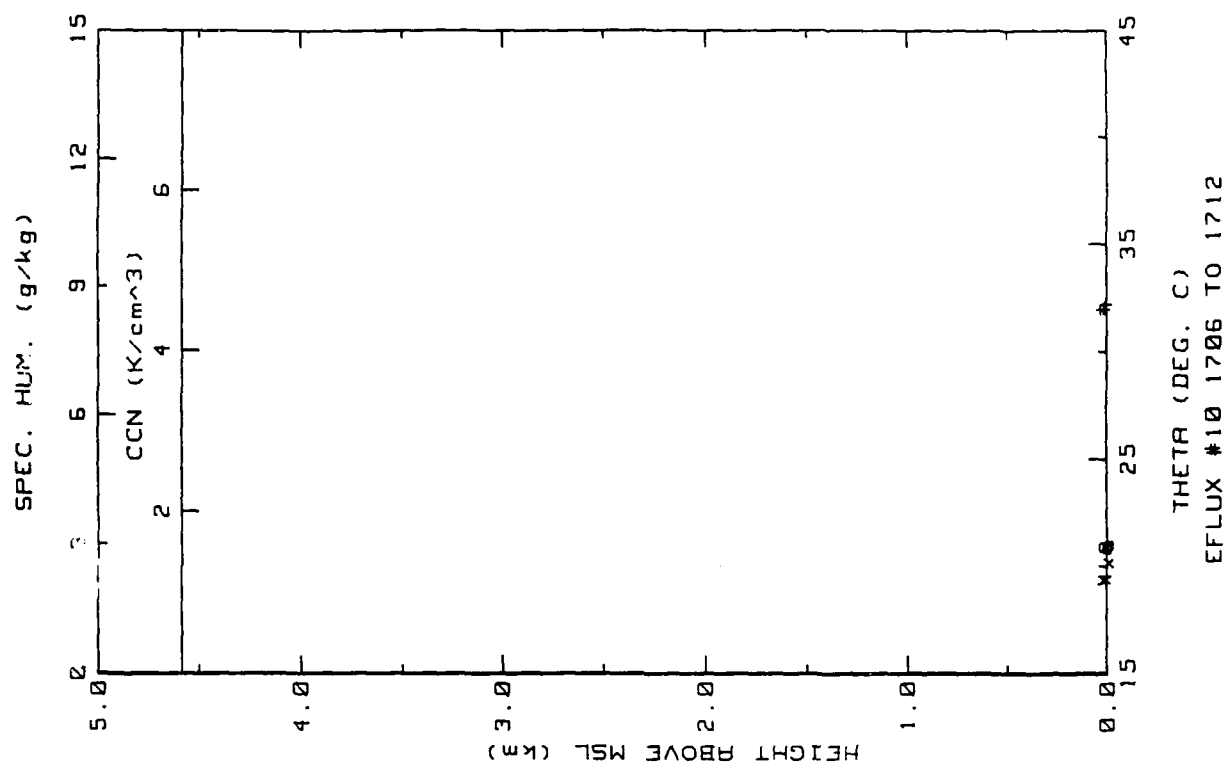


Figure 30b. RSD Flight 10 plot of level runs performed just E of RSD (ref. Fig. 5c).

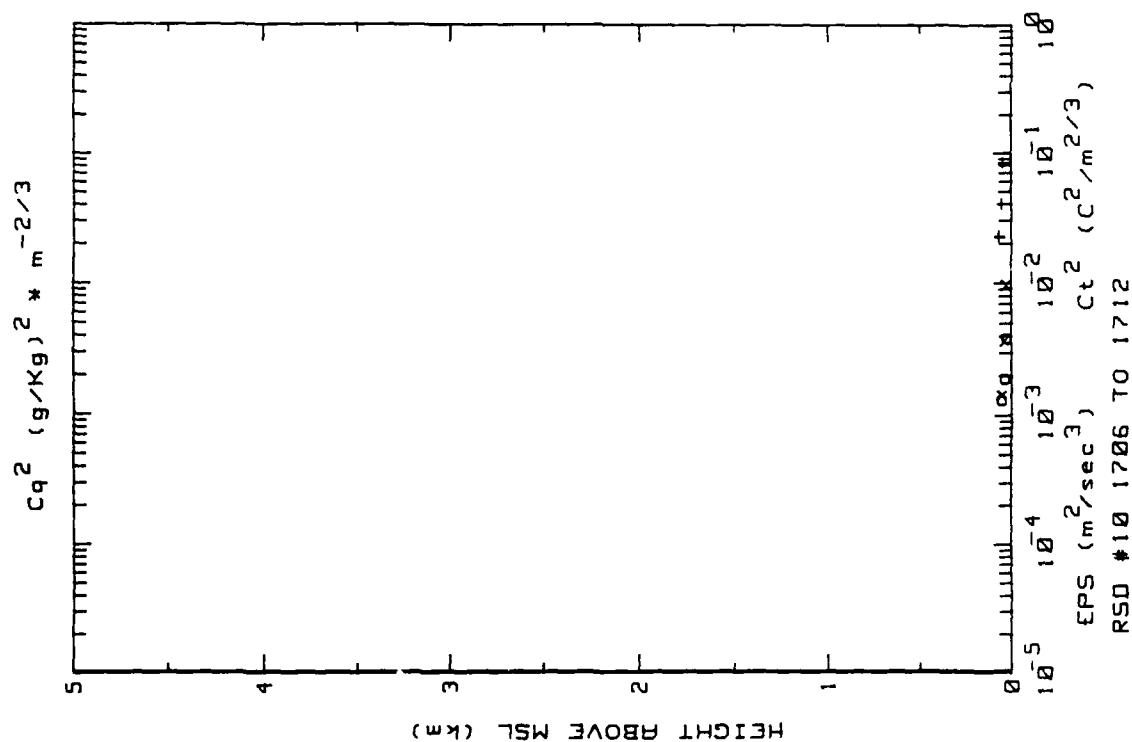


Figure 30c. RSD Flight 10 plot of level runs performed just E of RSD (ref. Fig. 5c).

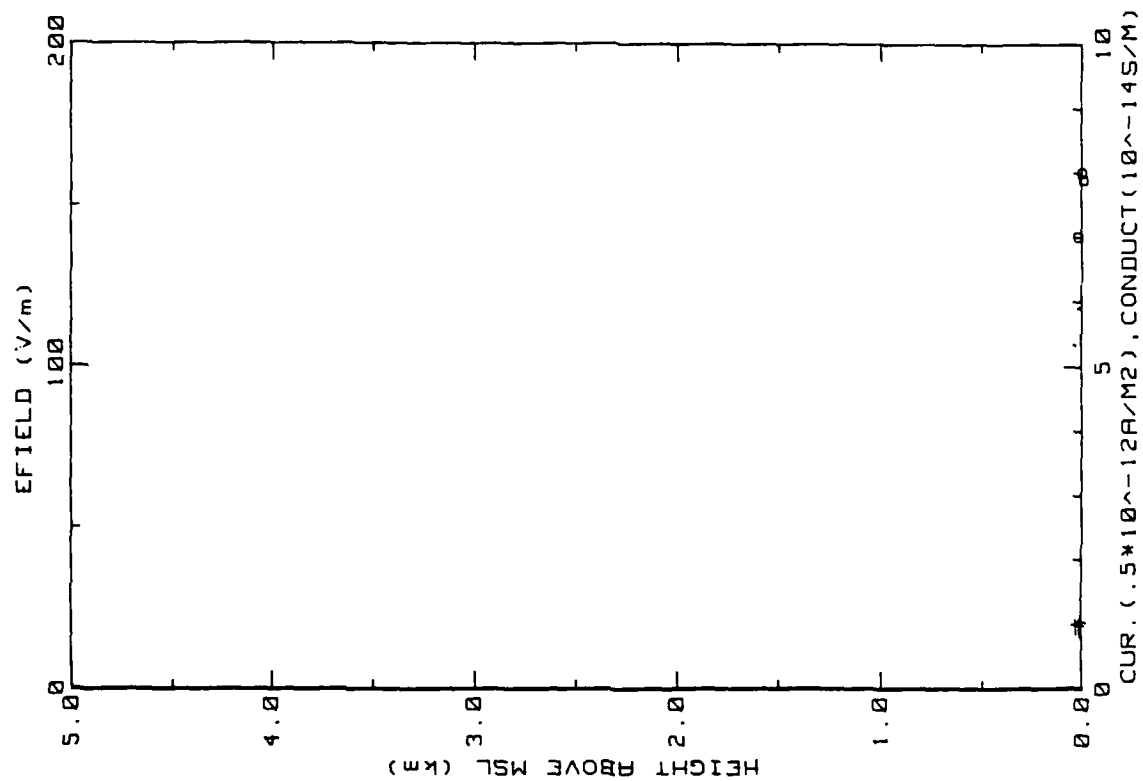


Figure 30c. RSD Flight 10 plot of level runs performed just E of RSD (ref. Fig. 5a).

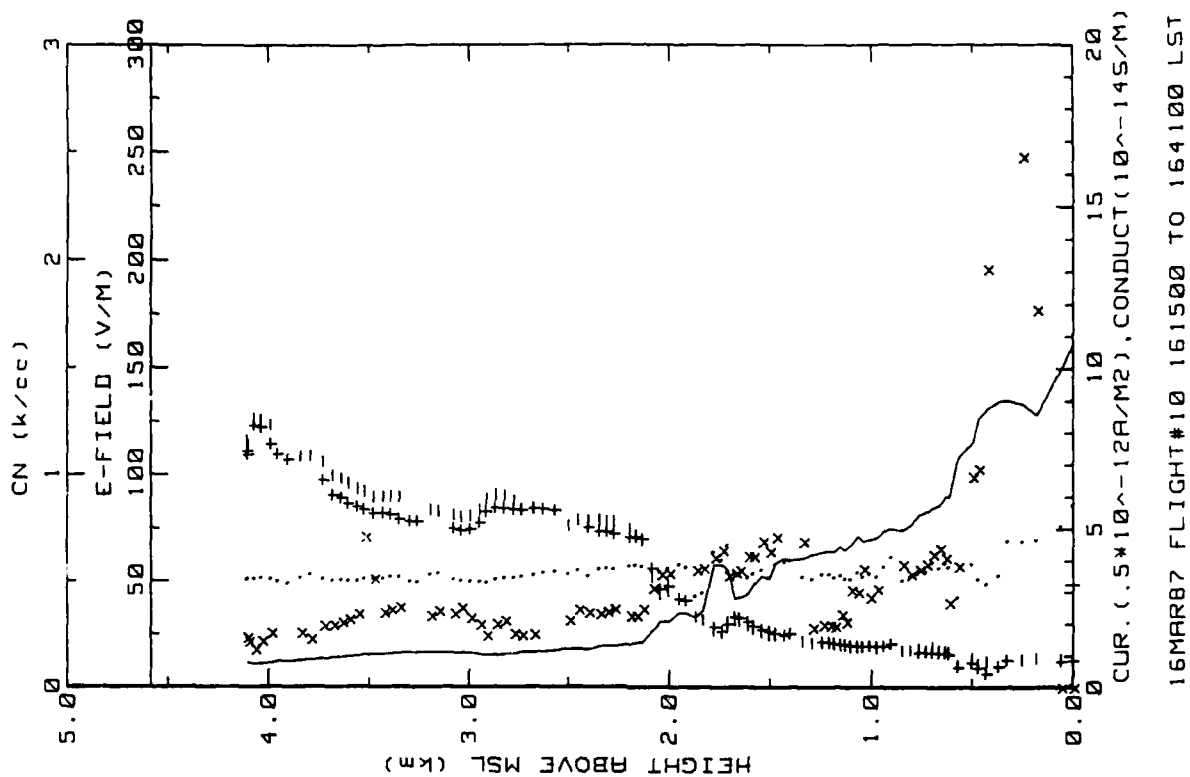


Figure 30d. RSD Flight 10 continuous upsonding between Nassau and RSD over shallow water (ref. Fig. 5e).

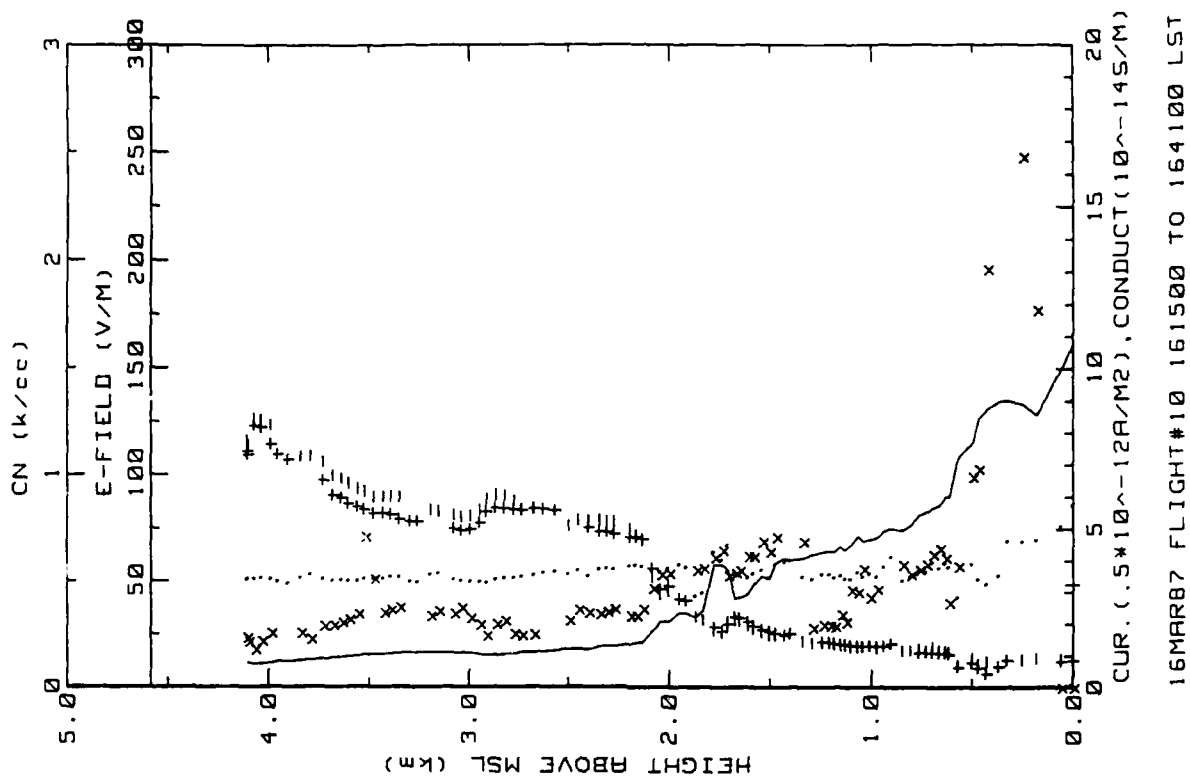


Figure 30e. RSD Flight 10 continuous upsonding between Nassau and RSD over shallow water (ref. Fig. 5f).

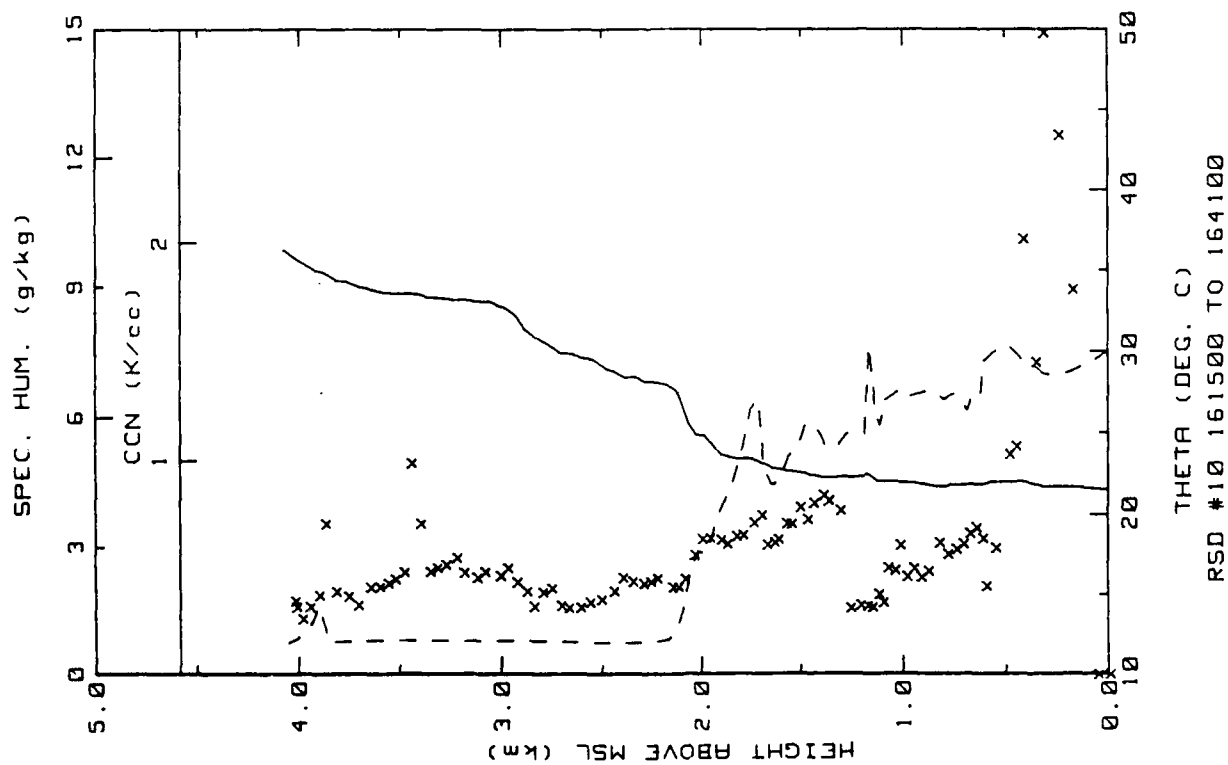


Figure 30f. RSD Flight 10 continuous upsounding between Nassau and RSD over shallow water (ref. Fig. 5h).

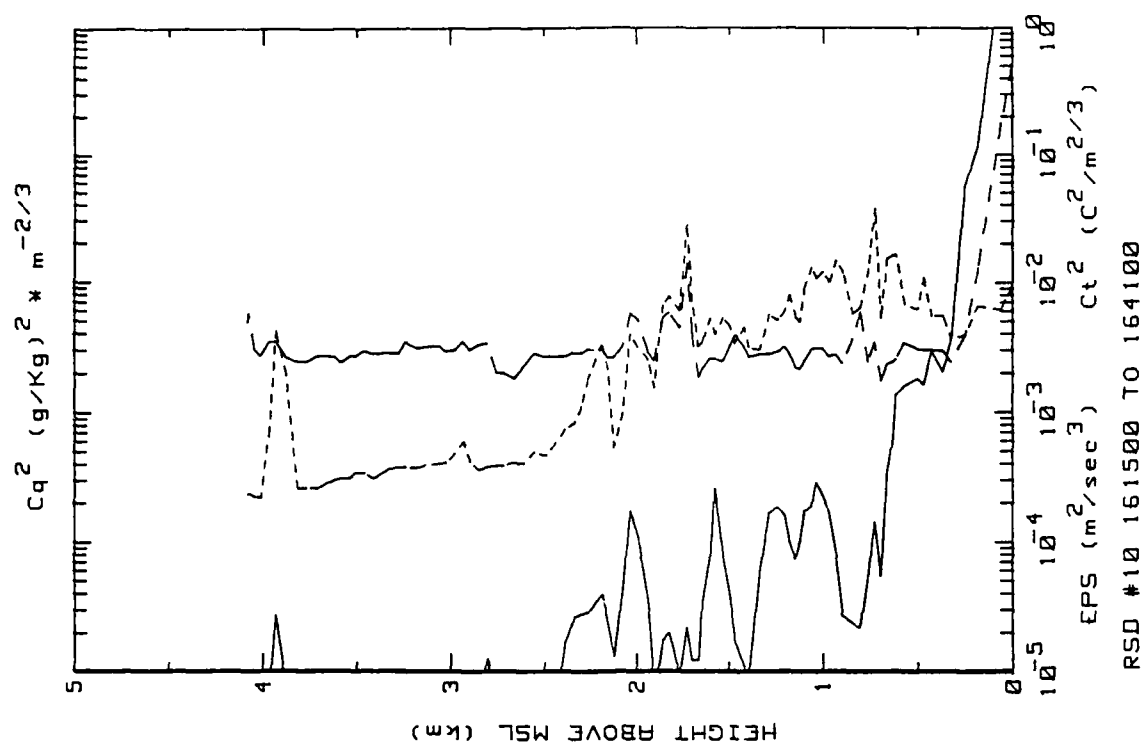
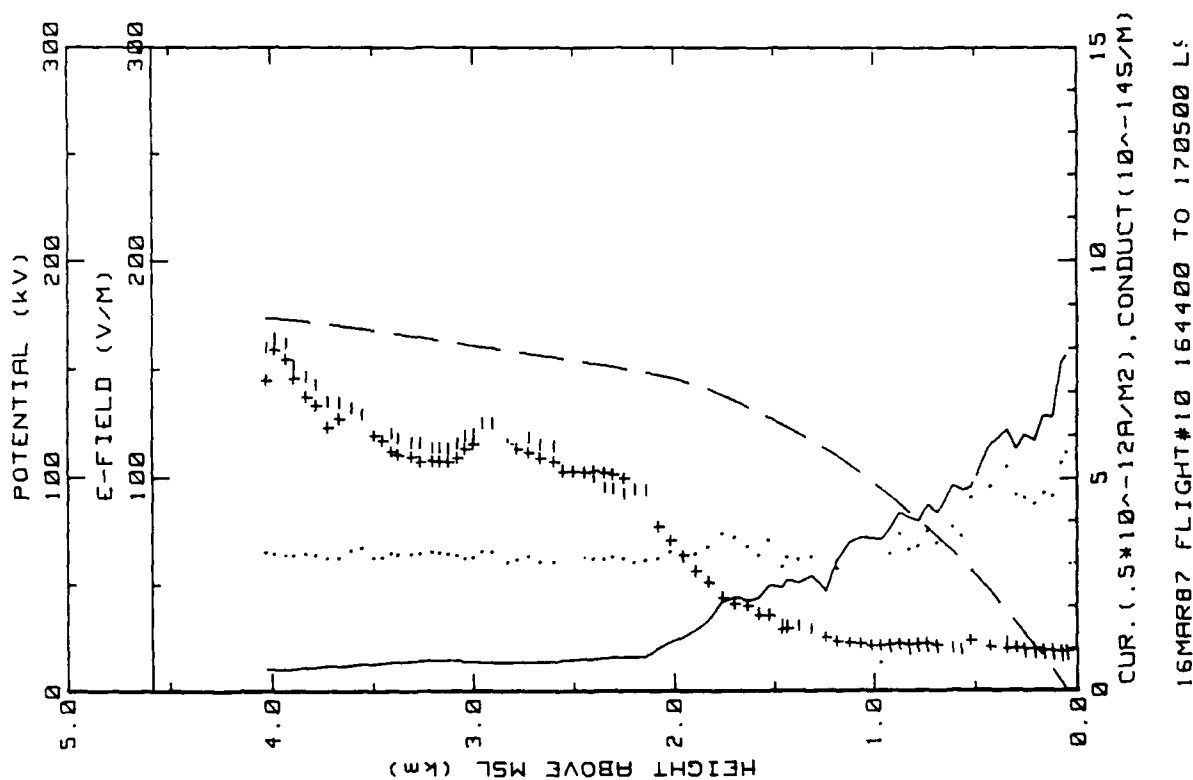
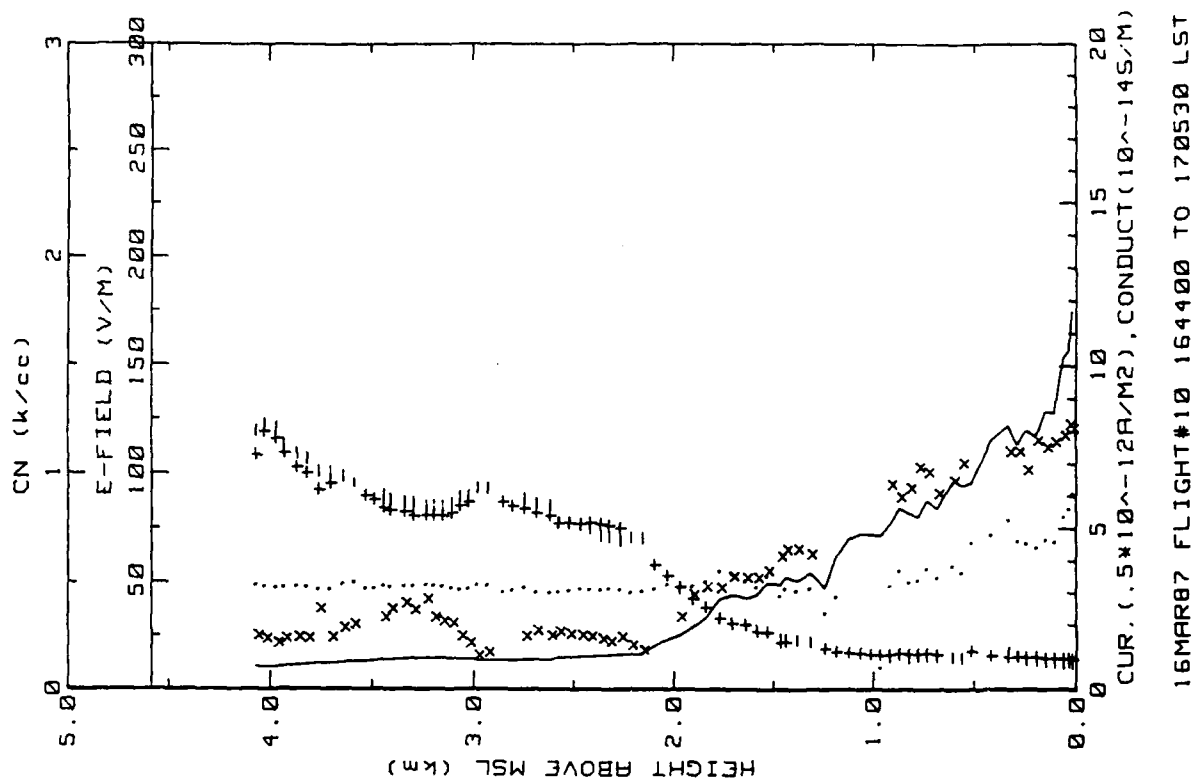


Figure 30g. RSD Flight 10 continuous upsounding between Nassau and RSD over shallow water (ref. Fig. 5g).





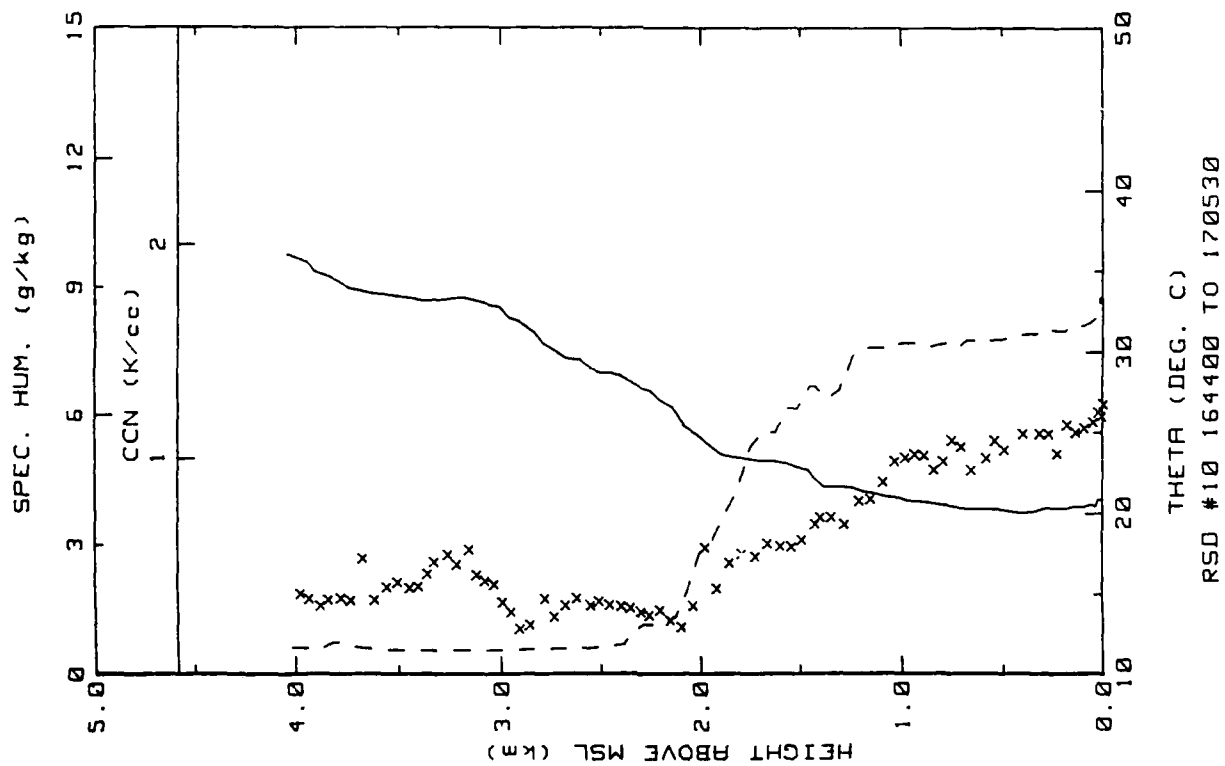


Figure 30j. RSD Flight 10 spiral down sounding just E of RSD (ref. Fig. 5h).

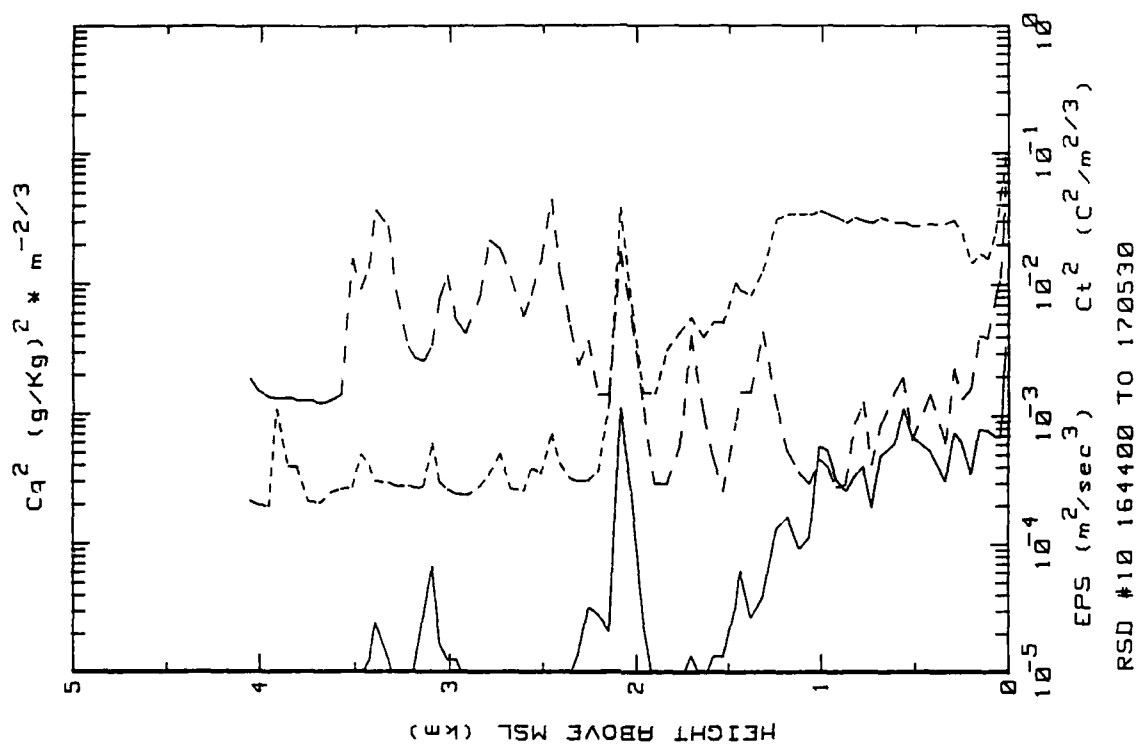


Figure 30k. RSD Flight 10 spiral down sounding just E of RSD (ref. Fig. 5g).

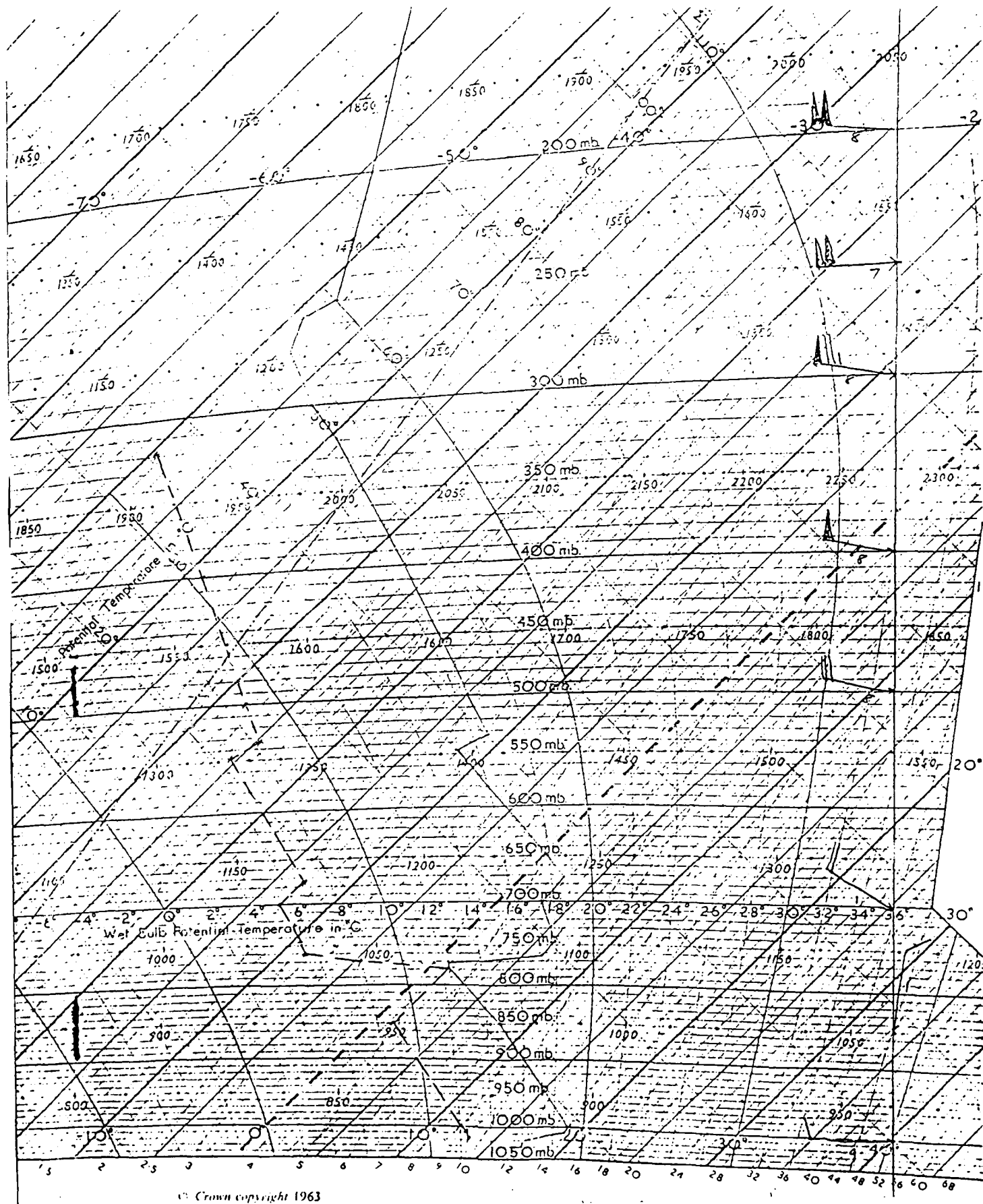


Figure 301. Meteorological sounding from Nassau, Bahamas, taken on the day of Flight 10 (16 March 1987).

Flight: 11

Date: 17 March 1987

Takeoff: 1107 LT from RSD

Landed: 1515 at RSD

Conditions: Clear skies with winds from ENE at 6 m/s (calculated from groundspeed and airspeed measurements); very few whitecaps and ocean swells <1 m.

Instruments: All worked properly.

Summary: Flight consisted of 2 data taking missions; 1) to obtain convection current profiles and 2) to record electric field and humidity fluctuations at various heights to examine the organization of convection. A ladder profile and spiral down sounding were performed recording all instruments over the ocean 40-80 km E of RSD. Then the computer sampling rate was increased to about 2 Hz and only electric field, polar conductivities, humidity fluctuations (passively bandpassed between about 0.1 and 5 Hz) and the epsilon RMS values were recorded. Constant altitude runs were made over the same region sampled earlier, each consisting of a crosswind and an up or downwind leg.

Table 24a. RSD Flight 11 averages for constant altitude runs performed E of RSD over deep water.

AVERAGES FROM LEVEL RUNS

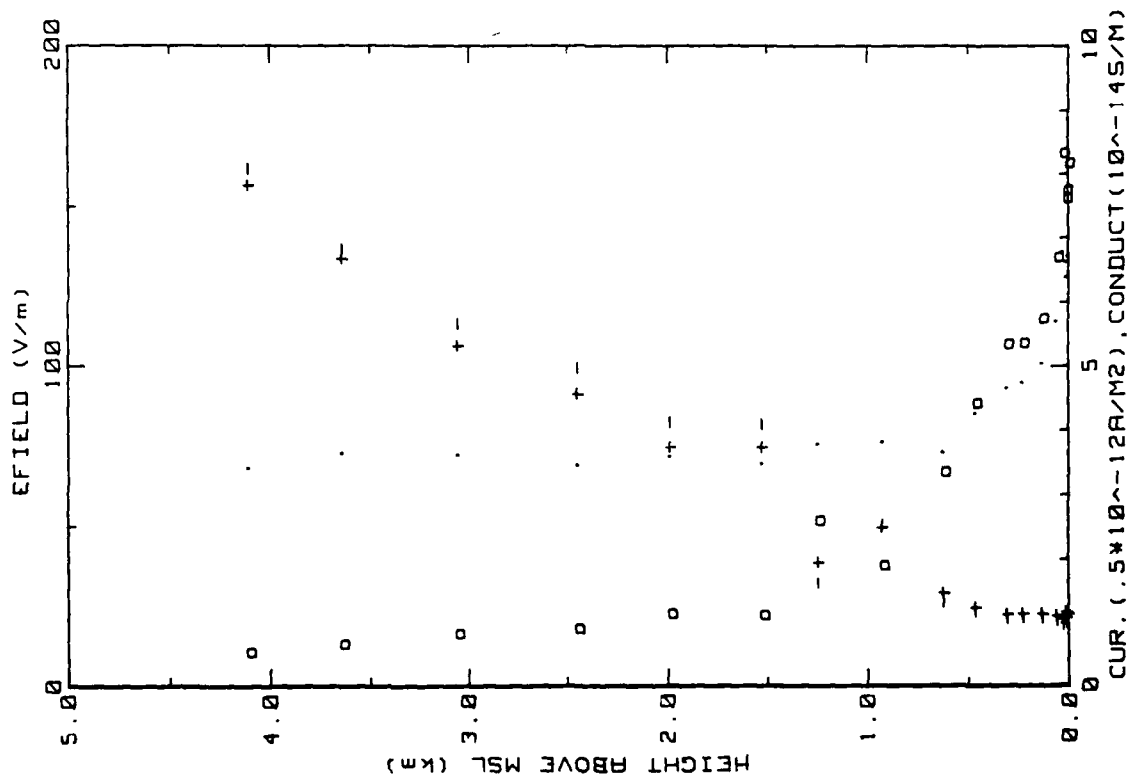
Time HHMM	N	Altitude km	E field V/m	Lam 10 <sup>-14</sup>	-Lam 10 <sup>-14</sup>	Con Curr 10 <sup>-12</sup>	Theta_v C	Rel Hum %	CNN k/cc
1116	47	.006	153.38	1.14	.91	3.36	21.5	55.1	1.44
1124	236	.015	152.32	1.17	1.00	3.31	21.2	54.4	1.46
1135	130	.015	154.94	1.09	.98	3.20	21.4	54.5	1.17
1140	54	.031	135.74	1.05	.93	3.35	21.4	56.2	1.27
1143	111	.061	134.03	1.11	1.03	2.85	21.1	56.7	1.12
1149	41	.133	114.80	1.14	1.07	2.52	20.9	55.8	1.23
1153	51	.229	107.23	1.15	1.07	2.37	21.1	58.2	1.10
1155	51	.303	105.89	1.14	1.06	2.33	21.3	61.0	1.06
1159	49	.462	88.33	1.24	1.16	2.13	21.5	50.2	1.06
1204	59	.620	57.05	1.47	1.32	1.83	21.7	52.4	.89
1207	69	.925	37.97	2.49	2.52	1.91	21.8	22.1	.50
1211	47	1.242	51.95	1.95	1.61	1.85	22.5	47.8	.83
1215	39	1.524	22.56	3.72	4.08	1.74	25.3	9.5	.51
1219	41	1.987	22.92	3.73	4.11	1.75	25.3	11.1	1.00
1223	39	2.448	18.14	4.54	4.55	1.72	30.3	13.0	.57
1225	37	3.056	15.55	5.31	5.35	1.81	32.7	14.6	.44
1230	44	3.542	13.36	6.67	6.81	1.82	34.9	15.2	.40
1234	11	4.107	10.72	7.83	8.08	1.71	36.3	15.4	.41

Time HHMM	N	Altitude km	EPS m2/s3	CT2 C2/m2/3	O g/kg	Co2 (g/kg)2m-2/3	Press mB	Trose C	T_IR C	T_dew C
1116	47	.006	1.07E-03	1.21E-02	7.9	5.79E+00	1010.9	19.9	24.1	10.6
1124	236	.015	5.86E-04	6.27E-03	7.6	3.12E-02	1009.1	19.5	23.8	10.1
1135	130	.015	5.40E-04	6.94E-03	7.7	2.86E-02	1009.0	19.7	23.9	10.2
1140	54	.031	5.89E-04	5.44E-03	7.9	2.34E-02	1007.3	19.5	23.9	10.6
1143	111	.061	4.15E-04	3.09E-03	7.5	1.05E-02	1001.5	18.8	23.9	10.0
1149	41	.133	3.41E-04	2.73E-03	7.3	9.33E-03	997.3	18.3	23.9	9.3
1153	51	.229	2.50E-04	2.82E-03	7.4	5.86E-03	986.2	17.5	23.8	9.2
1155	51	.303	2.27E-04	3.09E-03	7.5	8.74E-03	977.3	16.9	23.9	9.4
1159	49	.462	4.71E-04	4.77E-03	7.0	5.60E-02	959.5	15.9	23.9	8.0
1204	59	.620	2.50E-04	4.84E-03	6.8	1.96E-02	941.9	14.5	24.1	7.3
1207	69	.925	3.25E-05	3.30E-03	2.2	8.70E-03	908.7	12.4	24.2	-9.0
1211	47	1.242	2.09E-04	5.06E-03	4.1	1.71E-02	875.0	9.7	24.3	-9.9
1215	39	1.524	5.89E-06	2.21E-03	.5	3.65E-04	845.9	10.2	24.4	-20.7
1219	41	1.987	1.37E-05	2.00E-03	1.0	1.96E-03	793.9	9.4	24.1	-19.3
1223	39	2.448	1.32E-05	1.95E-03	1.0	3.91E-04	756.1	5.8	24.3	-20.6
1225	37	3.056	7.29E-06	3.53E-02	.3	2.28E-04	701.4	2.1	24.6	-22.2
1230	44	3.542	1.02E-05	3.87E-02	.3	1.56E-04	651.7	-1.7	24.8	-24.8
1234	11	4.107	1.41E-05	1.20E-01	.7	3.24E-04	614.3	-5.0	24.8	-27.3

Table 24b. RSD Flight 11 (standard deviations)/averages for  
constant altitude runs performed E of RSD over deep  
water.

STANDARD DEVIATIONS/MEAN VALUES

Time	E_Field	+Lam	-Lam	Con Curr	CON	EPS	CT2	Q	Co2
1116	.129	.076	.106	.149	.052	.317	.280	.050	6.769
1124	.160	.054	.068	.161	.114	.337	.332	.053	.415
1135	.130	.066	.071	.122	.188	.432	.391	.053	.574
1140	.103	.070	.062	.139	.147	.323	.270	.044	.406
1143	.142	.052	.057	.132	.051	.360	.331	.046	.406
1149	.059	.022	.044	.058	.381	.445	.289	.039	.472
1153	.036	.046	.039	.070	.043	.332	.135	.027	.250
1155	.043	.053	.035	.054	.094	.492	.176	.039	.360
1159	.061	.091	.124	.118	.124	.734	.453	.077	1.056
1204	.093	.107	.152	.128	.153	.517	.267	.108	.607
1207	.071	.079	.107	.043	.087	.913	.253	.255	1.420
1211	.097	.092	.062	.069	.091	.560	.319	.105	.705
1215	.018	.018	.034	.036	.325	.329	.142	.014	.159
1219	.035	.027	.034	.010	.119	.316	.255	.077	.722
1223	.019	.017	.019	.019	.153	.313	.232	.028	.389
1226	.068	.070	.063	.010	.256	.187	2.018	.031	.080
1230	.040	.020	.027	.017	.199	1.379	.406	.055	.121
1234	.018	.005	.006	.021	.094	.904	.776	.013	.532



17MAR87 FLIGHT#11 1116 TO 1234 LST

Figure 31a. RSD Flight 11 ladder profile over deep water  
E of RSD (ref. Fig. 5a).

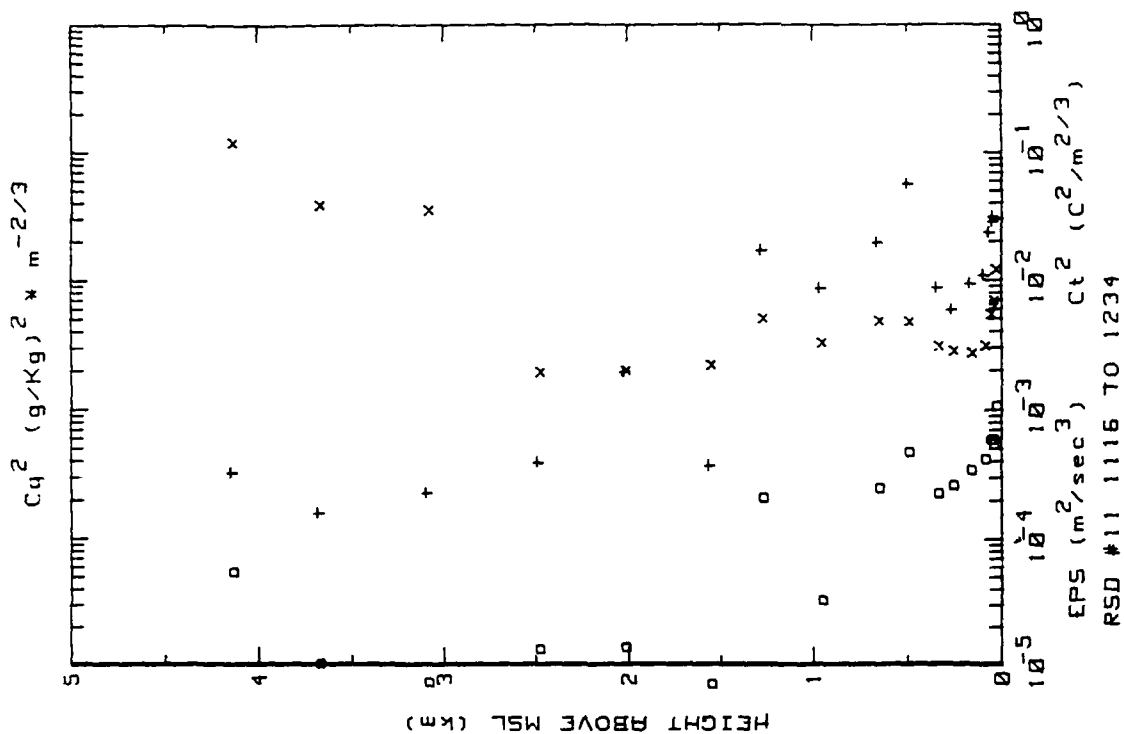


Figure 31b. RSD Flight 11 ladder profile over deep water  
E of RSD (ref. Fig. 5b).

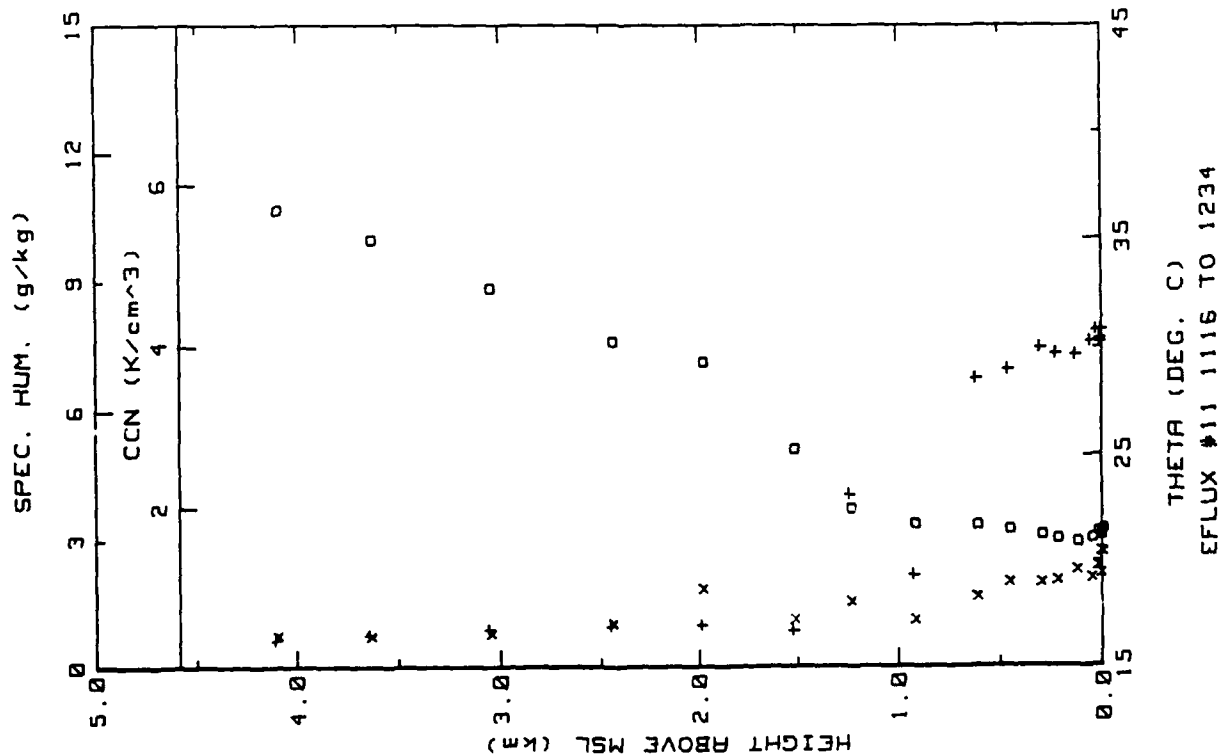


Figure 31c. RSD Flight 11 ladder profile over deep water E of RSD (ref. Fig. 5c).

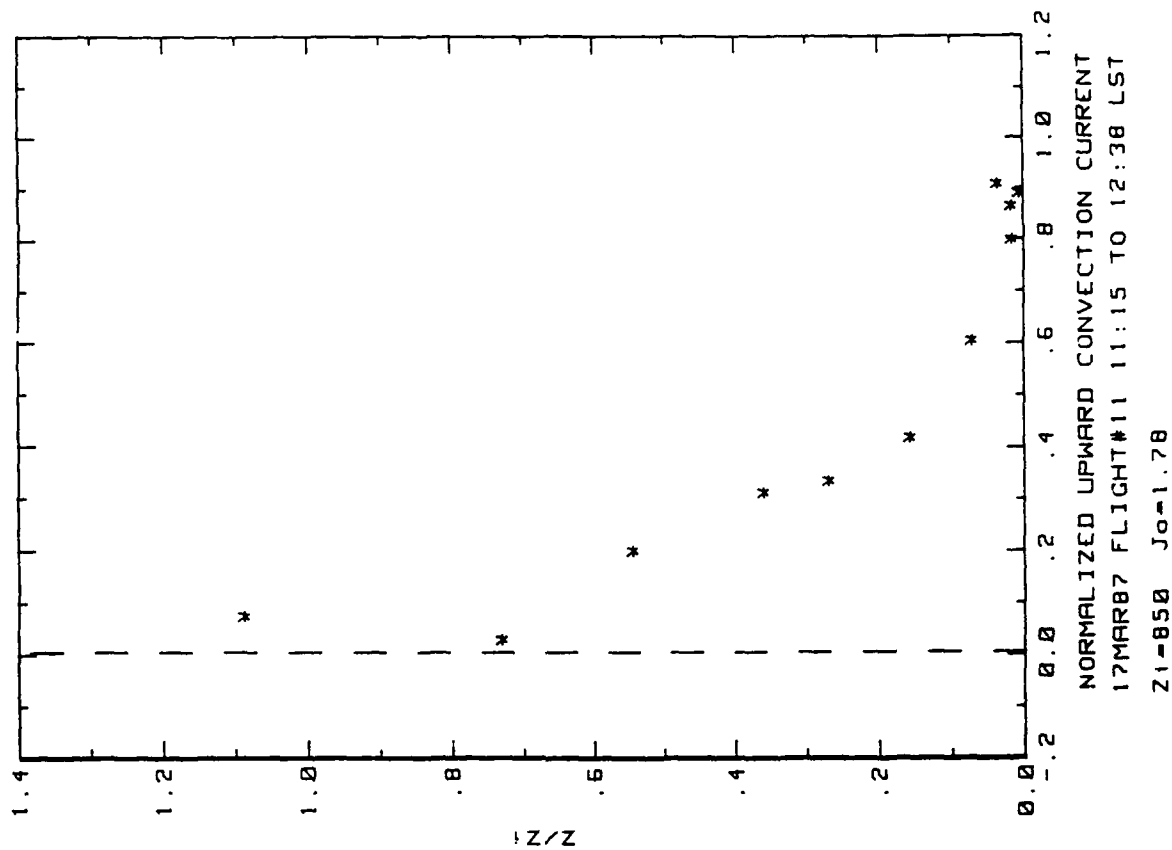


Figure 31d. RSD Flight 11 convection current profile over deep water E of RSD (ref. Fig. 5d).



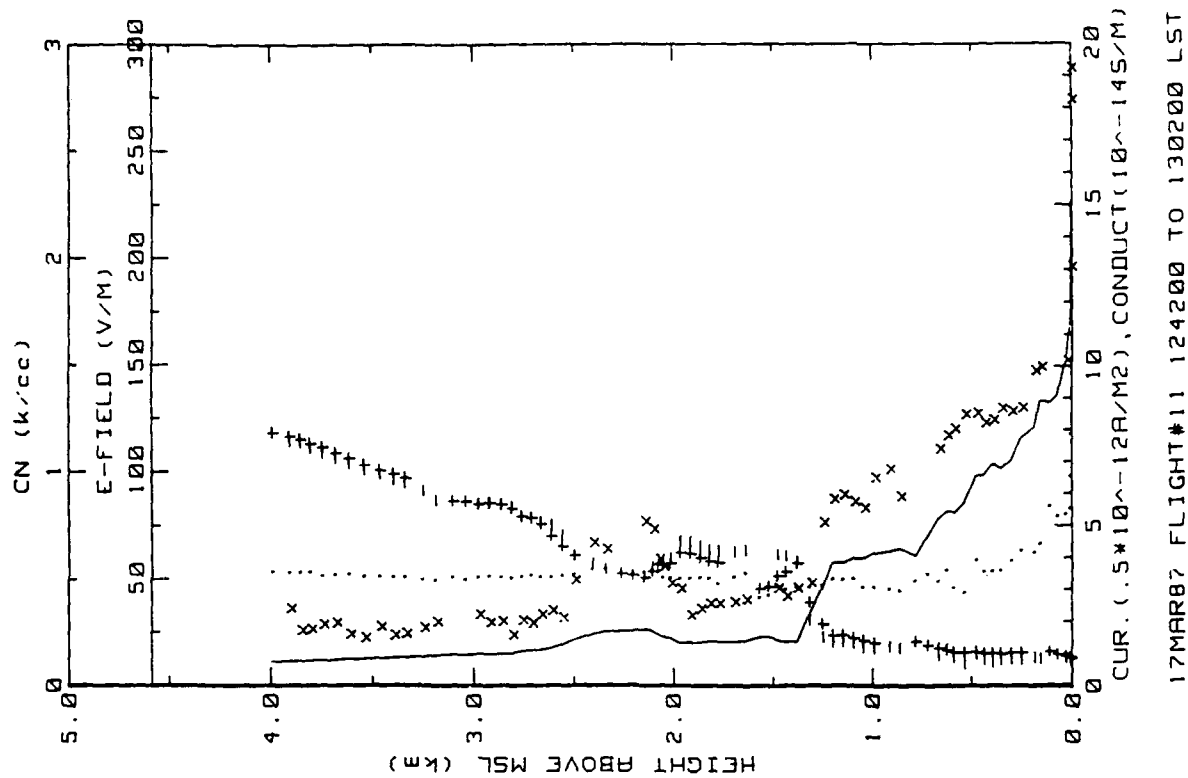


Figure 31f. RSD Flight 11 spiral down-sounding over deep water E of RSD (ref. Fig. 5f).

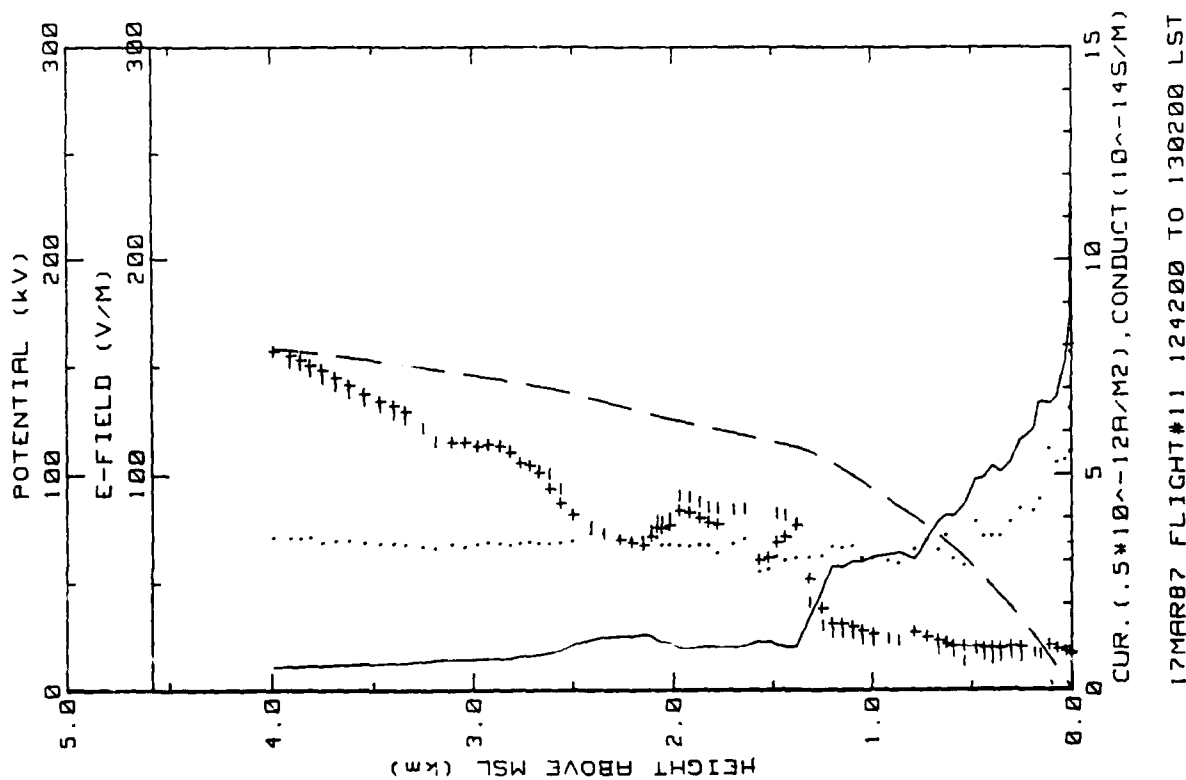


Figure 31e. RSD Flight 11 spiral down-sounding over deep water E of RSD (ref. Fig. 5e).

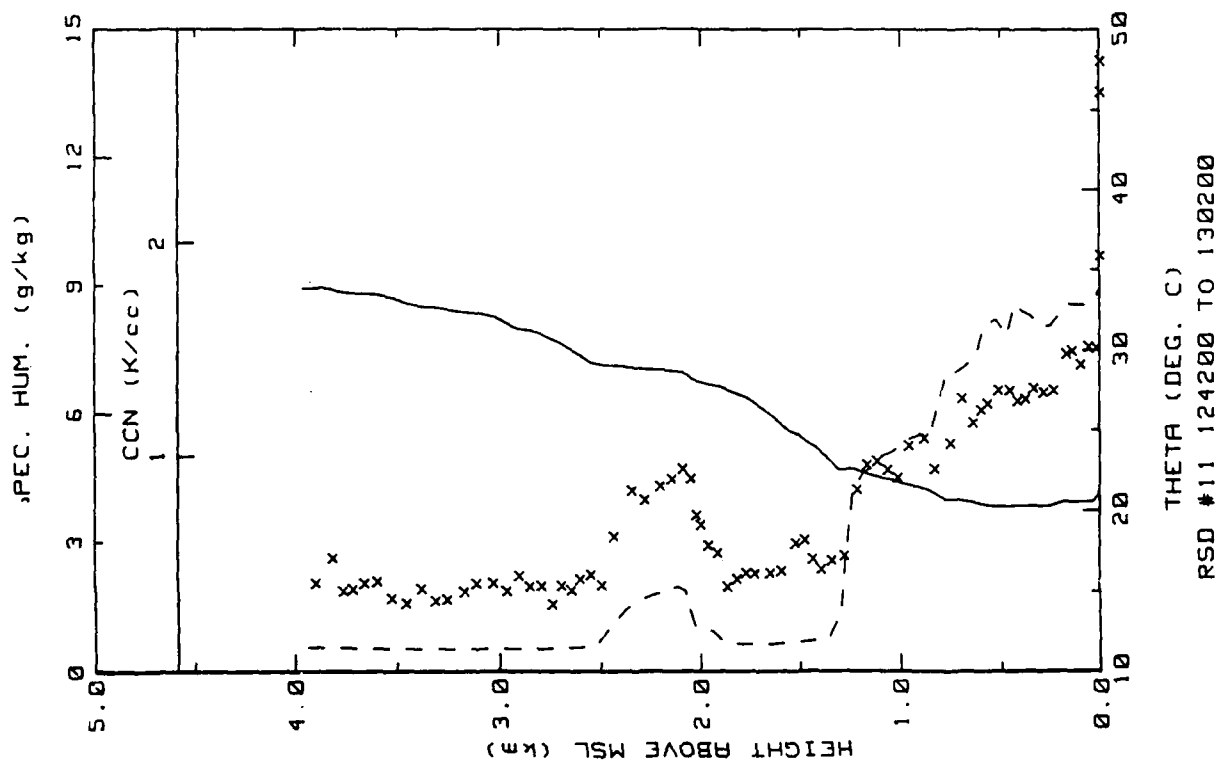


Figure 31g. RSD Flight 11 spiral down sounding over deep water E of RSD (ref. Fig. 5h).

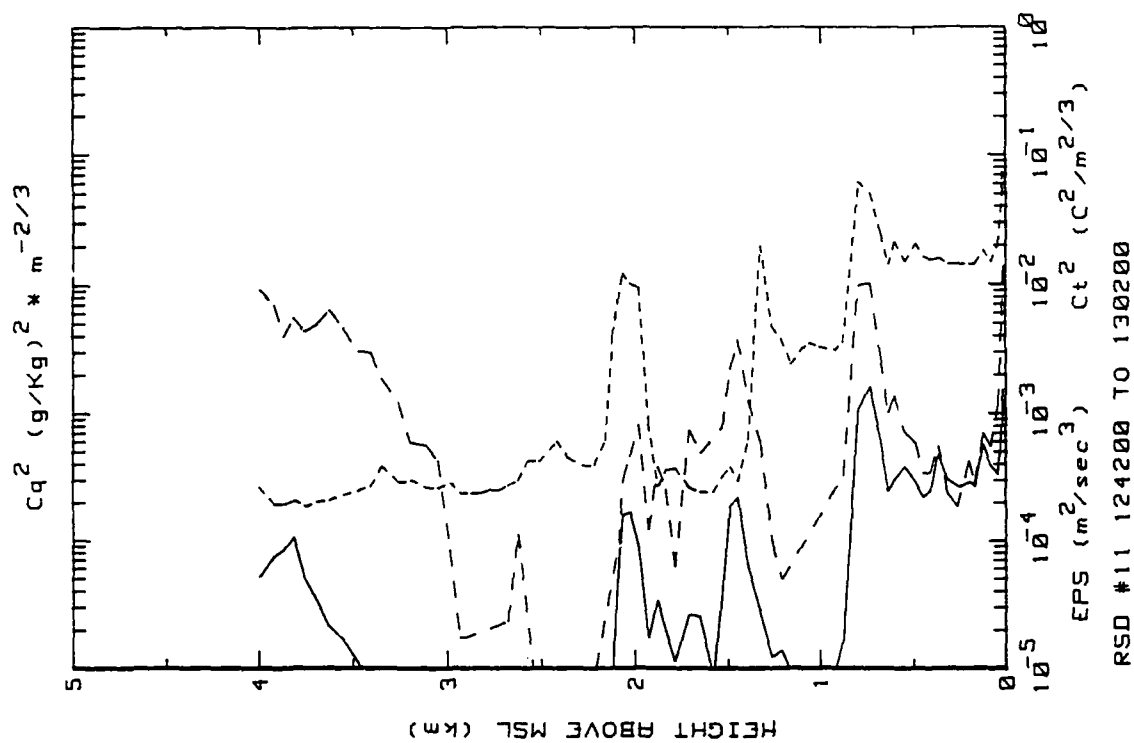


Figure 31h. RSD Flight 11 spiral down sounding over deep water E of RSD (ref. Fig. 5g).

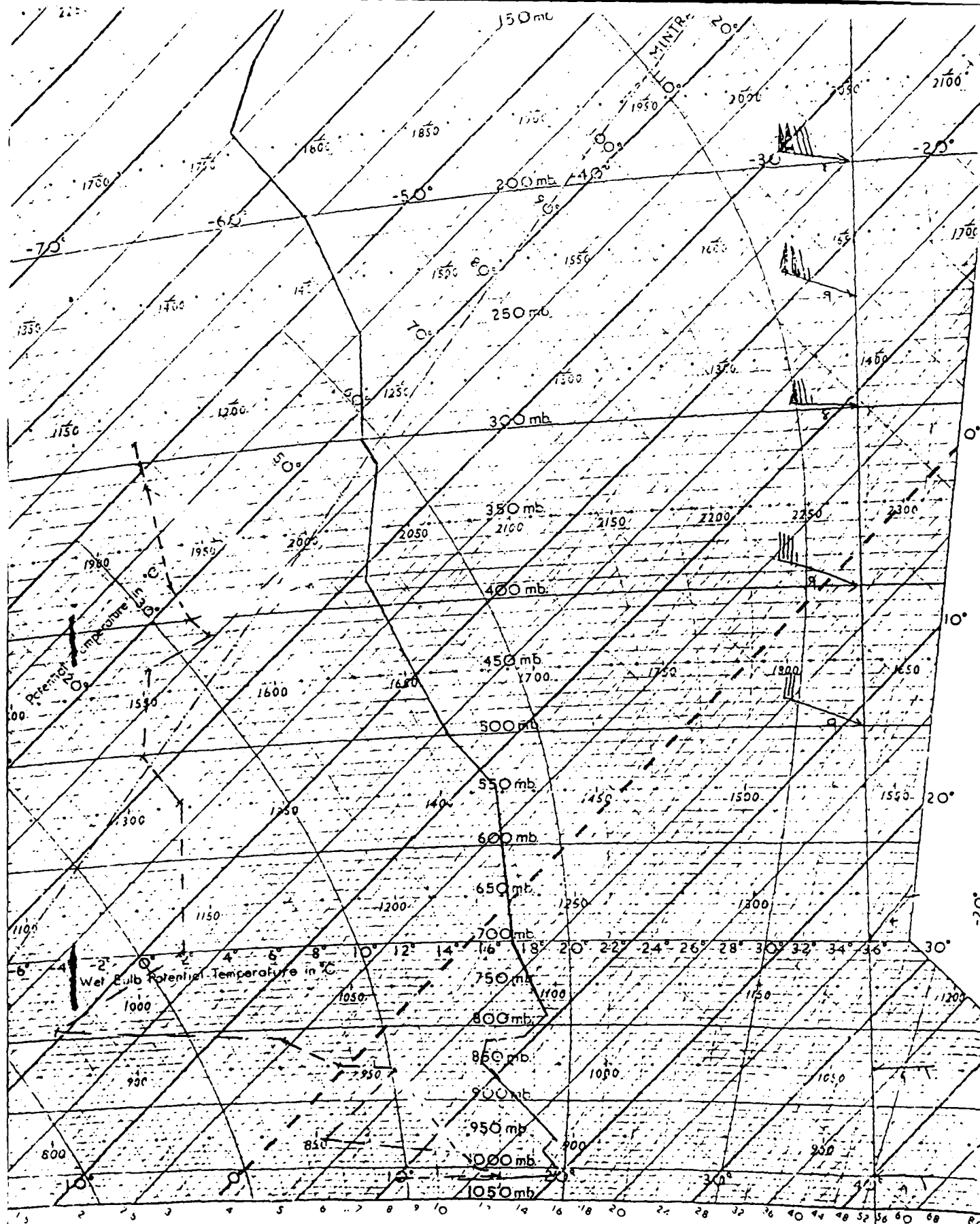


Figure 31i. Meteorological sounding from Nassau, Bahamas, taken on the day of Flight 11 (17 March 1987).

## VI. DATA SUMMARIES AND CONVECTION CURRENT PROFILES

This section contains summaries of turbulence, electrical, and model parameters for each flight in both deployments in addition to plots of convection current profiles. Definitions of symbols and references to pages where they are discussed are presented in Table 25. Parameters pertinent to evaluating the charge transport model calculated from ladder profile data can be found in Tables 26 and 27. Electrical parameters determined from spiral soundings are emphasized in Tables 28 and 29 and convection current profiles from both field deployment are presented in Figures 32 through 48.

As was indicated above, Tables 26 and 27 list values for parameters necessary for testing Willett's turbulent transport model. Data are only provided for flights where valid convection current profiles were obtained.

Table 26 lists results from the desert flights. The given times are when the aircraft was at 15 m height in the neighborhood of the ground station, either initiating or ending a ladder profile. Wind directions are from observations made by John Willett while operating the ground station and wind speeds were measured with an anemometer at 2 m height. Since there was some uncertainty in the aircraft determinations of  $\epsilon$ , the surface scaling parameters were calculated from ground station measurements (note the suffix "gs") using the dissipation method. Aircraft measurements of  $\epsilon$  were in most cases a factor of 3 to 4 larger than ground station values. We suspect a faulty RMS unit aboard the aircraft may have caused this problem and similar difficulties in determining  $C_T^2$  in the ocean flights.

Table 27 displays results from the ocean deployment. The listed times correspond to when the aircraft was 15 m above the surface either beginning or ending a ladder profile. Wind directions are from aircraft observations while the speeds were calculated from the surface friction velocity ( $u_*$ ) and surface drag coefficients. (Speeds calculated in this manner were generally within 10% of those observed from the aircraft.) Since there was some uncertainty in the  $C_T^2$  and  $C_q^2$  measurements in this

deployment, the listed temperature and humidity surface scaling parameters are those calculated using the bulk aerodynamic technique, hence the "\_blk" suffix. When  $C_T^2$  values were divided by 3,  $T_s$  values determined from the dissipation method were comparable in magnitude to those resulting from bulk calculations.

The aerosols values presented in Tables 26 and 27 have been corrected using the data of Figure 4. Since the calibration was performed prior to the experiment, the range of particle densities could not be anticipated. Therefore, some parts of the curve involve generous interpolation which could lead to errors in determining aerosol concentrations. This would have a deleterious effect on the calculated volume ionization rates and small ion lifetimes as well.

Two new variables,  $R_I$  and  $V_I$ , are introduced in Tables 28 and 29. Columnar resistance,  $R_I$ , was calculated from conductivity using the following equation:

$$R_I \text{ (ohm m}^2\text{)} = \int_0^{\text{apogee}} (\lambda_+ + \lambda_-)^{-1} dz + h (\lambda_+ + \lambda_-)^{-1}_{\text{apogee}}$$

where  $h$  is the electrical scale height (Gish, 1944) at the flight apogee and terms subscripted "apogee" denote measurements taken at the maximum flight altitude. The second term in the above equation accounts for the resistance between the top of the sounding and the ionosphere and in most of the data presented, represents less than 10% of  $R_I$ .

Ionospheric potential,  $V_I$ , was found from integrating the electric field and extrapolating it to the ionosphere as illustrated below:

$$V_I \text{ (Volts)} = \int_0^{\text{apogee}} E dz + h E_{\text{apogee}}$$

where, again,  $h$  is the electrical scale height at the maximum flight altitude. The second term contributed around 10% to typical  $V_I$  determinations. The data presented in this section uses the convention that fair weather electric fields are negative, thus  $V_I$  is negative.

Assuming Ohm's law to be operative in the atmosphere,  $V_1 = J_0 R_1$ . This, however, is true only in the absence of convection current. The ratio  $R_1 J_0 / V_1$  (convective factor, C.F.) when subtracted from 1 gives the fractional decrease of  $J_0$  due to convection. Tables 28 and 29 present values of C.F. for each spiral; a further discussion of its significance can be found in Appendix B.

Convection current profiles from the desert deployment are illustrated in Figures 32 through 39. These plots are only provided for the flights listed in Table 26.  $J_c$  values were calculated from averages of level runs (see data tables for individual flights) and were normalized using the  $J_0$  values listed in the table. The altitudes have been normalized by dividing each height by the boundary layer thickness,  $Z_1$ . Similar profiles for the ocean flights listed in Table 27 are presented in Figures 40 through 48.

Table 25. Summary of symbols used in Section VI tables.

<u>Variable</u>	<u>Definition</u>	<u>Units</u>	<u>ref. page</u>
$u_s$	Surface scaling parameter for velocity.	m/s	21
$T_s$	Surface scaling parameter for temperature.	°C	21
$q_s$	Surface scaling parameter for humidity.	g/Kg	21
$Z_i$	Boundary layer thickness.	m	20
$\tau_{lam}$	Electrical relaxation time.	s	19
Aerosols	Large particle concentration.	$m^{-3}$	12
$J_o$	Conduction current density.	pA/m <sup>2</sup>	18
$\hat{J}_{mx}$	Electrode effect efficiency factor.	-	18
$\hat{V}$	Dimensionless potential drop across the boundary layer.	-	19
$L$	Monin-Obukhov length.	m	22
$\tau_n$	Small ion lifetime.	s	19
$q$	Volume ionization rate.	$m^{-3}s^{-1}$	19
$R$	Dimensionless potential drop.	-	22
$-Z_i/L$	Convective scaling factor.	-	22
$\lambda_{tot}$	Total conductivity	$ohm^{-1}m^{-1}$	11
$RI$	Columnar resistance extrapolated to the ionosphere	$ohm m^2$	285
$VI$	Integrated electric field extrapolated to the ionosphere	V	285
C.F.	Convection Factor = $R_I J_o / V_I$	-	286

Table 26. Electrical, meteorological and model parameters from flights conducted over the desert near Hobbs, NM.

Flight	Date	Time @sfc (LT)	Wind Dir	Wind Speed (m/s)	U* gs (m/s)	-T* gs (C)	Zi (m)	tau lam (s)	Aerosols (1/m <sup>3</sup> )	-Jo (pA/m <sup>2</sup> )
4-1	5/18/86	1055	N	5	0.50	0.72	1300	189	2.0E+09	3.40
5-1	5/18/86	1610	N-NE	5	0.42	0.72	2300	216	2.7E+09	2.71
11-1	5/24/86	1202	NE-SE	3.4	0.37	0.78	900	284	2.3E+09	2.25
12-1	5/27/86	1704	N-NE	4.2	0.40	0.36	1500	183	2.0E+09	3.00
13-1	5/27/86	1755	N-NE	4	0.40	0.25	1400	159	1.9E+09	3.00
14-1	5/28/86	1005	SE-W	2.5	0.30	0.67	1400	257	3.2E+09	2.20
	5/28/86	1112	SE-W	2.8	0.34	0.79	1400	314	1.4E+10	1.90
15-1	5/28/86	1435	SE-SW	3.3	0.42	0.71	1900	466	1.0E+10	1.30
	5/28/86	1547	S-SW	3.4	0.35	0.66	1900	546	9.8E+09	1.30
16-1	5/29/86	0528	NE-E	2.3	0.24	0.15	400	227	2.3E+09	2.00
	5/29/86	0532	NE-E	2.3	0.24	0.15	400	221	1.7E+09	2.00
	5/29/86	0554	NE-E	2.1	0.19	0.12	400	221	1.7E+09	2.00
	5/29/86	0600	E	1.8	0.16	0.12	400	221	1.7E+09	2.00
	5/29/86	0640	E	2.3	0.22	0.11	400	221	1.7E+09	2.00
Averages.....					0.32	0.45	1143	266	4.1E+09	2.22

Flight	Date	Time @sfc (LT)	-Jo pA/m <sup>2</sup> )	Jmx	V	-L (m)	tau n (s)	q (1/m <sup>3</sup> s)	R	-Zi/L
4-1	5/18/86	1055	3.40	0.30	1.08	27	249	4.27E+06	0.073	48
5-1	5/18/86	1610	2.71	0.35	0.94	19	217	4.29E+06	0.039	123
11-1	5/24/86	1202	2.25	0.47	1.26	14	264	2.69E+06	0.117	65
12-1	5/27/86	1704	3.00	0.47	1.02	34	246	4.48E+06	0.049	44
13-1	5/27/86	1755	3.00	0.43	1.18	50	237	5.33E+06	0.045	28
14-1	5/28/86	1005	2.20	0.68	1.17	10	202	3.86E+06	0.055	134
	5/28/86	1112	1.90	0.71	1.16	11	60	1.06E+07	0.076	123
15-1	5/28/86	1435	1.30	0.68	1.42	19	82	5.27E+06	0.103	98
	5/28/86	1547	1.30	0.68	1.21	14	84	4.37E+06	0.101	131
16-1	5/29/86	0528	2.00	0.49		30	246	3.61E+06	0.136	13
	5/29/86	0532	2.00			30	243	3.74E+06	0.133	13
	5/29/86	0554	2.00			24	292	3.11E+06	0.107	16
	5/29/86	0600	2.00			16	292	3.11E+06	0.087	26
	5/29/86	0640	2.00			33	292	3.11E+06	0.120	12
Averages.....			2.22		1.16	24	215	4.42E+06	0.089	62



Table 27. Electrical, meteorological and model parameters from flights conducted over the ocean near the Bahamas Islands.

Flight	Date	Time @sfc (LT)	Wind Dir.	Wind Speed (m/s)	u* (m/s)	-T* blk (C)	-q* blk (g/Kg)	Zi (m)	tau lam (s)	Aerosols (1/m <sup>3</sup> )
2-1	3/8/1987	1307	W	3.5	0.11	0.03	0.22	500	325	1.0E+09
3-1	3/9/1987	1113	SW	3.3	0.10	0.06	0.29	800	354	1.1E+09
4-1	3/10/1987	1108	NNW	10.5	0.37	0.13	0.30	1100	973	2.3E+09
5-1	3/11/1987	1153	N	6.2	0.21	0.14	0.35	1000	420	1.1E+09
6-1	3/12/1987	1211	WNW	3.0	0.10	0.15	0.35	950	277	8.0E+08
7-1	3/13/1987	1342	NNE	6.0	0.20	0.17	0.38	1250	325	1.1E+09
8-1	3/14/1987	1431	NE	7.0	0.24	0.22	0.40	1400	812	1.3E+09
9-2	3/16/1987	1303	E-NE	5.3	0.18	0.22	0.40	950	571	1.4E+09
11-1	3/17/1987	1135	ENE	2.8	0.09	0.18	0.44	850	421	1.0E+09
AVERAGES.....				5.29	0.18	0.14	0.35	978	497	1.23E+09

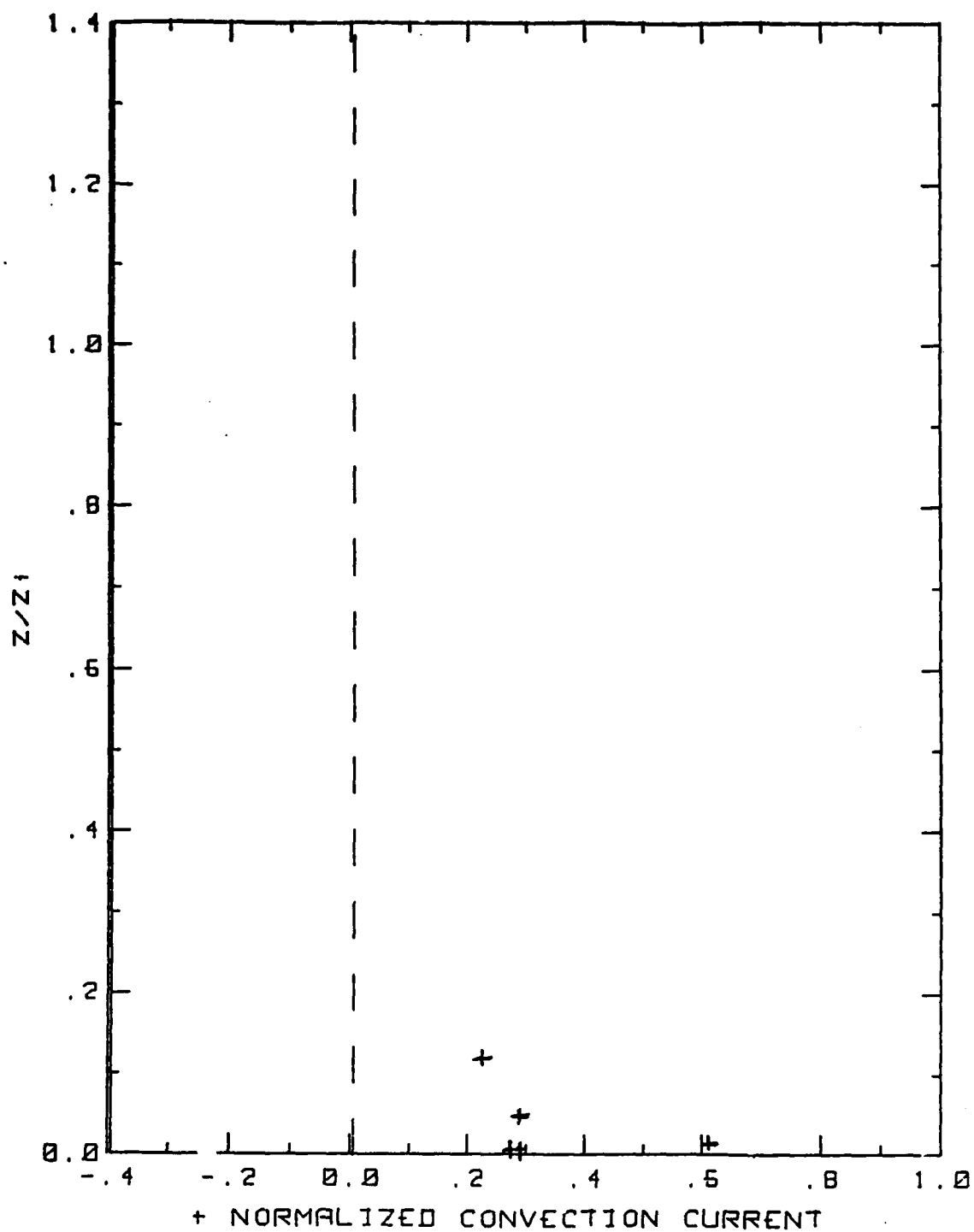
Flight	Date	Time @sfc (LT)	-Jo pA/m <sup>2</sup>	Jmx	V	-L blk (m)	tau n (s)	q (1/m <sup>3</sup> )	R	-zi/L
2-1	3/8/1987	1307	2.35	0.57	1.06	12.7	232	3.06E+06	0.072	39
3-1	3/9/1987	1113	2.13	0.75	1.06	7.0	220	2.95E+06	0.044	114
4-1	3/10/1987	1108	1.05	0.66	1.43	56.8	130	1.82E+06	0.327	19
5-1	3/11/1987	1153	2.05	0.93	1.09	16.6	229	2.40E+06	0.088	60
6-1	3/12/1987	1211	2.39	0.77	0.98	3.6	258	3.23E+06	0.029	265
7-1	3/13/1987	1342	1.96	0.71	1.03	12.8	216	3.28E+06	0.052	98
8-1	3/14/1987	1431	1.20	0.71	1.13	15.1	218	1.30E+06	0.139	93
9-2	3/16/1987	1303	1.65	0.67	1.20	8.5	196	2.06E+06	0.108	112
11-1	3/17/1987	1135	1.78	0.88	1.08	2.4	247	2.22E+06	0.045	356
AVERAGES.....			1.84	0.74	1.12	15.0	216	2.48E+06	0.10	129

Table 28. Electrical parameters obtained from continuous soundings  
on flights conducted over the desert near Hobbs, NM.

Flight	Date	Start Time (LT)	End Time (LT)	Maximum Altitude (km)	-Jo (pA/m <sup>2</sup> )	RI x10 <sup>-16</sup> (ohm*m)	-VI (kV)	Jo*RI/VI -
1	5/13/86	1842	1908	5.5	1.70	11.5	225.5	0.87
2a	5/14/86	1554	1632	7.5	2.95	10.7	285.6	1.11
2b	5/14/86	1641	1731	9.0	2.95	8.9	257.5	1.02
3	5/16/86	1853	1920	6.0	2.20	10.7	234.0	1.01
4a	5/18/86	1045	1121	4.5	2.90	7.2	226.2	0.92
4b	5/18/86	1121	1158	4.5	3.20	6.9	207.8	1.06
5	5/18/86	1535	1614	4.0	2.60	8.1	214.3	0.98
7	5/19/86	1419	1439	4.5	2.75	9.7	283.0	0.94
8	5/19/86	1710	1729	4.5	2.50	9.2	234.0	0.98
9a	5/22/86	1058	1113	7.0	2.45	7.8	182.0	1.05
11	5/24/86	1106	1122	8.0	2.20	10.1	246.0	0.90
12a	5/27/86	1544	1604	7.0	3.25	8.2	267.0	1.00
12b	5/27/86	1639	1701	7.0	3.00	8.1	232.0	1.05
13	5/27/86	1839	1859	7.0	2.95	7.7	216.8	1.05
14	5/28/86	1050	1110	7.0	2.00	10.1	212.2	0.95
15	5/28/86	1519	1543	7.0	2.00	17.0	256.0	1.33
AVERAGES.....				6.3	2.60	9.5	236.2	1.01

Table 29. Electrical parameters obtained from continuous soundings on flights conducted over the ocean near the Bahamas Islands.

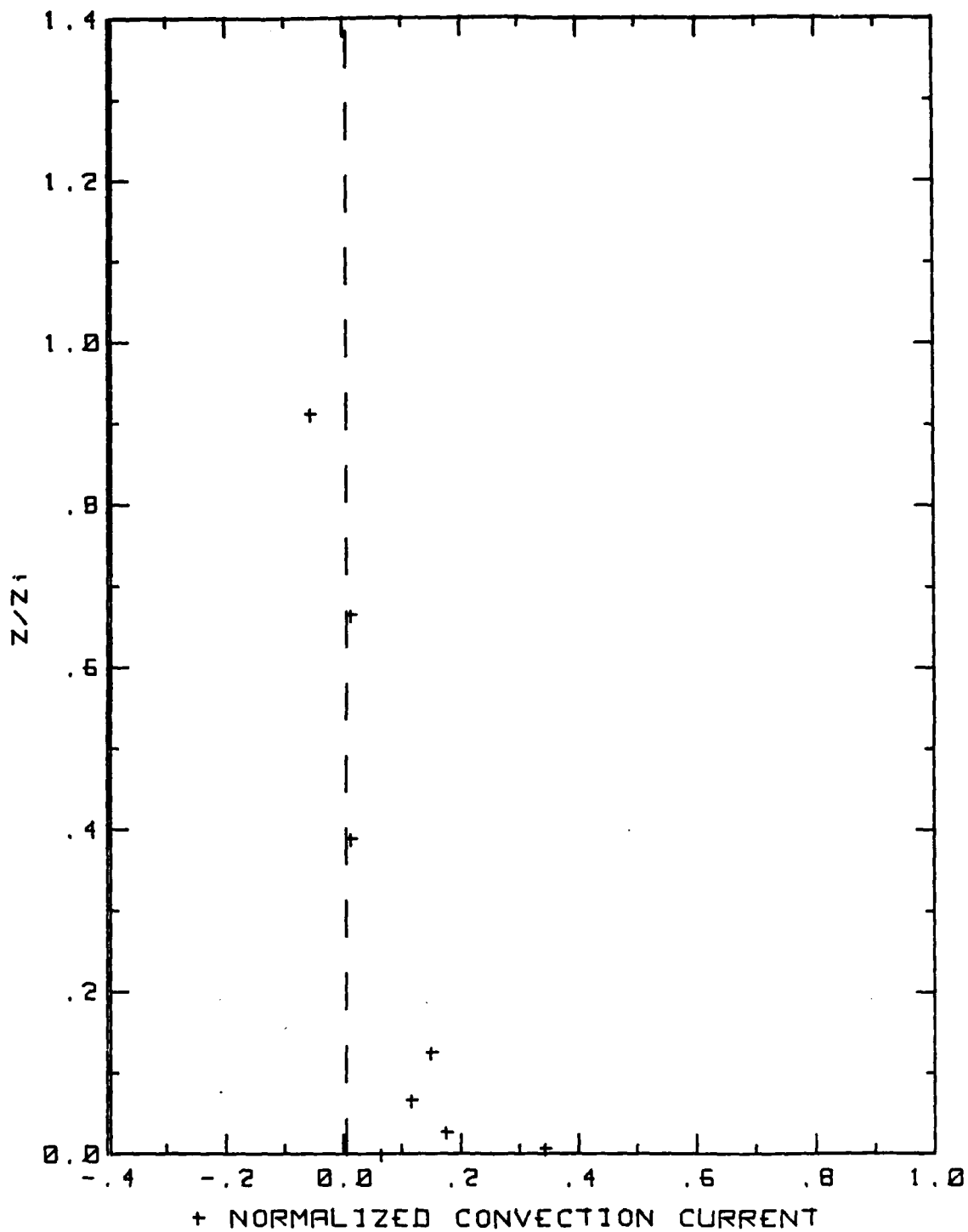
flight	date	Start Time (LT)	End Time (LT)	Maximum Altitude (km)	Inversion Height Zi (m)	-Jo (pA/m <sup>2</sup> )	-VI (kV)	RI x10 <sup>-16</sup> (ohm*m)	R*Jo/VI
2-1	3/8/87	1407	1423	4.1	500	2.15	229.6	9.7	0.91
2	"	1600	1633	4.0	900	2.50	235.9	9.0	0.95
3-1	3/9/87	1219	1238	4.1	800	2.19	225.9	10.2	0.99
4-1	3/10/87	1219	1239	4.1	1100	1.00	278.4	22.7	0.81
5-1	3/11/87	1252	1318	7.7	1000	2.10	274.5	11.8	0.90
7-1	3/13/87	1445	1508	4.1	1250	2.02	223.1	10.2	0.92
8-1	3/14/87	1516	1534	4.0	1400	1.05	264.4	19.5	0.77
2	"	1639	1658	4.1	1400	1.07	243.4	18.0	0.79
3	"	1659	1718	3.9	1400	1.09	241.8	18.3	0.82
9-1	3/16/87	1158	1220	4.0	950	1.62	241.0	13.0	0.88
2	"	1354	1412	3.9	950	1.77	254.3	12.8	0.89
10-1	"	1615	1640	4.1	950	1.71	237.1	12.9	0.93
2	"	1644	1705	4.1	1000	1.50	221.6	12.3	0.83
11-1	3/17/87	1242	1302	4.0	850	1.74	210.8	11.2	0.92
AVERAGES	.....	.....	.....	4.3	1032	1.68	241.6	13.7	0.88



18MAY86 FLIGHT#4 1044 TO 1110 LST

$Z_i = 1300$   $J_0 = 3.40$

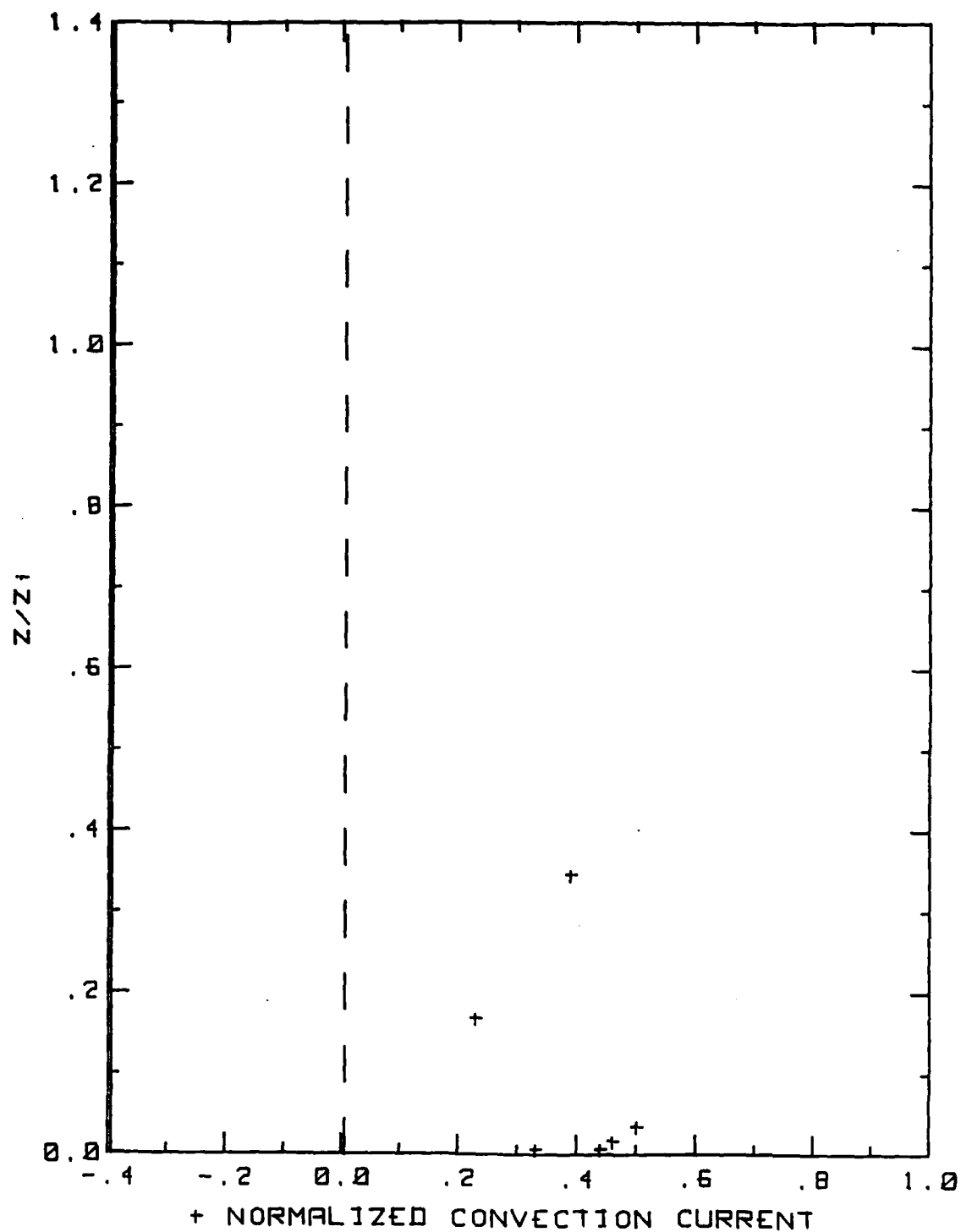
Figure 32. Hobbs Flight 4-1 normalized convection current profile.



18MAY86 FLIGHT#5 1531 TO 1614 LST

Zi=2300 Jo=2.71

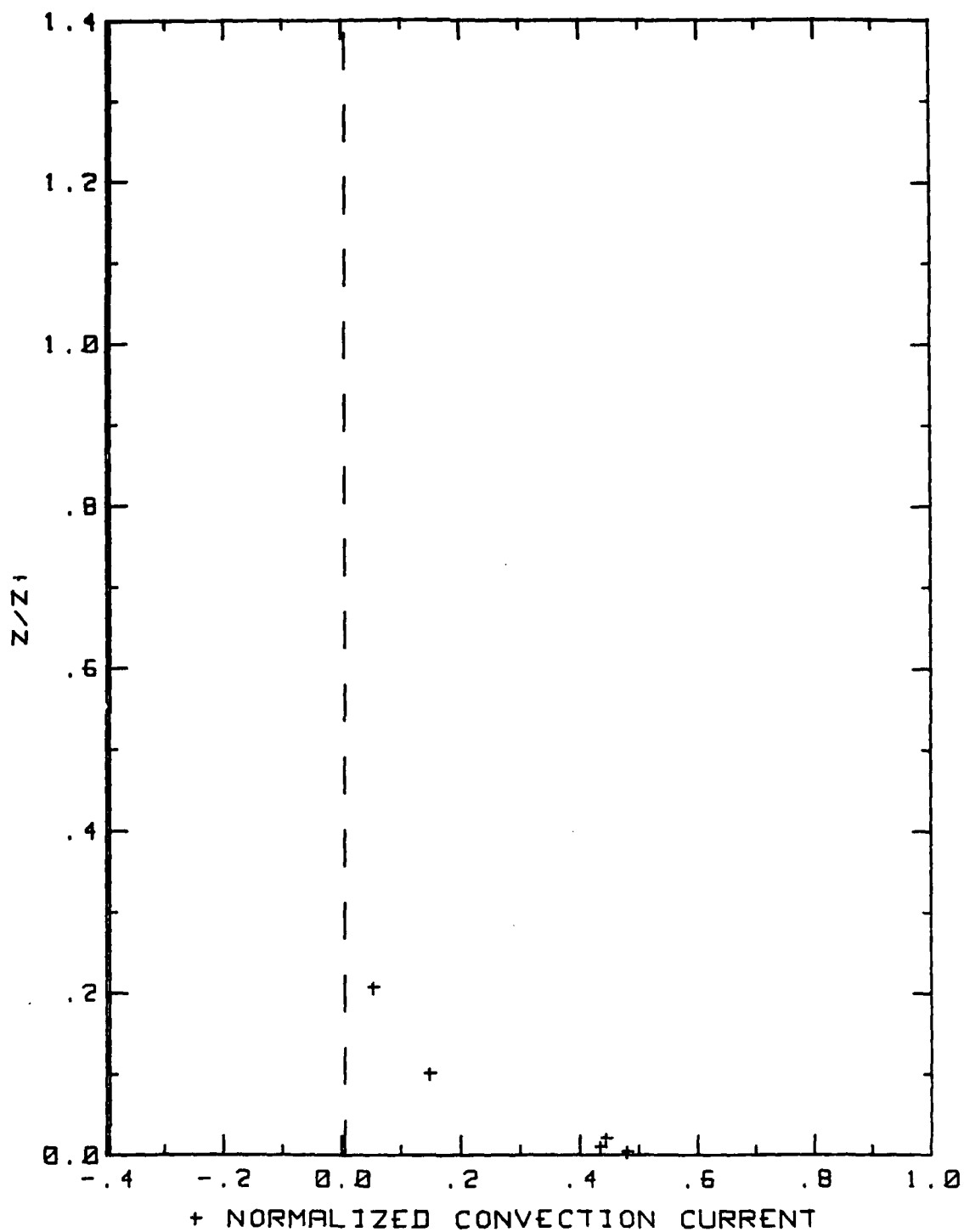
Figure 33. Hobbs Flight 5-1 normalized convection current profile.



24MAY86 FLIGHT#11 1156 TO 1212 LST

$Z_i=900$   $J_0=2.25$

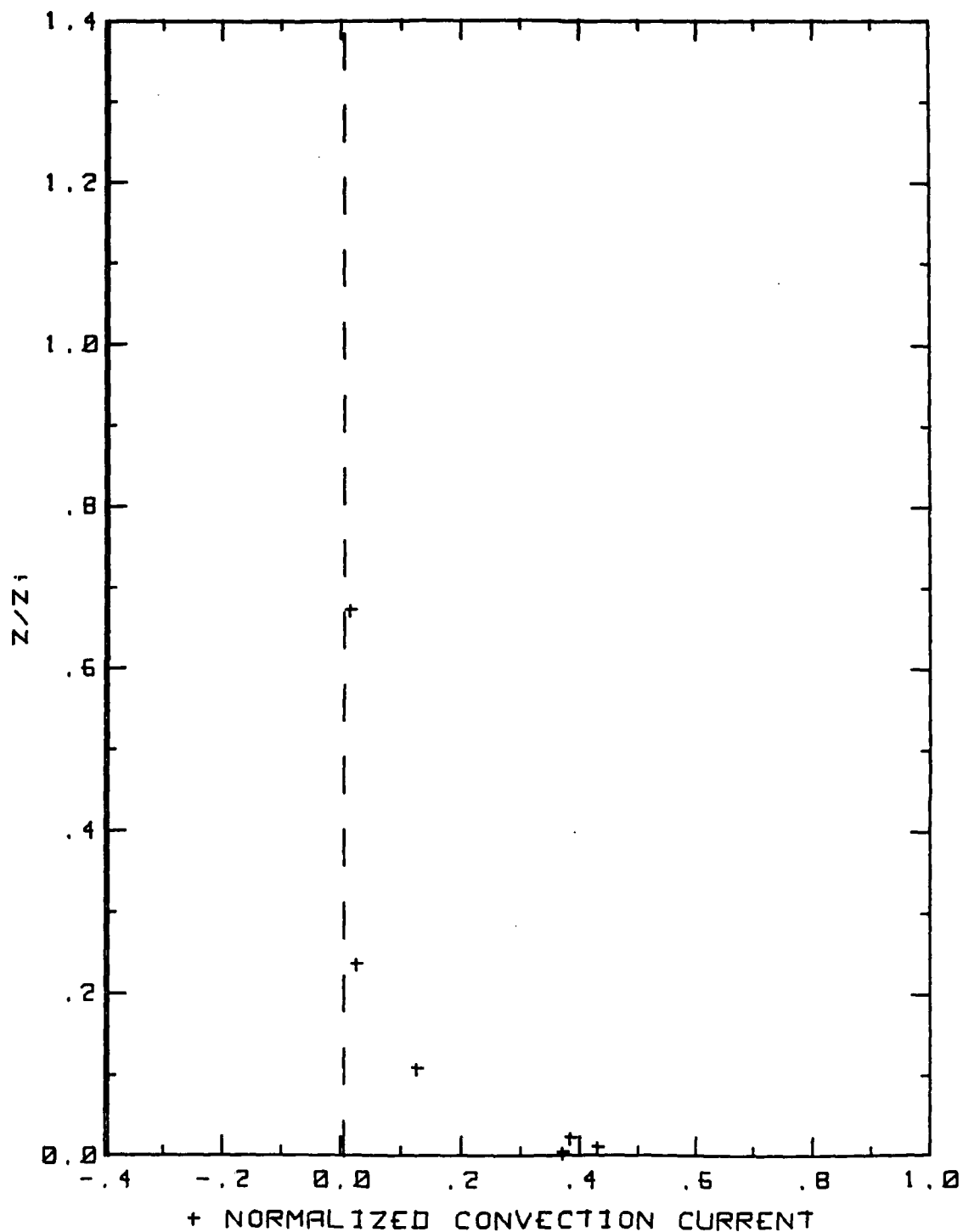
Figure 34. Hobbs Flight 11-1 normalized convection current profile.



27MAY86 FLIGHT#12 1702 TO 1711 LST

$Z_1=1500$   $J_0=3.00$

Figure 35. Hobbs Flight 12-1 normalized convection current profile.

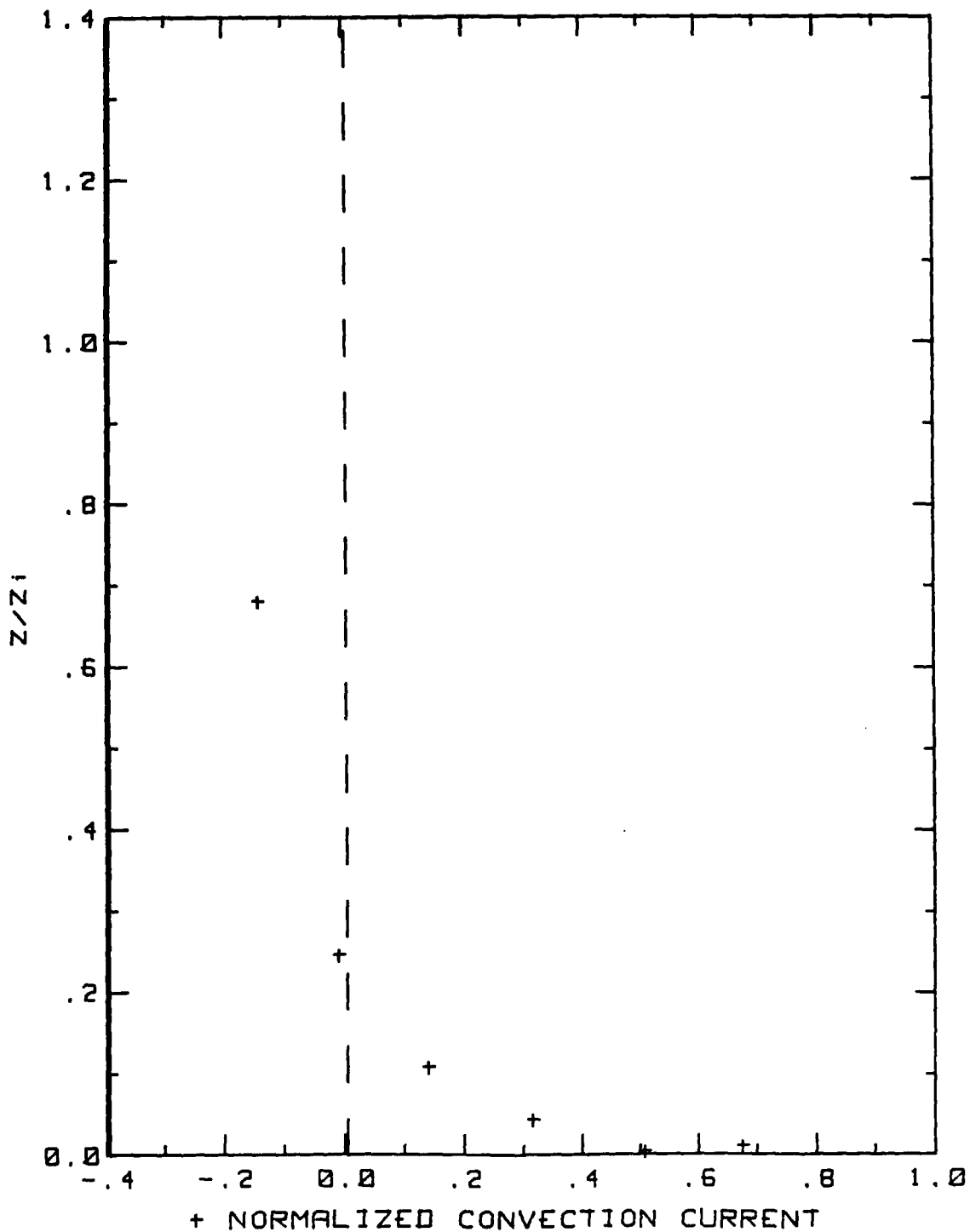


27MAY86 FLIGHT#13 1753 TO 1829 LST

$Z_i = 1400$   $J_0 = 3.00$

Figure 36. Hobbs Flight 13-1 normalized convection current profile.

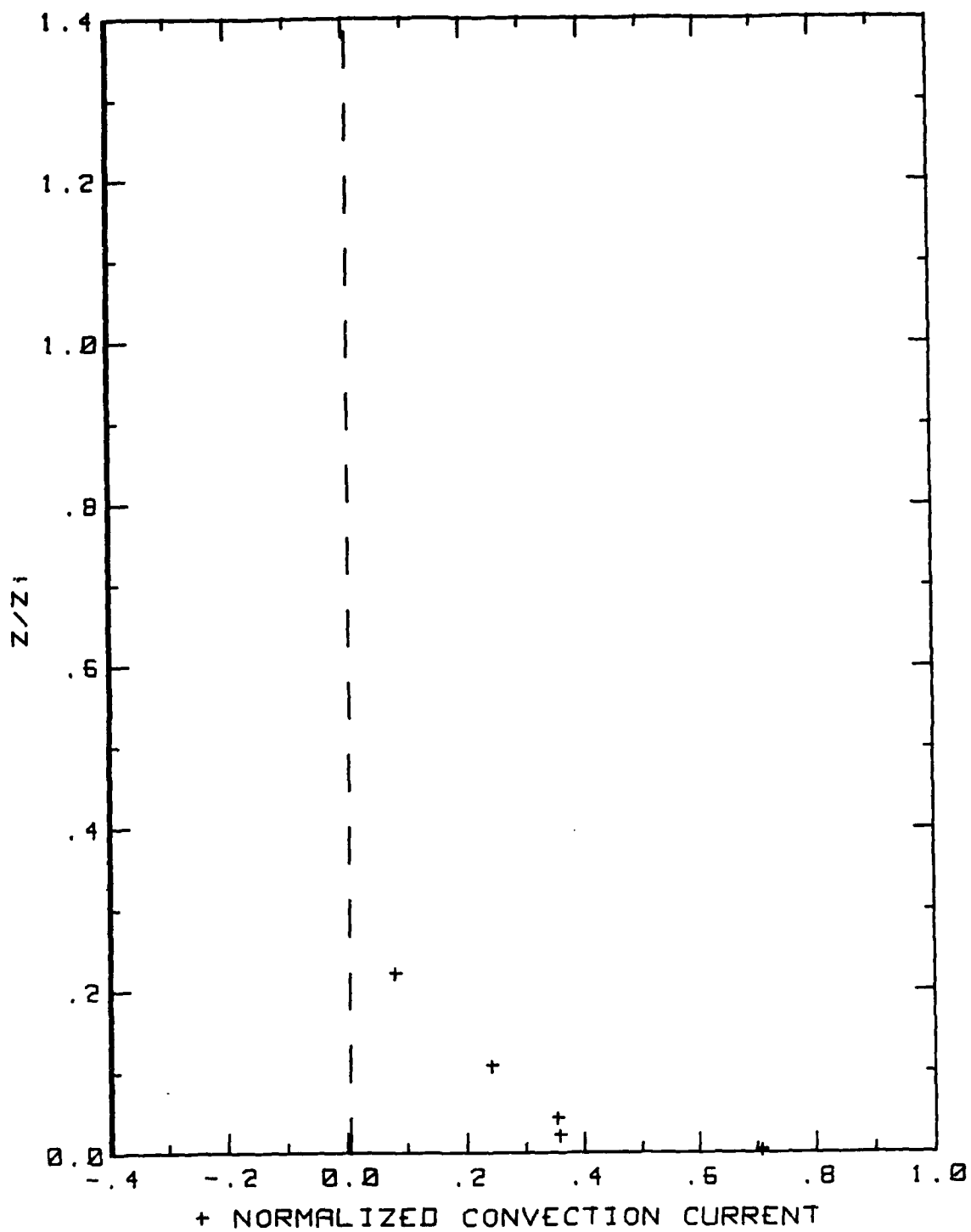




28MAY86 FLIGHT#14 1000 TO 1046 LST

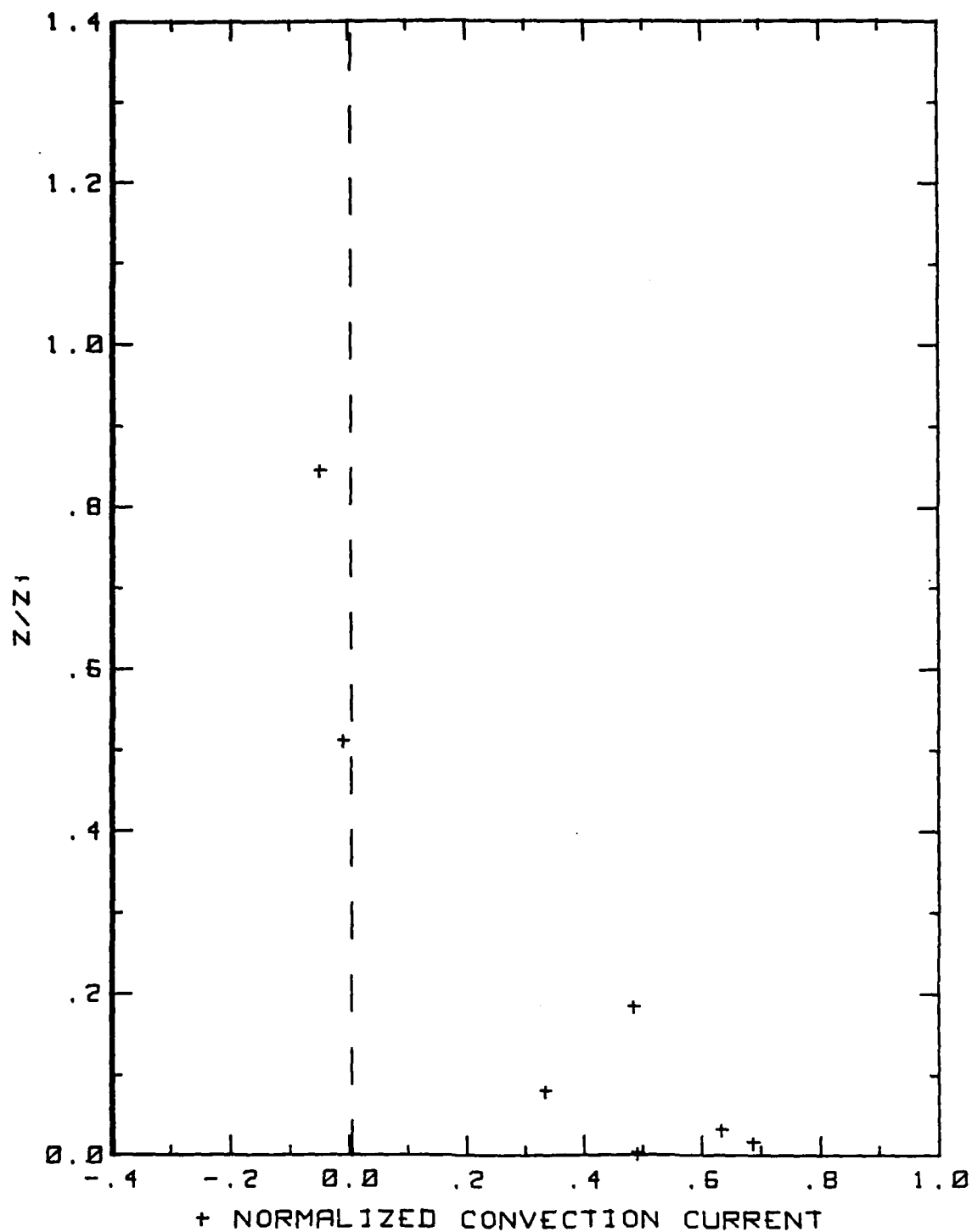
$Z_i = 1400$   $J_0 = 2.20$

Figure 37. Hobbs Flight 14-1 normalized convection current profile corresponding to 1005 LT.



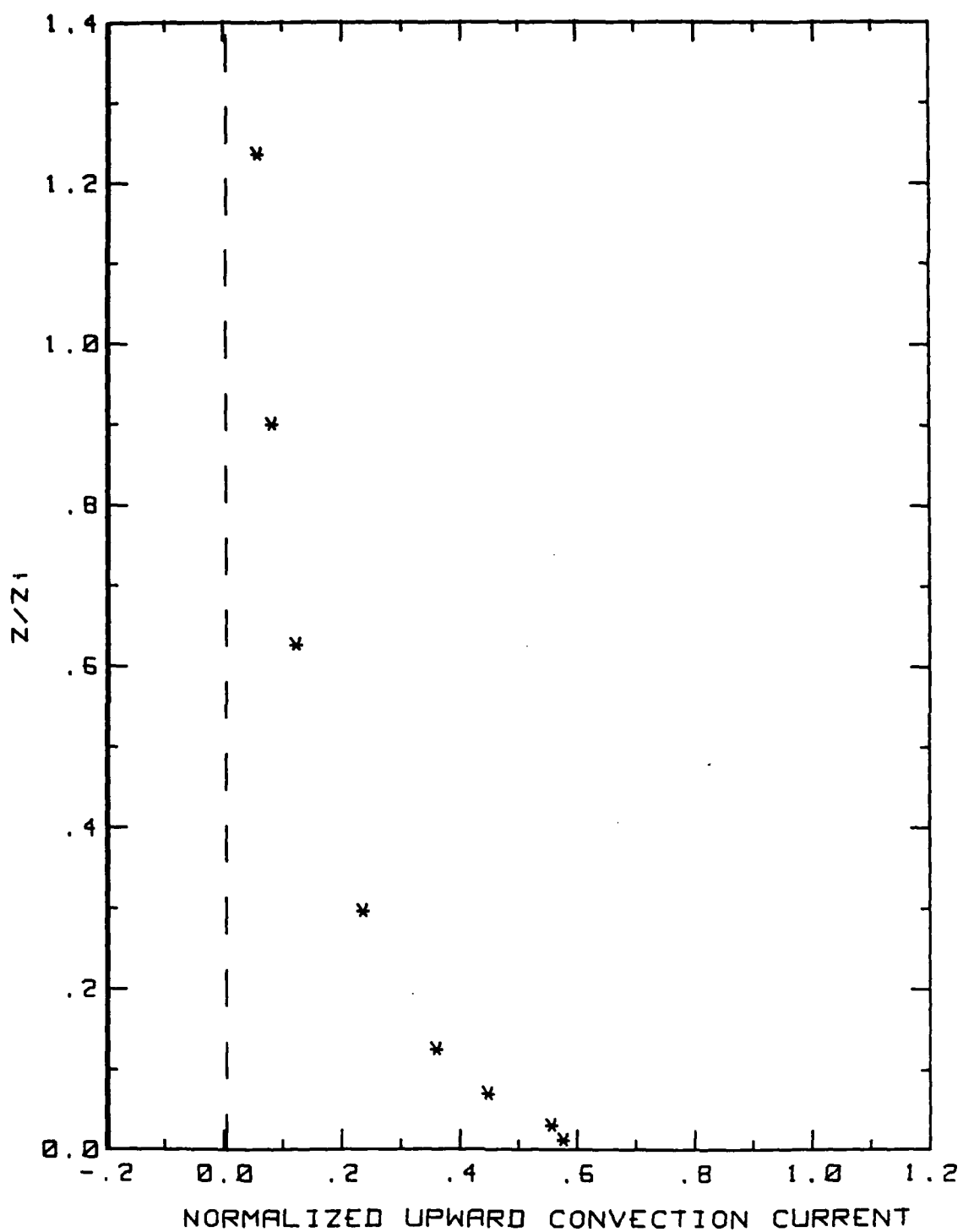
28MAY86 FLIGHT#14 1112 TO 1120 LST  
 $Z_i = 1400$   $J_0 = 1.90$

Figure 38. Hobbs Flight 14-1 normalized convection current profile corresponding to 1112 LT.



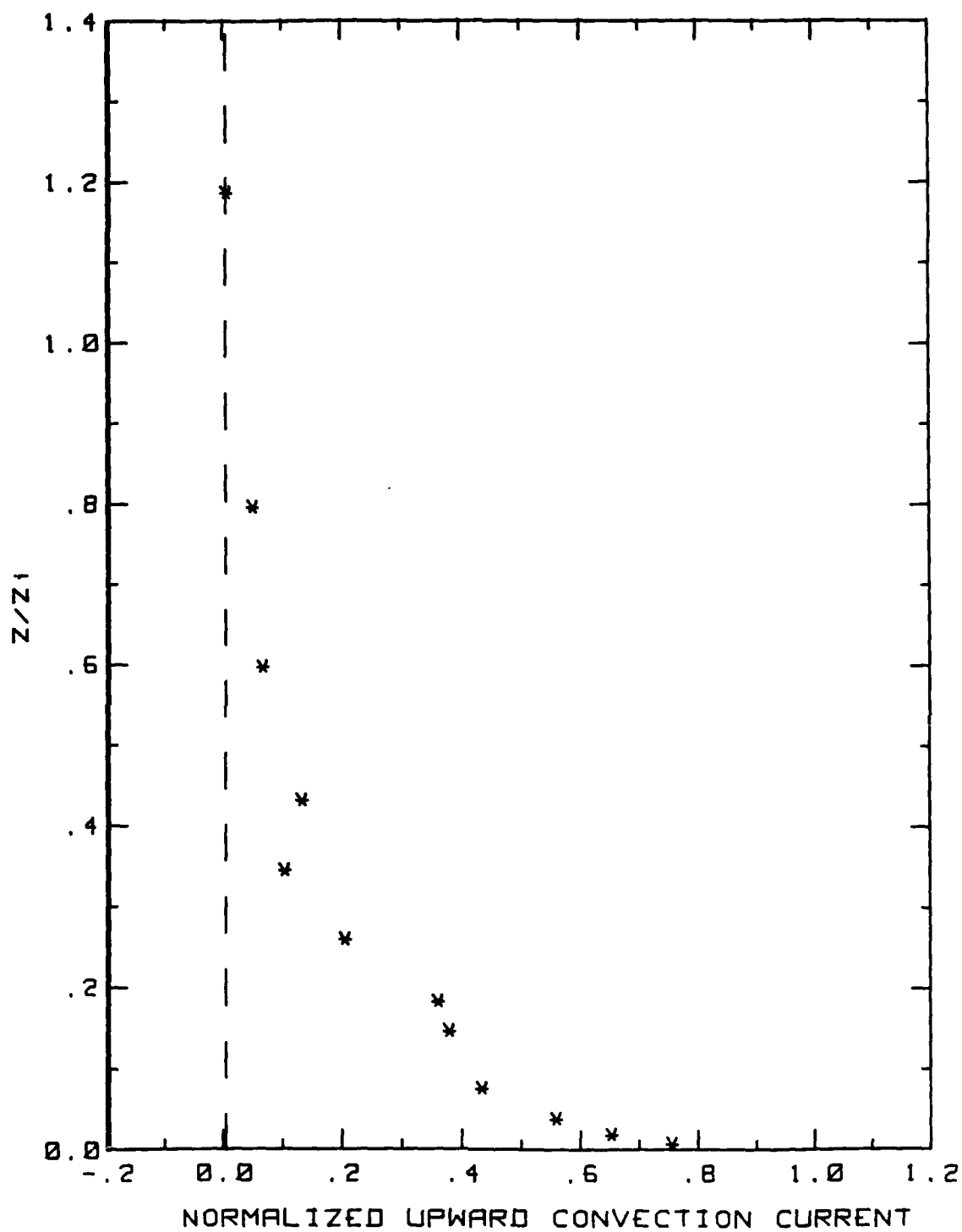
28MAY86 FLIGHT#15 1431 TO 1518 LST  
 Z<sub>1</sub>=1900 J<sub>0</sub>=1.30

Figure 39. Hobbs Flight 15-1 normalized convection current profile.



08MAR87 FLIGHT#2 13:04 TO 14:32 LST  
Z<sub>1</sub>=500 J<sub>0</sub>=2.35

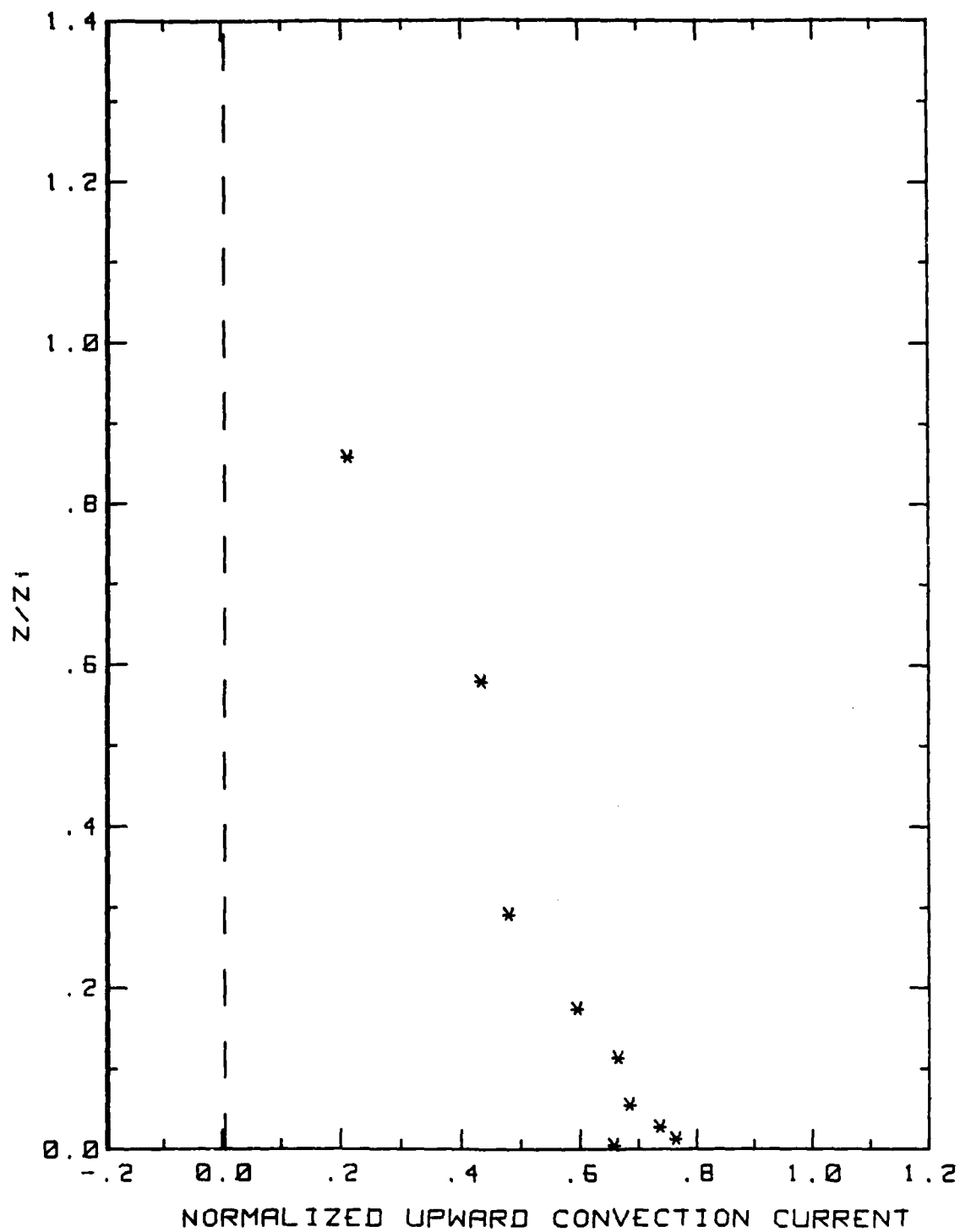
Figure 40. Bahamas Flight 2-1 normalized convection current profile.



09MAR87 FLIGHT#3 10:34 TO 12:14 LST

Z1=800 J0=2.13 T0=1110

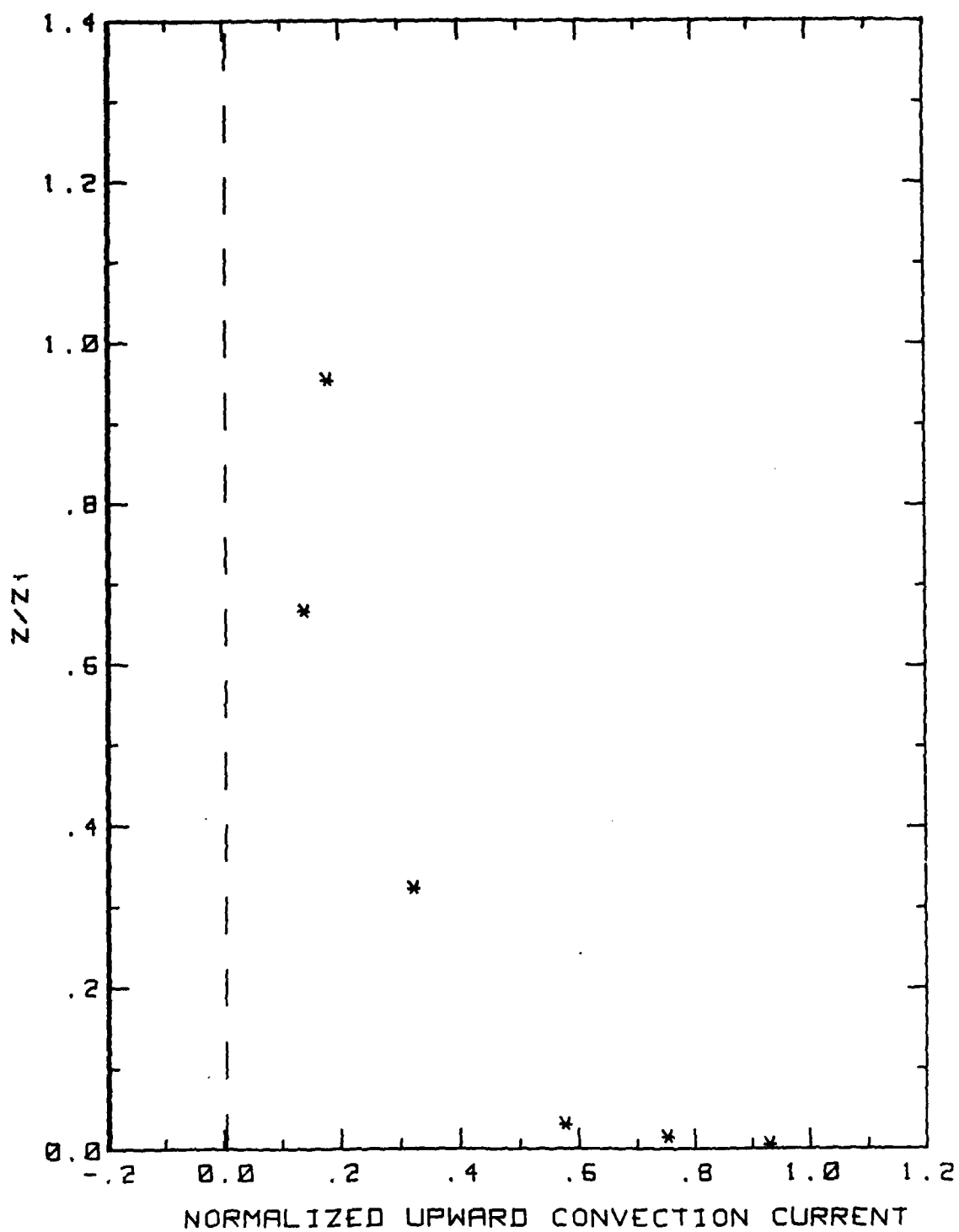
Figure 41. Bahamas Flight 3-1 normalized convection current profile.



10MAR87 FLIGHT#4 10:46 TO 12:16 LST

$Z_i = 1100$   $J_0 = 1.05$

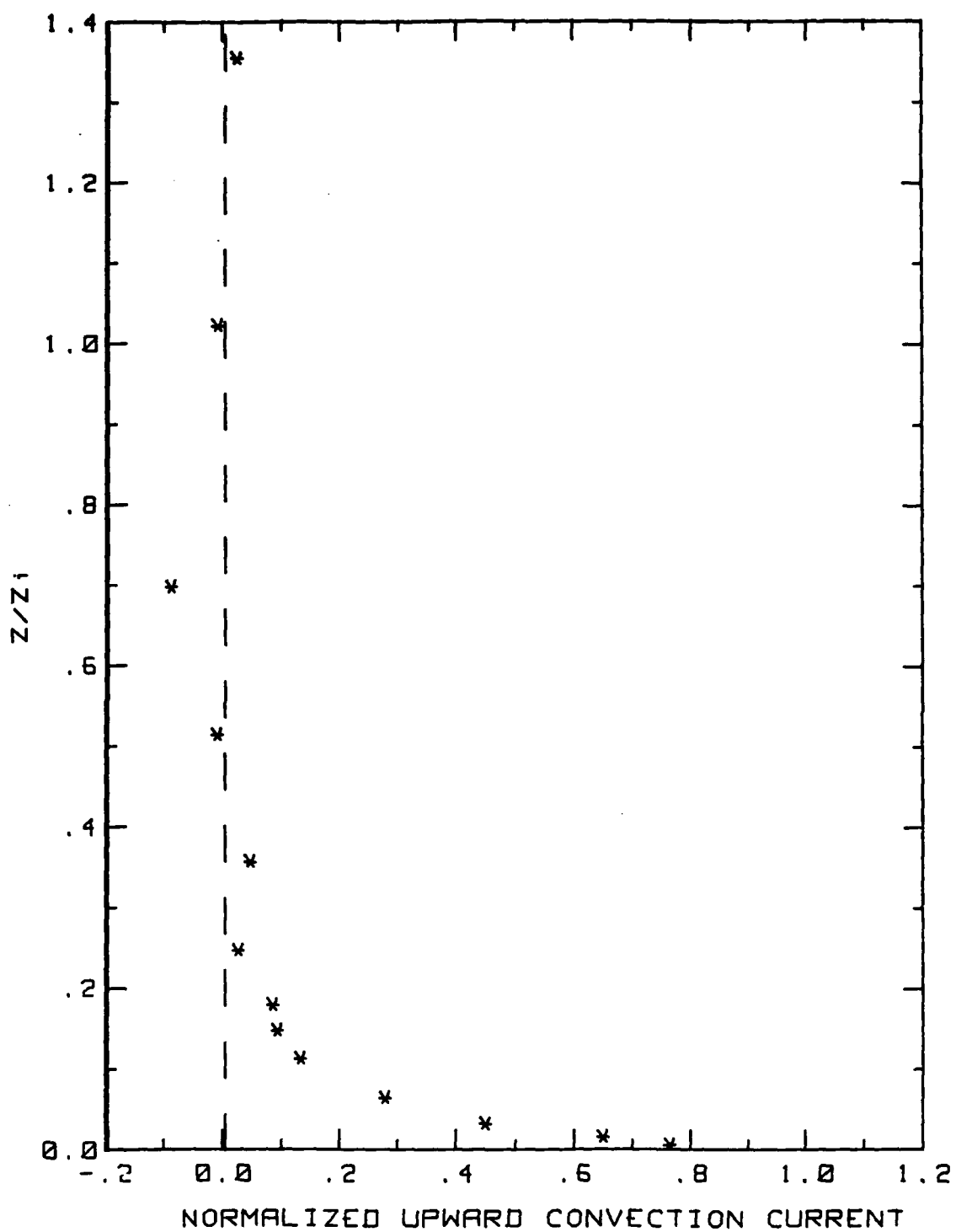
Figure 42. Bahamas Flight 4-1 normalized convection current profile.



11MAR87 FLIGHT#5 11:24 TO 12:37 LST

$Z_1=1000$   $J_0=2.05$  TIME=1148 TO 1233

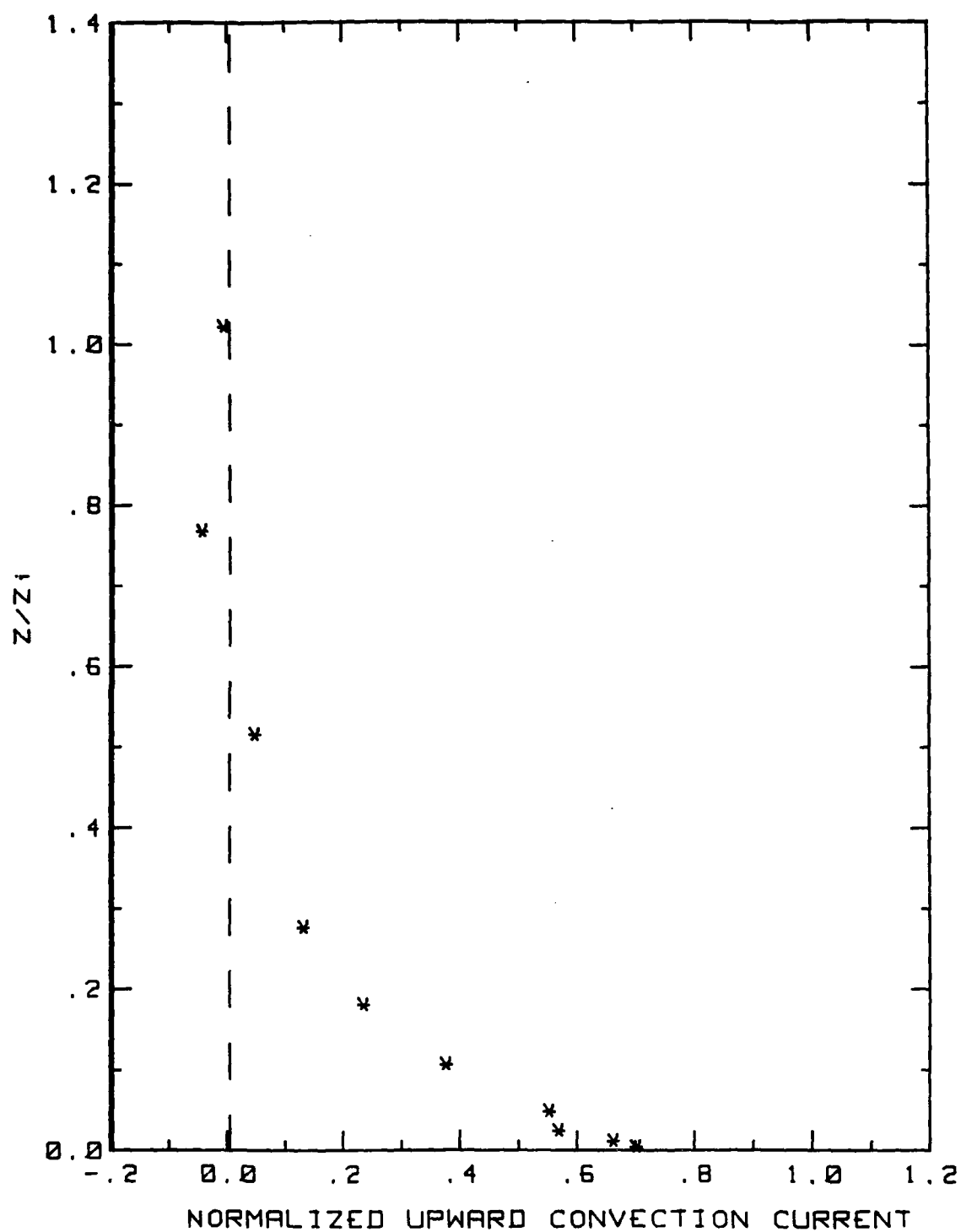
Figure 43. Bahamas Flight 5-1 normalized convection current profile.



12MAR87 FLIGHT#6 12:00 TO 12:52 LST  
Z<sub>i</sub>=950 J<sub>0</sub>=2.39

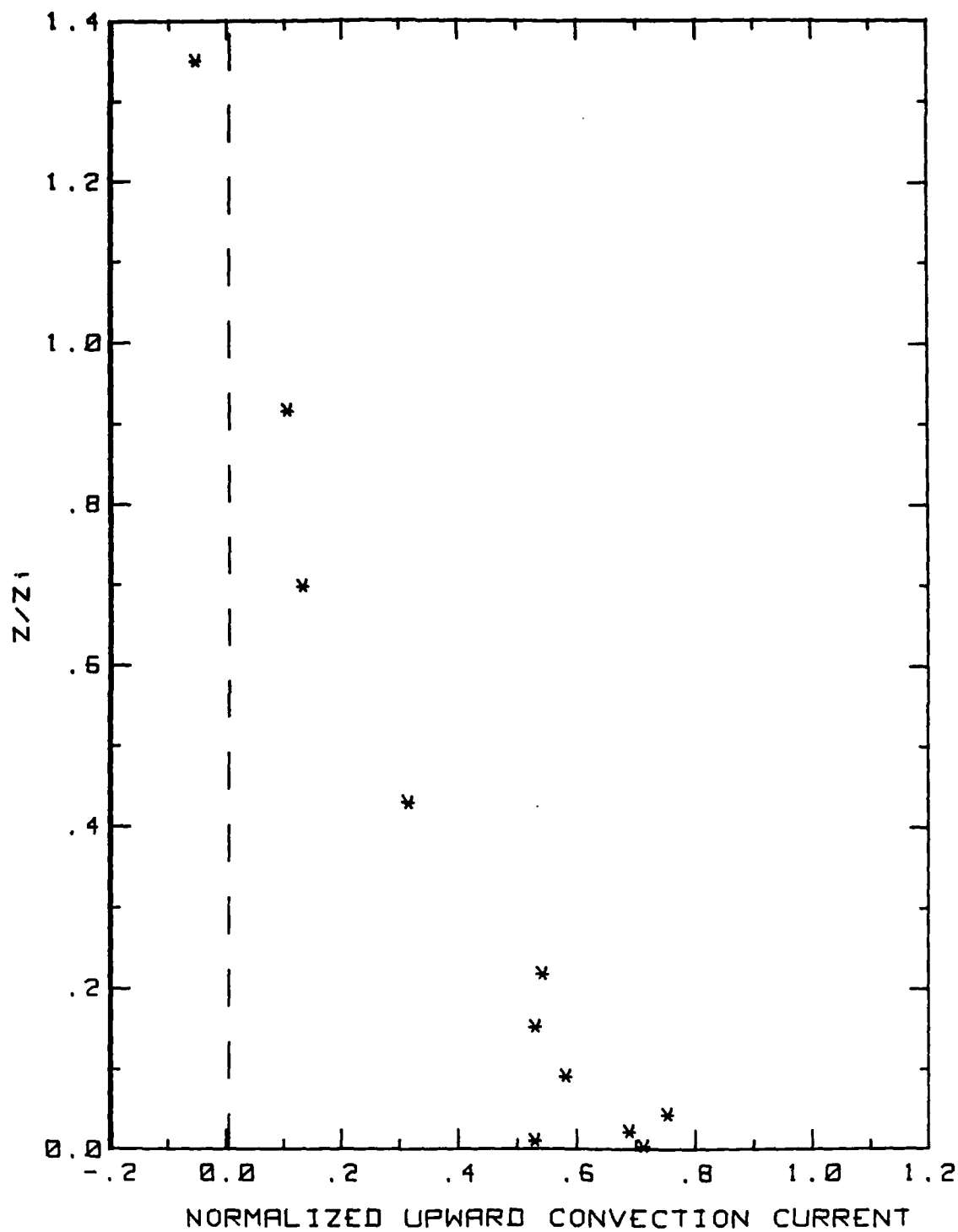
Figure 44. Bahamas Flight 6-1 normalized convection current profile.





13MAR87 FLIGHT#7 13:28 TO 15:14 LST  
 $J_0=2.0$   $Z_i=1250$  NEG. COND. ONLY

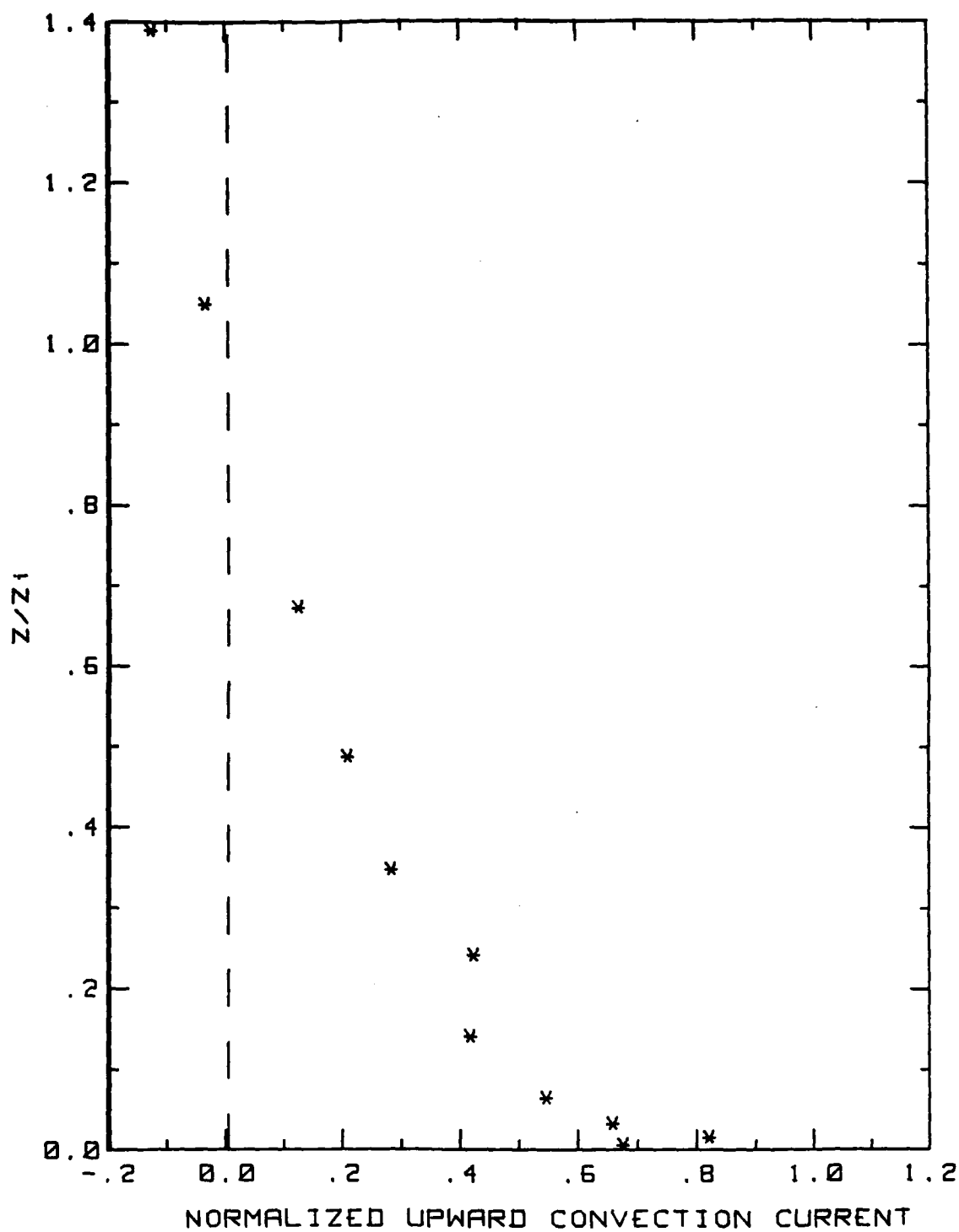
Figure 45. Bahamas Flight 7-1 normalized convection current profile.



14MAR87 FLIGHT#8 14:29 TO 15:18 LST

$Z_i=1400$   $J_0=1.2$  NEG COND ONLY

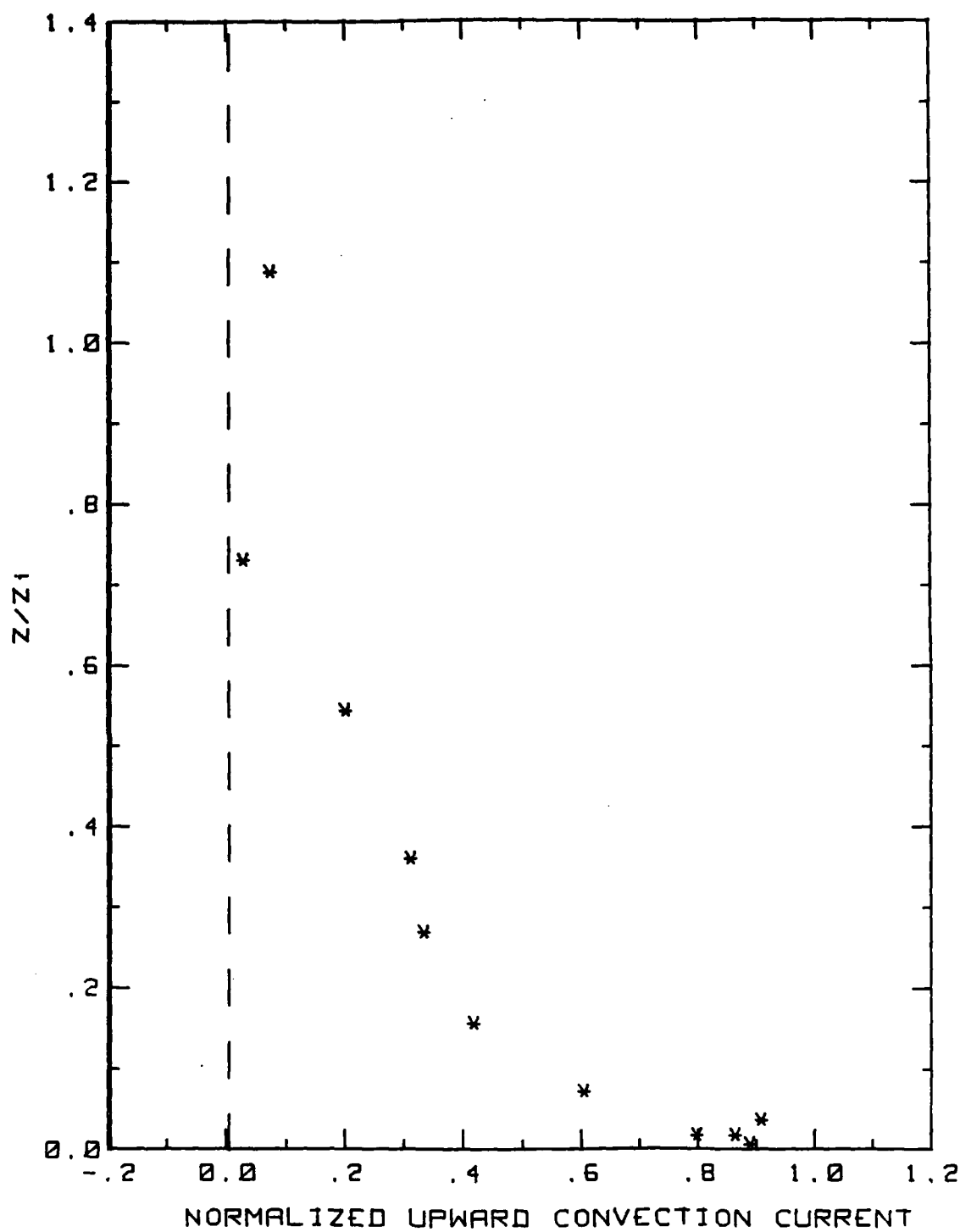
Figure 46. Bahamas Flight 8-1 normalized convection current profile.



16MAR87 FLIGHT#9 12:44 TO 13:56 LST

$Z_1=950$   $J_0=1.65$

Figure 47. Bahamas Flight 9-1 normalized convection current profile.



17MAR87 FLIGHT#11 11:15 TO 12:38 LST

$Z_1=850$   $J_0=1.78$

Figure 48. Bahamas Flight 11-1 normalized convection current profile.

## VII. APPENDICES

Appendix A. "Aircraft Investigation of Electric Charge Flux over Land and Sea", Anderson, B., R. Markson, C.W. Fairall and J.C. Willett, Proc. VIII Int. Conf. Atmos. Electricity, 782, Uppsala, Sweden, (June, 1988), Institute of High Voltage Research at Uppsala University, Sweden (accepted for publication by J. Geophys. Res.).

Appendix B. "Comparison of Ionospheric Potential and Air-Earth Current as Indicators of the Global Circuit Current", R. Markson, Proc. VIII Int. Conf. Atmos. Electricity, 814, Uppsala, Sweden, (June, 1988), Institute of High Voltage Research at Uppsala University, Sweden (accepted for publication by J. Geophys. Res.)

## Appendix A

### **AIRCRAFT INVESTIGATION OF ELECTRIC CHARGE FLUX OVER LAND AND SEA**

Bruce Anderson and Ralph Markson  
Airborne Research Associates, Weston, MA 02193

Christopher W. Fairall  
Pennsylvania State University, University Park, PA 16802

John C. Willett  
Naval Research Laboratory, Washington, DC 20375

**ABSTRACT:** Aircraft measurements of electric field, conductivity and turbulence parameters from heights of 3 m to several km have been made to examine the electrical and meteorological structure of the unstable planetary boundary layer (PBL). Our findings indicate that: 1) strong electrode layers form over the ocean but are often inhibited over land, apparently because of surface radioactivity, 2) convection-current profiles appear to be governed by electrical relaxation and turbulence intensity as predicted previously by a numerical model of turbulent charge transport, and 3) vertical electric field measurements, because of their sensitivity to volumes of space charge, show details of oceanic convective plume structure not evident in records of humidity or other in situ measurements.

#### **INTRODUCTION**

Positive charge can accumulate near the Earth's surface in fair weather because of the electrode effect. This is especially true over water; strong electrode layers have not been measured over land (Muhleisen, 1961).

Convection currents, formed when electrode-effect space charge is transported upward by turbulent mixing (Kraakevik, 1958; Markson et al., 1981), can comprise a significant fraction of the total current density near the ocean surface. This positive charge flux acts as an electrical generator which raises the potential in the PBL, effectively reducing the air-earth conduction-current density above the exchange layer (Willett, 1979).

Hoppel and Gathman (1971) modeled the electrode effect using an eddy-diffusion approximation which, though giving accurate predictions in some cases, fails to describe large convection currents. Willett's (1979) second-order-closure model of turbulent charge transport shows that, in addition to the electrical parameters, the surface fluxes of buoyancy and momentum and the PBL thickness are primary factors governing convection-current intensity. Aside from a limited number of measurements made in a thin, weakly convective PBL over the ocean (Markson et al., 1981), no previous attempts have been made to study the convective generator with a complete array of atmospheric electrical, meteorological and turbulence instruments.

#### **EXPERIMENTAL DESIGN**

Our primary experimental objectives were to determine the electrode-effect source strength over land and sea and to obtain convection-current profiles under a variety of atmospheric conditions in order to test Willett's model. To accomplish this, two sites were selected for the field experiments: 1) Hobbs, New Mexico, a flat desert region characterized by sparse vegetation, intense dry convection and an

unusually thick PBL, and 2) the ocean near Eleuthera, Bahamas, a classic trade-wind regime with clean air and atmospheric instability caused by warm water. Our aircraft was instrumented to measure vertical electric field, both polar conductivities, temperature, dew point, pressure, infrared surface temperature, cloud-condensation nuclei, and the turbulence-structure functions for velocity, temperature and humidity. These were used to derive conduction- and convection-current densities, electrical relaxation times, inversion heights, atmospheric stability, and surface fluxes of heat, momentum, and moisture. Mean winds were derived from airspeed and Loran groundspeed measurements. The use of a light aircraft allowed measurements to extend to within 3 m of the surface in both regimes.

A ground station was also operated during the land deployment to record wind profiles, turbulence-structure functions for temperature and velocity, and Wilson current. These provided a check on the aircraft data as well as an independent means for determining surface fluxes.

## DISCUSSION OF OBSERVATIONS

### Oceanic Regime

Figure 1a is a typical example of PBL electrical structure in the Bahamas; Fig. 1b depicts meteorological profiles for the same flight. The lower tropospheric structure consists of a well mixed PBL capped by a weak inversion near 700 m (Zi) and a secondary inversion at 1300 m. Within the PBL, the electric field increases with decreasing height while conductivity remains constant, indicating a convection current ( $J_C$ ). The magnitude of  $J_C$  can be derived through the relation  $J_C = J_0 - E\lambda$ , where  $J_0$  is the air-earth conduction-current density well above the inversion,  $E$  is electric field and  $\lambda$  is total conductivity. By the "physics" sign convention,  $E$  and  $J_0$  are negative while  $J_C$  is positive in fair weather. The shaded area in Fig. 1a indicates the increase in conduction-current density ( $E\lambda$ ) caused by  $J_C$ . The strength of the electrode effect charge source is characterized by the maximum  $J_C$  ( $J_{\max}$ ) value, which in this case is about  $1.1 \text{ pA/m}^2$ . Normalized  $J_{\max}$  values have been shown by Markson et al. (1981) to correlate with surface fluxes of moisture and momentum.

Preliminary results are summarized in Table 1. Nine soundings were obtained over water when measurements from the full complement of instrumentation were unambiguous.  $J_{\max}$  values ranged from 0.7 to  $1.8 \text{ pA/m}^2$  (57% to 93% of  $J_0$ ). The average  $J_{\max}/J_0$  of 0.74 is in fair agreement with theoretical predictions of 0.60 to 0.65 by Willett (1983). Volume ionization rates calculated from conductivity and aerosol measurements averaged  $1.5 \times 10^6 \text{ m}^{-3}$ , which is consistent with that due strictly to cosmic radiation (Israel, 1970). Air temperatures ranged to from 1 to 6 °C less than the sea-surface temperatures, resulting in significant convective mixing on each flight.

### Desert Deployment

Conditions were not as uniform in New Mexico. The PBL height through 10 flights ranged from 400 m (early morning) to 2800 m (afternoon) as surface heating controlled convection. Aerosol concentrations averaged about 4 times those over the ocean and varied by a factor of 10 due to natural and/or anthropogenic factors.

The electrode-effect charge source and related convection currents were generally much smaller in New Mexico.  $J_{\max}$  values ranged from 0 to  $1.3 \text{ pA/m}^2$  (0 to 65% of  $J_0$ ) and  $J_{\max}/J_0$  averaged 0.3, much less than the predicted range of 0.7 to 0.9 (Willett, 1983). PBL

volume-ionization rates averaged about  $8 \times 10^6 \text{ m}^{-3}$ , 5 times larger than the oceanic values, due to a combination of radioactive emanations, surface activity, and increased cosmic radiation (ground level was 1.1 km MSL). The soil probably emitted radon gas. This point is illustrated in Fig. 2, electrical profiles obtained in the early morning before the onset of convection. Conductivity values increased by 60% near the ground, causing a sharp decrease in electric field, and a shallow layer of negative space charge resulted. The onset of convection destroyed most of the conductivity gradient, although some afternoon profiles showed a small increase in conductivity near the surface. Thus, the electrode effect probably was inhibited by deposition of Radon daughters on the vegetation (Willett, 1985), Thoron gas emission from the soil, or some other form of surface radioactivity.

#### Effects of Turbulence

The columns in Table 1 headed R and  $-Zi/L$  are turbulence parameters used by Willett (1979) to predict the strength and shape of convection-current profiles. R is a ratio of electric to turbulent time scales given by  $R = u_* \tau_\lambda / Zi$ , where  $u_*$  is the friction velocity and  $\tau_\lambda$  is the electrical relaxation time. The larger  $u_*$  becomes, the shorter will be the mixing time in the PBL, and for a given  $\tau_\lambda$ , the higher charge will be transported before decaying. The ratio,  $-Zi/L$ , is an indicator of convection strength, where L is the Monin-Obukhov length and denotes approximately the height where mechanical and buoyant generation of turbulence are equal. L is dependent on the surface buoyancy flux (produced by both sensible heat and water-vapor fluxes) and  $u_*$ , and at constant wind velocity,  $-Zi/L$  becomes more positive with increasing convection.

As Table 1 indicates, both R and  $-Zi/L$  were larger in the ocean deployment. Small R values at Hobbs were caused mainly by the higher ionization rates and thicker PBLs, while  $-Zi/L$  ratios were affected by the latter and by stronger mechanical turbulence due to the greater surface roughness. Figure 3 displays normalized convection-current ( $J_c/J_o$ ) profiles from both locations with approximately the same  $-Zi/L$  ratios, but varying R values, while Fig. 4 depicts nearly constant R values and variable  $-Zi/L$ . Both are seen to systematically affect convection currents, in good qualitative agreement with the model (see Figs. 1 and 2 in Willett, 1979), although in some cases the model predicts currents which are larger by a factor of 2 or more.

Since these upward convection currents must be balanced (in the steady state) by increases in the downward conduction-current density within the mixed layer, they have the effect of increasing the electrostatic potential at the top of that layer, opposing the normal downward flow of charge in the fair weather atmosphere. The reduction in total downward current density ( $J_o$ ) due to convection currents alone averaged 12% over the ocean, but only a few percent in New Mexico (Markson, this conference).

#### Oceanic Convection

Horizontal variations in vertical electric field near the ocean surface were found to be highly correlated with humidity fluctuations ( $q'$ ) as illustrated in Fig. 5 ( $r=0.54$ ;  $N=288$ ), which is consistent with earlier findings (Markson, 1975). Moisture as well as electrode-effect space charge are accumulated by air motions into small plumes spaced at 200 to 400 m intervals and transported to the interior of the PBL where, on windy, convective days, larger scale organization occurs



(Kuettnner, 1971); cloud streets are a manifestation of this effect. Since space charge accumulates in these large updrafts, electric field measurements can provide a remote indicator of their size and spacing. This is illustrated by the 1 to 2 km periodicity also evident in E but missing in q' (Fig. 5).

The dependence of the relationship between E and q' on height further exemplifies the remote sensing capability of electric field measurements. When the aircraft flies below the electrical center of the plumes, E and q' increase together (Fig. 5); when most of the charge is beneath the aircraft, E and q' show a negative correlation (Fig. 6;  $r = -0.26$   $N = 188$ ).

## CONCLUSIONS

Preliminary analysis indicates that strong electrode layers and large convection currents can form over the ocean, confirming previous investigations (Kraakevik, 1958; Markson et al., 1981), but tend to be suppressed over land. In addition, electric field measurements, because they integrate space charge through a large volume, are good indicators of cloud scale convective patterns over the ocean.

## ACKNOWLEDGEMENTS

This work was supported by the Air Force Office of Scientific Research under Contract F49620-86-C-0013. We would like to thank the Bahamian government, Mr. Breon Leary and other personnel at the Rock Sound Airport, members of the Hobbs Soaring Society, and in particular, the late Mr. Jack Gomez for their assistance in the field deployments.

## REFERENCES

- Hoppel, W.A. and S.G. Gathman, 1971: Determination of eddy diffusion coefficients from atmospheric electrical measurements, J. Geophys. Res., 76, 1467-1477.
- Israel, H., 1970: Atmospheric Electricity, Vol I., Jerusalem, Israel Program for Scientific Translations.
- Kraakevik, J.H., 1958: Electrical conduction and convection current in the troposphere, in Recent Advances in Atmospheric Electricity, edited by L.G. Smith, Pergamon, New York, 75-88.
- Kuettnner, J.P., 1971: Cloud bands in the Earth's atmosphere, Tellus XXIII, 4-5, 404-426.
- Markson, R., 1975: Atmospheric electrical detection of organized convection, Science, 188, 1171-1177.
- Markson, R., J. Sedlacek and C.W. Fairall, 1981: Turbulent transport of electric charge in the marine atmospheric boundary layer, J. Geophys. Res., 86, 12115-12121.
- Markson, R.: Comparison of ionospheric potential and air-earth current as indicators of the global circuit current, this volume.
- Muhleisen, R.P., 1961: Electrode effect measurements above the sea, J. Atmos. Terr. Phys., 20, 79-81.
- Willett, J.C., 1979: Fair weather electric charge transfer by convection in an unstable planetary boundary layer, J. Geophys. Res., 84, 703-718.
- Willett, J.C., 1983: Effects of interfacial ion transfer on the turbulent electrode layer, J. Geophys. Res., 88, 8453-8469.
- Willett, J.C., 1985: Atmospheric-electrical implications of  $^{222}\text{Rn}$  daughter deposition on vegetated ground, J. Geophys. Res., 90, 5901-5908.

Table 1. Experimental averages.		
Location	Ocean	Desert
N	9	10
$Z_i$ (m)	980	1750
$J_0$ (pA/m <sup>2</sup> )	-1.84	-2.38
$J_{max}$ (pA/m <sup>2</sup> )	1.37	0.69
R	0.10	0.07
$-Z_i/L$	129	62

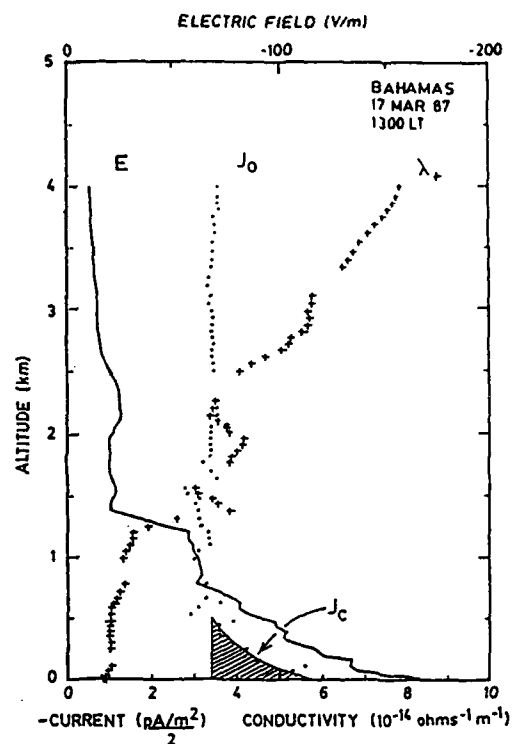


Fig. 1a. Profiles of electric field, conduction current and positive conductivity over the ocean.

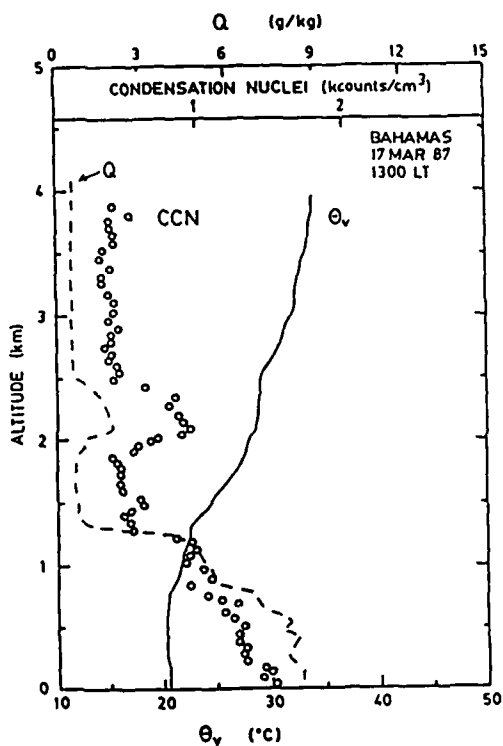


Fig. 1b. Profiles of specific humidity ( $Q$ ), virtual potential temperature ( $\theta_v$ ) and condensation nuclei (CCN) for Fig. 1a.

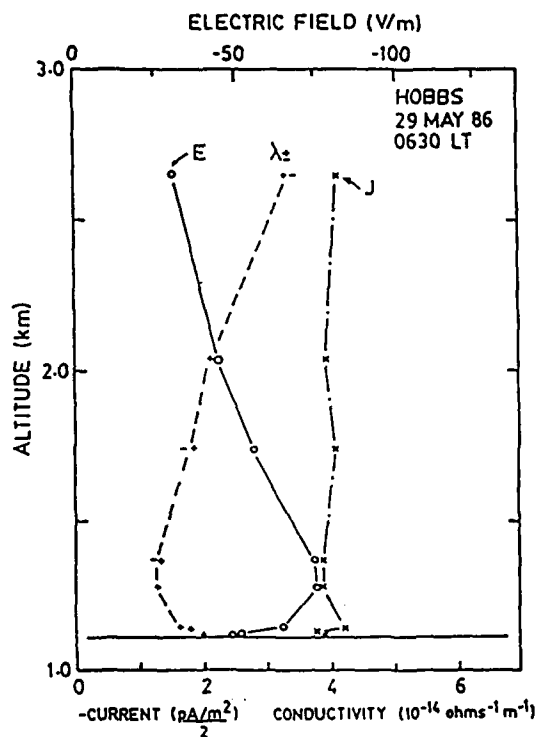


Fig. 2. Early morning sounding of electrical parameters over the desert.

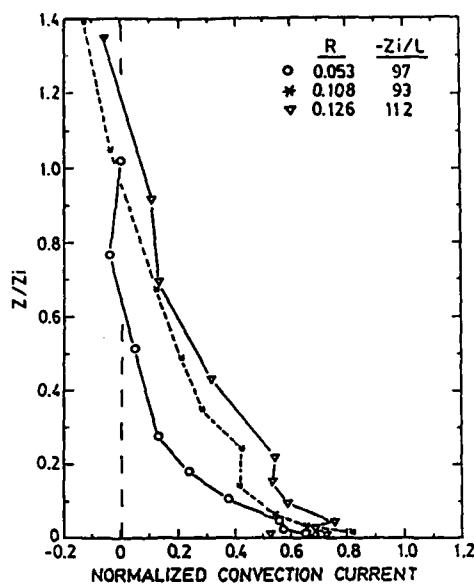


Fig. 3. Plots of  $-J_c/J_0$  versus normalized height illustrating the effect of varying  $R$ .

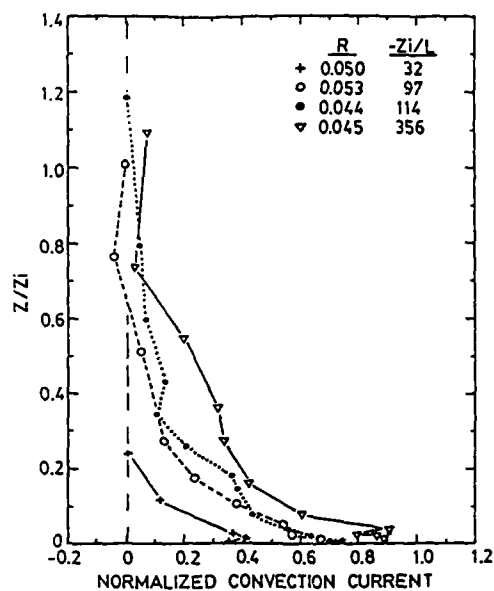


Fig. 4. Plots of  $-J_c/J_0$  versus normalized height showing effect of varying  $-Z_i/L$ .

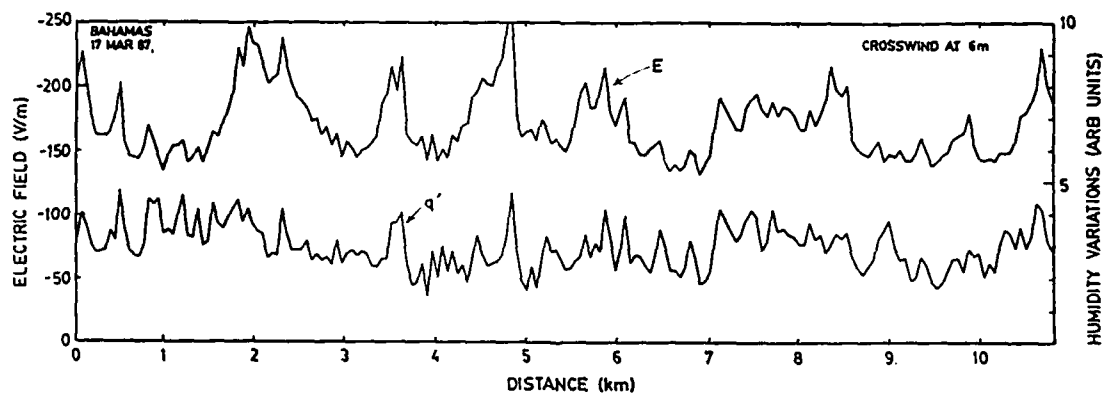


Fig. 5. Variation of electric field and humidity on crosswind pass over the ocean at 6 m.

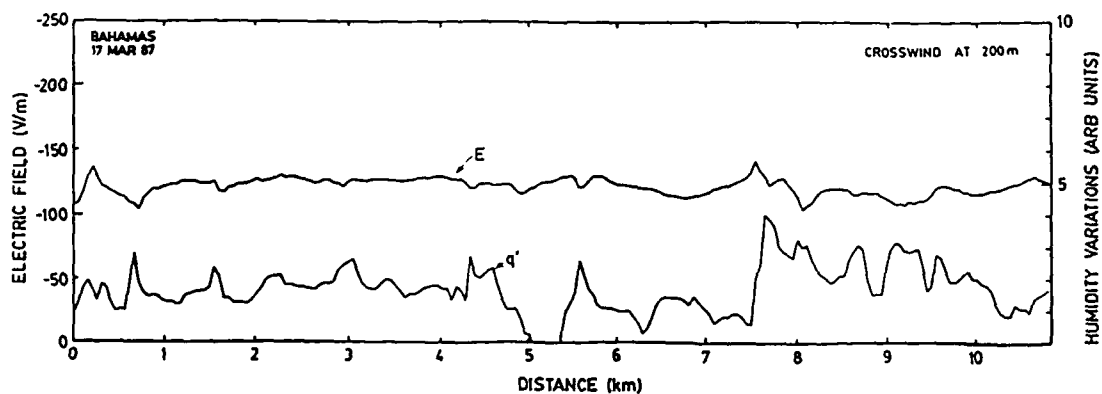


Fig. 6. The same as Fig. 5 at 200 m.

COMPARISON OF IONOSPHERIC POTENTIAL AND AIR-EARTH  
CURRENT AS INDICATORS OF THE GLOBAL CIRCUIT CURRENT

Ralph Markson

Center for Meteorology and Physical Oceanography  
Massachusetts Institute of Technology  
Cambridge, MA 02139

**ABSTRACT:** The sensitivity of ionospheric potential and air-earth conduction currents (above the exchange layer) to variation caused by processes in the planetary boundary layer are examined through analysis of atmospheric electrical soundings made over land and sea. It is found that the air-earth current is particularly sensitive to local variations in columnar resistance and convection of space charge as predicted by theory. It would not be a good parameter for measurement of temporal variation of the global circuit.

INTRODUCTION

A decade has passed since it was proposed that..."a Geoelectric Index representative of global thunderstorm currents should be established to complement the Geomagnetic Index which has proven invaluable in solar-terrestrial research" (Markson, 1979). Additional discussion in Markson and Muir (1980) concerned how such measurements could be obtained and utilized to test a proposed mechanism for solar control of the global circuit supply current through modulation of ionizing radiation over thunderclouds (Markson, 1978). There has been growing interest in establishing such an index, but no consensus exists on what the index or indices should be. Few and Weinheimer (1986) recommend measurement of the air-earth conduction current from a free balloon while Markson (1987) responded that ionospheric potential would be a better parameter because meteorological factors have appreciable influence on air-earth current.

Recently, in an investigation of the convective generator (Anderson et al., this volume), unique data sets have been obtained in which ionospheric potential ( $V_I$ ), air-earth current density above the exchange layer ( $J_O$ ), and the ionosphere-to-earth columnar resistance ( $R_I$ ) (as well as supporting data) have been measured simultaneously from an aircraft over land (Hobbs, New Mexico) and sea (the Bahamas). These measurements make it possible to quantitatively compare the effects of variations in  $R_I$  and vertical transport of space charge ( $J_C$ ), the convective generator, on  $V_I$  and  $J_O$ .

METEOROLOGICAL FACTORS

Columnar Resistance

By measuring conductivity profiles it is possible to compute columnar resistance which is the reciprocal of conductivity integrated between two heights; this is in effect the resistance of a column of 1 m<sup>2</sup> cross-section. A sounding between the ground and top of the sounding (apogee) provides the resistance in that column. The remainder of  $R_I$  to the ionosphere can be estimated by multiplying the resistivity (reciprocal of conductivity) and scale height at maximum altitude in the same way as electric field times scale height provides the voltage difference from apogee to the ionosphere when determining  $V_I$  (Markson, 1976). Thus, by adding the calculated increment to the

integrated value it is possible to estimate  $R_I$ . By Ohm's law, the air-earth current density  $J_I = V_I/R_I$ . Therefore, if  $V_I$  remains constant, an increase in  $R_I$  will cause a decrease in  $J_I$ . Since  $R_I$  is a function of aerosol loading and ionization rate, which in turn are modulated by numerous natural and man-made factors, it is expected that  $J_I$  will vary accordingly. Detailed discussion of how meteorological factors in the lower atmosphere affect  $V_I$  and  $J_O$  time-series are in Markson (1984; 1985).

### Convection Currents

The global electrical generator maintains the fair-weather conduction current above the exchange layer ( $J_O$ ) which is constant with altitude (Kraakevik, 1958; Markson, 1981; Anderson et al., this volume). This is because there are no generators in this region; changes in conductivity are exactly balanced by changes in electric field to maintain a constant current density from the ionosphere to the top of the planetary boundary layer (PBL). However, within the PBL (particularly over water) space charge is transported upward by air motions which constitutes a convective generator ( $J_C$ ) first described by Kasemir (1956). Thus, within the exchange layer the measured downward conduction current density (electric field times total conductivity) increases to balance the upward convection current. The potential at the top of the exchange layer is raised by  $J_C$  above what it would be if it were due only to  $J_O$ . Assuming  $V_I$  remains unaffected by local PBL processes, there must be an adjustment (reduction) in the potential gradient and  $J_O$  above the exchange layer because a smaller potential difference occurs between the PBL and the ionosphere (Willett, 1979). It is possible to determine the percent reduction in  $J_O$  above the PBL due to  $J_C$  through the fraction  $J_O/J_I = J_O/(V_I/R_I)$  which is the measured conduction current divided by what the current would have been if there were no  $J_C$ . We define this fraction as CF, the "convective factor".

In sum, changes in  $R_I$  and  $J_C$  within the exchange layer will affect the current density locally above the PBL, while at latitudes lower than the polar cap region (where there are no ionospheric or magnetospheric generators) the ionospheric potential will remain globally representative (Markson, 1985). This assumes  $J_C$  is a local generator; if  $J_C$  occupies a sufficiently large fraction of the Earth's surface,  $V_I$  could be increased. Time-series of  $J_O$  measured from a constant altitude balloon or aircraft well above the exchange layer crossing regions of variable  $R_I$  or  $J_C$  would undergo changes because of the factors described above.

### OBSERVATIONS AND DISCUSSION

Table I is a summary comparison between mean  $V_I$ ,  $J_O$ ,  $R_I$ , and CF values at Hobbs and the Bahamas. The effects of both the differences in  $R_I$  and CF between the locations is readily apparent. While the mean  $V_I$  was slightly larger (2%) in the Bahamas,  $J_O$  was 56% lower in the Bahamas, i.e.,  $(J_{\text{Hobbs}} - J_{\text{Bahamas}})/J_{\text{Bahamas}}$ . This was mostly caused by  $R_I$  at Hobbs being 32% lower than in the Bahamas causing an increase in current. It is also seen that the range of variations of  $J_O$  are appreciably larger at Hobbs as would be expected from a location where variations in aerosols, conductivity and convection are larger.

Table I. Comparison of Mean Hobbs vs Bahamas Data		
Parameters	Hobbs	Bahamas
$V_I$ (kV)	237	242
$J_I$ ( $\text{pA/m}^2$ ) measured	2.62	1.68
$J_O$ ( $\text{pA/m}^2$ ) range	1.4-3.2=128%	1.05-2.1)=100%
$R_I \times 10^{-16}$ ( $\text{ohm-m}^2$ )	9.36	13.7
$(J_O/J_I) = CF$	1.00	0.88

#### Bahamas Measurements

Figure 1 summarizes the relevant parameter time-series for the Bahamas data. Correlation coefficients have been computed and for 14 soundings (12 d.f.) the 5% and 1% levels of significance are  $r = 0.53$  and  $0.66$  respectively. The most obvious feature is the inverse correlation between  $J_I$  and  $R_I$  ( $r = -0.92$ ). It is also seen that  $J_I$  is positively correlated with  $CF$  ( $r = 0.89$ ). Thus both variations in  $R_I$  and  $J_O$  strongly modulate  $J_I$  in the expected directions. Considering the effects on the  $V_I$  measurement. It also is found that  $V_I$  is correlated with  $R_I$  ( $r = 0.63$ ), but not as strongly as  $R_I$  is with  $J_O$ , and the correlation is positive. This suggests that the soundings were not made sufficiently high and error was introduced into the  $V_I$  estimate because of aerosols affecting the electric field at apogee. The average height of the Bahamas soundings was 4.3 km. A summary of conductivity profiles from all sources (Fig. 3 of Markson, 1985) shows that it is necessary to make a sounding to 6 or 7 km to get into the region of exponential increase in conductivity with height which the scale height increment estimation procedure assumes. The effect of convection ( $CF$ ) on  $V_I$  is not statistically significant ( $r = -0.47$ ). There is a negative, but not statistically significant, correlation between  $V_I$  and  $J_O$  ( $r = -0.38$ ). Summarizing the Bahamas data, Fig. 1 indicates that  $R_I$  variations cause about 2/3 and  $J_O$  causes about 1/3 of the  $J_O$  variation.

#### Hobbs Measurements

The Hobbs data have been treated in the same manner. Fifteen soundings were made to a mean apogee of 6.3 km. Correlation coefficients (13 d.f.) at the 5% and 1% levels of significance are  $r = 0.51$  and  $0.64$ . The inverse correlation between  $J_I$  and  $R_I$  ( $r = -0.79$ ) is seen by inspection. Similarly there is a positive correlation between  $J_I$  and  $CF$  ( $r = 0.56$ ).  $J_I$  is affected as expected by  $R_I$  and  $J_O$ . Considering effects on  $V_I$ , the correlation with  $R_I$  ( $r = 0.42$ ) is again positive but smaller and not significant. This could be explained by the fact that the soundings were made to higher altitudes and there was less aerosol effects at Hobbs. There was no effect of  $CF$  on  $V_I$  ( $r = -0.11$ ) and no correlation between  $V_I$  and  $J_O$  ( $r = 0.09$ ).

Differences between the Bahamas and Hobbs results can be interpreted in view of differences in conditions between these regions as discussed in the companion paper by Anderson et al. At Hobbs there was very little  $J_O$  and the  $CF$  average was 1.00 (compared to 0.88 due to  $J_O$  in the Bahamas). Also the data for Hobbs had somewhat larger sources of error because of instrumentation factors and the fact that there was less horizontal homogeneity in the convectively unstable atmosphere. The latter affects the aircraft spiral soundings which are made over a region of about 5 to 10 km diameter.

## CONCLUSION

The above analysis indicates that measurements of  $J_0$  from a platform well above the exchange layer would be an unreliable method for observing the variation of current in the global circuit. Typical local variations caused by the combined effects of changes in  $R_1$  and convection of space charge could introduce variations on the order of 50%. It should also be recognized that regional and global variations in  $R_1$  from cosmic radiation ionization and aerosol loading will strongly modulate  $J_0$  which is twice as large at Spitsbergen and Greenland as in the Bahamas because of these factors (Markson, 1985).

## REFERENCES

- Anderson, B., R. Markson, C.W. Fairall and J.C. Willett, 1988: Aircraft investigation of electric charge flux over land and sea, this volume.
- Few, A.A. and A.J. Weinheimer, 1986: Factor of 2 error in balloon-borne atmospheric conduction current measurements, J. Geophys. Res., 91, 10937.
- Kasemir, H., 1956: Der Austauschgenerator, Archiv. Met. Geophys. Biokl., 9, 357.
- Kraakevik, J.H., 1958: Electrical conduction and convection currents in the troposphere, in Recent Advances in Atmospheric Electricity, edited by L.G. Smith, p. 75, Pergamon, New York.
- Markson, R., 1976: Ionospheric potential variations obtained from aircraft measurements of potential gradient, J. Geophys. Res., 81, 1980.
- Markson, R., 1978: Solar modulation of atmospheric electrification and possible implications for the sun-weather relationship, Nature, 273, 103.
- Markson, R., 1979: Atmospheric electricity and the sun-weather problem, in Solar-Terrestrial Influences on Weather and Climate, editors B.M. McCormac and T.A. Seliga, Reidel, Hingham, MA.
- Markson, R. and M. Muir, 1980: Solar wind control of the Earth's electric field, Science, 208, 979.
- Markson, R., J. Sedlacek and C.W. Fairall, 1981: Turbulent transport of electric charge in the marine atmospheric boundary layer, J. Geophys. Res., 86, 12115.
- Markson, R., 1984: Comment on "Hy-Wire measurements of atmospheric potential" by R.H. Holzworth, J. Geophys. Res., 89, 2629.
- Markson, R., 1985: Aircraft measurements of the atmospheric electrical global circuit during the period 1971-1984, J. Geophys. Res., 90, 5967.
- Markson, R., 1987: Comment on "Factor of 2 error in balloon-borne atmospheric conduction current measurements" by A.A. Few and A.J. Weinheimer, J. Geophys. Res., 92, 11003.
- Willett, J.C., 1979: Fair weather electric charge transfer by convection in an unstable planetary boundary layer, J. Geophys. Res., 84, 703.

## ACKNOWLEDGMENTS

I wish to thank to B. Anderson, C.W. Fairall and J.C. Willett who participated in the Hobbs and Bahamas field periods. B. Anderson and A. Kendra assisted in data reduction and analysis. I am particularly grateful to J. Willett for his insights into the problems discussed here during an ongoing dialogue over many years. Partial support for this research was under Air Force Office of Scientific Research Contract F49620-86-C-0013.

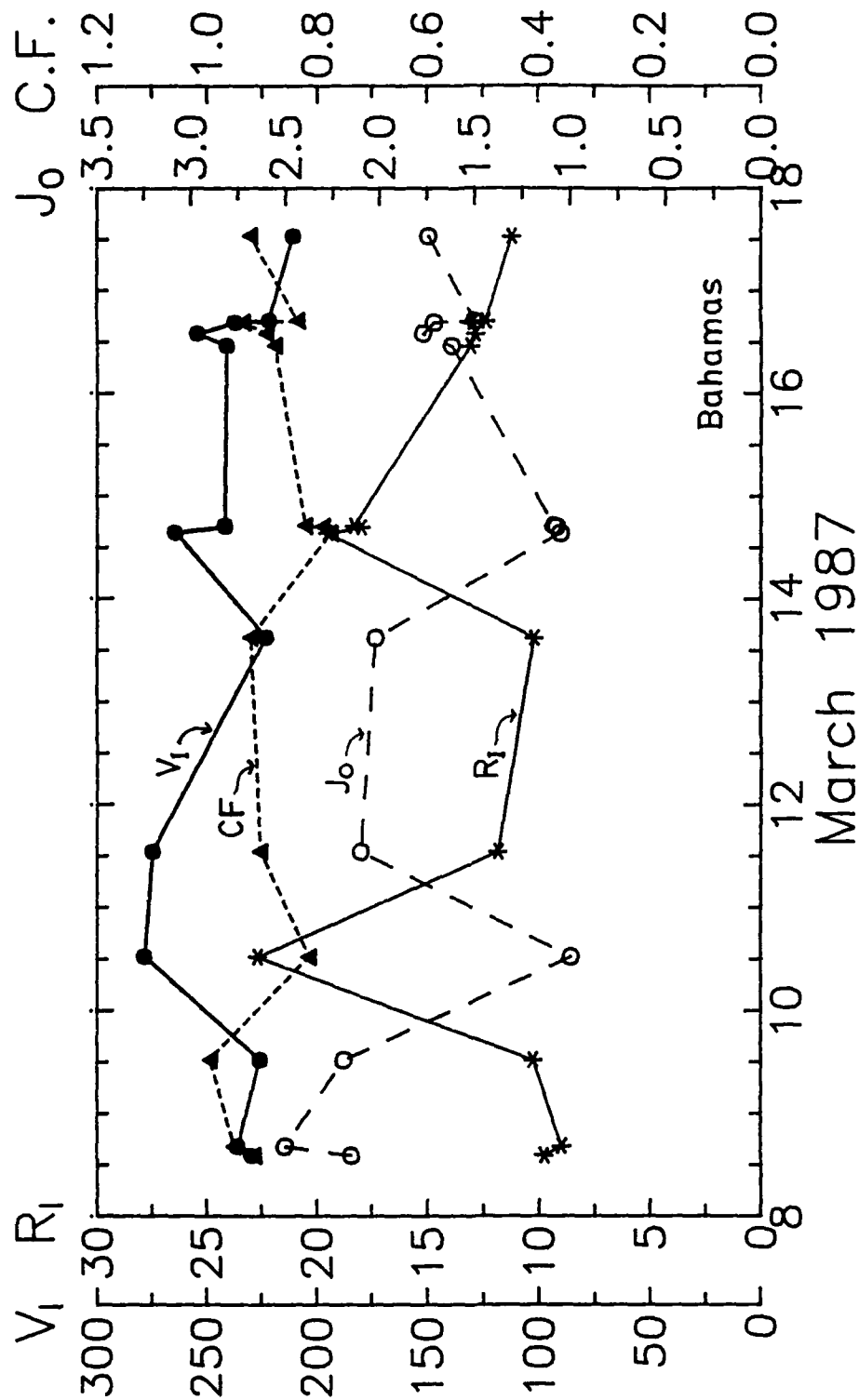


Fig. 1. Summary of means ( $n=14$ ) of ionospheric potential ( $V_1$ ), air-earth conduction current density above the exchange layer ( $J_0$ ), total columnar resistance ( $R_1$ ), and the "convection factor" ( $CF$ ), a measure of the effect of the convective generator on current above the exchange layer, in the Bahamas.



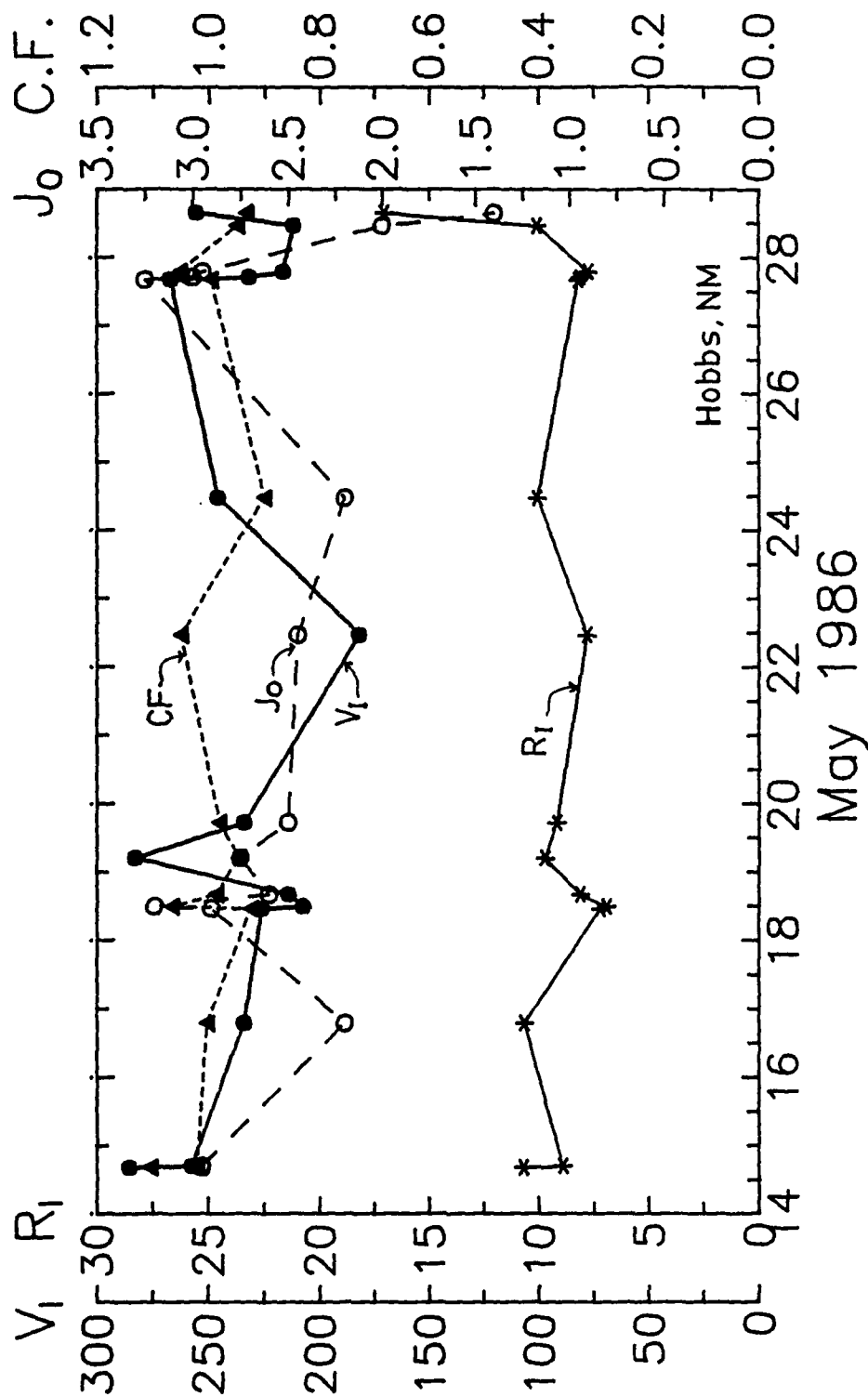


Fig. 2. Summary of means ( $n=15$ ) of ionospheric potential ( $V_I$ ), air-earth conduction current density above the exchange layer ( $J_o$ ), total columnar resistance ( $R_I$ ), and the "convection factor" (CF), a measure of the effect of the convective generator on current above the exchange layer, at Hobbs.